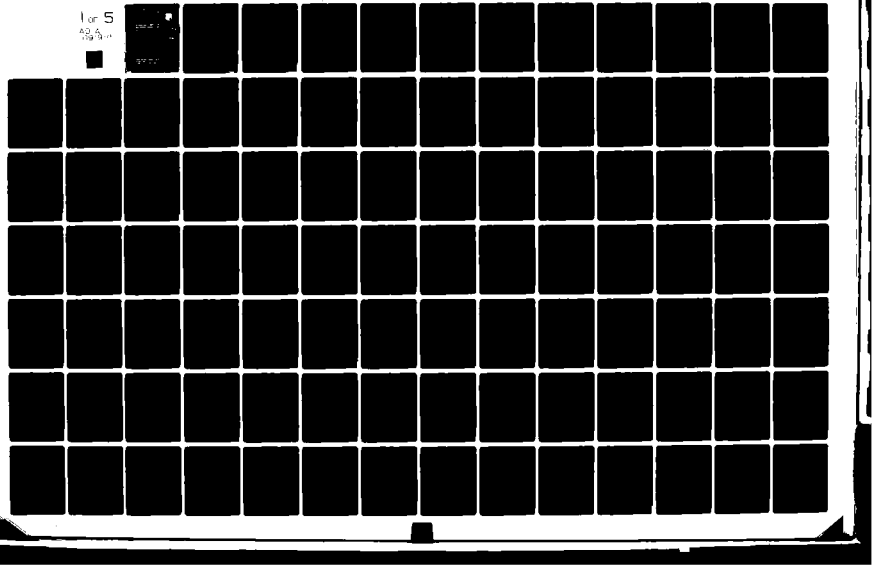
AD-A091 985 CNR INC NEEDHAM MA F/G 17/4
INTEGRATED CODING AND WAVEFORM DESIGN STUDY.(U)
AUG 80 D CHASE F30602-78-C-0309
UNCLASSIFIED RADC-TR-80-282 NL



LEVEL II

12

RADC-TR-80-282
Final Technical Report
August 1980

AD A091985

INTEGRATED CODING AND WAVEFORM DESIGN STUDY

CNR, Inc.

Dr. David Chase

DTIC
ELECTE
NOV 18 1980
S C

APPROVED FOR PUBLIC RELEASE; DISTRIBUTION UNLIMITED

ROME AIR DEVELOPMENT CENTER
Air Force Systems Command
Griffiss Air Force Base, New York 13441

80 11 18 053

INTEGRATED CODING AND WAVEFORM DESIGN

This report has been reviewed by the RADC Public Affairs Office (PA) and is releasable to the National Technical Information Service (NTIS). At NTIS it will be releasable to the general public, including foreign nations.

RADC-TR-80-282 has been reviewed and is approved for publication.

APPROVED: Frederick Schmandt

FREDERICK SCHMANDT
Project Engineer

APPROVED: Fred I. Diamond

FRED I. DIAMOND, Technical Director
Communications and Control Division

FOR THE COMMANDER: John P. Huss

JOHN P. HUSS
Acting Chief, Plans Orfice

SUBJECT TO EXPORT CONTROL LAWS

This document contains information for manufacturing or using munitions of war. Export of the information contained herein, or release to foreign nationals within the United States, without first obtaining an export license, is a violation of the International Traffic in Arms Regulations. Such violation is subject to a penalty of up to 2 years imprisonment and a fine of $100,000 under 22 U.S.C 2778.

Include this notice with any reproduced portion of this document.

If your address has changed or if you wish to be removed from the RADC mailing list, or if the addressee is no longer employed by your organization, please notify RADC (DCCT) Griffiss AFB NY 13441. This will assist us in maintaining a current mailing list.

Do not return this copy. Retain or destroy.

UNCLASSIFIED

SECURITY CLASSIFICATION OF THIS PAGE (When Data Entered)

REPORT DOCUMENTATION PAGE

READ INSTRUCTIONS BEFORE COMPLETING FORM

1. REPORT NUMBER: RADC-TR-80-282	2. GOVT ACCESSION NO.: AD-A091 985
3. RECIPIENT'S CATALOG NUMBER:	
4. TITLE (and Subtitle): INTEGRATED CODING AND WAVEFORM DESIGN STUDY	5. TYPE OF REPORT & PERIOD COVERED: Final Technical Report, Oct 78 — Oct 79
	6. PERFORMING ORG. REPORT NUMBER: N/A
7. AUTHOR(s): Dr. David Chase	8. CONTRACT OR GRANT NUMBER(s): F30602-78-C-0309
9. PERFORMING ORGANIZATION NAME AND ADDRESS: CNR, Inc. 220 Reservoir Street Needham MA 02194	10. PROGRAM ELEMENT, PROJECT, TASK AREA & WORK UNIT NUMBERS: 62702F 45192129
11. CONTROLLING OFFICE NAME AND ADDRESS: Rome Air Development Center (DCCT) Griffiss AFB NY 13441	12. REPORT DATE: August 1980
	13. NUMBER OF PAGES: 400
14. MONITORING AGENCY NAME & ADDRESS(if different from Controlling Office): Same	15. SECURITY CLASS. (of this report): UNCLASSIFIED
	15a. DECLASSIFICATION/DOWNGRADING SCHEDULE: N/A

16. DISTRIBUTION STATEMENT (of this Report)

Approved for public release; distribution unlimited.

17. DISTRIBUTION STATEMENT (of the abstract entered in Block 20, if different from Report)

Same

18. SUPPLEMENTARY NOTES

RADC Project Engineer: Frederick D. Schmandt (DCCT)

19. KEY WORDS (Continue on reverse side if necessary and identify by block number)

Error correction coding
Multiple-Access Concepts
Pulse interference with Adaptive Arrays

20. ABSTRACT (Continue on reverse side if necessary and identify by block number)

It is shown that error-correcting codes capable of correcting random/burst errors play a critical role in the design of reliable multiple-access and adaptive-array ECCM systems. A comprehensive investigation of effective block and convolutional coding techniques, as well as combinations of the above, is conducted for worst-case interference models which are applicable to a wide variety of digital communications systems. It is shown that essentially error-free communications are possible, even when sig-

DD FORM 1 JAN 73 1473 EDITION OF 1 NOV 65 IS OBSOLETE UNCLASSIFIED (Cont'd)

SECURITY CLASSIFICATION OF THIS PAGE (When Data Entered)

4107852

501

Item 20 (Cont'd)

nificant portions of the received data are completely destroyed by interference, providing a proper code rate and decoding technique are selected. The results in this report may be used to select error-correcting codes to improve the performance of existing systems as well as to optimize the integration of the coding and waveform design in new digital communications network.

PREFACE

This final report, covering the period October 1978 to October 1979, was prepared by CNR, Inc. of Needham, Massachusetts, under Contract No. F30602-78-C-0309 with Rome Air Development Center, Griffiss Air Force Base, New York.

The principal investigator and manager for this project was Dr. David Chase. Contributions to this report were made by Dr. John O'Donnell, Mr. Einar Gudjohnsen, and Mr. Robert Pinto.

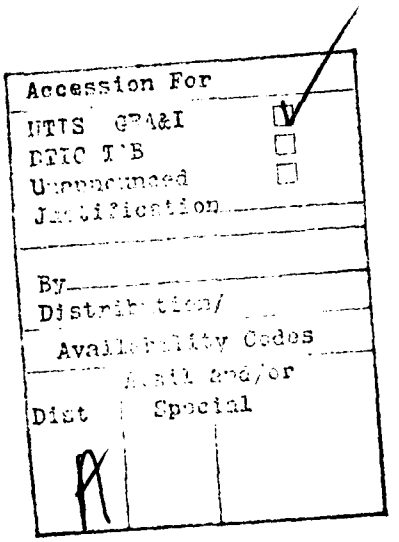


TABLE OF CONTENTS

Section		Page
1	INTRODUCTION	1-1
2	MULTIPLE-ACCESS CONCEPTS FOR BURSTY COMMUNICATIONS SOURCES	2-1
	2.1 Introduction	2-1
	2.2 Multiple-Access Channel Definitions	2-1
	2.3 Code Division (Direct Sequence Spread Spectrum) Multiple-Access (CDMA) Systems	2-5
	2.4 Slotted Aloha Multiple-Access System	2-8
	2.5 Versatile Multiple-Access (VMA) System	2-11
	2.6 Summary	2-17
3	PULSE JAMMING OF AN ADAPTIVE ANTENNA	3-1
	3.1 Background for Single Adaptive Loop	3-1
	3.2 Development of Steady-State Solution	3-8
	3.3 Loop Performance Data	3-12
	3.4 Extension to Sidelobe Canceller	3-30
4	PERFORMANCE ANALYSIS FOR ERROR-CORRECTING CODES OPERATING IN THE PRESENCE OF INTERFERENCE	4-1
	4.1 Channel Models for Interference	4-1
	4.2 Probability of Error between Two Sequences	4-5
	4.2.1 Binary Decoding	4-5
	4.2.2 Binary Decoding with Interference (Model 2)	4-7
	4.2.3 Binary Decoding with Interference and Erasure Information (Model 4)	4-7
	4.2.4 Channel Measurement Decoding	4-8
	4.2.5 Channel Measurement Decoding with Interference (Model 1)	4-10
	4.2.6 Channel Measurement Decoding with Interference and Erasure Information (Model 3)	4-11
	4.3 Probability of Error for Convolutional Codes	4-11
	4.4 Probability of an Error for Block Codes	4-17
	4.4.1 Binary Decoding	4-18
	4.4.2 Binary Decoding with Interference (Model 2)	4-19

TABLE OF CONTENTS (continued)

Section		Page
	4.4.3 Binary Decoding with Interference and Erasure Information (Model 4)	4-19
	4.5 Two-Stage Coding Approaches	4-22
	4.5.1 Interleaved Inner and Outer Coding Approaches (Nonadaptive)	4-22
	4.5.2 Adaptive Inner and Outer Coding Techniques	4-26
5	PERFORMANCE OF BLOCK CODES IN THE PRESENCE OF INTERFERENCE	5-1
6	PERFORMANCE OF CONVOLUTIONAL CODES IN THE PRESENCE OF INTERFERENCE	6-1
7	TWO-STAGE CODING APPROACHES BASED ON A LONG INNER BLOCK CODE	7-1
8	TWO-STAGE CODING APPROACH BASED ON A CONVOLUTIONAL INNER CODE	8-1
9	TWO-STAGE CODING APPROACH BASED ON A REED-SOLOMON OUTER CODE	9-1
10	CONCLUSIONS AND RECOMMENDATIONS FOR FUTURE WORK	10-1
Appendix		
A	EVALUATION OF CONVOLUTIONAL CODES FOR AN AVERAGE POWER-LIMITED PULSE JAMMING MODEL	A-1
B	EFFECTS OF QUANTIZATION ON THE PERFORMANCE OF CONVOLUTIONAL CODES IN THE PRESENCE OF INTERFERENCE	B-1
C	RANDOMIZED INTERLEAVER CONCEPTS	C-1

LIST OF ILLUSTRATIONS

Figure		Page
1.1	Block Diagram of the Communication System of Interest	1-2
2.1	Examples of Channel Allocations with M Degrees of Freedom	2-2
3.1	Two-Element Array with Single Adaptive Loop	3-2
3.2	Signal Phase Reference Diagram for Two-Element Array	3-4
3.3	Loop Performance at Jammer Angle of 5^{o}	3-16
3.4	Loop Performance at Jammer Angle of 10^{o}	3-17
3.5	Loop Performance at Jammer Angle of 20^{o}	3-18
3.6	Loop Performance at Jammer Angle of 30^{o}	3-19
3.7	Loop Performance at Jammer Angle of 40^{o}	3-20
3.8	Loop Performance at Jammer Angle of 50^{o}	3-21
3.9	Loop Performance at Jammer Angle of 60^{o}	3-22
3.10	Loop Performance at Jammer Angle of 70^{o}	3-23
3.11	Loop Performance at Jammer Angle of 80^{o}	3-24
3.12	Signal Phase Reference Diagram for Main Antenna with Auxiliary	3-33
3.13	Output Noise Increase as a Function of Angle Off Boresight for Sidelobe Canceller (m = 4)	3-36
4.1	Block Diagram of an Interleaved Inner and Outer Coding Approach	4-23
4.2	Comparison of Error Rate Performance for R = 0.9 Codes	4-27

LIST OF ILLUSTRATIONS (continued)

Figure		Page
5.1	Decoded Performance of a Block Code Dimensions (24,12;8); No Interference; No Erasure Information	5-4
5.2	Decoded Performance of a Block Code Dimensions (24,12;8); Interference Occurs with Probability 0.05; No Erasure Information	5-5
5.3	Decoded Performance of a Block Code Dimensions (24,12;8); Interference Occurs with Probability 0.10; No Erasure Information	5-6
5.4	Decoded Performance of a Block Code Dimensions (24,12;8); Interference Occurs with Probability 0.15; No Erasure Information	5-7
5.5	Decoded Performance of a Block Code Dimensions (24,12;8); Interference Occurs with Probability 0.20; No Erasure Information	5-8
5.6	Decoded Performance of a Block Code Dimensions (24,12;8); Interference Occurs with Probability 0.05; Erasure Information Employed	5-9
5.7	Decoded Performance of a Block Code Dimensions (24,12;8); Interference Occurs with Probability 0.10; Erasure Information Employed	5-10
5.8	Decoded Performance of a Block Code Dimensions (24,12;8); Interference Occurs with Probability 0.15; Erasure Information Employed	5-11
5.9	Decoded Performance of a Block Code Dimensions (24,12;8); Interference Occurs with Probability 0.20; Erasure Information Employed	5-12
5.10	Decoded Performance of a Block Code Dimensions (128,64;22); No Interference, No Erasure Information	5-13

LIST OF ILLUSTRATIONS (continued)

Figure		Page
5.11	Decoded Performance of a Block Code Dimensions (128,64;22); Interference Occurs with Probability 0.05; No Erasure Information	5-14
5.12	Decoded Performance of a Block Code Dimensions (128,64;22); Interference Occurs with Probability 0.10; No Erasure Information	5-15
5.13	Decoded Performance of a Block Code Dimensions (128,64;22); Interference Occurs with Probability 0.15; No Erasure Information	5-16
5.14	Decoded Performance of a Block Code Dimensions (128,64;22); Interference Occurs with Probability 0.20; No Erasure Information	5-17
5.15	Decoded Performance of a Block Code Dimensions (128,64;22); Interference Occurs with Probability 0.05; Erasure Information Employed	5-18
5.16	Decoded Performance of a Block Code Dimensions (128,64;22); Interference Occurs with Probability 0.10; Erasure Information Employed	5-19
5.17	Decoded Performance of a Block Code Dimensions (128,64;22); Interference Occurs with Probability 0.15; Erasure Information Employed	5-20
5.18	Decoded Performance of a Block Code Dimensions (128,64;22); Interference Occurs with Probability 0.20; Erasure Information Employed	5-21
5.19	Decoded Performance of a Block Code Dimensions (24,12;8); No Interference, No Erasure Information	5-22
5.20	Decoded Performance of a Block Code Dimensions (24,12;8); Interference Occurs with Probability 0.05; No Erasure Information	5-23

LIST OF ILLUSTRATIONS (continued)

Figure		Page
5.21	Decoded Performance of a Block Code Dimensions (24,12;8); Interference Occurs with Probability 0.10; No Erasure Information	5-24
5.22	Decoded Performance of a Block Code Dimensions (24,12;8); Interference Occurs with Probability 0.15; No Erasure Information	5-25
5.23	Decoded Performance of a Block Code Dimensions (24,12;8); Interference Occurs with Probability 0.20; No Erasure Information	5-26
5.24	Decoded Performance of a Block Code Dimensions (24,12;8); Interference Occurs with Probability 0.05; Erasure Information Employed	5-27
5.25	Decoded Performance of a Block Code Dimensions (24,12;8); Interference Occurs with Probability 0.10; Erasure Information Employed	5-28
5.26	Decoded Performance of a Block Code Dimensions (24,12;8); Interference Occurs with Probability 0.15; Erasure Information Employed	5-29
5.27	Decoded Performance of a Block Code Dimensions (24,12;8); Interference Occurs with Probability 0.20; Erasure Information Employed	5-30
6.1	Decoded Performance of a Convolutional Code Rate 1/2; Constraint Length = 7; No Interference No Erasure Information	6-3
6.2	Decoded Performance of a Convolutional Code Rate 1/2; Constraint Length = 7; Interference Occurs with Probability 0.05; No Erasure Information	6-4

LIST OF ILLUSTRATIONS (continued)

Figure		Page
6.3	Decoded Performance of a Convolutional Code Rate 1/2; Constraint Length = 7; Interference Occurs with Probability 0.10; No Erasure Information	6-5
6.4	Decoded Performance of a Convolutional Code Rate 1/2; Constraint Length = 7; Interference Occurs with Probability 0.15; No Erasure Information	6-6
6.5	Decoded Performance of a Convolutional Code Rate 1/2; Constraint Length = 7; Interference Occurs with Probability 0.20; No Erasure Information	6-7
6.6	Decoded Performance of a Convolutional Code Rate 1/2; Constraint Length = 7; Interference Occurs with Probability 0.05; Erasure Information Employed	6-8
6.7	Decoded Performance of a Convolutional Code Rate 1/2; Constraint Length = 7; Interference Occurs with Probability 0.10; Erasure Information Employed	6-9
6.8	Decoded Performance of a Convolutional Code Rate 1/2; Constraint Length = 7; Interference Occurs with Probability 0.15; Erasure Information Employed	6-10
6.9	Decoded Performance of a Convolutional Code Rate 1/2; Constraint Length = 7; Interference Occurs with Probability 0.20; Erasure Information Employed	6-11
6.10	Decoded Performance of a Convolutional Code Rate 1/4; Constraint Length = 7; No Interference; No Erasure Information	6-12

LIST OF ILLUSTRATIONS (continued)

Figure		Page
6.11	Decoded Performance of a Convolutional Code Rate 1/4; Constraint Length = 7; Interference Occurs with Probability 0.05; No Erasure Information	6-13
6.12	Decoded Performance of a Convolutional Code Rate 1/4; Constraint Length = 7; Interference Occurs with Probability 0.10; No Erasure Information	6-14
6.13	Decoded Performance of a Convolutional Code Rate 1/4; Constraint Length = 7; Interference Occurs with Probability 0.15; No Erasure Information	6-15
6.14	Decoded Performance of a Convolutional Code Rate 1/4; Constraint Length = 7; Interference Occurs with Probability 0.20; No Erasure Information	6-16
6.15	Decoded Performance of a Convolutional Code Rate 1/4; Constraint Length = 7; Interference Occurs with Probability 0.05; Erasure Information Employed	6-17
6.16	Decoded Performance of a Convolutional Code Rate 1/4; Constraint Length = 7; Interference Occurs with Probability 0.10; Erasure Information Employed	6-18
6.17	Decoded Performance of a Convolutional Code Rate 1/4; Constraint Length = 7; Interference Occurs with Probability 0.15; Erasure Information Employed	6-19
6.18	Decoded Performance of a Convolutional Code Rate 1/4; Constraint Length = 7; Interference Occurs with Probability 0.20; Erasure Information Employed	6-20

LIST OF ILLUSTRATIONS (continued)

Figure		Page
6.19	Decoded Performance of a Convolutional Code Rate 1/8; Constraint Length = 7; No Interference; No Erasure Information	6-21
6.20	Decoded Performance of a Convolutional Code Rate 1/8; Constraint Length = 7; Interference Occurs with Probability 0.05; No Erasure Information	6-22
6.21	Decoded Performance of a Convolutional Code Rate 1/8; Constraint Length = 7; Interference Occurs with Probability 0.10; No Erasure Information	6-23
6.22	Decoded Performance of a Convolutional Code Rate 1/8; Constraint Length = 7; Interference Occurs with Probability 0.15; No Erasure Information	6-24
6.23	Decoded Performance of a Convolutional Code Rate 1/8; Constraint Length = 7; Interference Occurs with Probability 0.20; No Erasure Information	6-25
6.24	Decoded Performance of a Convolutional Code Rate 1/8; Constraint Length = 7; Interference Occurs with Probability 0.05; Erasure Information Employed	6-26
6.25	Decoded Performance of a Convolutional Code Rate 1/8; Constraint Length = 7; Interference Occurs with Probability 0.10; Erasure Information Employed	6-27
6.26	Decoded Performance of a Convolutional Code Rate 1/8; Constraint Length = 7; Interference Occurs with Probability 0.15; Erasure Information Employed	6-28

LIST OF ILLUSTRATIONS (continued)

Figure		Page
6.27	Decoded Performance of a Convolutional Code Rate 1/8; Constraint Length = 7; Interference Occurs with Probability 0.20; Erasure Information Employed	6-29
6.28	Convolutional Coding Performance with Code Rate as a Parameter; Channel Measurement Decoding-No Erasure Information	6-32
6.29	Convolutional Coding Performance with Code Rate as a Parameter; Binary Decoding-No Erasure Information	6-33
6.30	Convolutional Coding Performance with Code Rate as a Parameter; Channel Measurement Decoding-Erasure Information Available	6-34
6.31	Convolutional Coding Performance with Code Rate as a Parameter; Binary Decoding-Erasure Information Available	6-35
6.32	Convolutional Coding Performance with Interference Probability as a Parameter; Channel Measurement-Decoding-No Erasure Information	6-36
6.33	Convolutional Coding Performance with Interference Probability as a Parameter; Binary Decoding-No Erasure Information	6-37
6.34	Convolutional Coding Performance with Interference Probability as a Parameter; Channel Measurement Decoding-Erasure Information Available	6-38
6.35	Convolutional Coding Performance with Interference Probability as a Parameter; Binary Decoding-Erasure Information Available	6-39
6.36	Minimum E_b/N_0 for the Gaussian Channel and Channel Measurement Decoding	6-40

LIST OF ILLUSTRATIONS (continued)

Figure		Page
6.37	Minimum E_b/N_0 for the Gaussian Channel and Binary Decoding	6-41
6.38	Minimum E_b/N_0 for the Gaussian Channel and Channel Measurement Decoding with an Erasure Signal	6-42
6.39	Minimum E_b/N_0 for the Gaussian Channel and Binary Decoding with an Erasure Signal	6-43
7.1	Decoded Performance of a Two-Stage Coding Approach Outer Decoder: BCH Code (240,216;7) Inner Decoder: Block Code (128,64;22) δ=0.0 and No Erasure Information Employed	7-3
7.2	Decoded Performance of a Two-Stage Coding Approach Outer Decoder: BCH Code (240,216;7) Inner Decoder: Block Code (128,64;22) δ=0.05 and No Erasure Information Employed	7-4
7.3	Decoded Performance of a Two-Stage Coding Approach Outer Decoder: BCH Code (240,216;7) Inner Decoder: Block Code (128,64;22) δ=0.10 and No Erasure Information Employed	7-5
7.4	Decoded Performance of a Two-Stage Coding Approach Outer Decoder: BCH Code (240,216;7) Inner Decoder: Block Code (128,64;22) δ=0.15 and No Erasure Information Employed	7-6
7.5	Decoded Performance of a Two-Stage Coding Approach Outer Decoder: BCH Code (240,216;7) Inner Decoder: Block Code (128,64;22) δ=0.20 and No Erasure Information Employed	7-7
7.6	Decoded Performance of a Two-Stage Coding Approach Outer Decoder: BCH Code (240,216;7) Inner Decoder: Block Code (128,64;22) δ=0.05 and Erasure Information is Employed	7-8

LIST OF ILLUSTRATIONS (continued)

Figure		Page
7.7	Decoded Performance of a Two-Stage Coding Approach Outer Decoder: BCH Code (240,216;7) Inner Decoder: Block Code (128,64;22) δ=0.10 and Erasure Information is Employed	7-9
7.8	Decoded Performance of a Two-Stage Coding Approach Outer Decoder: BCH Code (240,216;7) Inner Decoder: Block Code (128,64;22) δ=0.15 and Erasure Information is Employed	7-10
7.9	Decoded Performance of a Two-Stage Coding Approach Outer Decoder: BCH Code (240,216;7) Inner Decoder: Block Code (128,64;22) δ=0.20 and Erasure Information is Employed	7-11
7.10	Decoded Performance of a Two-Stage Coding Approach Outer Decoder: BCH Code (128,64;22) Inner Decoder: Block Code (128,64;22) δ=0.00 and No Erasure Information Employed	7-12
7.11	Decoded Performance of a Two-Stage Coding Approach Outer Decoder: BCH Code (128,64;22) Inner Decoder: Block Code (128,64;22) δ=0.05 and No Erasure Information Employed	7-13
7.12	Decoded Performance of a Two-Stage Coding Approach Outer Decoder: BCH Code (128,64;22) Inner Decoder: Block Code (128,64;22) δ=0.10 and No Erasure Information Employed	7-14
7.13	Decoded Performance of a Two-Stage Coding Approach Outer Decoder: BCH Code (128,64;22) Inner Decoder: Block Code (128,64;22) δ=0.15 and No Erasure Information Employed	7-15
7.14	Decoded Performance of a Two-Stage Coding Approach Outer Decoder: BCH Code (128,64;22) Inner Decoder: Block Code (128,64;22) δ=0.20 and No Erasure Information Employed	7-16

LIST OF ILLUSTRATIONS (continued)

Figure		Page
7.15	Decoded Performance of a Two-Stage Coding Approach Outer Decoder: BCH Code (128,64;22) Inner Decoder: Block Code (128,64;22) δ=0.05 and Erasure Information is Employed	7-17
7.16	Decoded Performance of a Two-Stage Coding Approach Outer Decoder: BCH Code (128,64;22) Inner Decoder: Block Code (128,64;22) δ=0.10 and Erasure Information is Employed	7-18
7.17	Decoded Performance of a Two-Stage Coding Approach Outer Decoder: BCH Code (128,64;22) Inner Decoder: Block Code (128,64;22) δ=0.15 and Erasure Information is Employed	7-19
7.18	Decoded Performance of a Two-Stage Coding Approach Outer Decoder: BCH Code (128,64;22) Inner Decoder: Block Code (128,64;22) δ=0.20 and Erasure Information is Employed	7-20
7.19	Decoded Performance of a Two-Stage Coding Approach Adaptive Technique Outer Decoder: BCH Code (240,216;7) Inner Decoder: Block Code (128,64;22) δ=0.00 and No Erasure Information Employed	7-21
7.20	Decoded Performance of a Two-Stage Coding Approach Adaptive Technique Outer Decoder: BCH Code (240,216;7) Inner Decoder: Block Code (128,64;22) δ=0.05 and No Erasure Information Employed	7-22
7.21	Decoded Performance of a Two-Stage Coding Approach Adaptive Technique Outer Decoder: BCH Code (128,64;22) Inner Decoder: Block Code (128,64;22) δ=0.00 and No Erasure Information Employed	7-23

LIST OF ILLUSTRATIONS (continued)

Figure		Page
7.22	Decoded Performance of a Two-Stage Coding Approach Adaptive Technique Outer Decoder: BCH Code (128,64;22) Inner Decoder: Block Code (128,64;22) δ=0.05 and No Erasure Information Employed	7-24
7.23	Decoded Performance of a Two-Stage Coding Approach Adaptive Technique Outer Decoder: BCH Code (128,64;22) Inner Decoder: Block Code (128,64;22) δ=0.10 and No Erasure Information Employed	7-25
8.1	Decoded Performance of a Two-Stage Coding Approach Outer Decoder: BCH Code (240,216;7) Inner Decoder: Convolutional Code; Rate=1/2; K=7 δ=0.00 and No Erasure Information Employed	8-3
8.2	Decoded Performance of a Two-Stage Coding Approach Outer Decoder: BCH Code (240,216;7) Inner Decoder: Convolutional Code; Rate=1/2; K=7 δ=0.05 and No Erasure Information Employed	8-4
8.3	Decoded Performance of a Two-Stage Coding Approach Outer Decoder: BCH Code (240,216;7) Inner Decoder: Convolutional Code; Rate=1/2; K=7 δ=0.10 and No Erasure Information Employed	8-5
8.4	Decoded Performance of a Two-Stage Coding Approach Outer Decoder: BCH Code (240,216;7) Inner Decoder: Convolutional Code; Rate=1/2; K=7 δ=0.15 and No Erasure Information Employed	8-6
8.5	Decoded Performance of a Two-Stage Coding Approach Outer Decoder: BCH Code (240,216;7) Inner Decoder: Convolutional Code; Rate=1/2; K=7 δ=0.20 and No Erasure Information Employed	8-7
8.6	Decoded Performance of a Two-Stage Coding Approach Outer Decoder: BCH Code (240,216;7) Inner Decoder: Convolutional Code; Rate=1/2; K=7 δ=0.05 and Erasure Information is Employed	8-8

LIST OF ILLUSTRATIONS (continued)

Figure		Page
8.7	Decoded Performance of a Two-Stage Coding Approach Outer Decoder: BCH Code (240,216;7) Inner Decoder: Convolutional Code; Rate=1/2; K=7 δ=0.10 and Erasure Information is Employed	8-9
8.8	Decoded Performance of a Two-Stage Coding Approach Outer Decoder: BCH Code (240,216;7) Inner Decoder: Convolutional Code; Rate=1/2; K=7 δ=0.15 and Erasure Information is Employed	8-10
8.9	Decoded Performance of a Two-Stage Coding Approach Outer Decoder: BCH Code (240,216;7) Inner Decoder: Convolutional Code; Rate=1/2; K=7 δ=0.20 and Erasure Information is Employed	8-11
8.10	Decoded Performance of a Two-Stage Coding Approach Outer Decoder: BCH Code (240,216;7) Inner Decoder: Convolutional Code; Rate=1/4; K=7 δ=0.00 and No Erasure Information is Employed	8-12
8.11	Decoded Performance of a Two-Stage Coding Approach Outer Decoder: BCH Code (240,216;7) Inner Decoder: Convolutional Code; Rate=1/4; K=7 δ=0.05 and No Erasure Information Employed	8-13
8.12	Decoded Performance of a Two-Stage Coding Approach Outer Decoder: BCH Code (240,216;7) Inner Decoder: Convolutional Code; Rate=1/4; K=7 δ=0.10 and No Erasure Information Employed	8-14
8.13	Decoded Performance of a Two-Stage Coding Approach Outer Decoder: BCH Code (240,216;7) Inner Decoder: Convolutional Code; Rate=1/4; K=7 δ=0.15 and No Erasure Information Employed	8-15
8.14	Decoded Performance of a Two-Stage Coding Approach Outer Decoder: BCH Code (240,216;7) Inner Decoder: Convolutional Code; Rate=1/4; K=7 δ=0.20 and No Erasure Information Employed	8-16

LIST OF ILLUSTRATIONS (continued)

Figure		Page
8.15	Decoded Performance of a Two-Stage Coding Approach Outer Decoder: BCH Code (240,216;7) Inner Decoder: Convolutional Code; Rate=1/4; K=7 δ=0.05 and Erasure Information is Employed	8-17
8.16	Decoded Performance of a Two-Stage Coding Approach Outer Decoder: BCH Code (240,216;7) Inner Decoder: Convolutional Code; Rate=1/4; K=7 δ=0.10 and Erasure Information is Employed	8-18
8.17	Decoded Performance of a Two-Stage Coding Approach Outer Decoder: BCH Code (240,216;7) Inner Decoder: Convolutional Code; Rate=1/4; K=7 δ=0.15 and Erasure Information is Employed	8-19
8.18	Decoded Performance of a Two-Stage Coding Approach Outer Decoder: BCH Code (240,216;7) Inner Decoder: Convolutional Code; Rate=1/4; K=7 δ=0.20 and Erasure Information is Employed	8-20
8.19	Decoded Performance of a Two-Stage Coding Approach Outer Decoder: BCH Code (240,216;7) Inner Decoder: Convolutional Code; Rate=1/8; K=7 δ=0.00 and No Erasure Information Employed	8-21
8.20	Decoded Performance of a Two-Stage Coding Approach Outer Decoder: BCH Code (240,216;7) Inner Decoder: Convolutional Code; Rate=1/8; K=7 δ=0.05 and No Erasure Information Employed	8-22
8.21	Decoded Performance of a Two-Stage Coding Approach Outer Decoder: BCH Code (240,216;7) Inner Decoder: Convolutional Code; Rate=1/8; K=7 δ=0.10 and No Erasure Information Employed	8-23
8.22	Decoded Performance of a Two-Stage Coding Approach Outer Decoder: BCH Code (240,216;7) Inner Decoder: Convolutional Code; Rate=1/8; K=7 δ=0.15 and No Erasure Information Employed	8-24

LIST OF ILLUSTRATIONS (continued)

Figure		Page
8.23	Decoded Performance of a Two-Stage Coding Approach Outer Decoder: BCH Code (240,216;7) Inner Decoder: Convolutional Code; Rate=1/8; K=7 δ=0.20 and No Erasure Information Employed	8-25
8.24	Decoded Performance of a Two-Stage Coding Approach Outer Decoder: BCH Code (240,216;7) Inner Decoder: Convolutional Code; Rate=1/8; K=7 δ=0.05 and Erasure Information is Employed	8-26
8.25	Decoded Performance of a Two-Stage Coding Approach Outer Decoder: BCH Code (240,216;7) Inner Decoder: Convolutional Code; Rate=1/8; K=7 δ=0.10 and Erasure Information is Employed	8-27
8.26	Decoded Performance of a Two-Stage Coding Approach Outer Decoder: BCH Code (240,216;7) Inner Decoder: Convolutional Code; Rate=1/8; K=7 δ=0.15 and Erasure Information is Employed	8-28
8.27	Decoded Performance of a Two-Stage Coding Approach Outer Decoder: BCH Code (240,216;7) Inner Decoder: Convolutional Code; Rate=1/8; K=7 δ=0.20 and Erasure Information is Employed	8-29
8.28	Decoded Performance of a Two-Stage Coding Approach Outer Decoder: Convolutional Code, Rate=1/2; K=7 Inner Decoder: Convolutional Code, Rate=1/2; K=7 δ=0.00 and No Erasure Information Employed	8-30
8.29	Decoded Performance of a Two-Stage Coding Approach Outer Decoder: Convolutional Code, Rate=1/2; K=7 Inner Decoder: Convolutional Code, Rate=1/2; K=7 δ=0.05 and No Erasure Information Employed	8-31
8.30	Decoded Performance of a Two-Stage Coding Approach Outer Decoder: Convolutional Code, Rate=1/2; K=7 Inner Decoder: Convolutional Code, Rate=1/2; K=7 δ=0.10 and No Erasure Information Employed	8-32

LIST OF ILLUSTRATIONS (continued)

Figure		Page
8.31	Decoded Performance of a Two-Stage Coding Approach Outer Decoder: Convolutional Code, Rate=1/2; K=7 Inner Decoder: Convolutional Code, Rate=1/2; K=7 δ=0.15 and No Erasure Information Employed	8-33
8.32	Decoded Performance of a Two-Stage Coding Approach Outer Decoder: Convolutional Code, Rate=1/2; K=7 Inner Decoder: Convolutional Code, Rate=1/2; K=7 δ=0.20 and No Erasure Information Employed	8-34
8.33	Decoded Performance of a Two-Stage Coding Approach Outer Decoder: Convolutional Code, Rate=1/2; K=7 Inner Decoder: Convolutional Code, Rate=1/2; K=7 δ=0.05 and Erasure Information is Employed	8-35
8.34	Decoded Performance of a Two-Stage Coding Approach Outer Decoder: Convolutional Code, Rate=1/2; K=7 Inner Decoder: Convolutional Code, Rate=1/2; K=7 δ=0.10 and Erasure Information is Employed	8-36
8.35	Decoded Performance of a Two-Stage Coding Approach Outer Decoder: Convolutional Code, Rate=1/2; K=7 Inner Decoder: Convolutional Code, Rate=1/2; K=7 δ=0.15 and Erasure Information is Employed	8-37
8.36	Decoded Performance of a Two-Stage Coding Approach Outer Decoder: Convolutional Code, Rate=1/2; K=7 Inner Decoder: Convolutional Code, Rate=1/2; K=7 δ=0.20 and Erasure Information is Employed	8-38
8.37	Two-Stage Coding Results Outer Decoder: BCH (240,216;7) Inner Decoder: Convolutional Code, K=7 Channel Measurement Decoding-No Erasure Information	8-42
8.38	Two-Stage Coding Results Outer Decoder: BCH (240,216;7) Inner Decoder: Convolutional Code, K=7 Binary Decoding-No Erasure Information	8-43

LIST OF ILLUSTRATIONS (continued)

Figure		Page
8.39	Two-Stage Coding Results Outer Decoder: BCH (240,216;7) Inner Decoder: Convolutional Code, K=7 Binary Decoding-Erasure Information Employed	8-44
8.40	Two-Stage Coding Results Outer Decoder: BCH (240,216;7) Inner Decoder: Convolutional Code, K=7 Channel Measurement Decoding-Erasure Information Employed	8-45
9.1	Comparison of Error Rate Performance for R=0.9 Codes	9-2
9.2	Decoded Performance of a Two-Stage Coding Approach Outer Decoder: Reed-Solomon Code (60,54;7) Bit Interleaver Employed Inner Decoder: Convolutional Code, Rate=1/2; K=7 δ=0.00 and No Erasure Information Employed	9-3
9.3	Decoded Performance of a Two-Stage Coding Approach Outer Decoder: Reed-Solomon Code (60,54;7) Bit Interleaver Employed Inner Decoder: Convolutional Code, Rate=1/2; K=7 δ=0.05 and No Erasure Information Employed	9-4
9.4	Decoded Performance of a Two-Stage Coding Approach Outer Decoder: Reed-Solomon Code (60,54;7) Bit Interleaver Employed Inner Decoder: Convolutional Code, Rate=1/2; K=7 δ=0.10 and No Erasure Information Employed	9-5
9.5	Decoded Performance of a Two-Stage Coding Approach Outer Decoder: Reed-Solomon Code (60,54;7) Bit Interleaver Employed Inner Decoder: Convolutional Code, Rate=1/2; K=7 δ=0.15 and No Erasure Information Employed	9-6

LIST OF ILLUSTRATIONS (continued)

Figure		Page
9.6	Decoded Performance of a Two-Stage Coding Approach Outer Decoder: Reed-Solomon Code (60,54;7) Bit Interleaver Employed Inner Decoder: Convolutional Code, Rate=1/2; K=7 δ=0.20 and No Erasure Information Employed	9-7
9.7	Decoded Performance of a Two-Stage Coding Approach Outer Decoder: Reed-Solomon Code (60,54;7) Bit Interleaver Employed Inner Decoder: Convolutional Code, Rate=1/2; K=7 δ=0.05 and Erasure Information is Employed	9-8
9.8	Decoded Performance of a Two-Stage Coding Approach Outer Decoder: Reed-Solomon Code (60,54;7) Bit Interleaver Employed Inner Decoder: Convolutional Code, Rate=1/2; K=7 δ=0.10 and Erasure Information is Employed	9-9
9.9	Decoded Performance of a Two-Stage Coding Approach Outer Decoder: Reed-Solomon Code (60,54;7) Bit Interleaver Employed Inner Decoder: Convolutional Code, Rate=1/2; K=7 δ=0.15 and Erasure Information is Employed	9-10
9.10	Decoded Performance of a Two-Stage Coding Approach Outer Decoder: Reed-Solomon Code (60,54;7) Bit Interleaver Employed Inner Decoder: Convolutional Code, Rate=1/2; K=7 δ=0.20 and Erasure Information is Employed	9-11
9.11	Decoded Performance of a Two-Stage Coding Approach Outer Decoder: Reed-Solomon Code (60,54;7) Symbol Interleaver Employed Inner Decoder: Convolutional Code, Rate=1/2; K=7 δ=0.00 and No Erasure Information is Employed	9-12
9.12	Decoded Performance of a Two-Stage Coding Approach Outer Decoder: Reed-Solomon Code (60,54;7) Symbol Interleaver Employed Inner Decoder: Convolutional Code, Rate=1/2; K=7 δ=0.05 and No Erasure Information is Employed	9-13

LIST OF ILLUSTRATIONS (continued)

Figure		Page
9.13	Decoded Performance of a Two-Stage Coding Approach Outer Decoder: Reed-Solomon Code (60,54;7) Symbol Interleaver Employed Inner Decoder: Convolutional Code, Rate=1/2; K=7 δ=0.10 and No Erasure Information Employed	9-14
9.14	Decoded Performance of a Two-Stage Coding Approach Outer Decoder: Reed-Solomon Code (60,54;7) Symbol Interleaver Employed Inner Decoder: Convolutional Code, Rate=1/2; K=7 δ=0.15 and No Erasure Information Employed	9-15
9.15	Decoded Performance of a Two-Stage Coding Approach Outer Decoder: Reed-Solomon Code (60,54;7) Symbol Interleaver Employed Inner Decoder: Convolutional Code, Rate=1/2; K=7 δ=0.20 and No Erasure Information Employed	9-16
9.16	Decoded Performance of a Two-Stage Coding Approach Outer Decoder: Reed-Solomon Code (60,54;7) Symbol Interleaver Employed Inner Decoder: Convolutional Code, Rate=1/2; K=7 δ=0.05 and Erasure Information is Employed	9-17
9.17	Decoded Performance of a Two-Stage Coding Approach Outer Decoder: Reed-Solomon Code (60,54;7) Symbol Interleaver Employed Inner Decoder: Convolutional Code, Rate=1/2; K=7 δ=0.10 and Erasure Information is Employed	9-18
9.18	Decoded Performance of a Two-Stage Coding Approach Outer Decoder: Reed-Solomon Code (60,54;7) Symbol Interleaver Employed Inner Decoder: Convolutional Code, Rate=1/2; K=7 δ=0.15 and Erasure Information is Employed	9-19
9.19	Decoded Performance of a Two-Stage Coding Approach Outer Decoder: Reed-Solomon Code (60,54;7) Symbol Interleaver Employed Inner Decoder: Convolutional Code, Rate=1/2; K=7 δ=0.20 and Erasure Information is Employed	9-20

LIST OF ILLUSTRATIONS (continued)

Figure		Page
9.20	Decoded Performance of a Two-Stage Coding Approach Outer Decoder: Reed-Solomon Code (40,36;5) Bit Interleaver Employed Inner Decoder: Convolutional Code, Rate=1/2; K=7 δ=0.00 and No Erasure Information Employed	9-21
9.21	Decoded Performance of a Two-Stage Coding Approach Outer Decoder: Reed-Solomon Code (40,36;5) Bit Interleaver Employed Inner Decoder: Convolutional Code, Rate=1/2; K=7 δ=0.05 and No Erasure Information Employed	9-22
9.22	Decoded Performance of a Two-Stage Coding Approach Outer Decoder: Reed-Solomon Code (40,36;5) Bit Interleaver Employed Inner Decoder: Convolutional Code, Rate=1/2; K=7 δ=0.10 and No Erasure Information Employed	9-23
9.23	Decoded Performance of a Two-Stage Coding Approach Outer Decoder: Reed-Solomon Code (40,36;5) Bit Interleaver Employed Inner Decoder: Convolutional Code, Rate=1/2; K=7 δ=0.15 and No Erasure Information Employed	9-24
9.24	Decoded Performance of a Two-Stage Coding Approach Outer Decoder: Reed-Solomon Code (40,36;5) Bit Interleaver Employed Inner Decoder: Convolutional Code, Rate=1/2; K=7 δ=0.20 and No Erasure Information Employed	9-25
9.25	Decoded Performance of a Two-Stage Coding Approach Outer Decoder: Reed-Solomon Code (40,36;5) Bit Interleaver Employed Inner Decoder: Convolutional Code, Rate=1/2; K=7 δ=0.05 and Erasure Information is Employed	9-26
9.26	Decoded Performance of a Two-Stage Coding Approach Outer Decoder: Reed-Solomon Code (40,36;5) Bit Interleaver Employed Inner Decoder: Convolutional Code, Rate=1/2; K=7 δ=0.10 and Erasure Information Employed	9-27

LIST OF ILLUSTRATIONS (continued)

Figure		Page
9.27	Decoded Performance of a Two-Stage Coding Approach Outer Decoder: Reed-Solomon Code (40,36;5) Bit Interleaver Employed Inner Decoder: Convolutional Code, Rate=1/2; K=7 δ=0.15 and Erasure Information is Employed	9-28
9.28	Decoded Performance of a Two-Stage Coding Approach Outer Decoder: Reed-Solomon Code (40,36;5) Bit Interleaver Employed Inner Decoder: Convolutional Code, Rate=1/2; K=7 δ=0.20 and Erasure Information is Employed	9-29
9.29	Decoded Performance of a Two-Stage Coding Approach Outer Decoder: Reed-Solomon Code (40,36;5) Symbol Interleaver Employed Inner Decoder: Convolutional Code, Rate=1/2; K=7 δ=0.00 and No Erasure Information Employed	9-30
9.30	Decoded Performance of a Two-Stage Coding Approach Outer Decoder: Reed-Solomon Code (40,36;5) Symbol Interleaver Employed Inner Decoder: Convolutional Code, Rate=1/2; K=7 δ=0.05 and No Erasure Information Employed	9-31
9.31	Decoded Performance of a Two-Stage Coding Approach Outer Decoder: Reed-Solomon Code (40,36;5) Symbol Interleaver Employed Inner Decoder: Convolutional Code, Rate=1/2; K=7 δ=0.10 and No Erasure Information Employed	9-32
9.32	Decoded Performance of a Two-Stage Coding Approach Outer Decoder: Reed-Solomon Code (40,36;5) Symbol Interleaver Employed Inner Decoder: Convolutional Code, Rate=1/2; K=7 δ=0.15 and No Erasure Information Employed	9-33
9.33	Decoded Performance of a Two-Stage Coding Approach Outer Decoder: Reed-Solomon Code (40,36;5) Symbol Interleaver Employed Inner Decoder: Convolutional Code, Rate=1/2; K=7 δ=0.20 and No Erasure Information Employed	9-34

LIST OF ILLUSTRATIONS (continued)

Figure		Page
.9.34	Decoded Performance of a Two-Stage Coding Approach Outer Decoder: Reed-Solomon Code (40,36;5) Symbol Interleaver Employed Inner Decoder: Convolutional Code, Rate=1/2; K=7 δ=0.05 and Erasure Information is Employed	9-35
9.35	Decoded Performance of a Two-Stage Coding Approach Outer Decoder: Reed-Solomon Code (40,36;5) Symbol Interleaver Employed Inner Decoder: Convolutional Code, Rate=1/2; K=7 δ=0.10 and Erasure Information is Employed	9-36
9.36	Decoded Performance of a Two-Stage Coding Approach Outer Decoder: Reed-Solomon Code (40,36;5) Symbol Interleaver Employed Inner Decoder: Convolutional Code, Rate=1/2; K=7 δ=0.15 and Erasure Information is Employed	9-37
9.37	Decoded Performance of a Two-Stage Coding Approach Outer Decoder: Reed-Solomon Code (40,36;5) Symbol Interleaver Employed Inner Decoder: Convolutional Code, Rate=1/2; K=7 δ=0.20 and Erasure Information is Employed	9-38
9.38	Decoded Performance of a Two-Stage Coding Approach Outer Decoder: Reed-Solomon Code (60,54;7) Bit Interleaver Employed Inner Decoder: Block Code (128,64;22) δ=0.00 and No Erasure Information Employed	9-39
9.39	Decoded Performance of a Two-Stage Coding Approach Outer Decoder: Reed-Solomon Code (60,54;7) Bit Interleaver Employed Inner Decoder: Block Code (128,64;22) δ=0.05 and No Erasure Information Employed	9-40
9.40	Decoded Performance of a Two-Stage Coding Approach Outer Decoder: Reed-Solomon Code (60,54;7) Bit Interleaver Employed Inner Decoder: Block Code (128,64;22) δ=0.10 and No Erasure Information Employed	9-41

LIST OF ILLUSTRATIONS (continued)

Figure		Page
9.41	Decoded Performance of a Two-Stage Coding Approach Outer Decoder: Reed-Solomon Code (60,54;7) Bit Interleaver Employed Inner Decoder: Block Code (128,64;22) δ=0.15 and No Erasure Information Employed	9-42
9.42	Decoded Performance of a Two-Stage Coding Approach Outer Decoder: Reed-Solomon Code (60,54;7) Bit Interleaver Employed Inner Decoder: Block Code (128,64;22) δ=0.20 and No Erasure Information Employed	9-43
9.43	Decoded Performance of a Two-Stage Coding Approach Outer Decoder: Reed-Solomon Code (60,54;7) Bit Interleaver Employed Inner Decoder: Block Code (128,64;22) δ=0.05 and Erasure Information is Employed	9-44
9.44	Decoded Performance of a Two-Stage Coding Approach Outer Decoder: Reed-Solomon Code (60,54;7) Bit Interleaver Employed Inner Decoder: Block Code (128,64;22) δ=0.10 and Erasure Information is Employed	9-45
9.45	Decoded Performance of a Two-Stage Coding Approach Outer Decoder: Reed-Solomon Code (60,54;7) Bit Interleaver Employed Inner Decoder: Block Code (128,64;22) δ=0.15 and Erasure Information is Employed	9-46
9.46	Decoded Performance of a Two-Stage Coding Approach Outer Decoder: Reed-Solomon Code (60,54;7) Bit Interleaver Employed Inner Decoder: Block Code (128,64;22) δ=0.20 and Erasure Information is Employed	9-47
9.47	Decoded Performance of a Two-Stage Coding Approach Outer Decoder: Reed-Solomon Code (60,54;7) Symbol Interleaver Employed Inner Decoder: Block Code (128,64;22) δ=0.00 and No Erasure Information Employed	9-48

LIST OF ILLUSTRATIONS (continued)

Figure		Page
9.48	Decoded Performance of a Two-Stage Coding Approach Outer Decoder: Reed-Solomon Code (60,54;7) Symbol Interleaver Employed Inner Decoder: Block Code (128,64;22) δ=0.05 and No Erasure Information Employed	9-49
9.49	Decoded Performance of a Two-Stage Coding Approach Outer Decoder: Reed-Solomon Code (60,54;7) Symbol Interleaver Employed Inner Decoder: Block Code (128,64;22) δ=0.10 and No Erasure Information Employed	9-50
9.50	Decoded Performance of a Two-Stage Coding Approach Outer Decoder: Reed-Solomon Code (60,54;7) Symbol Interleaver Employed Inner Decoder: Block Code (128,64;22) δ=0.15 and No Erasure Information Employed.	9-51
9.51	Decoded Performance of a Two-Stage Coding Approach Outer Decoder: Reed-Solomon Code (60,54;7) Symbol Interleaver Employed Inner Decoder: Block Code (128,64;22) δ=0.20 and No Erasure Information Employed	9-52
9.52	Decoded Performance of a Two-Stage Coding Approach Outer Decoder: Reed-Solomon Code (60,54;7) Symbol Interleaver Employed Inner Decoder: Block Code (128,64;22) δ=0.05 and Erasure Information is Employed	9-53
9.53	Decoded Performance of a Two-Stage Coding Approach Outer Decoder: Reed-Solomon Code (60,54;7) Symbol Interleaver Employed Inner Decoder: Block Code (128,64;22) δ=0.10 and Erasure Information is Employed	9-54
9.54	Decoded Performance of a Two-Stage Coding Approach Outer Decoder: Reed-Solomon Code (60,54;7) Symbol Interleaver Employed Inner Decoder: Block Code (128,64;22) δ=0.15 and Erasure Information is Employed	9-55

LIST OF ILLUSTRATIONS (continued)

Figure		Page
9.55	Decoded Performance of a Two-Stage Coding Approach Outer Decoder: Reed-Solomon Code (60,54;7) Symbol Interleaver Employed Inner Decoder: Block Code (128,64;22) δ=0.20 and Erasure Information is Employed	9-56
9.56	Decoded Performance of a Two-Stage Coding Approach Outer Decoder: Reed-Solomon Code (40,36;5) Bit Interleaver Employed Inner Decoder: Block Code (128,64;22) δ=0.00 and No Erasure Information Employed	9-57
9.57	Decoded Performance of a Two-Stage Coding Approach Outer Decoder: Reed-Solomon Code (40,36;5) Bit Interleaver Employed Inner Decoder: Block Code (128,64;22) δ=0.05 and No Erasure Information Employed	9-58
9.58	Decoded Performance of a Two-Stage Coding Approach Outer Decoder: Reed-Solomon Code (40,36;5) Bit Interleaver Employed Inner Decoder: Block Code (128,64;22) δ=0.10 and No Erasure Information Employed	9-59
9.59	Decoded Performance of a Two-Stage Coding Approach Outer Decoder: Reed-Solomon Code (40,36;5) Bit Interleaver Employed Inner Decoder: Block Code (128,64;22) δ=0.15 and No Erasure Information Employed	9-60
9.60	Decoded Performance of a Two-Stage Coding Approach Outer Decoder: Reed-Solomon Code (40,36;5) Bit Interleaver Employed Inner Decoder: Block Code (128,64;22) δ=0.20 and No Erasure Information Employed	9-61
9.61	Decoded Performance of a Two-Stage Coding Approach Outer Decoder: Reed-Solomon Code (40,36;5) Bit Interleaver Employed Inner Decoder: Block Code (128,64;22) δ=0.05 and Erasure Information is Employed	9-62

LIST OF ILLUSTRATIONS (continued)

Figure		Page
9.62	Decoded Performance of a Two-Stage Coding Approach Outer Decoder: Reed-Solomon Code (40,36;5) Bit Interleaver Employed Inner Decoder: Block Code (128,64;22) δ=0.10 and Erasure Information Employed	9-63
9.63	Decoded Performance of a Two-Stage Coding Approach Outer Decoder: Reed-Solomon Code (40,36;5) Bit Interleaver Employed Inner Decoder: Block Code (128,64;22) δ=0.15 and Erasure Information is Employed	9-64
9.64	Decoded Performance of a Two-Stage Coding Approach Outer Decoder: Reed-Solomon Code (40,36;5) Bit Interleaver Employed Inner Decoder: Block Code (128,64;22) δ=0.20 and Erasure Information is Employed	9-65
9.65	Decoded Performance of a Two-Stage Coding Approach Outer Decoder: Reed-Solomon Code (40,36;5) Symbol Interleaver Employed Inner Decoder: Block Code (128,64;22) δ=0.00 and No Erasure Information Employed	9-66
9.66	Decoded Performance of a Two-Stage Coding Approach Outer Decoder: Reed-Solomon Code (40,36;5) Symbol Interleaver Employed Inner Decoder: Block Code (128,64;22) δ=0.05 and No Erasure Information Employed	9-67
9.67	Decoded Performance of a Two-Stage Coding Approach Outer Decoder: Reed-Solomon Code (40,36;5) Symbol Interleaver Employed Inner Decoder: Block Code (128,64;22) δ=0.10 and No Erasure Information Employed	9-68
9.68	Decoded Performance of a Two-Stage Coding Approach Outer Decoder: Reed-Solomon Code (40,36;5) Symbol Interleaver Employed Inner Decoder: Block Code (128,64;22) δ=0.15 and No Erasure Information Employed	9-69

LIST OF ILLUSTRATIONS (continued)

Figure		Page
9.69	Decoded Performance of a Two-Stage Coding Approach Outer Decoder: Reed-Solomon Code (40,36;5) Symbol Interleaver Employed Inner Decoder: Block Code (128,64;22) δ=0.20 and No Erasure Information Employed	9-70
9.70	Decoded Performance of a Two-Stage Coding Approach Outer Decoder: Reed-Solomon Code (40,36;5) Symbol Interleaver Employed Inner Decoder: Block Code (128,64;22) δ=0.05 and Erasure Information Employed	9-71
9.71	Decoded Performance of a Two-Stage Coding Approach Outer Decoder: Reed-Solomon Code (40,36;5) Symbol Interleaver Employed Inner Decoder: Block Code (128,64;22) δ=0.10 and Erasure Information Employed	9-72
9.72	Decoded Performance of a Two-Stage Coding Approach Outer Decoder: Reed-Solomon Code (40,36;5) Symbol Interleaver Employed Inner Decoder: Block Code (128,64;22) δ=0.15 and Erasure Information is Employed	9-73
9.73	Decoded Performance of a Two-Stage Coding Approach Outer Decoder: Reed-Solomon Code (40,36;5) Symbol Interleaver Employed Inner Decoder: Block Code (128,64;22) δ=0.20 and Erasure Information is Employed	9-74

LIST OF TABLES

Table		Page
2-1	Properties of Multiple-Access Systems	2-18
3-1	Output Noise Increase over Thermal Noise (dB) Average Power = 1	3-25
3-2	Output Noise Increase over Thermal Noise (dB) Average Power = 10	3-26
3-3	Output Noise Increase over Thermal Noise (dB) Average Power = 100	3-27
3-4	Output Noise Increase over Thermal Noise (dB) Average Power = 1000	3-28
3-5	Jammer Pulse Width (μ sec)	3-31
4-1	Summary of Results for the Probability of an Error Between Two Sequences	4-12
4-2	Best Rate-1/2 Constraint Length-3 Code	4-14
4-3	Best Rate-1/2 Constraint Length-5 Code	4-15
4-4	Best Rate-1/2 Constraint Length-7 Code	4-16
6-1	E_b/N_0 (dB) Required for a Bit Error Rate of 10^{-5} Interleaved Convolutional Codes: Constraint Length K = 7	6-30
7-1	E_b/N_0 (dB) Required for a Bit Error Rate of 10^{-5} for Rate-1/2 Inner Block Code with Rate-0.9 and Rate-1/2 Outer Codes	7-26
8-1	E_b/N_0 (dB) Required for a Bit Error Rate of 10^{-5} for a Rate-1/2 Inner Convolutional Code, with Rate-0.9 and Rate-1/2 Outer Codes	8-39

LIST OF TABLES (continued)

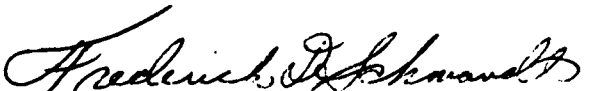
Table		Page
8-2	E_b/N_0 (dB) Required for a Bit Error Rate of 10^{-5} for Rate-1/4 and Rate-1/8 Inner Convolutional Code with a Rate-0.9 Outer Code	8-40
10-1	Coding Hardware Estimates	10-4

EVALUATION

The trend of the Tactical Air Force (TAF), in the future will be to many dispersed facilities to achieve increased survivability. This trend increases the requirement of developing waveform and coding concepts to minimize interference caused by multiple user spread spectrum signals and intentional jamming. Because of the anticipated widescale use of adaptive antennas and the influence such antennas have on the error characteristics the waveform and coding design should take into account their effects.

The results of this study indicate that burst error-correcting codes can be critical components in certain multiple-access and adaptive array systems. A thorough investigation of these codes under a variety of interference models has been conducted. It is shown that essentially error-free communication is possible even when large portions of the data are completely destroyed by interference. While typical coding gains in the presence of just additive noise are in the 5 dB range, coding gains in the presence of interference of 20 dB or more are to be expected.

The results, while applicable to a wide class of LOS channels, are most directly applicable to communication networks requiring multiple-access and ECCM capabilities. While no direct follow-on effort is planned the topics addressed in this effort provide relevant inputs to the Relay Communication and Distributed C^3 areas being investigated under TPO subthrusts R3B and R3C, respectively.



FREDERICK D. SCHMANDT
Project Engineer

SECTION 1

INTRODUCTION

For conventional digital communications systems, error-correcting codes have been used to improve the data reliability for a given link and, in some cases, the codes have been used to reduce the required transmission power to achieve a desired level of performance. For more sophisticated ECCM communication systems, such as those shown on Figure 1.1, the role of error-correcting codes is just beginning to be understood. The broad objective of this report is to determine the need and possible benefits of error-correcting codes for systems within the class defined by Figure 1.1.

Data is encoded and passed into a spread-spectrum modulator. Since the encoder and the spread-spectrum modulator both increase the required bandwidth of the system, an optimum integration of these two functions should exist. This optimum integration is a strong function of the type of interference the system is expected to tolerate. For example, in Section 2, several multiple-access systems are considered with vastly different coding and waveform requirements. The pseudo-random noise multiple-access system, discussed in Section 2.3, is shown to require a conventional random error-correcting code of moderate redundancy, i.e., rate-1/2, with maximum bandwidth expansion to be used by the spread-spectrum modulator. The new versatile multiple-access system, introduced in Section 2.5, is shown to require a minimum of bandwidth expansion by the spread-spectrum modulator and to require burst error-correcting codes of rates on the order of 1/4. When noncontinuous (pulse-type) intentional interference is considered, the choice of coding techniques and waveforms may be further altered. Finally, the capabilities of an adaptive array to null-out intentional interference must be considered before the final optimization of the system, such as illustrated in Figure 1.1, can be made. For completeness, dotted lines are used on this figure to indicate possible ways of integrating the adaptive array, spread-spectrum demodulator and the error-correcting decoder.

In order to bound the scope of this investigation, we first show, in Sections 2 and 3, that error-correcting codes capable

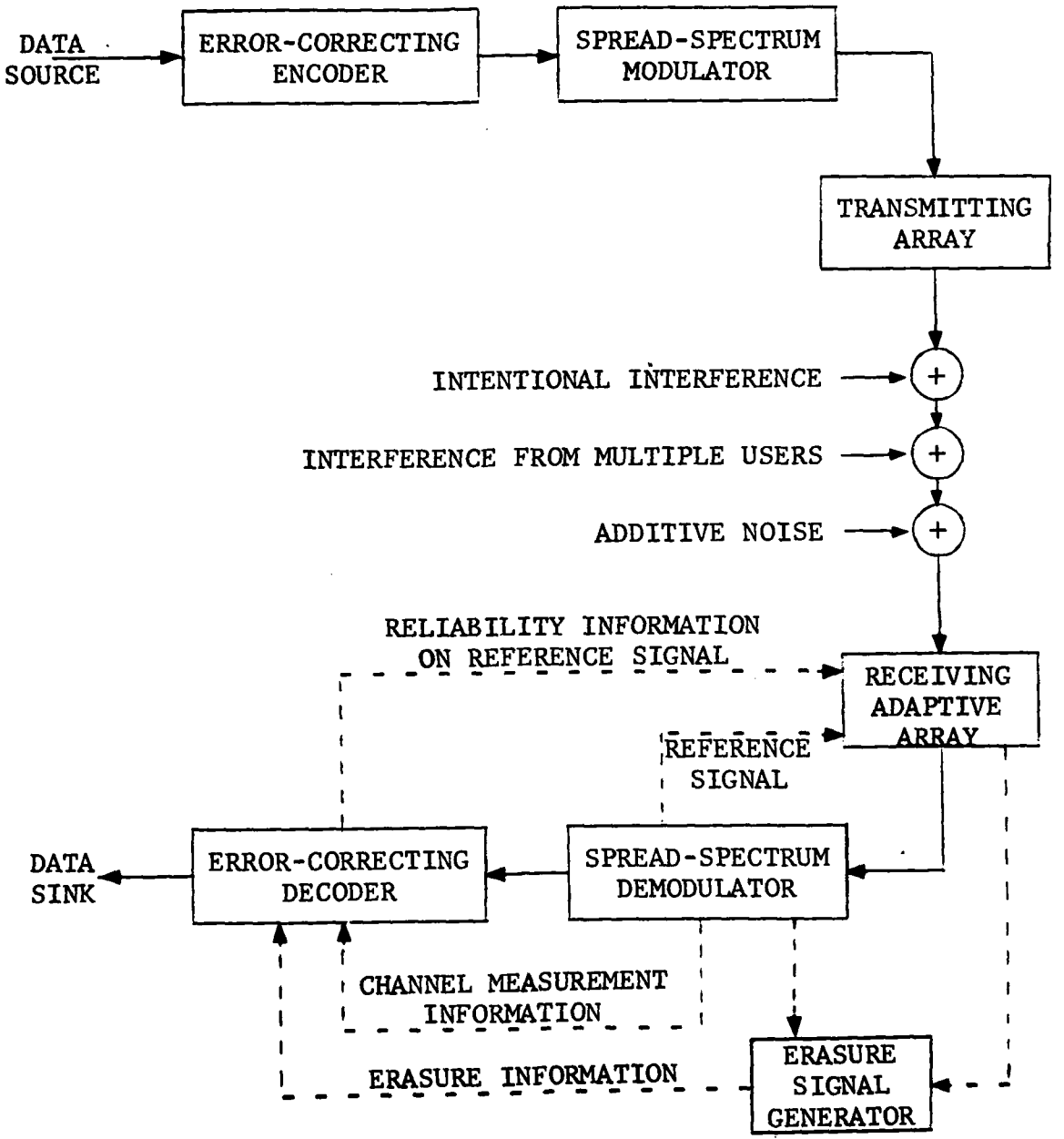


Figure 1.1 Block Diagram of the Communication System of Interest

of correcting both burst and random errors are critical components of advanced multiple-access and adaptive-array systems. In Section 4, a worst-case model is introduced for interference which assumes an error rate-1/2 during the presence of interference and an error rate determined by the available signal-to-noise ratio during the intervals of just additive noise. The following four different receiver configurations are considered:

(1) A receiver which supplies just binary data to the decoder.

(2) A receiver which supplies binary data and an external (erasure) signal indicating the presence of interference.

(3) A receiver which supplies channel measurement information to the decoder.

(4) A receiver which supplies channel measurement information and an external signal indicating the presence of interference.

The first configuration is relevant for applications where error-correction coding is added to an existing system and just binary bit interfacing is required. The last configuration assumes that coding is fully integrated into the design of the system and, thus, channel measurement (unquantized soft-decision) information and an erasure signal indicating the intervals when interference occurs are available to the decoder. General expressions for the performance of block, convolutional, and two-stage coding approaches, based on combinations of block and/or convolutional codes, are obtained in Section 4 for all four configurations given above.

Sections 5 through 9 apply the results of Section 4 to obtain performance tradeoffs for various possible coding techniques and levels of interference. Conclusions and recommendations for additional work are provided in Section 10.

SECTION 2

MULTIPLE-ACCESS CONCEPTS FOR BURSTY COMMUNICATION SOURCES

2.1 Introduction

An emphasis on multiple-access systems for bursty (low duty factor) sources is given in this section. A baseline fixed assignment system, such as TDMA or FDMA, is considered first. Systems such as these lose their inefficiency linearly as the duty factor of the multiple users decreases. Next, a code division (pseudo-noise) multiple-access system is shown to have a channel efficiency which is independent of the users' duty factor; and, thus, the number of allowable users increases inversely with the duty factor. Unfortunately, this system is restricted to applications where the received power from multiple users must be uniformly distributed. The slotted Aloha is attractive in that the channel efficiency is independent of the users' duty factor, and a uniform received power distribution is not required. However, this system requires a perfect feedback to detect collisions and has a variable data throughput delay. Finally, a new versatile multiple-access (VMA) system is introduced which has all the advantages of the previous systems and none of their disadvantages. Efficiency is independent of the user duty factor, and a uniform received power distribution is not required. This system uses burst/random feed-forward error-correcting codes as discussed in Sections 4 through 9. The theoretical channel efficiency of VMA is 37%, which is identical to the limit for the slotted Aloha system and yet no feedback link is required for VMA.

2.2 Multiple-Access Channel Definitions

A channel with M degrees of freedom (independent communication slots) per T seconds will be assumed. Thus, as shown in Figure 2.1, various combinations of time- and frequency-division allocation schemes can support M simultaneous users, all with a duty factor of 1. Each degree of freedom is assumed to support a packet of information. Thus, full utilization (maximum throughput) is achieved when a data rate of

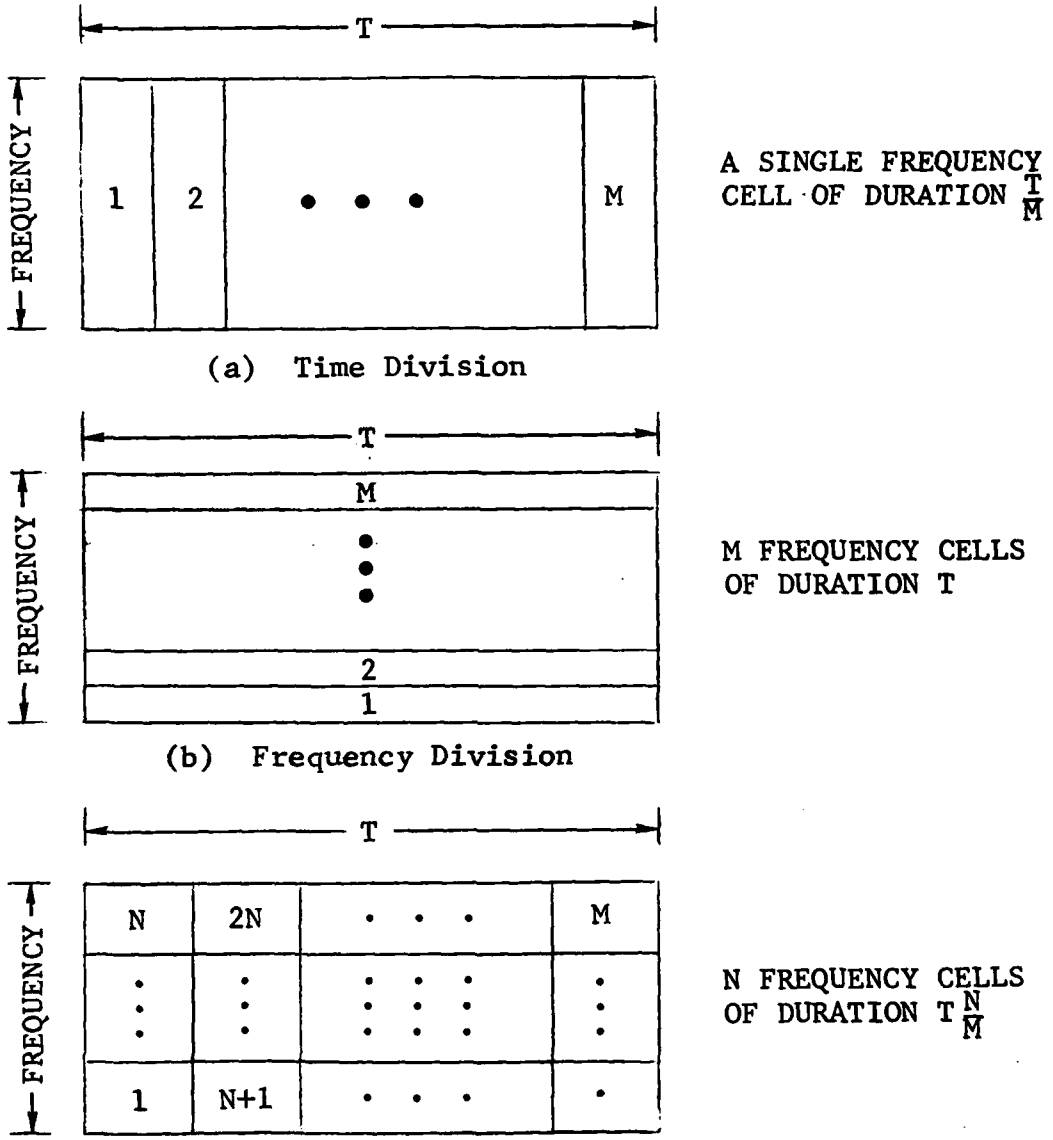


Figure 2.1 Examples of Channel Allocations with M Degrees of Freedom

$$R_{max} = \frac{M}{T} \text{ packets/second} \tag{2.1}$$

is transmitted over the channel. It should be noted that, for the special case where each packet is defined as a single (binary) symbol, the value of M is given by the time-bandwidth product WT. For the more general case with k bits per packet, M is a factor of k less than the time-bandwidth product.

The signal-to-noise ratio available per packet is in the general case assumed to be a variable, given by

$$\text{SNR}(i^{th} \text{ packet}) = \frac{E_p(i)}{N_0(i)} \tag{2.2}$$

where $E_p(i)$ is the received energy for the i^{th} user, and N_0 is the noise power density. This signal-to-noise ratio can also be written in terms of the data rate per user

$$R_p = \frac{1}{T} \text{ packets/second} \tag{2.3}$$

and the received power per user, P(i), as

$$\frac{E_p(i)}{N_0(i)} = \frac{P(i)}{N_0(i)\ R_p} = \frac{P(i)\ T}{N_0(i)} \tag{2.4}$$

For most communication applications, modulation/coding performance curves are given in terms of the signal-to-noise ratio per information bit. If there are k information bits per packet, the bit data rate per user is given by

$$R_b = \frac{k}{T} \text{ bits/second} \tag{2.5}$$

and, thus, the two SNR's are related simply by

$$\frac{E_b(i)}{N_0(i)} = \frac{P(i)}{N_0(i)\ R_b} = \frac{P(i)\ T}{N_0(i)\ k} = \frac{1}{k}\frac{E_p(i)}{N_0(i)} \tag{2.6}$$

For the special case when the total power, P_0, is divided equally among the M users, and the noise power per Hz, N_0, is constant, we have

$$\frac{E_p(i)}{N_0(i)} = \frac{P_0(\text{Time per Frequency Cell})}{(\text{Number of Frequency Cells})N_0} = \frac{P_0\ T}{M\ N_0} \qquad (2.7)$$

for all of the time-frequency allocations illustrated in Figure 2.1. In general, Eq. (2.7) can be obtained by noting that the average power per user is given by P_0/M and the data rate per user is 1/T packets/second. For this case, the signal-to-noise ratio per information bit is given by

$$\frac{E_b(i)}{N_0(i)} = \frac{P_0\ T}{k M N_0} \qquad (2.8)$$

In addition to considering users with various received power levels, each user can have a duty factor (i.e., probability of transmission), $\epsilon(i)$, which is less than or equal to 1. If each user is assigned a fixed degree of freedom, the channel allocations illustrated in Figure 2.1 can support M users. Assuming that all users have the same duty factor, the average data rate per user is now given by

$$\bar{R}(i) = \frac{\epsilon}{T} \text{ packets/second} \qquad (2.9)$$

The channel efficiency, defined as the ratio of the total average data rate divided by the maximum possible data rate, is given by

$$\eta = \frac{\bar{R}}{R_{max}} = \frac{\frac{\epsilon M}{T}}{\frac{M}{T}} = \epsilon \qquad (2.10)$$

Needless to say, for users with low duty factors (bursty communication sources), the use of a conventional time-division multiple access (TDMA) or frequency-division multiple access (FDMA) system, which is limited to a maximum of M users, can be quite inefficient. Furthermore, for certain applications, the network timing for conventional multiple-access systems

may dictate the use of the less conventional approaches. In the remainder of this section, multiple-access systems, which are efficient for bursty communications sources, are discussed.

2.3 Code Division (Direct Sequence Spread Spectrum) Multiple-Access (CDMA) Systems

For CDMA, each packet is transmitted in T seconds and is assumed to occupy the entire frequency band. The received signal-to-noise ratio per information bit when the i^{th} packet is transmitted is

$$\frac{E_b(i)}{N_0(i)} = \frac{P(i)}{\frac{N_0 k}{T} + \frac{\sum_{j \neq i} P(j)\,\epsilon(j)}{PG}} \tag{2.11}$$

The average noise power density is N_0 (watts/Hz), and P(i) is the desired received power (watts) at the terminal for the i^{th} packet. The unwanted received power, $\sum_{j \neq i} P(j)$, is attenuated by the processing gain, PG, of the spread-spectrum system which is given by M for our case. Note that for a packet composed of k bits, each bit only occupies a period of T/k and, thus, occupies M available data bit slots. While the results in this section will be in terms of E_b/N_0, for completeness, the signal-to-noise ratio per packet is given by

$$\frac{E_p(i)}{N_0(i)} = \frac{P(i)}{\frac{N_0}{T} + \frac{\sum_{j \neq i} P(j)\,\epsilon(j)}{kM}} \tag{2.12}$$

which is consistent with (2.6). Note that the processing gain for a packet of k bits is given by the full time-bandwidth product of the channel, which is kM.

It is interesting to determine the channel efficiency and the maximum number of users that can be supported with a CDMA system. The total number of users is denoted as U, which yields an average data rate per user of

$$\bar{R}_b = \frac{\epsilon(j)\,k}{T} \quad \text{bits/second} \tag{2.13}$$

The maximum data rate in terms of bits, rather than packets, is given by

$$\mathcal{R}_{max} = \frac{M k}{T} \qquad \text{bits/second} \tag{2.14}$$

and, thus, the channel efficiency is given by

$$\eta = \frac{\bar{\mathcal{R}}}{\mathcal{R}_{max}} = \frac{\sum_{j=1}^{U} \epsilon(j)}{M} \tag{2.15}$$

To find the maximum number of users, we first rewrite Eq. (2.11) as

$$\frac{\sum_{j \neq 1} P(j)\, \epsilon(j)}{P(i)} = M\left[\frac{1}{\frac{E_b(i)}{N_0(i)}} - \frac{1}{\frac{P(i)\, T}{N_0\, k}}\right] \tag{2.16}$$

To evaluate the above, several assumptions will now be made. The term, $\frac{P(i)\, T}{N_0 k}$, which represents the signal-to-noise ratio per bit when all (U-1) interfering users are not transmitting, will be assumed much larger than the actual received $\frac{E_b(i)}{N_0(i)}$. Furthermore, all users will be assumed to be received at all terminals with equal power and also to have the same duty factors, given by ϵ. Thus, we can write

$$U = \frac{M}{\epsilon} \frac{1}{E_b/N_0} + 1 \tag{2.17}$$

Note that the uniform received power assumption is critical in obtaining a reasonably large value for U.

For a communications system with a well-designed modulation and error-correction coding format, a bit error rate of

below 10^{-5} can be obtained at an $E_b/N_0 = 3$ (4.77 dB) when the link can be approximated as an additive noise nonfading Gaussian channel. (See Sections 5 through 9.) Line-of-sight and satellite channels with direct sequence spread-spectrum modulation formats generally fall into this class.

Assuming all of the above,

$$U = 1 + \frac{M}{3\epsilon} \quad - \quad \text{Practical Systems} \tag{2.18}$$

and

$$\eta = \frac{U\epsilon}{M} = \frac{\epsilon}{M} + \frac{1}{3} \quad - \quad \text{Practical Systems} \tag{2.19}$$

Thus, for typically large values of M, CDMA offers an efficiency of around 33%. Comparing these numbers to the fixed assigned system given in Section 2.2, we note that for the above case when the duty factor is below 33% a CDMA can support more users (and also have a higher channel efficiency) than a TDMA system. However, the TDMA system has the desirable property that all received power levels do not have to be equal. It is interesting to note that we lose channel efficiency in a TDMA system if binary error-correction coding is applied. Thus, a TDMA must also operate with large values of $\frac{P(i)}{N_0 R}$. Of course, if high alphabet symbol coding is applied to a TDMA system, it is possible to reduce the required signal-to-noise ratio.

A curious result is obtained by assuming an ideal system with codes that can satisfy channel capacity. In this case, the minimum received SNR is given by

$$\frac{E_b}{N_0} = \ell n(2) = -1.6 \text{ dB} \tag{2.20}$$

and Eq. (2.17) can be written as

$$U-1 = \frac{M}{\epsilon} \frac{1}{\ell n(2)} = \frac{1.44M}{\epsilon} \tag{2.21}$$

In this limiting case, the number of simultaneous users yields a channel efficiency of greater than 1. The original assumptions used to obtain Eq. (2.11) may be questioned in this limiting case. Needless to say, CDMA systems have to be designed with care for successful operations.

2.4 Slotted Aloha Multiple-Access System

For this multiple-access system, the following set of assumptions is made:

- A feed-forward link, such as described in Section 2.2, is used with infinite SNR.
- A perfect (error-free) broadcast feedback exists such that all users can determine when two or more packets collide.
- Each user has an infinite buffer to store packets until they are transmitted collision-free.

Needless to say, there are many communications applications where these assumptions cannot be satisfied.

For this multiple-access system, the i^{th} user transmits a single packet with probability p(i). Thus, the probability of no collision, given the i^{th} user is transmitting in a given slot, is

$$P_{nc}(i) = \prod_{j \neq i} [1 - p(j)] \tag{2.22}$$

The average data rate, or throughput, for the i^{th} user is given by

$$\bar{R}_p(i) = p(i)\ P_{nc}(i)\ \frac{M}{T} \quad \text{packets/second} \tag{2.23}$$

Note that all M slots in the T second interval can be accessed by each user.

The total data rate for U users is given by

$$\bar{R} = \sum_{i=1}^{U} R_p(i) \tag{2.24}$$

which, with the aid of Eq. (2.1), yields a channel efficiency of

$$\eta = \frac{\bar{R}}{R_{max}} = \sum_{i=1}^{U} p(i)\, P_{nc}(i) \tag{2.25}$$

For the special case when all U users access the channel with the same probability p,

$$P_{nc} = (1-p)^{U-1} \tag{2.26}$$

and

$$\boxed{\eta = Up(1-p)^{U-1} = G\left(1-\frac{G}{U}\right)^{U-1} \xrightarrow[U\to\infty]{} G\,e^{-G}} \tag{2.27}$$

The quantity G=Up represents the total traffic entering the channel of which only a fraction, given by P_{nc}, is received.

The efficiency is maximized when the number of users satisfies

$$\boxed{U_{opt} = \frac{-1}{\ell n(1-p)} = \frac{1}{\ell n(1-p)^{-1}}} \tag{2.28}$$

which yields a probability of no collision of

$$P_{nc} = e^{-\frac{U-1}{U}} \xrightarrow[U\to\infty]{} e^{-1} \tag{2.29}$$

and an efficiency of

$$\eta_{opt} = U\left(1 - e^{-\frac{1}{U}}\right) e^{-\frac{U-1}{U}} \xrightarrow[U\to\infty]{} e^{-1} \approx 0.37 \qquad (2.30)$$

At the maximum efficiency, the quantity G is given by

$$G_{opt} = U\left(1 - e^{-\frac{1}{U}}\right) \xrightarrow[U\to\infty]{} 1 \qquad (2.31)$$

which indicates that the offered traffic is 100%, with collisions occurring at a rate of 63%. It also can be shown that as the efficiency approaches 37%, the delay required to receive a given packet approaches infinity.

An attractive feature of this multiple-access system is that the number of users can grow inversely with the users' duty factor. This duty factor, calculated over a T second (M slot) period, is

$$\epsilon = M p \qquad (2.32)$$

which is the average number of packets transmitted in T seconds. In terms of this duty factor, which is consistent with the notation used in this section, we can write

$$U_{opt} = \frac{1}{\ell n\left(1 - \frac{\epsilon}{M}\right)^{-1}} \leq \frac{M}{\epsilon} \qquad (2.33)$$

and, in general, the efficiency is given by

$$\eta = \frac{UM}{\epsilon}\left(1 - \frac{M}{\epsilon}\right)^{U-1} \qquad (2.34)$$

Choosing $U = G\frac{M}{\epsilon}$, with $G < 1$, we obtained the desirable result that the efficiency given by Eq. (2.27) is independent of ϵ, and the number of users are inversely proportional to ϵ.

2.5 Versatile Multiple-Access (VMA) System

In this section we introduce a new multiple-access system which is called a versatile multiple-access system since uniform received power is not required (as is true for TDMA), and is efficient for bursty communication sources (as is true for CDMA). This system uses feed-forward error-correcting codes with randomly placed code digits to correct self-interference and interference from other multiple-access users. Unlike the Aloha system discussed in Section 2.4, infinite SNR and a perfect feedback link are not required for this VMA system.

The VMA system can be used with channel allocations, such as those given in Figure 2.1. Every T seconds, the i^{th} user randomly occupies (transmits over) s of the available M packet slots with probability $\epsilon(i)$. The value of the integer s represents the inverse of the code rate r actually transmitted by each user, i.e.,

$$r = \frac{1}{s} \quad - \quad \text{code rate} \tag{2.35}$$

The s slots are truly chosen at random, with no attempt made to avoid choosing the same packet slot more than once in a given T-second interval. Thus, the probability of a single user not interfering with itself is given by

$$\Pr[\text{no self-interference}] = 1\left(1 - \frac{1}{M}\right)\left(1 - \frac{2}{M}\right) \cdots \left(1 - \frac{s-1}{M}\right) \tag{2.36}$$

The advantage of allowing a truly random placement of packets comes about when the interference from other multiple users is considered.

The probability of no interference within a given packet channel from U-1 additional users, each transmitting with probability $\epsilon(j)$, is given by

$$\Pr[\text{no external interference}] = \prod_{j \neq i} \left\{ [1 - \epsilon(j)] + \epsilon(j)\left(1 - \frac{1}{M}\right)^{s} \right\} \tag{2.37}$$

If we allow each user to select s individual packet channels so that the self-interference probability would be zero, the probability of no external interference is given by

$$\Pr[\text{no external interference}] = \prod_{j \neq i} \left\{ [1 - \epsilon(j)] + \epsilon(j) \prod_{\ell=1}^{s} \left(1 - \frac{\ell}{M}\right) \right\} \quad (2.38)$$

which is greater than Eq. (2.37) for all $s > 1$. To optimize the performance of the VMA system, it is necessary to maximize

$$\Pr[\text{no self-interference}] \cdot \Pr[\text{no external interference}] \quad (2.39)$$

For applications where the number of users is large, the second term, which involves U-1 products, dominates. Thus, a true random selection of s packet channels represents the preferred VMA system design.

For a VMA system to be effective, codes capable of operating in the presence of high levels of interference must be used. Fundamentally, channel capacity limits have been found [2.1] which show that binary codes can offer error-free communication in the presence of interference occurring with a probability of δ when

$$r < (1 - \delta) \quad (2.40)$$

for a binary and channel measurement decoding with erasure information, and

$$r < 1 + \left(\frac{\delta}{2}\right) \log_2 \left(\frac{\delta}{2}\right) + \left(1 - \frac{\delta}{2}\right) \log_2 \left(1 - \frac{\delta}{2}\right) \quad (2.41)$$

for a modulation format which allows only binary decoding. Equation (2.40) has also been shown to be true when no erasure information is present but channel measurement decoding is allowable (see model 1 of reference [2.1]).

Practical coding techniques also exist (see Sections 5 through 9) which offer performance in the presence of interference, providing the code rate, $1/s$, is small enough. For

example, if erasure information is present, a probability of error below 10^{-5} is possible with an interleaved, K=7, rate-1/4, convolutional code at E_b/N_0 = 5.7 dB when the interference probability δ = 0.2 (see Figure 6.18). An even more impressive result is obtained by using a rate-1/2, K=7 convolutional code with a rate-0.9 (240,216;7) BCH outer code. This overall rate-0.45 code is capable of yielding a probability of 10^{-5} with δ = 0.2 at an E_b/N_0 = 5.2 dB. (See Figure 8.9) While these codes operate considerably below the capacity limits given by Eq. (2.40), it is encouraging to know that practical codes do exist which operate in the presence of high levels of interference.

One possible way to obtain the desired erasure information for a VMA system is to use high-rate detection codes for packets. Unfortunately, techniques such as these usually require large signal-to-noise ratios to ensure that a packet is not falsely erased. Some form of error correction and detection, such as is used in adaptive coding, should represent an effective coding approach for this multiple-access system. It should be noted that channel measurement decoding, such as that used in model 1 of reference [2.1], is generally not applicable to this system unless we are guaranteed to receive just additive noise (and no signal energy) during the presence of interference. Optimizing the coding approach for a VMA system is an important topic of current interest.

In order to determine the number of possible users, and, hence, the channel efficiency, the behavior of Eq. (2.37) must be determined. For the case when the duty factors of all users are identically given by ϵ, we may rewrite Eq. (2.37) as

$$\Pr[\text{no external interference}] = 1 - \delta = \left[(1 - \epsilon) + \epsilon\left(1 - \frac{1}{M}\right)^S\right]^{U-1} \quad (2.42)$$

Solving for the number of multiple users U in terms of the external interference probability δ yields

$$U = 1 + \frac{\ln(1 - \delta)}{\ln\left[(1 - \epsilon) + \epsilon\left(1 - \frac{1}{M}\right)^S\right]} \quad (2.43)$$

Note that for large values of M and U, the self-interference probability can be neglected relative to δ.

The term in the denominator can be simplified when

$$1 >> \epsilon\left[1 - \left(1 - \frac{1}{M}\right)^{S}\right] \tag{2.44}$$

since the $\ell n(1+x) \leq x$, when $x \ll 1$.

Similarly, when M is large, the term

$$1 - \left(1 - \frac{1}{M}\right)^{S} \leq \frac{S}{M} \tag{2.45}$$

Thus, we can approximate the number of multiple users by

$$U \approx 1 + \frac{\ell n(1-\delta)}{-\frac{\epsilon S}{M}} = 1 + \frac{M\,\ell n\left(\frac{1}{1-\delta}\right)}{\epsilon S} \tag{2.46}$$

A strict upper bound on U cannot be obtained by the above approximations since x is a negative number which implies that a lower bound is needed for the expression given by Eq. (2.45).

Finally, with the aid of Eq. (2.35), we may write

$$\boxed{U \approx 1 + \frac{r M\,\ell n\left(\frac{1}{1-\delta}\right)}{\epsilon}} \tag{2.47}$$

which has the desirable property that the number of allowable users is inversely proportional to ϵ.

The code data rate per user is given by

$$\overline{R} = \frac{\epsilon}{T} \qquad \text{packets/second} \tag{2.48}$$

since, for a code rate of r, only one information packet is transmitted every T seconds. The maximum data rate is given by Eq. (2.1) so that the channel efficiency becomes

$$\eta = \frac{\bar{R}\,U}{\frac{M}{T}} \approx \frac{\epsilon}{M} + r\,\ell n\left(\frac{1}{1-\delta}\right) \tag{2.49}$$

If, for example, a r = 1/4, K=7, convolutional code is used with erasure information, at an E_b/N_0 = 7 dB an error rate of 10^{-5} can be obtained for δ = 0.33. Thus, for large values of M, for δ = 1/3 and r = 1/4, we obtain

$$U \approx \frac{0.1M}{\epsilon} \quad - \quad \text{Practical Systems} \tag{2.50}$$

and

$$\eta \approx 0.1 \quad - \quad \text{Practical Systems} \tag{2.51}$$

Somewhat greater efficiency is even possible if a two-stage coding approach based on a combination of convolutional and block codes is considered. For example, a rate-1/2 convolutional code and a rate-0.9 block code can be combined to require an E_b/N_0 = 6.9 dB, for δ = 0.30 as indicated in Section 6. For this coding approach, an efficiency of 16% is possible.

While an efficiency of 10% (or 16% for more sophisticated coding approaches) is somewhat lower than the 33% obtained with a CDMA system, the fact that the VMA system does not require uniformly-received power at all terminals is quite relevant. If the uniform receiver power assumption is not true, the efficiency of the CDMA system drops below 10% quite rapidly. Similarly, if the duty factor of each user, ϵ, is below 10%, the efficiency of a fixed assignment system (such as TDMA) is also below that obtainable for the VMA system.

For an optimum code with $r \rightarrow (1 - \delta)$, we have

$$U_{opt} \rightarrow 1 + \frac{M}{\epsilon}(1-\delta)\ \ell n\left(\frac{1}{1-\delta}\right) \tag{2.52}$$

and

$$\eta_{opt} \to \frac{\epsilon}{M} + (1 - \delta)\ \ell n\left(\frac{1}{1 - \delta}\right) \tag{2.53}$$

The above expressions are maximized at

$$(1 - \delta) = r_{opt} = e^{-1} \approx 0.37 \tag{2.54}$$

to yield

$$\boxed{U_{opt} \to 1 + \frac{M}{\epsilon} e^{-1}} \tag{2.55}$$

and

$$\boxed{\eta_{opt} \to \frac{\epsilon}{M} + e^{-1}} \tag{2.56}$$

The best practical results are at rates close to r_{opt}, i.e., a rate-1/4 convolutional code and a rate-0.45 two-stage coding approach yields efficiencies of 10% and 16%, respectively. It is interesting to note that the maximum efficiency of this VMA system is identical to the maximum efficiency of the slotted Aloha system discussed in Section 2.4, which does require a perfect feedback link and an infinite signal-to-noise ratio. However, to achieve the capacity limits given above, long codes are required which imply complex decoders and long delays. Fortunately, as is also true for the Aloha system, practical systems do not attempt to operate at rates approaching the maximum limit.

For pure (unslotted) Aloha, the users are not required to transmit synchronously within a given slot. Thus, the probability of a collision is increased due to partial overlaps of packets. A loss in efficiency of a factor of 2 results in this case. A similar loss also results for the VMA system,

since the probability of interference within a given slot is a function of the factor 1/2M rather than 1/M as given by Eq. (2.37). Note that this is true for the time-division format given in Figure 2.1(a). If we allow random time and frequency placements of packets, overlaps in time and frequency will force the probability of interference to behave as a factor 1/4M. For antijam applications, where high efficiency is not warranted, systems of this nature still may be of interest.

2.6 Summary

The salient features of the four multiple-access systems are given in Table 2-1, the summary chart. While the typical efficiency of the VMA is somewhat lower than that for the Aloha and CDMA systems, the fact that the VMA system does not require a perfect feedback link, nor do the users have to be received with equal power, makes this multiple-access system attractive for a wide range of applications. While not emphasized in this section, it should be noted that the VMA system also has desirable ECCM features since high levels of interference can be tolerated by the burst/random error-correcting codes used in this system.

TABLE 2-1

PROPERTIES OF MULTIPLE-ACCESS SYSTEMS

Multiple-Access System	Number of Multiple Users in M Available Channels	Channel Efficiency for Users with a Duty Factor of ϵ	Number of Multiple Users Increases as the Duty Factor Decreases	Features			
				Received Power Distribution	Feedback Link Required	Required Transmit SNR	Variable Throughput Delay
Fixed Assignment Systems; i.e., TDMA, FDMA	M	ϵ	No	Arbitrary	No	High	No
CDMA	$\frac{M}{\epsilon}\frac{1}{E_b/N_0}+1$ Typically: $\frac{M}{3\epsilon}$	$\frac{1}{E_b/N_0}+\frac{\epsilon}{M}$ Typically: $\frac{1}{3}$	Yes	Uniform	No	High	No
Slotted Aloha	$\frac{GM}{\epsilon}$ with $G \le 1$ Typically: $\frac{M}{2\epsilon}$	$Ge^{-G} \le e^{-1}$ Typically: $\frac{e^{-1}}{2}$	Yes	Arbitrary	Yes	Very High	Yes
VMA	$\frac{rM\,\ell n(1-\delta)^{-1}}{\epsilon}+1$ Typically: $\frac{M}{10\epsilon}$	$r\,\ell n(1-\delta)^{-1}+\frac{\epsilon}{M} \le e^{-1}$ Typically: $\frac{1}{10}$	Yes	Arbitrary	No	Moderate to Low	No

REFERENCE

[2.1] D. Chase and L. H. Ozarow, "Capacity Limits for Binary Codes in the Presence of Interference," IEEE Trans. on Communications, Vol. COM-27, No. 2, February 1979.

SECTION 3

PULSE JAMMING OF AN ADAPTIVE ANTENNA

The effectiveness of a pulsed jammer against an adaptive antenna is developed through analysis of a single adaptive loop. Specific numerical results are presented for the use of the single loop in a two element array; the extension of these results to a sidelobe canceller situation is sketched. The basic loop design and analysis are due to Gabriel [3.1]. Using his results, a solution is developed for the steady-state performance under periodic pulsed jamming. Through appropriate normalizations the results are made independent of specific system parameter values, and are presented as a function of jammer properties only.

The results presented in this section indicate that even a low power jammer with a small duty factor can increase the output noise significantly during the occurrence of the jamming pulse. These array results serve to justify the worst-case pulse jamming models considered in Section 4 which assume an error rate of 1/2 during the presence of interference and just thermal noise during the pulse-off time.

3.1 Background for Single Adaptive Loop

Following Gabriel [3.1] the single adaptive loop in a two-element array is shown in Figure 3.1. The behavior of the adjustable weight W_2 is governed by a first order differential equation which Gabriel solves as

$$W_2(t) = \left[W_2(0) - W_2(\infty)\right] e^{-t/\tau_L} + W_2(\infty) \qquad (3.1)$$

where τ_L is the loop time constant. It is assumed that B_2, the beam-steering command in Figure 3.1, is such that $W_2 = W_I^*$ in the absence of a jammer; thus with jammer turn-on at time zero,

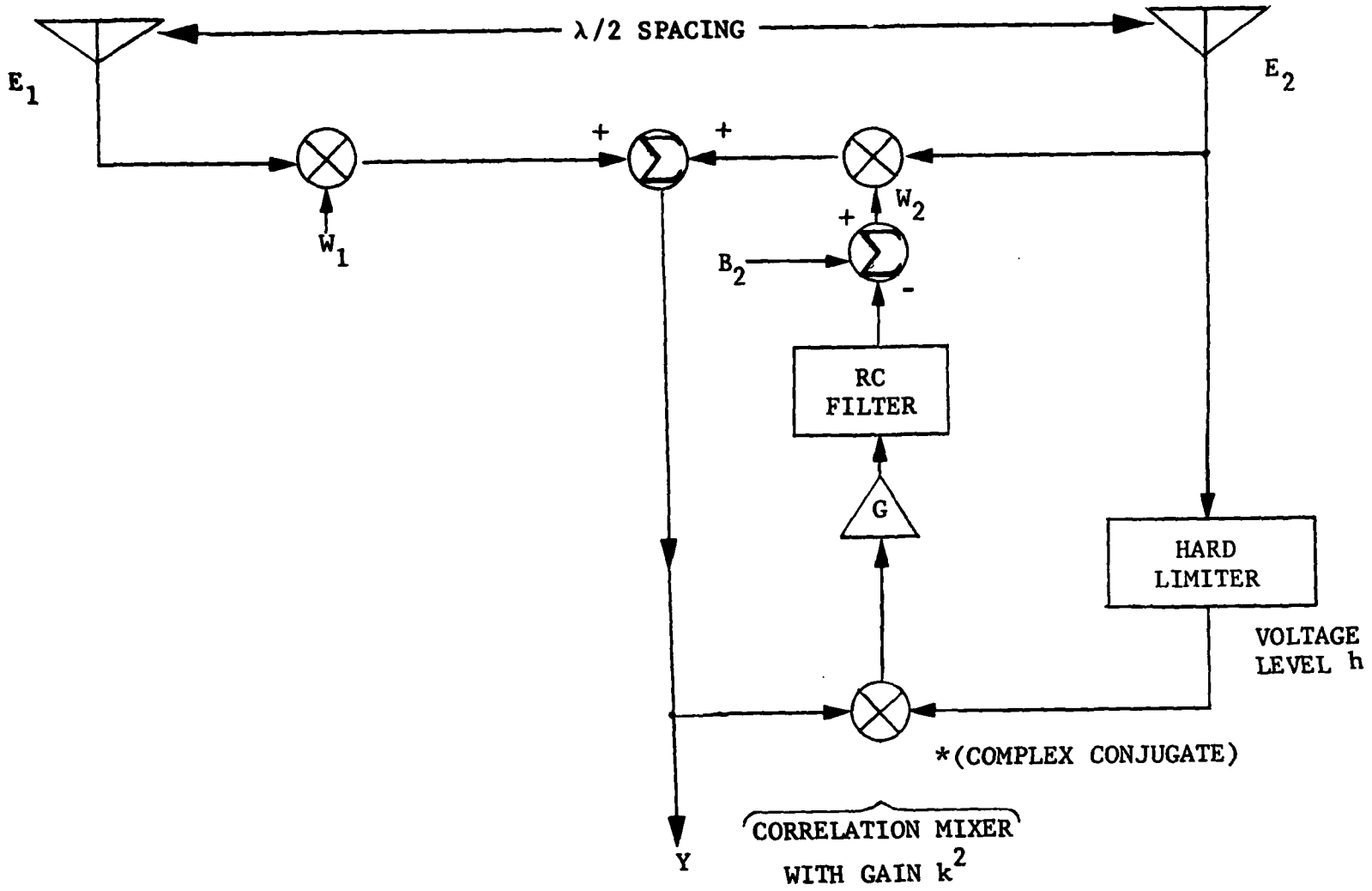


Figure 3.1 Two-Element Array with Single Adaptive Loop

$$W_2(0) = W_1^* \tag{3.2}*$$

Let J_i denote the jammer level, and n the thermal noise level, at the output of each array element. From Figure 3.2, in which the phase reference is chosen to be midway between the elements, the output of each element can be written as

$$\left.\begin{aligned} E_1 &= J_i e^{-ju} + n_1 \\ E_2 &= J_i e^{ju} + n_2 \end{aligned}\right\} \tag{3.3}$$

where u is the phase shift at angle θ. Only when the bandwidth of each array element channel is small relative to the center frequency of the array can the time delay between element outputs be represented as a phase shift for noiselike jammers. The noise power out of the array, due to thermal noise alone, is

$$\overline{|Y_0|^2} = \overline{\left|W_1 n_1 + W_2^0 n_2\right|^2} = \left(|W_1|^2 + |W_2^0|^2\right)\overline{|n|^2} \tag{3.4}$$

(where W_2^0 indicates the value of W_2 in the absence of jamming) under the assumption that n_1 and n_2 are uncorrelated and zero mean, but of equal power density. The value of W_1, and the beam-steering command B_2 determine the pointing direction of the array in the absence of a jammer. For this two-element array, it will always be true that $W_2^0 = W_1^*$. There is no loss in generality from choosing a pointing direction of 0^o, so that

$$W_2^0 = W_1^* = W_1 = 1 \tag{3.5}$$

*In Gabriel's paper W_2 is used for the weight in a loop without the hard limiter, whereas W_2' denotes the weight in the loop with a hard limiter. Because only the latter case is considered here the prime is dropped from W_2.

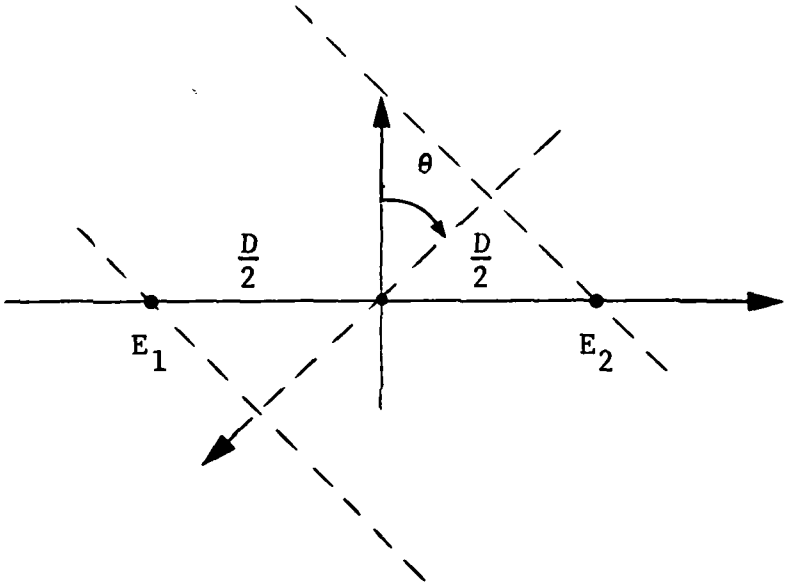


Figure 3.2 Signal Phase Reference Diagram for Two-Element Array

and Eq. (3.4) becomes

$$\overline{|Y_0|^2} = 2\overline{|n|^2} \tag{3.6}$$

With jamming, the output is

$$Y = W_1E_1 + W_2E_2$$

or, from Eq. (3.3),

$$Y = J_i e^{-ju} + n_1 + W_2 J_i e^{ju} + W_2 n_2 \tag{3.7}$$

Assuming J_i and n_1, n_2 to be all uncorrelated and of zero mean, the output noise level is

$$\overline{|Y|^2} = \left(1 + |W_2|^2\right)\overline{|n|^2} + \overline{|J_i|^2}\,|e^{-ju} + W_2 e^{ju}|^2 \tag{3.8}$$

Of primary interest in assessing the performance of the adaptive loop is the increase in output noise due to jamming. Thus, by defining

$$N = \left\{\begin{matrix}\text{Increase in output} \\ \text{noise due to jamming}\end{matrix}\right\} = \overline{|Y|^2}\Big/\overline{|Y_0|^2} \tag{3.9}$$

Eqs. (3.6) and (3.8) give

$$N = \frac{1}{2}\left[1 + |W_2|^2 + P_i|1 + W_2 e^{j2u}|^2\right] \tag{3.10}$$

where

$$P_i = \overline{|J_i|^2}\Big/\overline{|n|^2}$$

is the ratio of jammer to thermal noise levels.

From Figure 3.2 it is possible to develop the fact that

$$u = \frac{\pi D}{\lambda} \sin \theta$$

where λ is the wavelength corresponding to the center frequency of the array. By choosing $D = \lambda/2$

$$u = \frac{\pi}{2} \sin \theta \tag{3.11}$$

and the array has a gain in the absence of jamming of the form

$$G_0(\theta) = \cos u \tag{3.12}$$

so the nulls exist at $\theta = \pm 90^{\circ}$.

Complete cancellation of the jammer would result in $\overline{|Y|^2} = \overline{|Y_0|^2}$, or N = 1. To see the conditions under which this perfect cancellation could exist, consider the following reasoning: because of the phase difference between E_1 and E_2 it is necessary that the optimum W_2, denoted by W_{0_2}, have the form

$$W_{0_2} = -Ae^{-j2u} \tag{3.13}$$

where the lag of 2u will bring the phase of J_1 at E_2 into phase with that at E_1, and the negative value will provide cancellation. Thus, substitution of Eq. (3.13) into Eq. (3.10) gives

$$N = \frac{1}{2}\left[1 + A^2 + P_i(1 - A)^2\right] \tag{3.14}$$

Recognizing the positive nature of A, minimization of Eq. (3.14) with respect to A results in

$$W_{0_2} = -\frac{P_i}{1 + P_i} e^{-j2u} \tag{3.15}$$

and

$$N_{min} = \frac{1}{2}\left[1 + \frac{P_i}{(i + P_i)^2} + \frac{P_i^2}{(1 + P_i)^2}\right] \tag{3.16}$$

Only when $P_i \gg 1$ will $N_{min} = 1$.

Returning to Eq. (3.1), the values of τ_L and $W_2(\infty)$ in that equation have been shown by Gabriel to be expressible as

$$W_2(\infty) = \frac{1 + \mu_0}{1 + \mu_0\sqrt{1 + P_i}} + \frac{\mu_0\sqrt{1 + P_i}}{1 + \mu_0\sqrt{1 + P_i}} W_{0_2} \tag{3.17}$$

$$\tau_L = \frac{\tau_0}{1 + \mu_0\sqrt{1 + P_i}} \tag{3.18}$$

where

$$\mu_0 = h\, k^2\, G\, \overline{|n|^2} \tag{3.19}$$

and τ_0 is the time constant of the RC filter (see Figure 3.1). As a guide in choosing τ_0 Gabriel proposes the design rule that the loop bandwidth, $1/\tau_L$, should not exceed one tenth of the array channel bandwidth (principally to ensure that the average weight behavior is adequately represented by Eq. (3.1), and to ensure that the weight noise is not a dominant consideration). If the array element channel has a bandpass of B_c Hz, then the maximum value of the two-sided loop bandwidth is

$$2\frac{1}{(\tau_L)_{max}} = 2\frac{1 + \mu_0\sqrt{1 + P_{im}}}{\tau_0} = \frac{2\pi B_c}{10}$$

or

$$\tau_0 = \frac{10}{\pi B_c}\left(1 + \mu_0\sqrt{1 + P_{im}}\right) \tag{3.20}$$

where now P_{im} must be the maximum anticipated value of the jammer to thermal noise power ratio, P_i.

In summary, Gabriel has developed a model for a single adaptive loop in a two-element array such that the weight behavior is governed by Eq. (3.1), with the parameters in Eq. (3.1) defined by Eqs. (3.2), (3.5), (3.11), (3.15), (3.17), (3.18), (3.19), and (3.20). The performance of the loop in minimizing jammer output noise relative to thermal noise is given by Eq. (3.10), with the minimum attainable value in Eq. (3.16). Only in Eqs. (3.19) and (3.20) are explicit values for system parameters required; for the pulsed jamming case to be considered next, only a value for μ_0 will be required in order to generate numerical performance data.

3.2 Development of Steady-State Solution

Let pulses occur at t = kT and last for τ_p seconds. The duty factor is $d = \tau_p/T$ so that $T = \tau_p/d$. For a pulse beginning at $t = (k - 1)T$ the value of the weight at the end of the pulse is, from Eq. (3.1),

$$W_2\left[(k - 1)T + \tau_p\right] = \left\{W_2\left[(k - 1)T\right] - W_2(\infty)\right\}e^{-\tau_p/\tau_L} + W_2(\infty) \tag{3.21}$$

From $t = (k - 1)T + \tau_p$ to t = kT the jammer is off and the loop behavior is governed by a different time constant. Let τ_{off} denote the time constant with no jammer; from Eq. (3.18), with $P_i = 0$ the time constant becomes

$$\tau_{off} = \frac{\tau_0}{1 + \mu_0}$$

which is better expressed as the ratio

$$\tau_{off} = \tau_L/K \tag{3.22}$$

with

$$K = \frac{1 + \mu_0}{1 + \mu_0\sqrt{1 + P_i}} \tag{3.23}$$

The time that the jammer is off is

$$kT - \left[(k-1)T + \tau_p\right] = T - \tau_p = \frac{\tau_p}{d} - \tau_p = (\frac{1}{d} - 1)\tau_p$$

so that the weight at the beginning of the next pulse is

$$W_2(kT) = \left\{W_2\left[(k-1)T + \tau_p\right] - W_1^*\right\} e^{-K(1/d-1)\tau_p/\tau_L} + W_1^* \tag{3.24}$$

where the exponent has been obtained from

$$\frac{kT - \left[(k-1)T + \tau_p\right]}{\tau_{off}} = K(\frac{1}{d} - 1)\tau_p/\tau_L$$

In Eq. (3.24) the more general final value for W_2 of W_1^* has been used, even though for an initial beam-steering direction of 0^o, $W_1^* = W_1 = 1$.

To simplify notation, define the normalized pulse width

$$p = \tau_p/\tau_L \tag{3.25}$$

Now the adaptive loop behavior is characterized by the two difference equations

$$\left.\begin{aligned} W_2\left[(k-1)T+\tau_p\right] &= \left\{W_2\left[(k-1)T\right]-W_2(\infty)\right\}e^{-p}+W_2(\infty) \\ W_2(kT) &= \left\{W_2\left[(k-1)T+\tau_p\right]-W_1^*\right\}e^{-Kp\left(\frac{1}{d}-1\right)}+W_1^* \end{aligned}\right\} \quad (3.26)$$

with $W_2(0) = W_1^*$.

In order to characterize the loop performance it is necessary to establish a definition of the steady-state weight value. Clearly, from Eq. (3.26), the steady-state weight behavior is periodic, with well-defined values at two epochs -- the beginning and end of a jammer pulse. Specifically, steady-state implies that $W(kT) = W[(k-1)T]$ and thus that $W_2[(k-1)T+\tau_p] = W_2(kT+\tau_p)$. However, a meaningful performance evaluation is not possible if the change in W_2 over the pulse-on time causes a change in N, the output noise increase due to jamming, of more than, say, 2 dB. The value of p which would cause such a change in W_2, and thus N, will not be a constant but will depend upon the jammer parameters P_i, d, and θ. Determining the optimum value of p could only be done recursively and would represent a serious computational problem. This problem has been resolved by numerical exploration using Eqs. (3.26) and (3.10), and covering the significant range of values of the jammer parameters. A choice of p = 0.25 was made, based upon this numerical exploration; a more detailed discussion of this choice of p will be given with the presentation of the numerical results.

A steady-state solution may be developed from Eq. (3.26) in either of two ways: by setting $W_2(kT) = W_2[(k-1)T] = W_{ss}$ and solving for W_{ss} by elimination of $W_2[(k-1)T+\tau_p]$, or by cycling through the two difference equations from t = 0 to obtain an explicit expression for $W_2(kT+\tau_p)$. Both results are of interest and will be given, but the details of the second approach will be suppressed.

To reduce typographical complexity, the following notation will be adopted:

$$\left.\begin{aligned} W_k &\equiv W_2(kT),\ W_{k-1+p} \equiv W_2\left[(k-1)\,T + \tau_p\right] \\ W_\infty &\equiv W_2(\infty),\ e_1 \equiv e^{-p},\ e_2 \equiv e^{-Kp(1/d-1)} \end{aligned}\right\} \tag{3.27}$$

Using Eq.. (3.27) in Eq. (3.26) gives

$$\left.\begin{aligned} W_{k-1+p} &= \left[W_{k-1} - W_\infty\right] e_1 + W_\infty \\ W_k &= \left[W_{k-1+p} - W_1^*\right] e_2 + W_1^* \end{aligned}\right\} \tag{3.28}$$

By setting

$$W_{ss} = W_{k-1} = W_k$$

and eliminating W_{k-1+p} between the equations in Eq. (3.28), there is obtained after suitable algebraic manipulations

$$W_{ss} = \frac{1 - e_2}{1 - e_1 e_2} W_1^* + \frac{e_2(1 - e_1)}{1 - e_1 e_2} W_\infty \tag{3.29}$$

Before any discussion of Eq. (3.29) is undertaken, the second solution is presented; by using $W_2(0) = W_1^*$, and cycling the equations in Eq. (3.26) there can be obtained

$$W_2(nT) = \left[\sum_{k=0}^{n-1} (e_1 e_2)^k\right]\left[(1 - e_2)W_1^* + e_2(1-e_1)W_\infty\right] + (e_1 e_2)^n W_1^* \tag{3.30}$$

By recognizing that

$$\lim_{n \to \infty} \sum_{k=0}^{n-1} (e_1 e_2)^k = \frac{1}{1 - e_1 e_2}$$

and that

$$\lim_{n \to \infty} (e_1 e_2)^n = 0$$

it is seen that Eq. (3.30) reduces to Eq. (3.29) for large n; the utility of Eq. (3.30) is in allowing estimates of the transient settling time to be made from knowledge of e_1 and e_2 only.

The steady-state weight value in Eq. (3.29) has two intuitively satisfying components: the first component depends upon the beam-steering value W_1^*; when the jammer pulse length and duty factor are small so that $e_2 \approx 0$, the value of W_2 will not be much different from its nonjammed value of W_1^*. When the jammer pulse is long with respect to the loop time constant, so that p is large, then $e_1 \approx 0$; if, at the same time, the duty factor approaches unity, then $e_2 \approx 1$ and W_2 will attain the jammer-adapted value $W_2(\infty)$.

To obtain quantitative performance data it is necessary to use only Eqs. (3.29) and (3.10), together with values for the parameters μ_0, θ, P_i, p, and d. Except for μ_0 which is a composite of loop parameters, the remainder are related strictly to specification of jammer properties.

3.3 Loop Performance Data

It is desirable to summarize here the equations and parameter definitions which have been used in obtaining the performance data. Some slight modifications will be made to the form of some previously stated equations. Also, the specific values $W_1 = 1$, $D = \lambda/2$ are being used.

Output Noise Increase over Thermal Noise:

$$N = \frac{1}{2}\left[1 + P_i + (1 + P_i)A_2^2 + 2P_i A_2 \cos(2u + \varphi)\right] \qquad (3.31)$$

where

$$\left(W_2\right)_{ss} = W_{ss} = A_2 e^{j\varphi} \qquad (3.32)$$

and

$$P_i = \overline{|J_i|^2} \Big/ \overline{|n|^2} \tag{3.33}$$

Steady-State Weight

$$W_{ss} = \alpha + \beta W_2(\infty) \tag{3.34}$$

where

$$\alpha = \frac{1 - e_2}{1 - e_1 e_2} \tag{3.35}$$

$$e_1 = e^{-p} , \quad e_2 = e^{-Kp(\frac{1}{d}-1)} \tag{3.36}$$

$$\beta = \frac{e_2(1-e_1)}{1 - e_1 e_2} \tag{3.37}$$

and

$$W_2(\infty) = K - Me^{-j2u} \tag{3.38}$$

with

$$K = \frac{1 + \mu_0}{1 + \mu_0\sqrt{1 + P_i}} \tag{3.39}$$

$$M = \frac{\mu_0\sqrt{1 + P_i}}{1 + \mu_0\sqrt{1 + P_i}} \cdot \frac{P_i}{1 + P_i} \tag{3.40}$$

and

$$u = \frac{\pi}{2} \sin \theta \tag{3.41}$$

The parameters which specify the jammer are

p = pulse width as a multiple of loop time constant with jammer on

d = duty factor

P_i = jammer to thermal noise ratio at output of array element

and

θ = jammer angle off boresight

To obtain numerical results it is necessary to give fixed values to the parameters μ_0 and p. Gabriel recommends that $\mu_0 = 100$ be used; the effect of μ_0 is principally in the minimum value achievable for N. This minimum value is of course realized only for continuous jamming. To see how the value of μ_0 affects pulsed jamming performance, it is necessary to consider Eqs. (3.34) to (3.40). The value of W_{ss} is affected by μ_0 through $W_2(\infty)$, which itself depends upon μ_0 in a relatively complicated fashion through K and M. For the range of values of P_i, d, and θ considered in generating the numerical data, a value of $\mu_0 > 10$ was determined to be sufficient in the sense that further increase in μ_0 caused less than 1 dB change in computed N values. Obviously, values of $\mu_0 < 10$ caused greater change in N values, with $\mu_0 = 1$ causing N to be generally 5 or more dB greater than values computed with $\mu_0 = 10$.

Some aspects of the problem of choosing a value of p have been discussed already. Essentially, p should not be so small that it would violate any bandwidth assumption [such as that made in developing Eq. (3.20)] , nor should it be so large that the values of N at the beginning and end of the pulse differ by more than 2 or 3 dB. The minimum condition for a p value is not invoked here because of the normalization procedure which results in no direct need for values of τ_0. To properly implement the maximum condition would require that

for each value of P_i, d, and θ a search be made for that p value which would result in a 2 to 3 dB variation in N over the pulse duration (note that the second of the equations in Eq. (3.28) would have to be used to compute W_2 at the end of the pulse). Because such a search would result in a variable value for p, and thus considerably complicate the data presentation, a fixed value of $p = 0.25$ was chosen after exploration of a range of values for p. For the ranges considered for the parameters P_i, d, and θ, use of $p \leq 0.25$ ensured a difference in N over the pulse duration of less than 3 dB. In fact, as is necessary for precision in the results, for values of N under 10 dB the variation over the pulse duration is less than 1 dB.

The final topic before presentation of the numerical results is the nature of the jammer. It has been assumed that the jammer is average power limited. Thus, with P_{ave} denoting the average jammer power relative to the thermal noise level, the pulsed jammer power is $P_i = P_{ave}/d$. By choosing a maximum P_{ave} of 1000, and a minimum d of 0.01, the maximum value of P_i is 10^5; the minimum value used is 1.

The numerical performance data for the single adaptive loop will be presented in two formats: first as a set of curves parametrized by jammer angle θ, and then as a set of tables parametrized by P_{ave}.

In Figures 3.3 through 3.11, and in Tables 3-1 through 3-4, loop performance is measured by the increase in output noise level above that which is due to thermal noise alone. Eq. (3.31) is the basis for the computation. A fact to remember when interpreting the data in these curves and tables is that the outputs of two array elements are being summed (refer to Figure 3.1). Thus the combined output power can be up to 3 dB greater than the power delivered by one element, with the 3 dB limit being attained when $W_2 = W_1 = 1$. This latter condition is nearly obtained for $d = 0.01$ and $P_{ave} = 1$ (because the loop accomplished very little adaptation, so that $W_2 \approx W_1$) so that the indicated value of N is 22 dB (see Table 3-1), representing a 2 dB increase over $P_i = 1/0.01 = 20$ dB. An additional fact to remember when interpreting the data is that the quiescent null is at 90^o. Consequently, it is not the jammer angle off boresight, but its complement with respect to 90^o, which is the proper indicator of loop performance.

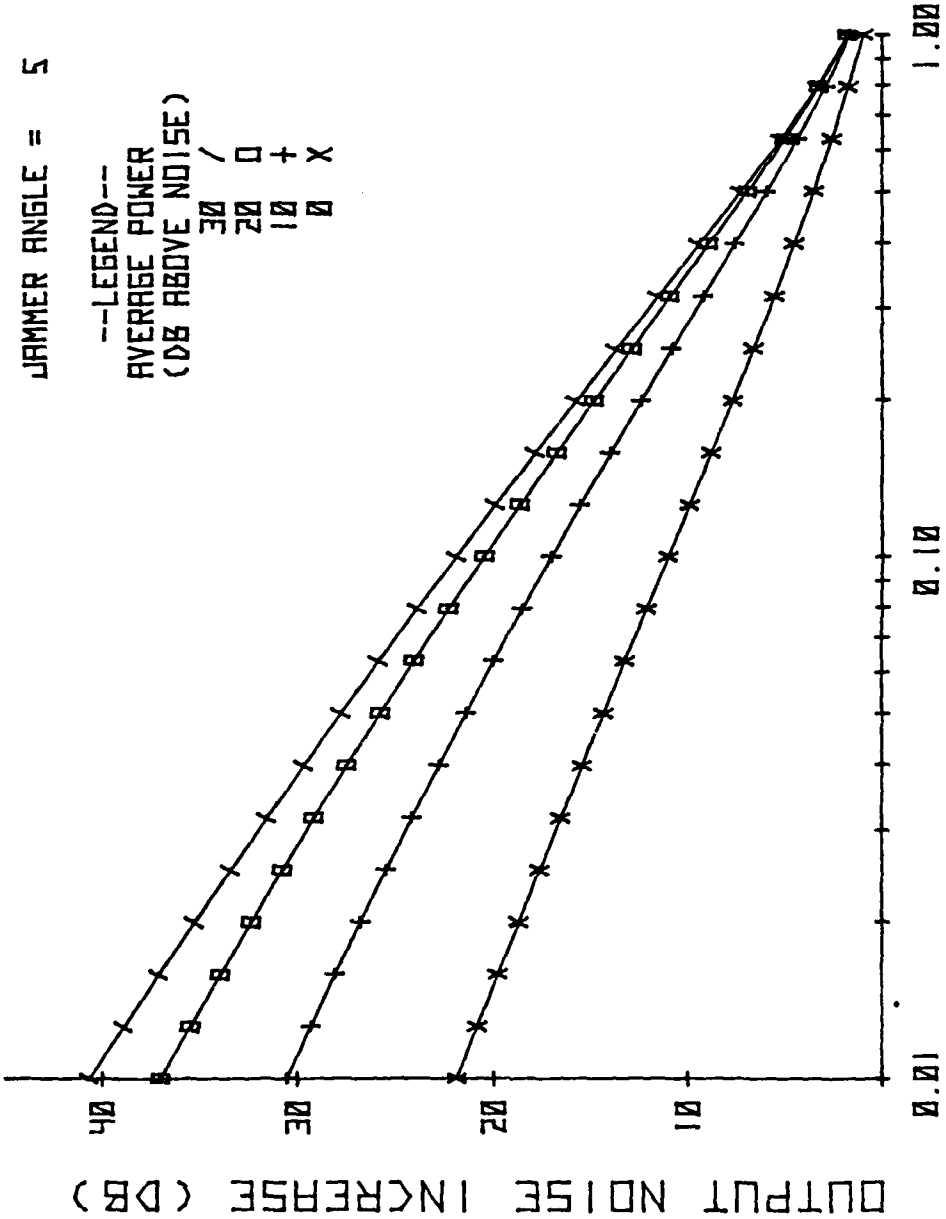


Figure 3.3 Loop Performance at Jammer Angle of 5°

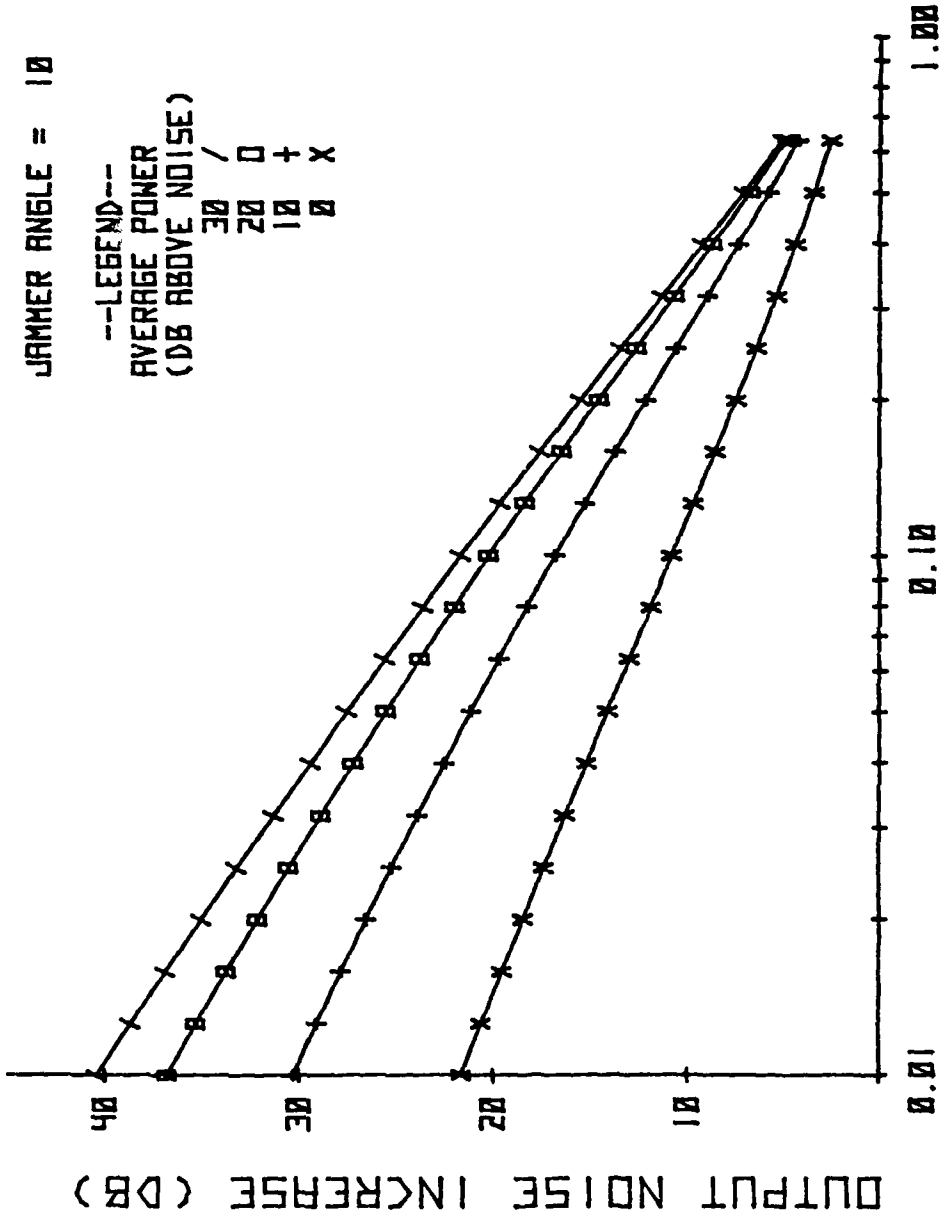


Figure 3.4 Loop Performance At Jammer Angle of 10°

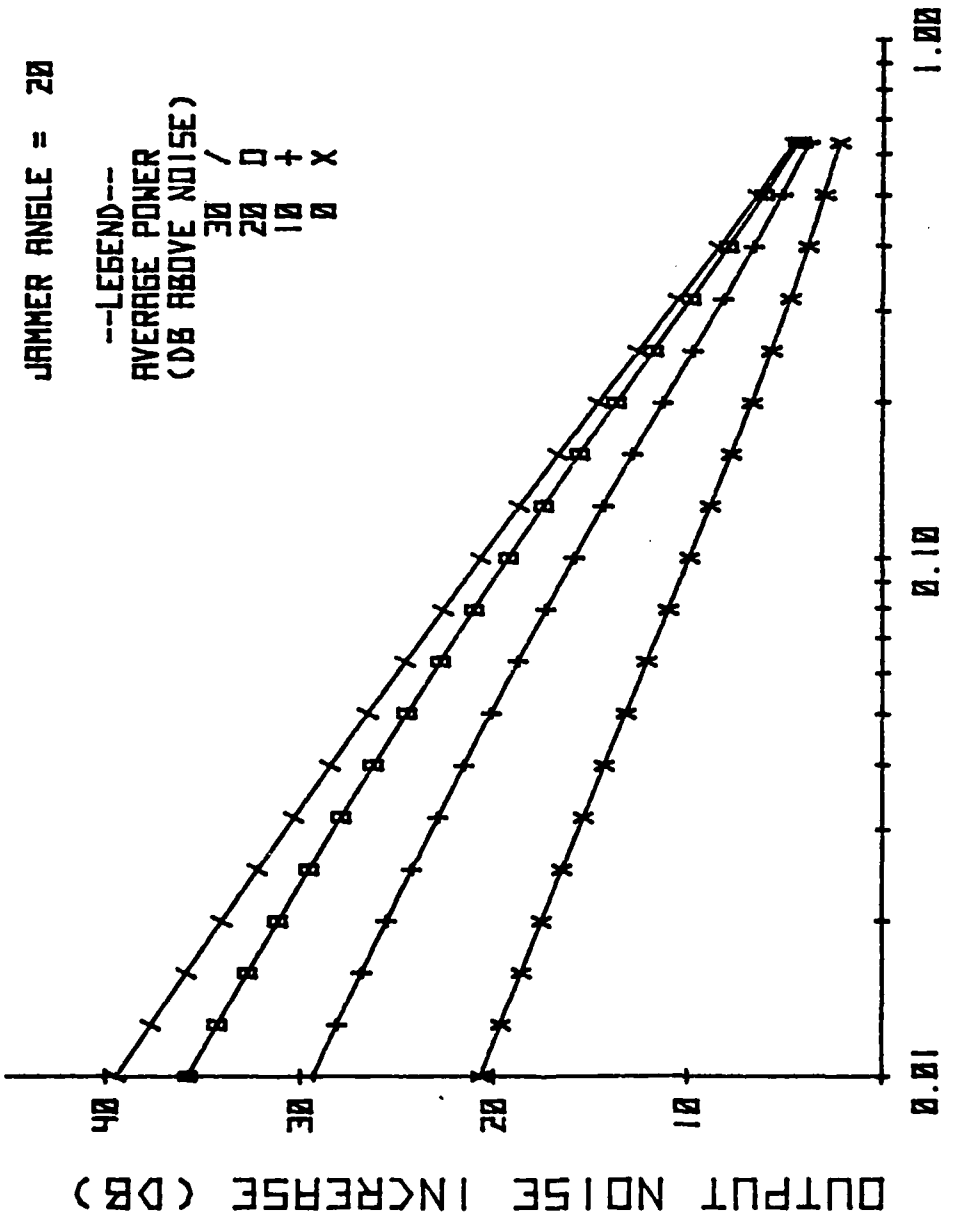


Figure 3.5 Loop Performance at Jammer Angle of 20°

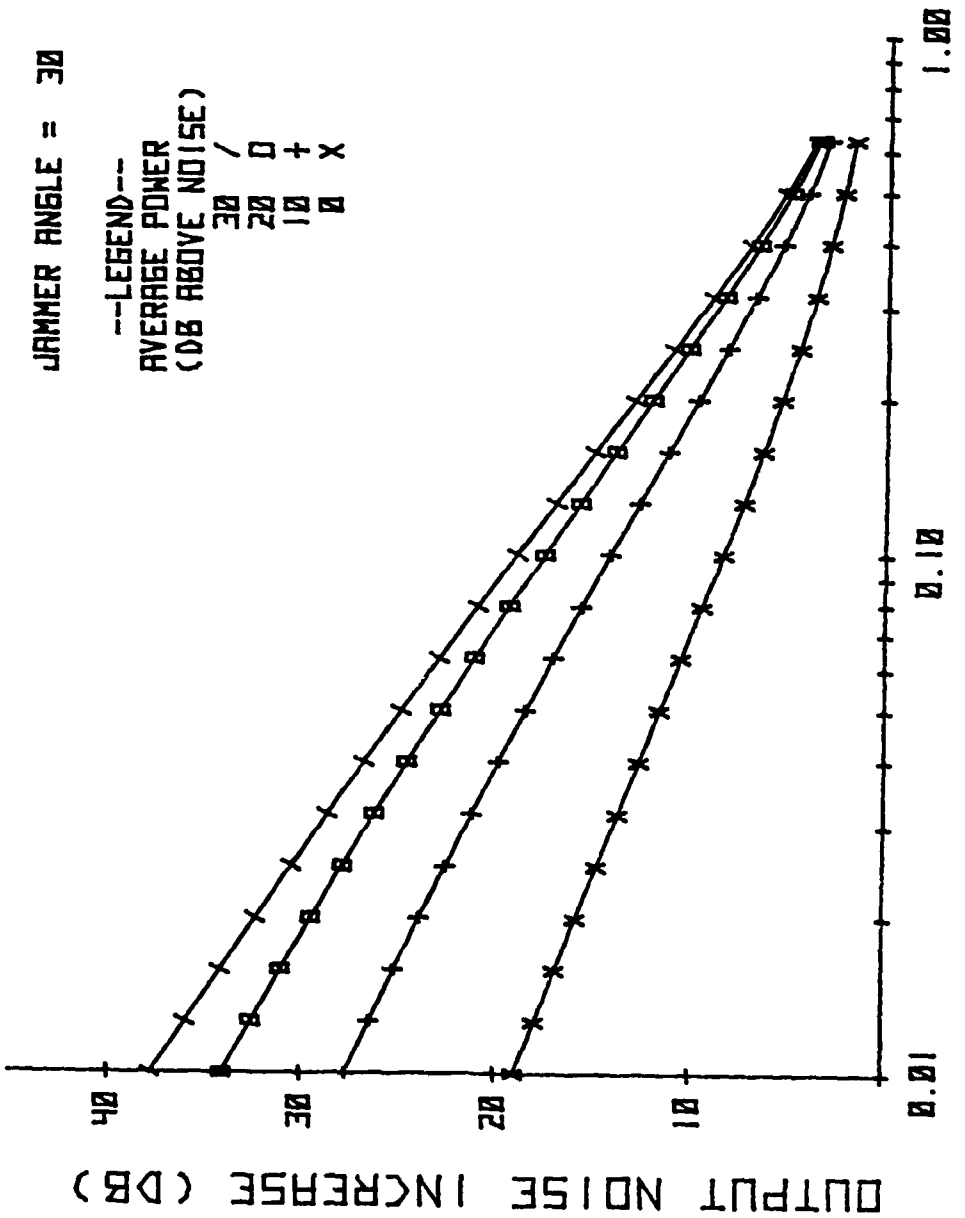


Figure 3.6 Loop Performance at Jammer Angle of 30°

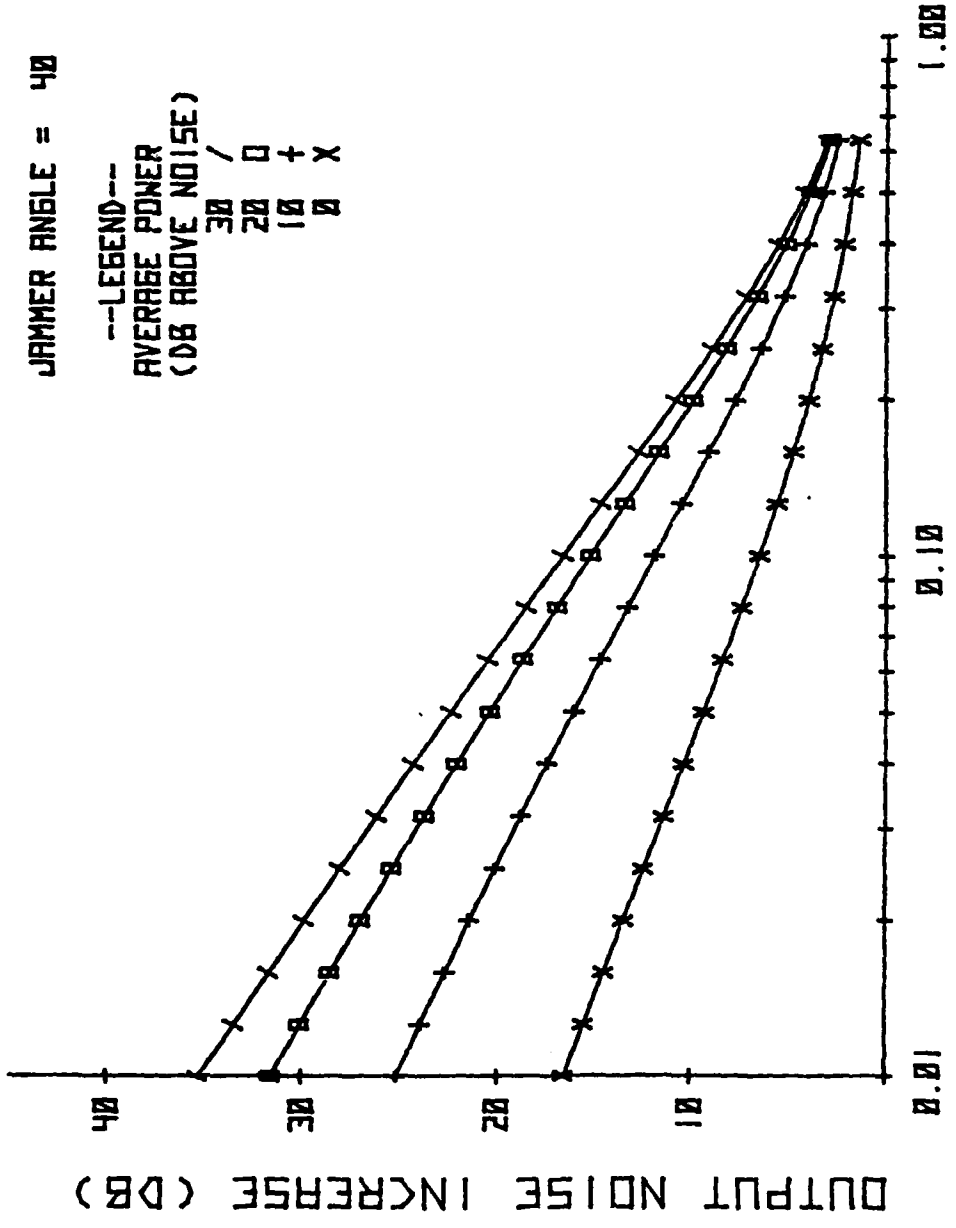


Figure 3.7 Loop Performance at Jammer Angle of 40°

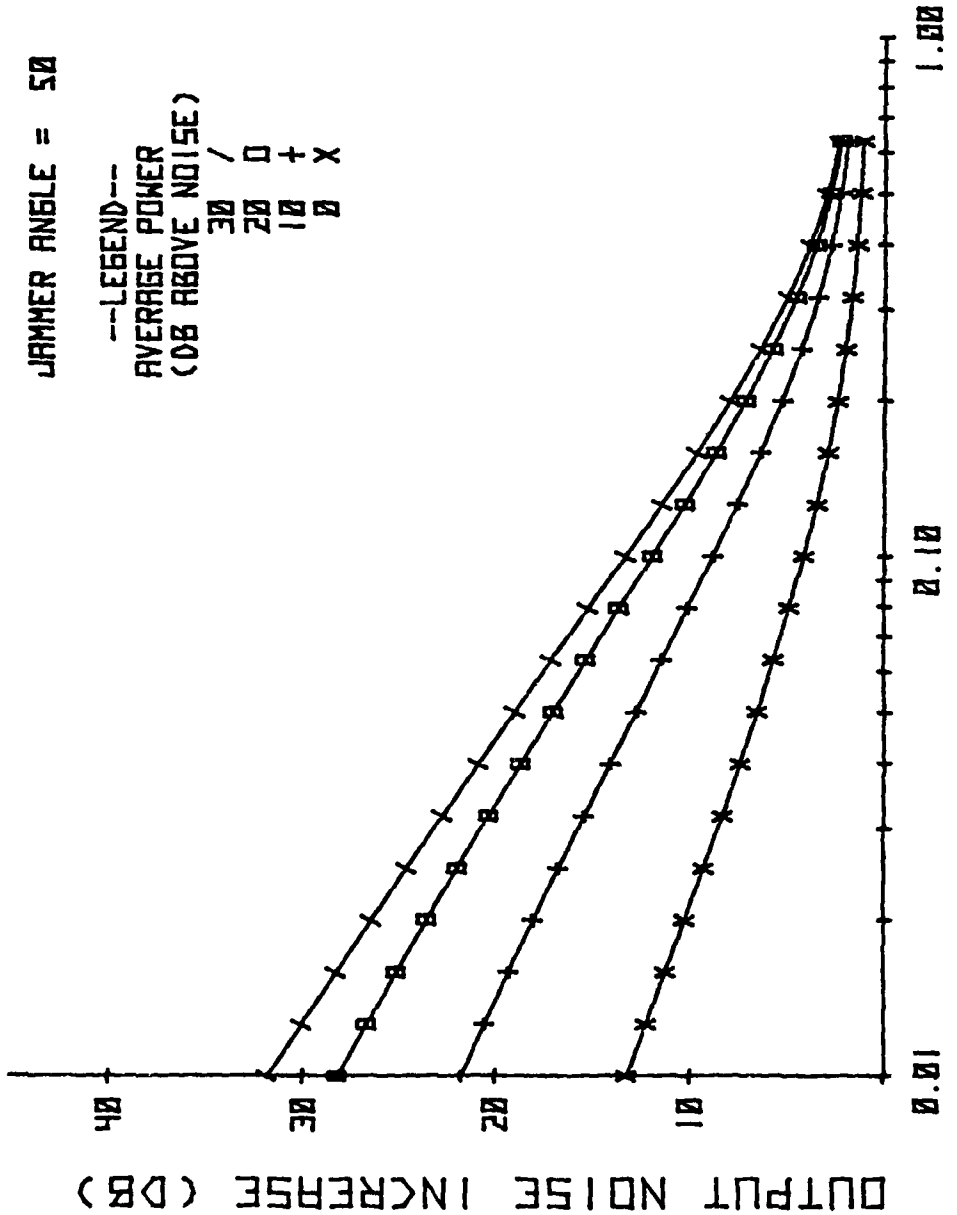


Figure 3.8 Loop Performance at Jammer Angle of 50°

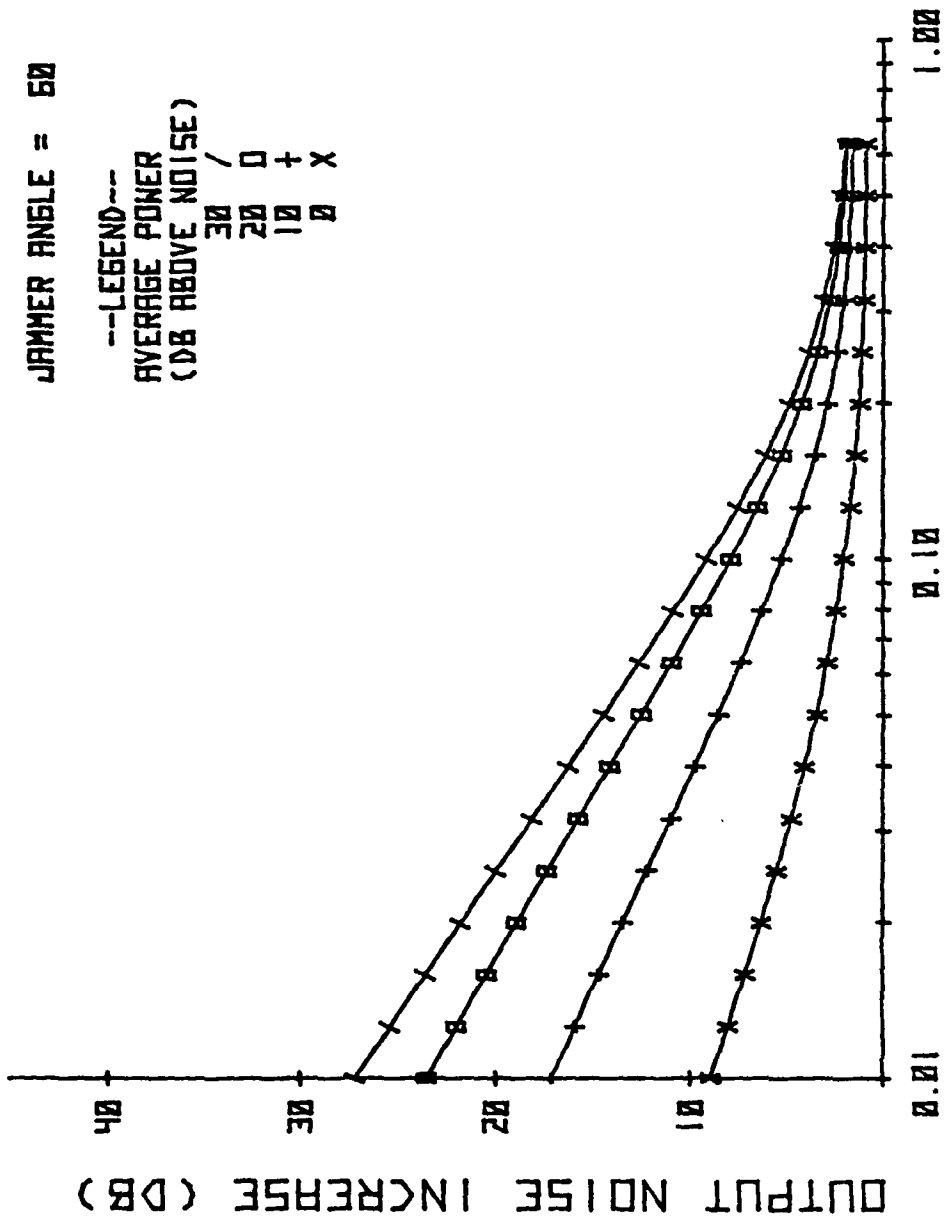


Figure 3.9 Loop Performance at Jammer Angle of 60°

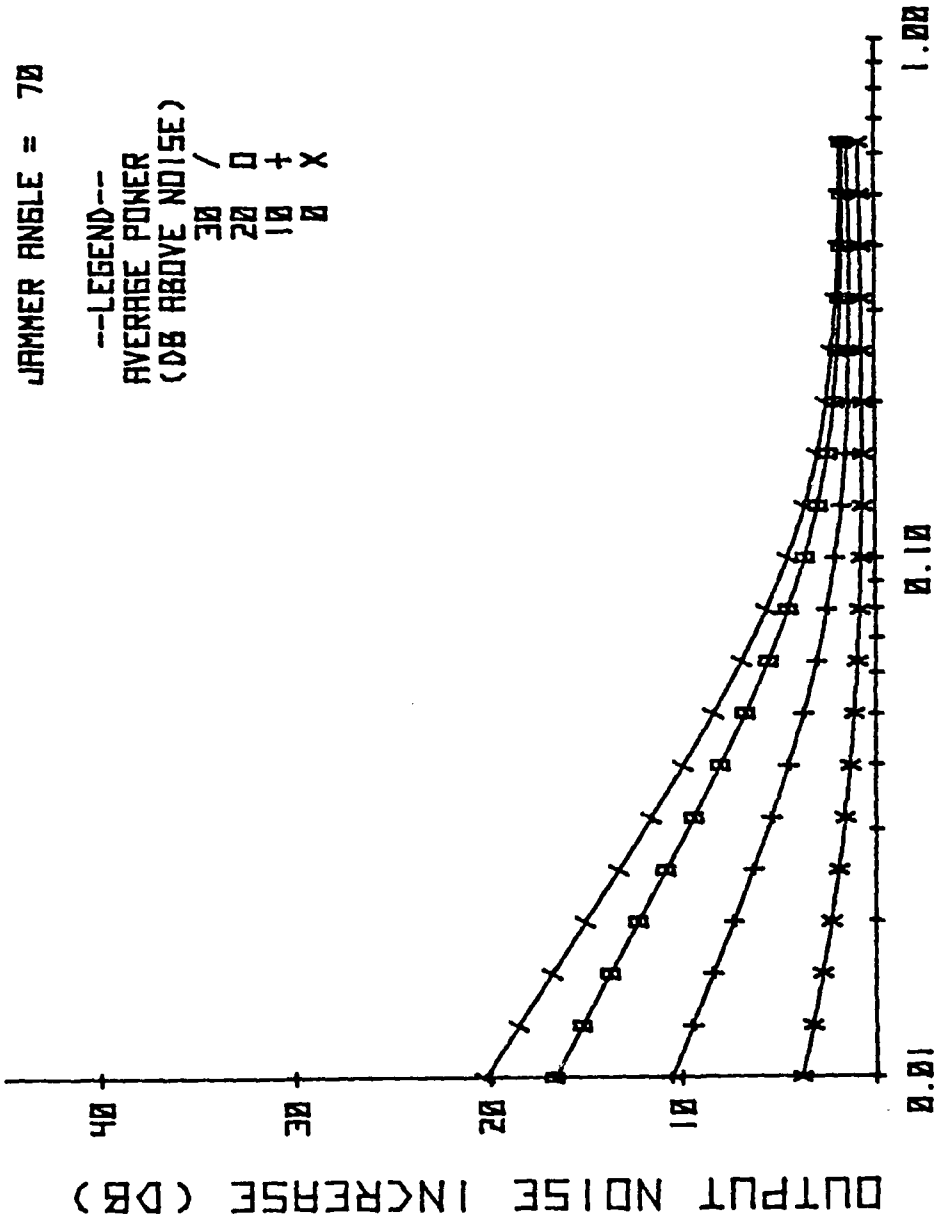


Figure 3.10 Loop Performance at Jammer Angle of 70°

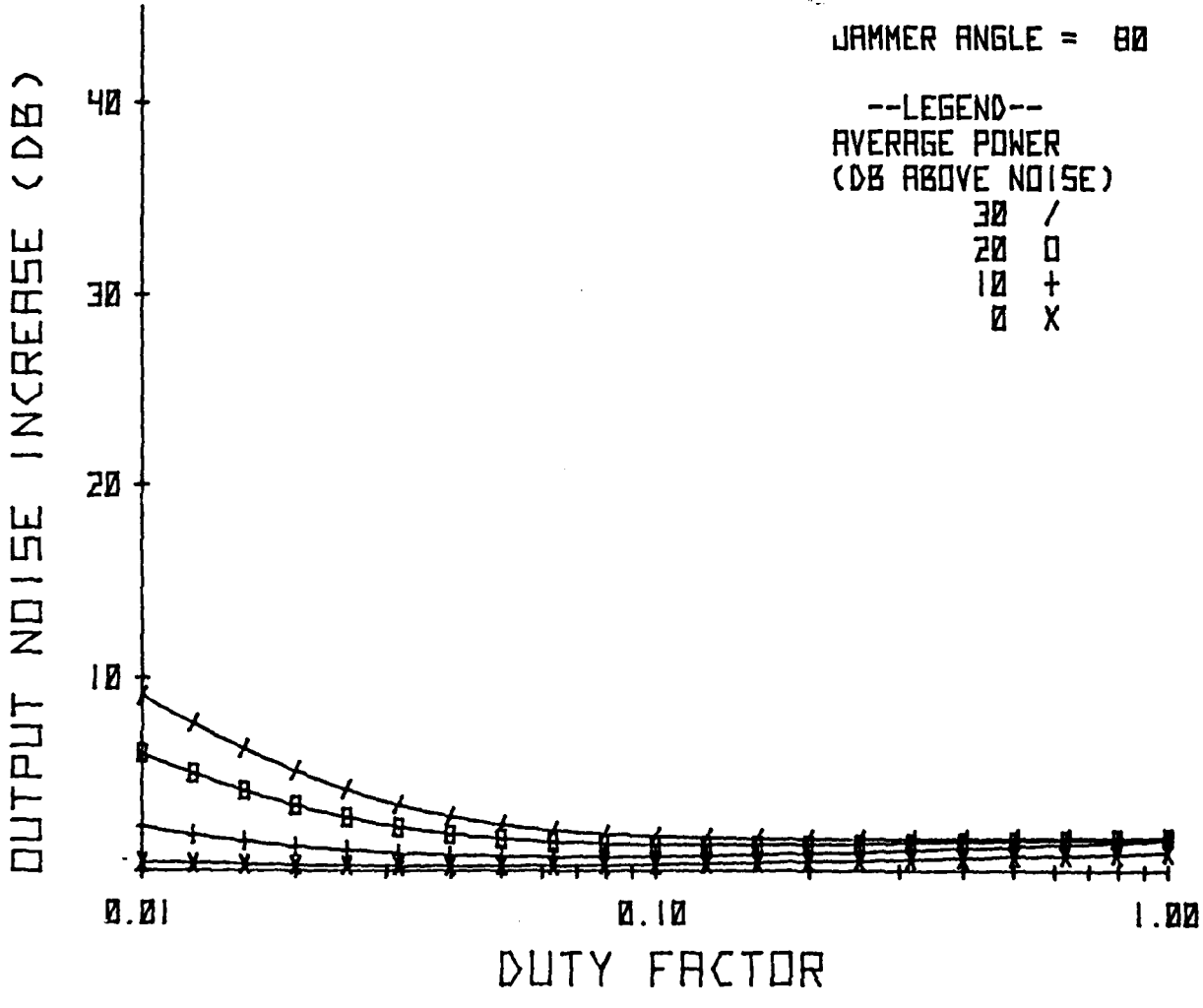


Figure 3.11 Loop Performance at Jammer Angle of 80^{o}

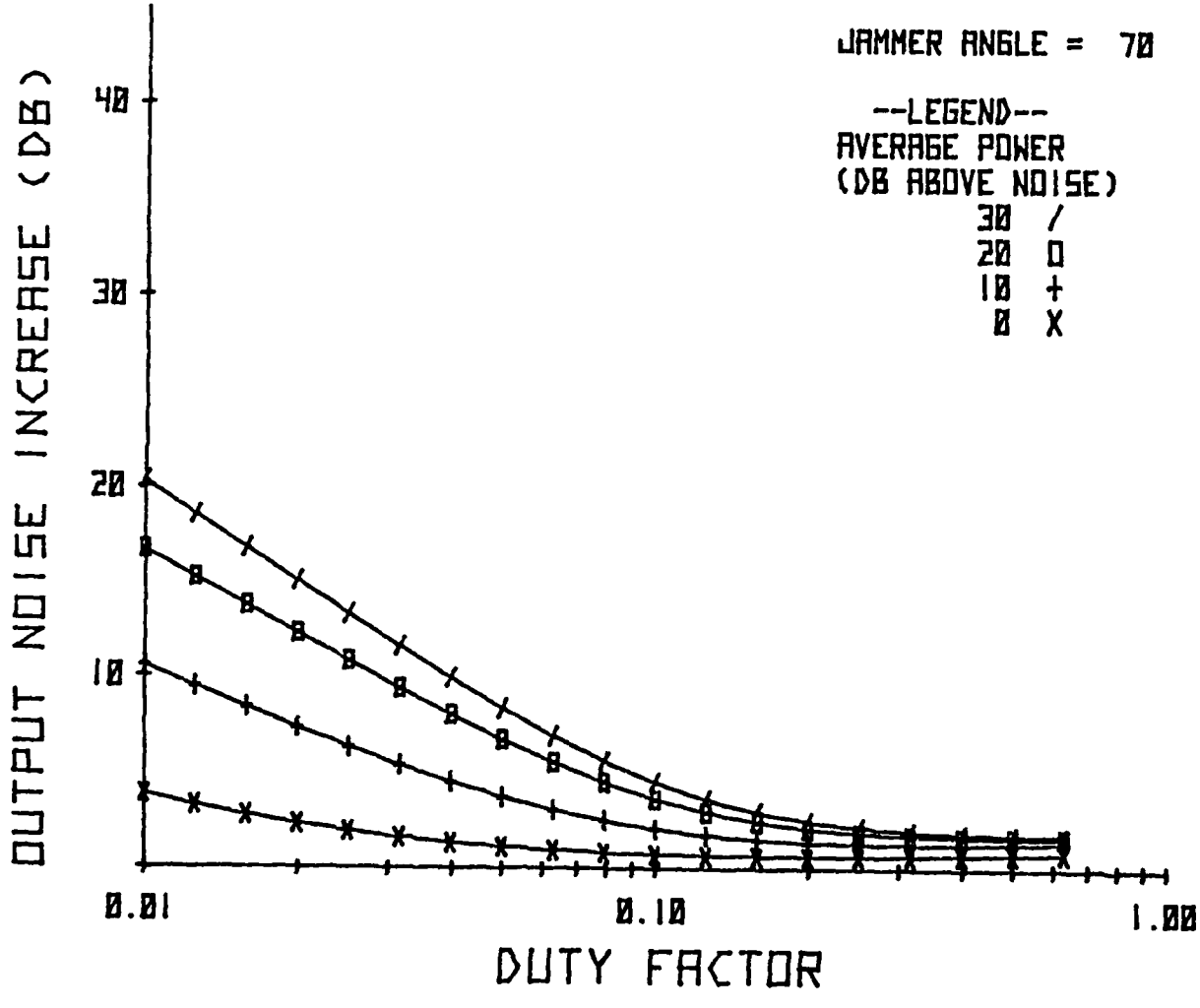


Figure 3.10 Loop Performance at Jammer Angle of 70°

TABLE 3-1

OUTPUT NOISE INCREASE OVER THERMAL NOISE (DB)
AVERAGE POWER = 1

ANGLE (DEG)	DUTY FACTOR .01			.05				.1				.5				.9	
0	22	19	17	16	14	14	13	12	12	11	8	6	5	4	3	2	2	2
5	22	19	17	15	14	14	13	12	12	11	8	6	4	4	3	2	2	2
10	22	18	17	15	14	13	13	12	11	11	7	6	4	3	3	2	2	2
15	21	18	16	15	14	13	12	12	11	10	7	5	4	3	3	2	2	2
20	21	17	16	14	13	12	12	11	10	10	7	5	4	3	2	2	2	2
25	20	17	15	14	12	12	11	10	10	9	6	4	3	3	2	2	2	2
30	19	16	14	13	12	11	10	9	9	8	5	4	3	2	2	2	2	2
35	18	15	13	12	11	10	9	8	8	8	5	3	3	2	2	2	2	2
40	17	13	12	10	9	9	8	7	7	6	4	3	2	2	2	2	2	2
45	15	12	10	9	8	7	7	6	6	5	3	2	2	2	2	2	2	2
50	13	10	9	7	7	6	5	5	4	4	2	2	2	2	2	2	2	2
55	11	8	7	6	5	4	4	4	3	3	2	2	2	2	2	2	2	2
60	9	6	5	4	3	3	3	2	2	2	2	2	2	2	2	2	2	2
65	6	4	3	3	2	2	2	2	2	2	2	2	2	2	2	2	2	2
70	4	2	2	2	2	2	2	2	2	2	2	2	2	2	2	2	2	2
75	2	2	2	2	2	2	2	2	2	2	2	2	2	2	2	2	2	2
80	2	2	2	2	2	2	2	2	2	2	2	2	2	2	2	2	2	2
85	2	2	2	2	2	2	2	2	2	2	2	2	2	2	2	2	2	2
90	2	2	2	2	2	2	2	2	2	2	2	2	2	2	2	2	2	2

TABLE 3-2

OUTPUT NOISE INCREASE OVER THERMAL NOISE (DB)
AVERAGE POWER = 10

ANGLE (DEG)	DUTY FACTOR .01			.05				.1			.5					.9
0	31	27	25	23	21	20	19	19	18	17	12	10	8	6	5	4	3	2
5	31	27	24	23	21	20	19	18	18	17	12	10	7	6	5	4	3	2
10	30	27	24	23	21	20	19	18	17	17	12	9	7	6	5	4	3	2
15	30	26	24	22	21	20	19	18	17	16	12	9	7	5	4	3	3	2
20	29	26	23	22	20	19	18	17	17	16	11	8	7	5	4	3	3	2
25	29	25	22	21	19	18	17	17	16	15	11	8	6	5	4	3	2	2
30	28	24	22	20	19	17	16	16	15	14	10	7	5	4	3	3	2	2
35	26	23	20	19	17	16	15	15	14	13	9	6	5	4	3	2	2	2
40	25	21	19	17	16	15	14	13	13	12	8	5	4	3	3	2	2	2
45	24	20	18	16	15	13	13	12	11	10	6	5	3	3	2	2	2	2
50	22	18	16	14	13	12	11	10	9	9	5	4	3	2	2	2	2	2
55	20	16	14	12	11	10	9	8	8	7	4	3	2	2	2	2	2	2
60	17	13	11	10	9	8	7	6	6	5	3	2	2	2	2	2	2	2
65	14	11	9	7	6	5	5	4	4	4	2	2	2	2	2	2	2	2
70	11	7	6	4	4	3	3	2	2	2	2	2	2	2	2	2	2	2
75	6	4	3	2	2	2	2	2	2	2	2	2	2	2	2	2	2	2
80	2	2	2	2	2	2	2	2	2	2	2	2	2	2	2	2	2	2
85	2	2	2	2	2	2	2	2	2	2	2	2	2	2	2	2	2	2
90	2	2	2	2	2	2	2	2	2	2	2	2	2	2	2	2	2	2

TABLE 3-3

OUTPUT NOISE INCREASE OVER THERMAL NOISE (DB)
AVERAGE POWER = 100

ANGLE (DEG)	DUTY FACTOR .01			.05			.1			.5			.9		
0	37	32	30	27	26	24	23	22	21	21	15	11	9	7	5	4	3	2
5	37	32	29	27	26	24	23	22	21	20	15	11	9	7	5	4	3	2
10	37	32	29	27	26	24	23	22	21	20	15	11	9	7	5	4	3	2
15	36	32	29	27	25	24	23	22	21	20	14	11	8	6	5	4	3	2
20	36	31	28	26	25	23	22	21	20	19	14	10	8	6	5	4	3	2
25	35	30	27	25	24	22	21	20	19	18	13	10	7	6	4	3	3	2
30	34	29	27	24	23	21	20	19	18	18	12	9	7	5	4	3	2	2
35	33	28	25	23	22	20	19	18	17	16	11	8	6	4	3	3	2	2
40	32	27	24	22	20	19	18	17	16	15	10	7	5	4	3	3	2	2
45	30	25	23	20	19	17	16	15	14	14	9	6	4	3	3	2	2	2
50	28	24	21	19	17	16	15	14	13	12	7	5	4	3	2	2	2	2
55	26	21	19	17	15	14	13	12	11	10	6	4	3	2	2	2	2	2
60	23	19	16	14	13	11	10	9	9	8	4	3	2	2	2	2	2	2
65	20	16	13	11	10	9	8	7	6	6	3	2	2	2	2	2	2	2
70	17	12	10	8	7	6	5	4	4	4	2	2	2	2	2	2	2	2
75	12	8	6	5	4	3	3	2	2	2	2	2	2	2	2	2	2	2
80	6	3	2	2	2	2	2	2	2	2	2	2	2	2	2	2	2	2
85	2	2	2	2	2	2	2	2	2	2	2	2	2	2	2	2	2	2
90	2	2	2	2	2	2	2	2	2	2	2	2	2	2	2	2	2	2

TABLE 3-4

OUTPUT NOISE INCREASE OVER THERMAL NOISE (DB)
AVERAGE POWER = 1000

ANGLE (DEG)	DUTY FACTOR .01				.05				.1				.5				.9	
0	41	35	32	30	28	26	25	24	23	22	16	12	9	7	6	4	3	2
5	41	35	32	30	28	26	25	24	23	22	16	12	9	7	6	4	3	2
10	40	35	32	29	28	26	25	24	23	22	15	12	9	7	5	4	3	2
15	40	35	31	29	27	26	24	23	22	21	15	11	9	7	5	4	3	2
20	39	34	31	28	27	25	24	23	22	21	15	11	8	6	5	4	3	2
25	39	33	30	28	26	24	23	22	21	20	14	10	8	6	5	4	3	2
30	38	32	29	27	25	23	22	21	20	19	13	9	7	5	4	3	3	2
35	37	31	28	26	24	22	21	20	19	18	12	9	6	5	4	3	2	2
40	35	30	27	24	22	21	20	18	17	17	11	7	5	4	3	3	2	2
45	34	28	25	23	21	19	18	17	16	15	9	6	5	4	3	2	2	2
50	32	26	23	21	19	18	16	15	14	13	8	5	4	3	2	2	2	2
55	30	24	21	19	17	15	14	13	12	11	6	4	3	3	2	2	2	2
60	27	22	19	16	14	13	12	11	10	9	5	3	3	2	2	2	2	2
65	24	19	16	13	12	10	9	8	7	7	3	2	2	2	2	2	2	2
70	20	15	12	10	8	7	6	6	5	4	2	2	2	2	2	2	2	2
75	15	10	8	6	5	4	4	3	3	3	2	2	2	2	2	2	2	2
80	9	5	4	3	2	2	2	2	2	2	2	2	2	2	2	2	2	2
85	2	2	2	2	2	2	2	2	2	2	2	2	2	2	2	2	2	2
90	2	2	2	2	2	2	2	2	2	2	2	2	2	2	2	2	2	2

The major conclusions to be drawn from Figures 3.1 through 3.11 are two in number. The first relates to jammer power level; the compression in curve spacing for increasing P_{ave} shows the decreasing marginal utility of raising jammer power. From Eqs. (3.38) through (3.40), it can be deduced that, for $\mu_0 \leq 100$ and $P_i \geq 1000$, $K \approx 0$ and $M \approx 1$; thus, at sufficiently high jammer levels, $W_2(\infty)$ and hence W_{ss} become independent of P_{ave}, and are affected by jammer angle only. The second conclusion has been anticipated by the remark above relating to the quiescent null location; namely, that loop performance improves rapidly as the jammer angle exceeds 50^o.

Tables 3-1 through 3-4 provide a different perspective on pulse jammer performance. For a specific P_{ave}, and a specific system margin against noise, it is possible to trace a contour in the (jammer angle)-(duty factor) plane which establishes the boundary between acceptable and unacceptable performance. For example, if the jammer is willing to use a duty factor as low as 1%, then a 10 dB margin will be exceeded for all jammer angles up to 55^o for $P_{ave} = 1$, and for all angles up to 80^o for $P_{ave} = 1000$.

Because the results are normalized, it is instructive to consider an example for a specific loop design; the principal task is to establish a numeric value for the jammer pulse width which has been assumed to be $\tau_p = 0.25\tau_L$. Development of values for τ_0, and hence τ_L, was discussed previously, and the results presented in Eqs. (3.18) and (3.20). Consider an I.F. or channel bandwidth of $B_c = 20$ MHz. Also needed in Eq. (3.20) are values for μ_0 and P_{im}; all data in the curves and tables were based on $\mu_0 = 100$. Because $P_{ave} \leq 1000$ and $d \geq 0.01$, a maximum value for P_i of $P_{im} = 10^6$ is appropriate. Hence, from Eq. (3.20), $\tau_0 = 15.92$ msec and Eq. (3.18) gives

$$\tau_L = \frac{15.92}{1 + 100\sqrt{1 + P_{ave}/d}} \text{ msec}$$

so that

$$\tau_p = \frac{3.98}{1 + 100\sqrt{1 + P_{ave}/d}} \text{ msec} \qquad (3.42)$$

Eq. (3.42) has been used to construct Table 3-5. The cross-hatched portion of the table represents pulse widths too small to be consistent with the bandwidth of 20 MHz. Implicit in the use of Eq. (3.1) is the condition that pulse rise time be small relative to pulse width. A conservative requirement, therefore, is that pulse width be greater than $10/B_c$, which, in this example, is 500 nsec. In fact, if the condition

$$\tau_p = \frac{\tau_L}{4} \geq \frac{10}{B_c} \tag{3.43}$$

is imposed, then it is possible to combine Eq. (3.43) with Eqs. (3.18) and (3.20) to obtain

$$P_i \leq \left[\frac{1 - 4\pi + \mu_0\sqrt{1 + P_{im}}}{4\pi\,\mu_0}\right]^2 - 1 \tag{3.44}$$

For this example, with $\mu_0 = 100$ and $P_{im} = 10^6$, Eq. (3.44) gives the bound $P_i \leq 6330$, which agrees with the cross-hatched region of Table 3-5. It should be emphasized that the bound in Eq. (3.44) is to be used only to determine the range of applicable performance data in Figures 3.3 through 3.11 and Tables 3-1 through 3-4, for a particular choice of P_{im}. If P_i does not satisfy the bound in Eq. (3.44) then the assumptions underlying the numerical data are violated and the data cannot be used.

The discussion surrounding Eq. (3.44) does not consider the role played by P_{im} in determining system performance. From Eqs (3.18) and (3.20) it is clear that the value of P_{im} affects the absolute time behavior of the loop. This time behavior is of importance for the primary function of the loop, which is the nulling of a continuous jammer. Choosing P_{im} too large will result in sluggish performance against low-level jammers. Choosing P_{im} too small will invalidate Gabriel's analysis for jammers which exceed the expected maximum, so that loop performance cannot easily be determined analytically (simulation will be required).

3.4 Extension to Sidelobe Canceller

By considering the single adaptive loop and its associated array element to be an auxiliary antenna employed to cancel jamming in the sidelobes of a main antenna, the numerical data

TABLE 3-5

JAMMER PULSE WIDTH (μ sec)

AVERAGE JAMMER POWER RELATIVE TO THERMAL NOISE	DUTY FACTOR						
	.01	.02	.05	.1	.2	.5	.9
30 dB	.13	.18	.3	.4	.6	.9	1.2
20 dB	.4	.6	.9	1.3	1.8	2.8	3.8
10 dB	1.3	1.8	2.8	4.0	5.6	8.7	11.0
0 dB	4.0	5.6	8.7	12.0	16.0	23.0	27.0

[Parameter Values Used: $\mu_0 = 100$, $B_c = 20$ MHz, $P_{im} = 10^6$]

just presented may be interpreted as describing the performance of a sidelobe canceller against a pulsed jammer. Consider the diagram in Figure 3.12, where M is the main antenna and A the auxiliary. The phase reference is the phase center of the main antenna. It will be assumed that the gains of the auxiliary antenna and the main antenna have been chosen and normalized so that the auxiliary antenna can be considered to have unit, isotropic gain, and the main antenna a gain denoted by $G_M(\theta)$. For proper operation of the sidelobe canceller it will be necessary that $G_M(\theta) = 1$ in the sidelobe region.

Using the notation of Figure 3.1 the outputs of the main and auxiliary beams may be written as

$$\left.\begin{aligned} E_1 &= G_M(\theta)J_i + n_1 \\ E_2 &= J_i e^{ju_S} + n_2 \end{aligned}\right\} \qquad (3.45)$$

where

$$u_S = \frac{2\pi D}{\lambda} \sin\theta \qquad (3.46)$$

and D will now be many wavelengths long. It is now possible to parallel the development of Eqs. (3.3) to (3.10). Specifically

$$Y_0 = W_1^0 n_1 + W_2^0 n_2$$

and

$$Y = W_1 n_1 + W_2 n_2 + \left[G_M(\theta)W_1 + W_2 e^{ju_S}\right]J_i$$

so that

$$\overline{|Y_0|^2} = \left(|W_1^0|^2 + |W_2^0|^2\right)\overline{|n|^2} \qquad (3.47)$$

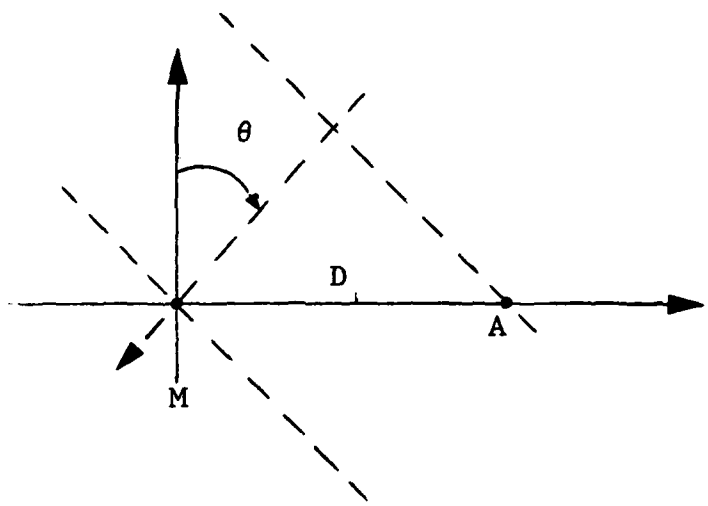


Figure 3.12 Signal Phase Reference Diagram for Main Antenna with Auxiliary

and

$$\overline{|Y|^2} = \left(|W_1|^2 + |W_2|^2\right)\overline{|n|^2} + \left|G_M(\theta)W_1 + W_2 e^{ju_S}\right|^2 \overline{|J_i|^2} \quad (3.48)$$

It is reasonable to choose $W_1 = 1$; choosing the quiescent value, W_2^0, of W_2 presents a problem. The auxiliary antenna serves no purpose in the absence of a jammer so that W_2^0 could simply be set to zero. But to use the numerical data for the two-element array, it would be necessary to consider $W_2^0 = 1$. The 15 to 20 dB difference between main beam and sidelobe level should minimize any effects arising from a non-zero quiescent value for W_2. Consequently, the output noise increase due to jamming can be written as

$$N_S = \frac{\overline{|Y|^2}}{\overline{|Y_0|^2}} = \frac{1}{2}\left[1 + |W_2|^2 + P_i \left|G_M(\theta) + W_2 e^{ju_S}\right|^2\right] \quad (3.49)$$

where the "S" subscript is used to distinguish between the sidelobe canceller case and the two-element array case. Reference to Eq. (3.10) discloses the fact that N_S differs from N mostly by the presence of $G_M(\theta)$. An additional difference lies in the relationship between θ and u_S. The spacing D between auxiliary and main antenna will be many wavelengths -- typically more than 40 or 50 -- so that the relationship between u and θ will be different for the sidelobe canceller than it was for the two-element array.

Numerical results similar to those in Figure 3.3 through Figure 3.11 and Tables 3-1 through 3-4 can be generated for the sidelobe canceller once a value for D is chosen. Simplification can result if θ is restricted to the sidelobe region so that $G_M(\theta) = 1$. The sidelobe canceller results will be similar in form to those for the two-element array, with only the angle θ demonstrating a different influence.

Specifically, consider the spacing D to be an integral number of wavelengths,

$$D = m\lambda$$

so that

$$u_S = m2\pi \sin \theta$$

Recall that for the two-element array the appropriate quantity in N [Eq. (3.10)] is $2u = \pi \sin \theta$. Thus for the sidelobe canceller, the range of u_S is 0 to 2π, and this range is repeated m times. As a result, the curve of N_S versus θ will not be a monotone decreasing curve as in Figures 3.3 to 3.11, but will consist of m similarly-shaped segments, having the same range of N_S values, but with different ranges of θ. The domains covered by these segments have boundaries given by the values of θ

$$\theta_r = \sin^{-1}\left(\frac{r}{m}\right), \quad r = 0, 1, 2, \ldots \tag{3.50}$$

Between the values θ_r and θ_{r+1}, u_S will change by 2π, so that N_S will range from its maximum to minimum values. We give a sketch of the kind of performance curve to be expected, for $m = 4$, in Figure 3.13. The shape of the segments is not meant to be accurate, only representative.

Actual values for N_S are the same as those for N given in Tables 3-1 to 3-4, except that the values for the angles no longer agree.

When the auxiliary antenna is much farther than 4λ from the phase center of the main antenna, there will be many more "periods" for the curve of N_S versus θ. Under those circumstances, the change in N_S for a change in θ will be greatly different from the two-element array characteristics. Put another way, the increased sensitivity as D increases leads to the practical conclusion that loop performance is essentially equal to that which occurs for values of θ away from the minima. This means that for D equal to a sufficiently large number of wavelengths the loop performance is not much better than that given in Tables 3-1 through 3-4 for an angle of 0^o. Thus, an auxiliary antenna located many wavelengths from the phase center of the main antenna will give a sidelobe canceller performance which is essentially described by Figure 3.3, where each of the curves in that figure can be interpreted as providing, for the duty factor chosen, an upper bound on the actual multi-segment curve of N_S versus θ.

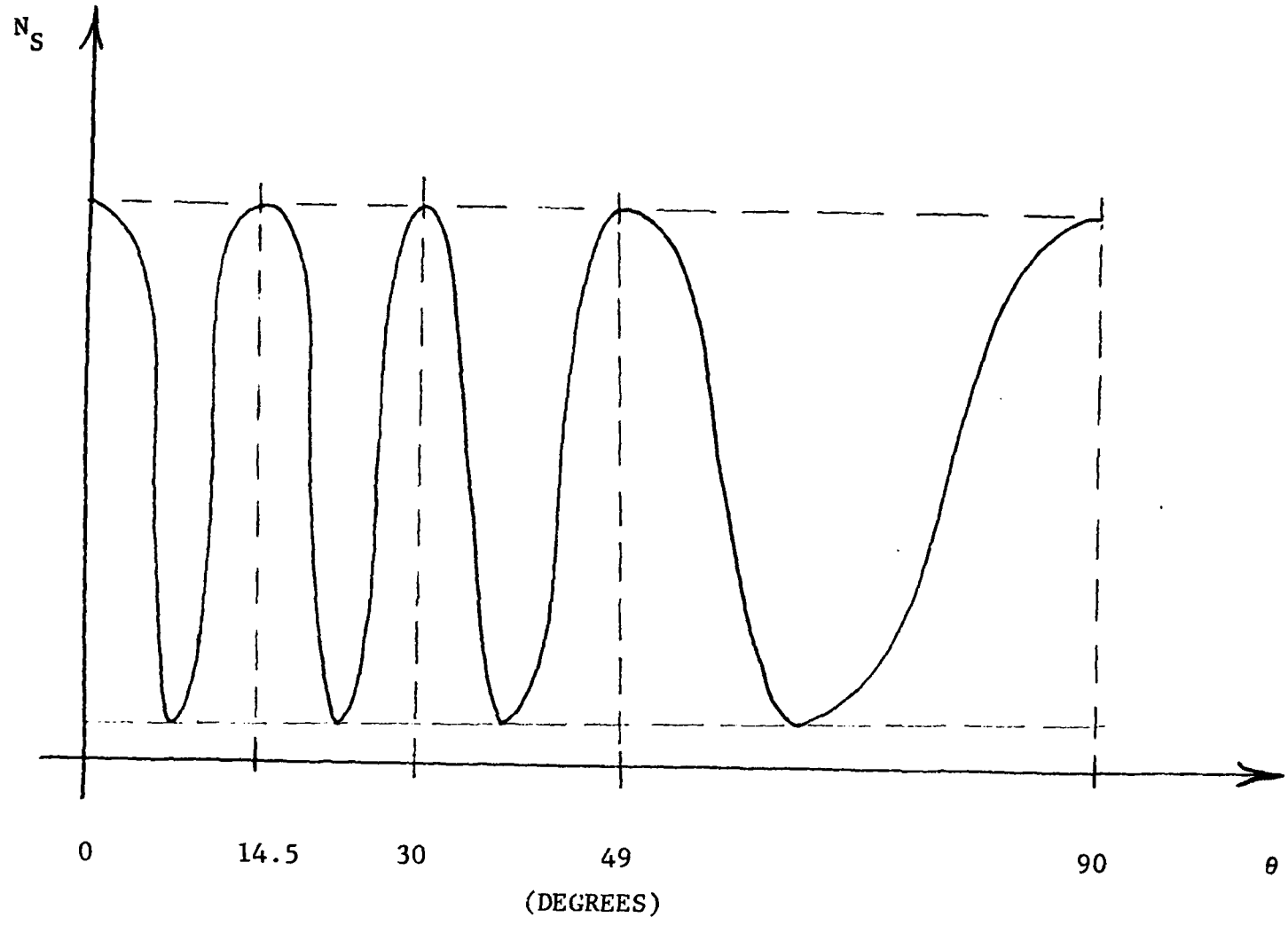
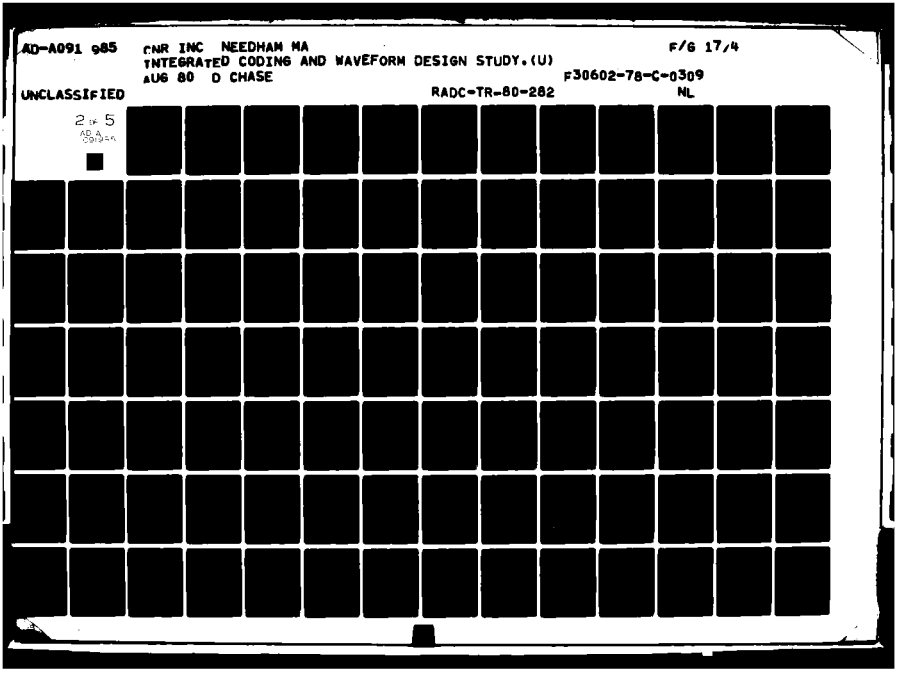


Figure 3.13 Output Noise Increase as a Function of Angle Off Boresight for Sidelobe Canceller (m = 4)

AD-A091 985 CNR INC NEEDHAM MA F/G 17/4
INTEGRATED CODING AND WAVEFORM DESIGN STUDY.(U)
AUG 80 D CHASE F30602-78-C-0309
UNCLASSIFIED RADC-TR-80-282 NL



REFERENCE

[3.1] William F. Gabriel, "Adaptive Array - An Introduction," Proc IEEE, Vol. 64, No. 2, February 1976, Pp. 239-272.

SECTION 4

PERFORMANCE ANALYSIS FOR ERROR-CORRECTING CODES OPERATING IN THE PRESENCE OF INTERFERENCE

4.1 Channel Models for Interference

In this section, four channel models for operating in the presence of interference are considered. Performance bounds are obtained for practical convolutional and block codes as well as for two-stage coding approaches based on combinations of block and/or convolutional codes.

For all four models considered, the interference is modeled by a single parameter δ, which represents the probability that the interference coincides with a code symbol. Furthermore, it is assumed that the code symbol is completely destroyed by the interference. Thus, the models evaluated in this section are worst-case models, which can readily be modified to include situations where the interference-to-signal power is some finite number during the presence of interference. An alternate model considered in Appendix A, based on an average power constraint for the interfering signal, is shown to offer performance results which are considerably more optimistic than the conservative results obtained based on this worst-case model. The philosophy taken in this report is to design coding concepts for worst-case models in an effort to ensure reliable communications for real channel applications where the exact interference model is generally a complex function of the actual waveform and jamming threat.

The additive noise during the period when no pulse-type interference is present is assumed to be Gaussian for all channel models considered. This assumption is valid for many LOS and satellite links and can even be justified when the additive noise is non-Gaussian and a spread-spectrum pseudo-random noise modem is used. Note that, after despreading, narrow non-Gaussian channel noise appears as Gaussian noise to the baseband demodulator and decoder [4.1].

The four models considered are as follows:*

- Model 1 - Gaussian Noise and Channel Measurement Decoding

For this model, a decoder capable of using received channel measurement information is assumed. When the channel measurement information is quantized, a decoder of this nature is sometimes referenced to a soft-decision decoder. When the quantization is limited to a single bit, as in Model 2, a binary or hard decoder results.

When no interference is present, the received continuous variable y is given by

$$y = x + n \tag{4.1}$$

where $x = \pm\sqrt{E_s}$ and n is a zero-mean Gaussian variable with variance given by $N_0/2$. The signal-to-noise ratio per symbol is given by

$$E_s/N_0 = \frac{\langle x^2 \rangle}{2\langle n^2 \rangle} \tag{4.2}$$

and the signal-to-noise ratio per information bit is given by

$$E_b/N_0 = \left(\frac{E_s}{N_0}\right)\frac{1}{R} \tag{4.3}$$

All results will be presented in terms of E_b/N_0 calculated as above, i.e., in the presence of no interference. For the worst-case models, $E_b/N_0 = 0$ is assumed, i.e., $y = n$, when interference is present. Note that the average value of E_b/N_0 is actually lower than that given in (4.3) when interference is present.

A simple example of the applicability of this model is given by a communications system with a front-end blanker such that during the presence of detected interference the signal path is opened. Model 1 assumes that the status of this blanking signal is unavailable to the decoder.

---

*Channel capacity limits have been recently obtained for these models [4.2], which will be compared to the results for practical coding approaches obtained in this report.

A more sophisticated example of the applicability of this model is given by a direct sequence spread-spectrum satellite repeater link with interference present on the uplink. As a consequence of the power-sharing properties of the repeater, a large interfering signal can severely limit the received signal power which is assumed to be zero for this model.

Before proceeding, it is instructive to consider this general communications link and determine the conditions when the proposed model is valid.

The total received satellite power P_0 in the presence of interference can be written as the sum of the signal power P_s and the interference power P_I as

$$P_0 = P_s + P_I \tag{4.4}$$

The relationship between P_I/P_s and the ratio of the interference to signal power I/S at the input to the satellite is given by

$$\frac{I}{S} = L\left(\frac{P_I}{P_s}\right) \tag{4.5}$$

where L is the loss in signal power due to the effects of hard-limiting [4.3]. For large interfering signals, this loss approaches 1/4.

Using (4.4) and (4.5), the received power can be written as

$$P_s = \frac{P_0}{1 + \frac{P_I}{P_s}} = \frac{P_0}{1 + \frac{I}{LS}} \tag{4.6}$$

and the received interference can be written as

$$P_I = P_0\left(1 - \frac{P_s}{P_0}\right) = P_0\left(\frac{\frac{I}{LS}}{1 + \frac{I}{LS}}\right) \tag{4.7}$$

In the presence of a direct sequence spread-spectrum system of process gain M [4.1], the signal-to-noise ratio per information bit can be written as

$$\frac{E_b}{N_0} = \frac{P_s}{N_0 R + \frac{P_I}{M}} \tag{4.8}$$

Equations (4.6), (4.7), and (4.8) may be used to characterize this link for arbitrary I/S ratios and spread-spectrum processing gains.

For the model of interest we assume

$$N_0 R >> \frac{P_I}{M} \tag{4.9}$$

and, thus, the noise power is essentially constant as the interference is varied. Furthermore, we assume that when the interference is present we have

$$\frac{I}{S} >> 1 \tag{4.10}$$

so that the received signal power given by (4.6) may be neglected in the presence of interference.

Mathematically, this channel model can be viewed as a binary input-continuous output channel with the signal-to-noise ratio per symbol given by E_s/N_0. Of course, when interference occurs, this signal-to-noise ratio drops to zero.

- Model 2 - Gaussian Noise and Binary Decoding

It is of practical interest to limit the decoder to the use of only binary information and to determine the loss in performance in the presence of interference. For a Gaussian channel, this loss in performance is generally less than 3 dB and typically on the order of only 2 dB [4.4] - [4.6]. As our results will indicate, the losses due to binary decoding in the presence of interference can be substantially greater than those incurred over the nonjammed Gaussian channel.

- Model 3 - Gaussian Noise and Channel Measurement Decoding with an Erasure Signal

For this model, an erasure signal coincident with the interfering signal is assumed available. A model of this type becomes valid when the received interference has a power level

much higher than the received signal level; thus, it is possible to detect the presence of interference without the use of the decoder. The detection probability is assumed to be 1 for this model. Interference from a high-power radar signal represents an example of the applicability of this channel model. More generally, this model is applicable whenever the interference signals have special properties which distinguish them from the communications signals.

- Model 4 - Gaussian Noise and Binary Decoding with an Erasure Signal

For this discrete output model, the presence of interference is modeled by the signal causing an erasure with a probability given δ. This model is equivalent to a noisy erasure channel, and the binary decoder operating with an erasure signal is, in fact, a binary error/erasure decoder.

4.2 Probability of Error between Two Sequences

In this section the probability of error between two binary sequences of Hamming distance d is found. These results are applied to convolutional codes in Section 4.3 and to block codes in Section 4.4. In all cases, the occurrence of interference is assumed statistically-independent over the code symbols. Results of this nature are applicable to systems which do not exploit the burst properties of the interfering signals, such as a system which interleaves the code symbols so that they appear random relative to the interference.* Again, this assumption represents a worst-case model since information concerning the time variations of the interfering signals is not utilized by the decoder.

4.2.1 Binary Decoding

For this binary symmetric channel, a maximum-likelihood receiver [4.5],[4.7] will decode on the transmitted sequence by simply picking the sequence with the minimum number of disagreements. For the two-sequence case, a decision is based on the d symbols which differ. Thus, the probability of error for odd values of d is given by

$$P_e(d) = \sum_{i=\left(\frac{d+1}{2}\right)}^{d} \binom{d}{i} p^i (1-p)^{d-i} \quad ; \quad d \text{ odd} \qquad (4.11)$$

*Appendix C discusses some techniques for randomizing the interference by interleaving.

where p is the probability of error for this binary symmetric channel. For even values of d, we have

$$P_e(d) = \frac{1}{2}\binom{d}{d/2}p^{d/2}(1-p)^{d/2} + \sum_{i=\frac{d}{2}+1}^{d}\binom{d}{i}p^i(1-p)^{d-i} \quad ; \text{ d even} \tag{4.12}$$

Note that when we have exactly d/2 errors, the probability of an error is 1/2 since both sequences are equally likely.

For the additive Gaussian channel with binary coherent phase-shift keying (CPSK), the probability of a bit error before binary decoding is given by

$$p = \Pr\left[y < 0 \,|\, x = \sqrt{E_s}\right] = \Pr\left[y > 0 \,|\, x = -\sqrt{E_s}\right] \tag{4.13}$$

The transmitted symbol is assumed to be given by

$$\begin{aligned} x &= \sqrt{E_s} \qquad \text{for a binary 1} \\ x &= -\sqrt{E_s} \qquad \text{for a binary 0} \end{aligned} \tag{4.14}$$

Thus, the probability of a bit error can be written as

$$p = \int_0^\infty \frac{\exp\left\{-\frac{\left(y+\sqrt{E_s}\right)^2}{N_0}\right\}}{\sqrt{\pi N_0}}\,dy = \int_{\sqrt{\frac{2E_s}{N_0}}}^\infty \frac{\exp\left\{-\frac{\alpha^2}{2}\right\}}{\sqrt{2\pi}}\,d\alpha$$

$$\doteq Q\left(\sqrt{\frac{2E_s}{N_0}}\right)$$

$$\doteq Q\left(\sqrt{\frac{\text{Mean of the Decision Statistic Squared}}{\text{Variance of the Noise}}}\right) \tag{4.15}$$

4.2.2 Binary Decoding with Interference (Model 2)

During the occurrence of interference, each binary symbol is assumed to have a probability of error of 1/2 and a probability of error, given by (4.15) occurs when interference is not present. Assuming

$$\Pr[\text{Interference is Present}] = \delta \tag{4.16}$$

we can write

$$p_I = \frac{1}{2}\delta + p(1-\delta) \tag{4.17}$$

This probability of an error also represents the performance of an uncoded system in the presence of interference.

To obtain the value of $P_e(d)$ for a channel with interference occurring with a probability of δ, we assume that the probability of errors between symbols within a sequence is statistically independent. We now can write

$$P_e(d) = \sum_{i=\frac{d+1}{2}}^{d} \binom{d}{i} p_I^i \left(1-p_I\right)^{d-i} \quad ; \quad d \text{ odd} \tag{4.18}$$

and

$$P_e(d) = \frac{1}{2}\binom{d}{d/2} p_I^{d/2} \left(1-p_I\right)^{d/2} + \sum_{i=\frac{d}{2}+1}^{d} \binom{d}{i} p_I^i \left(1-p_I\right)^{d-i} \tag{4.19}$$

4.2.3 Binary Decoding with Interference and Erasure Information (Model 4)

For this case we assume that an erasure signal, coincident with the interference, is available. Since the probability of an error is assumed to be 1/2 during the occurrence of interference, we can simply ignore those μ code symbols which are destroyed by interference and base our decision on the $(d-\mu)$ meaningful symbols.

The probability of having μ symbols destroyed by interference within the d symbols used in our decision rule is given by

$$f(\mu) = \binom{d}{\mu} \delta^{\mu} (1 - \delta)^{d-\mu} \tag{4.20}$$

where, as before, δ is the probability of interference occurring which, in this case, is also the probability of an erasure.

The probability of an error between two sequences is now given by

$$P_e(d) = \sum_{\mu=0}^{d} f(\mu) \; P_e[(d - \mu) | \mu] \tag{4.21}$$

where

$$P_e[(d - \mu) | \mu] = \sum_{i=\frac{d+1-\mu}{2}}^{d-\mu} \binom{d-\mu}{i} p^i (1 - p)^{d-\mu-i} \; ; \quad (d-\mu) \text{ odd} \tag{4.22}$$

and

$$P_e[(d - \mu) | \mu] = \frac{1}{2} \binom{d-\mu}{\frac{d-\mu}{2}} p^{\frac{d-\mu}{2}} \left(1 - p\right)^{\frac{d-\mu}{2}} + \sum_{i=\frac{d-\mu}{2}+1}^{d-\mu} \binom{d-\mu}{i} p^i (1 - p)^{d-\mu-i}$$

$$; \quad (d-\mu) \text{ even} \tag{4.23}$$

The value of p is just the binary error probability for a channel without interference and is thus given by (4.15). For this model, p is also the conditional probability of error given that an erasure is not present.

4.2.4 Channel Measurement Decoding

For this model, a decoder capable of using received channel measurement information is assumed.

Assuming maximum-likelihood decoding is used, the probability of errors between two sequences of Hamming distance d is given by

$$P_e(d) = \Pr[p(\underline{y}|\underline{x}_{m'}) > p(\underline{y}|\underline{x}_m)] \tag{4.24}$$

where, for a Gaussian channel,

$$p(\underline{y}|\underline{x}_m) = \frac{\exp\left\{-\sum_i \frac{(y_i - x_{m_i})^2}{N_0}\right\}}{\prod_i (\pi N_0)} \tag{4.25}$$

is the conditional probability density function for the transmitted sequence, and $p(\underline{y}|\underline{x}_{m'})$ is the corresponding function for the sequence of distance d from the transmitted sequence.

Taking logs and dropping irrelevant terms enables one to write

$$P_e(d) = \Pr\left[\sum_i y_i\left(x_{m_i} - x_{m_i'}\right) < 0\right] \tag{4.26}$$

The relevant terms in (4.26) are composed only of the d terms with i such that $x_{m_i} \neq x_{m_i'}$ which can be written as

$$P_e(d) = \Pr\left[\left(2\,d\,E_s + 2\sqrt{E_s}\sum_{i=1}^{d} n_i\right) < 0\right] \tag{4.27}$$

The Gaussian variables, n_i, are independent zero mean variables with a variance given by $N_0/2$. Since the weighted sum of these d Gaussian random variables has a variance of $2E_s\,d\,N_0$, the probability of error can be calculated as in (4.15) to give

$$P_e(d) = Q\left(\sqrt{\frac{(2\,d\,E_s)^2}{2\,E_s\,d\,N_0}}\right) = Q\left(\sqrt{\frac{2\,d\,E_s}{N_0}}\right) \tag{4.28}$$

4.2.5 Channel Measurement Decoding with Interference (Model 1)

For this model we will assume that the received signal is just given by additive noise alone during the occurrence of interference.

During the occurrence of interference with a probability of δ, the received decision statistic

$$y_i = n_i \tag{4.29}$$

With no interference, which occurs with a probability of $(1 - \delta)$, we have

$$y_i = \pm \sqrt{E_s} + n_i \tag{4.30}$$

Following the analysis given in Section 4.2.4, we can modify (4.27) for the case when μ symbols are destroyed by interference to give

$$P_e(d|\mu) = \Pr\left[2(d - \mu)E_s + 2\sqrt{E_s} \sum_{i=1}^{d} n_i < 0\right] \tag{4.31}$$

Note that the contribution from the noise terms remains unchanged but the mean of the decision statistic is decreased because of the interference.

The conditional probability of an error between two sequences is now given by

$$P_e(d|\mu) = Q\left(\sqrt{\frac{2^2(d - \mu)^2 E_s^2}{2E_s d N_0}}\right) = Q\left(\frac{d - \mu}{\sqrt{d}}\sqrt{\frac{2E_s}{N_0}}\right) \tag{4.32}$$

and the probability of error between two sequences is given by

$$P_e(d) = \sum_{\mu=0}^{d} \binom{d}{\mu} \delta^{\mu} (1 - \delta)^{d-\mu} P_e(d|\mu) \tag{4.33}$$

where $P_e(d|\mu)$ is given by (4.32).

4.2.6 Channel Measurement Decoding with Interference and Erasure Information (Model 3)

For this model we assume that an erasure signal is available during the occurrence of interference. Thus, the μ symbols affected by interference can be omitted from the decision rule to give

$$P_e(d|\mu) = \Pr\left[2(d-\mu)E_s + 2\sqrt{E_s}\sum_{i=1}^{d-\mu} n_i < 0\right] \tag{4.34}$$

In this case we obtain

$$P_e(d|\mu) = Q\left(\sqrt{\frac{\left[2(d-\mu)E_s\right]^2}{2E_s(d-\mu)N_0}}\right) = Q\left(\sqrt{\frac{2(d-\mu)E_s}{N_0}}\right) \tag{4.35}$$

with the probability of error given by (4.33) when (4.35) is used.

Table 4-1 summarizes the results in Sections 4.2.1 through 4.2.6.

4.3 Probability of Error for Convolutional Codes

Following the analyses given in [4.8], [4.9], and [4.10], the probability of a bit error for convolutional codes can be upper bounded by

$$P_e < \sum_{d=d_f}^{\infty} a_d\, P_e(d) \tag{4.36}$$

where d_f is the minimum free distance of a given convolutional code and a_d is the total number of information bit errors occurring in all sequences of Hamming distance d away from the transmitted sequence. Fortunately, for the short convolutional codes of interest, a_d can readily be found. Tables 4-2, 4-3, and 4-4 (from [4.9]) illustrate these results for some popular rate-1/2 codes. Effective lower rate codes can be simply obtained by the repeating taps of the rate-1/2 convolutional codes, i.e., a rate-1/4 code of twice the free distance is obtained by transmitting each coded symbol twice.

TABLE 4-1

SUMMARY OF RESULTS FOR THE PROBABILITY OF AN ERROR BETWEEN TWO SEQUENCES

Model Assumed	Error Probability
Binary Decoding	$P_e(d) = \sum_{i=\frac{d+1}{2}}^{d} \binom{d}{i} p^i (1-p)^{d-i}$; d odd where $P = Q\left(\sqrt{\frac{2E_s}{N_0}}\right)$ $P_e(d) = \frac{1}{2}\binom{d}{d/2} p^{d/2}(1-p)^{d/2} + \sum_{i=\frac{d}{2}+1}^{d} \binom{d}{i} p^i (1-p)^{d-i}$; d even
Binary Decoding with Interference Occurring with Probability δ	$P_e(d) = \sum_{i=\frac{d+1}{2}}^{d} \binom{d}{i} p_I^i (1-p_I)^{d-i}$; d odd where $P_I = \frac{1}{2}\delta + p(1-\delta)$ $P_e(d) = \frac{1}{2}\binom{d}{d/2} p_I^{d/2}(1-p_I)^{d/2} + \sum_{i=\frac{d}{2}+1}^{d} \binom{d}{i} p_I^i (1-p_I)^{d-i}$; d even
Binary Decoding with Interference and Erasure Information	$P_e(d) = \sum_{\mu=0}^{d} f(\mu)\, P_e(d-\mu \mid \mu)$ where $P_e[(d-\mu)\mid\mu] = P_e[(d-\mu)$ - for binary decoding] and $f(\mu) = \binom{d}{\mu} \delta^{\mu} (1-\delta)^{d-\mu}$

TABLE 4-1 (Continued)

Model Assumed	Error Probability
Channel Measurement Decoding	$P_e(d) = Q\left(\sqrt{\frac{2\,d\,E_s}{N_0}}\right)$
Channel Measurement Decoding with Interference	$P_e(d) = \sum_{\mu=0}^{d} f(\mu)\, Q\left(\frac{d-\mu}{\sqrt{d}}\sqrt{\frac{2E_s}{N_0}}\right)$
Channel Measurement Decoding with Interference and Erasure Information	$P_e(d) = \sum_{\mu=0}^{d} f(\mu)\, Q\left(\sqrt{\frac{2(d-\mu)E_s}{N_0}}\right)$

TABLE 4-2

BEST RATE-1/2 CONSTRAINT LENGTH-3 CODE

Code $\begin{matrix} 1 & 1 & 1 \\ 1 & 0 & 1 \end{matrix}$

Minimum free distance = 5

Weight	Number of Adversaries	a_d = Number of Bit Errors in the Adversaries
5	1	1
6	2	4
7	4	12
8	8	32
9	16	80
10	32	192
11	64	448
12	128	1024

TABLE 4-3

BEST RATE-1/2 CONSTRAINT LENGTH-5 CODE

Code 1 1 1 0 1
1 0 0 1 1

Minimum free distance = 7

Weight	Number of Adversaries	a_d = Number of Bit Errors in the Adversaries
7	2	4
8	3	12
9	4	20
10	16	72
11	37	225
12	68	500
13	176	1324
14	432	3680

TABLE 4-4

BEST RATE-1/2 CONSTRAINT LENGTH-7 CODE

Code 1 1 1 1 0 0 1
1 0 1 1 0 1 1

Minimum free distance = 10

Weight	Number of Adversaries	a_d = Number of Bit Errors in the Adversaries
10	11	36
11	0	0
12	38	211
13	0	0
14	193	1404
15	0	0
16	1331	11633
17	0	0

4.4 Probability of an Error for Block Codes

When channel measurement decoding is used, the results in Section 4.2 can be directly applied by following the analyses in [4.11] which gives an approximation for the probability of a bit error by

$$P_e \approx \frac{d}{N} n_d P_e(d) \tag{4.37}$$

where d is the minimum distance of a block code of length N which contains n_d words of minimum distance d. A strict union upper bound is given by

$$P_e \leq \sum_{i=d}^{N} \frac{i}{N} n_i P_e(i) \tag{4.38}$$

Two rate-1/2 codes of interest are the (24,12;8) Golay code with

$$d = 8, \quad N = 24, \quad n_d = 759 \tag{4.39}$$

and the (128,64;22) BCH code with

$$d = 22, \quad N = 128, \quad n_d \approx 243{,}840^* \tag{4.40}$$

For the Golay code, (4.38) can be used since the weight distribution is known and is given by

$$n_0 = 1, \; n_d = n_8 = 759, \; n_{12} = 2576, \; n_{16} = 759, \; n_{24} = 1 \tag{4.41}$$

Lower-rate block codes can be obtained by repeating these codewords, which is similar to repeating the taps in a convolutional code. Alternatively, the large class of BCH codes can be used to select low-rate codes, as illustrated in [4.13].

For binary decoding, direct use of Section 4.2 can be made by using (4.37) or (4.38), as is the case for the channel

*This number has been obtained with "almost certainty" in [4.12].

measurement decoding expression. However, it should be noted that the bounds are for maximum-likelihood decoding, which is generally not used for decoding binary block codes. Performance bounds for bounded distance decoding have been obtained in [4.11] which are more suitable for predicting the performance of binary decoding of block codes. Bounds of this nature will be obtained for binary decoding operating with and without interference.

4.4.1 Binary Decoding

For the case when d is odd, a simple bound is given by

$$P_e \leq \frac{1}{N} \sum_{i=e+1}^{N} \binom{N}{i} (i+e)\, p^i (1-p)^{N-i} \quad ; \quad d \text{ odd} \tag{4.42}$$

Note that whenever there are e+1 or more errors, the decoder may at most produce an extra e errors. The error-correcting capability of a binary code of minimum distance d is, of course, given by

$$e = \left\lfloor \frac{d-1}{2} \right\rfloor \tag{4.43}$$

When the number of codewords of minimum weight d is known to be n_d, the upper bound given in (4.42) can be tightened to

$$P_e \leq \frac{\Delta d + (1-\Delta)(e+1)}{N} \binom{N}{e+1} p^{e+1} (1-p)^{N-e-1} + \frac{1}{N} \sum_{i=e+2}^{N} \binom{N}{i} (i+e)\, p^i (1-p)^{N-i} \tag{4.44}$$

where

$$\Delta = \left[n_d \binom{d}{e+1} \right] \Big/ \binom{N}{e+1} \quad ; \quad d \text{ odd} \tag{4.45}$$

Note that when there are e+1 errors in a codeword, there is a probability Δ that the pattern is not detected and results in d decoded errors; and a probability 1-Δ that the pattern is detected and the e+1 errors remain unchanged. The expression for Δ is obtained by noting that for each codeword of minimum

distance d away from the transmitted codeword, $\binom{d}{e+1}$ patterns of e+1 errors are undetected. [There are $\binom{N}{e+1}$ possible error patterns of weight e+1.]

For the case where d is even, the upper bound on the decoded bit error rate is given by

$$p_b \leq \frac{e+1}{N}\binom{N}{e+1} p^{e+1}(1-p)^{N-e-1} + \frac{1}{N}\sum_{i=e+2}^{N}\binom{N}{i}(i+e)\, p^i(1-p)^{N-1}; \quad d \text{ even} \qquad (4.46)$$

The first term of (4.46) is due to the fact that all possible e+1 = d/2 errors can be detected for even d. Equation (4.46) is as tight as the bound given by (4.44); however, in (4.46) the value of n_d is not required.

4.4.2 Binary Decoding with Interference (Model 2)

For this case, we simply replace p in Eqs. (4.42), (4.44), and (4.46) by

$$p_I = \frac{1}{2}\delta + (1-\delta)\, p \qquad (4.47)$$

which is the overall probability of a binary error due to interference or Gaussian noise.

4.4.3 Binary Decoding with Interference and Erasure Information (Model 4)

The standard way of treating this problem is to use the trinomial probability function. We will proceed in this formal manner and eventually relate the trinomial probabilities to the actual probability of interest to us.

Let P_s and P_t be the respective (unconditional) probability of erasure and probability of error. Thus,

$$P_s + P_t \leq 1$$

The probability that there are i erasures and j errors among independent bits is given by

$$f(N;i,j) = \binom{N}{i,j} P_s^i \, P_t^j (1 - P_s - P_t)^{N-i-j}$$

$$= \binom{N}{i}\binom{N-i}{j} P_s^i \, P_t^j (1 - P_s - P_t)^{N-i-j} \qquad (4.48)$$

where $\binom{N}{i,j}$ is the trinomial coefficient.

This function may also be written as

$$f(N;i,j) = \Pr[i \text{ erasures}] \Pr[j \text{ errors} | i \text{ erasures}]$$

$$= \binom{N}{i} P_s^i (1 - P_s)^{N-i} \binom{N-i}{j} \left(\frac{P_t}{1 - P_s}\right)^j \left(1 - \frac{P_t}{1 - P_s}\right)^{N-i-j} \qquad (4.49)$$

where $[P_t/(1 - P_s)]$ is the conditional probability of a symbol error given that no erasure is present.

A decoding error results if there are i erasures and j errors such that

$$i + 2j \geq d \qquad (4.50)$$

If there are i erasures with $i \leq d-1$, the decoder may produce as many as

$$e = \left\lfloor \frac{d - i - 1}{2} \right\rfloor \qquad (4.51)$$

additional errors in decoding.* When the number of i erasures is equal to d or greater, no additional errors are introduced by the assumed bounded distance decoder which corrects only up to e errors.

---

*A somewhat tighter bound can be obtained by noting that when (d-i) is even, no additional errors are introduced when $j = (d-i)/2$. However, this refinement is only of secondary importance and, at most, tightens the bound by a factor of 2.

The probability of a bit error, P_E, can be upper bounded by the following expression:

$$\frac{1}{N}\sum_{i=0}^{d-1}\sum_{j=e+1}^{N-i}(i+j+e)\binom{N}{i}\binom{N-i}{j}P_s^i\,P_t^j(1-P_s-P_t)^{N-i-j}$$

$$+\frac{1}{N}\sum_{i=d}^{N}\sum_{j=0}^{N-i}(i+j)\binom{N}{i}\binom{N-i}{j}P_s^i\,P_t^j(1-P_s-P_t)^{N-i-j}$$

$$=\frac{1}{N}\sum_{i=0}^{d-1}\binom{N}{i}P_s^i(1-P_s)^{N-i}\sum_{j=e+1}^{N-i}(i+j+e)\binom{N-i}{j}\left(\frac{P_t}{1-P_s}\right)^j\left(1-\frac{P_t}{1-P_s}\right)^{N-i-j}$$

$$+\frac{1}{N}\sum_{i=d}^{N}\binom{N}{i}P_s^i(1-P_s)^{N-i}\sum_{j=0}^{N-i}(i+j)\binom{N-i}{j}\left(\frac{P_t}{1-P_s}\right)^j\left(1-\frac{P_t}{1-P_s}\right)^{N-i-j} \tag{4.52}$$

Note that

$$\sum_{j=0}^{n}(i+j)\binom{n}{j}P_x^j(1-P_x)^{n-j}=i+n\sum_{j=0}^{n}\binom{n-1}{j-1}P_x^j(1-P_x)^{n-j}$$

$$=i+nP_x\sum_{j=1}^{n}\binom{n-1}{j-1}P_x^{j-1}(1-P_x)^{n-1-(j-1)}$$

$$=i+nP_x \tag{4.53}$$

enables one to write this upper bound as

$$\frac{1}{N}\sum_{i=0}^{d-1}\binom{N}{i}P_s^i(1-P_s)^{N-i}\sum_{j=e+1}^{N-i}(i+j+e)\binom{N-i}{j}\left(\frac{P_t}{1-P_s}\right)^j\left(1-\frac{P_t}{1-P_s}\right)^{N-i-j}$$

$$+\frac{1}{N}\sum_{i=d}^{N}\binom{N}{i}P_s^i(1-P_s)^{N-i}\left[i+(N-i)\frac{P_t}{1-P_s}\right] \tag{4.54}$$

For our problem, the probability of an erasure is given by

$$\delta = P_s \tag{4.55}$$

and the conditional probability of an error is given by

$$p = \frac{P_t}{1 - P_s} \tag{4.56}$$

Thus, (4.54) can readily be evaluated for any code with a known minimum distance.

4.5 Two-Stage Coding Approaches

Thus far we have established bounds on the performance of interleaved block and convolutional codes operating in the presence of interference. In this section, coding approaches based on the use of two separate levels of coding are discussed and applied to the interference problem. The use of two separate codes generally leads to an implementation which is less complex than the hardware required for a single level of coding of similar performance. Also, a two-level coding approach can be made adaptive by using the first level of coding to correct random errors and to detect interference, with the second level of coding used to fill in the data lost during the interference. A large number of coding techniques fall into this class, such as product (iterative) codes, concatenated codes, and multiple-rate codes.

4.5.1 Interleaved Inner and Outer Coding Approaches (Nonadaptive)

This coding approach uses an interleaved inner code and an interleaved outer code to improve the performance available with a single level of coding. A block diagram is illustrated on Figure 4.1.

The inner interleaver "randomizes" the interference, and the outer interleaver is used to randomize the error burst results from the inner decoder. For a convolutional inner decoder, error bursts of several constraint lengths must be randomized, while for a block code, the error burst is simply given by the block length.

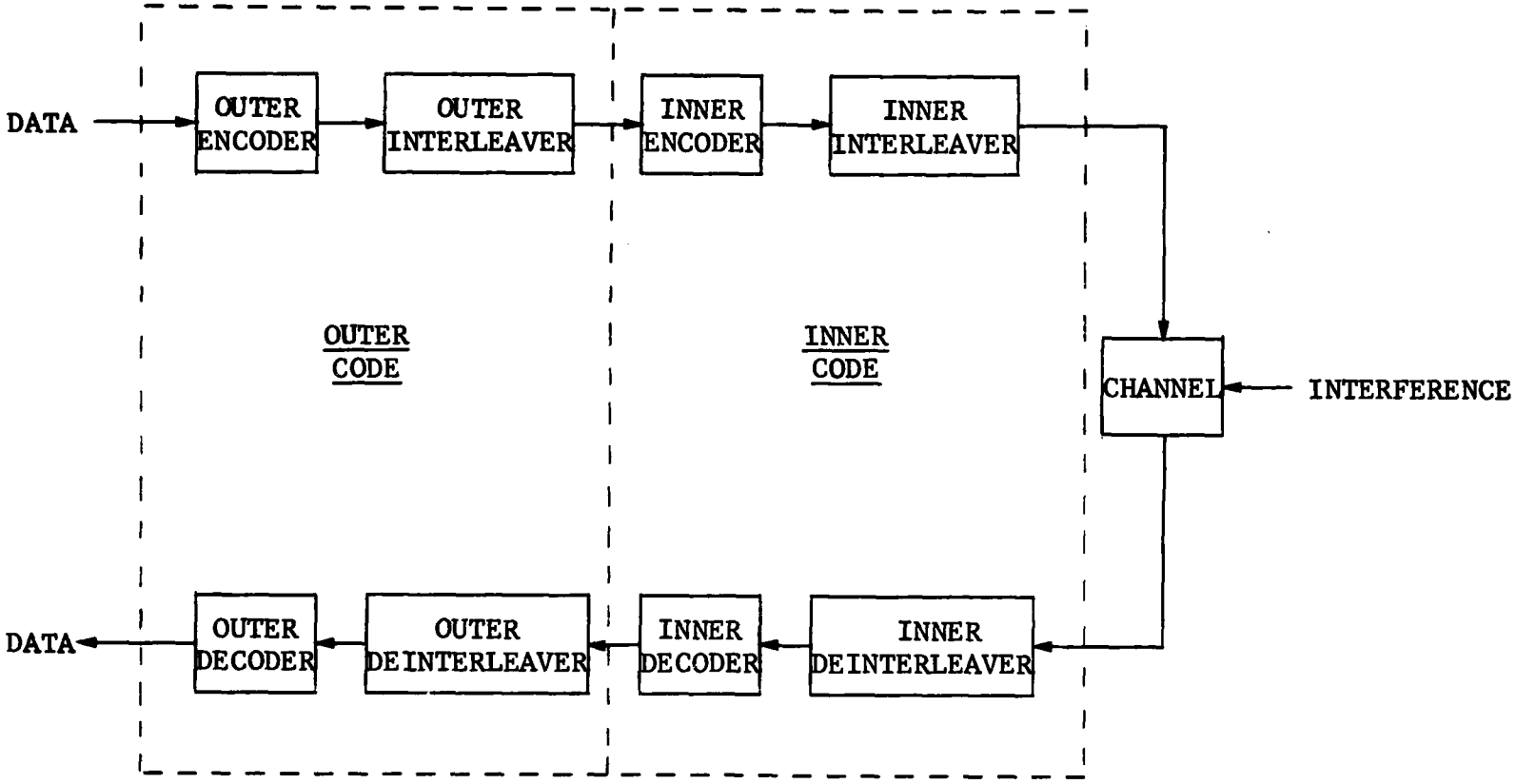


Figure 4.1 Block Diagram of an Interleaved Inner and Outer Coding Approach

Once the performance of the inner code is obtained, the performance of the outer code is obtained by noting that the inner code decoded bit error probability is just the error rate into the interleaved outer decoder.

For a bounded distance binary block outer decoder, the performance is given by Eqs. (4.42) - (4.46), where p is interpreted as the decoded error probability of the inner code. For a binary convolutional outer decoder, the performance is given by (4.36) with $P_e(d)$ given by (4.11) or (4.12).

For Reed-Solomon (R-S) outer codes, we work with symbols of α bits each. The symbol error probability before outer decoding is obtained in terms of the inner decoded bit error probability, denoted as p_d, as

$$p(s) = 1 - (1 - p_d)^{\alpha} < \alpha p_d \tag{4.57}$$

if an outer bit interleaver is used.

A lower value of p(s) is obtained if the outer interleaver is used to interleave α-bit blocks. In this case, we can write

$$p(s) = \Pr[\text{error burst}]\ P(\text{symbol error} \mid \text{error burst}) \tag{4.58}$$

by assuming inner decoded bit errors occur in bursts greater than α bits. The probability of an error burst is $2p_d$ when the probability of a bit error during an error burst is assumed to be 1/2.

Thus, we can calculate the symbol error probability as

$$p(s) = 2p_d\left[1 - \left(\frac{1}{2}\right)^{\alpha}\right] < 2p_d \tag{4.59}$$

when an α-bit block outer interleaver is used. The use of (4.59) to estimate the value for p(s) is somewhat optimistic since, generally, even when errors occur the bit is below 1/2.

The decoder symbol error rate, P_e(decoded symbol), is upper bounded by

$$P_e(\text{decoded symbol}) \le \frac{1}{N} \sum_{i=e+1}^{N} \binom{N}{i} (i+e)\, p^{i}(s)[1 - p(s)]^{N-i} \tag{4.60}$$

where d is odd with $e = \frac{d-1}{2}$. When d is even,

$$P_e(\text{decoded symbol}) \le \frac{e+1}{N}\binom{N}{e+1} p(s)^{e+1}[1-p)s)]^{N-e-1}$$

$$+ \frac{1}{N}\sum_{i=e+2}^{N}\binom{N}{i}(i+e)\, p(s)^{i}[1-p(s)]^{N-1} \quad (4.61)$$

where $e = \frac{d}{2} - 1$.

The final decoded bit error probability, P_e, is given by

$$P_e = \frac{P_e(\text{decoded symbol})}{2\left[1-\left(\frac{1}{2}\right)^{\alpha}\right]} \quad (4.62)$$

Note that when a symbol error occurs, one of $2^{\alpha}-1$ incorrect symbols can occur and, of those $2^{\alpha}/2 = 2^{\alpha-1}$ symbols will yield a bit error. The ratio of $2^{\alpha-1}/2^{\alpha}-1$ is just the factor used to convert the symbol error rate to a bit error rate.

Conventionally, an R-S code has been used as an outer code. However, it is interesting to note that binary block codes may actually be more suitable than the R-S codes. This is true in spite of the fact that R-S codes have the greatest minimum distance of any code of R with α bits per symbol. Note that an R-S code of length N symbols and K information symbols, $R = K/N$, has a minimum distance of N+K+1, which is the absolute maximum [4.7]. Since this result is for a code with α-bit symbols, it is of interest to compare an R-S code with a binary code of equal rate and an equal number of bits.

An interesting high-rate binary code is the rate-0.9 (240,216;7) code which is also a suitable outer code. For an R-S code of $R = 0.9$ and minimum distance 7, we must satisfy

$$R = \frac{K}{N} = 0.9 \quad (4.63)$$

and

$$D = N - K + 1 = 7 \quad (4.64)$$

which implies

$$N \geq 60 \text{ symbols} \tag{4.65}$$

A (60,54;7) R-S code must have at least six bits per symbol since the code length must satisfy

$$N \leq 2^{\alpha} \tag{4.66}$$

Thus, the shortest rate-0.9 R-S code of minimum distance 7 is $60 \times 6 = 360$ binary bits long.

If we restrict the R-S code to have the same length in binary digits as the (240,216) code, only the (40,36;5) R-S code with $\alpha = 6$ can exist.

A direct comparison of the performance of the rate-0.9 binary block code and the rate-0.9 R-S codes is given on Figure 4.2. Note that the (60,54;7) R-S code can out-perform the (240,216;7) BCH code only if we use symbol interleaving and are guaranteed that burst errors occur with an error rate of 1/2. If bit interleaving is used, the (60,54;7) R-S code offers inferior performance to that possible for the shorter (in binary bits) BCH code. The (40,36;5) R-S code, which is the same length as the BCH code, offers inferior performance for the case when a symbol interleaver, or bit interleaver, is used. The importance of binary block codes as outer codes should be clear from even these preliminary results.

4.5.2 Adaptive Inner and Outer Coding Techniques

Coding techniques in this class use an inner code to detect the presence of interference. The short rate-1/2, K=7 convolutional code is quite unsuitable for these techniques since most error are undetectable. However, the long rate-1/2 (128,64;22) BCH code is quite attractive since most errors are detectable either by the decoder or simply by comparing the analog weight of the selected error pattern to an appropriate threshold, such as one based on the analog weight of the sum of the r least reliable bits.

The inner decoder supplies binary errors and erasures to the outer decoder. To determine the probability of these events, we first note the probability of interference is given as

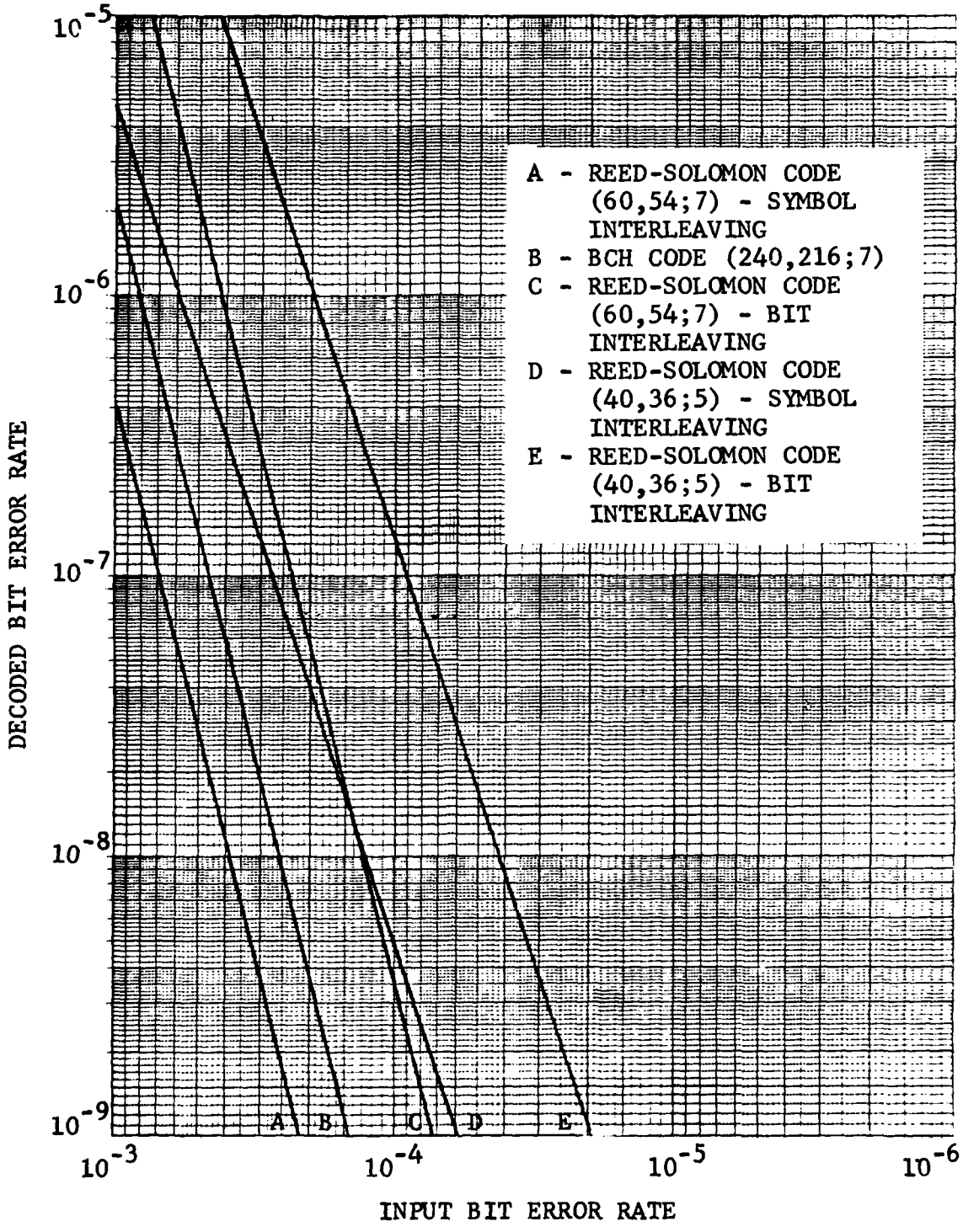


Figure 4.2 Comparison of Error Rate Performance for R = 0.9 Codes

$$\Pr[\text{interference}] = \delta \tag{4.67}$$

An undetected inner decoding error is most likely to occur in the presence of interference; but, in general, an undetected error can occur in the presence of noise as well. Thus, we can write

$$P_t = (1 - \delta)\ P(e|\text{noise}) + \delta\ P(e|\text{interference}) \tag{4.68}$$

Similarly, the probability of an erasure is given by

$$P_s = (1 - \delta)\ P(E|\text{noise}) + \delta\ P(E|\text{interference}) \tag{4.69}$$

In the above equations, P_t and P_s are unconditional probabilities, as defined in Section 4.4.3.

For a long block code with good detection capabilities to a first approximation, we can assume that

$$P_t \approx 0 \tag{4.70}$$

and

$$P_s = (1 - \delta)\ P(E|\text{noise}) + \delta \tag{4.71}$$

The probability of an erasure (detected block error) in the presence of noise only is given by

$$P(E|\text{noise}) \approx n_d Q\left(\sqrt{\frac{2dE_s}{N_0}}\right) \text{ - channel measurement decoding} \tag{4.72}$$

$$P(E|\text{noise}) = \sum_{i=e+1}^{N} \binom{N}{i} p^i (1-p)^{N-i} \text{ - binary decoding} \tag{4.73}$$

For the (128,64) block code, $n_d = 243{,}840$; $e+1 = 11$; $d = 22$.

In the general case, the probability of error after decoding is given by (4.54) for an outer code with N bits (or symbols) and of minimum distance d.

When (4.70) and (4.71) are satisfied, Eq. (4.54) is simplified to

$$P_e \leq \frac{1}{N} \sum_{i=d}^{N} i \binom{N}{i} P_s^i (1 - P_s)^{N-i} \tag{4.74}$$

For the (240,216) outer code, $d = 7$ and $N = 240$. Alternatively, a (128,64) outer code can be used in conjunction with a (128,64) inner code. For this case, $d = 22$ and $N = 128$.

Considerably more sophisticated adaptive coding techniques may also be considered by the analysis techniques similar to those used in this Section.

REFERENCES

[4.1] R. A. Scholtz, "The Spread Spectrum Concept," IEEE Trans. on Communications, Vol. COM-25, No. 8, August 1977.

[4.2] D. Chase and L. Ozarow, "Capacity Limits for Binary Codes in the Presence of Interference," IEEE Trans. on Communications, Vol. COM-27, No. 2, February 1979.

[4.3] J. J. Jones, "Hard-Limiting of Two Signals in Random Noise," IEEE Trans. on Information Theory, January 1963.

[4.4] D. Chase, "A Class of Algorithms for Decoding Block Codes with Channel Measurement Information," IEEE Trans. on Information Theory, Vol. IT-18, January 1972.

[4.5] J. M. Wozencraft and I. J. Jacobs, Principles of Communication Engineering, New York, Wiley, 1965.

[4.6] J. A. Heller and I. M. Jacobs, "Viterbi Decoding for Satellite and Space Communication," IEEE Trans. on Comm. Technology, Vol. COM-19, No. 5, October 1971.

[4.7] R. G. Gallager, Information Theory and Reliable Communication, New York, Wiley, 1968.

[4.8] A. J. Viterbi, "Convolutional Codes and Their Performance in Communication Systems," IEEE Trans. on Comm. Technology, Vol. COM-19, October 1971.

[4.9] J. P. Odenwalder, "Optimal Decoding of Convolutional Codes," Ph.D. Dissertation, UCLA, 1970.

[4.10] B. D. Trumpis and P. L. McAdam, "Performance of Convolutional Codes on Burst Noise Channels," National Telecommunications Conference, Los Angeles, CA, December 1977.

[4.11] D. Chase, "Digital Signal Design Concepts for a Time-Varying Rician Channel," IEEE Trans. on Communications, Vol. COM-24, No. 2, February 1976.

[4.12] L. D. Baumert and L. R. Welch, "Minimum Weight Codewords in the (128,64) BCH Code," The Deep Space Network Progress Report 42-42, Jet Propulsion Lab., Pasadena, CA, December 1977.

[4.13] D. Chase, et al., "Robust Waveforms for HF Communications," CNR, Inc. Final Report on Contract No. N00173-76-C-0168, November 1976.

SECTION 5

PERFORMANCE OF BLOCK CODES IN THE PRESENCE OF INTERFERENCE

In this section, performance results for the rate-1/2 (24,12;8) and the (128,64;22) block codes are presented for the four interference models considered in Section 4. Results for other block codes such as the rate-0.9 BCH code and R-S codes are presented in Sections 7 - 9.

Throughout this section, as well as Section 6, the following format is used.

Each figure will contain the uncoded modulation results, denoted by A, binary decoding results (model 2 or 4) denoted by B, and channel measurement decoding results (model 1 or 3) denoted by C. When no erasure information is available, models 1 or 2 are applicable and when erasure information is available, models 3 and 4 are applicable. From each curve the benefits of binary and channel measurement decoding can be readily obtained. The coding gain defined as the reduction in E_b/N_0 for a specified level of performance, i.e., 10^{-5}, can be obtained directly from each figure. The amount of interference is varied over the values 0, 5%, 10%, 15%, and 20% and for each non-zero interference level two graphs, with or without erasure information, are obtained. Thus, nine curves are required to characterize a given code over the four interference models and over the 0 to 20% range of interference probabilities.

Figures 5.1 to 5.9 represent these results for the (24,12) Golay code and Figures 5.10 to 5.18 are the corresponding results for the (128,64) BCH code.

The results when no erasure information is available, Figures 5.1 to 5.5 and 5.10 to 5.14, are obtained from Eqs. (4.37) (channel measurement decoding) and (4.44) and (4.46) (bounded distance binary decoding). When erasure information is available, Figures 5.6 to 5.9 and 5.15 to 5.18, Eq. (4.37) still applies for the channel measurement decoded, with the appropriate $P_e(d)$ obtained from Table 4-1. For the bounded distance binary erasure decoded, Eq. (4.54) is used.

The equations used for the bounded distance binary decoding are very tight upper bounds [5.1] with the actual performance expected to be only a factor of a dB better than the mathematical upper bounds. The channel measurement equations represent very tight estimates for the Golay code [5.1] [5.2], but since the true maximum likelihood performance of the (128,64) BCH code is unknown, the tightness of these channel measurement equations is also unknown. Simulation results for various channel measurement decoding algorithms for the (128,64) BCH code [5.3] [5.4] are less than 1 dB off the equations used in this report.

The effects of quantization are not included in any of the equations developed in Section 4, however, Appendix B develops bounds for the loss in performance due to quantization.

The no interference case, Figures 5.1 and 5.10, can also be viewed as the performance in the presence of continuous jamming (non-pulse) jamming. Note, that at a bit error rate of 10^{-5}, the channel measurement decoding approach offers coding gains (curve A - curve C) of 4 dB for the Golay code and over 6 dB for the (128,64) BCH code. For binary decoding, the coding gains are 2 dB for the Golay code and 3.5 dB for the (128,64) BCH code.

The coding gains for the case when interference is present approach infinity for many of the interesting cases. Note that for this worst-case model, the uncoded system has an irreducible error of 1/2 during the presence of the assumed completely destructive pulses, i.e., regardless of the value of E_b/N_0, the uncoded system must have a bit error rate greater than $\delta/2$. The importance of channel measurement decoding and erasure information should be clear from these results.

While the Golay code offers inferior performance to the (128,64) BCH code, this short code has the property that true maximum likelihood decoding can be achieved since there are only 2^{12} codewords. Equations (4.38), (4.41) and Table 4-1 can be used to upper bound the performance of a maximum likelihood binary decoder for the Golay code. Note, that the channel measurement equations are approximations to maximum likelihood decoding and, thus, need not be modified.

Figures 5.19 to 5.27 include the maximum likelihood binary decoding upper bound, superimposed as curve D, on the performance figures for the Golay code.

For binary decoding without erasure information, the upper bounds for maximum likelihood decoding indicate a loss in performance. In fact, since the (24,12) Golay code is quasisphere-packed, the bounded distance decoder and the maximum likelihood decoder should offer essentially the same performance. The differences shown on Figures 5.19 to 5.23 are just a consequence of the fact that the bounded distance decoding bounds (as advertised in Section 4) are tighter than the maximum likelihood decoding bounds.

The importance of true maximum likelihood decoding is quite evident when erasure information is available. Even though the Golay code is quasisphere packed, a bounded distance decoder is <u>not</u> equivalent to a maximum likelihood decoder when erasure information is available. Note, that when $d = 8$. erasures are present, a bounded distance decoder will make errors, while a maximum likelihood decoder has a good chance of correcting a pattern with eight erasures. Figures 5.24 to 5.27 indicate the importance of maximum likelihood decoding in the presence of interference. Even binary decoding with erasure information has the same irreducible error as that for channel measurement decoding with erasure information.

The convolutional decoding results given in Section 6 are all for short convolutional codes and thus maximum likelihood decoding is assumed for both binary and channel measurement decoding.

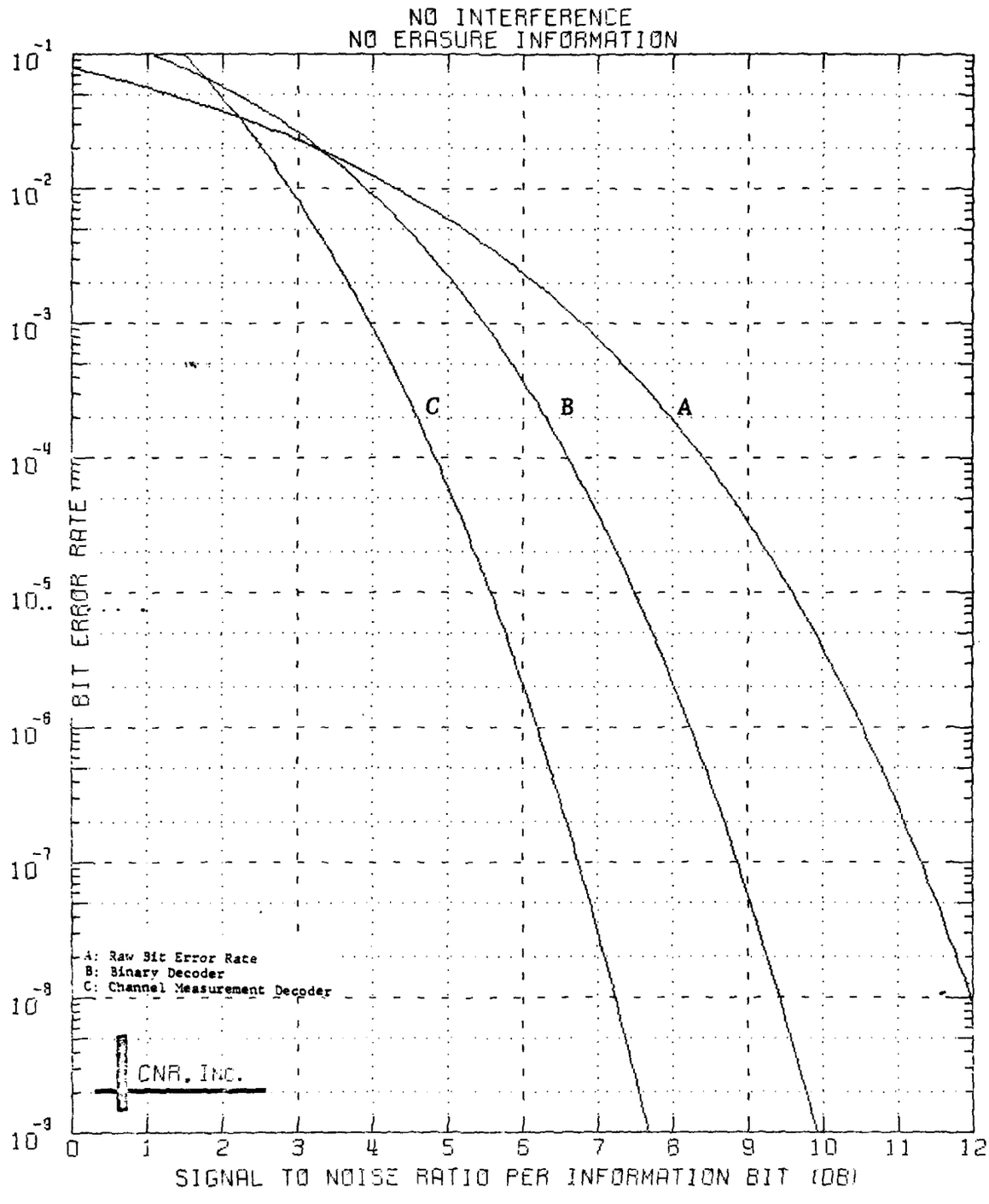


Figure 5.1 Decoded Performance of a Block Code Dimensions (24,12;8)

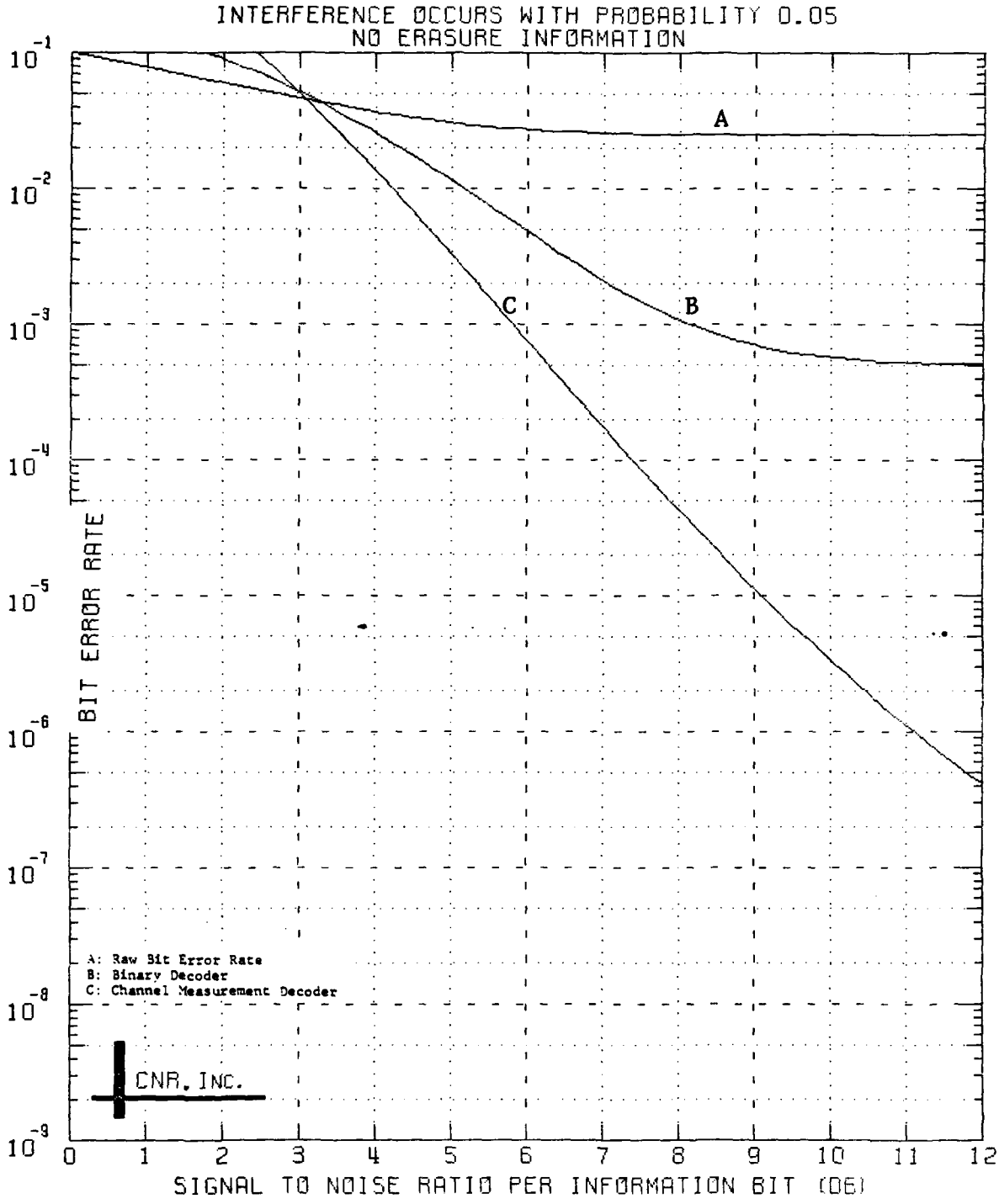


Figure 5.2 Decoded Performance of a Block Code Dimensions (24,12;8)

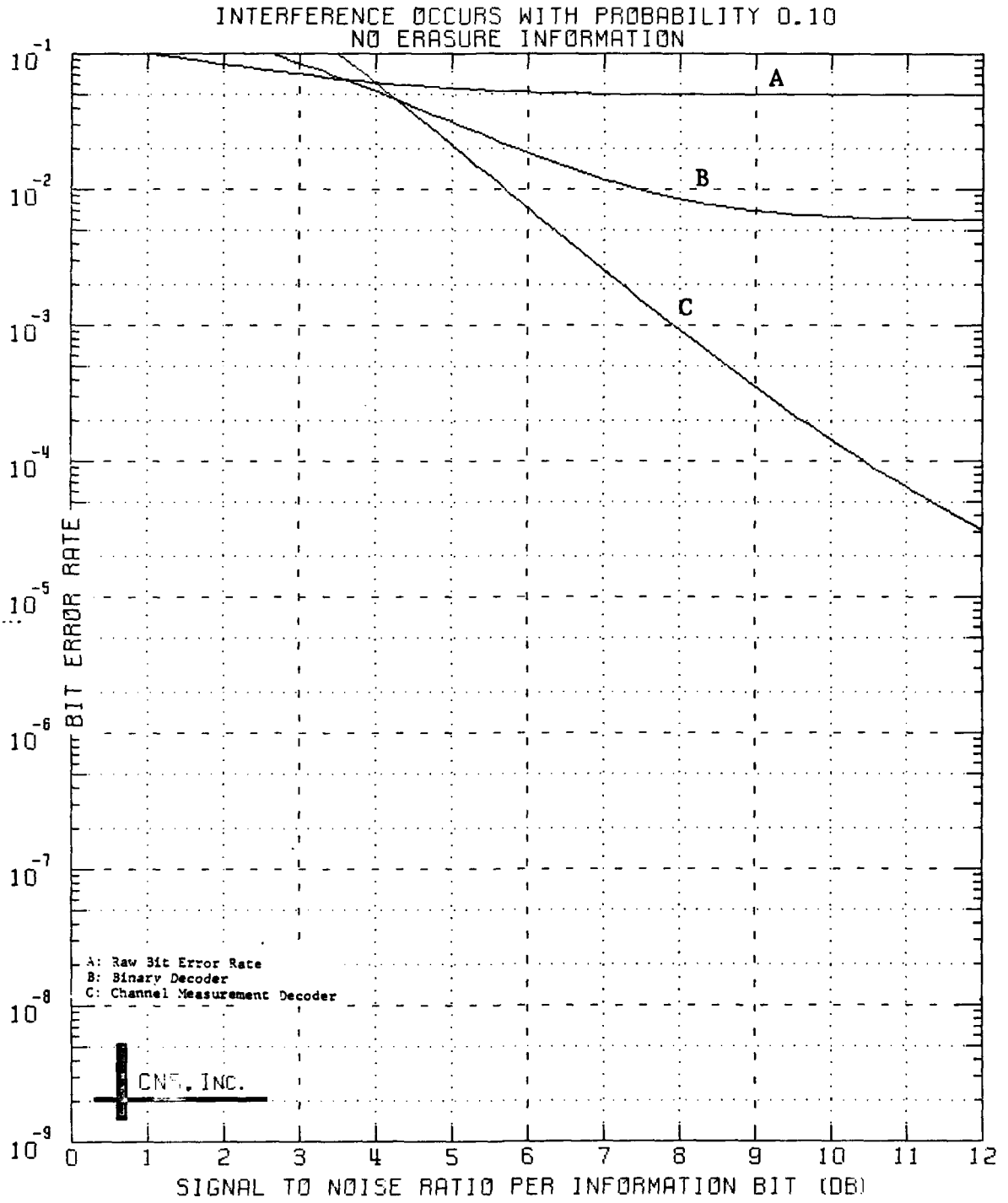


Figure 5.3 Decoded Performance of a Block Code Dimensions (24,12;8)

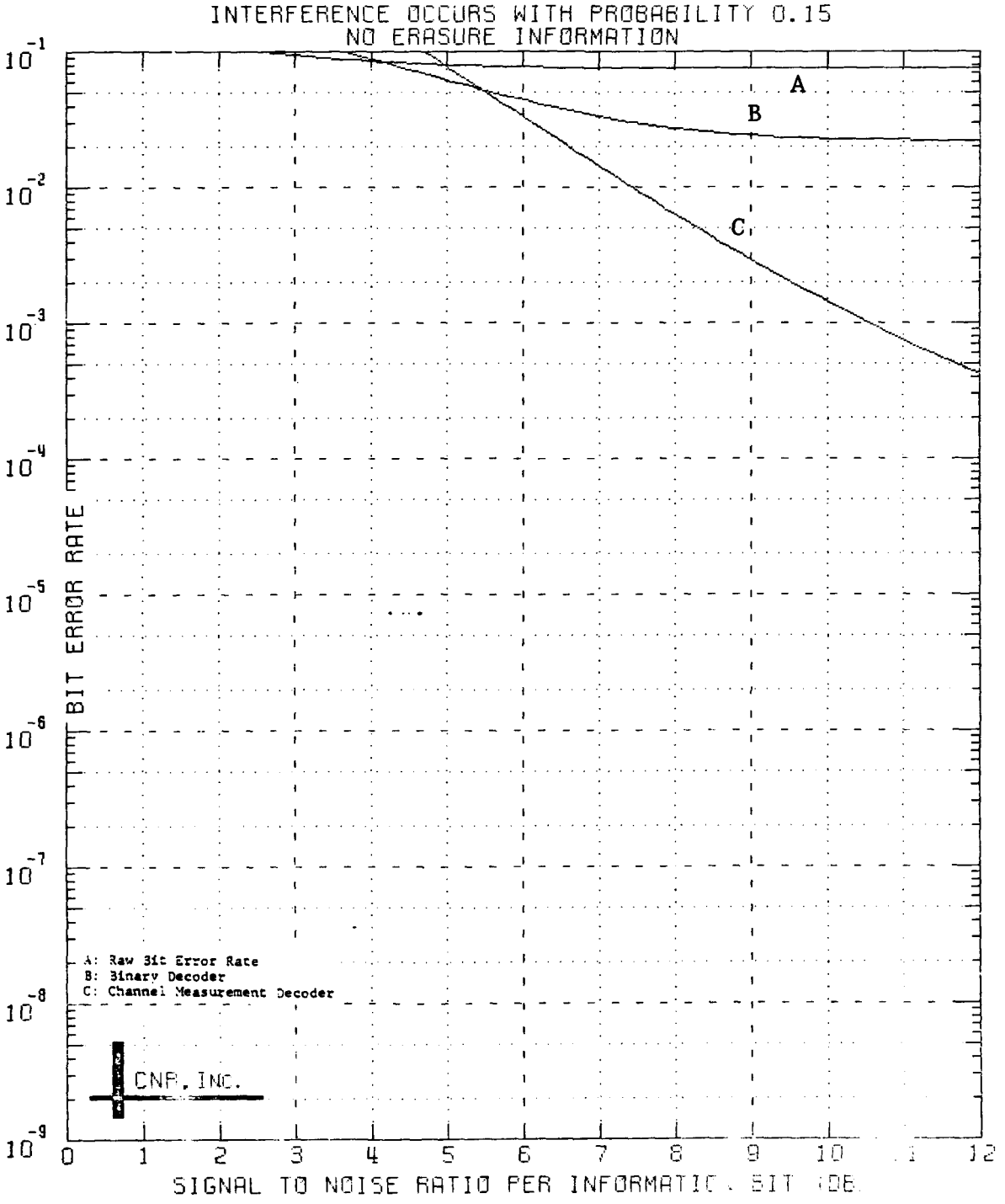


Figure 5.4 Decoded Performance of a Block Code Dimensions (24,12;8)

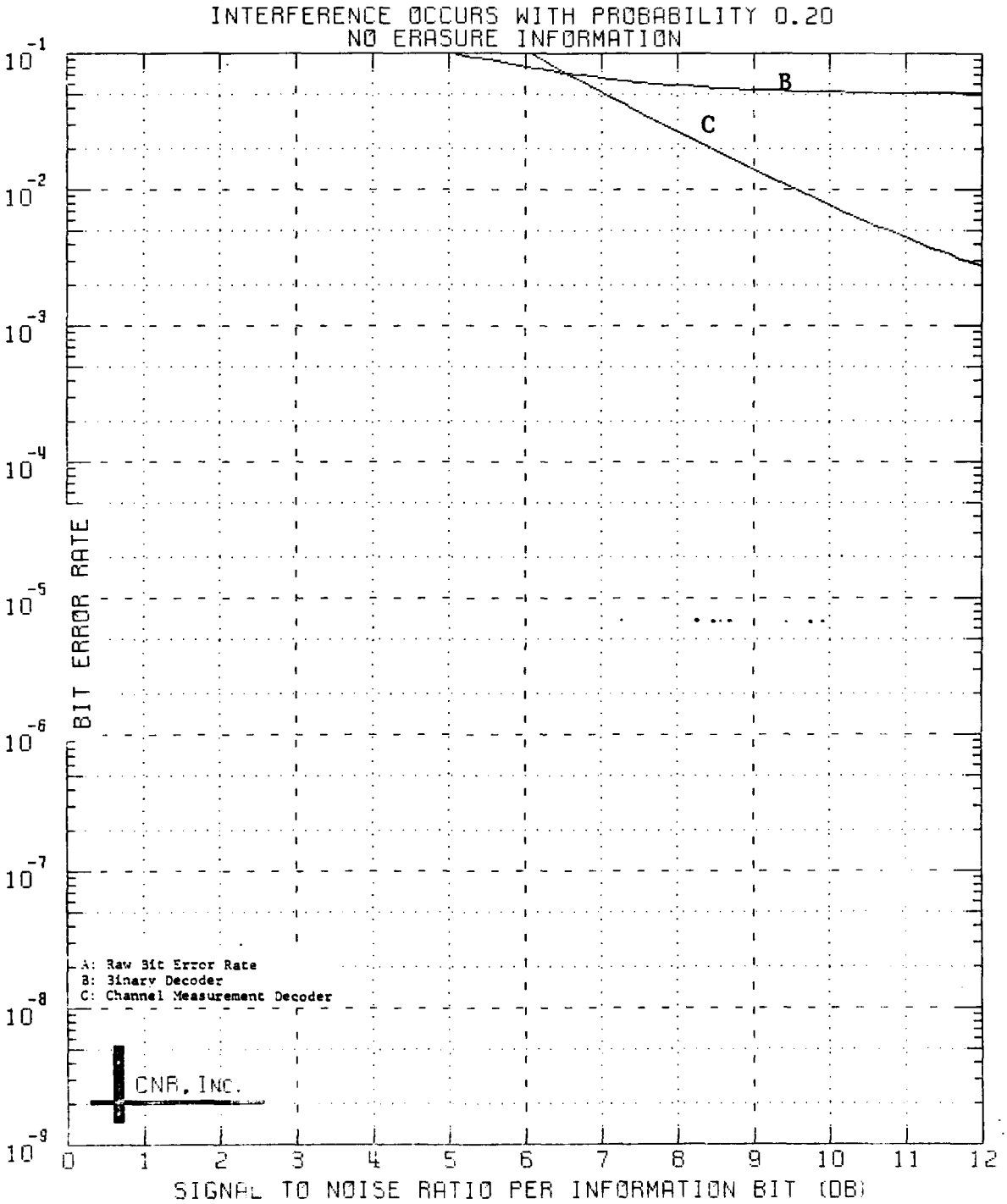


Figure 5.5 Decoded Performance of a Block Code Dimensions (24,12;8)

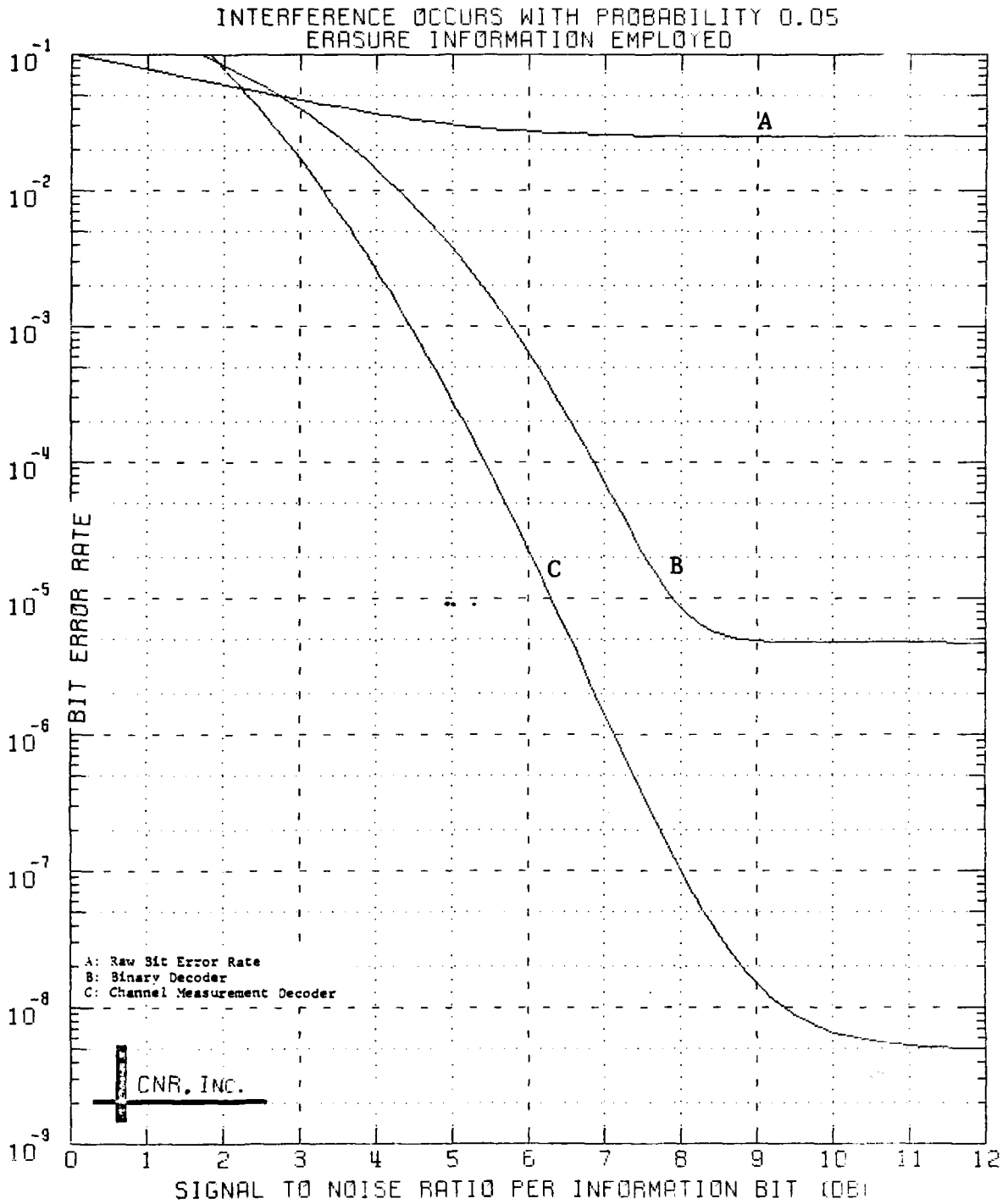


Figure 5.6 Decoded Performance of a Block Code Dimensions (24,12;8)

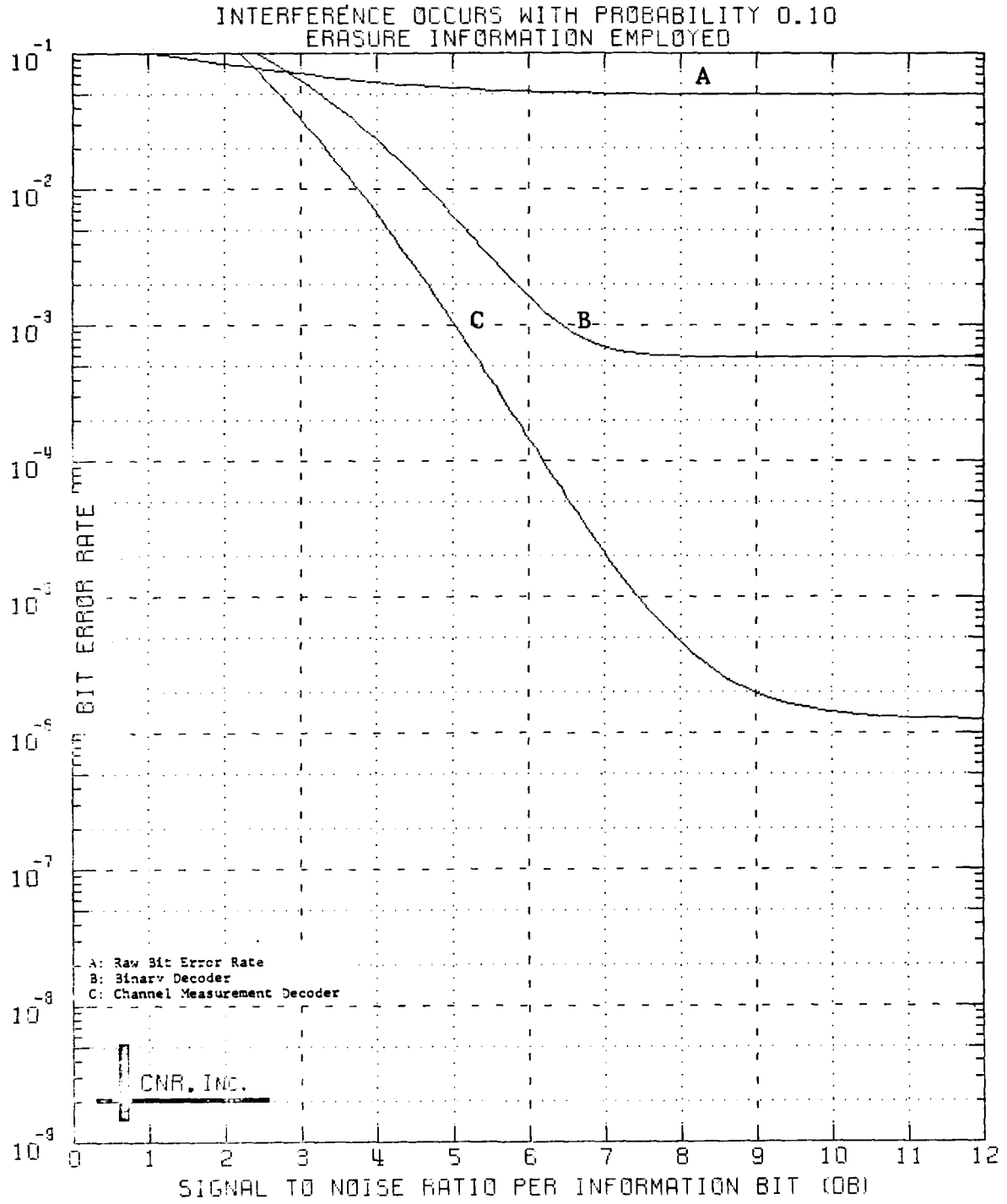


Figure 5.7 Decoded Performance of a Block Code Dimensions (24,12;8)

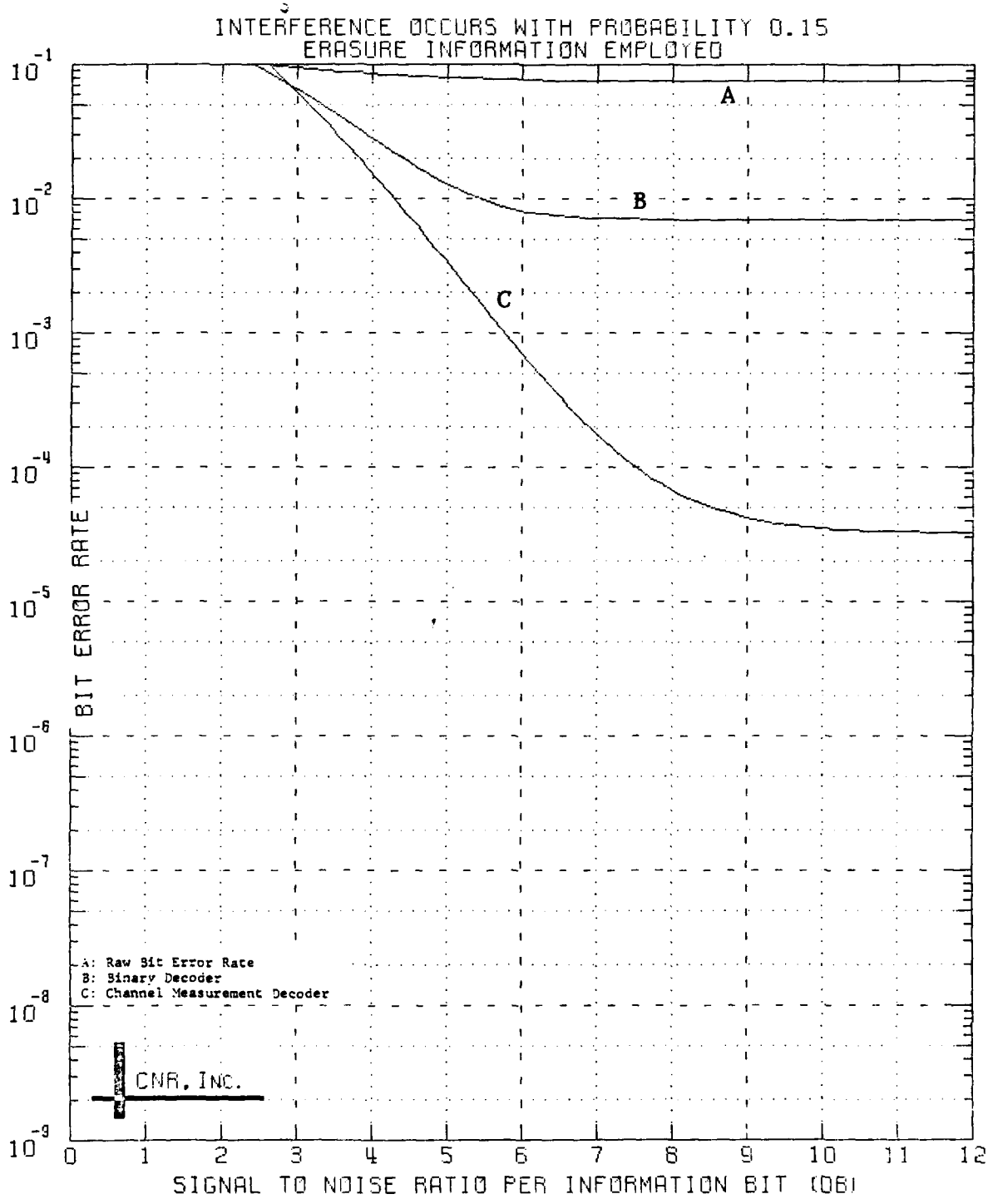


Figure 5.8 Decoded Performance of a Block Code Dimensions (24,12;8)

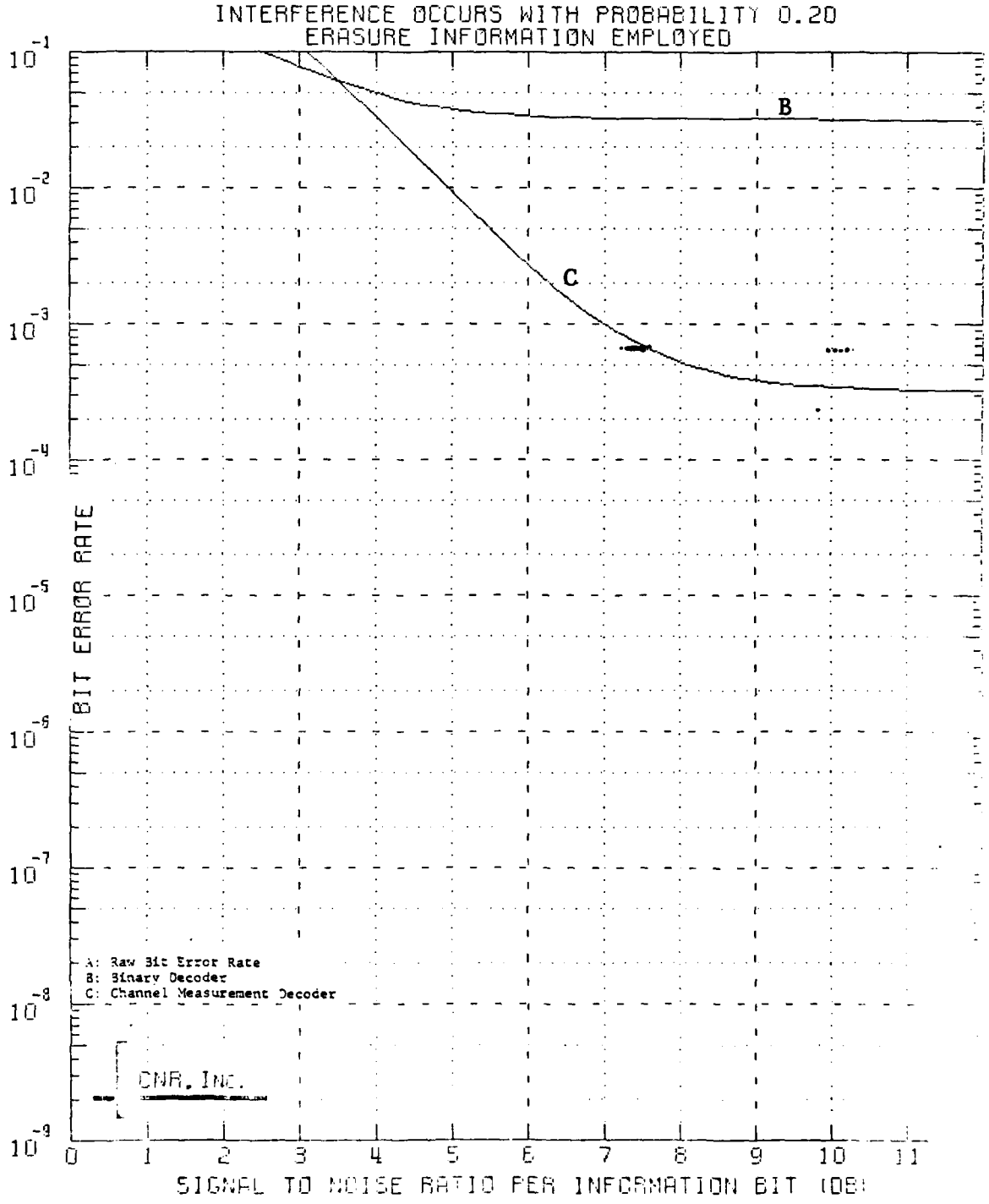


Figure 5.9 Decoded Performance of a Block Code Dimensions (24,12;8)

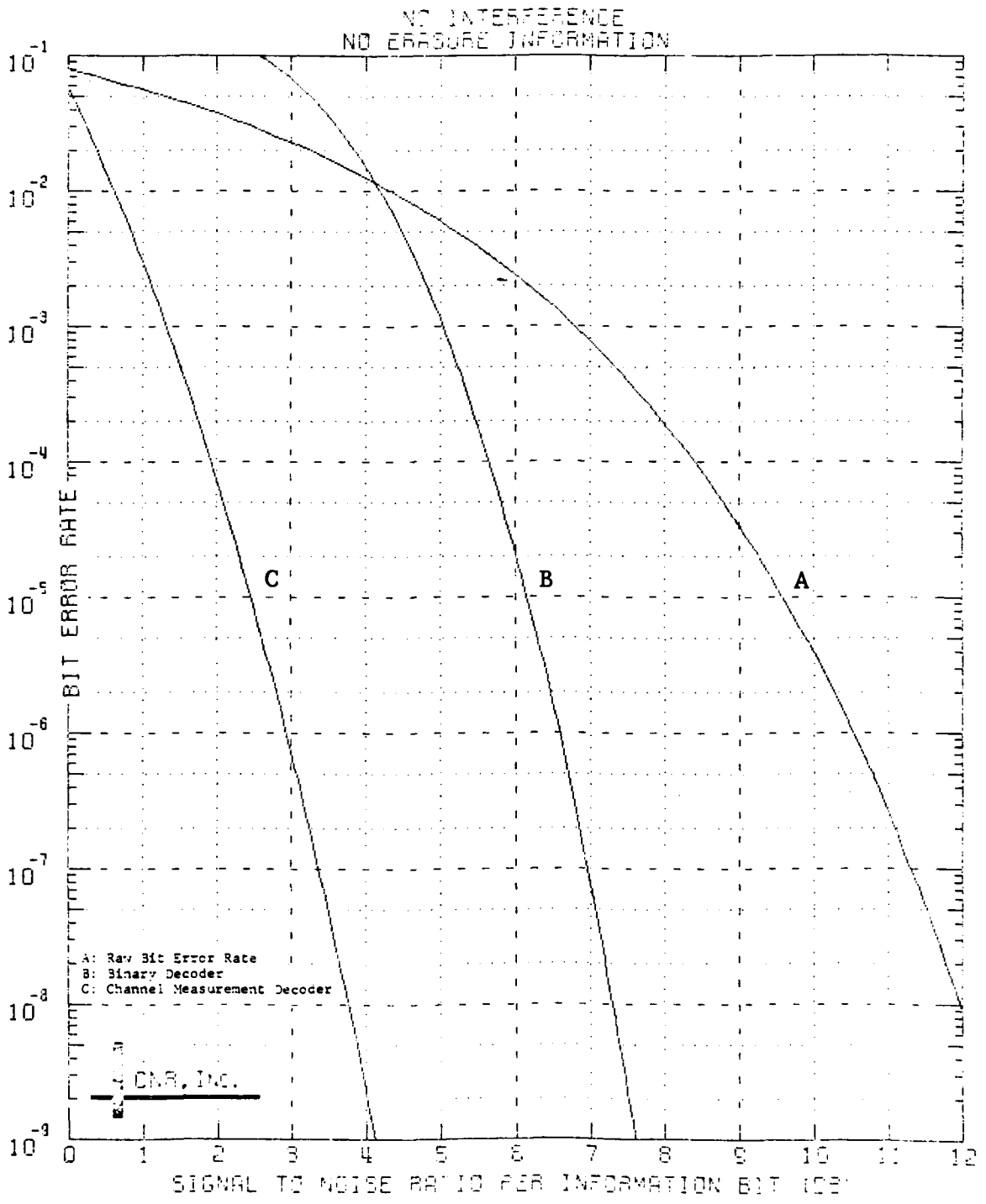


Figure 5.10 Decoded Performance of a Block Code Dimensions (128,64;22)

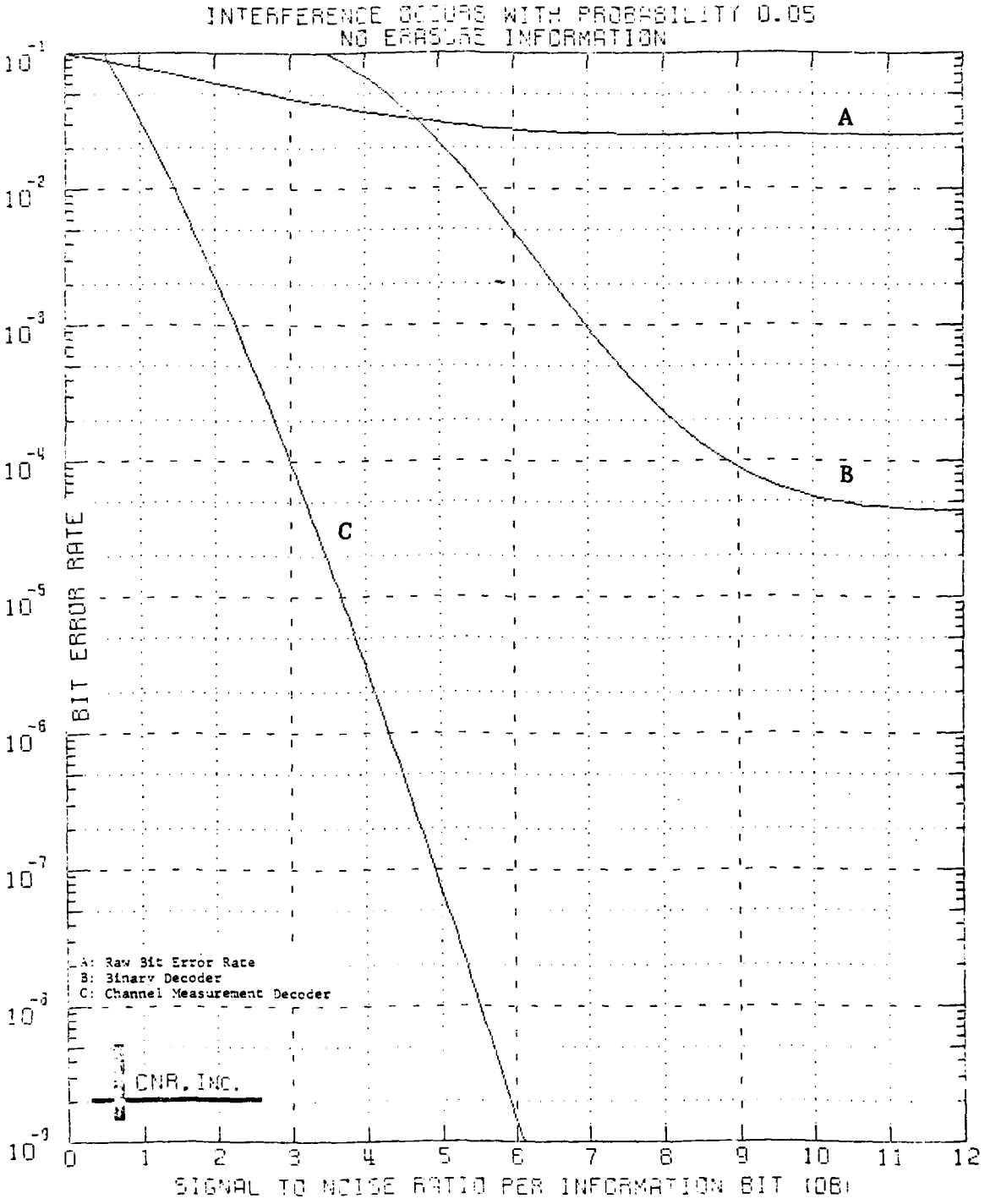


Figure 5.11 Decoded Performance of a Block Code Dimensions (128,64;22)

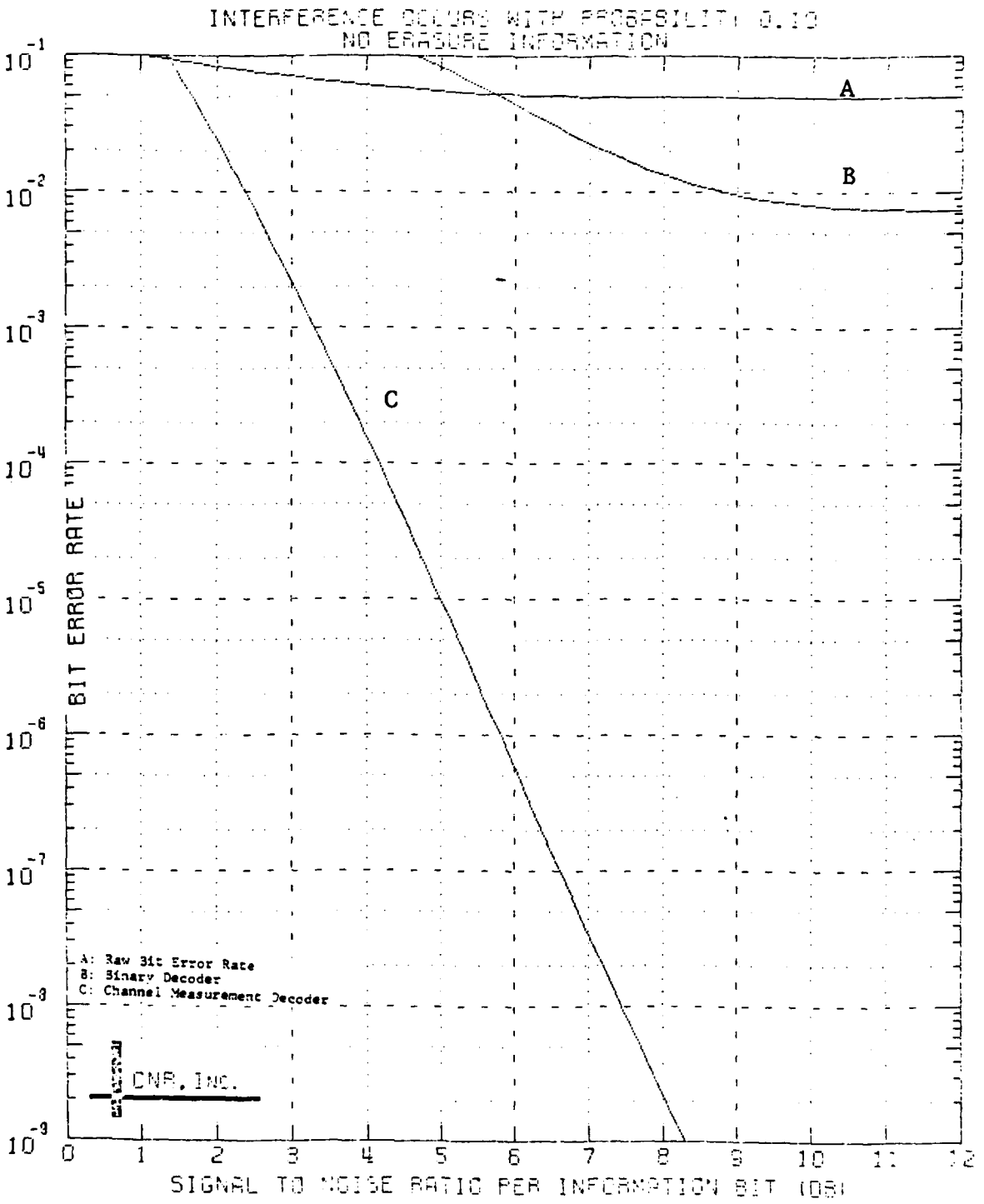


Figure 5.12 Decoded Performance of a Block Code Dimensions (128,64;22)

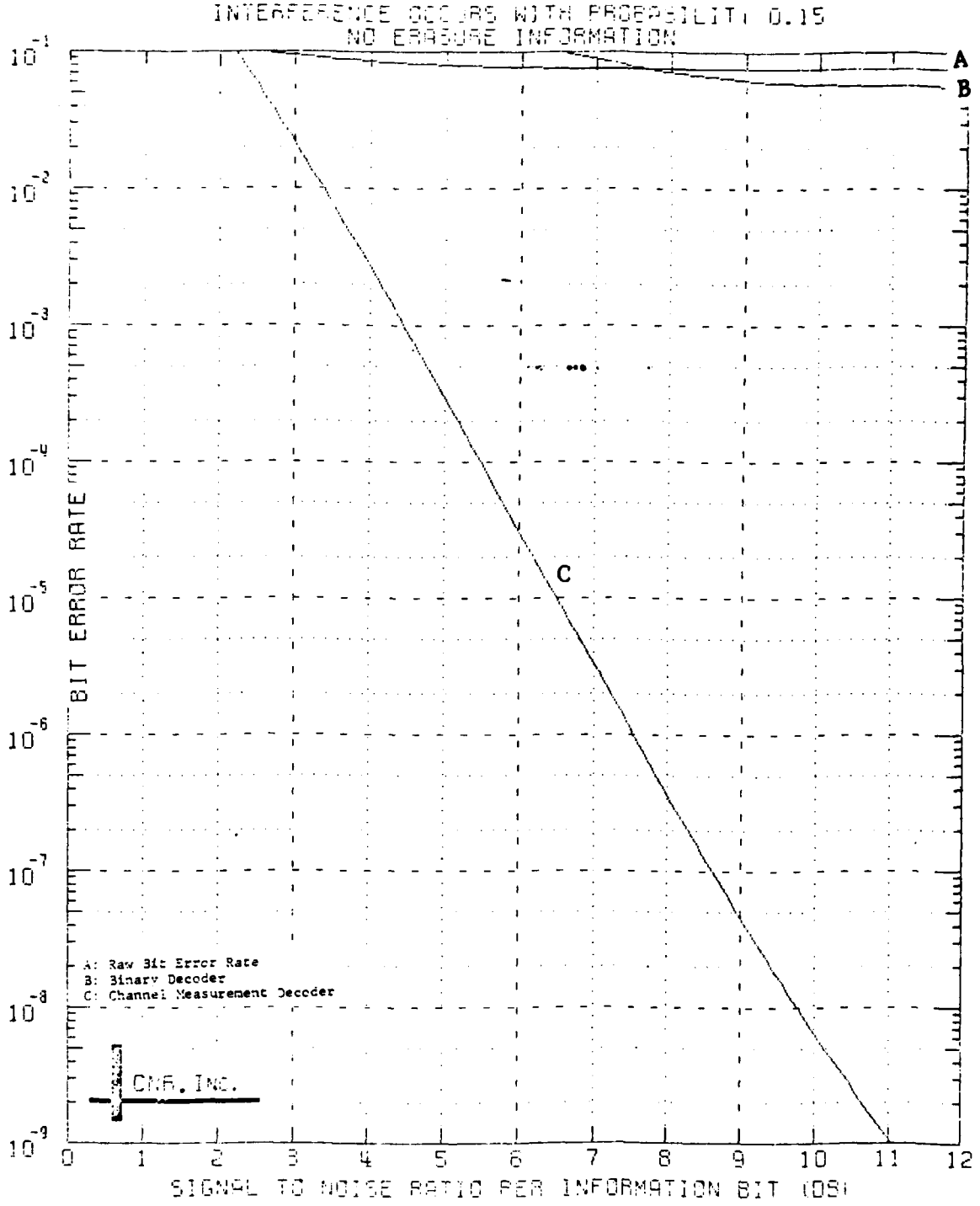


Figure 5.13 Decoded Performance of a Block Code Dimensions (128,64;22)

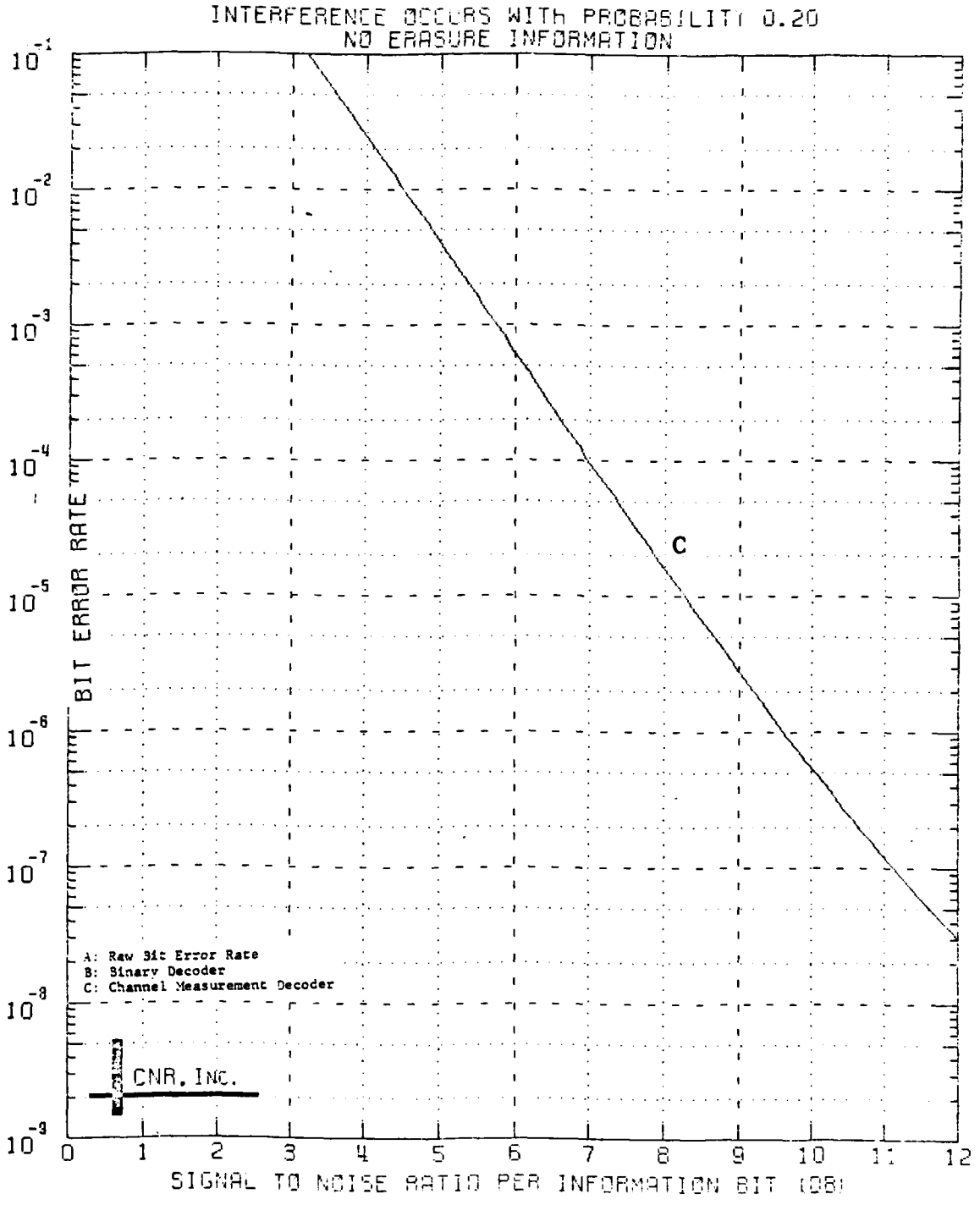


Figure 5.14 Decoded Performance of a Block Code Dimensions (128,64;22)

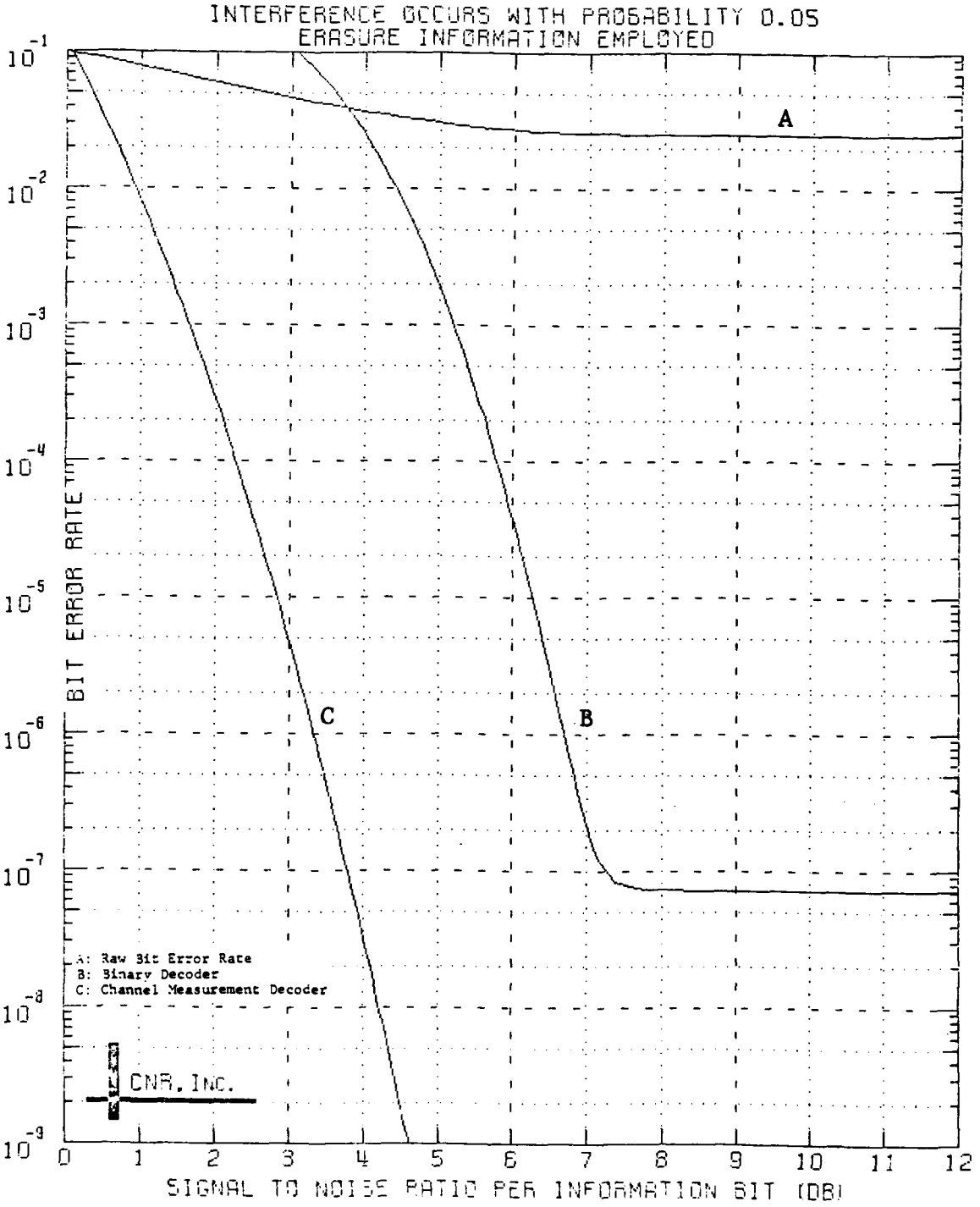


Figure 5.15 Decoded Performance of a Block Code Dimensions (128,64;22)

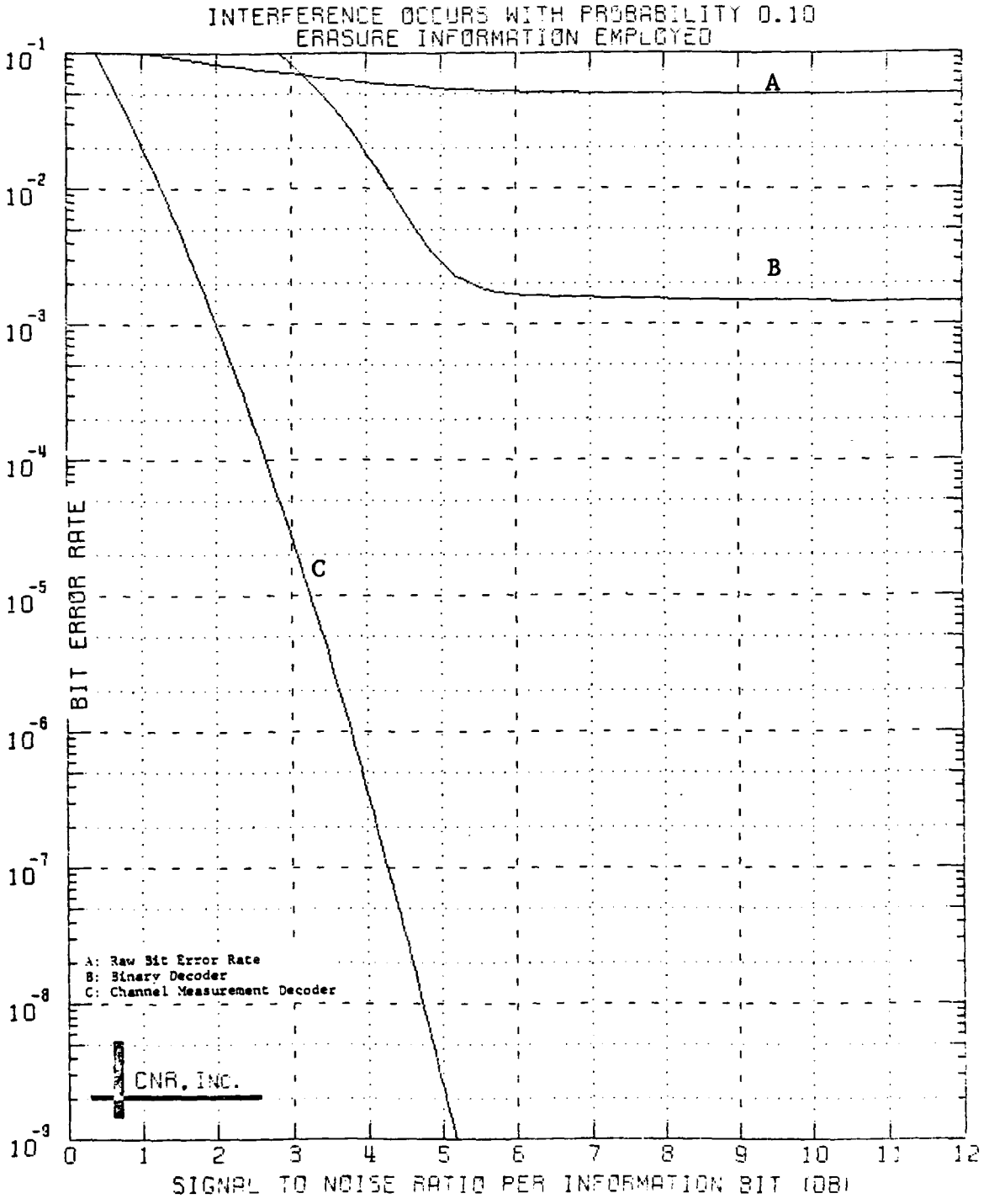


Figure 5.16 Decoded Performance of a Block Code Dimensions (128,64;22)

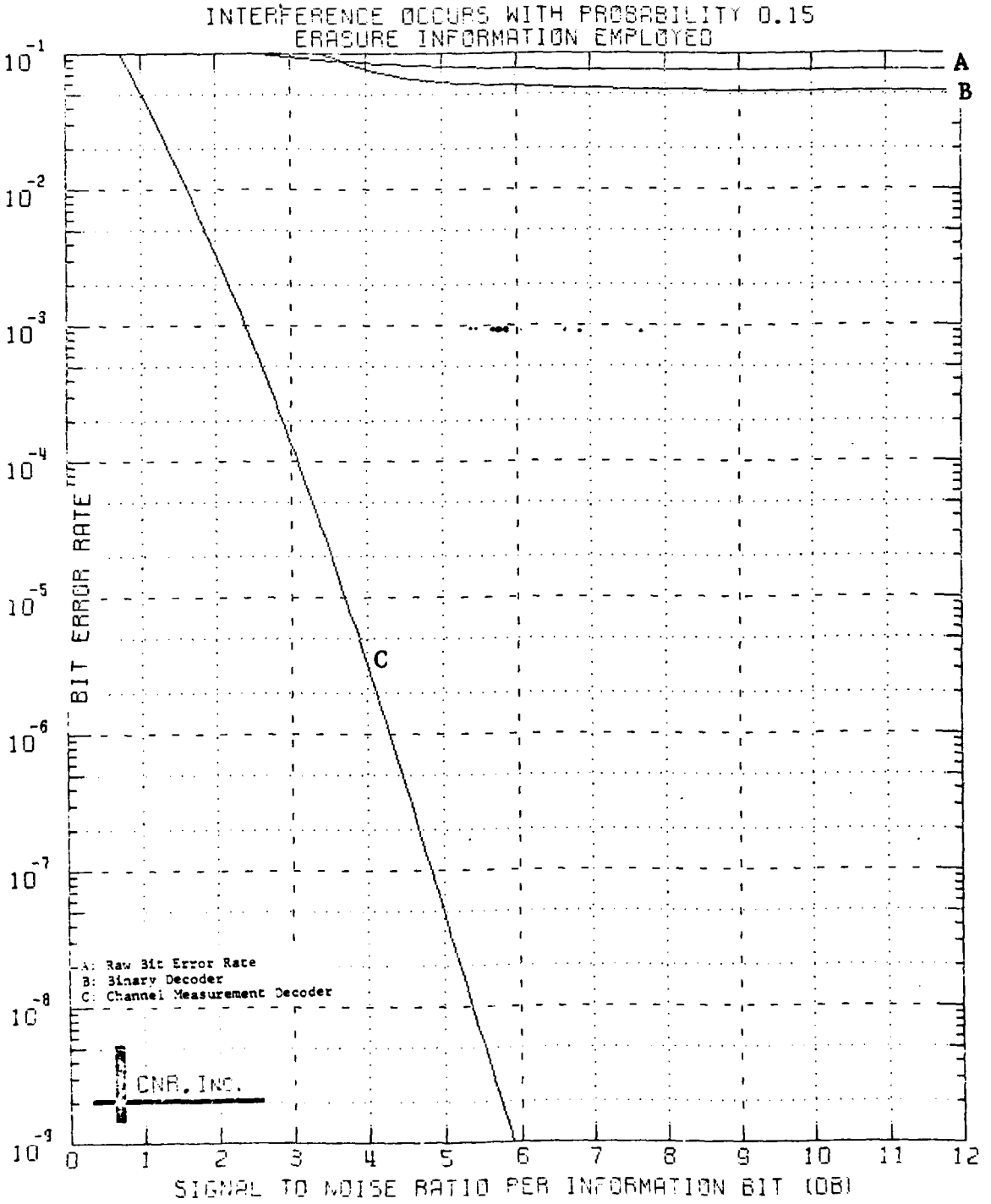


Figure 5.17 Decoded Performance of a Block Code Dimensions (128,64;22)

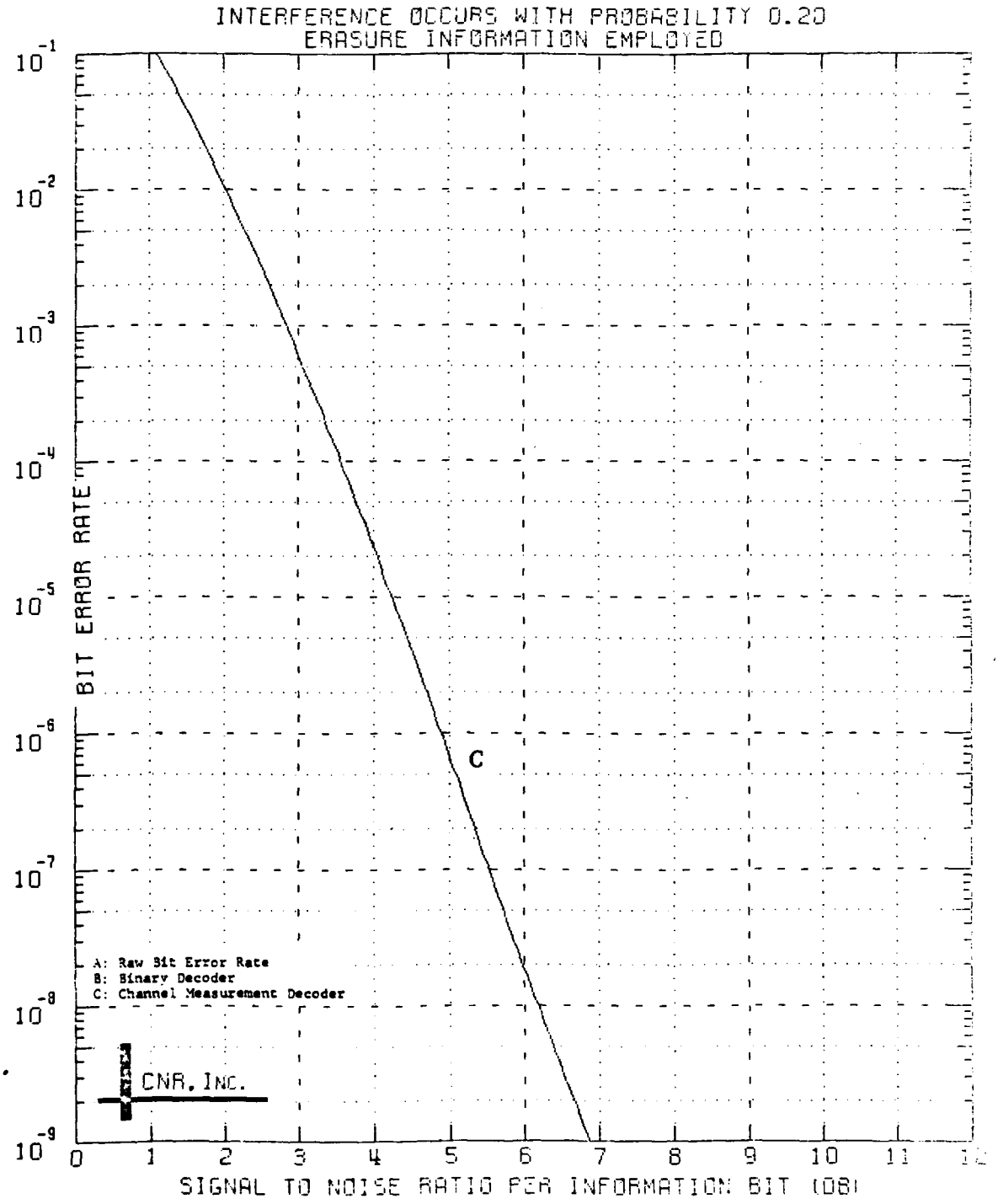


Figure 5.18 Decoded Performance of a Block Code Dimensions (128,64;22)

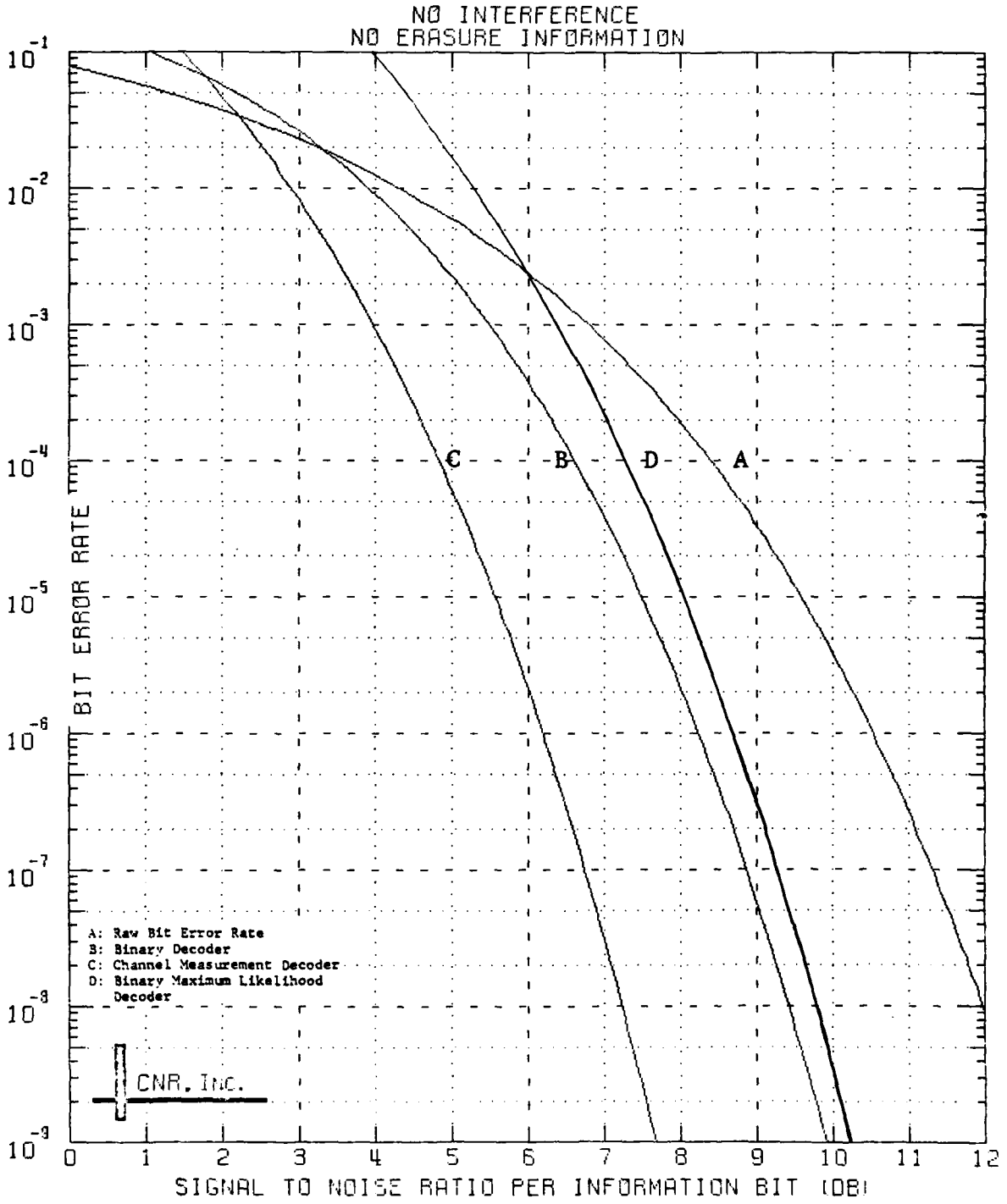


Figure 5.19 Decoded Performance of a Block Code Dimensions (24,12;8)

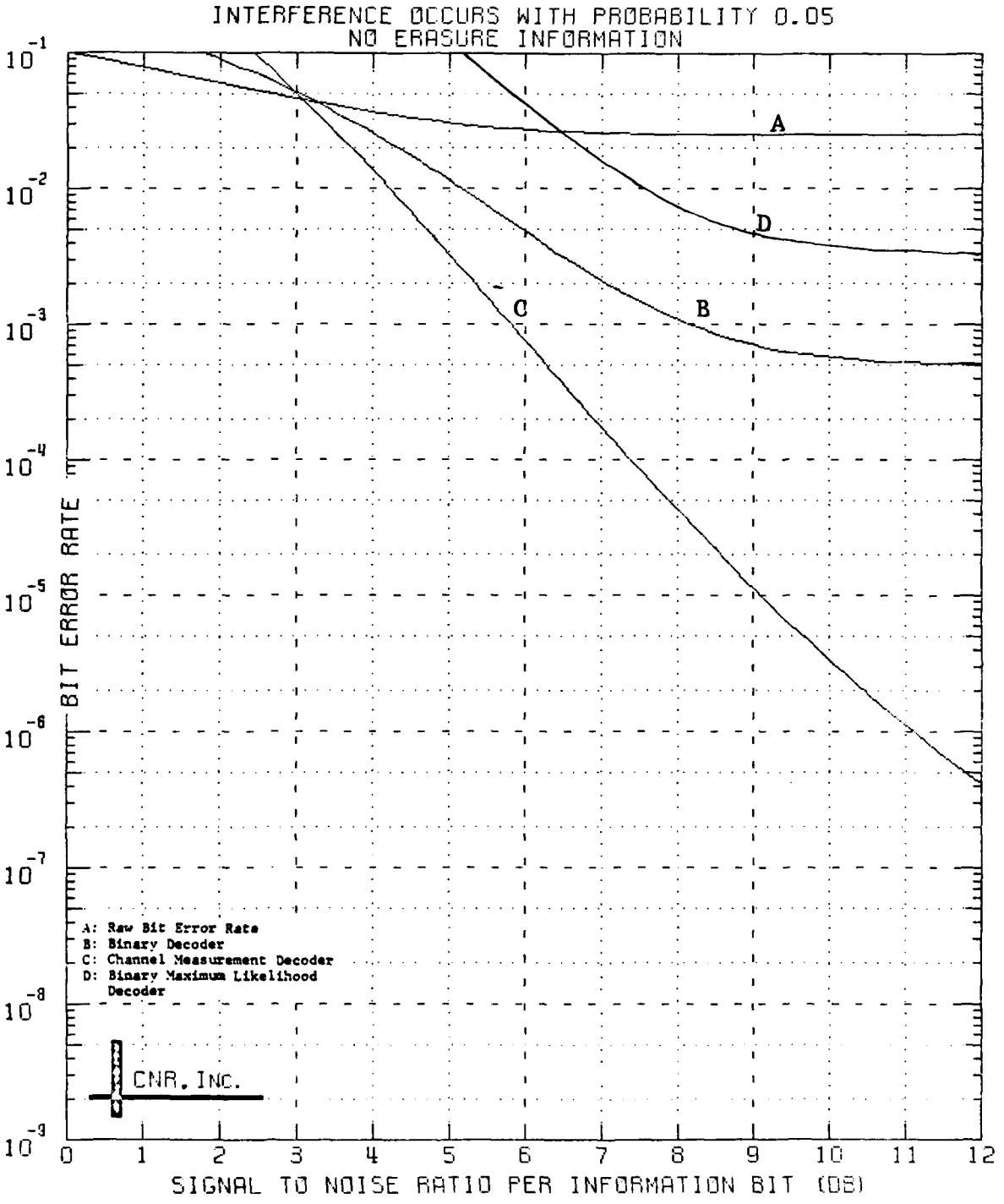


Figure 5.20 Decoded Performance of a Block Code Dimensions (24,12;8)

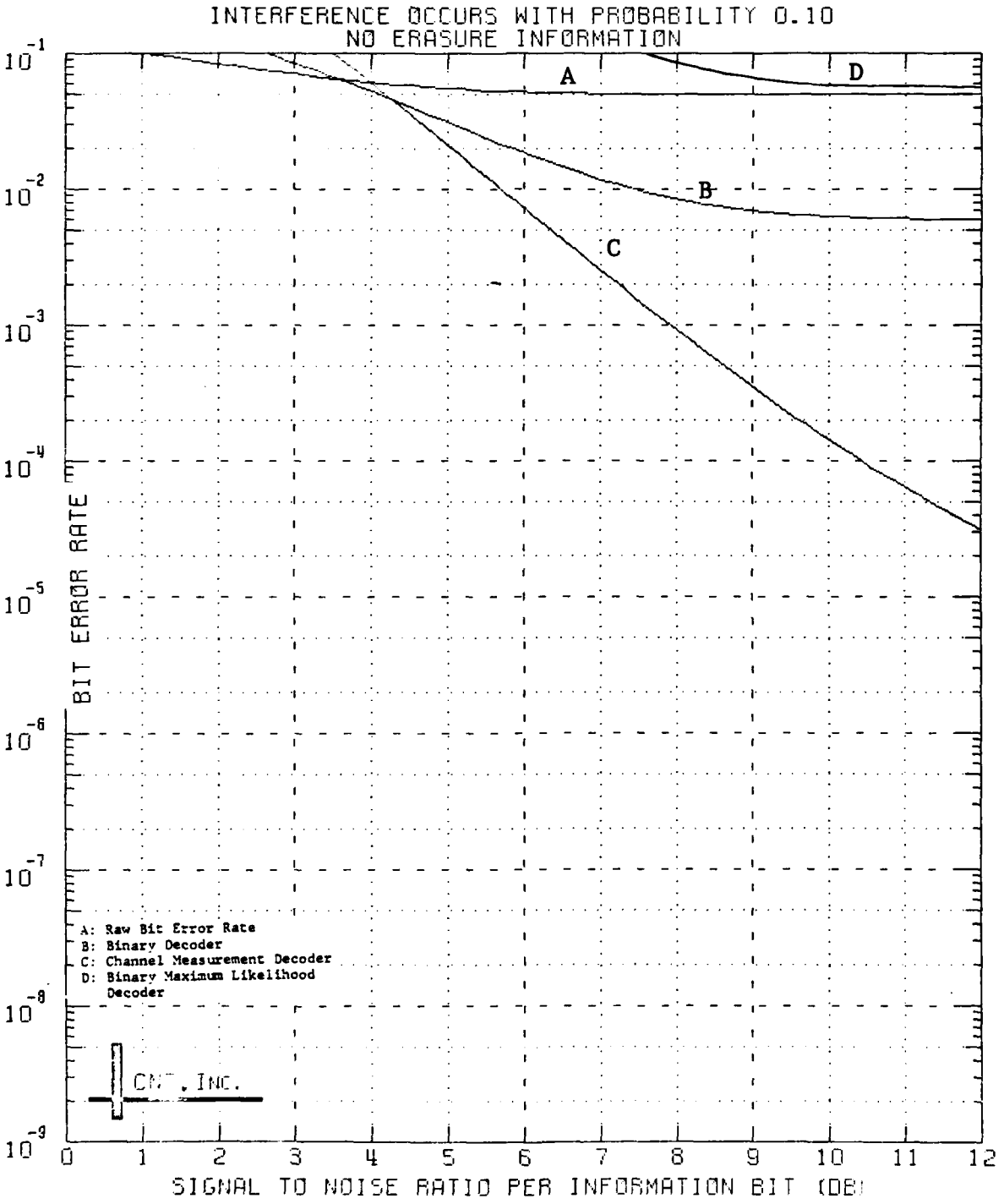


Figure 5.21 Decoded Performance of a Block Code Dimensions (24,12;8)

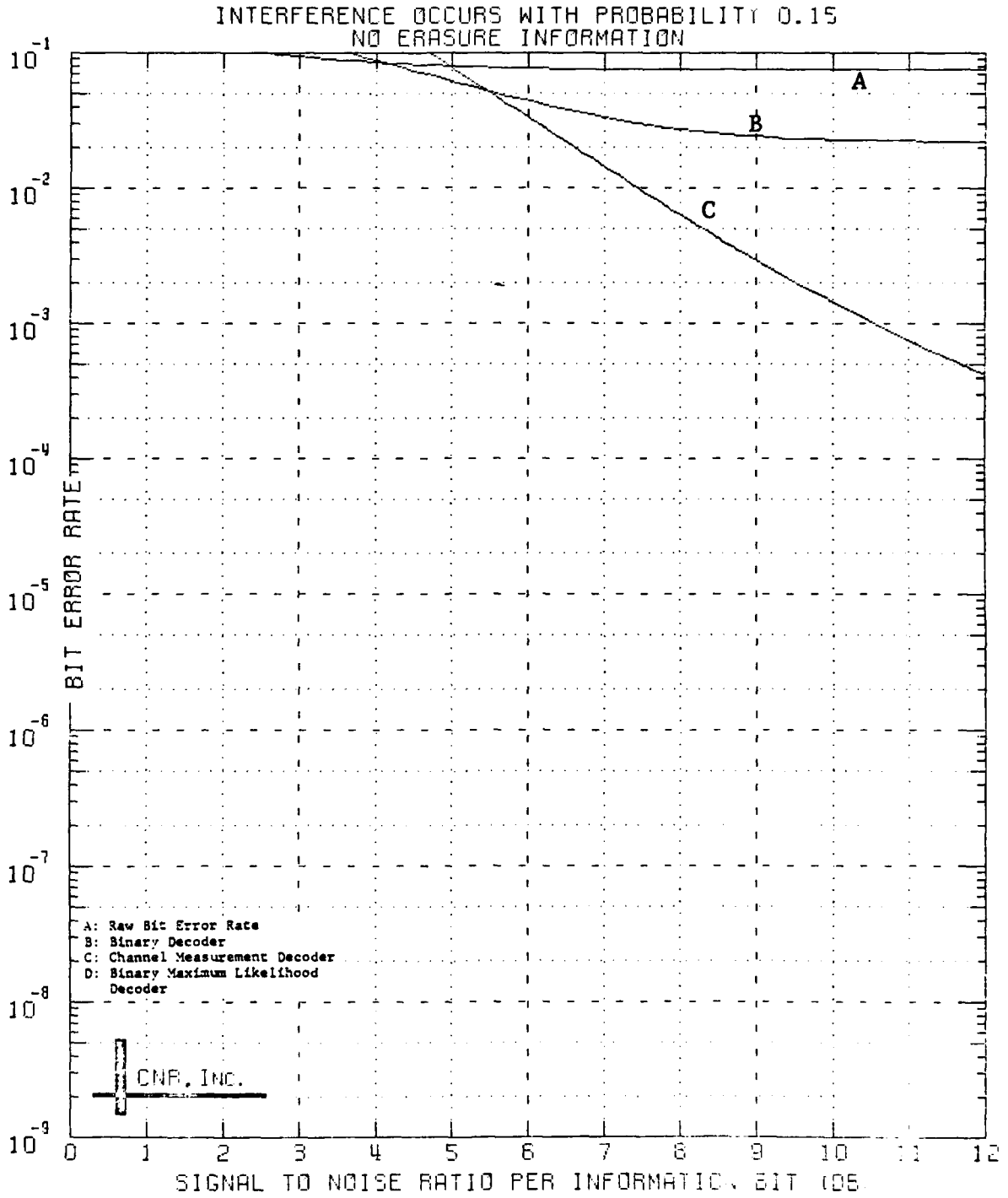


Figure 5.22 Decoded Performance of a Block Code Dimensions (24,12;8)

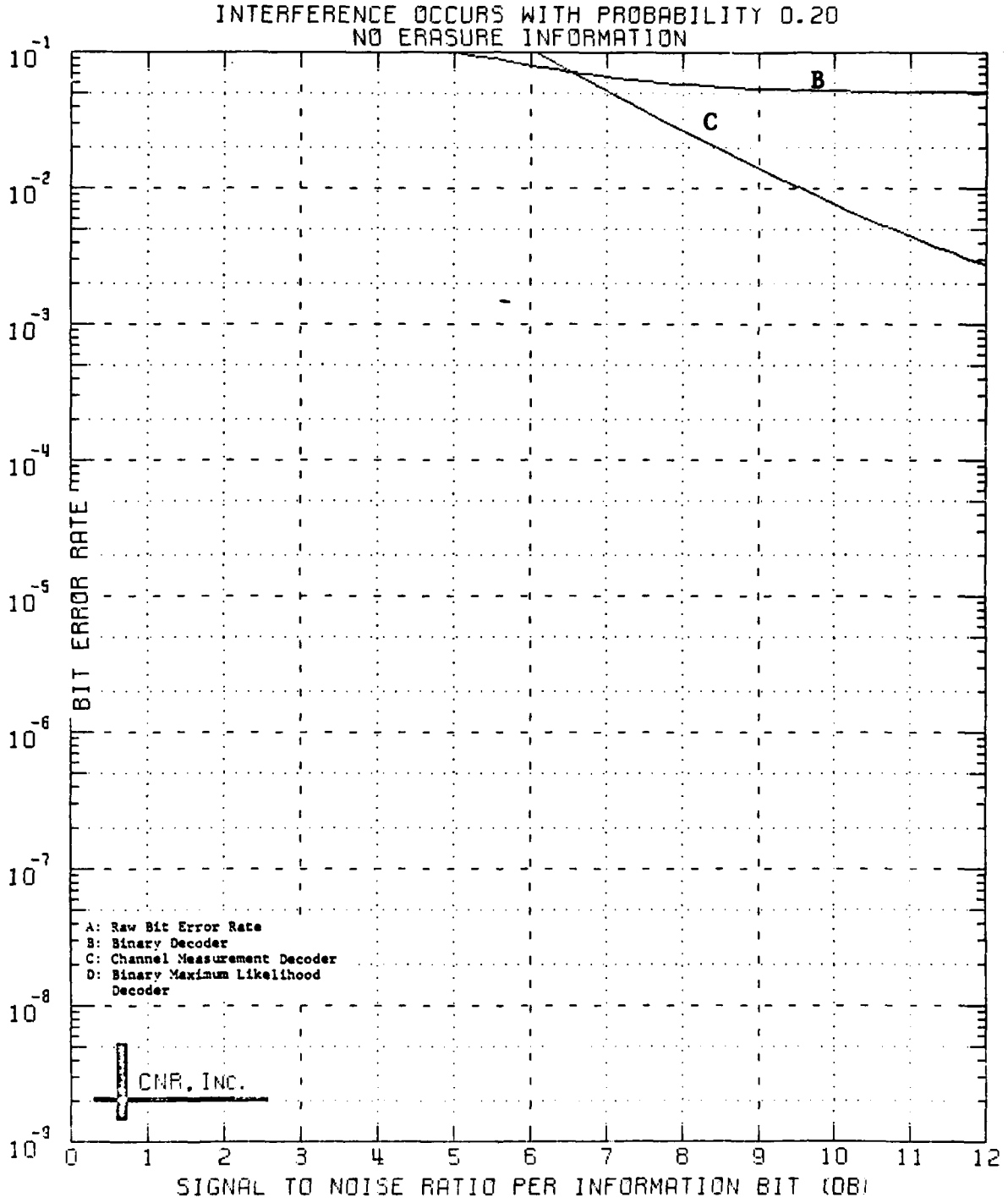


Figure 5.23 Decoded Performance of a Block Code Dimensions (24,12;8)

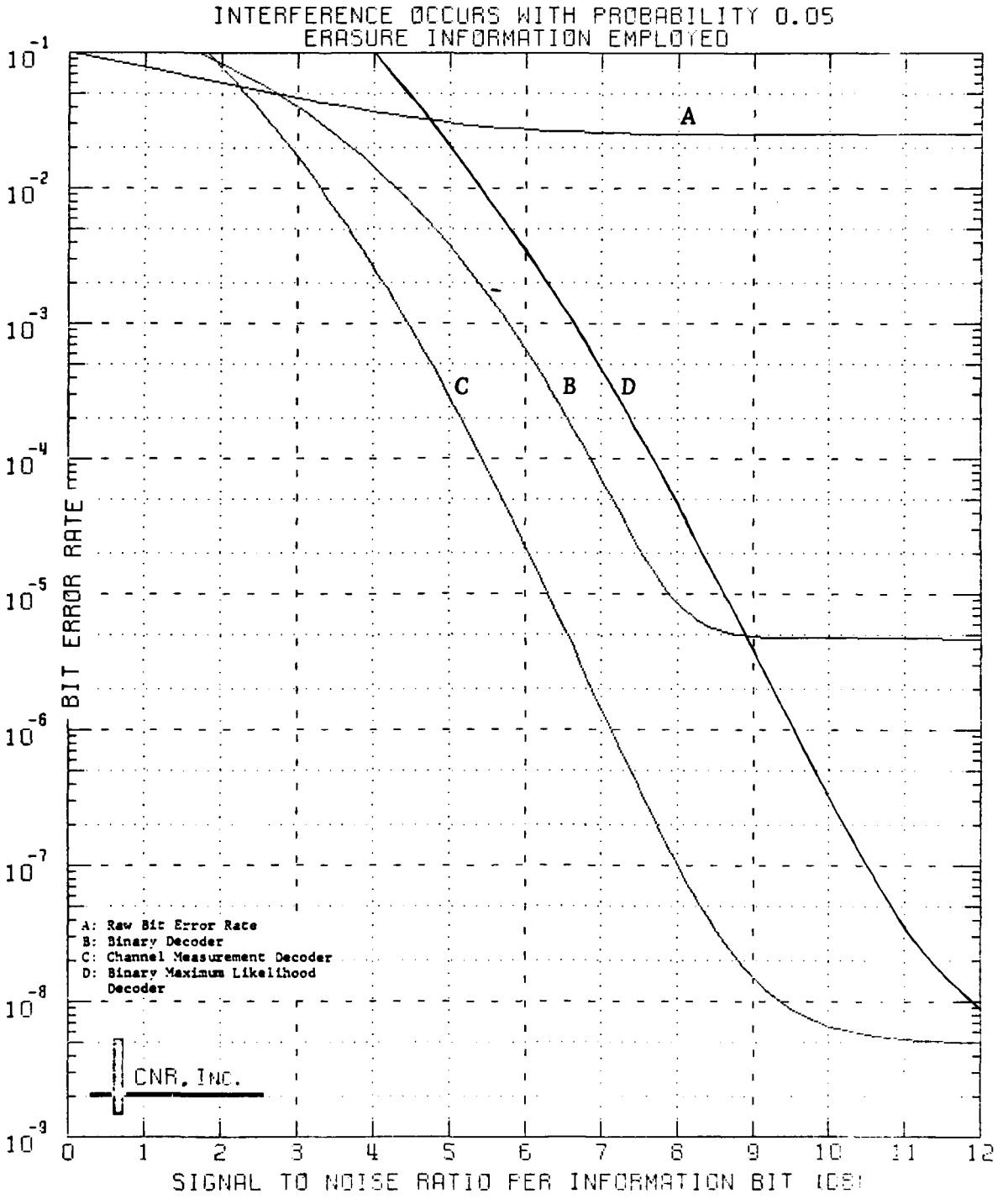


Figure 5.24 Decoded Performance of a Block Code Dimensions (24,12;8)

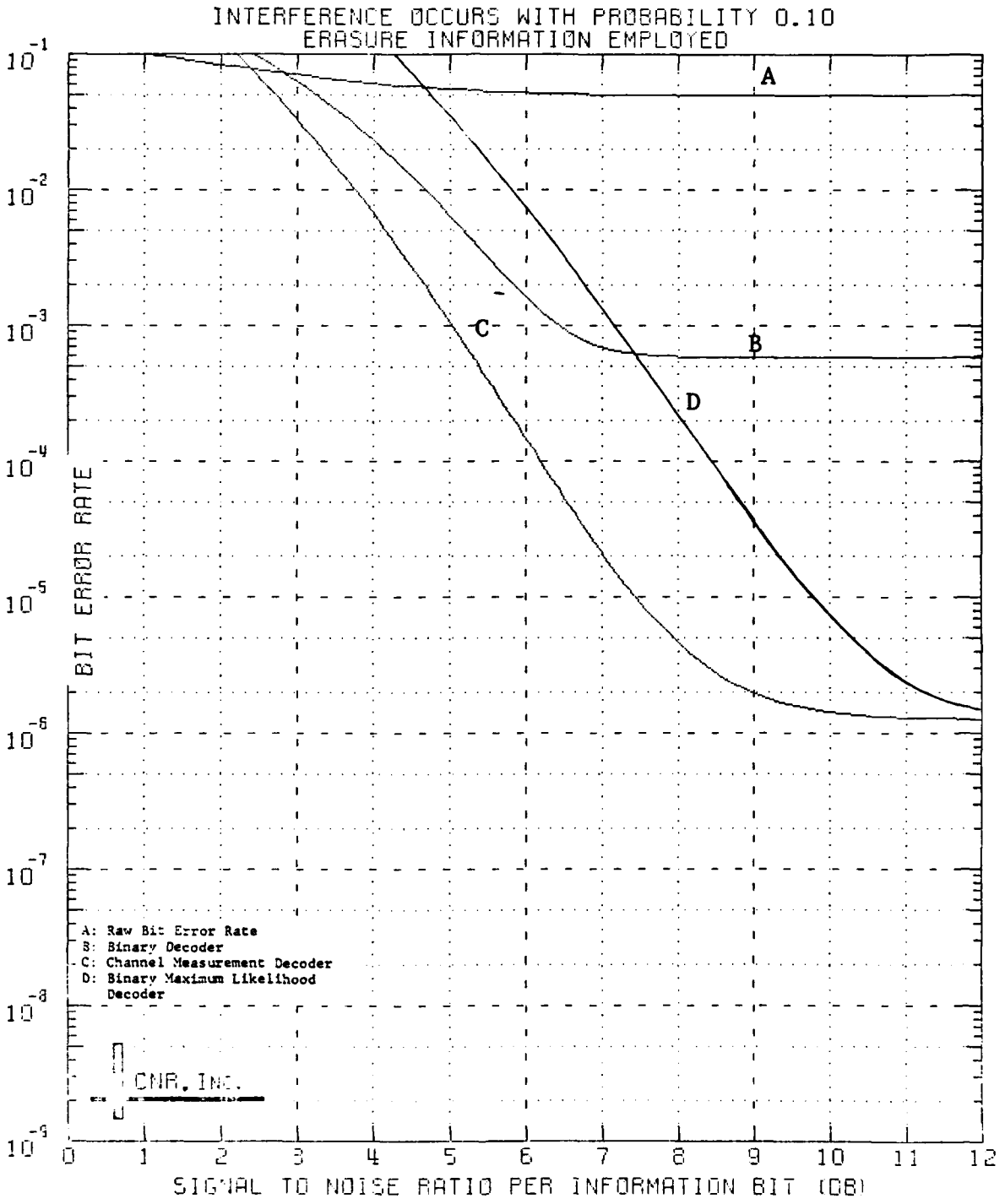


Figure 5.25 Decoded Performance of a Block Code Dimensions (24,12;8)

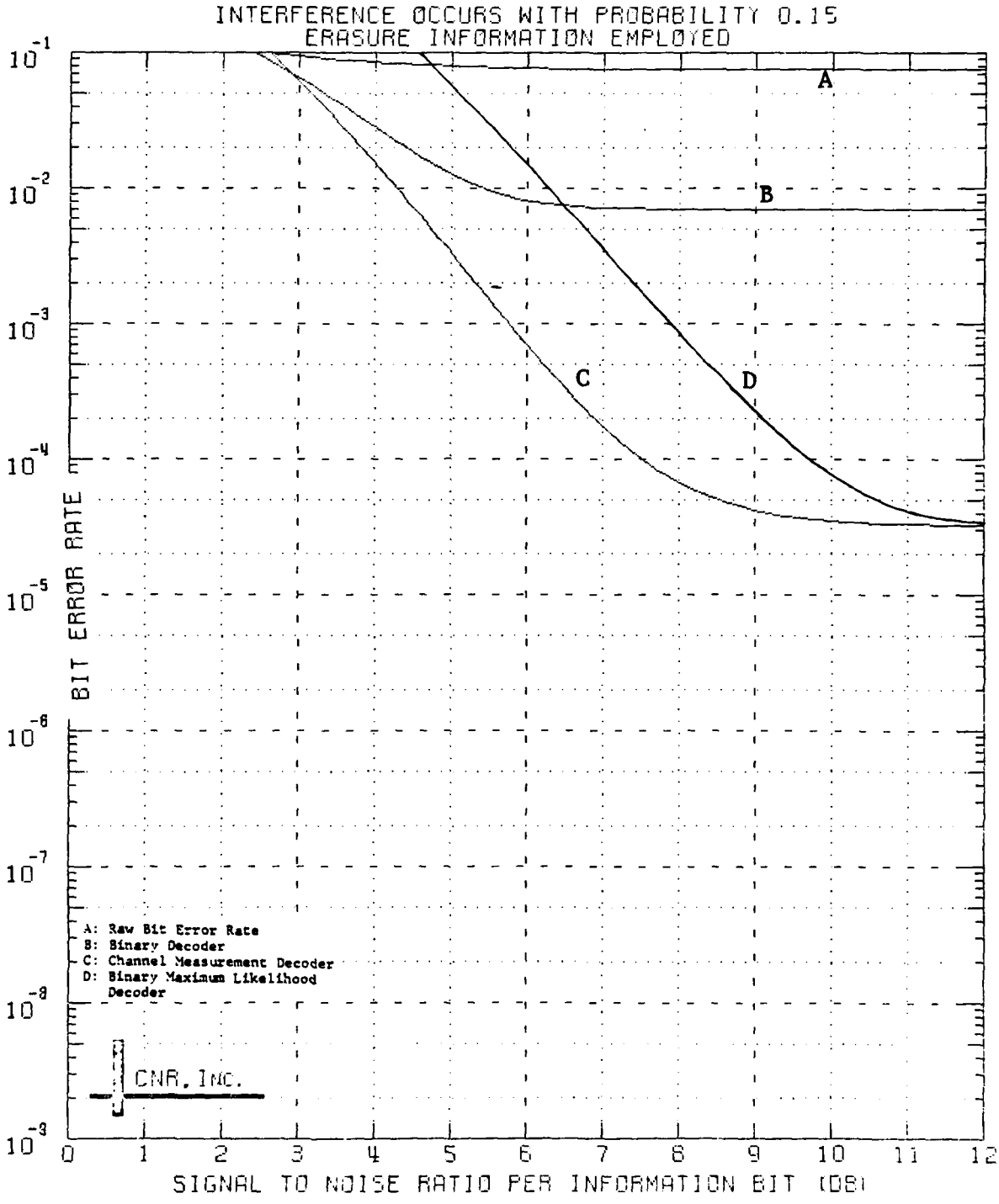


Figure 5.26 Decoded Performance of a Block Code Dimensions (24,12;8)

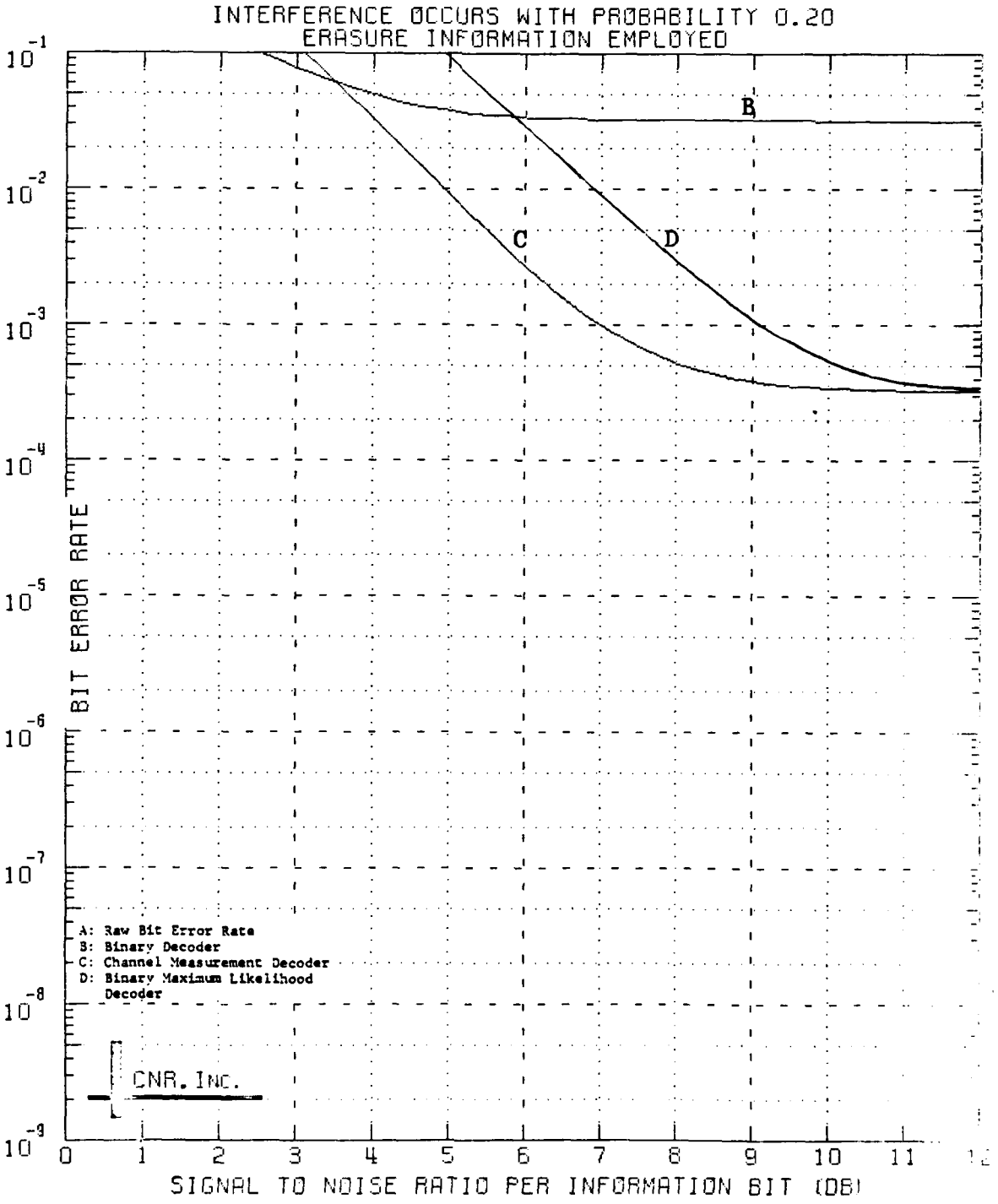


Figure 5.27 Decoded Performance of a Block Code Dimensions (24,12;8)

REFERENCES

[5.1] D. Chase, "Digital Signal Design Concepts for a Time-Varying Rician Channel," IEEE Trans. on Comm., Vol. COM-24, No. 2, pp. 164-172, February 1976.

[5.2] D. Chase, "A Class of Algorithms for Decoding Block Codes With Channel Measurement Information," IEEE Trans. on Information Theory, Vol. IT-18, pp. 170-182, January 1972.

[5.3] B. G. Dorsch, "A Decoding Algorithm for Binary Block Codes and J-ary Output Channels," IEEE Trans. on Information Theory, Vol. IT-20, pp. 391-394, May 1974.

[5.4] L. D. Baumert and R. J. McEliece, "Soft Decision Decoding of Block Codes," Proc. of 1978 International Telemetry Conf. (ITC), pp. 189-195, November 1978.

SECTION 6

PERFORMANCE OF CONVOLUTIONAL CODES IN THE PRESENCE OF INTERFERENCE

The performance for maximum likelihood decoding of the constraint length 7 convolutional codes is given in this section. Results are given for the four interference models under consideration and for code rates of 1/2, 1/4, 1/8, 1/16, and 1/32. These results follow from the analyses given in Sections 4.2 and 4.3.

Following the format introduced in Section 5, Figures 6.1 to 6.5 illustrate the results for rate-1/2 convolutional codes when no erasure information is present. The results for the case when an external erasure signal, coincident with the interference, are given in Figures 6.6 to 6.9. These results are quite comparable to those obtained for the block codes in Section 5. The (128,64) BCH code generally out performs the K=7 convolutional code and the Golay code offers somewhat inferior performance to the convolutional code.

As discussed in Section 4, the lower rate convolutional codes are obtained by simply repeating the taps, and thus, the unquantized additive noise performance (with no interference) is unchanged. However, the performance in the presence of interference improves as the code rate is reduced. Figures 6.10 to 6.18 illustrate the results from the rate-1/4 convolutional code and Figures 6.19 to 6.27 illustrate the corresponding results for the rate-1/8 convolutional code.

In order to compare convolutional coding results of different rates operating in the presence of different levels of interference, results have been tabulated in terms of the required E_b/N_0 for an error rate of 10^{-5}. A — on Table 6-1 indicates that this probability of error is not achievable for the given set of conditions. The notation BD indicates binary decoding and the notation CD indicates that a channel measurement decoder is used.

The results on Table 6-1 are illustrated in Figures 6.28, 6.29, 6.30 and 6.31 for the following four-channel models:

i) Channel Measurement Decoding - No Erasure Information

ii) Binary Decoding - No Erasure Information

iii) Channel Measurement Decoding - Erasure Information Available

iv) Binary Decoding - Erasure Information Available

Each curve is for a different code rate. The same results are illustrated in Figures 6.32, 6.33, 6.34, and 6.35 when a fixed value of δ is used for each curve.

These figures may be compared with the theoretical capacity results [6.1] given in Figures 6.36, 6.37, 6.38, and 6.39.

The general conclusions for the theoretical capacity results are applicable to the practical convolutional coding results. The importance of low rate codes and the advantage of erasure information (when available) is clear from both the practical and theoretical results.

It should be noted that these results have been obtained on an unquantized channel. As noted in Appendix B, a significant loss can result if a "standard" 3-bit quantizer is used when operating in the presence of interference without erasure information.

The results obtained in this section, based on our worst-case models, can be compared to the results given in Appendix A for rate-1/2 and 1/4 convolutional codes operating in the presence of the less severe average power-limited jamming model. Clearly, the choice of interference models can have a dramatic impact on the expected results. Thus, we have chosen to emphasize the worst-case interference models in this report since, in practice, the true characterization of the actual jamming waveform may be quite difficult.

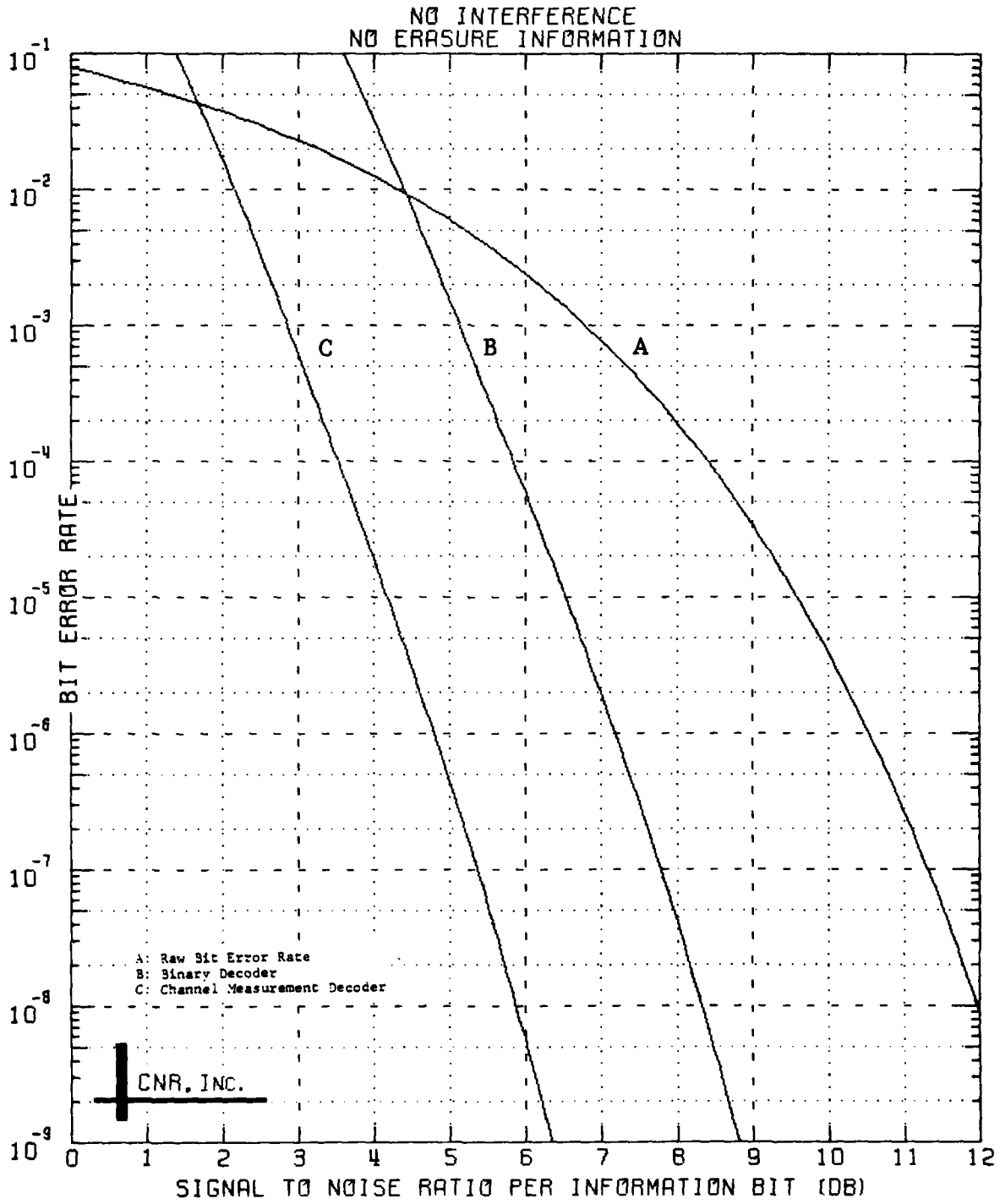


Figure 6.1 Decoded Performance of a Convolutional Code Rate 1/2; Constraint Length = 7

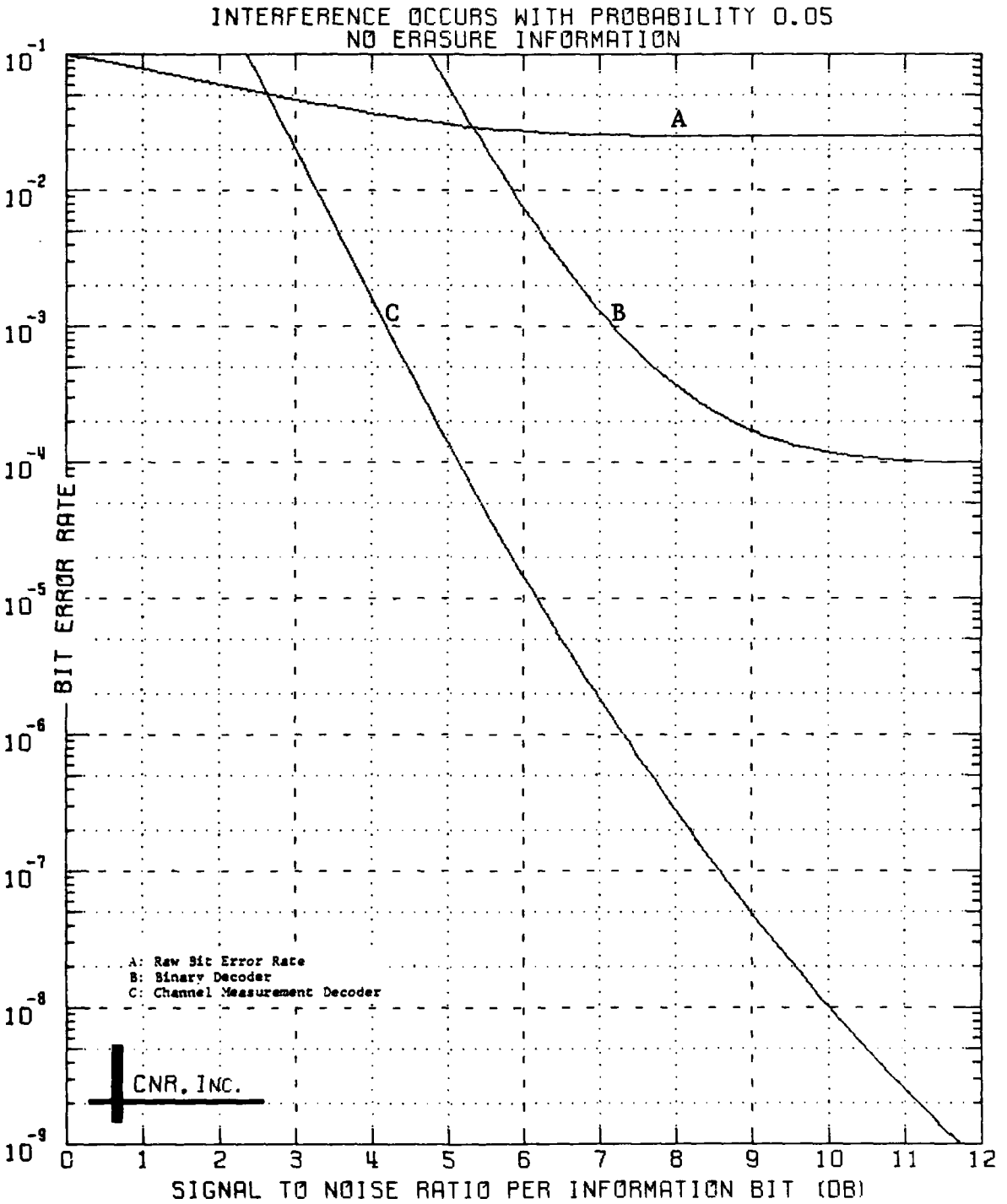


Figure 6.2 Decoded Performance of a Convolutional Code Rate 1/2; Constraint Length = 7

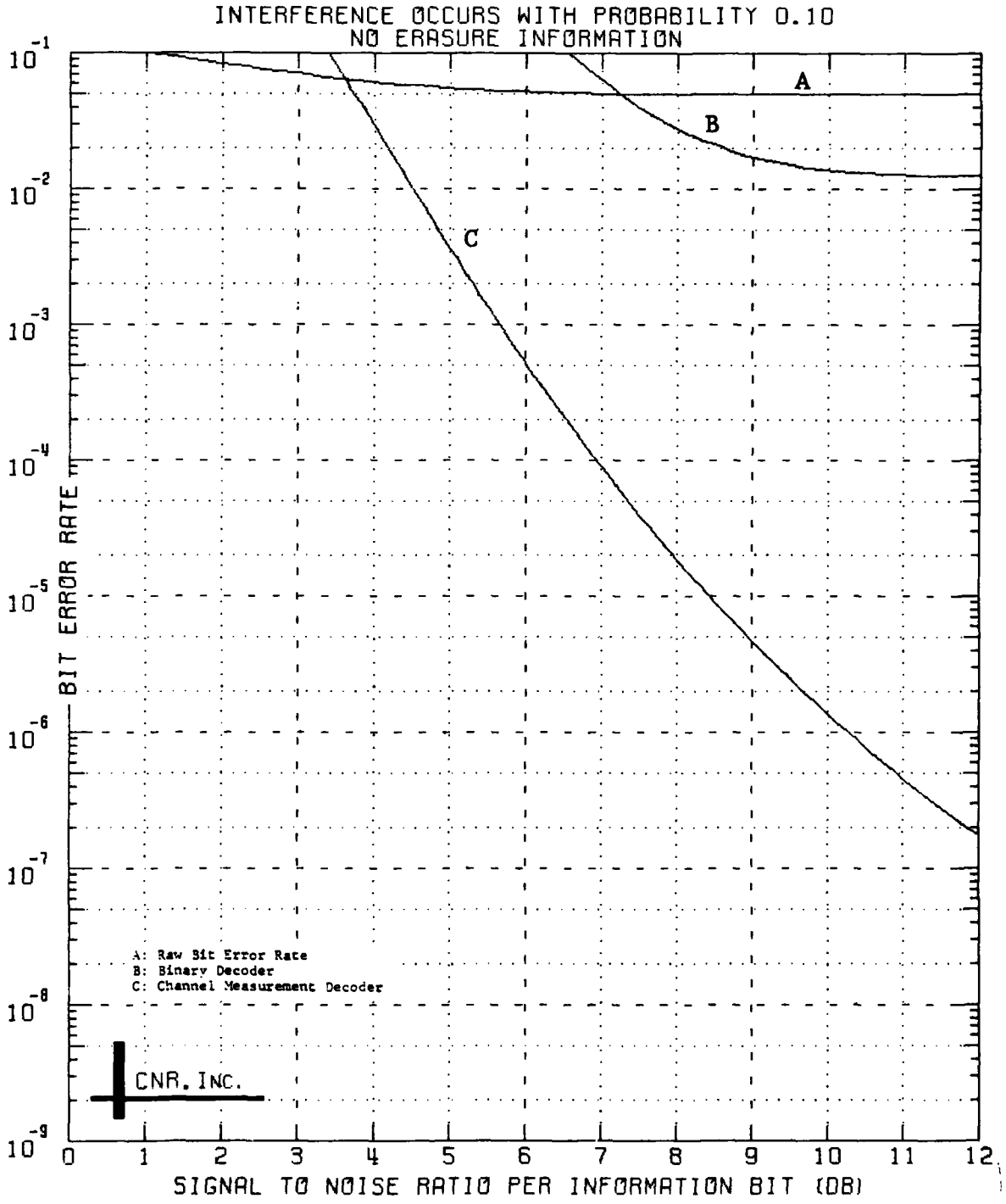


Figure 6.3 Decoded Performance of a Convolutional Code Rate 1/2; Constraint Length = 7

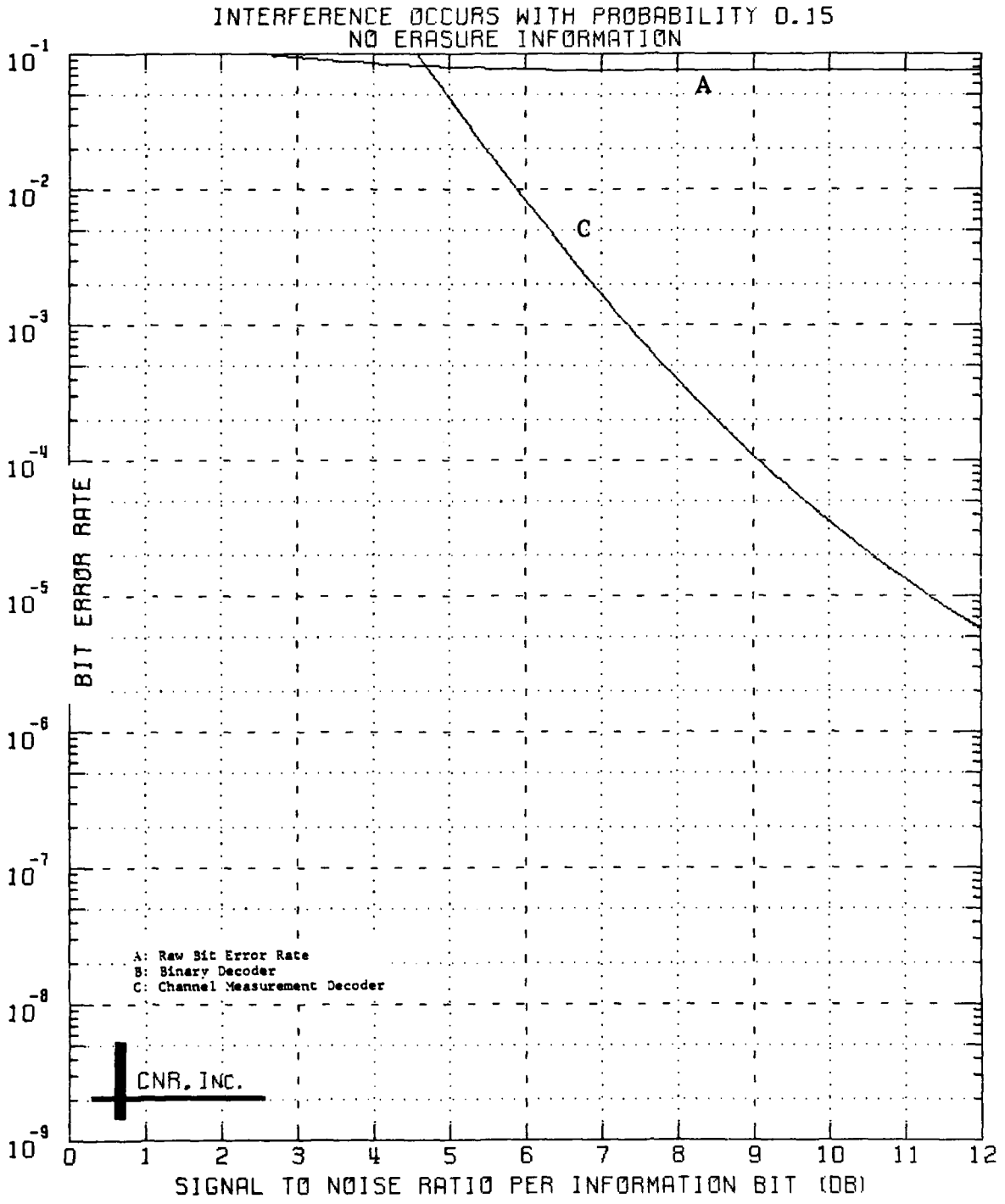


Figure 6.4 Decoded Performance of a Convolutional Code Rate 1/2; Constraint Length = 7

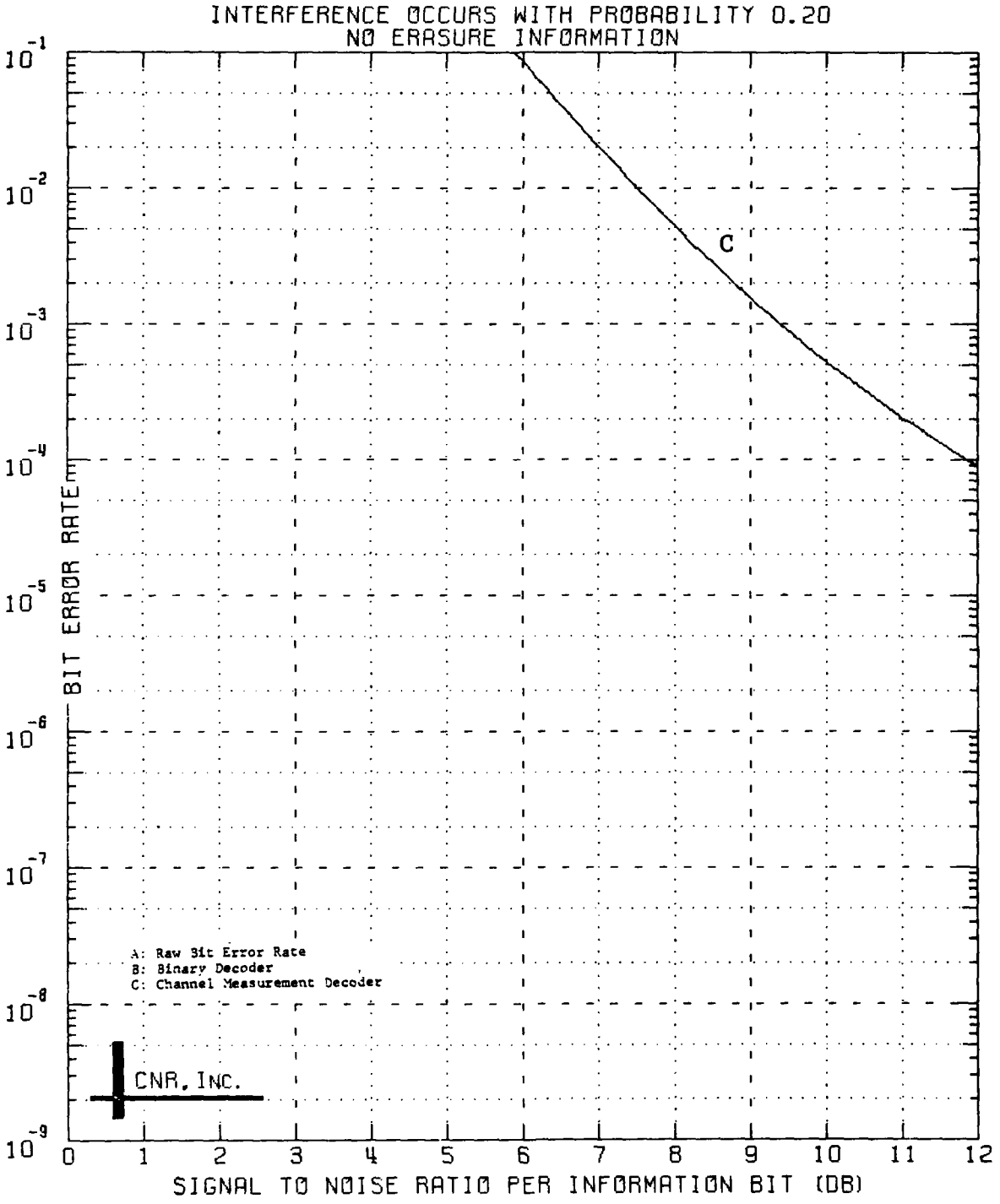


Figure 6.5 Decoded Performance of a Convolutional Code Rate 1/2; Constraint Length = 7

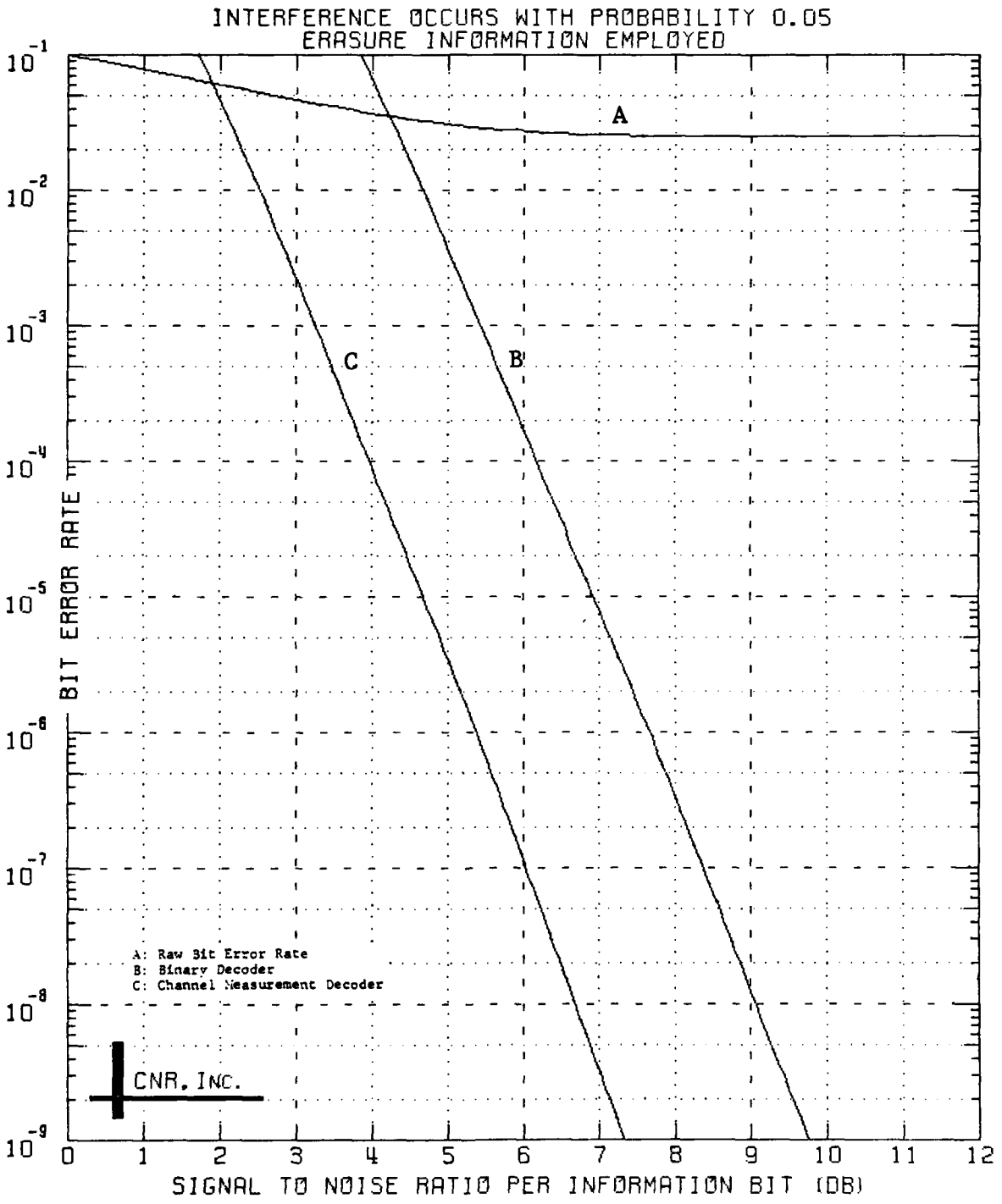


Figure 6.6 Decoded Performance of a Convolutional Code Rate 1/2; Constraint Length = 7

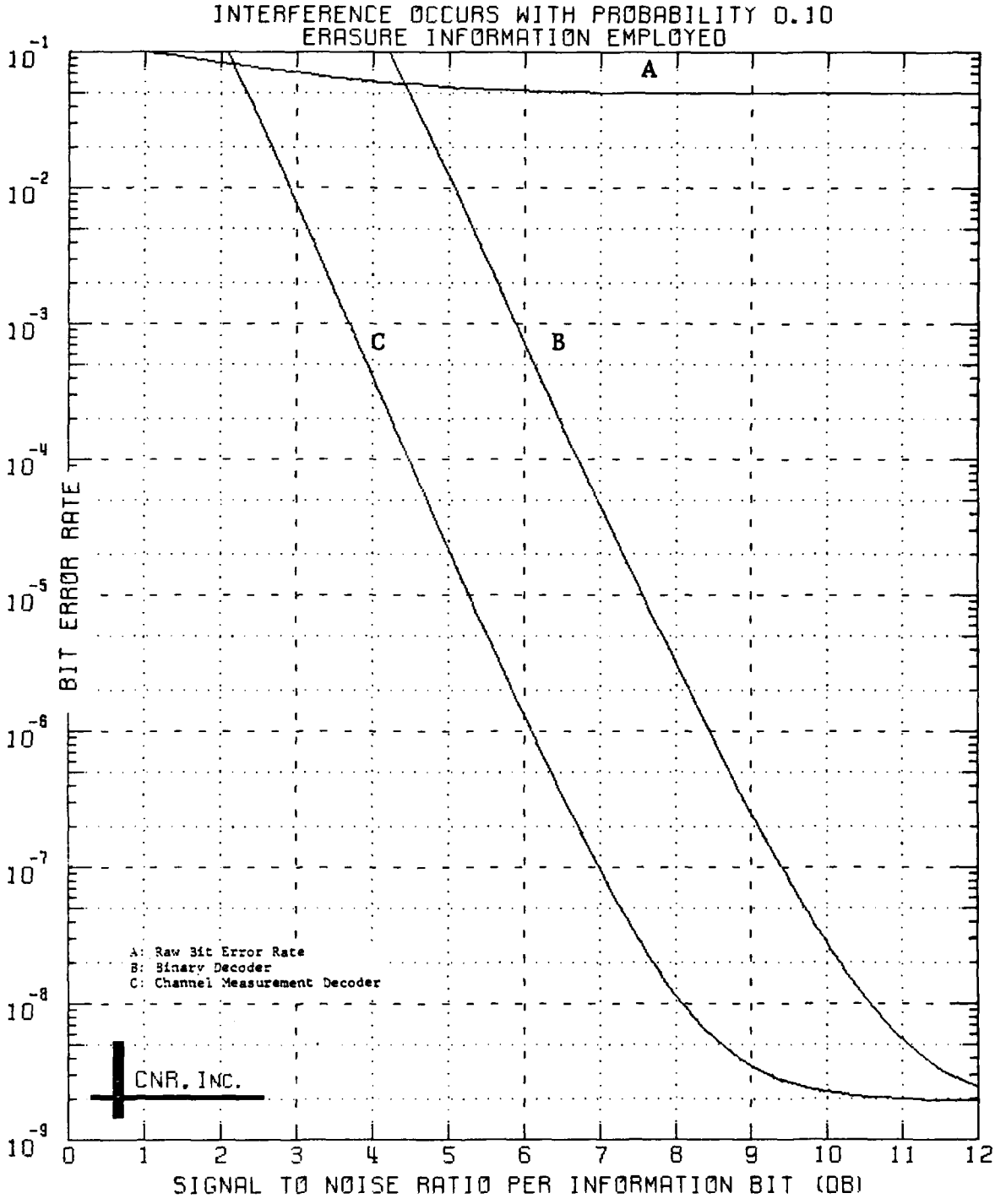


Figure 6.7 Decoded Performance of a Convolutional Code Rate 1/2; Constraint Length = 7

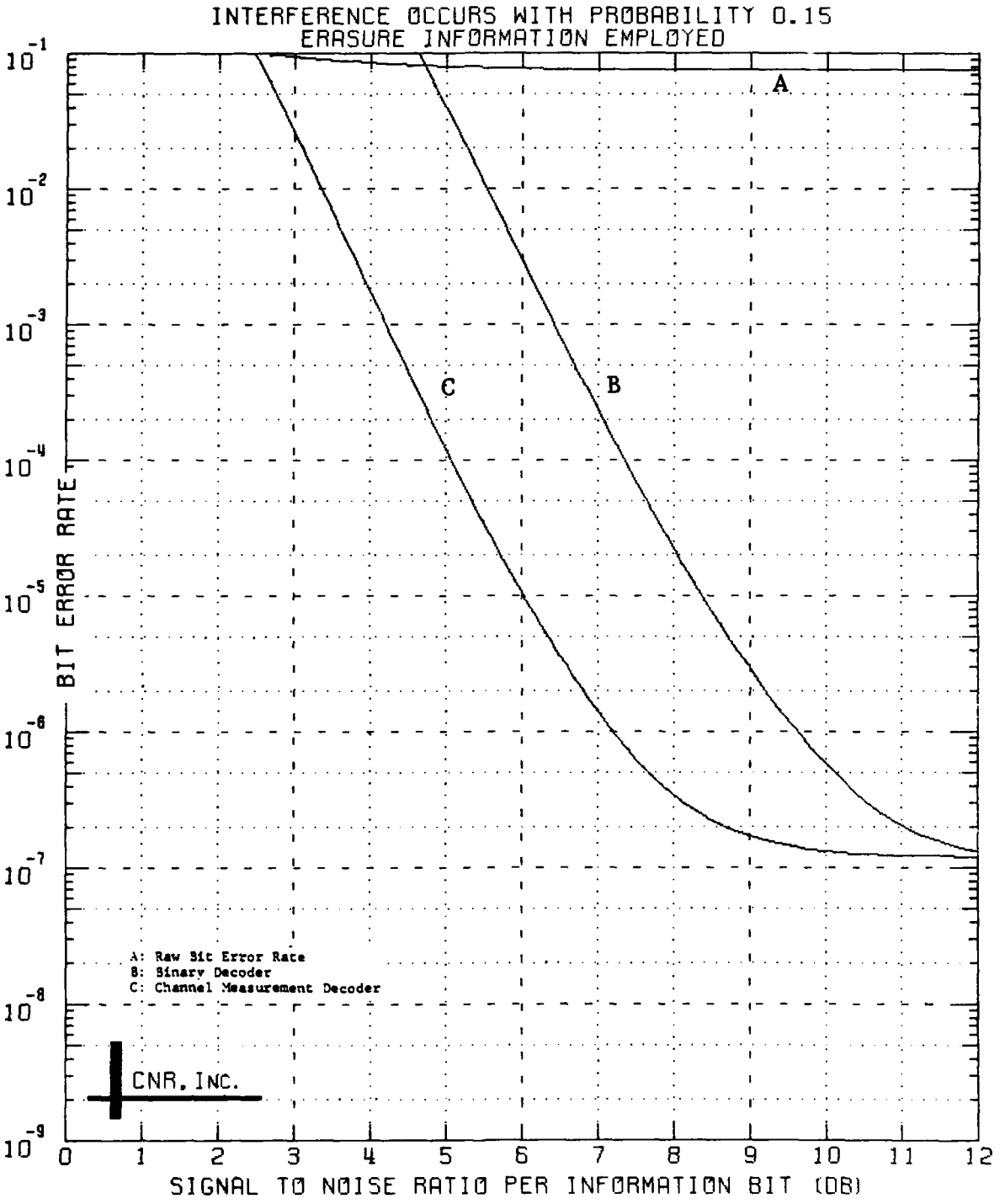


Figure 6.8 **Decoded Performance of a Convolutional Code Rate 1/2; Constraint Length = 7**

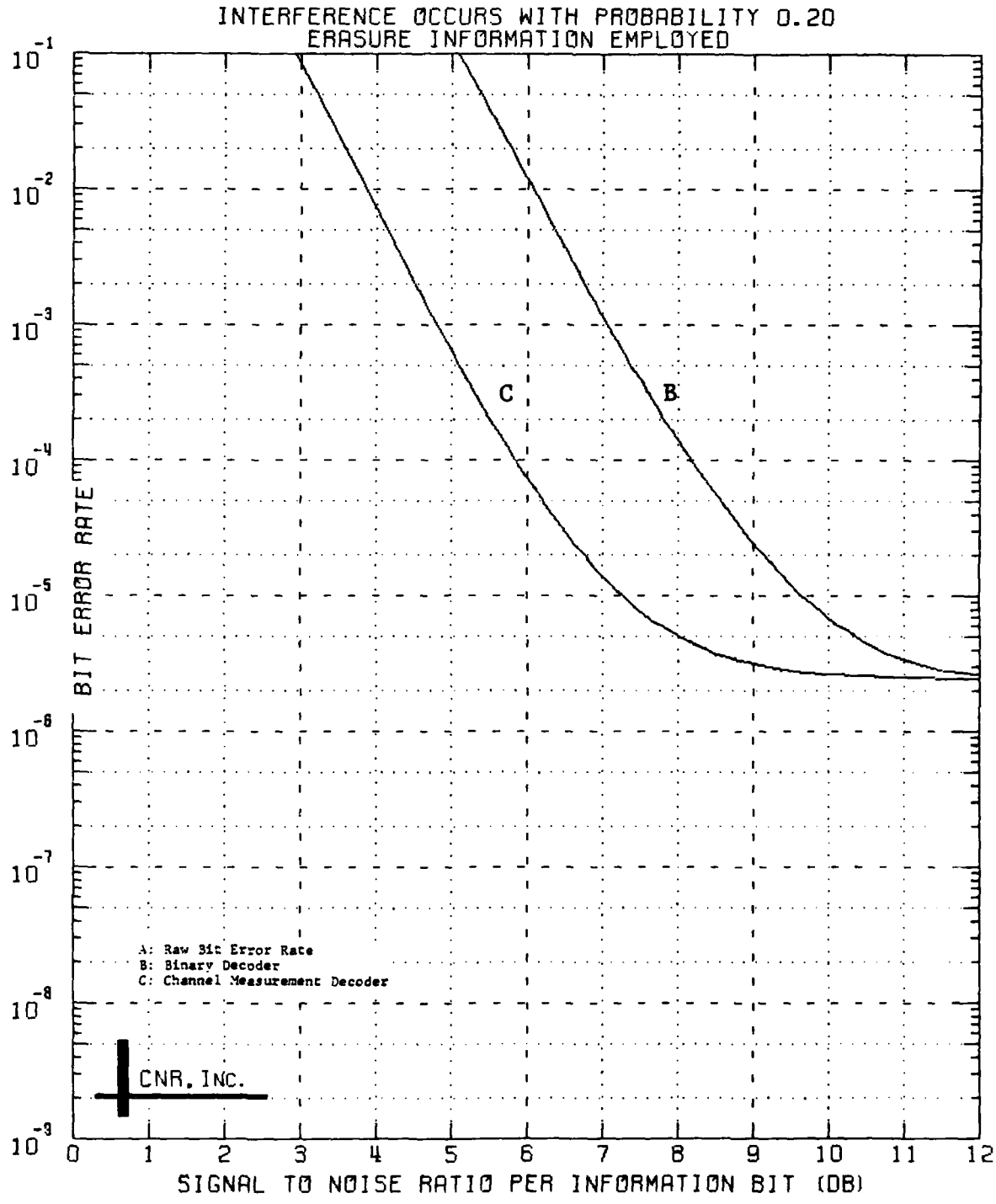


Figure 6.9 Decoded Performance of a Convolutional Code Rate 1/2; Constraint Length = 7

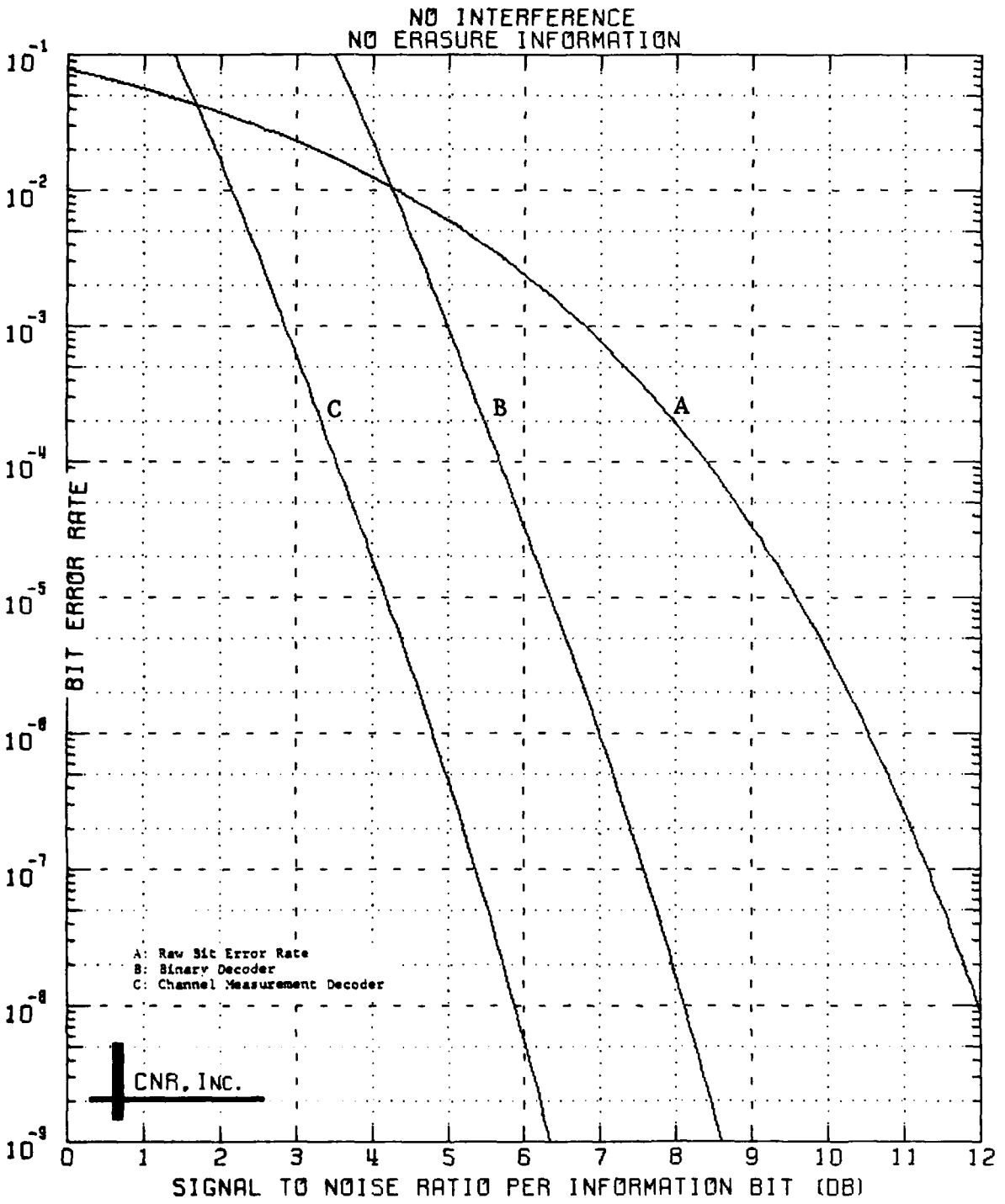


Figure 6.10 Decoded Performance of a Convolutional Code Rate 1/4; Constraint Length = 7

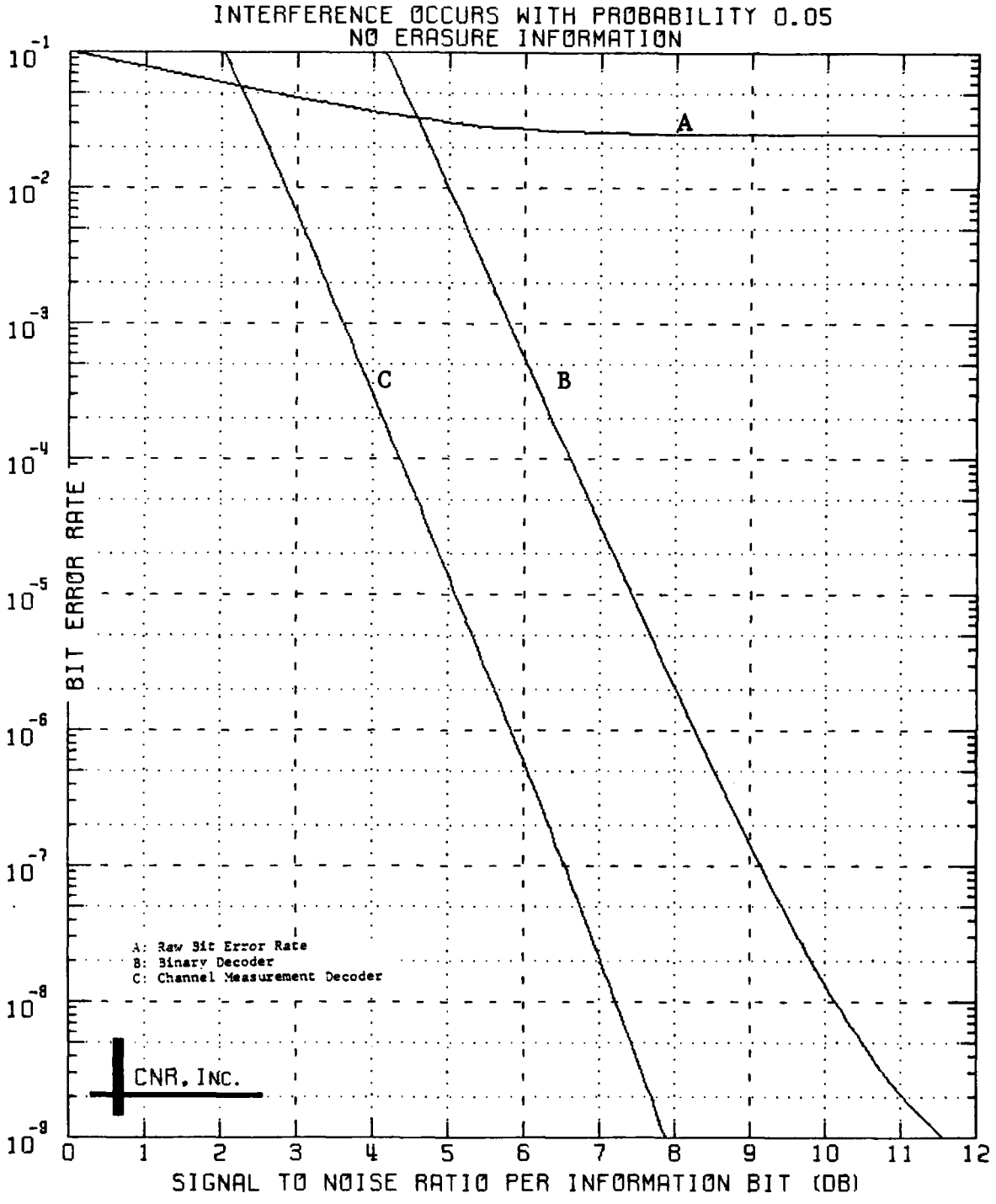


Figure 6.11 Decoded Performance of a Convolutional Code Rate 1/4; Constraint Length = 7

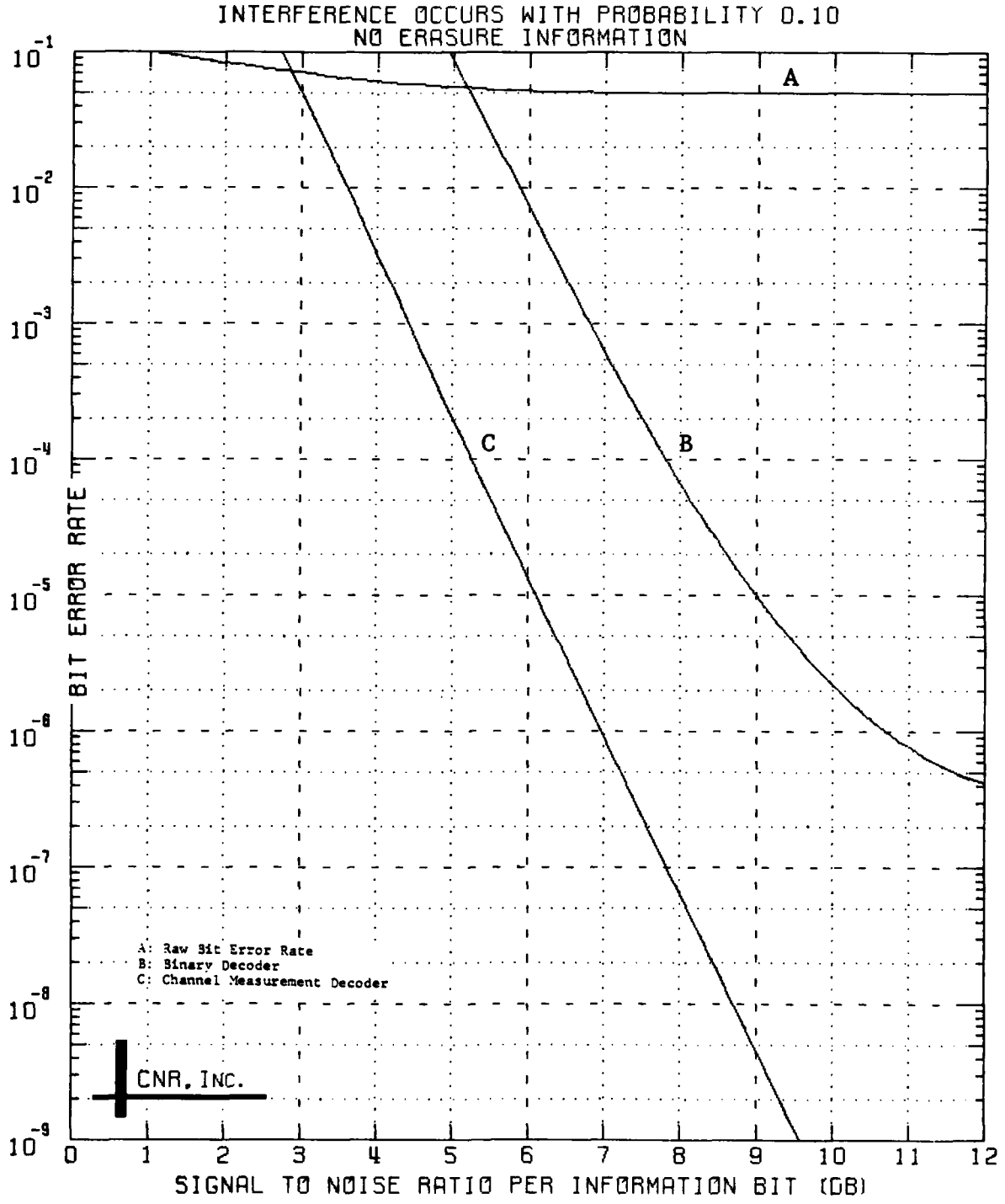


Figure 6.12 Decoded Performance of a Convolutional Code Rate 1/4; Constraint Length = 7

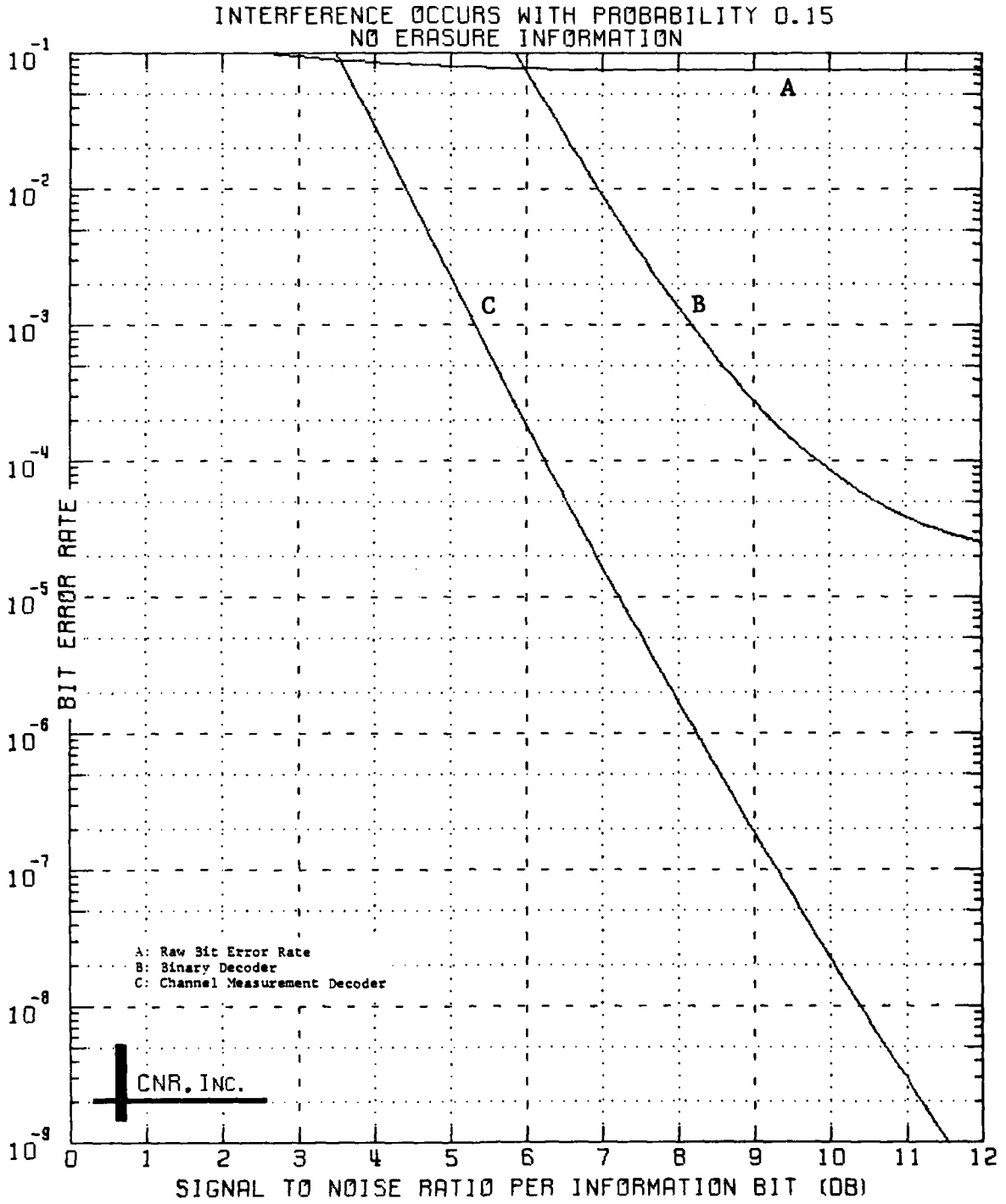


Figure 6.13 Decoded Performance of a Convolutional Code Rate 1/4; Constraint Length = 7

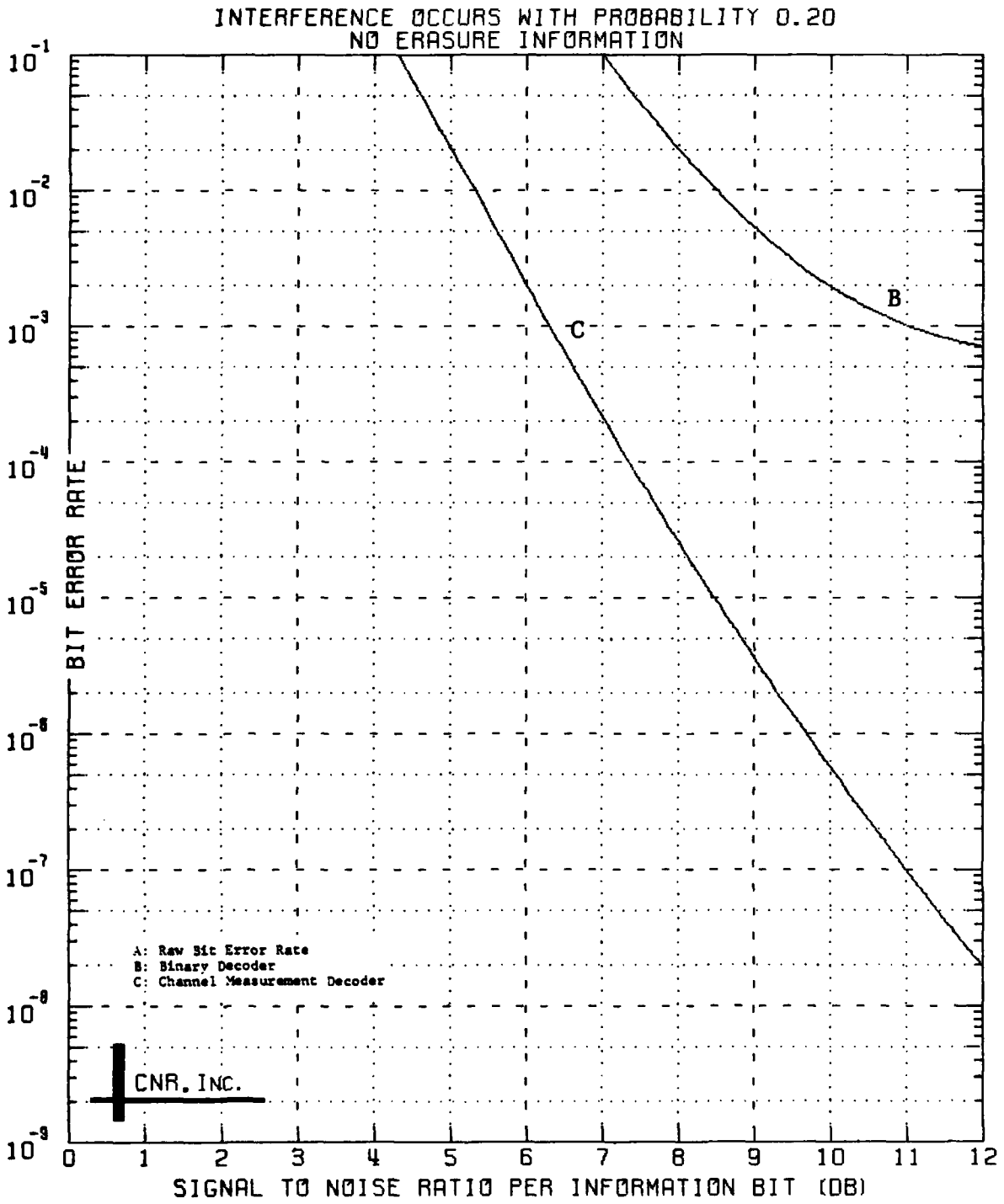


Figure 6.14 Decoded Performance of a Convolutional Code Rate 1/4; Constraint Length = 7

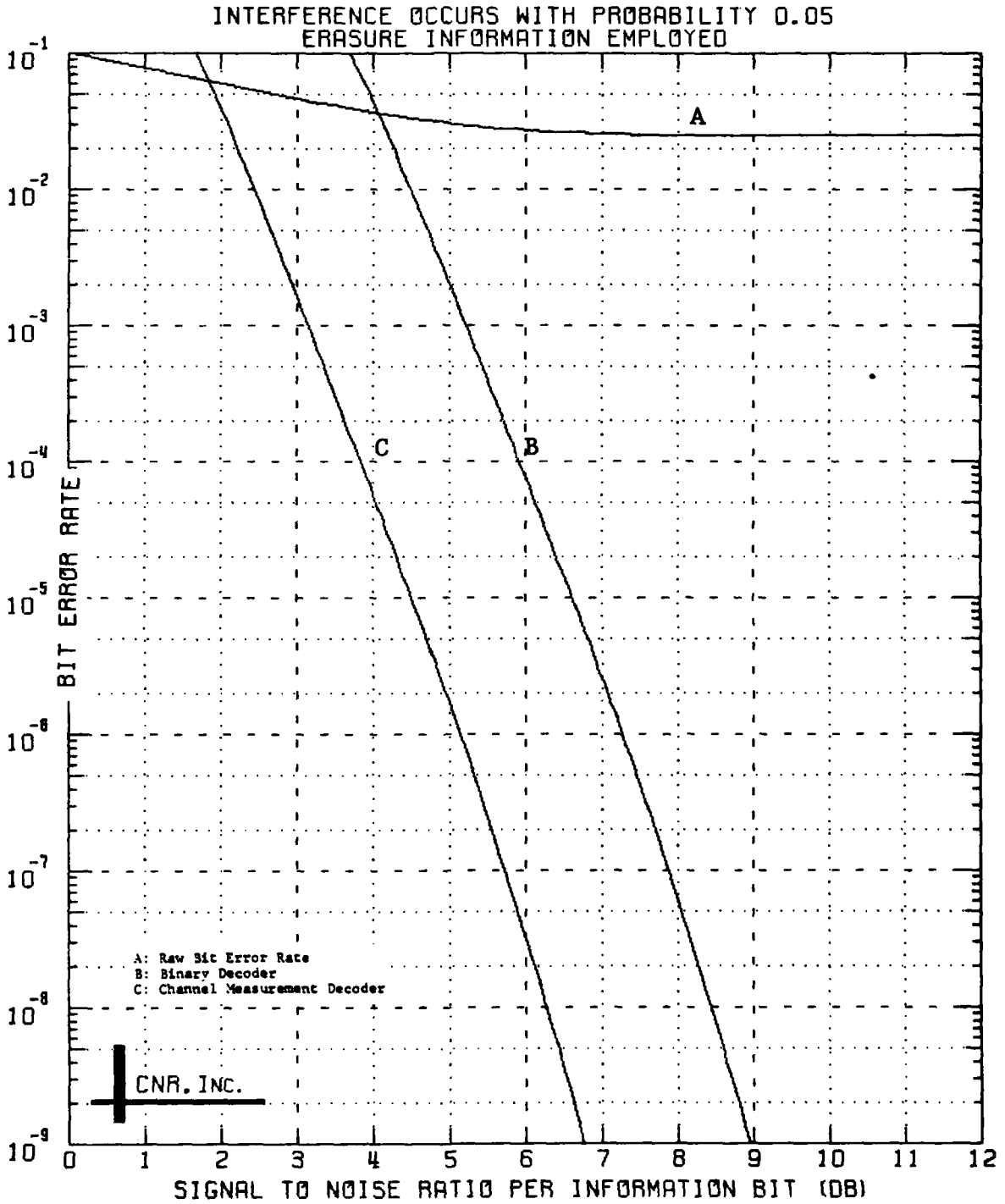


Figure 6.15 Decoded Performance of a Convolutional Code Rate 1/4; Constraint Length = 7

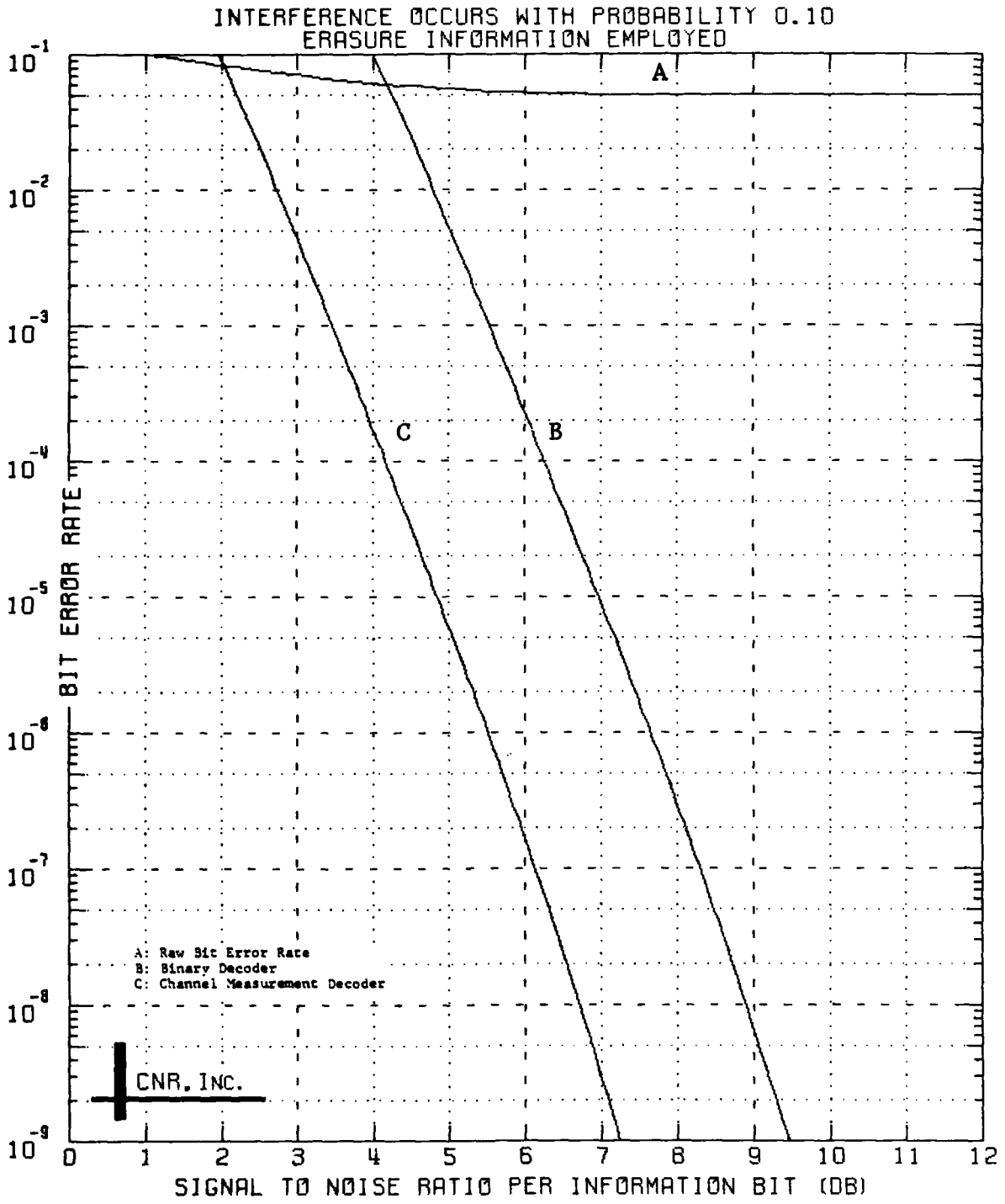


Figure 6.16 Decoded Performance of a Convolutional Code Rate 1/4; Constraint Length = 7

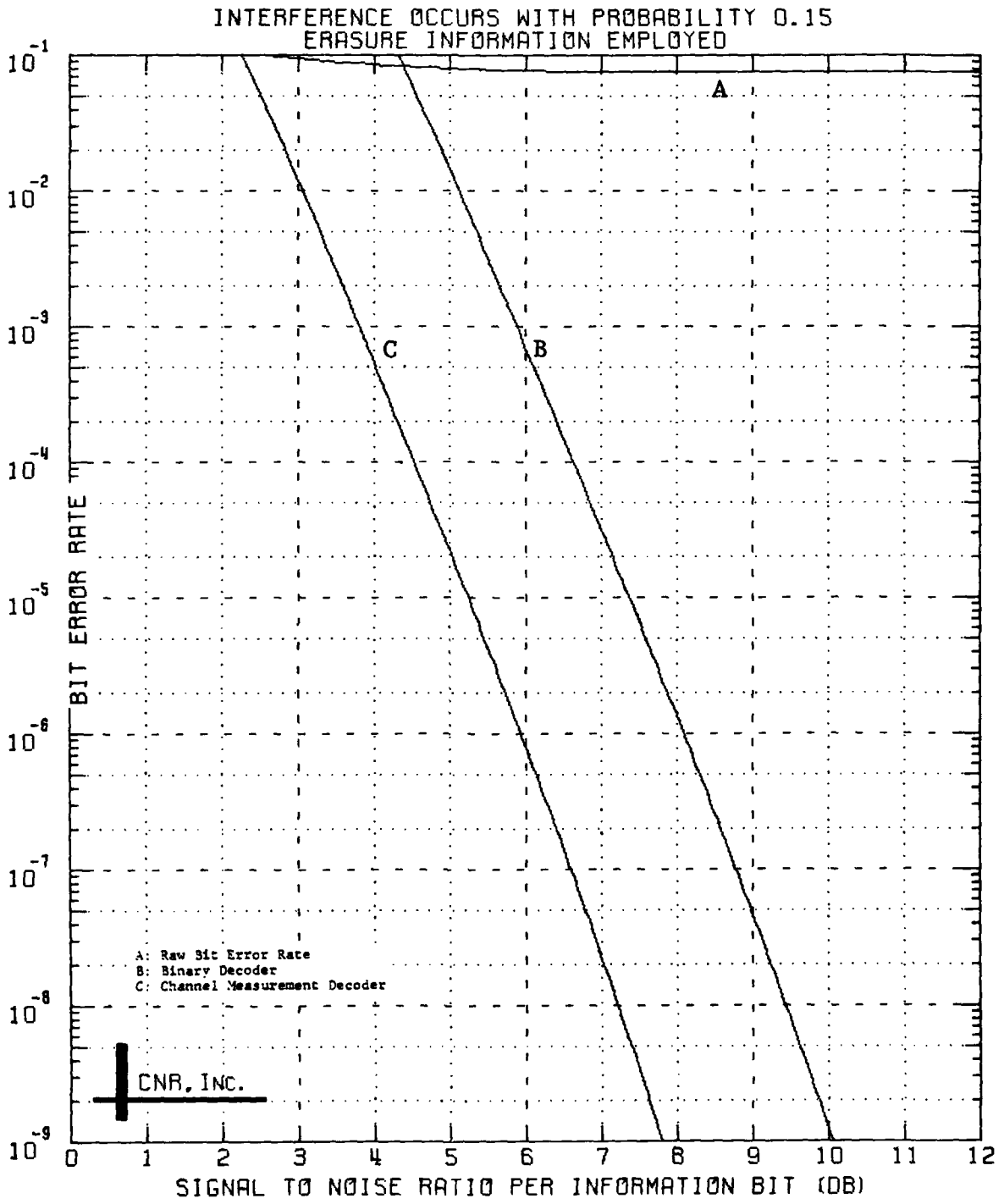


Figure 6.17 Decoded Performance of a Convolutional Code Rate 1/4; Constraint Length = 7

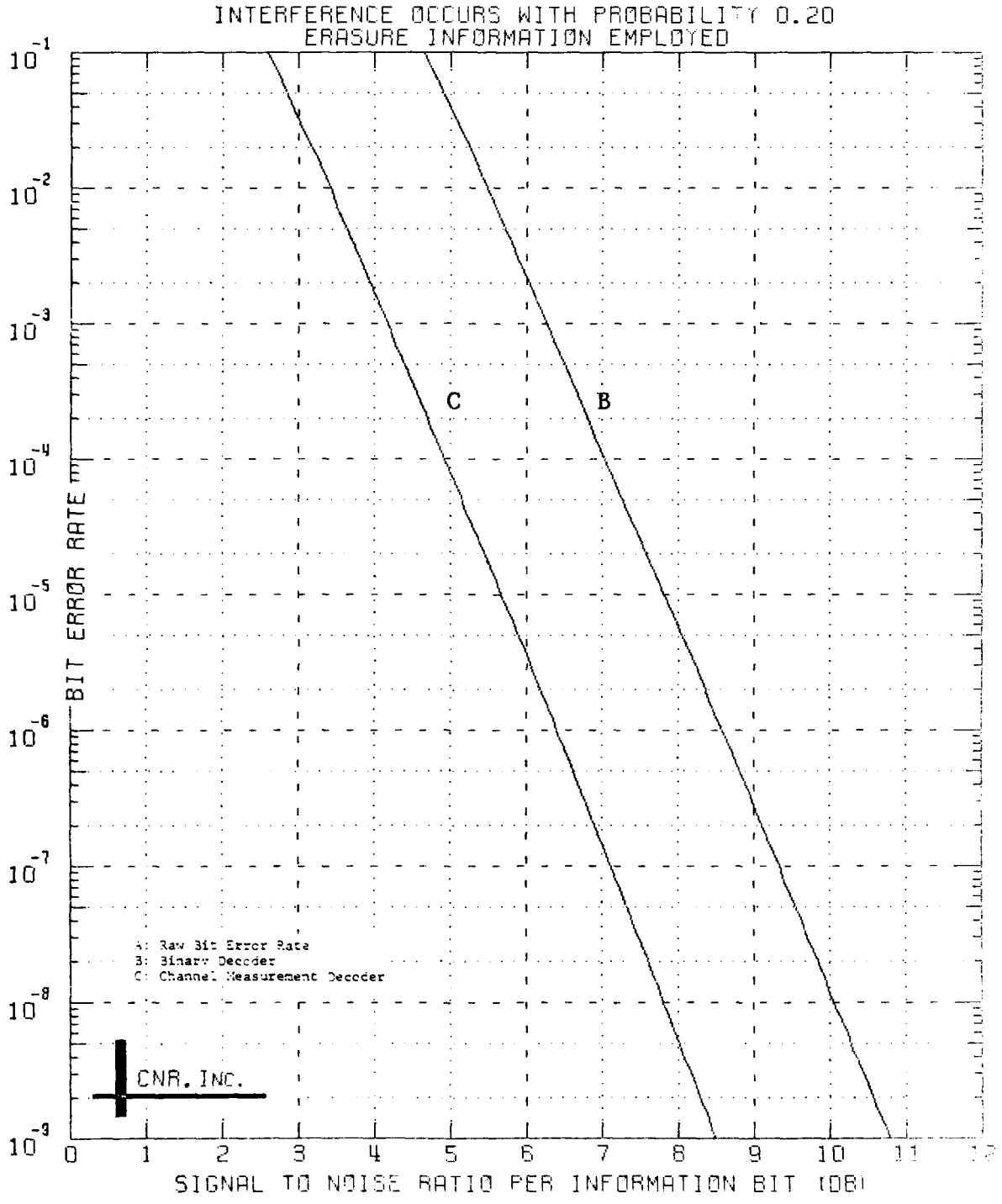
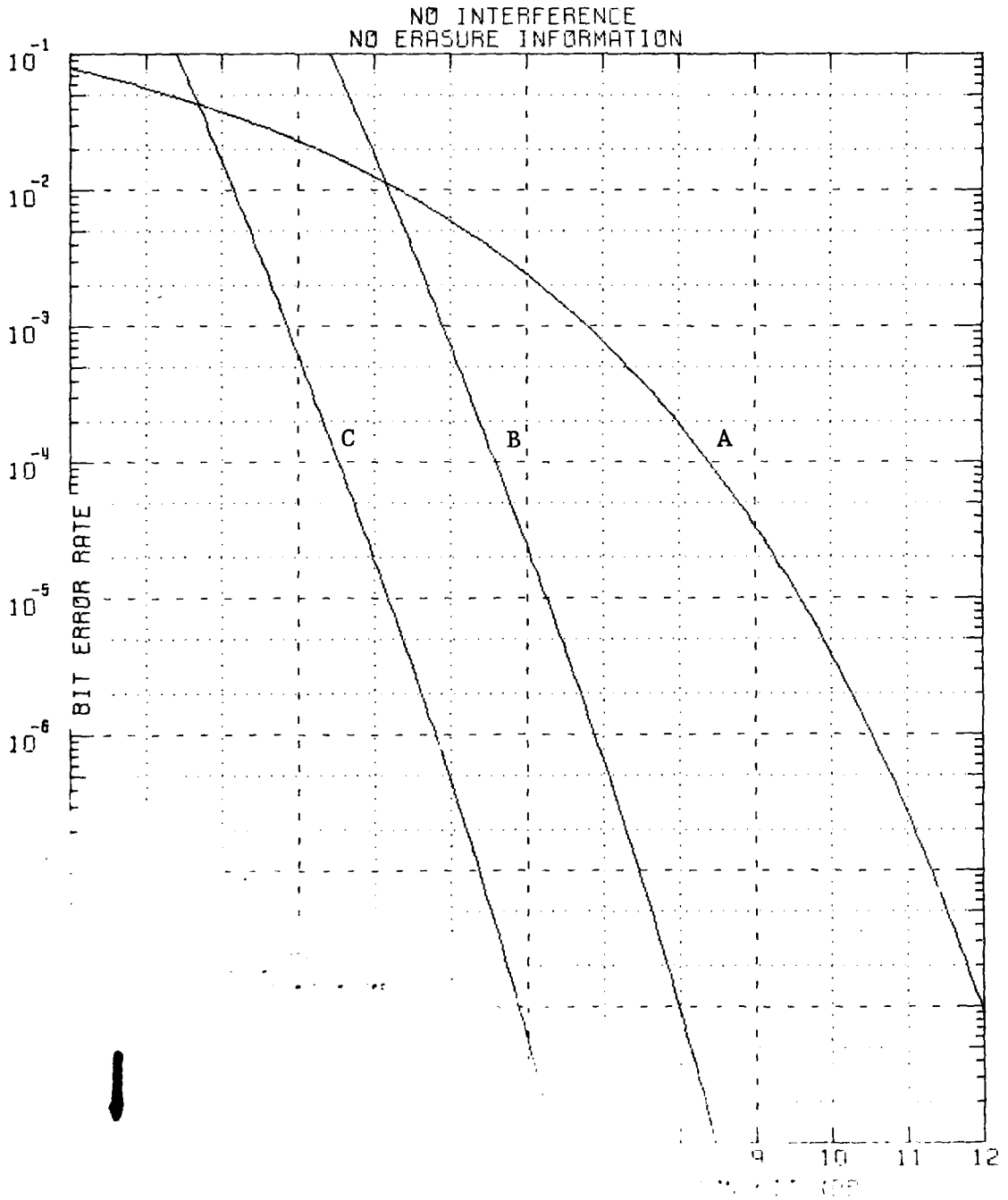


Figure 6.18 Decoded Performance of a Convolutional Code Rate 1/4; Constraint Length = 7



...nvolutional Code

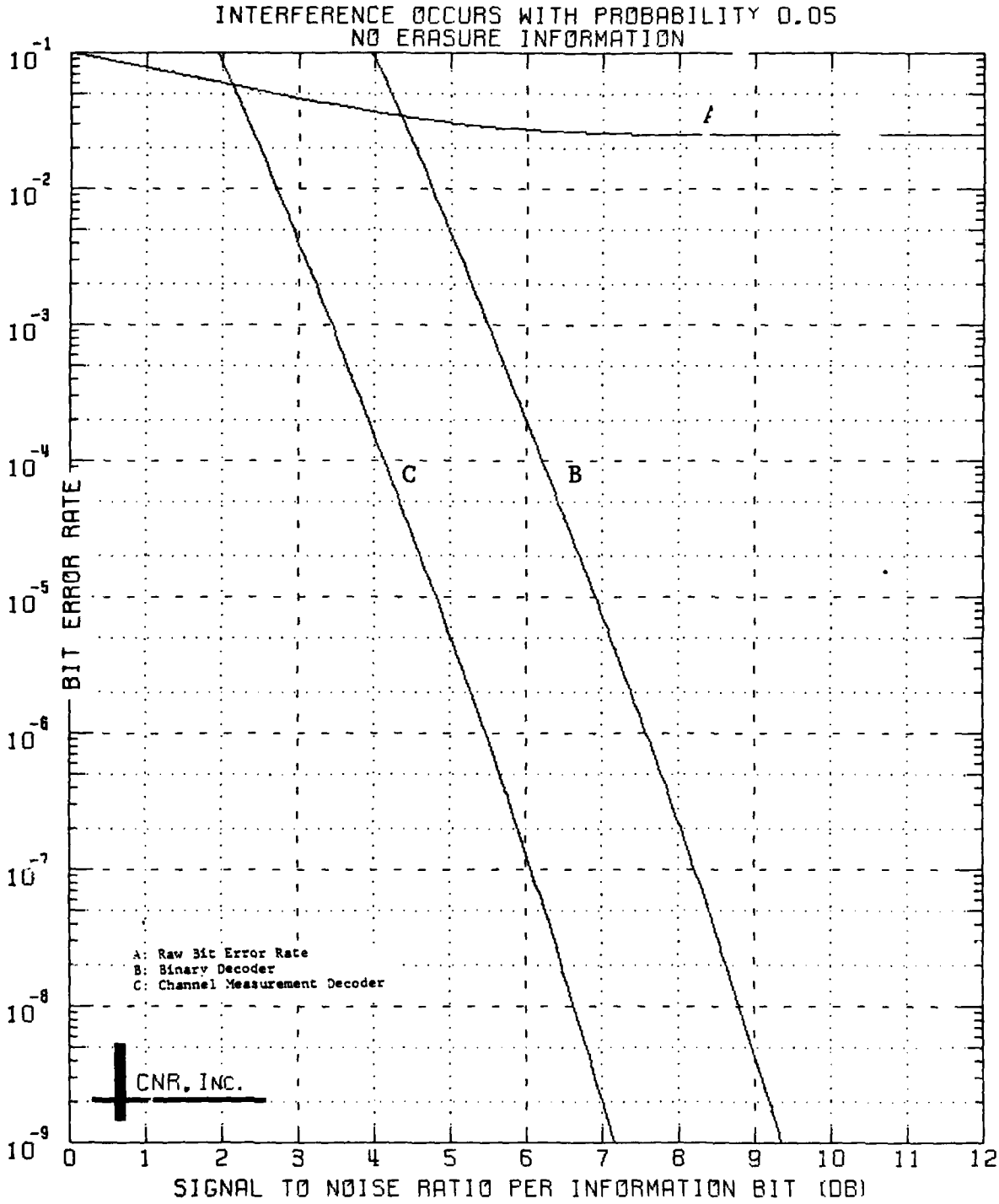


Figure 6.20 Decoded Performance of a Convolutional Code Rate 1/8; Constraint Length = 7

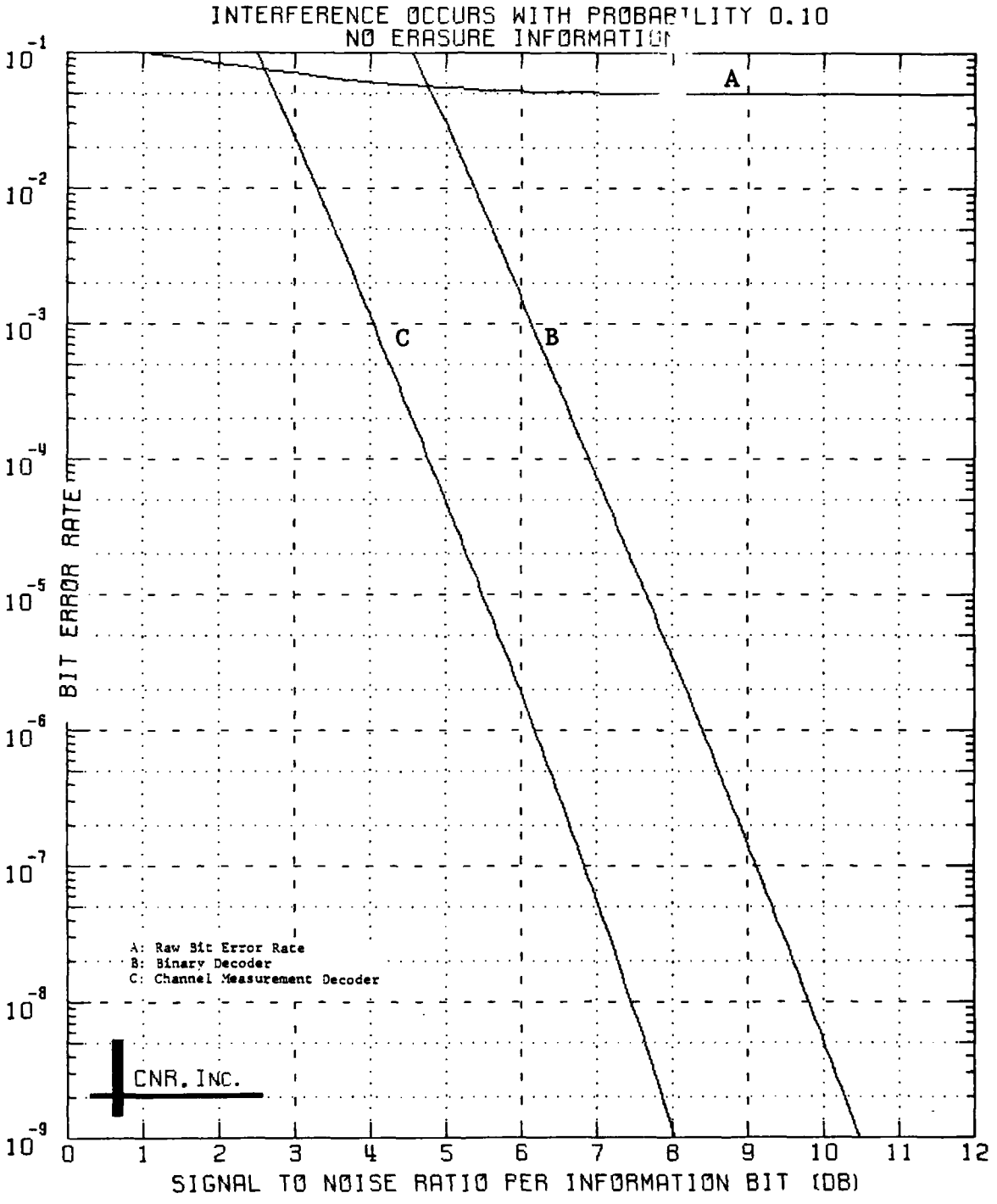


Figure 6.21 Decoded Performance of a Convolutional Code Rate 1/8; Constraint Length = 7

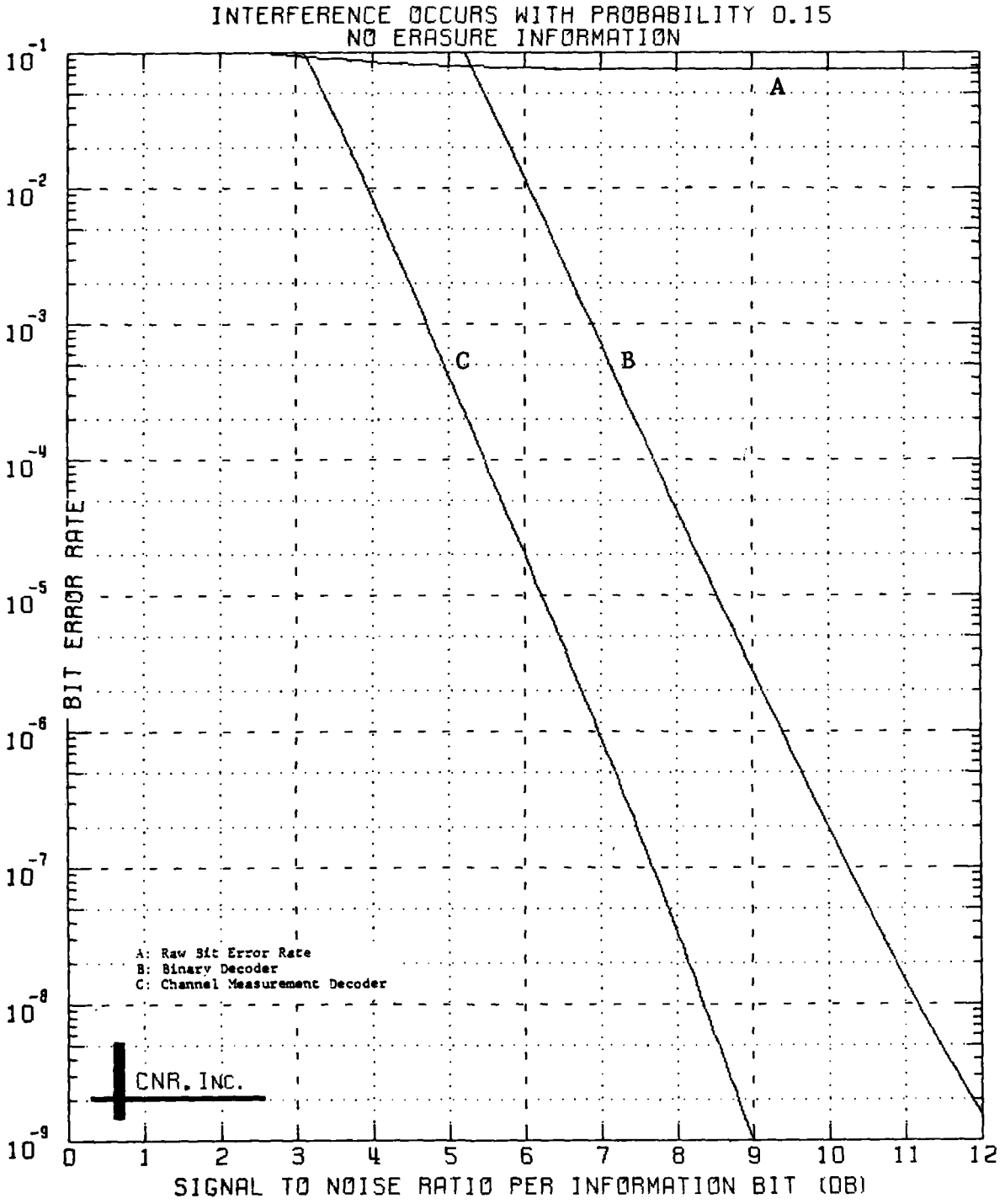


Figure 6.22 Decoded Performance of a Convolutional Code Rate 1/8; Constraint Length = 7

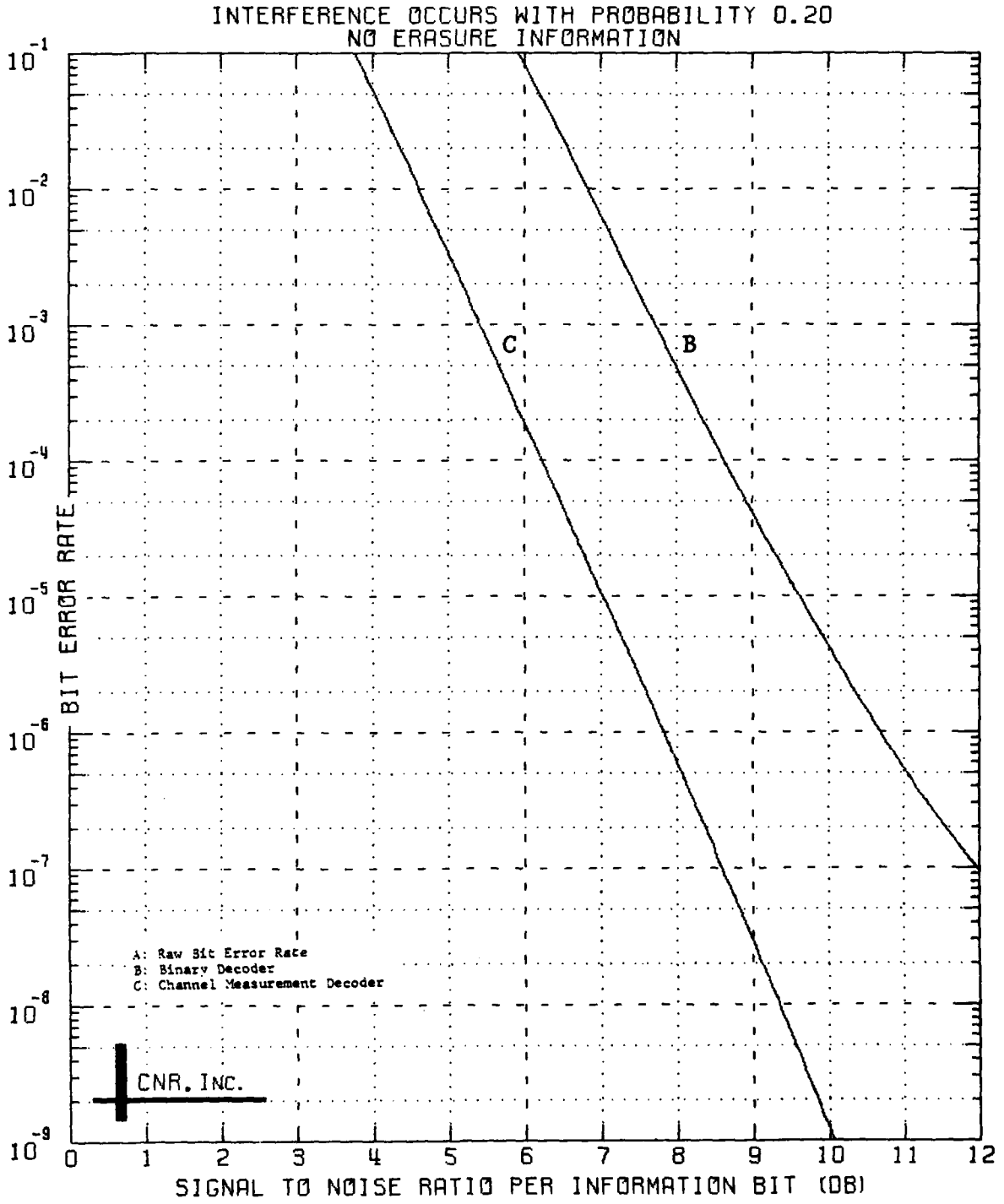


Figure 6.23 Decoded Performance of a Convolutional Code Rate 1/8; Constraint Length = 7

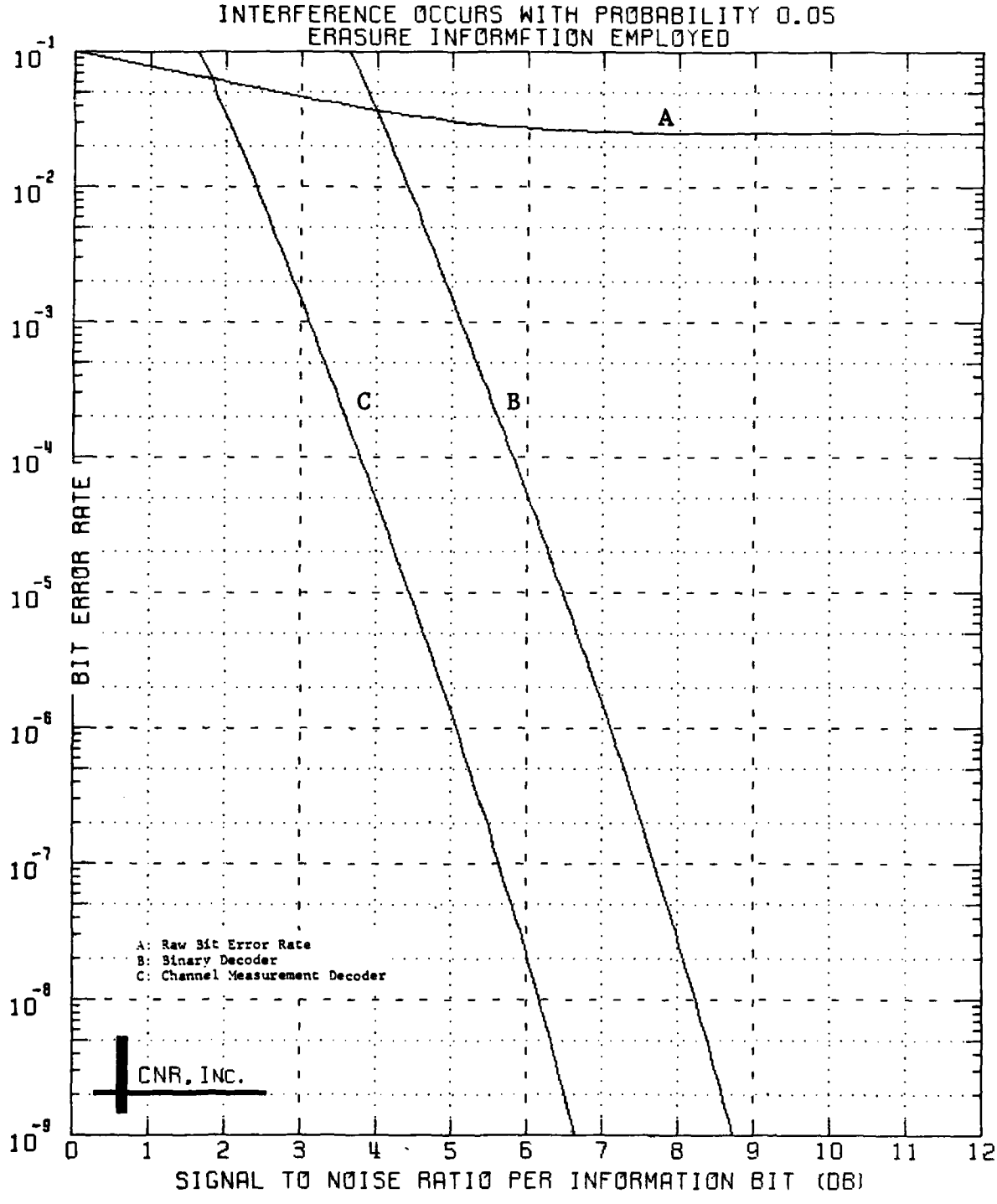


Figure 6.24 Decoded Performance of a Convolutional Code Rate 1/8; Constraint Length = 7

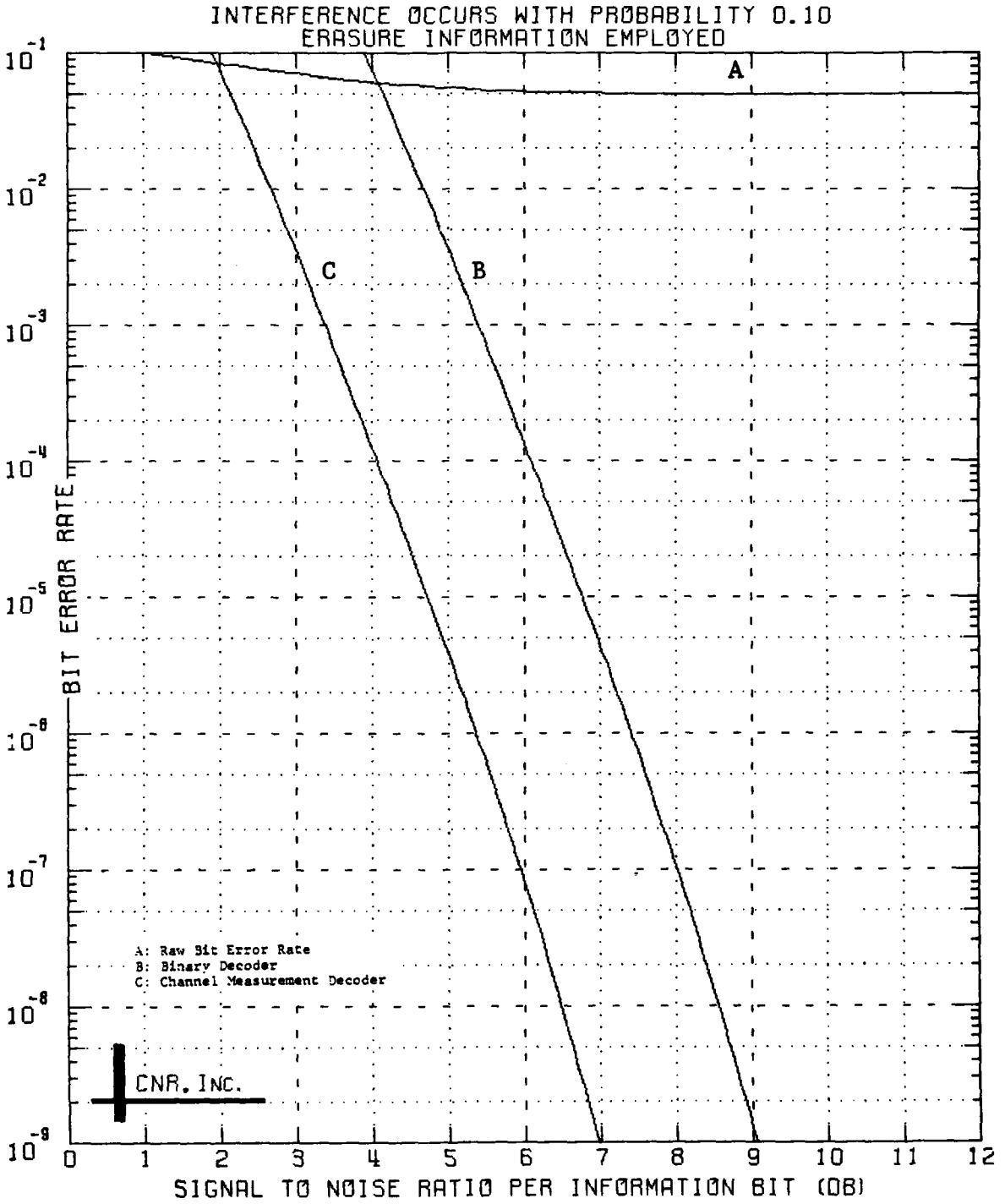


Figure 6.25 Decoded Performance of a Convolutional Code Rate 1/8; Constraint Length = 7

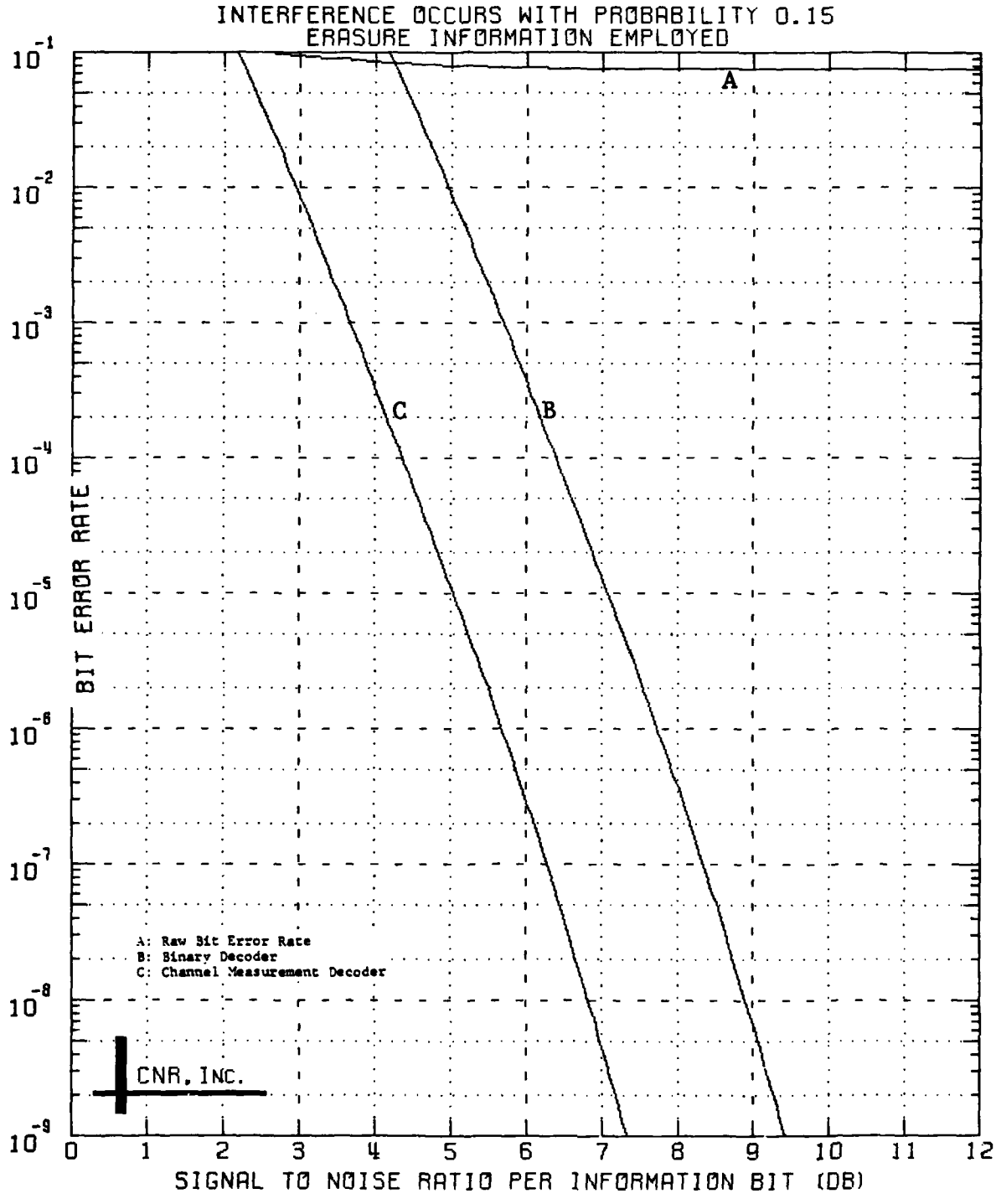


Figure 6.26 Decoded Performance of a Convolutional Code Rate 1/8; Constraint Length = 7

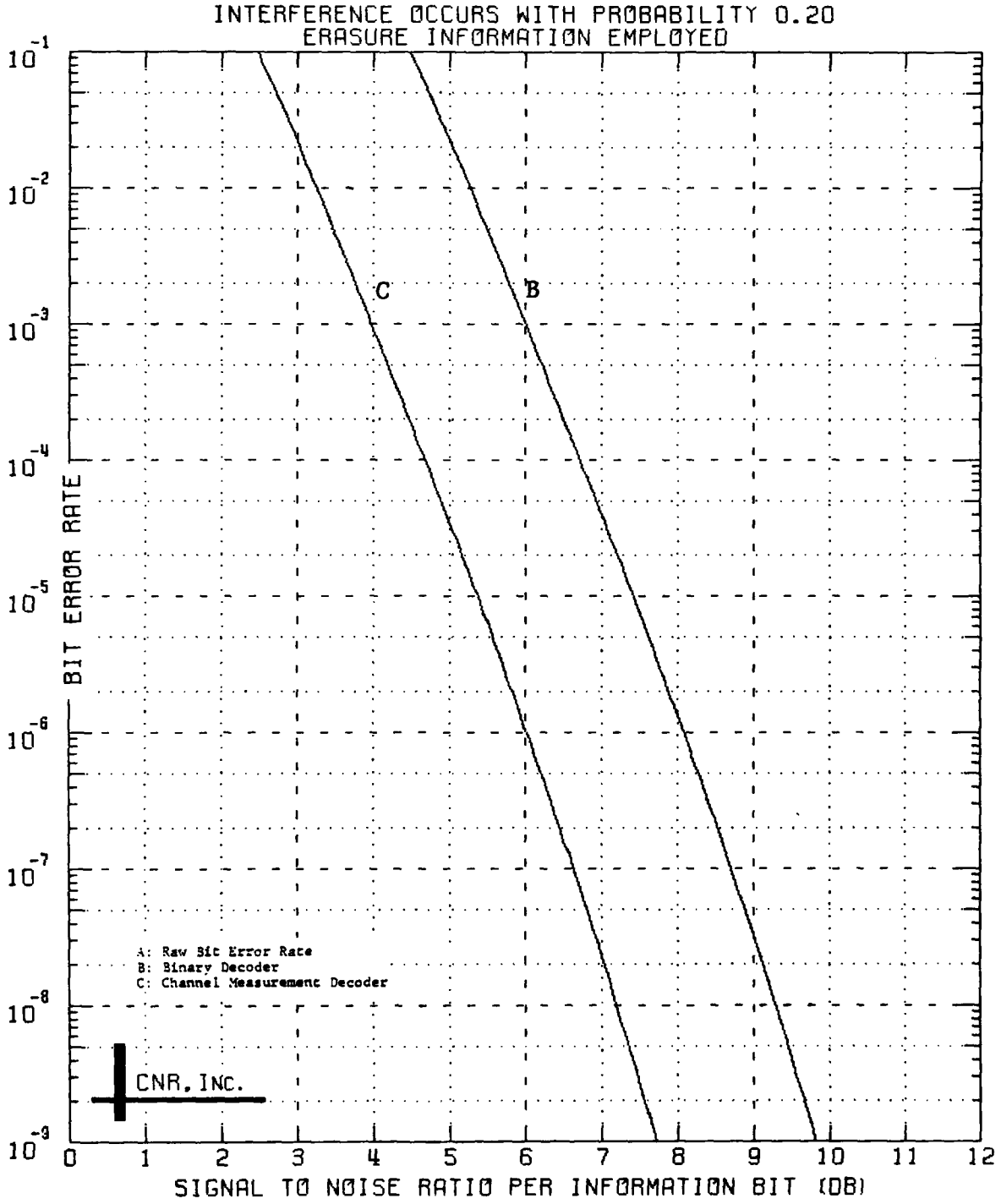


Figure 6.27 Decoded Performance of a Convolutional Code Rate 1/8; Constraint Length = 7

TABLE 6-1

E_b/N_0 (dB) REQUIRED FOR A BIT ERROR RATE OF 10^{-5}

INTERLEAVED CONVOLUTIONAL CODES: CONSTRAINT LENGTH K = 7

Rate		δ = 0.00		δ = 0.05		δ = 0.10		δ = 0.15		δ = 0.20		δ = 0.25		δ = 0.30		δ = 0.35		δ = 0.40		δ = 0.45	
		BD	CD	BD	CD	BD	CD	BD	CD	BD	CD	BD	CD	BD	CD	BD	CD	BD	CD	BD	CD
1/2	No Erasures	6.55	4.19	—	6.18	—	8.44	—	11.32	—	15.76	—	—	—	—	—	—	—	—	—	—
	Erasures	6.55	4.19	6.94	4.69	7.57	5.28	8.35	6.03	9.67	7.27	—	—	—	—	—	—	—	—	—	—
1/4	No Erasures	6.36	4.18	7.41	5.10	8.98	6.10	—	7.21	—	8.46	—	9.90	—	11.60	—	13.72	—	16.55	—	21.06
	Erasures	6.36	4.18	6.60	4.51	6.97	4.85	7.37	5.23	7.81	5.67	8.32	6.16	8.91	6.72	9.61	7.39	10.57	8.25	11.99	9.67
1/8	No Erasures	6.24	4.18	6.91	4.81	7.65	5.49	8.53	6.22	9.60	7.02	11.08	7.90	14.60	8.86	—	9.95	—	11.18	—	12.61
	Erasures	6.24	4.18	6.47	4.45	6.77	4.73	7.07	5.02	7.41	5.32	7.78	5.72	8.17	6.11	8.61	6.54	9.11	7.01	9.67	7.57
1/16	No Erasures	6.17	4.16	6.71	4.68	7.29	5.23	7.92	5.83	8.62	6.48	9.41	7.18	10.33	7.94	11.42	8.77	12.55	9.67	15.25	10.69
	Erasures	6.17	4.16	6.39	4.40	6.64	4.64	6.93	4.93	7.22	5.22	7.54	5.54	7.88	5.87	8.24	6.23	8.65	6.63	9.11	7.08
1/32	No Erasures	6.10	4.11	6.59	4.60	7.11	5.11	7.66	5.65	8.26	6.23	8.92	6.85	9.63	7.53	10.43	8.25	11.34	9.04	12.39	9.92
	Erasures	6.10	4.11	6.33	4.35	6.57	4.59	6.83	4.84	7.11	5.13	7.41	5.42	7.73	5.75	8.07	6.08	8.44	6.49	8.85	6.86

— $P[\epsilon] = 10^{-5}$ Not achievable

TABLE 6-1 (continued)

Rate		δ = 0.50		δ = 0.55		δ = 0.60		δ = 0.65		δ = 0.70		δ = 0.75		δ = 0.80		δ = 0.85		δ = 0.90		δ = 0.95	
		BD	CD	BD	CD	BD	CD	BD	CD	BD	CD	BD	CD	BD	CD	BD	CD	BD	CD	BD	CD
1/2	No Erasures	—	—	—	—	—	—	—	—	—	—	—	—	—	—	—	—	—	—	—	—
	Erasures	—	—	—	—	—	—	—	—	—	—	—	—	—	—	—	—	—	—	—	—
1/4	No Erasures	—	—	—	—	—	—	—	—	—	—	—	—	—	—	—	—	—	—	—	—
	Erasures	—	—	—	—	—	—	—	—	—	—	—	—	—	—	—	—	—	—	—	—
1/8	No Erasures	—	14.32	—	16.43	—	19.26	—	23.62	—	—	—	—	—	—	—	—	—	—	—	—
	Erasures	10.33	8.20	11.12	8.96	12.14	9.93	—	11.34	—	—	—	—	—	—	—	—	—	—	—	—
1/16	No Erasures	—	11.83	—	13.16	—	14.72	—	16.61	—	19.02	—	22.37	—	28.05	—	—	—	—	—	—
	Erasures	9.61	7.58	10.19	8.15	10.83	8.79	11.63	9.56	12.61	10.51	13.91	11.76	—	13.45	—	—	—	—	—	—
1/32	No Erasures	13.66	10.89	15.38	11.98	18.51	13.22	—	14.67	—	16.42	—	18.60	—	21.50	—	25.89	—	—	—	—
	Erasures	9.31	7.32	9.82	7.82	10.39	8.39	11.05	9.04	11.83	9.52	12.82	10.72	14.04	11.99	15.64	13.74	—	17.14	—	—

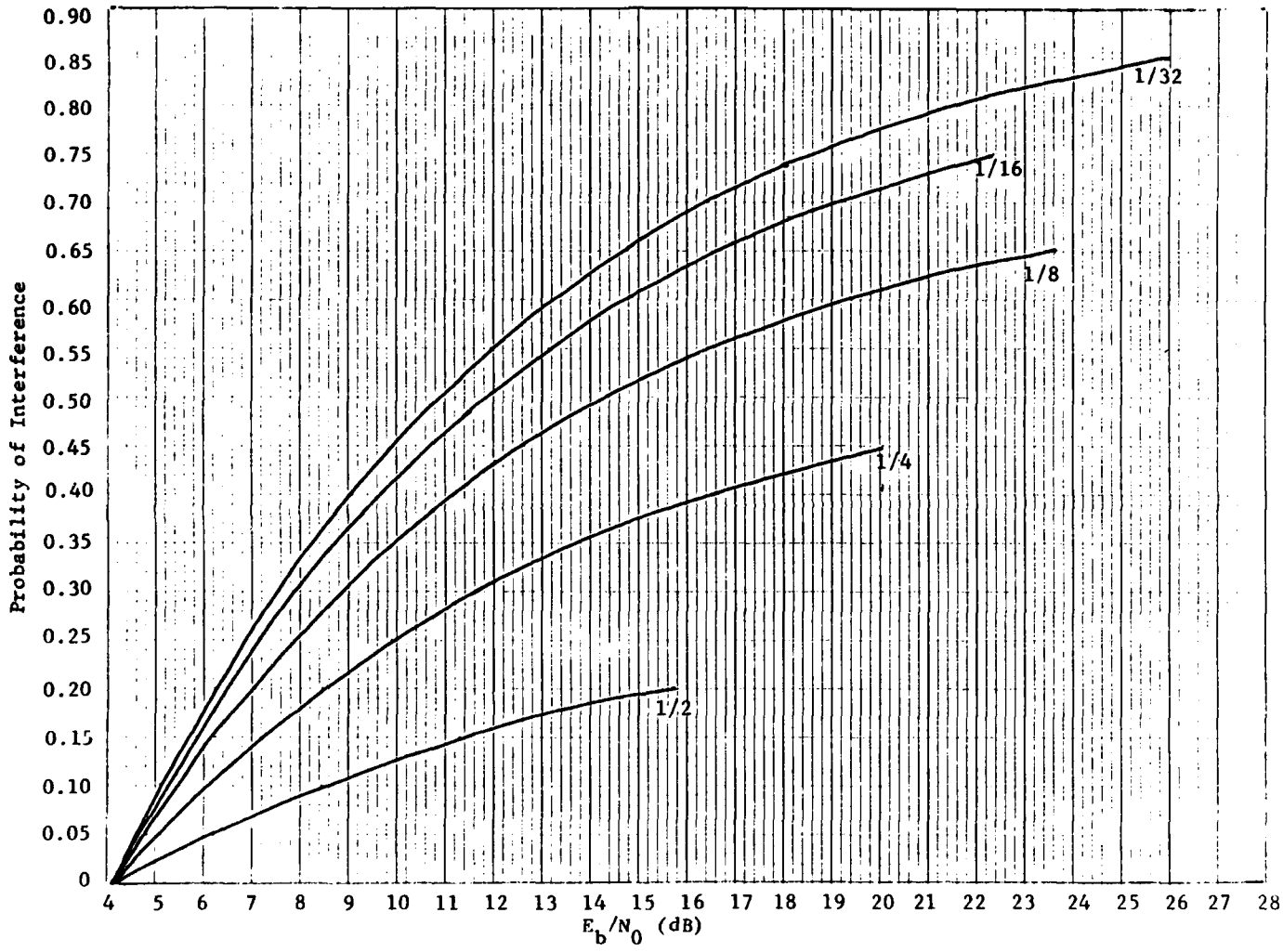


Figure 6.28 Convolutional Coding Performance with
Code Rate as a Parameter
Channel Measurement Decoding-No Erasure Information

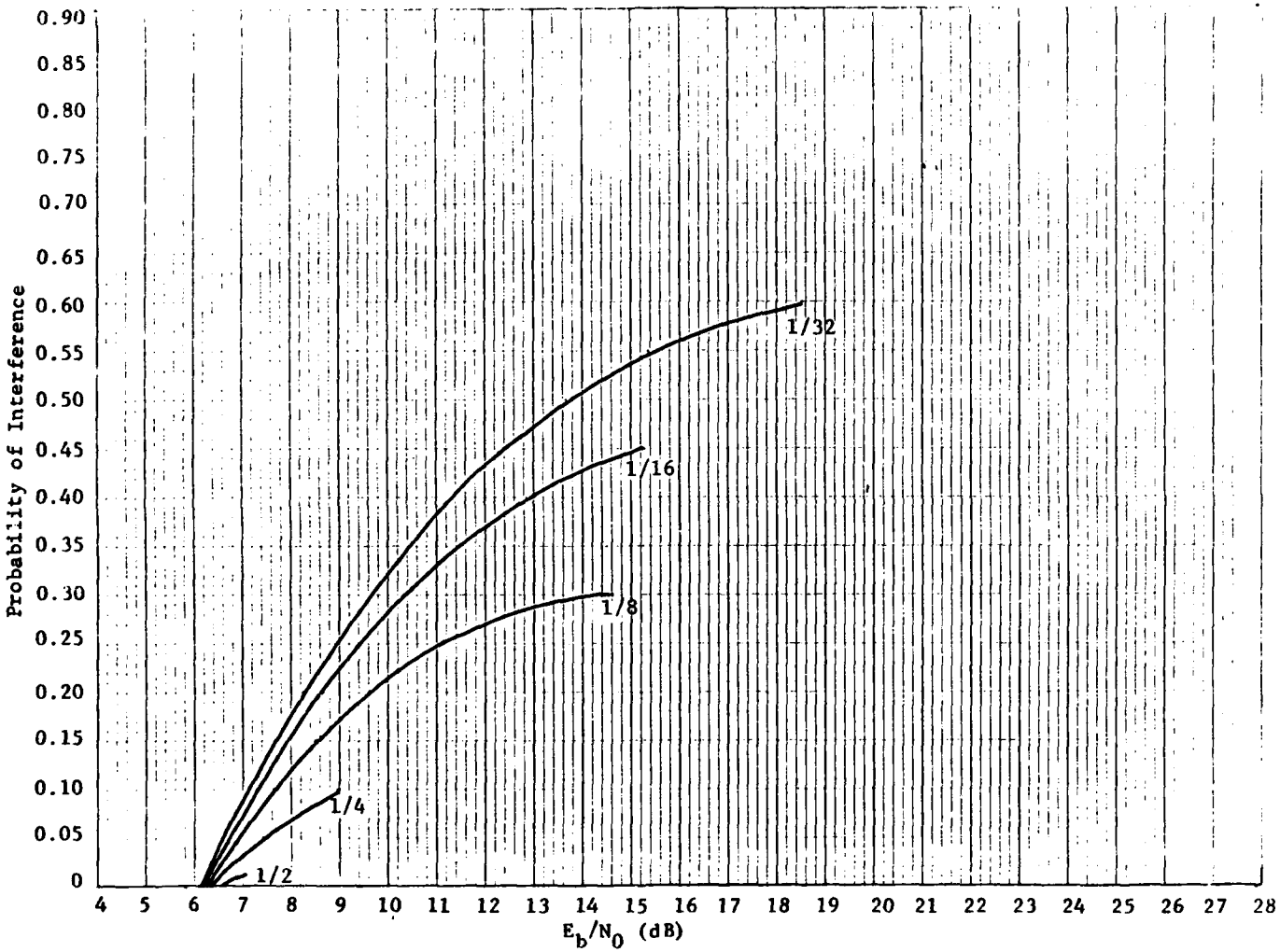


Figure 6.29 Convolutional Coding Performance with Code Rate as a Parameter Binary Decoding-No Erasure Information

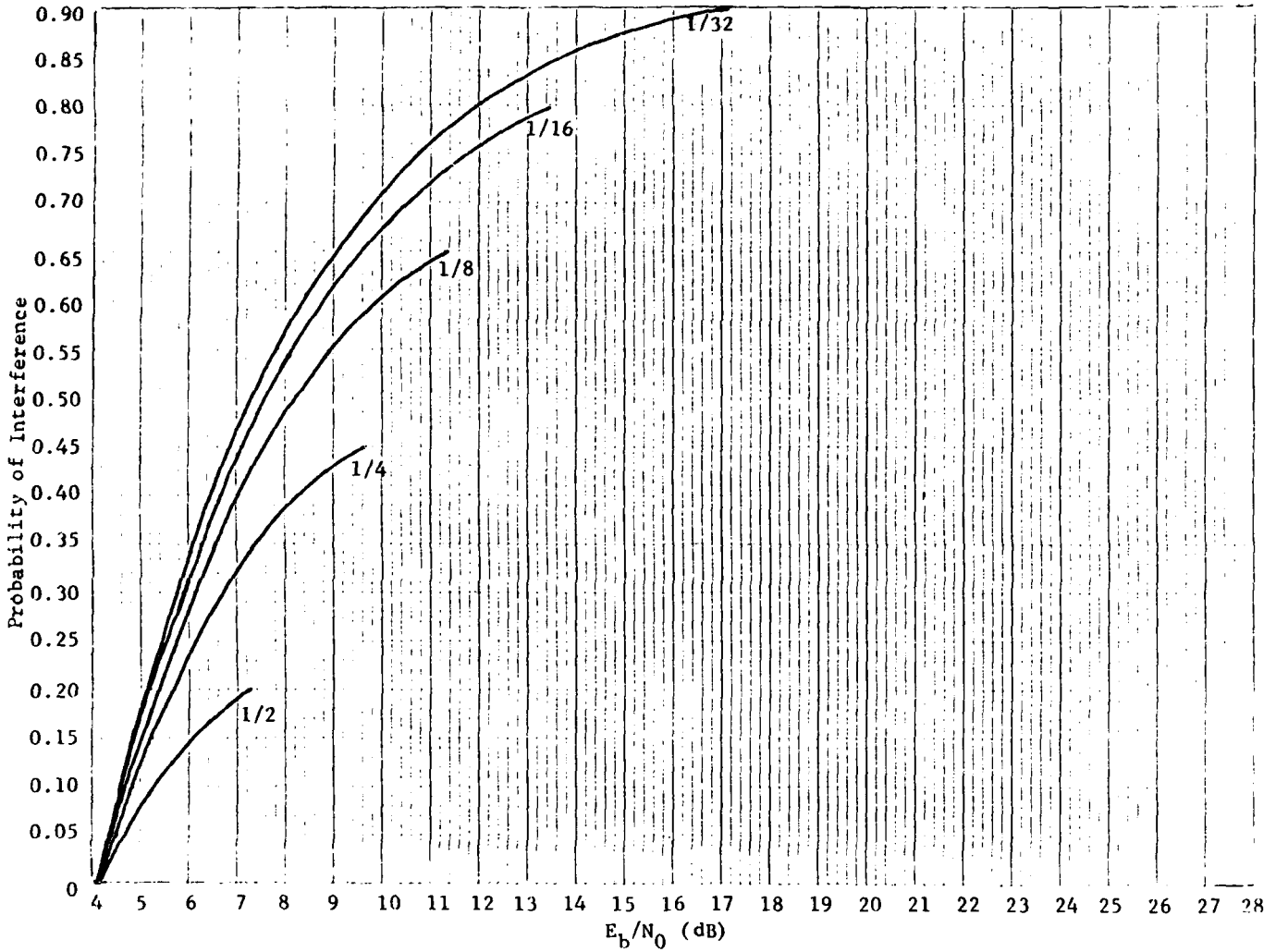
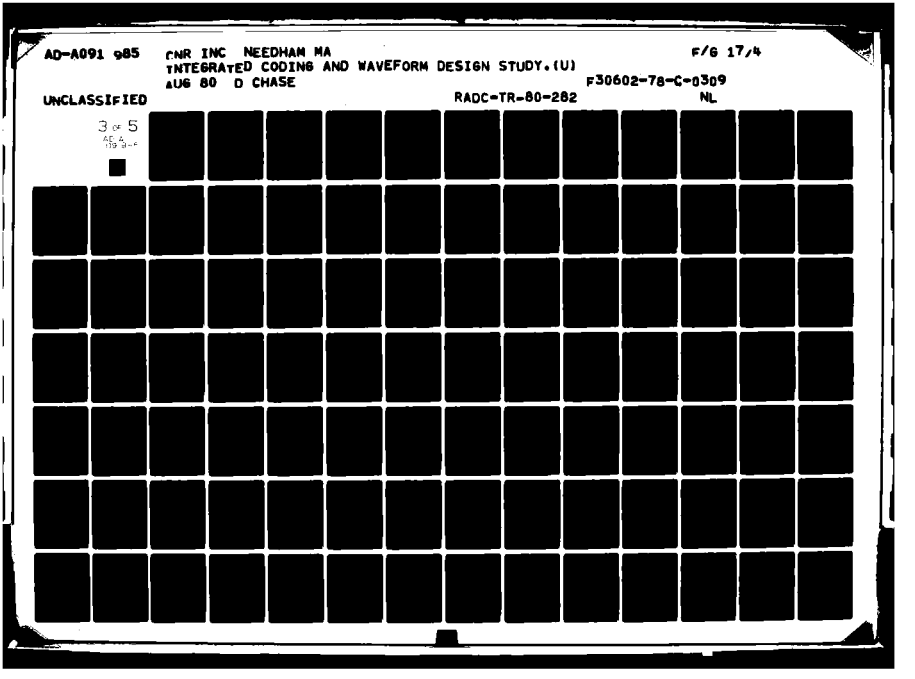


Figure 6.30 Convolutional Coding Performance with Code Rate as a Parameter Channel Measurement Decoding-Erasure Information Available


AD-A091 985
CNR INC NEEDHAM MA
INTEGRATED CODING AND WAVEFORM DESIGN STUDY.(U)
F/G 17/4
AUG 80 D CHASE
F30602-78-C-0309
UNCLASSIFIED
RADC-TR-80-282
NL
3 OF 5
AD A
091 985

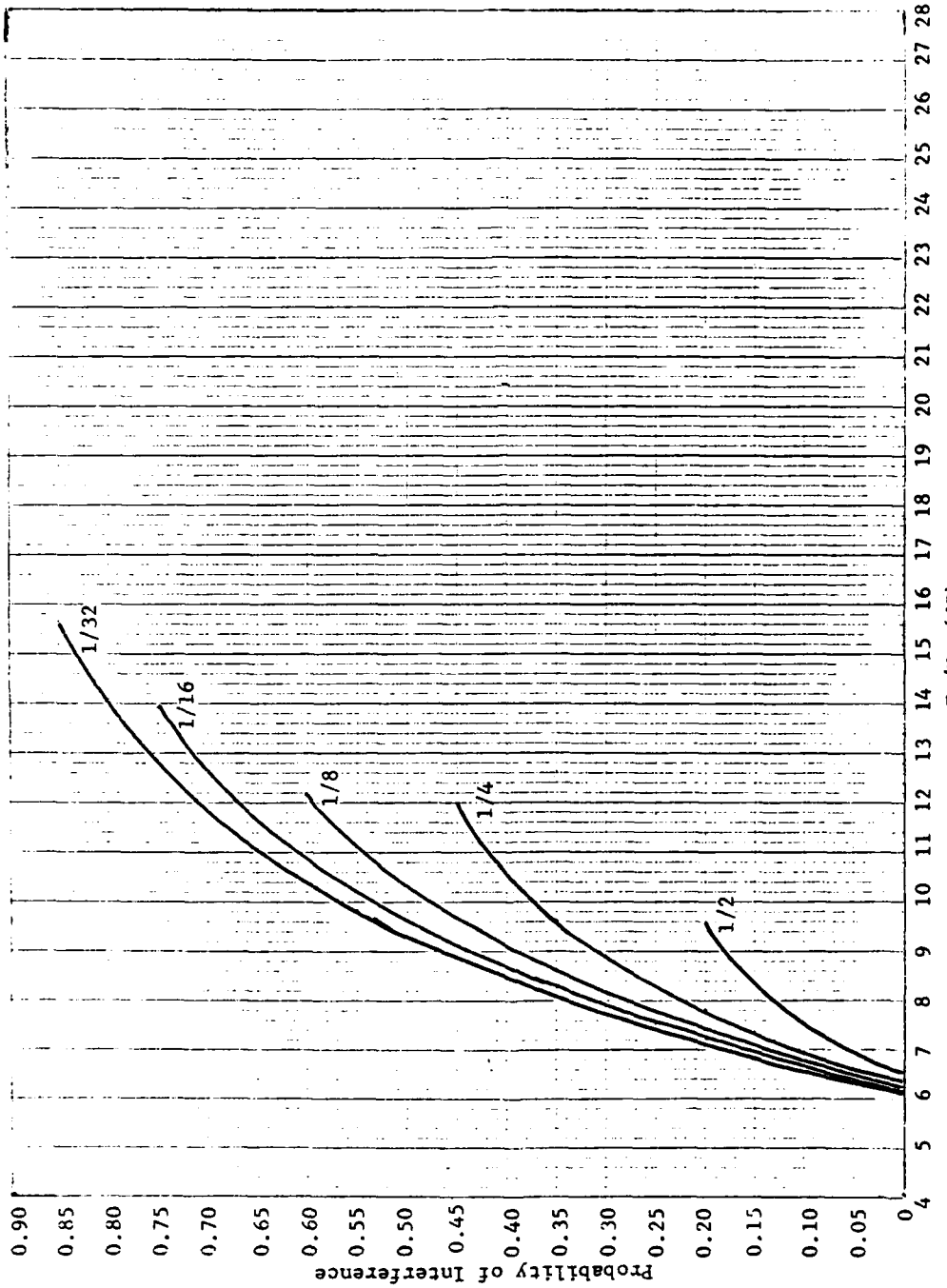


Figure 6.31 Convolutional Coding Performance with Code Rate as a Parameter Binary Decoding-Erasure Information Available

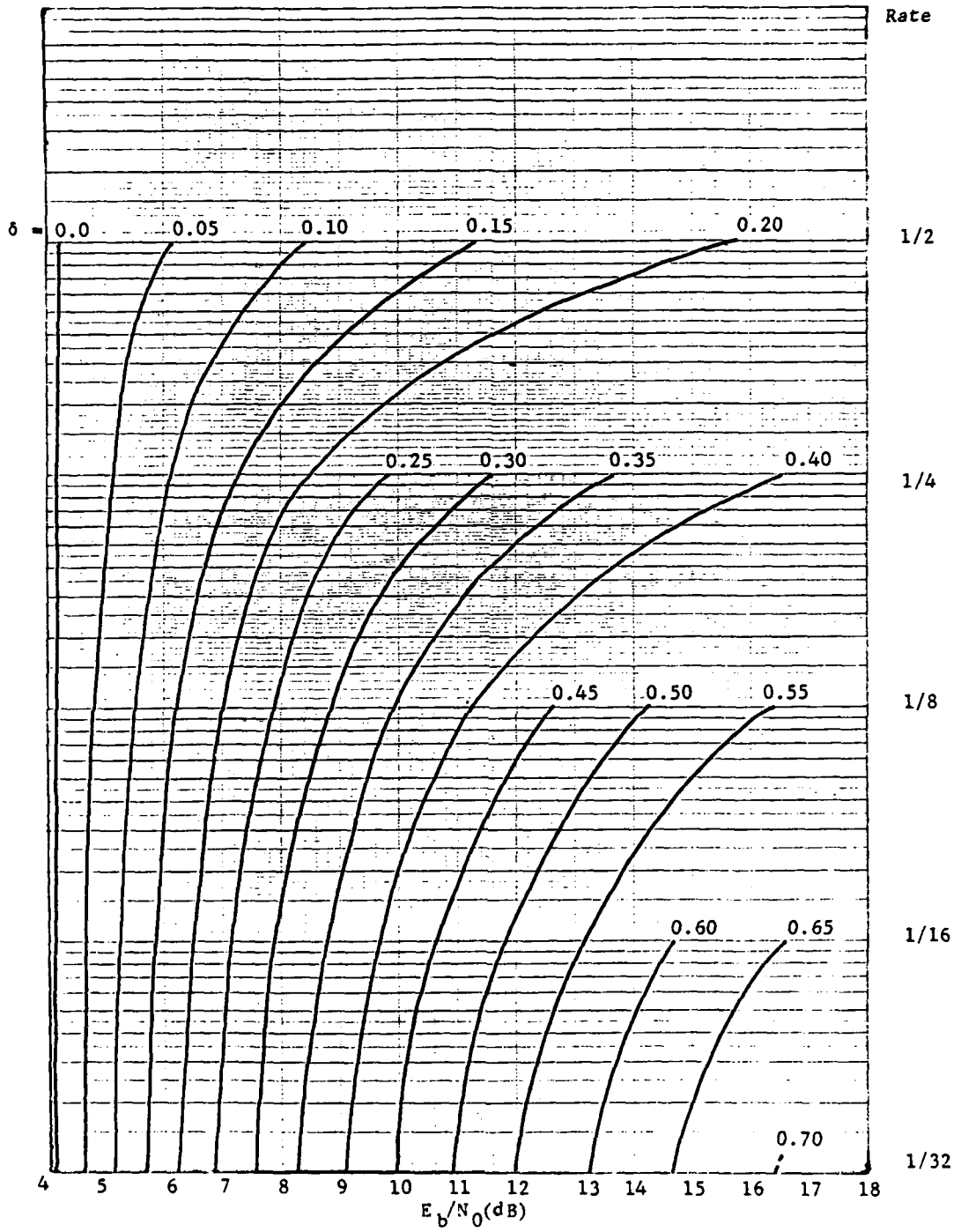


Figure 6.32 Convolutional Coding Performance with Interference Probability as a Parameter Channel Measurement Decoding-No Erasure Information

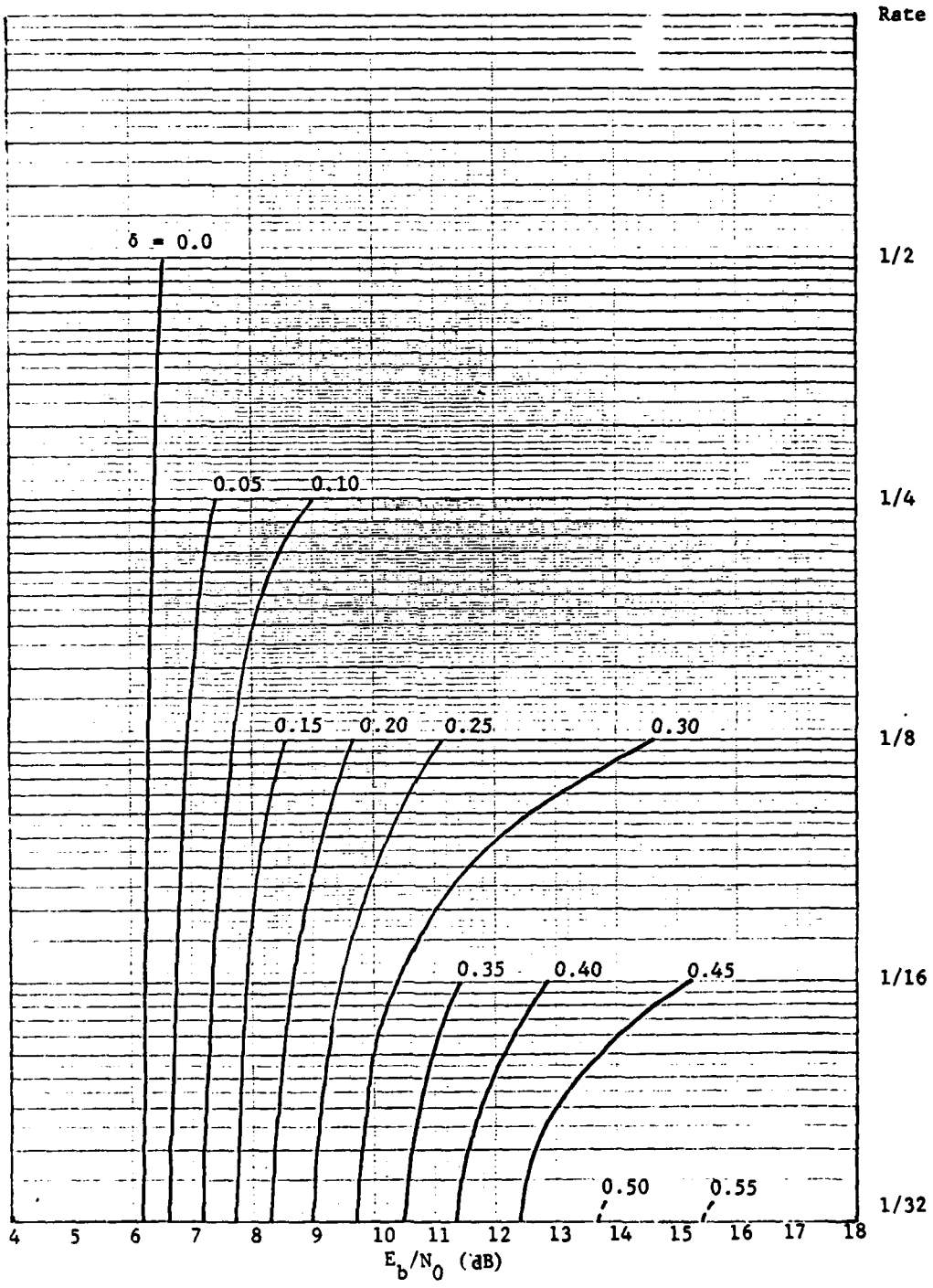


Figure 6.33 Convolutional Coding Performance with Interference Probability as a Parameter Binary Decoding-No Erasure Information

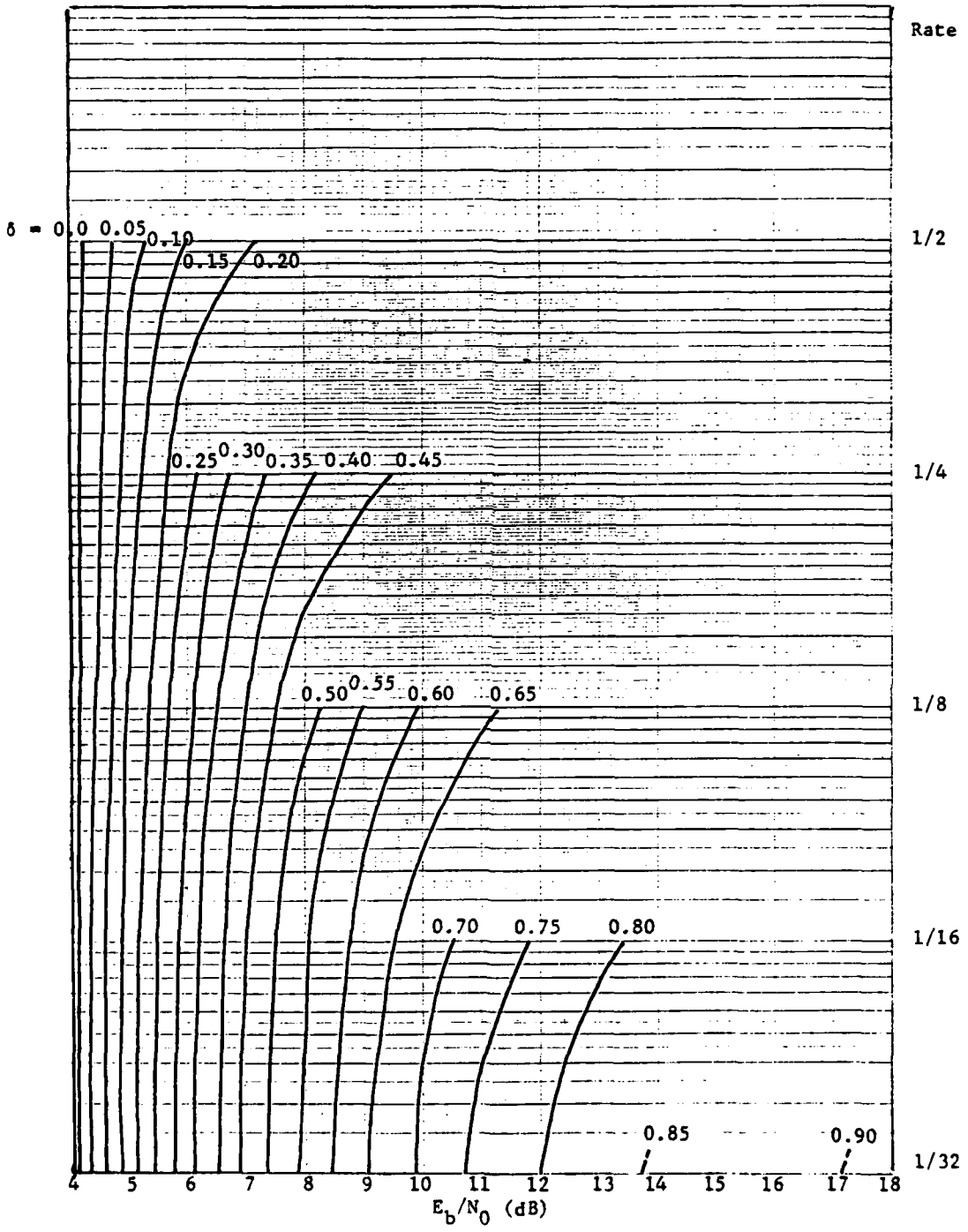


Figure 6.34 Convolutional Coding Performance with Interference Probability as a Parameter Channel Measurement Decoding-Erasure Information Available

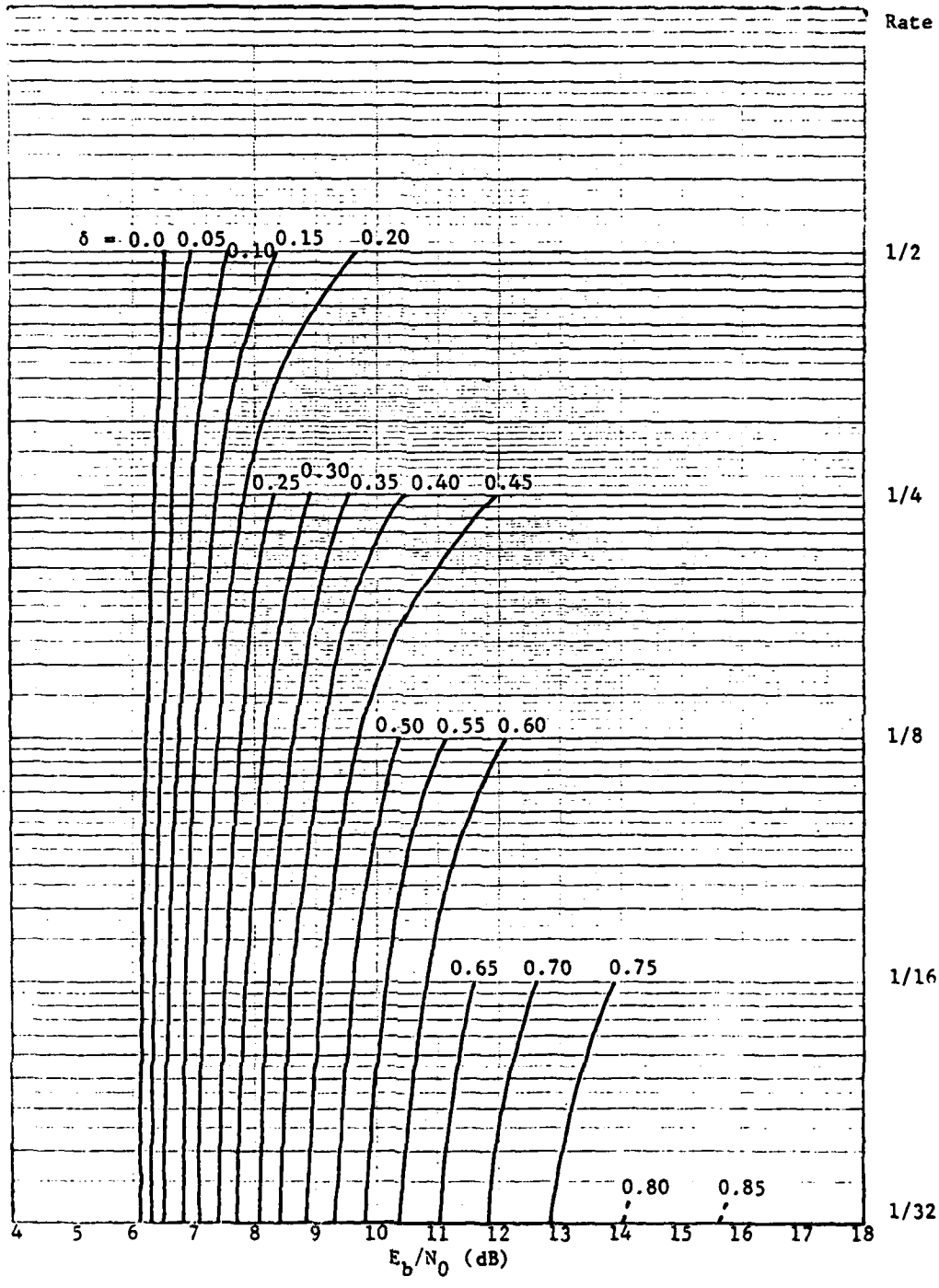


Figure 6.35 Convolutional Coding Performance with Interference Probability as a Parameter Binary Decoding-Erasure Information Available

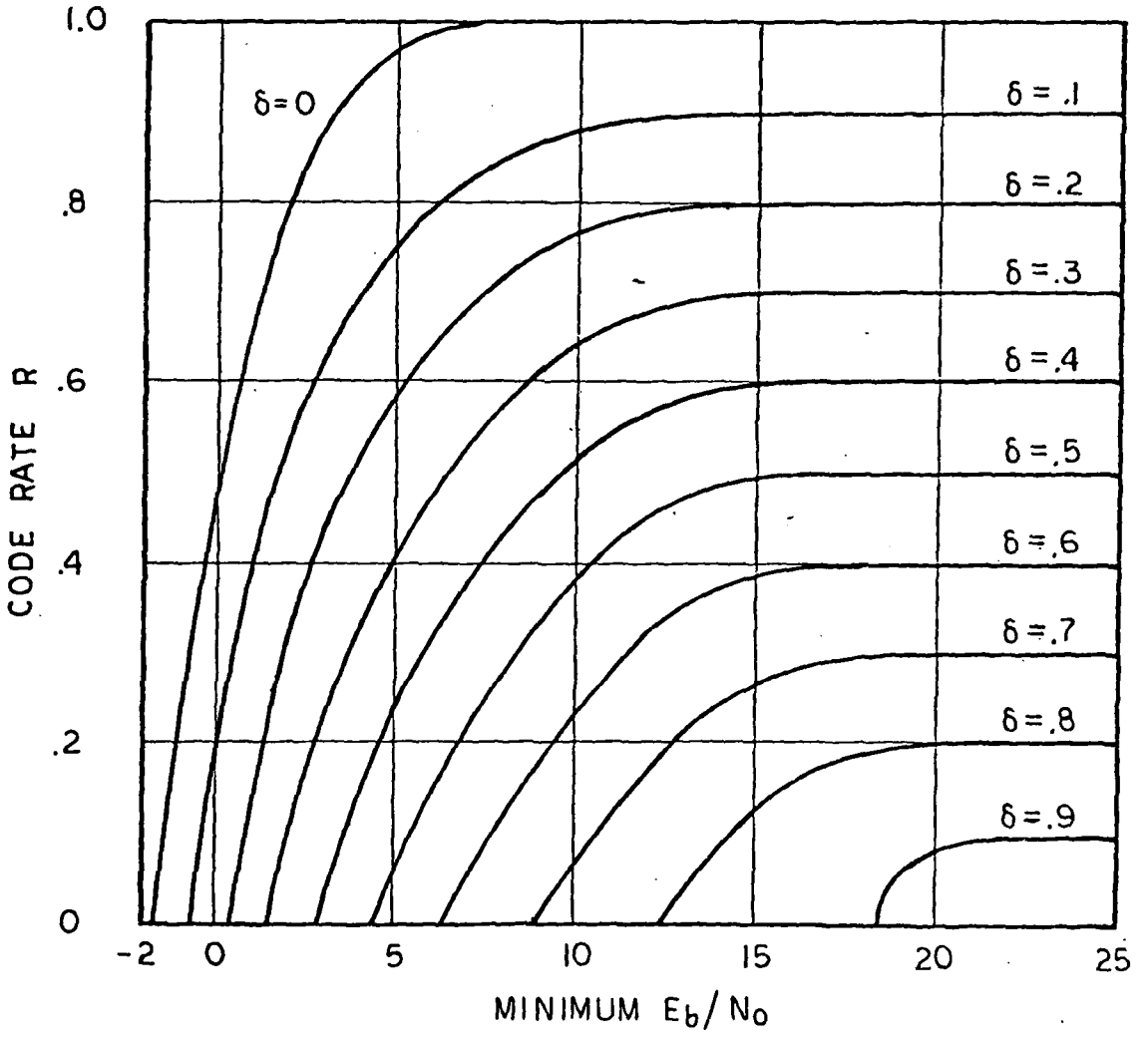


Figure 6.36 Minimum E_b/N_0 for the Gaussian Channel and Channel Measurement Decoding

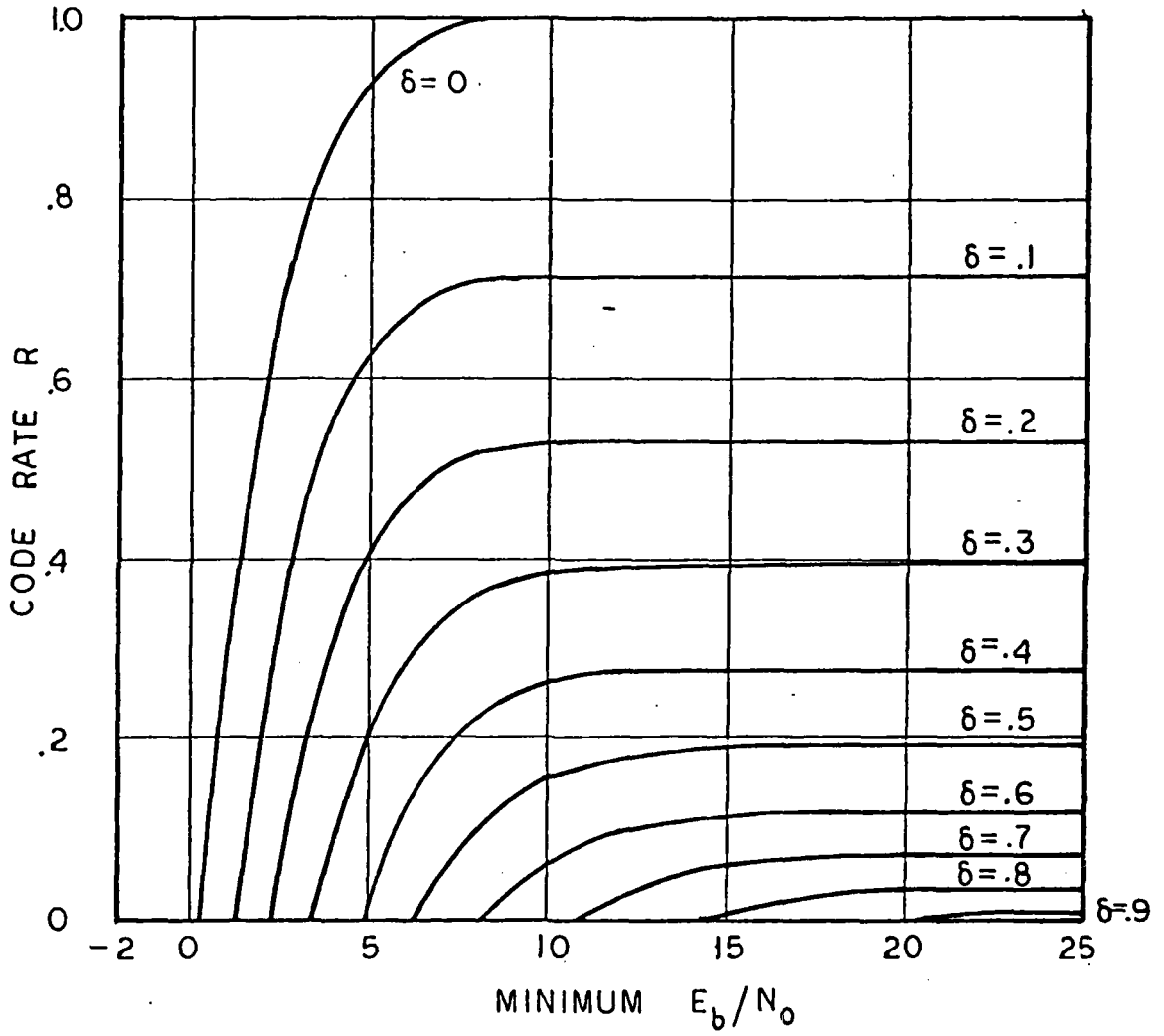


Figure 6.37 Minimum E_b/N_0 for the Gaussian Channel and Binary Decoding

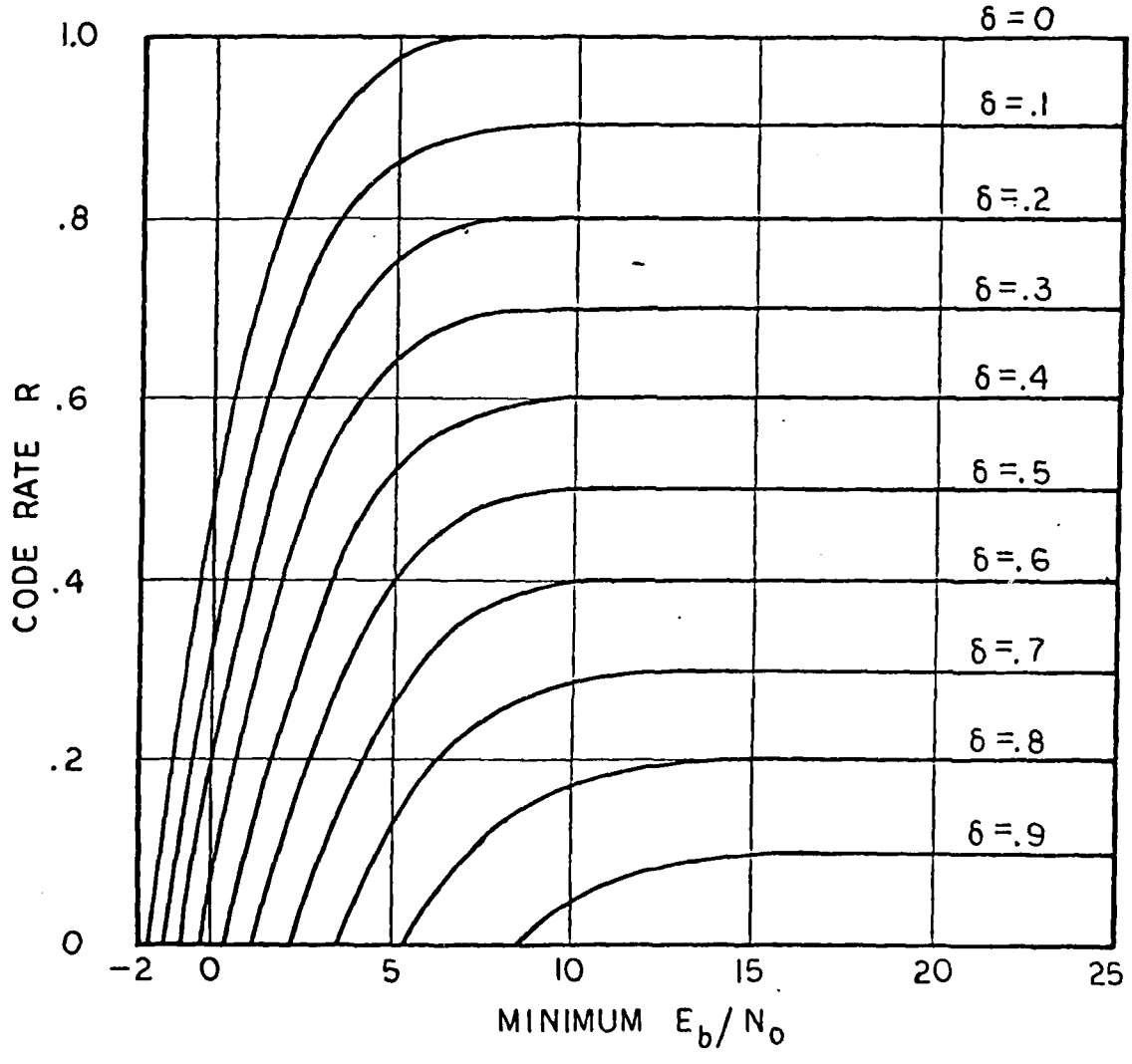


Figure 6.38 Minimum E_b/N_0 for the Gaussian Channel and Channel Measurement Decoding with an Erasure Signal

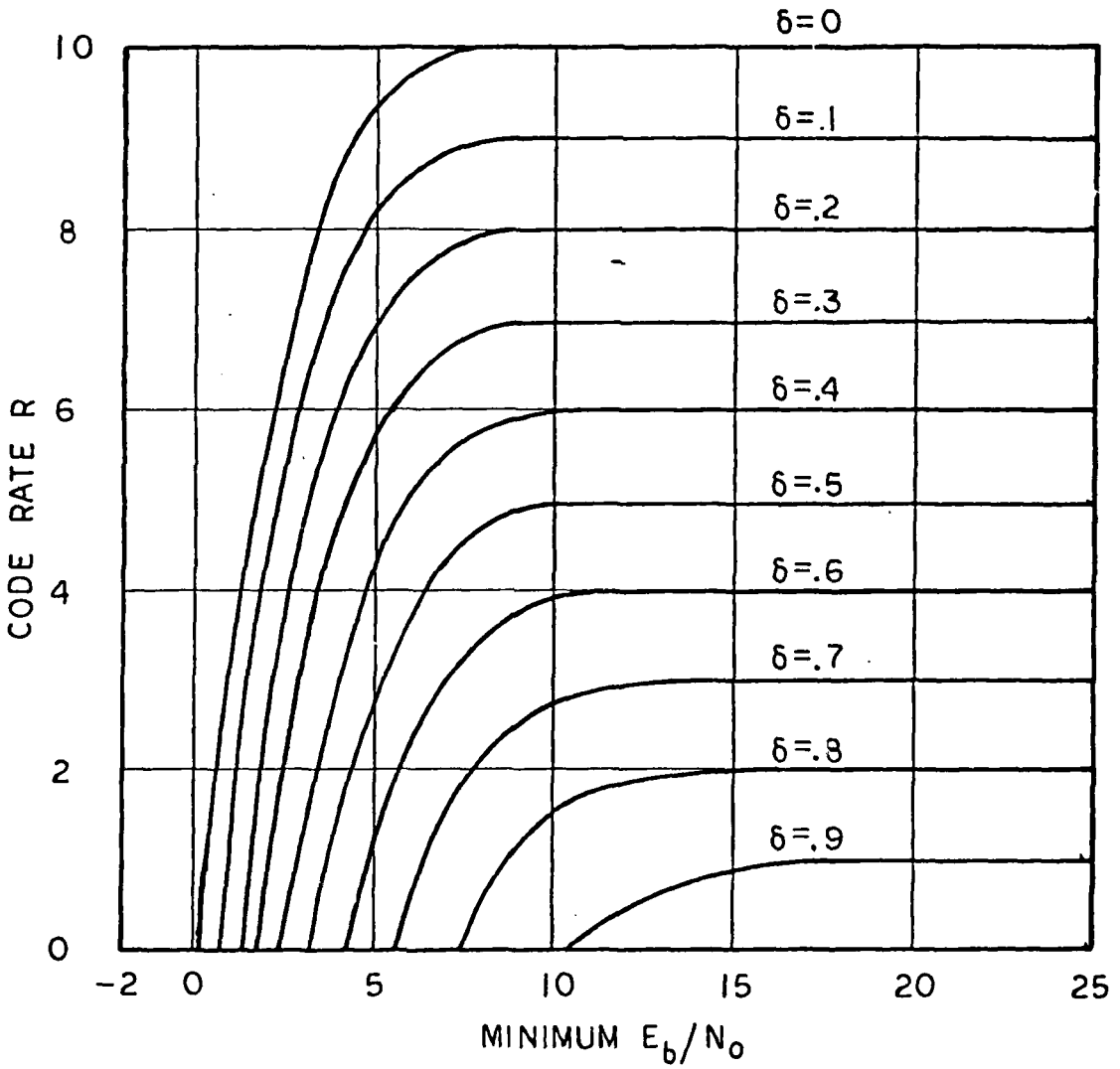


Figure 6.39 Minimum E_b/N_0 for the Gaussian Channel and Binary Decoding with an Erasure Signal

REFERENCE

[6.1] D. Chase and L. H. Ozarow, "Capacity Limits for Binary Codes in the Presence of Interference," IEEE Trans. on Communications, Vol. COM-27, No. 2, February 1979.

SECTION 7

TWO-STAGE CODING APPROACHES BASED ON A LONG INNER BLOCK CODE

The results in the previous section indicated that low rates are effective in combatting interference. In this section, we consider two-stage coding approaches based on a rate-1/2 (128,64) BCH inner code. The outer codes considered are the rate-0.9 (240,216) BCH code and the (128,64) BCH code. Thus, coding approaches of rate-0.45 and 0.25 are considered in this section.

We begin by considering the interleaved inner and outer decoding approach given by Figure 4.1 and analyzed in Section 4.5.

Typically, four curves will be shown on each figure. The uncoded modulation results (raw bit error rate) will be denoted by A. The binary decoding performance of the outer code alone will be denoted by B. Curves A and B act as reference curves for the two-stage coding approaches. Curve C gives the performance when a binary inner decoder is used (model 2 or 4). The performance when a channel measurement inner decoder is used (model 1 or 3) is given by curve D. The outer decoder is used to correct binary errors remaining after data is passed through the inner decoder.

Figures 7.1 to 7.9 illustrate the results when a rate-0.9 (240,216) outer code is assumed. The results when a rate-1/2 (128,64) outer code is used are given in Figures 7.10 to 7.18. It is interesting to note that the rate-1/2 $\otimes$ 0.9 combination generally outperforms the rate-1/2 $\otimes$ 1/2 combination. Furthermore, it should be noted that these two-stage coding approaches are considerably more efficient than the straight low-rate convolution coding approaches discussed in Section 6.

In an attempt to obtain the benefit of erasure information directly from the code, an adaptive coding approach has been investigated. This approach does not use an inner code interleaver and uses the inner code to detect the presence of pulse interference. This information is fed into the outer decoder as erasure information. An approach of this nature is

important for applications where delay must be minimized since no inner interleaver is required.

Figures 7.19 and 7.20 illustrate the results for the (128,64;22) inner code and the (240,216;7) outer code for $\delta = 0$ and $\delta = 0.05$. These results are based on the analysis given in Section 4.5.2. The reference curves A and B are omitted from these figures. For $\delta = 0$, the adaptive approach has a steeper slope than the non-adaptive approach, and thus, for low error rates, will offer superior results. For $\delta = 0.05$ and above, the adaptive code is not effective as a result of the fairly limited erasure-correcting capability of the (240,216;7) code.

A stronger outer code, the (128,64;22) is considered in Figures 7.21 to 7.23. Even this code suffers from an irreducible error for pulse interference with large duty factors, but is attractive for application when the duty factor is expected to be below 5% and no erasure information is available.

Table 7-1 summarizes the main results for the two-stage coding approaches which are based on an interleaved inner and outer code. Comparing the required E_b/N_0 needed to achieve 10^{-5} to the same results given in Table 6-1 illustrates the importance of two-stage coding approaches for applications where the code rate must be maximized because of systems requirements.

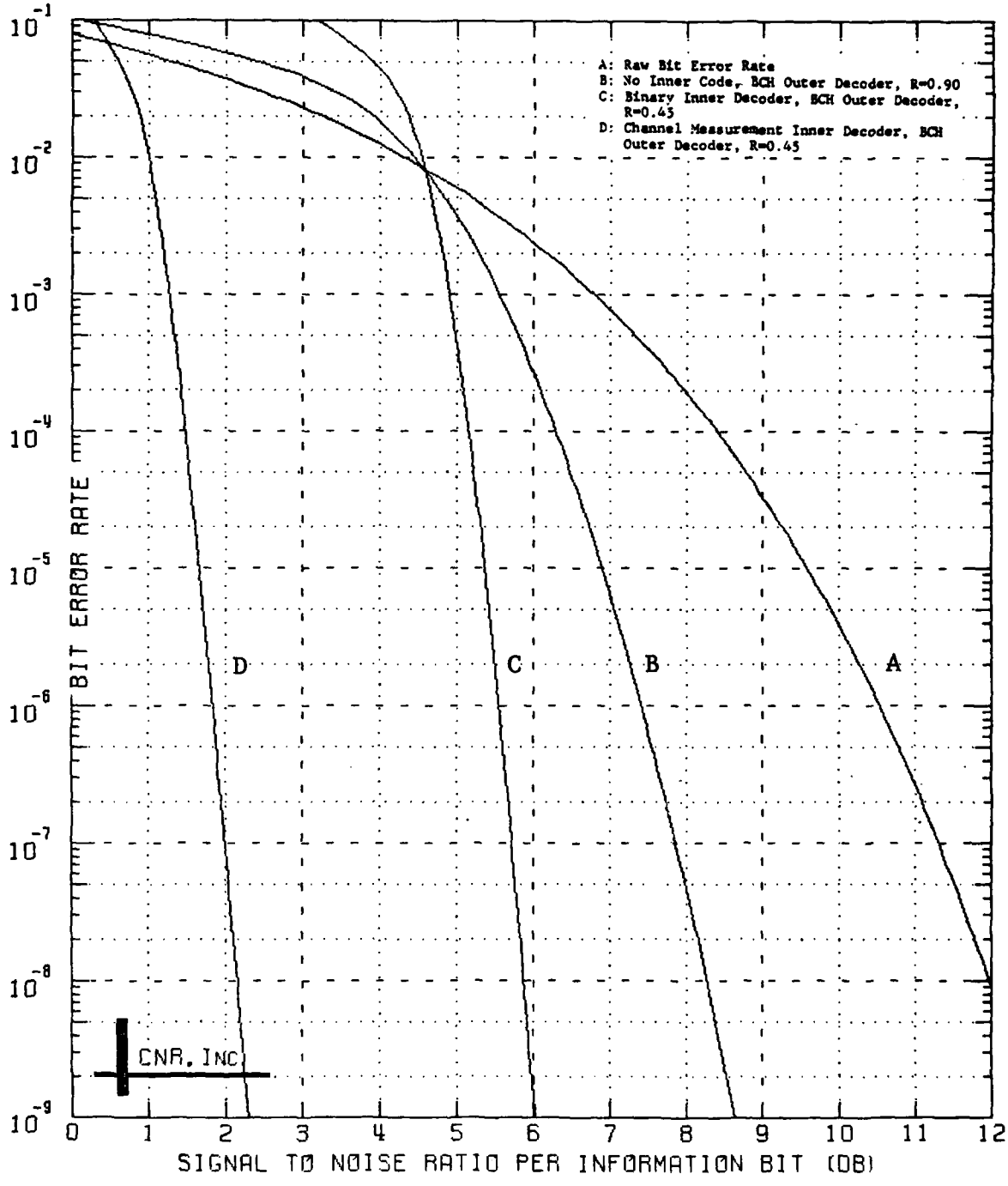


Figure 7.1 Decoded Performance of a Two-Stage Coding Approach
Outer Decoder: BCH Code (240,216;7)
Inner Decoder: Block Code (128,64;22)
δ=0.0 and No Erasure Information Employed

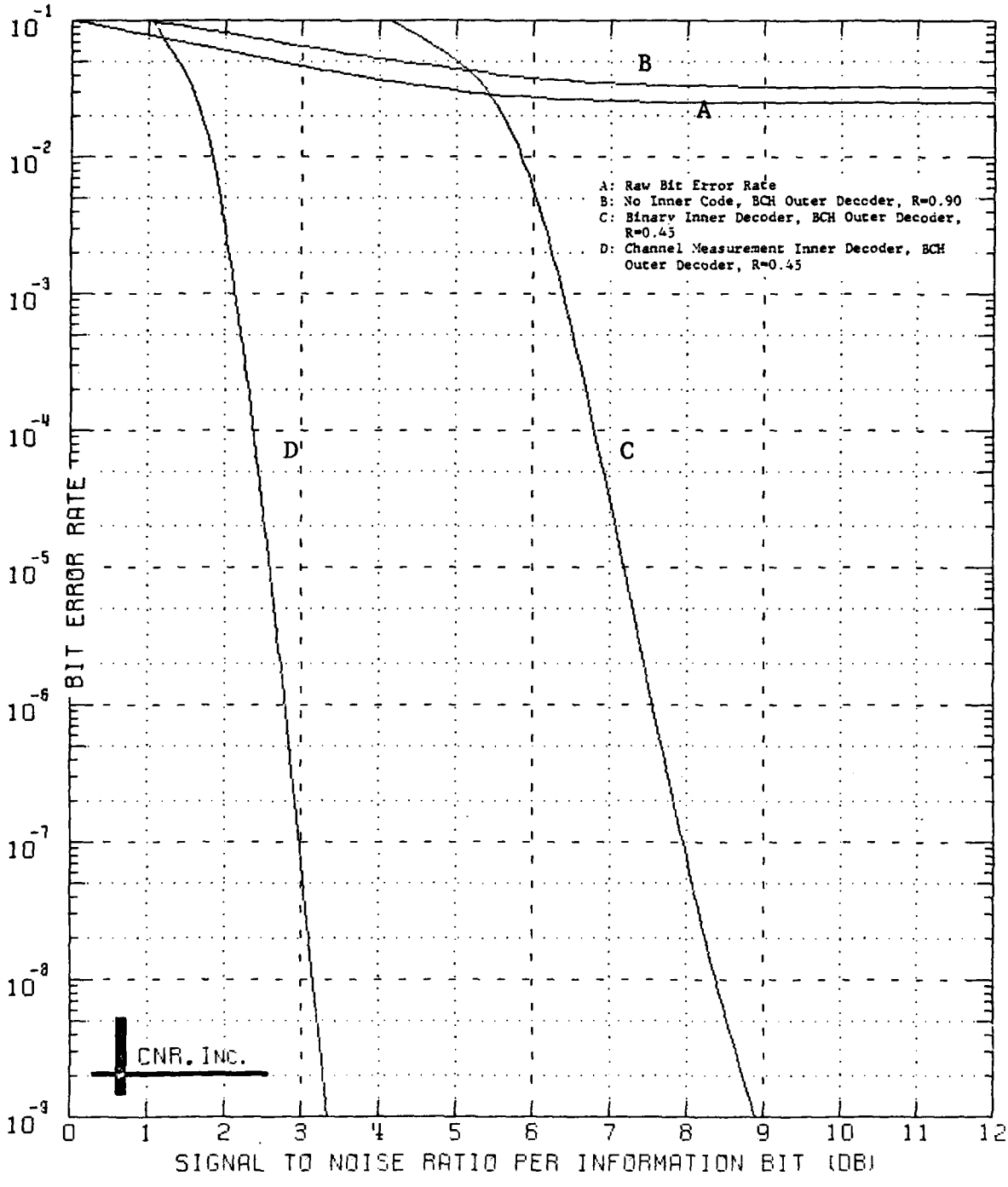


Figure 7.2 Decoded Performance of a Two-Stage Coding Approach
Outer Decoder: BCH Code (240,216;7)
Inner Decoder: Block Code (128,64;22)
δ=0.05 and No Erasure Information Employed

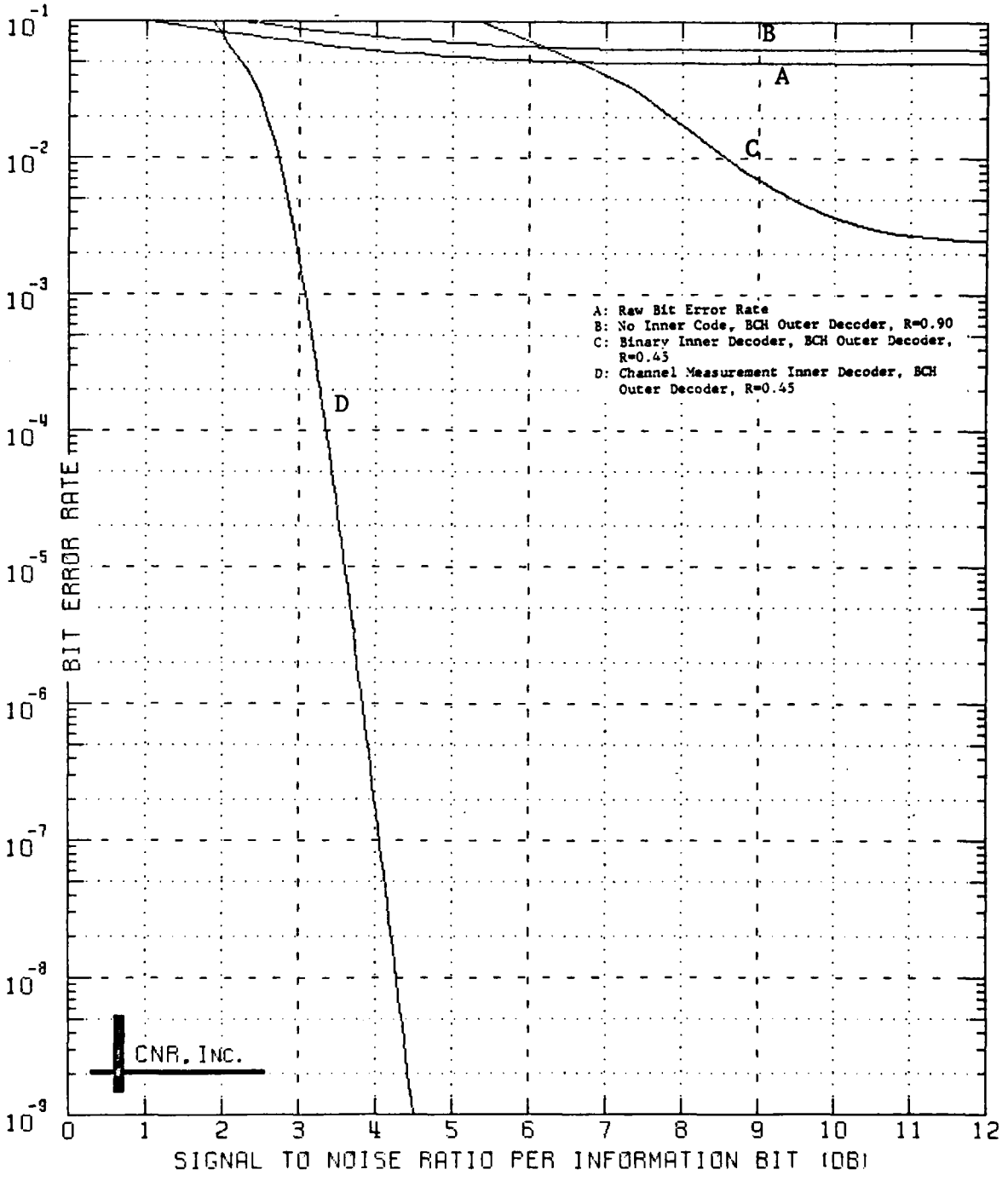


Figure 7.3 Decoded Performance of a Two-Stage Coding Approach
Outer Decoder: BCH Code (240,216;7)
Inner Decoder: Block Code (128,64;22)
δ=0.10 and No Erasure Information Employed

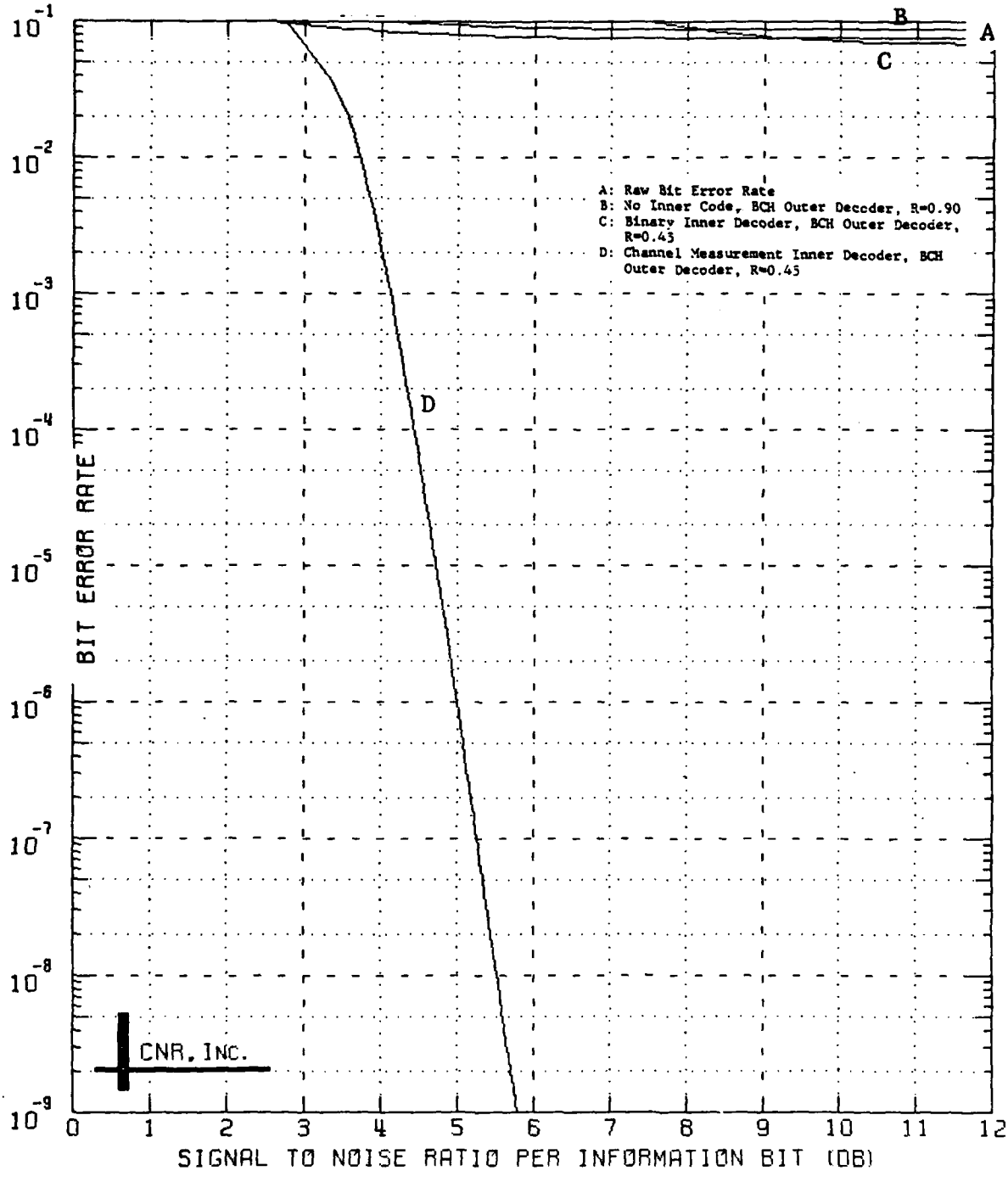


Figure 7.4 Decoded Performance of a Two-Stage Coding Approach
Outer Decoder: BCH Code (240,216;7)
Inner Decoder: Block Code (128,64;22)
δ=0.15 and No Erasure Information Employed

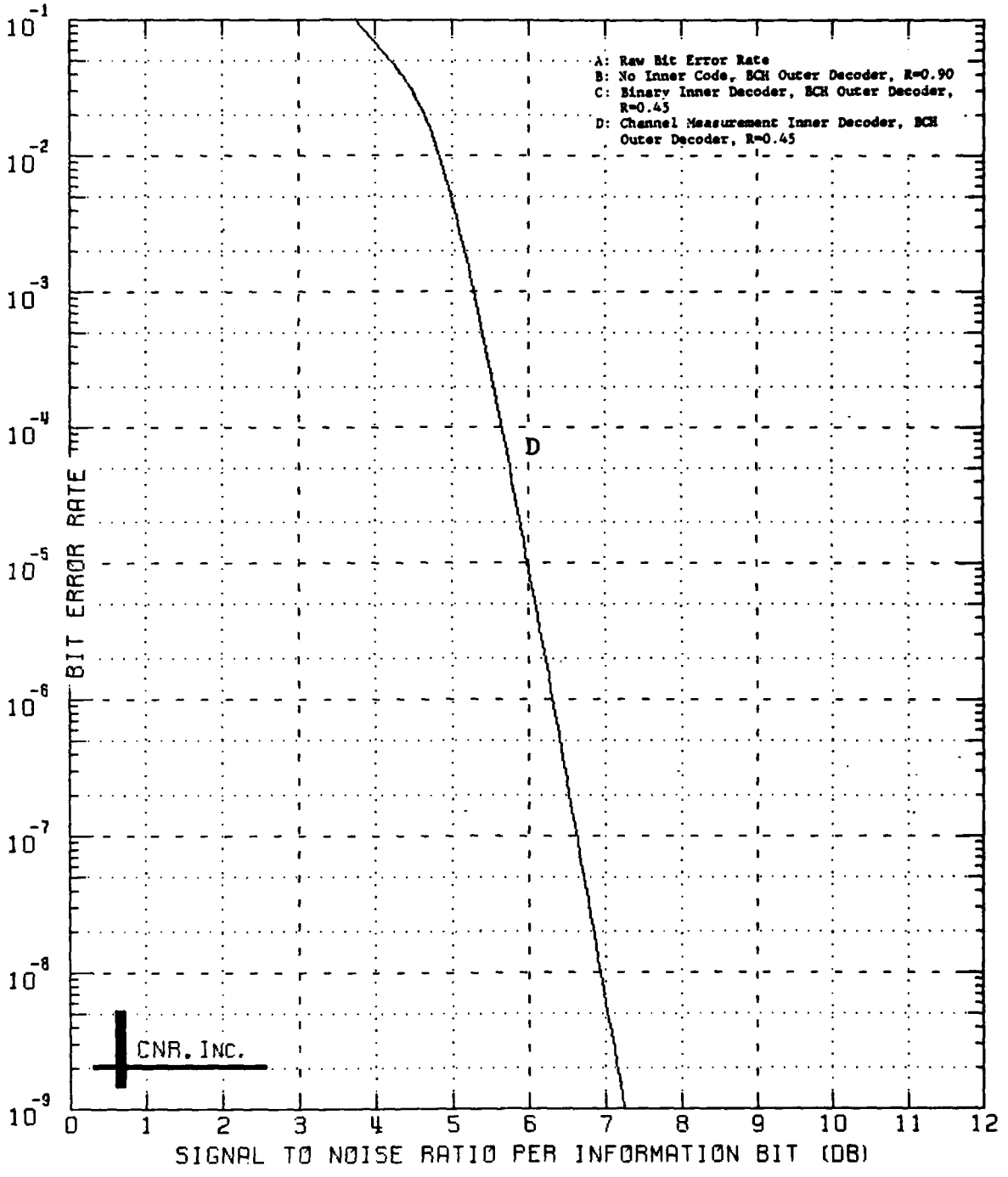


Figure 7.5 Decoded Performance of a Two-Stage Coding Approach
Outer Decoder: BCH Code (240,216;7)
Inner Decoder: Block Code (128,64;22)
δ=0.20 and No Erasure Information Employed

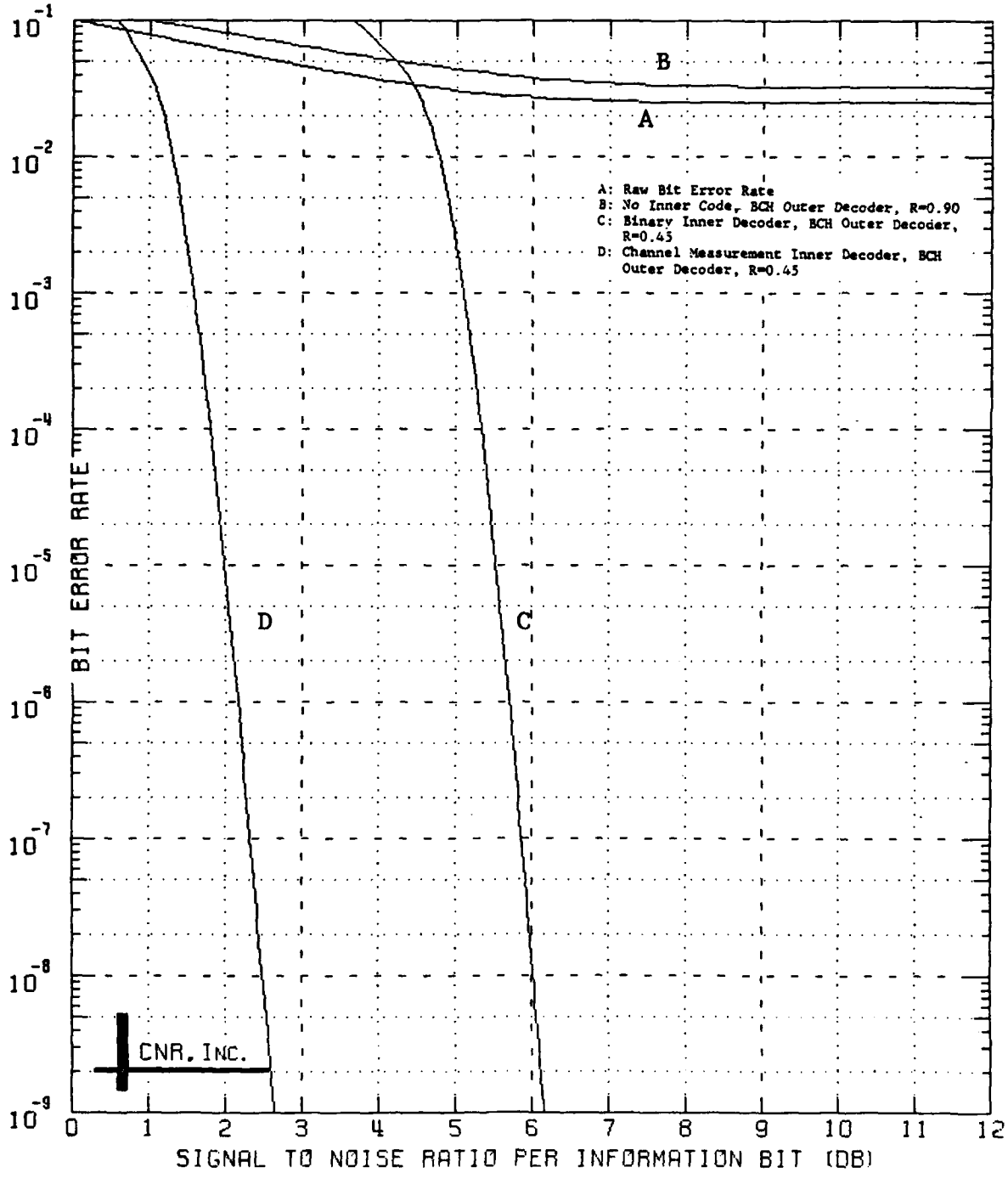


Figure 7.6 Decoded Performance of a Two-Stage Coding Approach
Outer Decoder: BCH Code (240,216;7)
Inner Decoder: Block Code (128,64;22)
δ=0.05 and Erasure Information is Employed

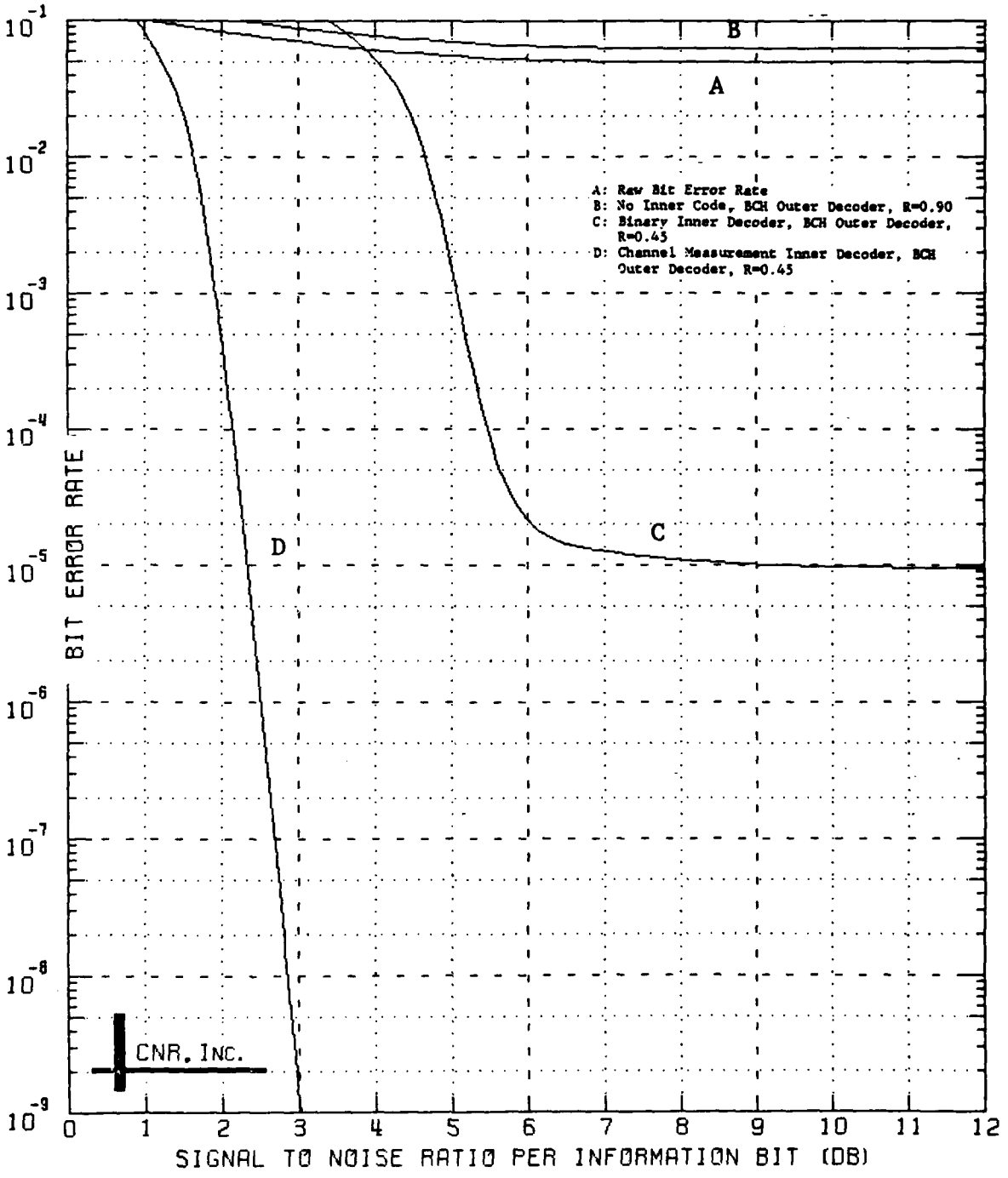


Figure 7.7 Decoded Performance of a Two-Stage Coding Approach
Outer Decoder: BCH Code (240,216;7)
Inner Decoder: Block Code (128,64;22)
δ=0.10 and Erasure Information is Employed

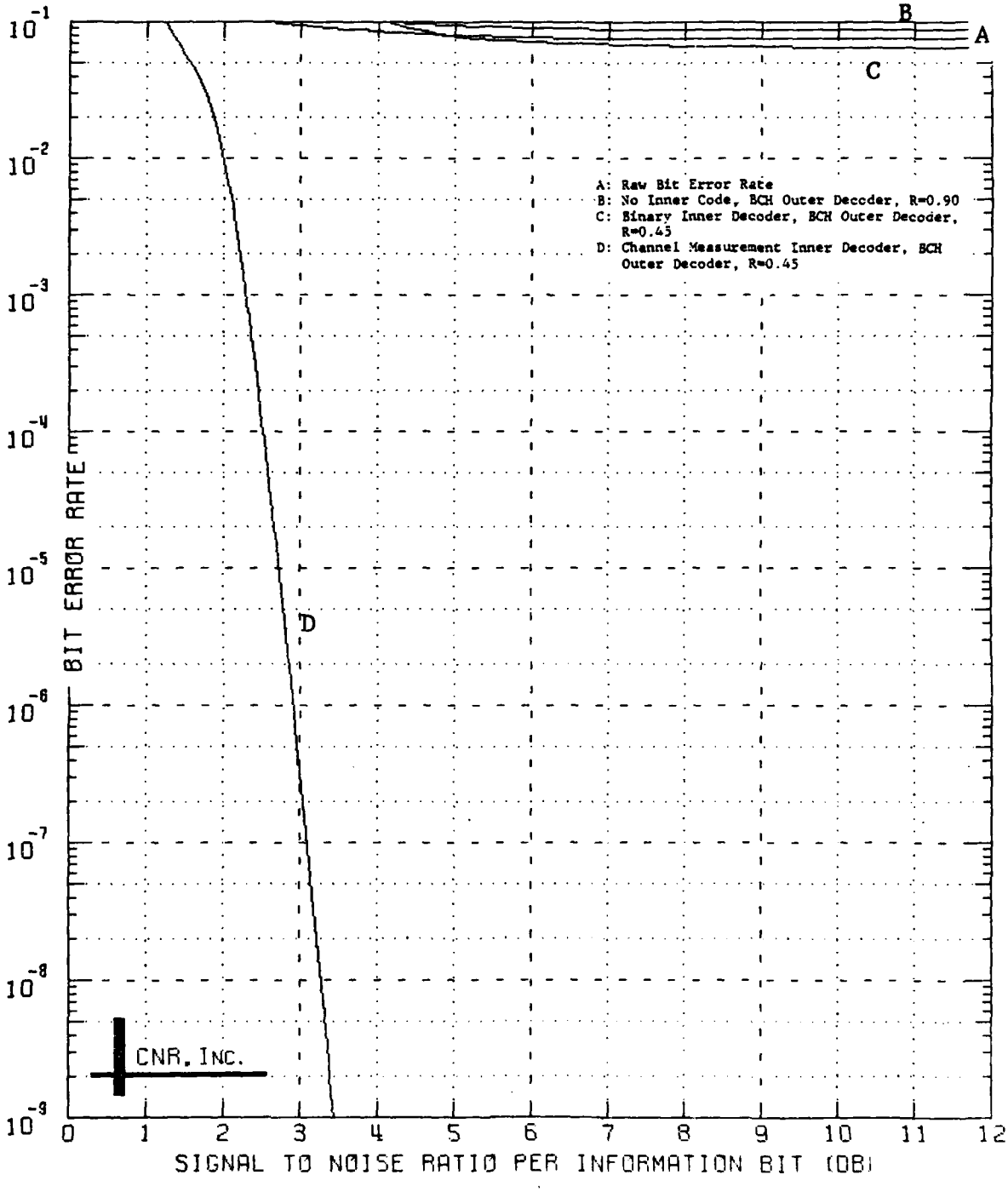


Figure 7.8 Decoded Performance of a Two-Stage Coding Approach
Outer Decoder: BCH Code (240,216;7)
Inner Decoder: Block Code (128,64;22)
δ=0.15 and Erasure Information is Employed

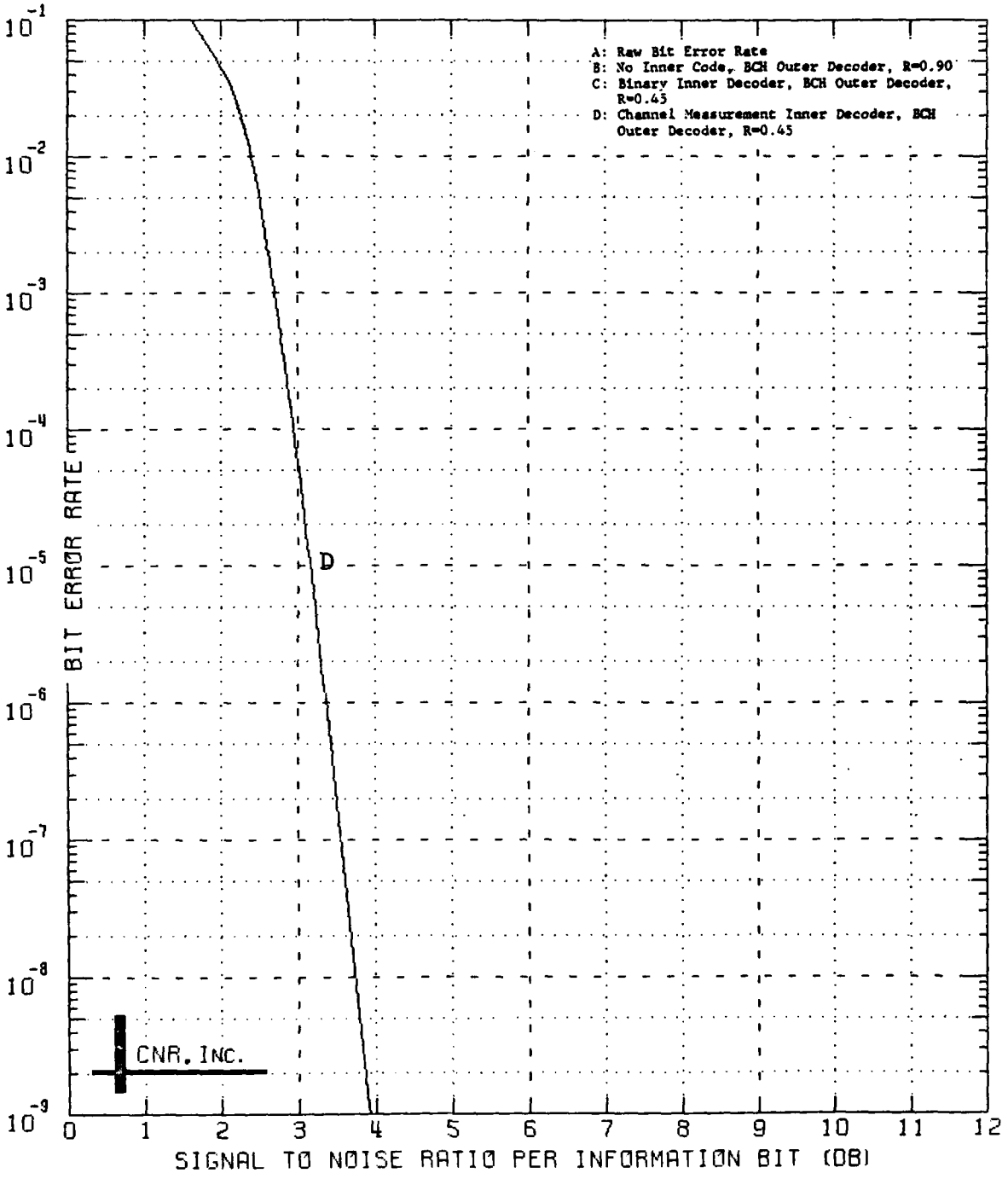


Figure 7.9 Decoded Performance of a Two-Stage Coding Approach
Outer Decoder: BCH Code (240,216;7)
Inner Decoder: Block Code (128,64;22)
δ=0.20 and Erasure Information is Employed

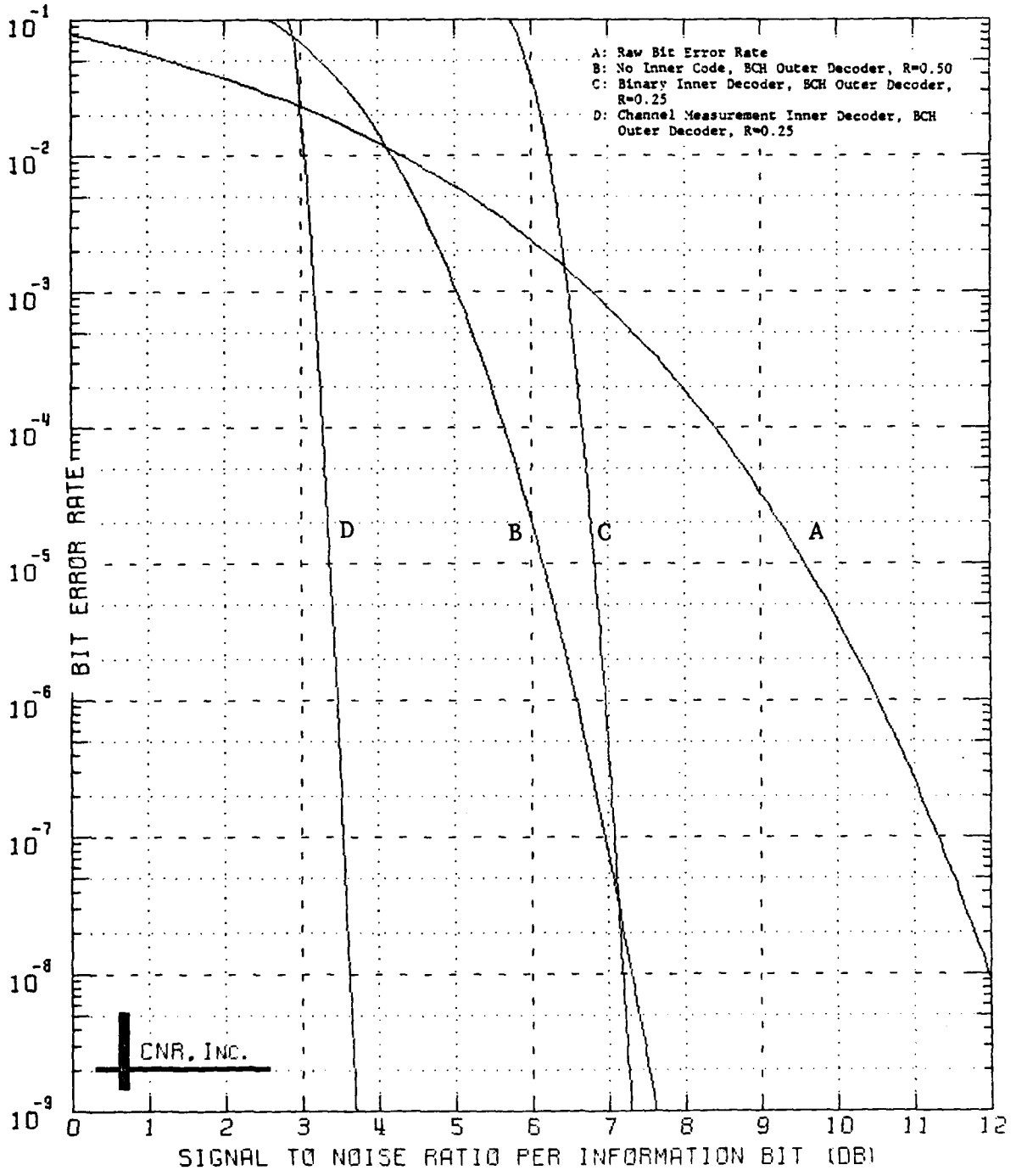


Figure 7.10 Decoded Performance of a Two-Stage Coding Approach
Outer Decoder: BCH Code (128,64;22)
Inner Decoder: Block Code (128,64;22)
δ=0.00 and No Erasure Information Employed

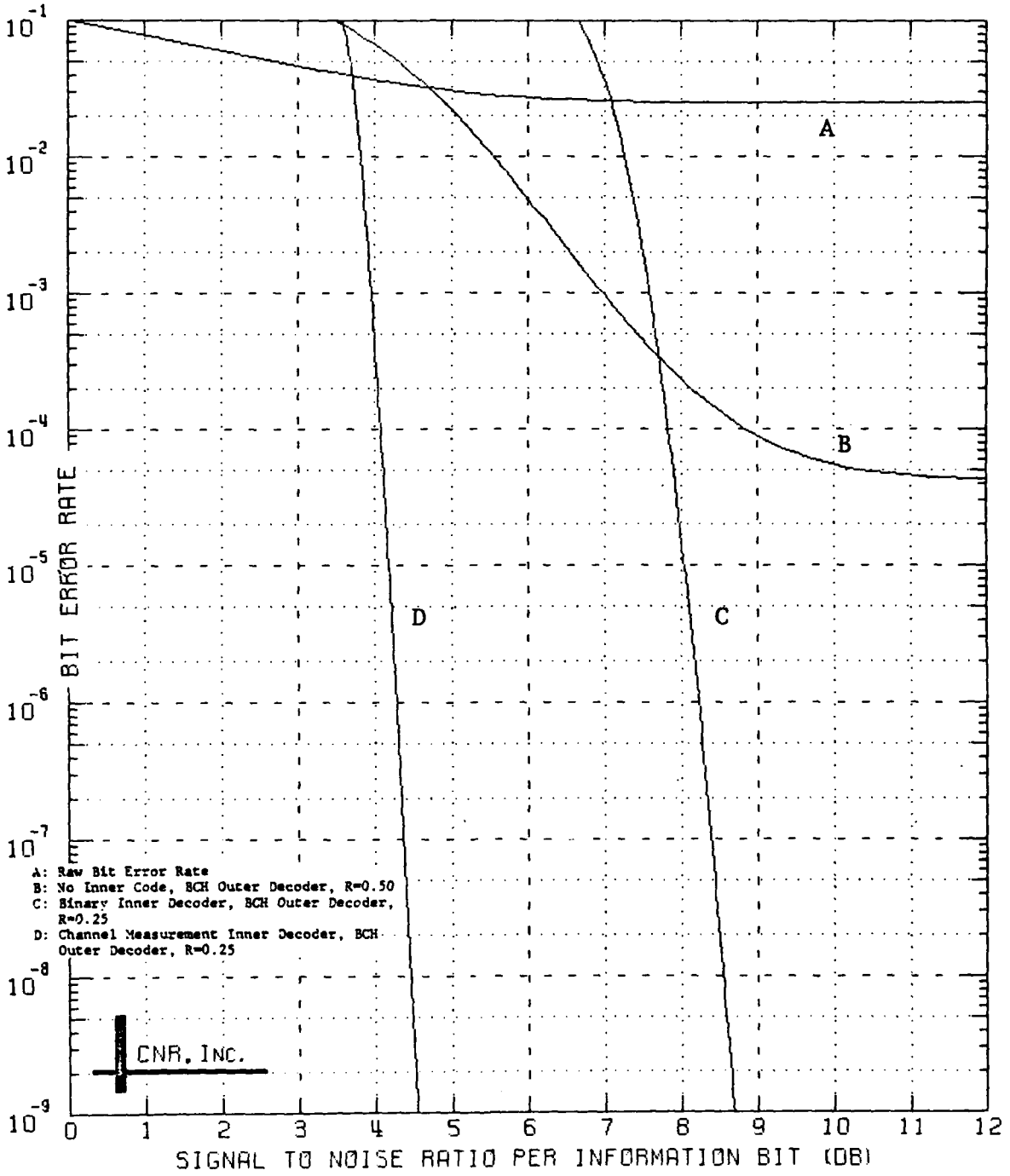


Figure 7.11 Decoded Performance of a Two-Stage Coding Approach
Outer Decoder: BCH Code (128,64;22)
Inner Decoder: Block Code (128,64;22)
δ=0.05 and No Erasure Information Employed

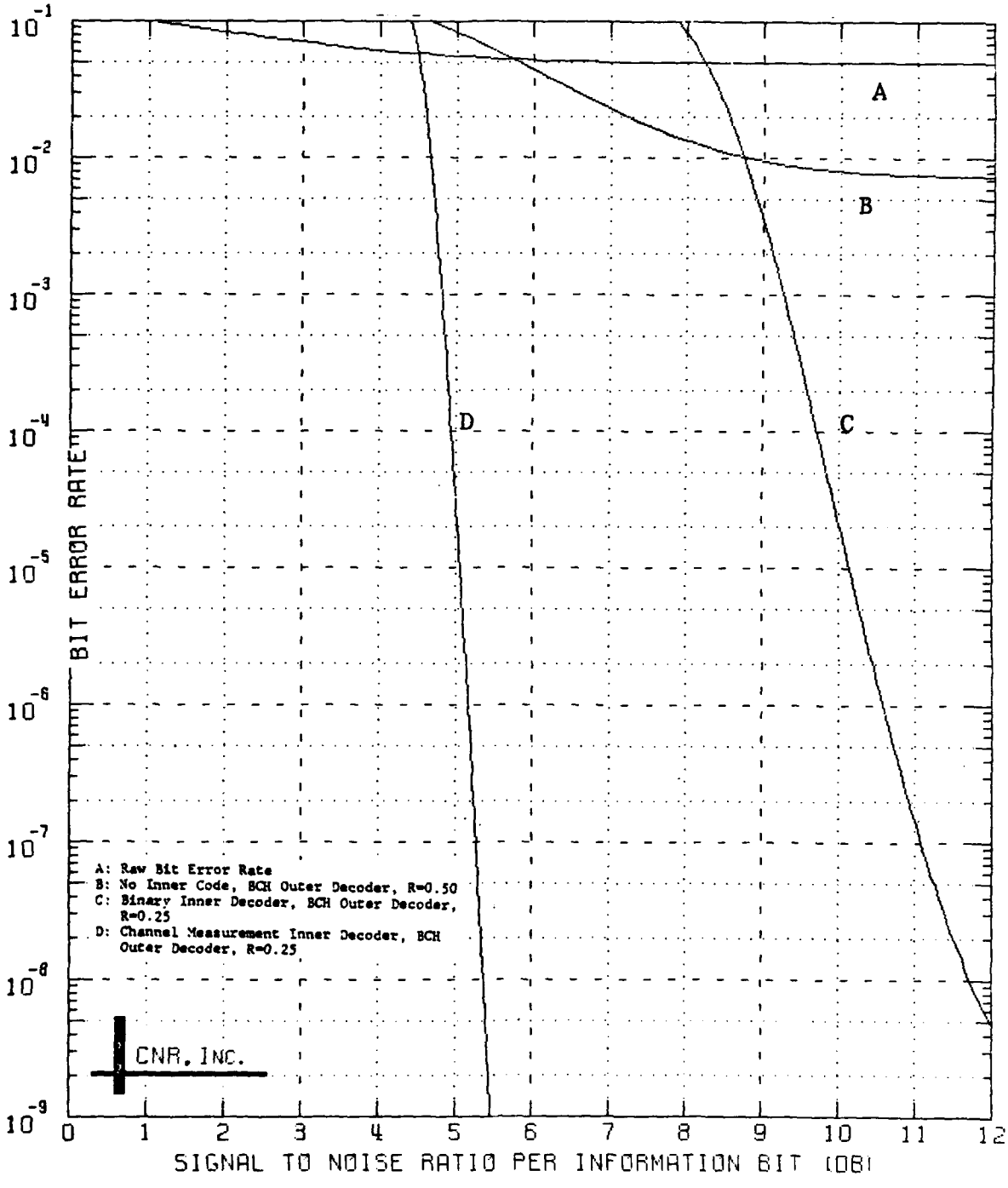


Figure 7.12 Decoded Performance of a Two-Stage Coding Approach
Outer Decoder: BCH Code (128,64;22)
Inner Decoder: Block Code (128,64;22)
δ=0.10 and No Erasure Information Employed

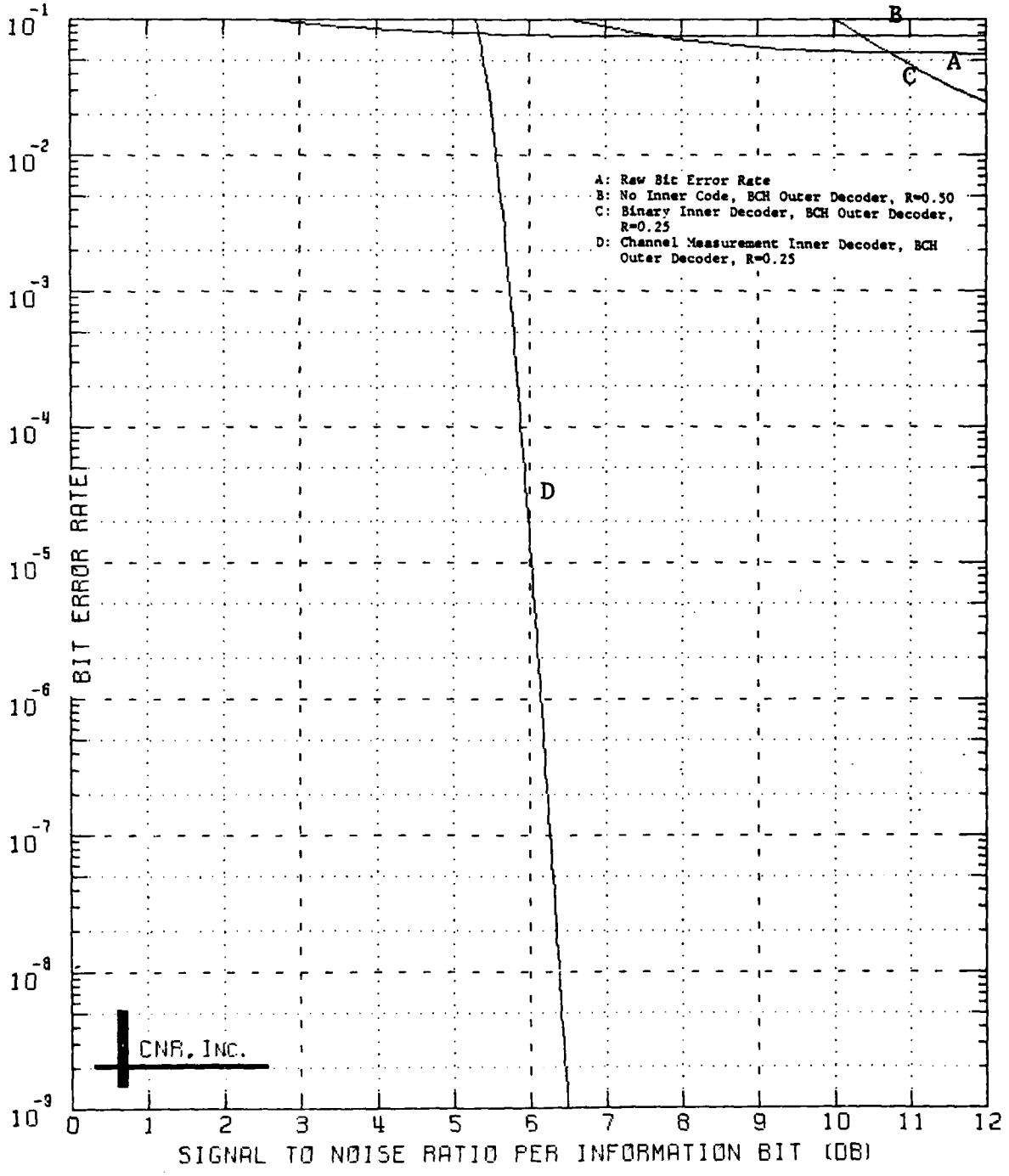


Figure 7.13 Decoded Performance of a Two-Stage Coding Approach
Outer Decoder: BCH Code (128,64;22)
Inner Decoder: Block Code (128,64;22)
δ=0.15 and No Erasure Information Employed

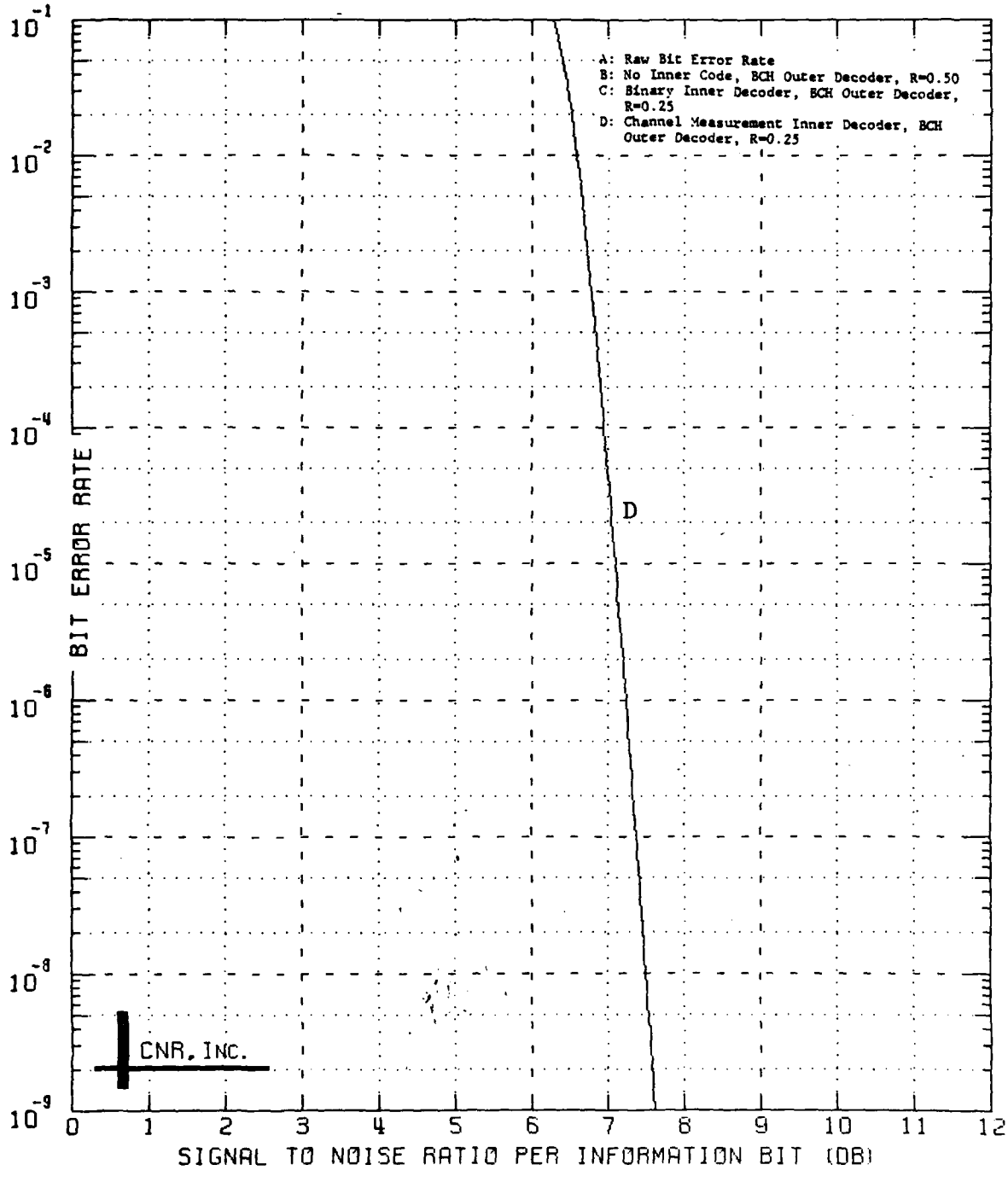


Figure 7.14 Decoded Performance of a Two-Stage Coding Approach
Outer Decoder: BCH Code (128,64;22)
Inner Decoder: Block Code (128,64;22)
δ=0.20 and No Erasure Information Employed

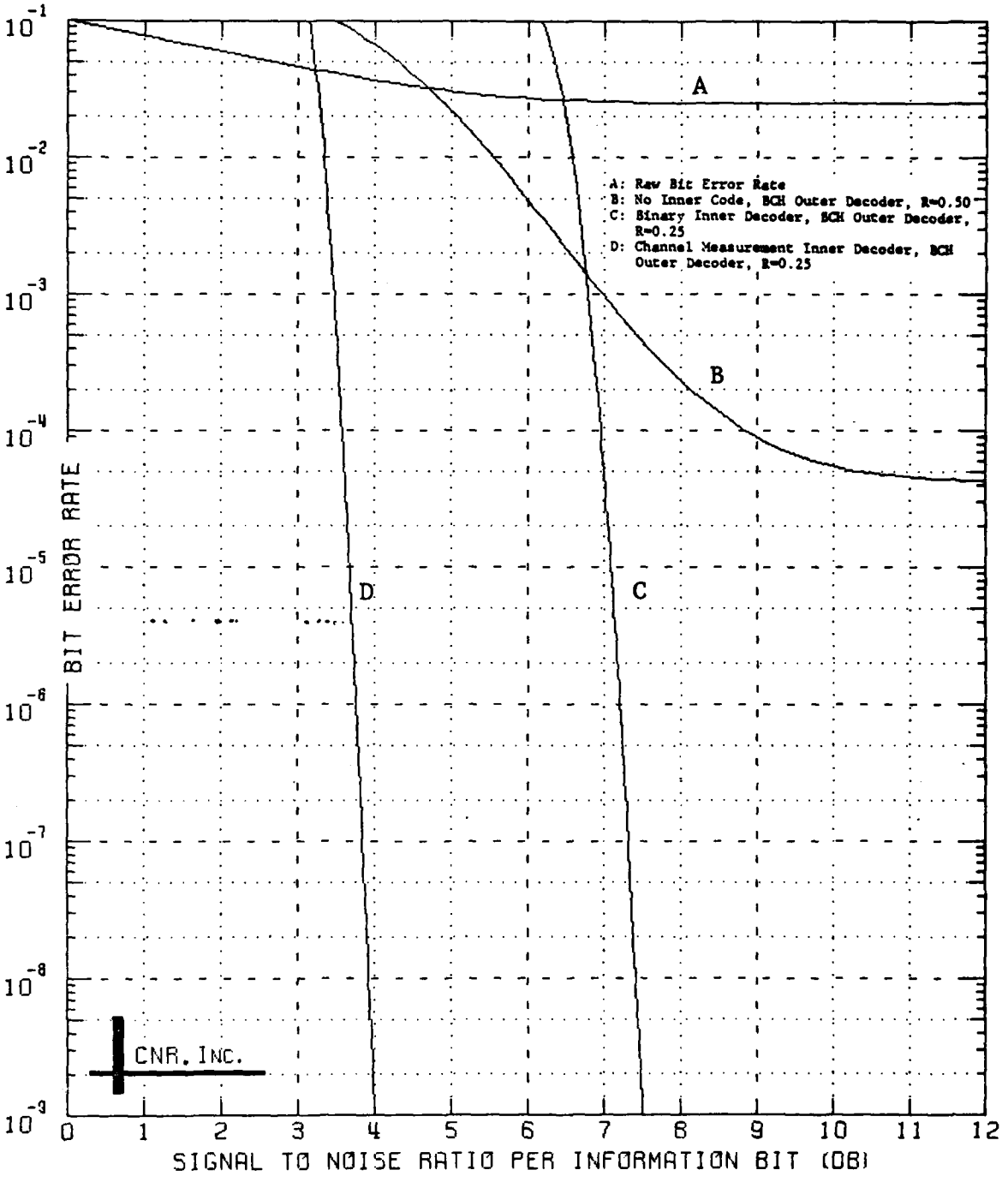


Figure 7.15 Decoded Performance of a Two-Stage Coding Approach
Outer Decoder: BCH Code (128,64;22)
Inner Decoder: Block Code (128,64;22)
δ=0.05 and Erasure Information is Employed

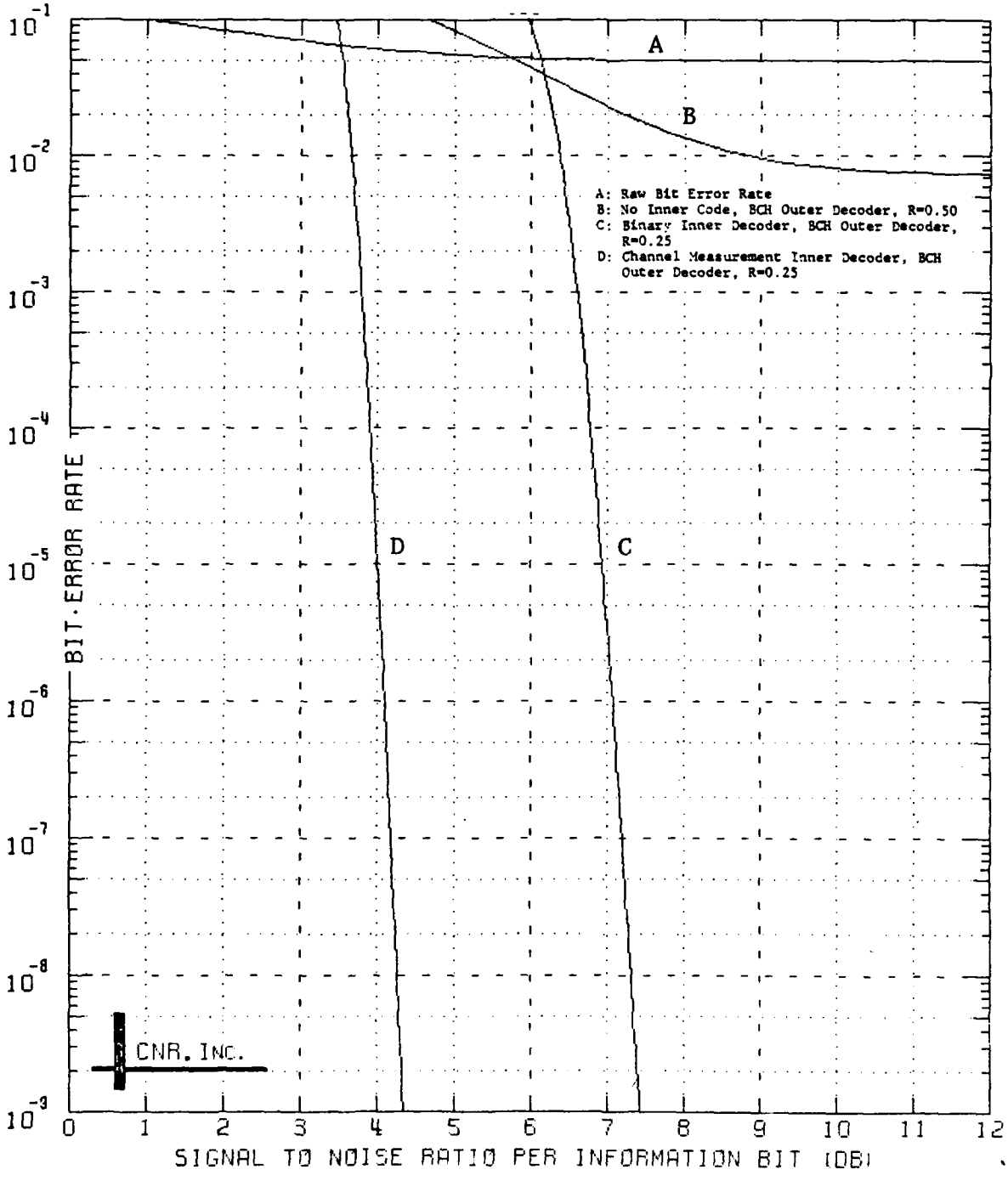


Figure 7.16 Decoded Performance of a Two-Stage Coding Approach
Outer Decoder: BCH Code (128,64;22)
Inner Decoder: Block Code (128,64;22)
δ=0.10 and Erasure Information is Employed

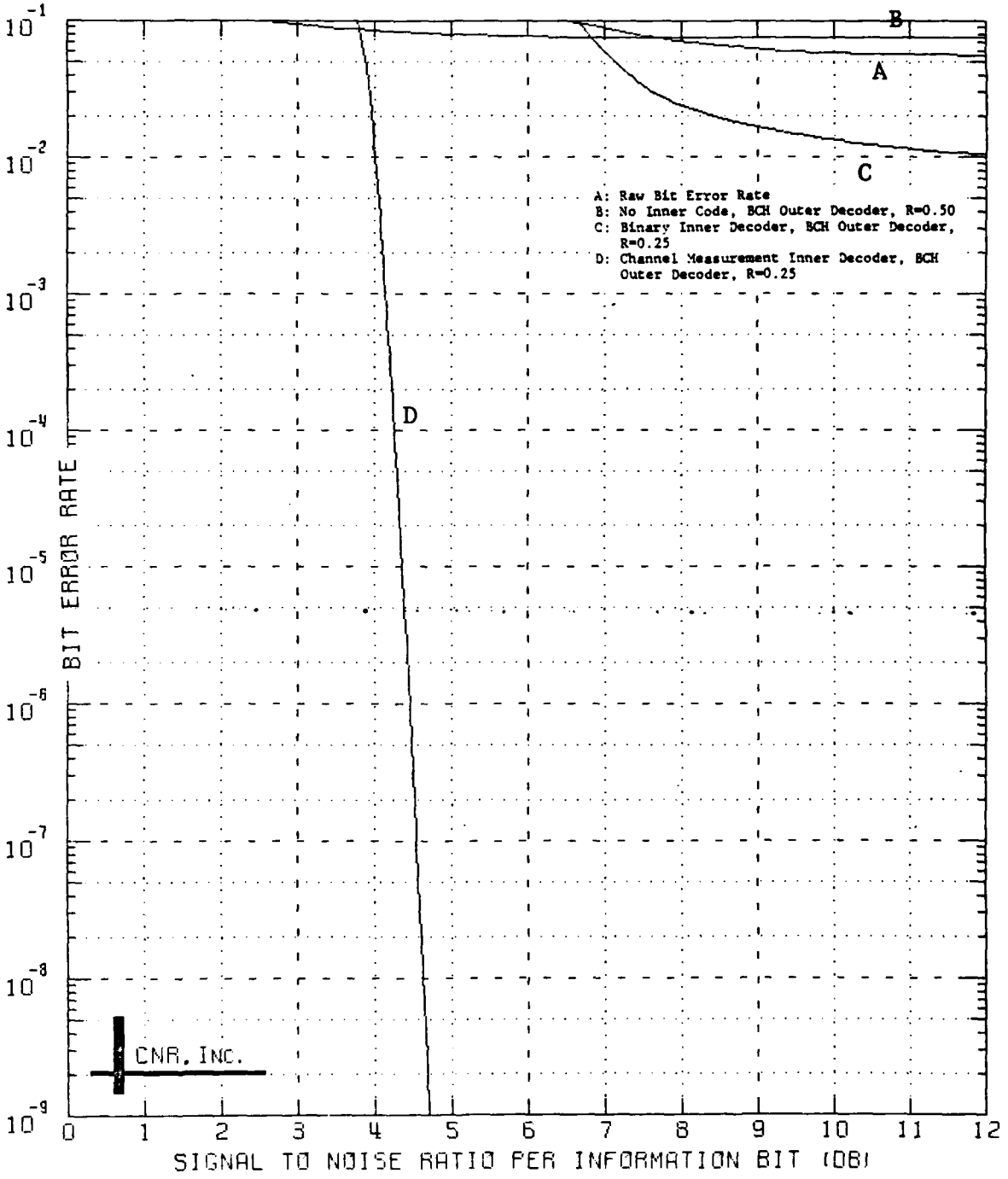


Figure 7.17 Decoded Performance of a Two-Stage Coding Approach
Outer Decoder: BCH Code (128,64;22)
Inner Decoder: Block Code (128,64;22)
δ=0.15 and Erasure Information is Employed

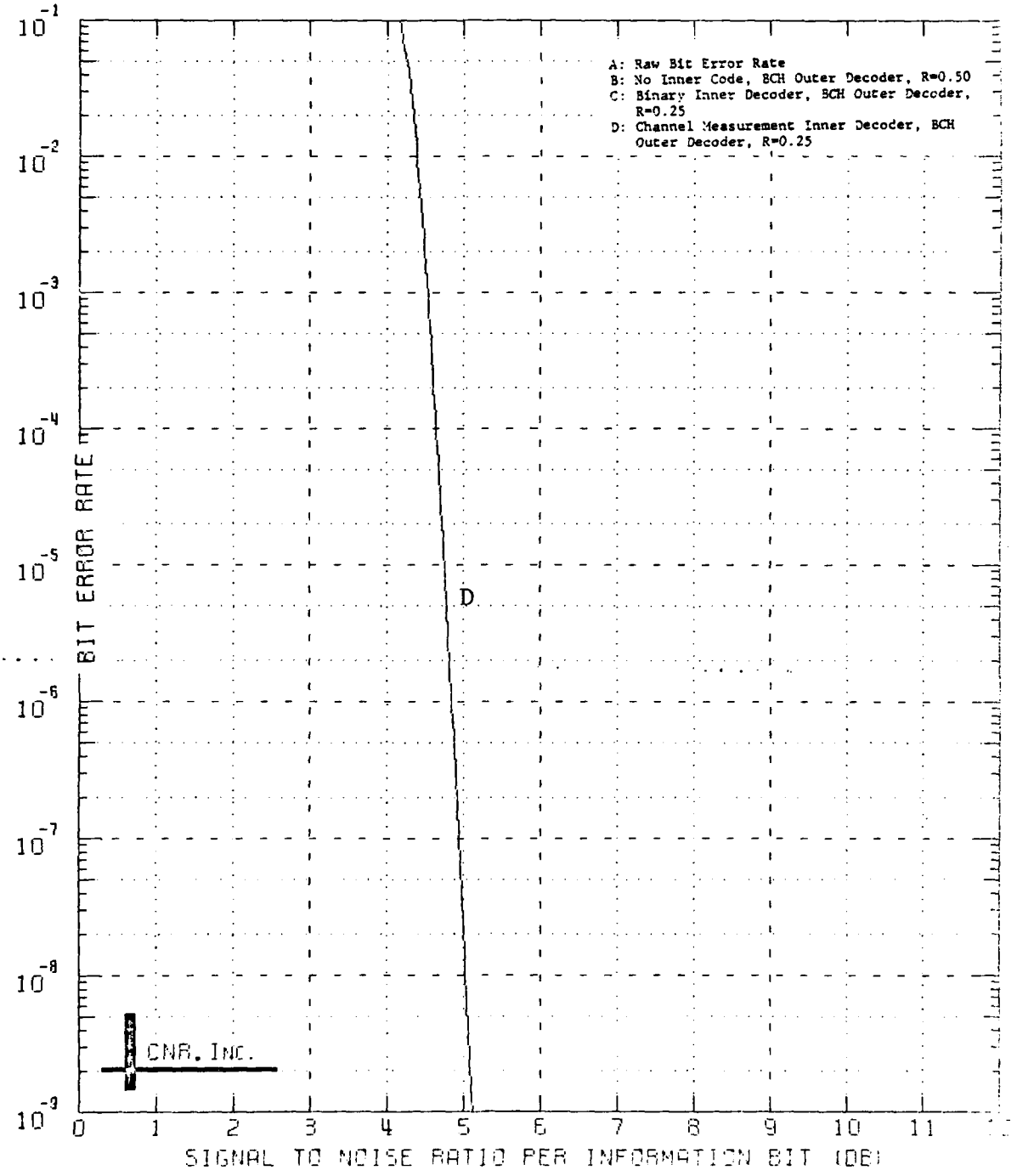


Figure 7.18 Decoded Performance of a Two-Stage Coding Approach
Outer Decoder: BCH Code (128,64;22)
Inner Decoder: Block Code (128,64;22)
δ=0.20 and Erasure Information is Employed

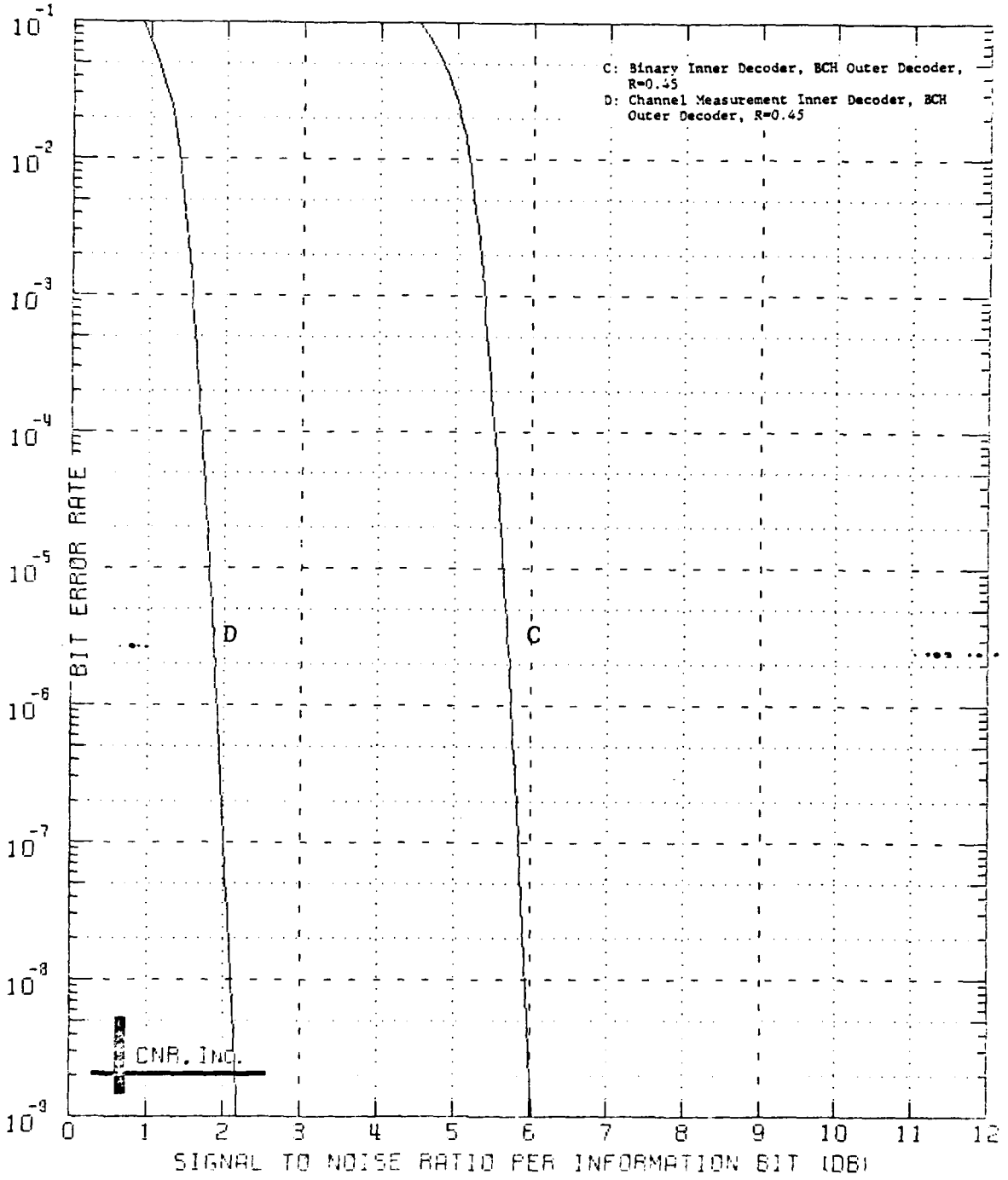


Figure 7.19 Decoded Performance of a Two-Stage Coding Approach Adaptive Technique
Outer Decoder: BCH Code (240,216;7)
Inner Decoder: Block Code (128,64;22)
δ=0.00 and No Erasure Information Employed

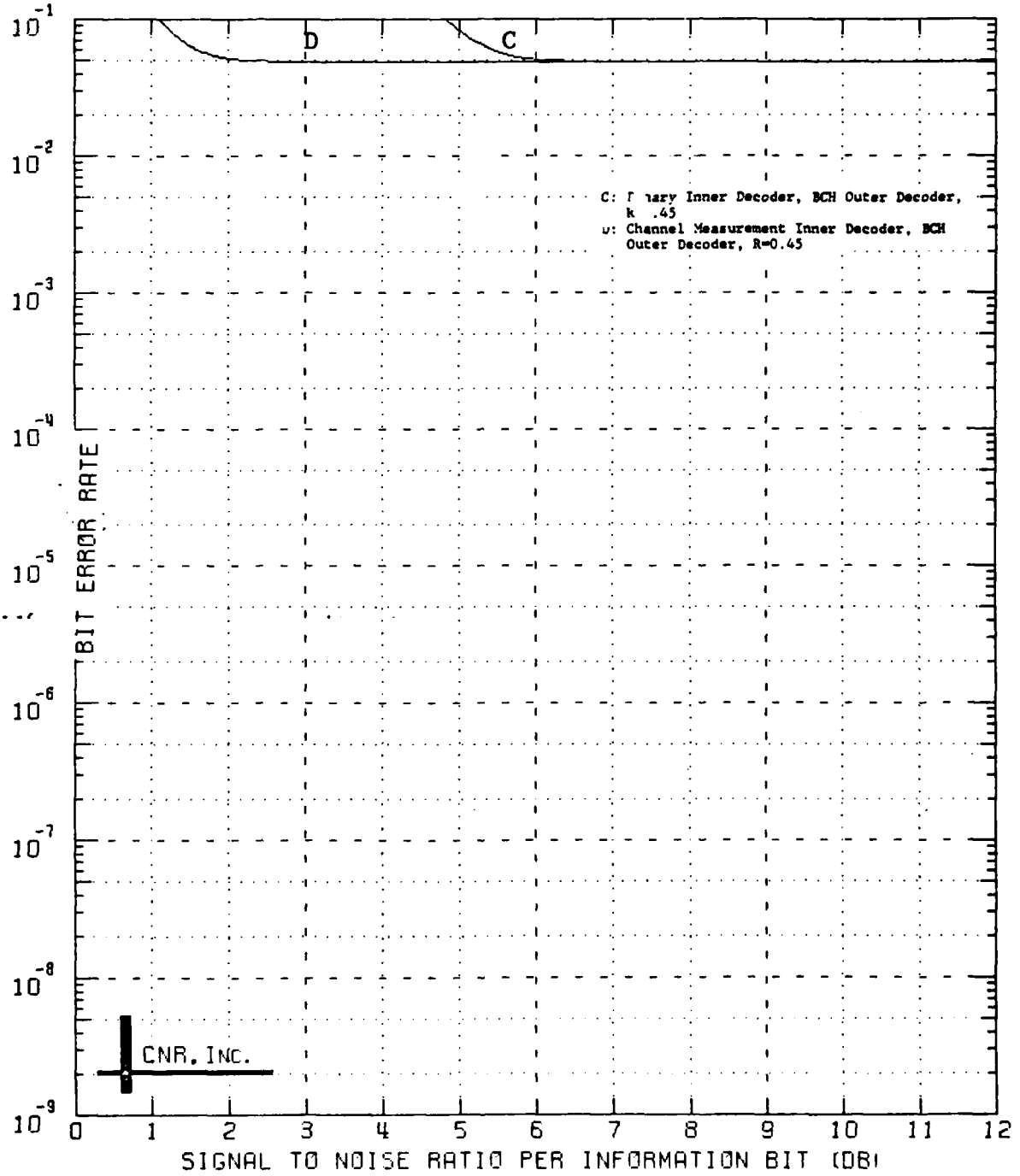


Figure 7.20 Decoded Performance of a Two-Stage Coding Approach Adaptive Technique
Outer Decoder: BCH Code (240,216;7)
Inner Decoder: Block Code (128,64;22)
δ=0.05 and No Erasure Information Employed

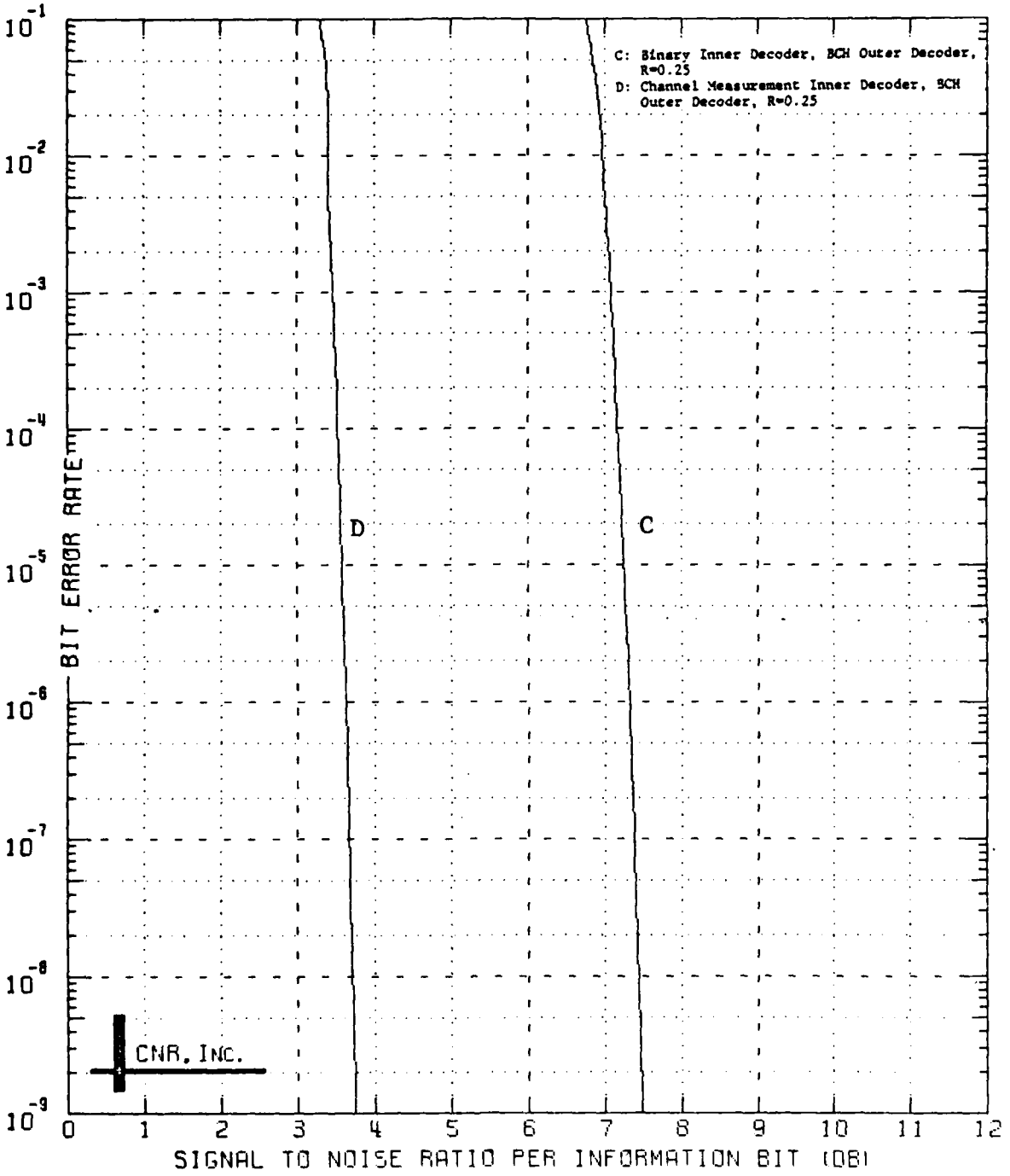


Figure 7.21 Decoded Performance of a Two-Stage Coding Approach Adaptive Technique
Outer Decoder: BCH Code (128,64;22)
Inner Decoder: Block Code (128,64;22)
δ=0.00 and No Erasure Information Employed

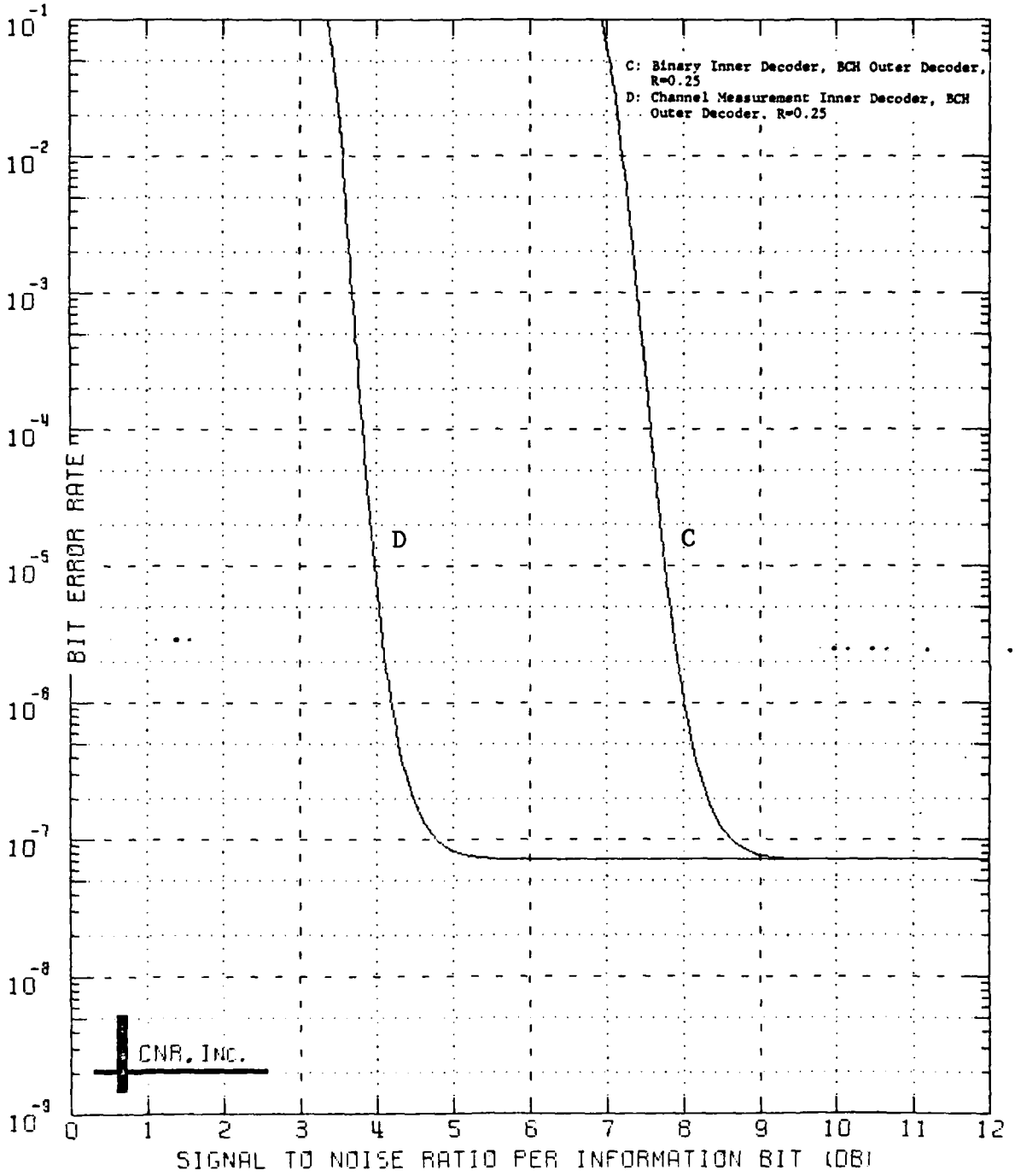


Figure 7.22 Decoded Performance of a Two-Stage Coding Approach Adaptive Technique
Outer Decoder: BCH Code (128,64;22)
Inner Decoder: Block Code (128,64;22)
δ=0.05 and No Erasure Information Employed

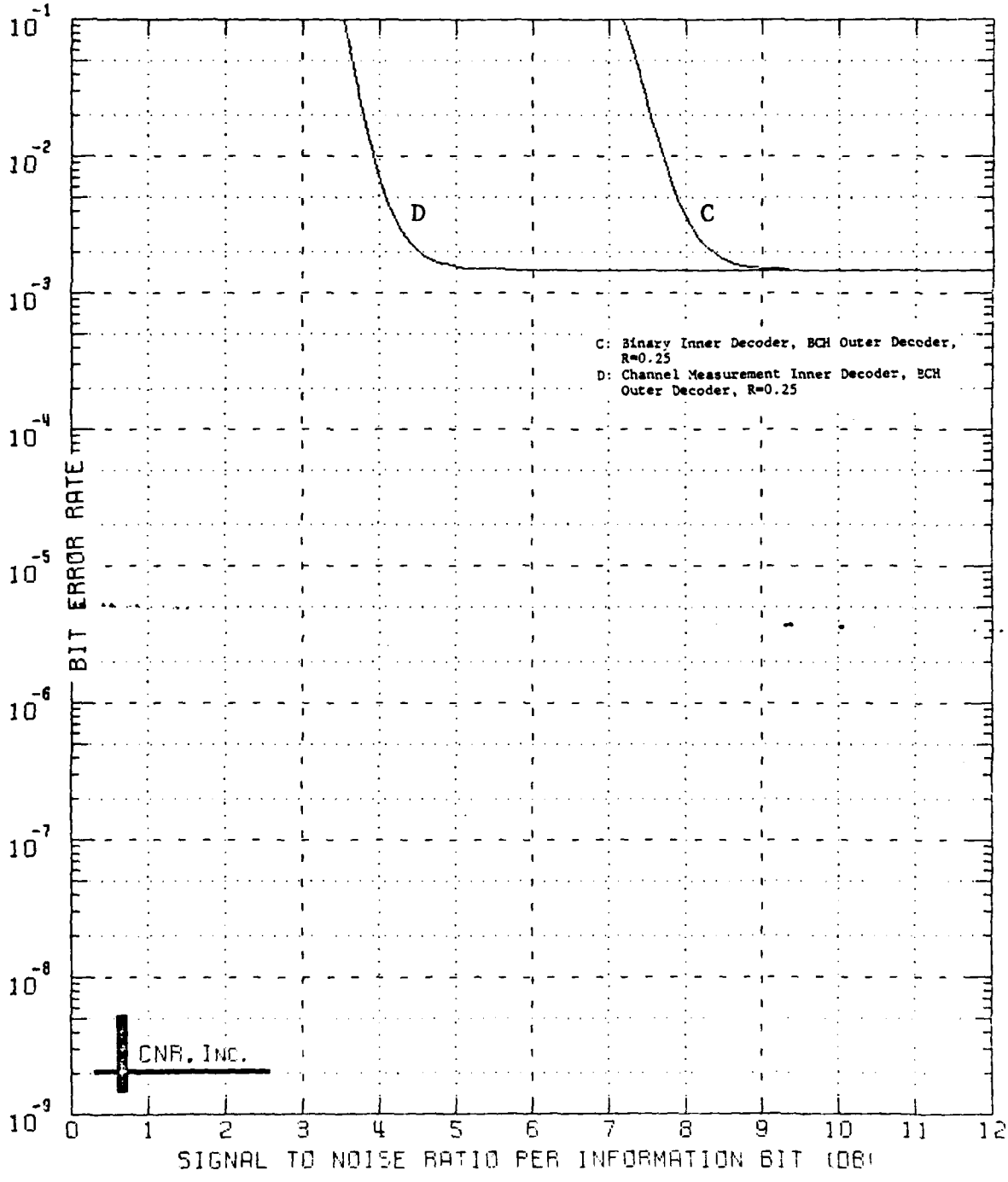


Figure 7.23 Decoded Performance of a Two-Stage Coding Approach Adaptive Technique
Outer Decoder: BCH Code (128,64;22)
Inner Decoder: Block Code (128,64;22)
δ=0.10 and No Erasure Information Employed

TABLE 7-1

E_b/N_0 (dB) REQUIRED FOR A BIT ERROR RATE OF 10^{-5} FOR RATE-1/2 INNER BLOCK CODE WITH RATE-0.9 AND RATE-1/2 OUTER CODES

Inner Decoder/Outer Decoder	Erasure Availability	δ=0.00		δ=0.05		δ=0.10		δ=0.15		δ=0.20	
		BD	CD	BD	CD	BD	CD	BD	CD	BD	CD
Block (128,64;22)/BCH (240,216;7)	No Erasures	5.3	1.6	7.2	2.6	----	3.6	----	4.7	----	6.0
Rate = 1/2 ⊗ 0.9 = 0.45	Erasures	5.3	1.6	5.5	2.0	9.5	2.3	----	2.7	----	3.2
Block (128,64;22)/BCH (128,64;22)	No Erasures	6.8	3.4	8.1	4.2	10.0	5.1	----	6.0	----	7.1
Rate = 1/2 ⊗ 1/2 = 0.25	Erasures	6.8	3.4	7.0	3.6	6.9	4.0	----	4.4	----	4.8

δ=0.25		δ=0.30		δ=0.35		δ=0.40		δ=0.45		δ=0.50		δ=0.55	
BD	CD	BD	CD	BD	CD	BD	CD	BD	CD	BD	CD	BD	CD
----	7.4	----	9.1	----	11.3	----	14.2	----	18.9	----	----	----	----
3.7		4.2		4.9		5.7		7.3		----		----	
----	8.2	----	9.6	----	11.3	----	13.3	----	16.0	----	20.1	----	----
5.2		5.7		6.2		6.9		7.8		9.0		----	

---- Error Rate of 10^{-5} not achievable

SECTION 8

TWO-STAGE CODING APPROACH BASED ON A CONVOLUTIONAL INNER CODE

The encouraging results obtained in Section 7 for rate-0.45 and rate-0.25 two-stage coding approaches motivate additional study of these coding approaches.

Following the same format used in Section 7, we obtained results for the K=7 convolutional inner codes of rate-1/2, 1/4 and 1/8.

Figures 8.1 to 8.9 illustrate the performance of a rate-1/2 $\otimes$ 0.9 coding approach based on the inner convolutional code and the rate-0.9 (240,216) outer BCH code. Similar results are given by Figures 8.10 to 8.18 for the rate-1/4 convolutional inner code, and by Figures 8.19 to 8.27 for the rate-1/8 convolutional inner code. The results for the rate-1/8 $\otimes$ 0.9 = 0.1125 coding approach are quite impressive and relatively insensitive to the interference duty factor as it varies for 0 to 20%. For example, when erasure information is unavailable a 2-3 dB loss in performance results when interference with a duty factor of 20% is compared to the no interference case. When erasure information is available, this loss is only on the order of 1 dB. Needless to say, a system based on these low rate coding approaches is quite robust and thus should represent attractive ECCM coding approaches.

In addition to considering a rate-0.9 outer BCH code, a rate-1/2, K=7 outer convolutional code is considered. Figures 8.28 to 8.36 illustrate these results. As summarized in Table 8-1, the choice of a rate-1/2 convolutional outer code is generally inferior to the rate-0.9 outer code. Table 8-2 shows that the rate-1/4 $\otimes$ 0.9 and rate 1/8 $\otimes$ 0.9, two-stage coding approach can be effective in the presence of interference probabilities which are significantly greater than the δ = 0.20 illustrated graphically.

Figures 8.37 to 8.40 illustrate the results in Tables 8-1 and 8-2 where the more effective rate-0.9 outer code is used

with a rate-1/2, 1/4, and 1/8 inner convolutional code. Comparing these figures to their straight convolutional coding counterparts, Figures 6.28 to 6.31, further illustrates the importance of these two-stage coding approaches.

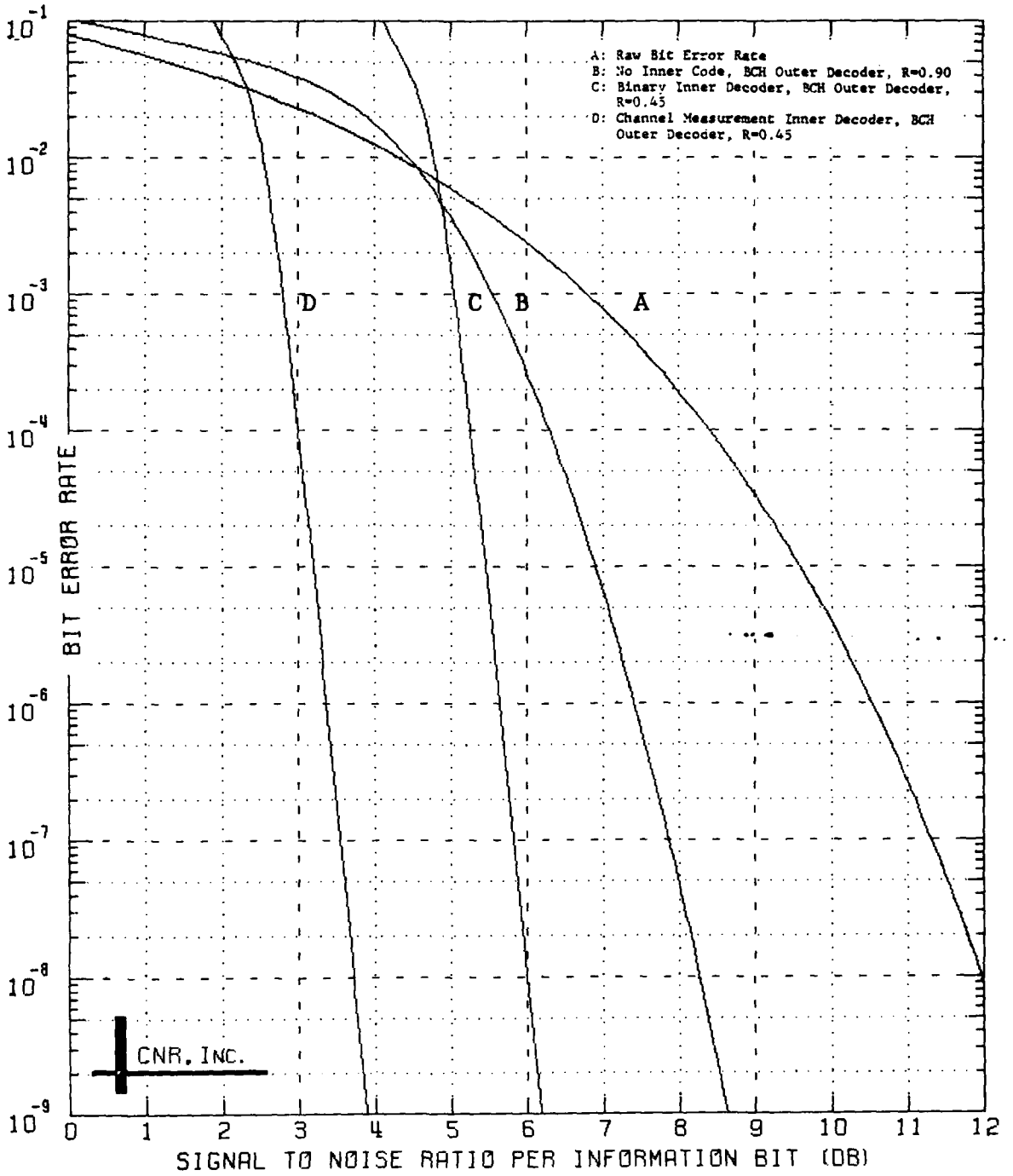


Figure 8.1 Decoded Performance of a Two-Stage Coding Approach
Outer Decoder: BCH Code (240,216;7)
Inner Decoder: Convolutional Code; Rate=1/2; K=7
δ=0.00 and No Erasure Information Employed

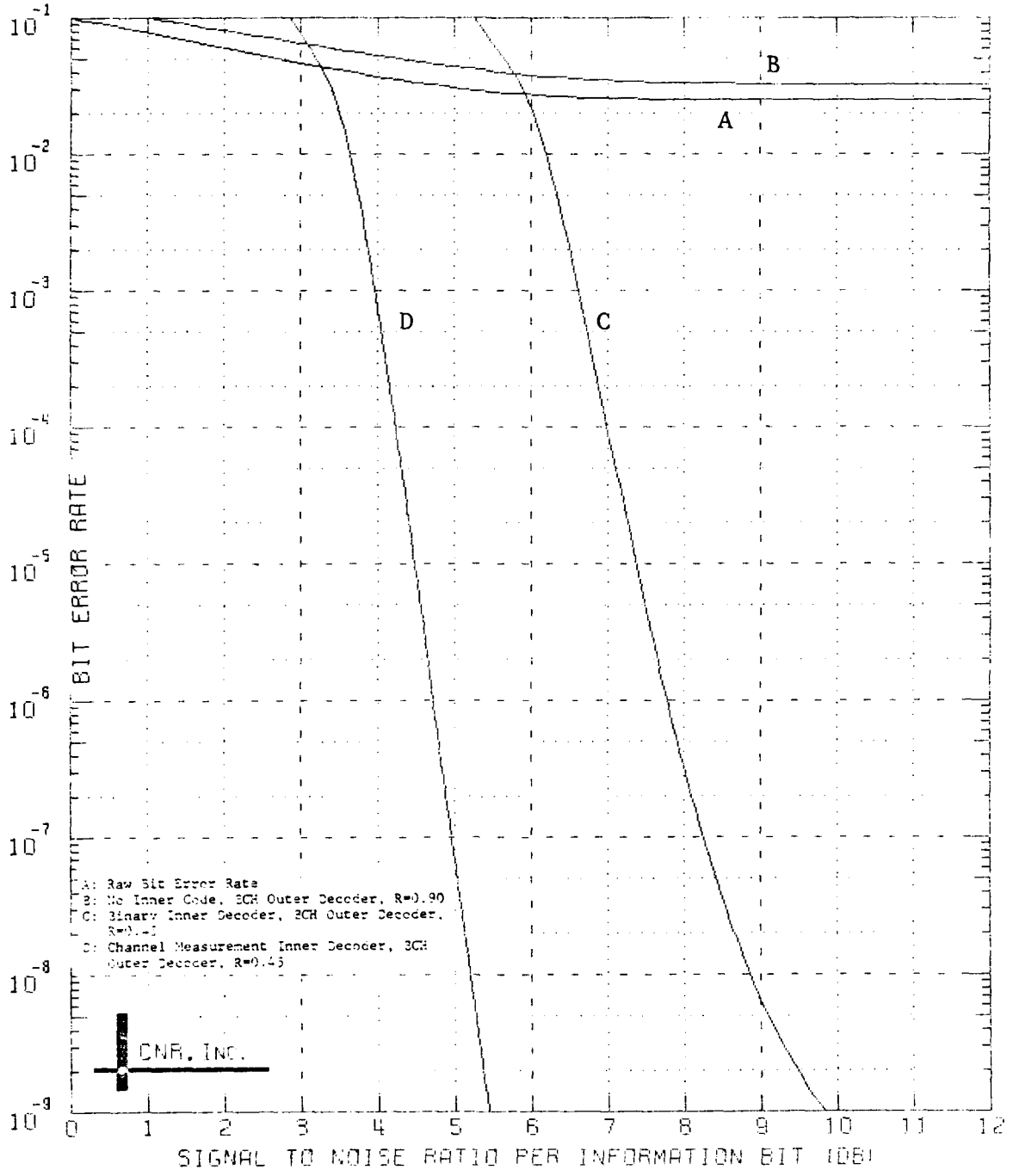


Figure 8.2 Decoded Performance of a Two-Stage Coding Approach
Outer Decoder: BCH Code (240,216;7)
Inner Decoder: Convolutional Code; Rate=1/2; K=7
δ=0.05 and No Erasure Information Employed

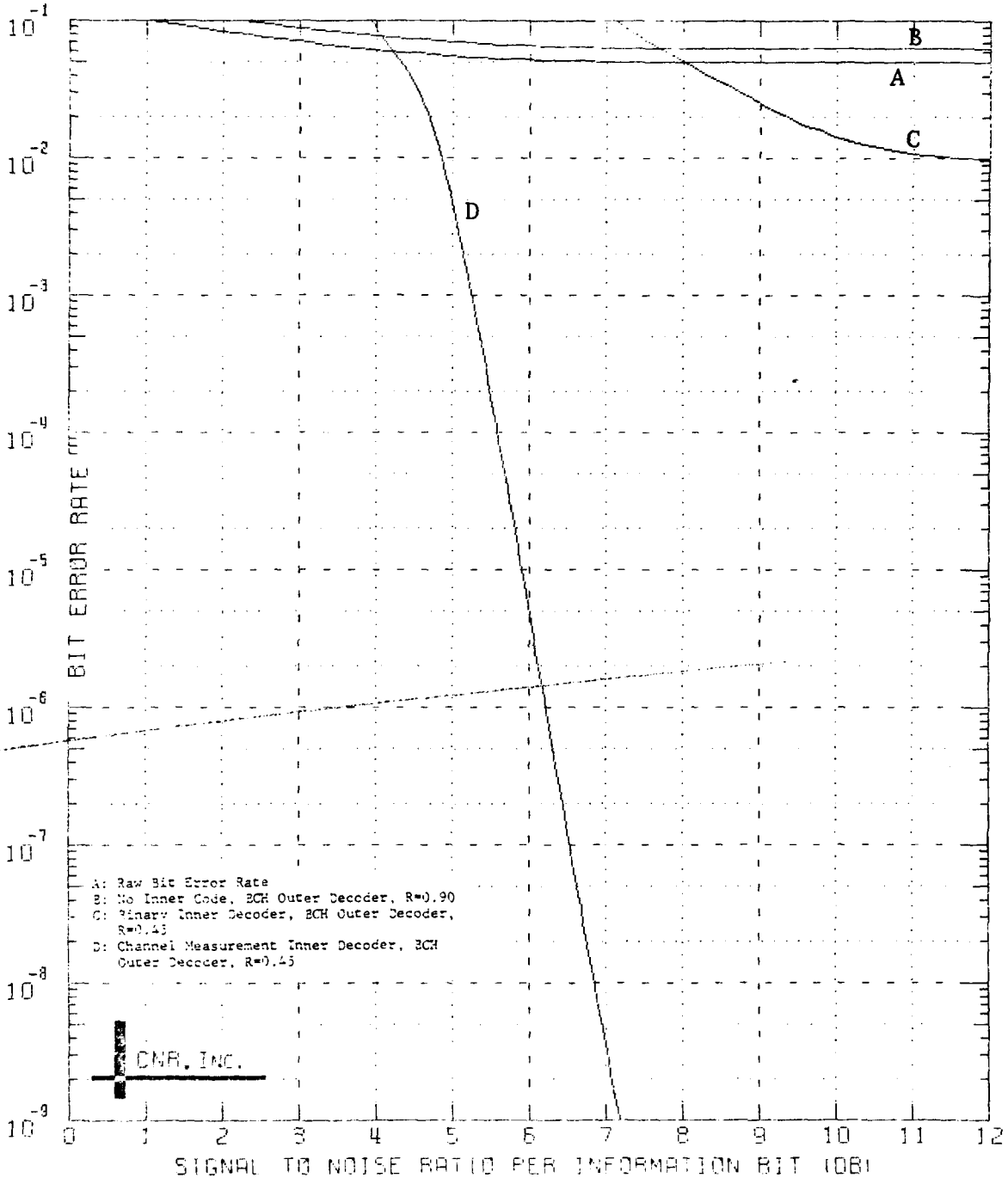


Figure 8.3 Decoded Performance of a Two-Stage Coding Approach
Outer Decoder: BCH Code (240,216;7)
Inner Decoder: Convolutional Code; Rate=1/2; K=7
δ=0.10 and No Erasure Information Employed

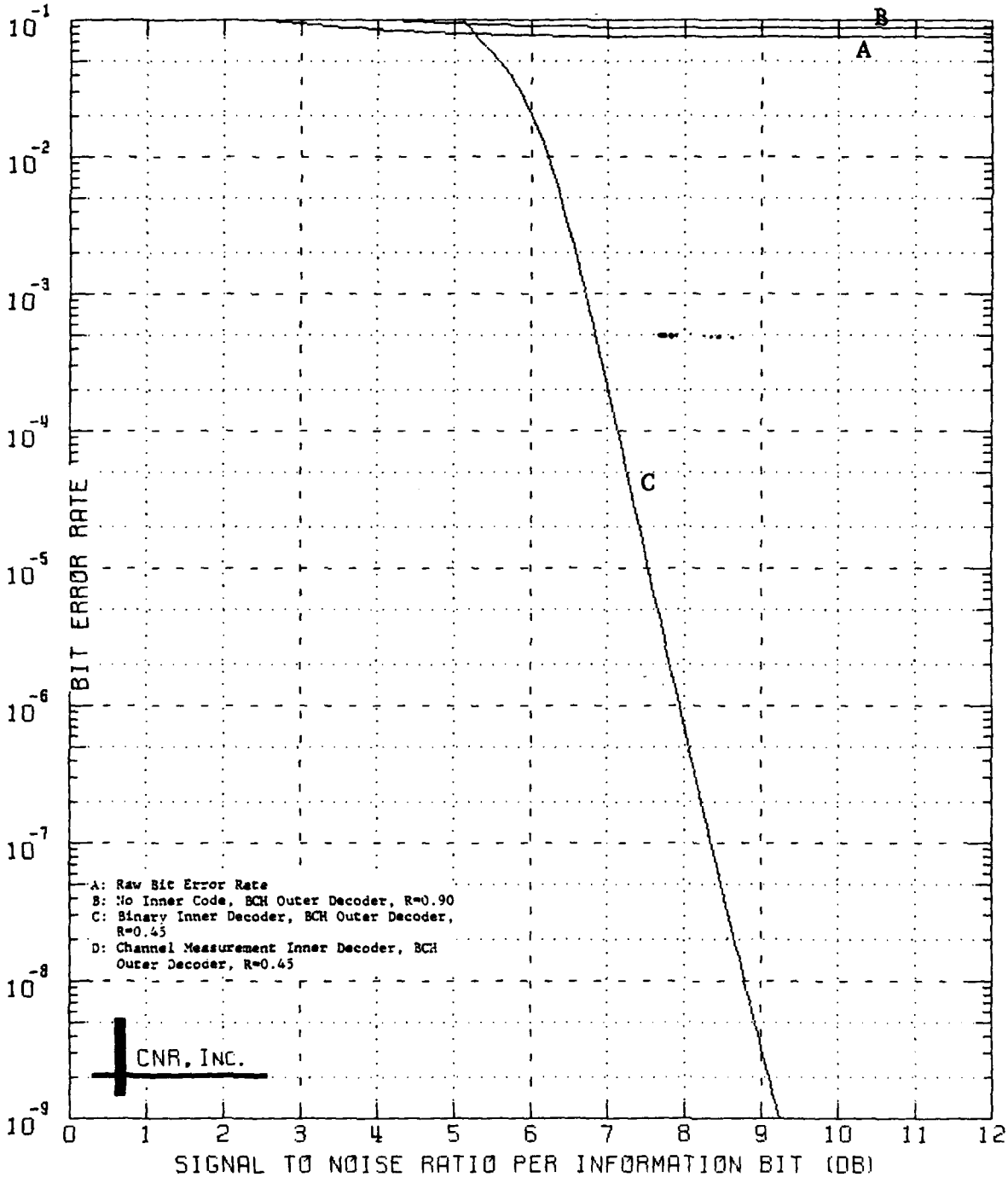


Figure 8.4 Decoded Performance of a Two-Stage Coding Approach
Outer Decoder: BCH Code (240,216;7)
Inner Decoder: Convolutional Code; Rate=1/2; K=7
δ=0.15 and No Erasure Information Employed

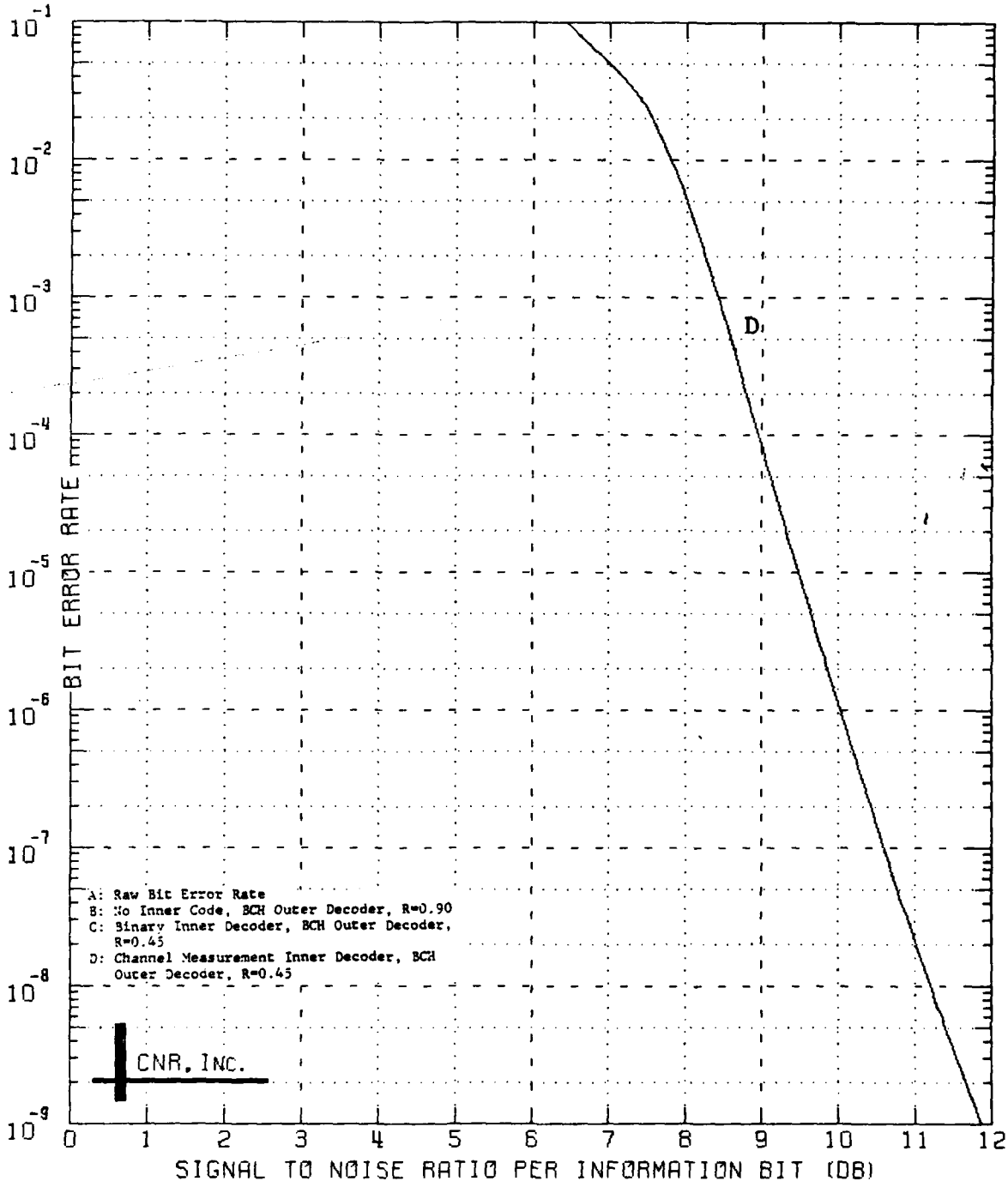


Figure 8.5 Decoded Performance of a Two-Stage Coding Approach
Outer Decoder: BCH Code (240,216;7)
Inner Decoder: Convolutional Code; Rate=1/2; K=7
δ=0.20 and No Erasure Information Employed

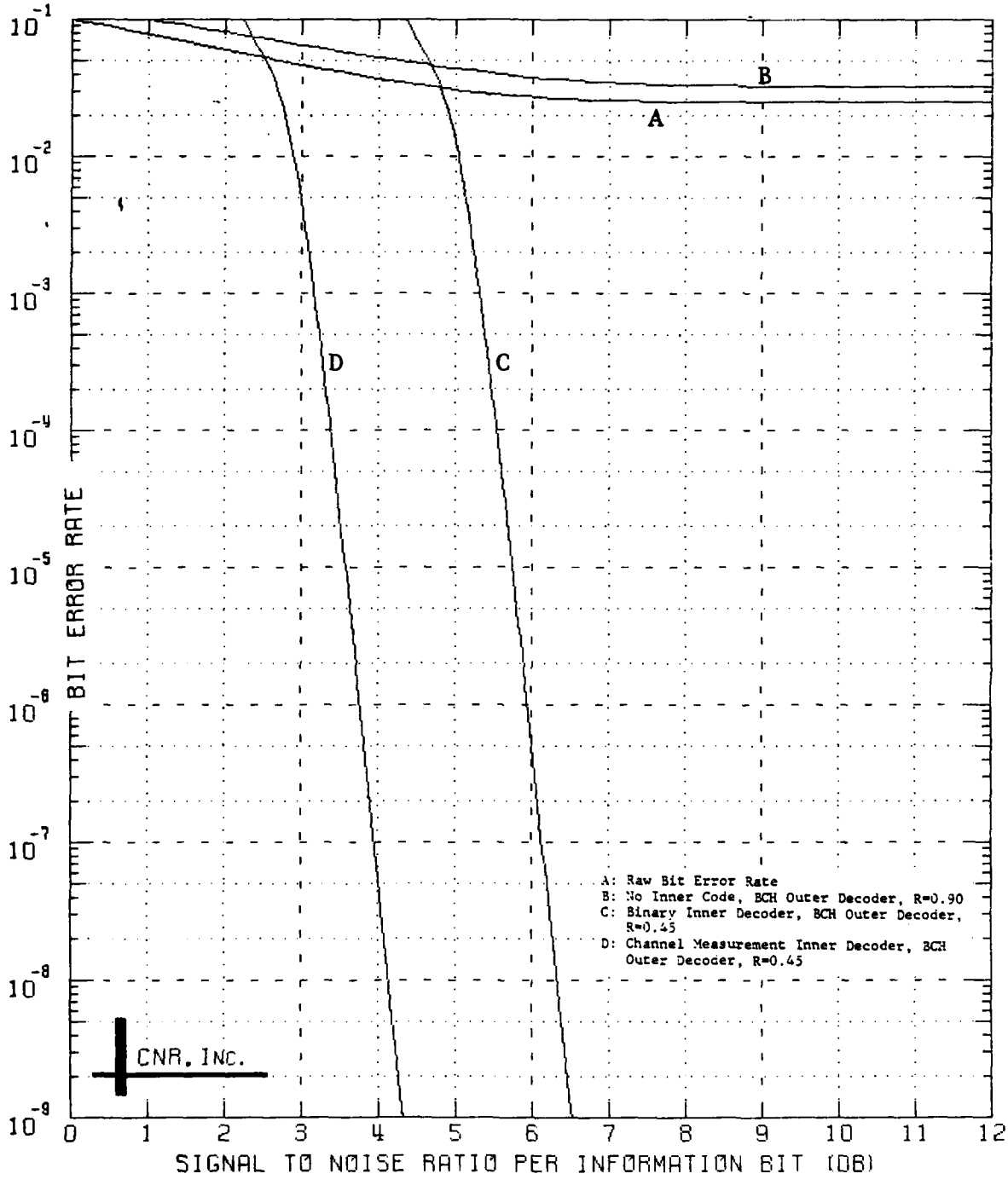


Figure 8.6 Decoder Performance of a Two-Stage Coding Approach
Outer Decoder: BCH Code (240,216;7)
Inner Decoder: Convolutional Code; Rate=1/2; K=7
δ=0.05 and Erasure Information is Employed

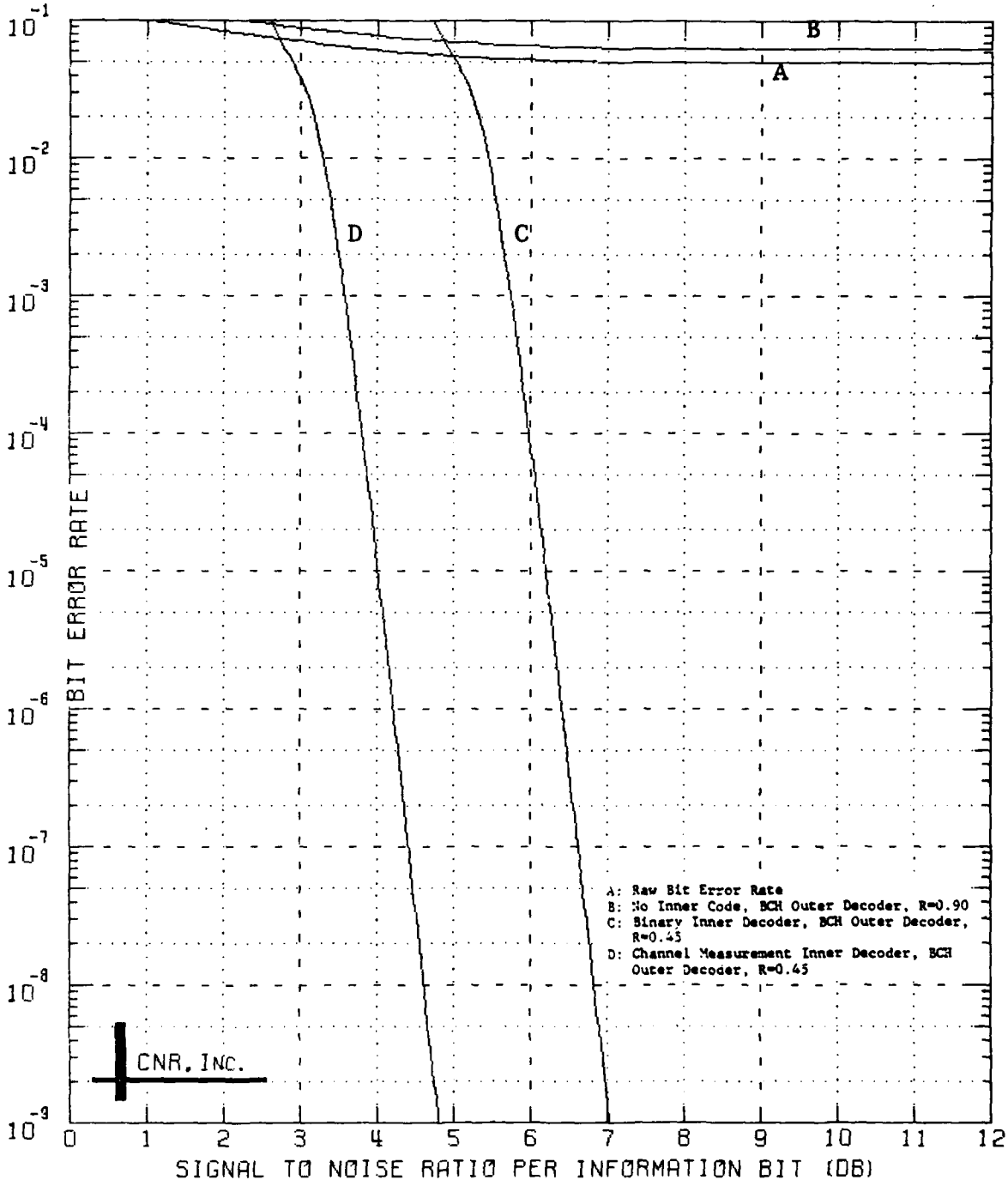


Figure 8.7 Decoded Performance of a Two-Stage Coding Approach
Outer Decoder: BCH Code (240,216;7)
Inner Decoder: Convolutional Code; Rate=1/2; K=7
δ=0.10 and Erasure Information is Employed

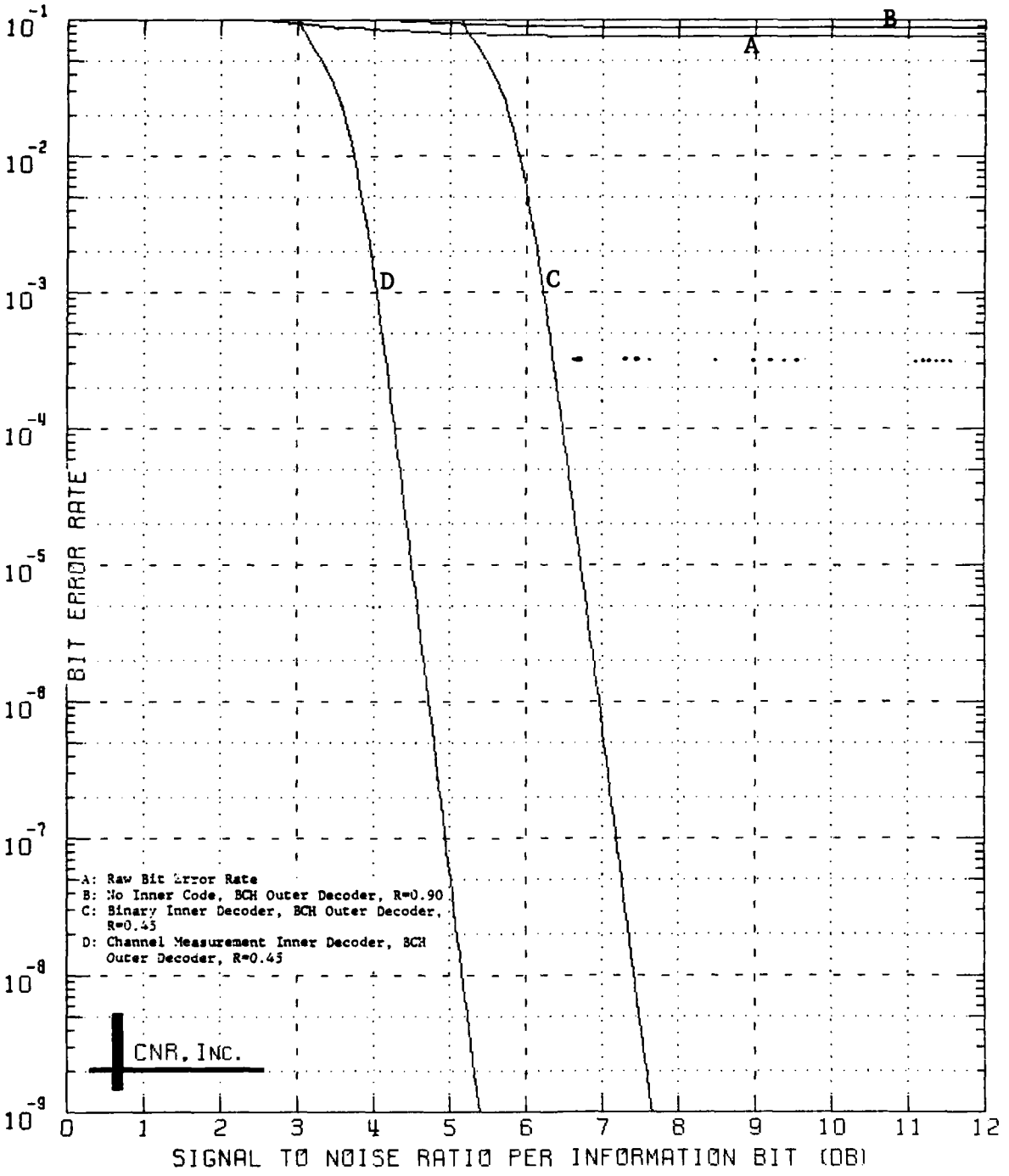


Figure 8.8 Decoded Performance of a Two-Stage Coding Approach
Outer Decoder: BCH Code (240,216;7)
Inner Decoder: Convolutional Code; Rate=1/2; K=7
δ=0.15 and Erasure Information is Employed

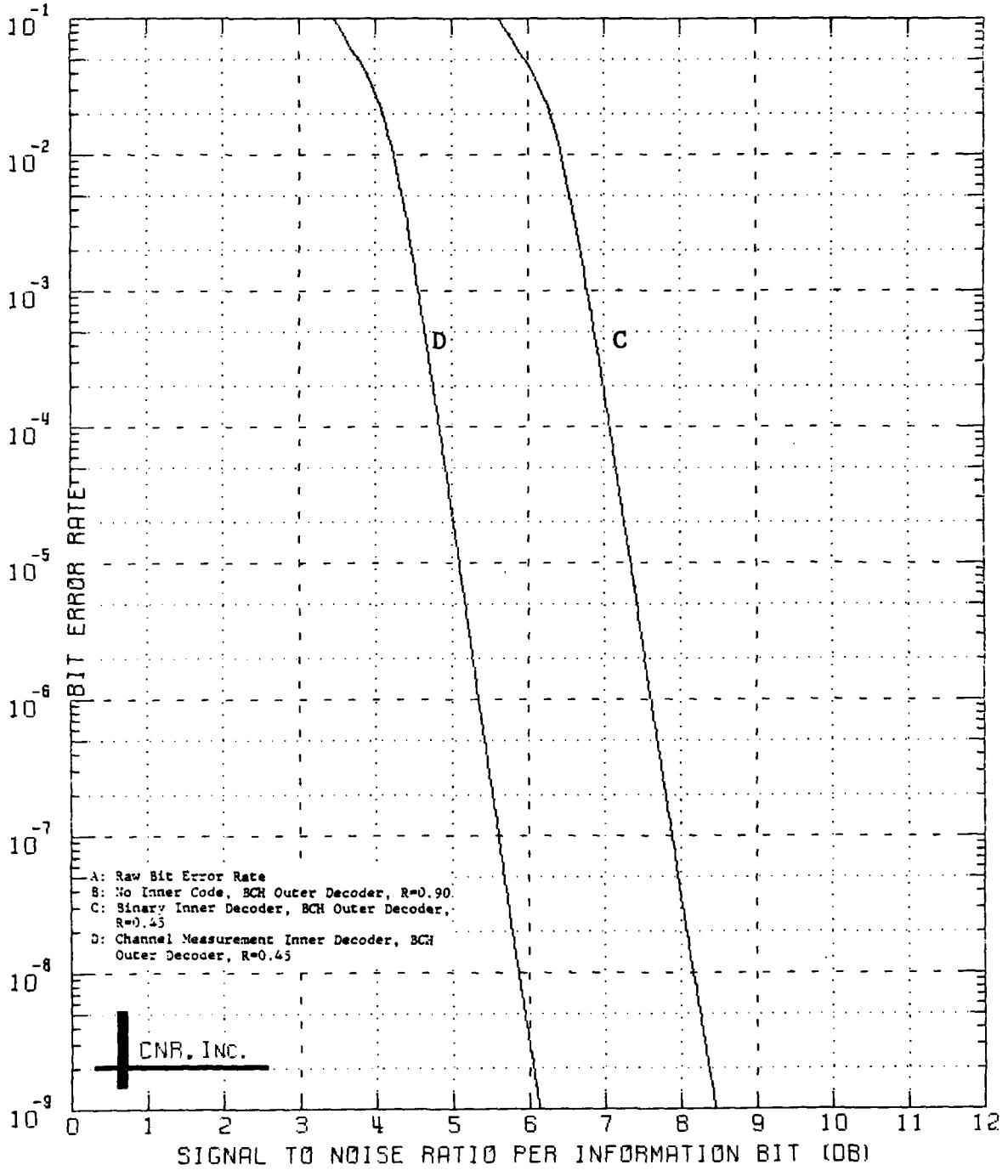


Figure 8.9 Decoded Performance of a Two-Stage Coding Approach
Outer Decoder: BCH Code (240,216;7)
Inner Decoder: Convolutional Code; Rate=1/2; K=7
δ=0.20 and Erasure Information is Employed

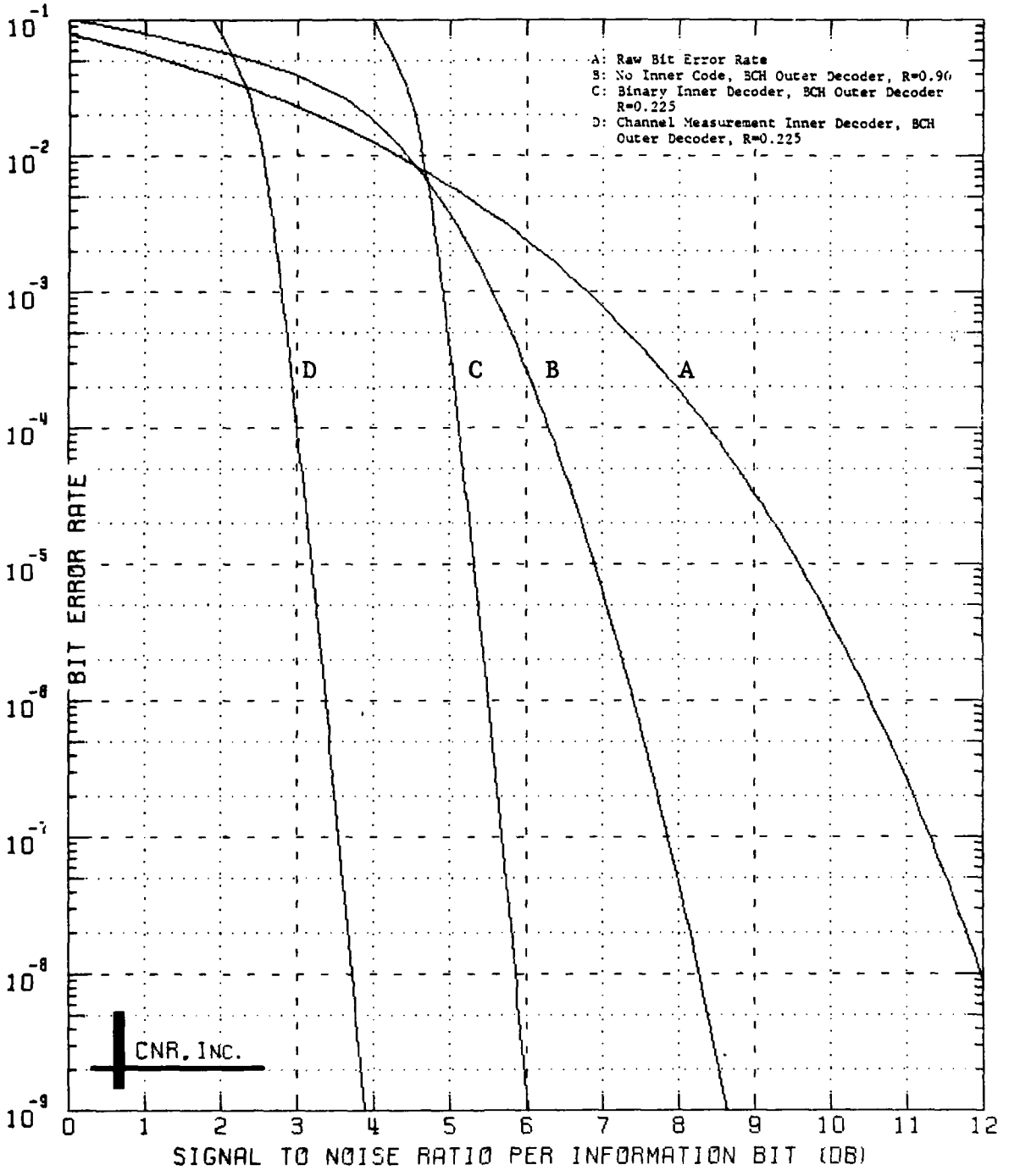


Figure 8.10 Decoded Performance of a Two-Stage Coding Approach
Outer Decoder: BCH Code (240,216;7)
Inner Decoder: Convolutional Code; Rate=1/4; K=7
δ=0.00 and No Erasure Information is Employed

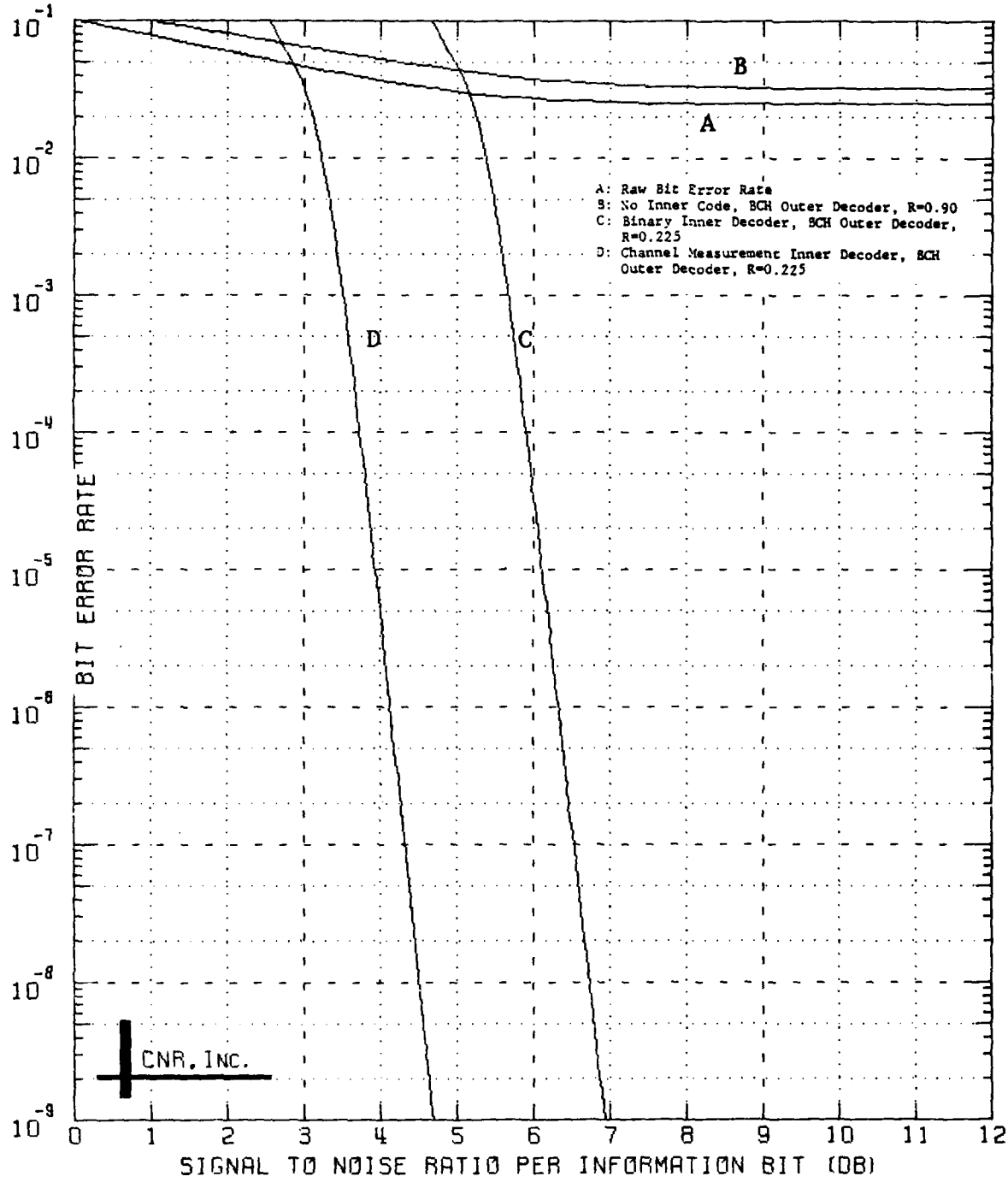


Figure 8.11 Decoded Performance of a Two-Stage Coding Approach
Outer Decoder: BCH Code (240,216;7)
Inner Decoder: Convolutional Code; Rate=1/4; K=7
δ=0.05 and No Erasure Information Employed

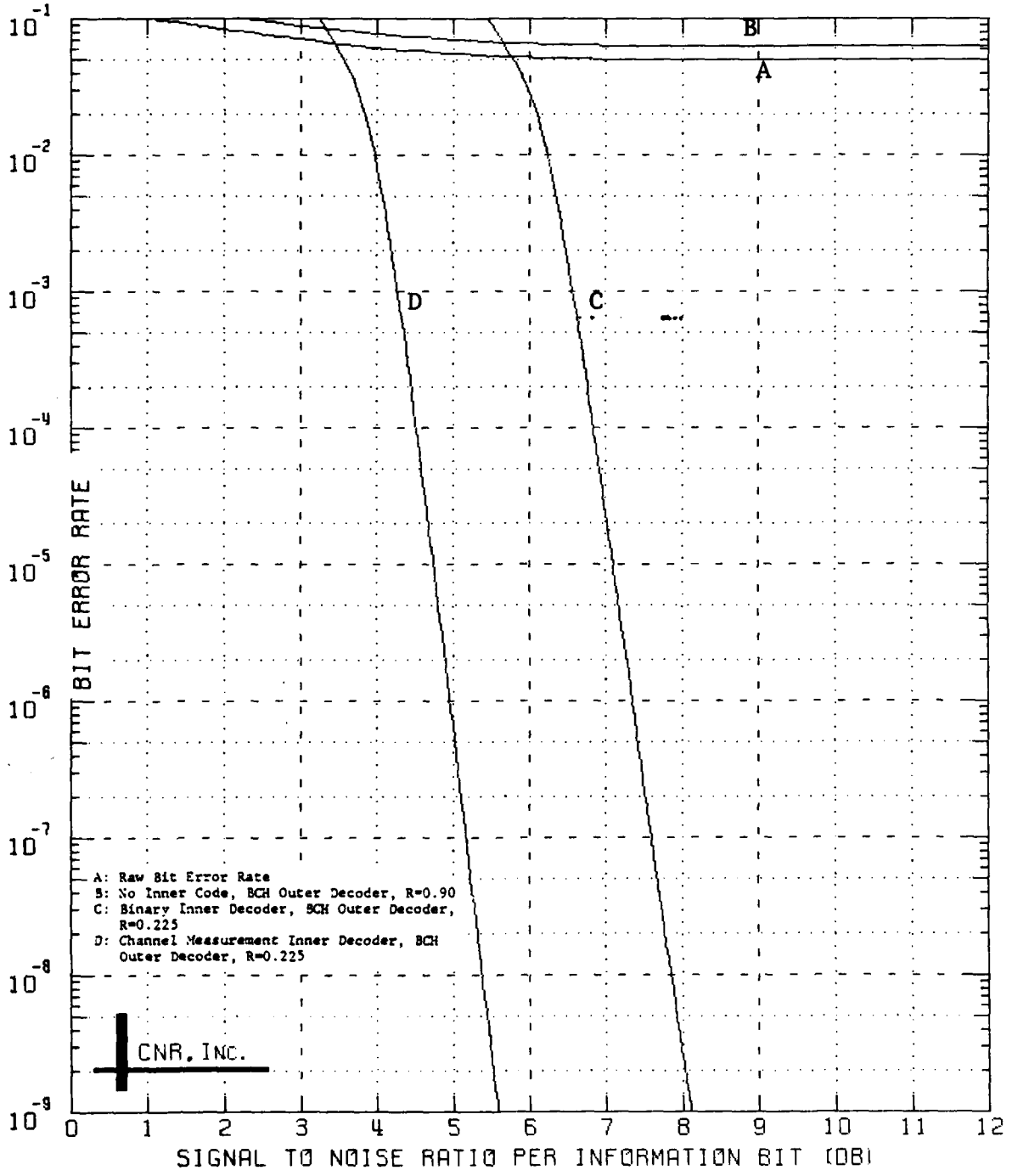


Figure 8.12 Decoded Performance of a Two-Stage Coding Approach
Outer Decoder: BCH Code (240,216;7)
Inner Decoder: Convolutional Code; Rate=1/4; K=7
δ=0.10 and No Erasure Information Employed

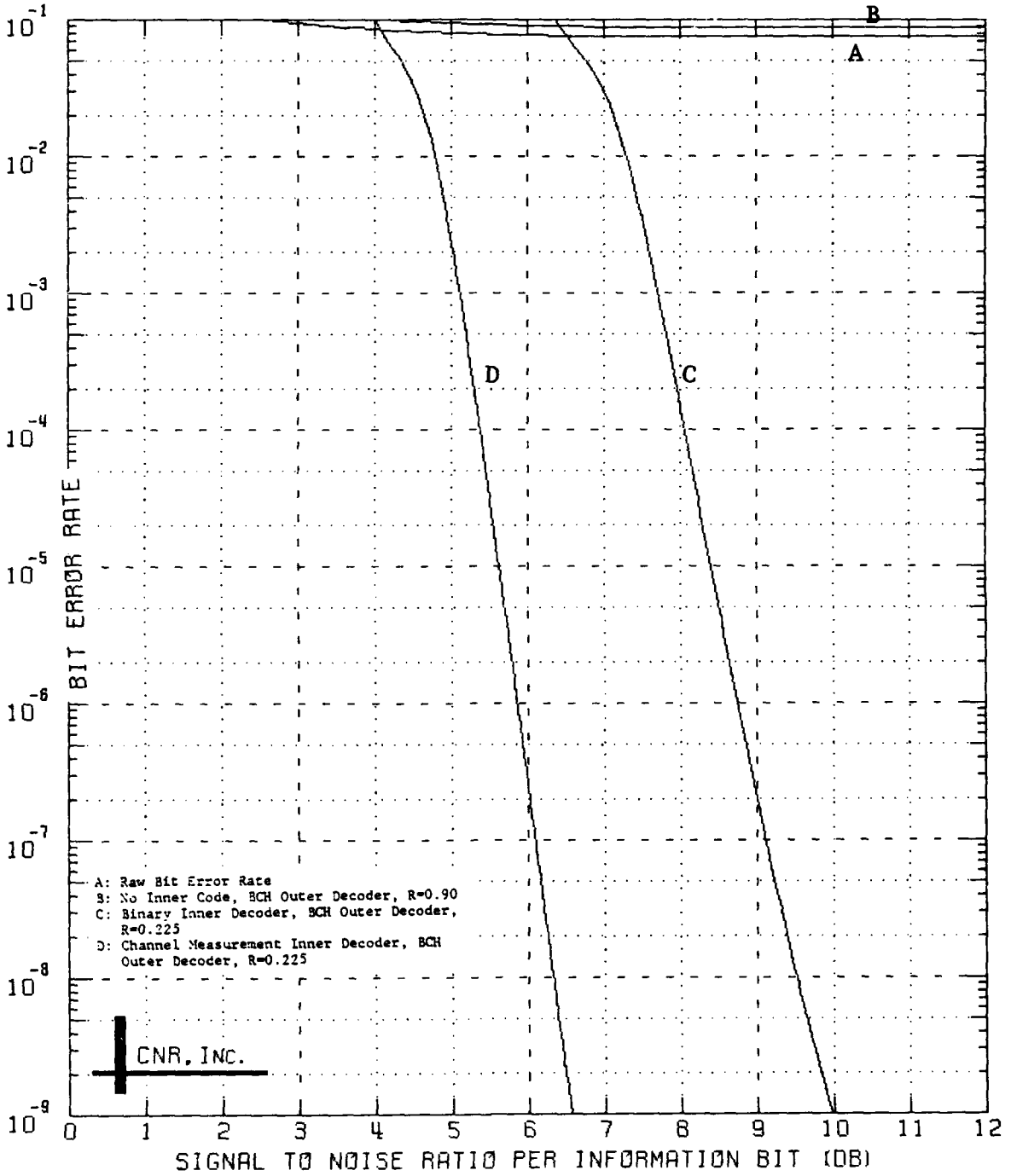


Figure 8.13 Decoded Performance of a Two-Stage Coding Approach
Outer Decoder: BCH Code (240,216;7)
Inner Decoder: Convolutional Code; Rate=1/4; K=7
δ=0.15 and No Erasure Information Employed

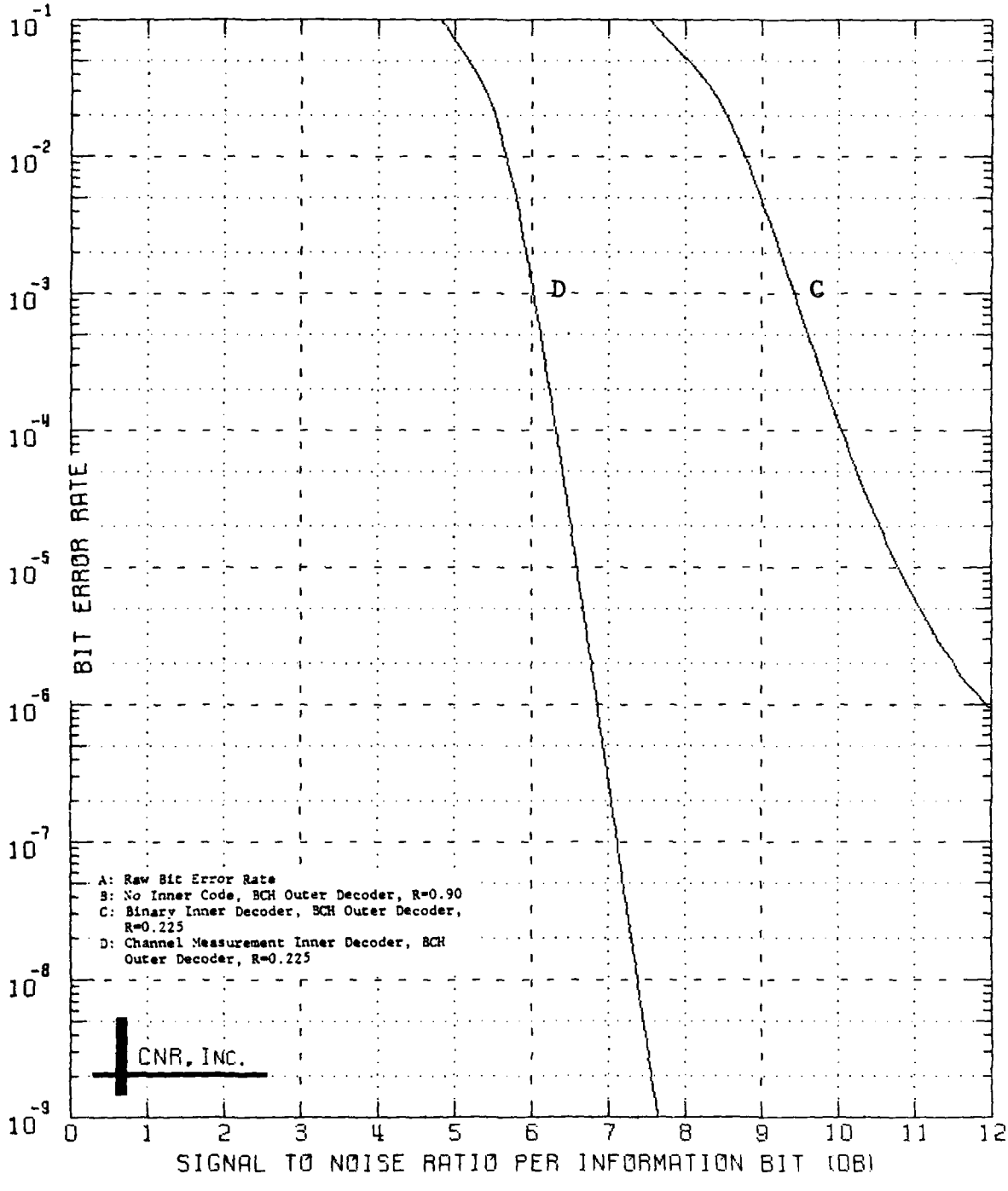


Figure 8.14 Decoded Performance of a Two-Stage Coding Approach
Outer Decoder: BCH Code (240,216;7)
Inner Decoder: Convolutional Code; Rate=1/4; K=7
δ=0.20 and No Erasure Information Employed

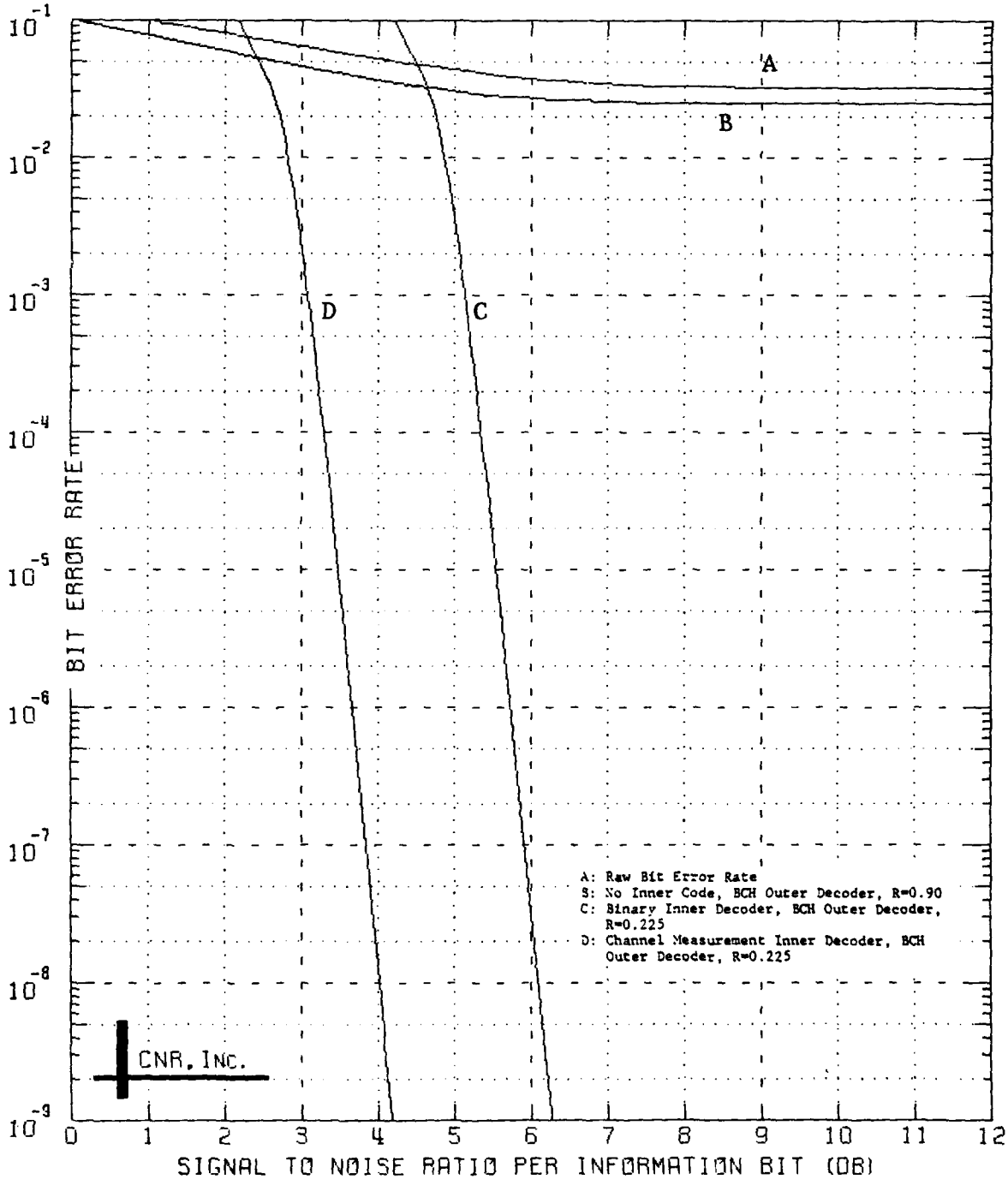


Figure 8.15 Decoded Performance of a Two-Stage Coding Approach
Outer Decoder: BCH Code (240,216;7)
Inner Decoder: Convolutional Code; Rate=1/4; K=7
δ=0.05 and Erasure Information is Employed

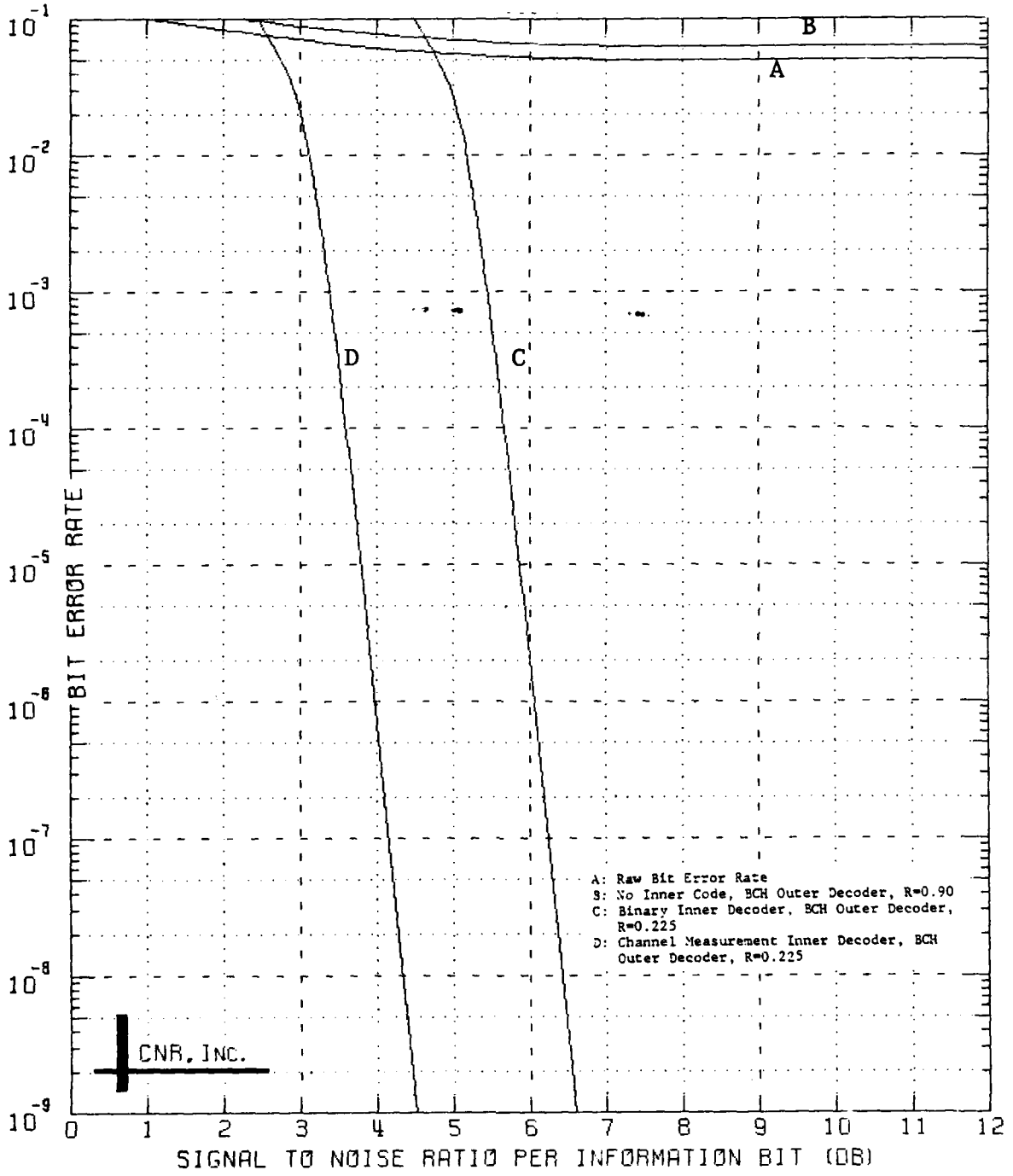


Figure 8.16 Decoded Performance of a Two-Stage Coding Approach
Outer Decoder: BCH Code (240,216;7)
Inner Decoder: Convolutional Code; Rate=1/4; K=7
δ=0.10 and Erasure Information is Employed

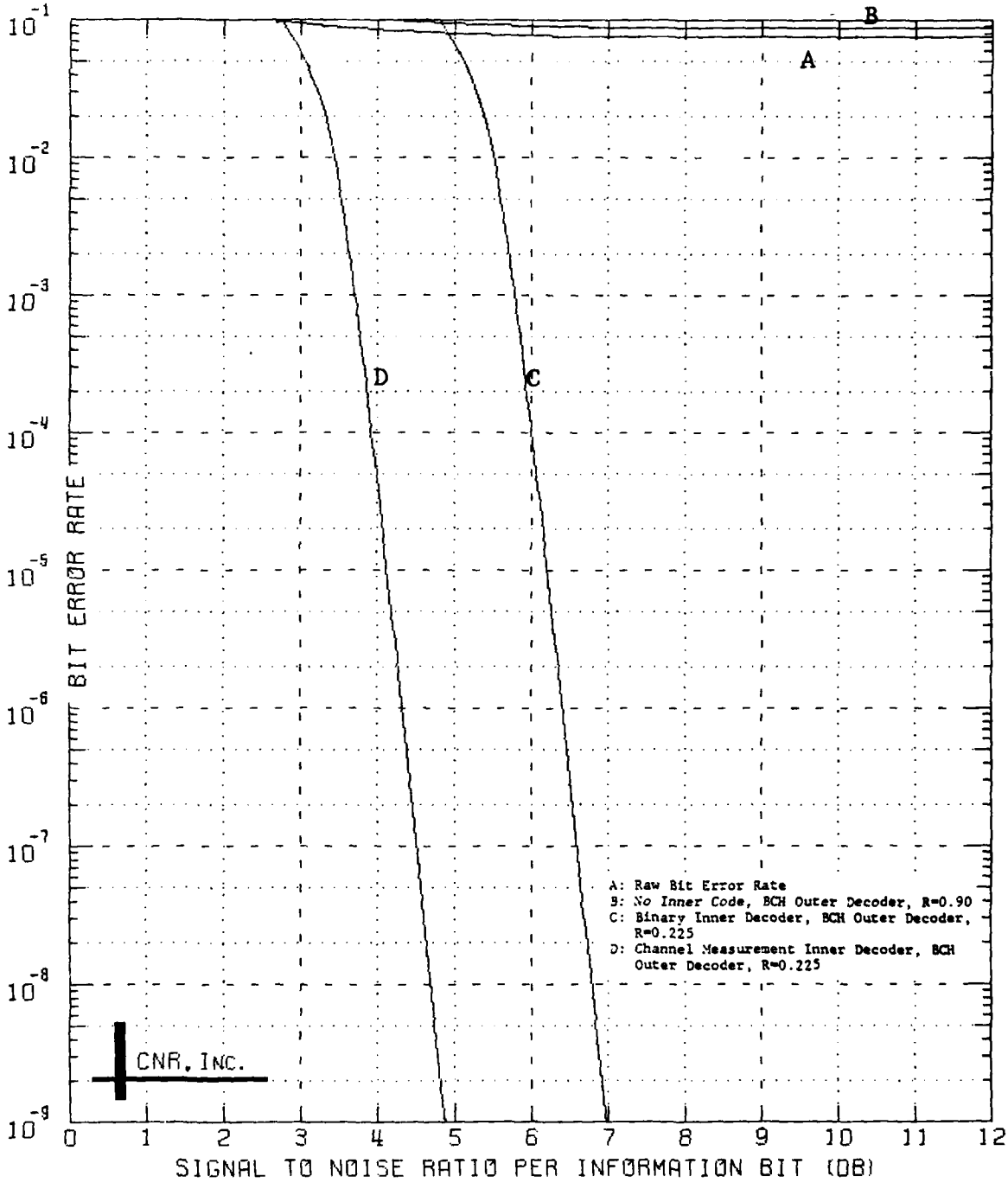


Figure 8.17 Decoded Performance of a Two-Stage Coding Approach
Outer Decoder: BCH Code (240,216;7)
Inner Decoder: Convolutional Code; Rate=1/4; K=7
δ=0.15 and Erasure Information is Employed

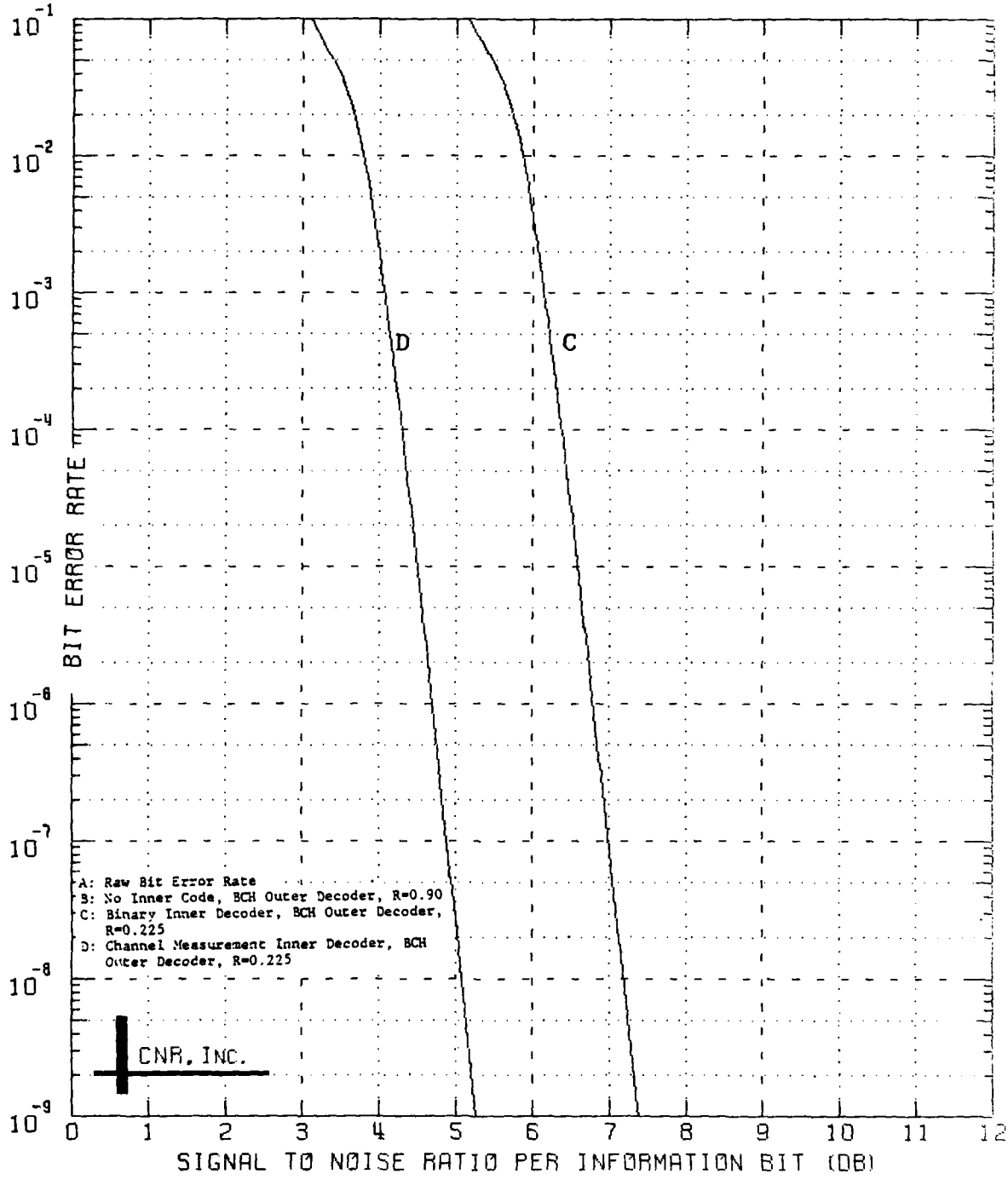


Figure 8.18 Decoded Performance of a Two-Stage Coding Approach
Outer Decoder: BCH Code (240,216;7)
Inner Decoder: Convolutional Code; Rate=1/4; K=7
δ=0.20 and Erasure Information is Employed

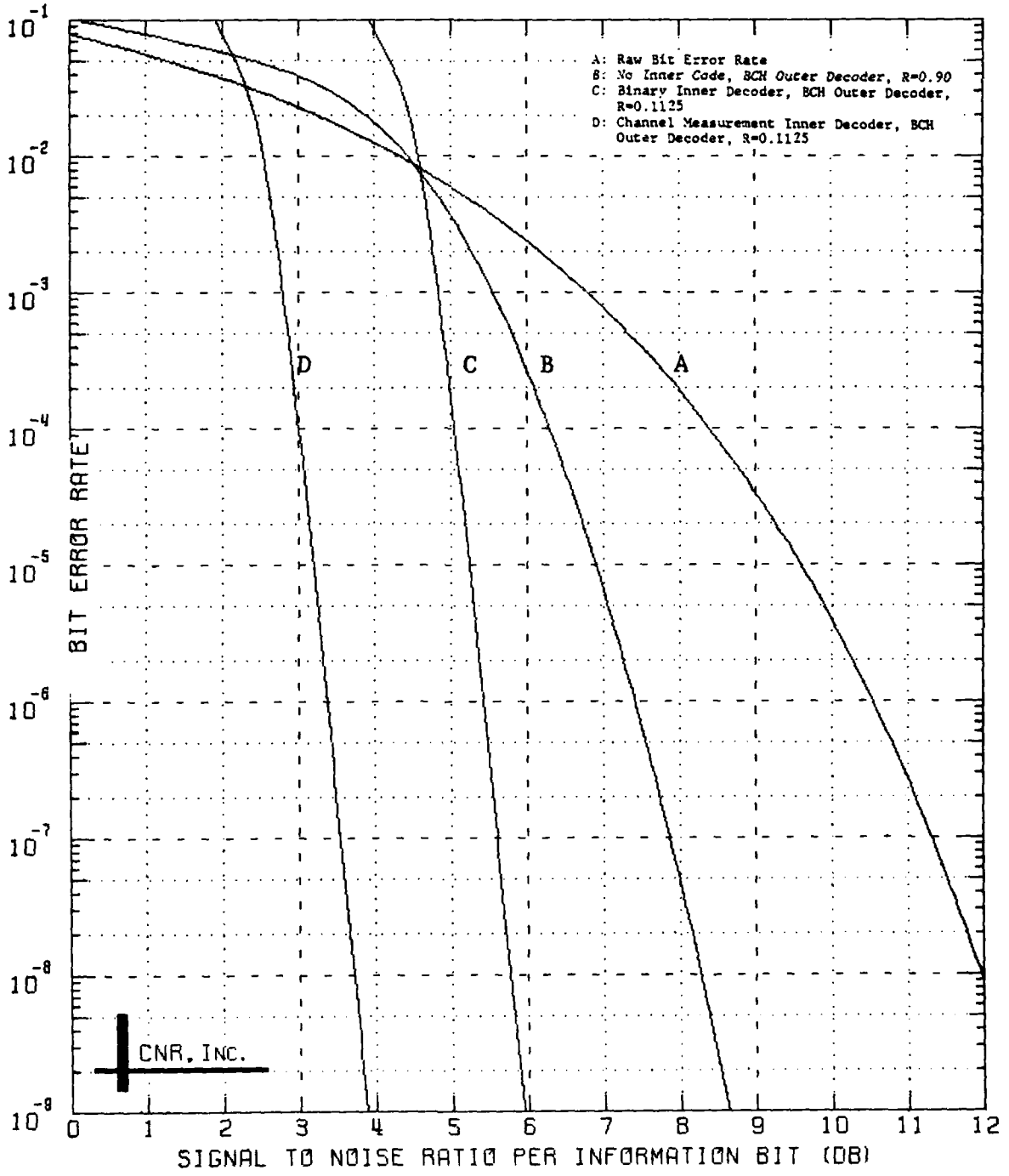


Figure 8.19 Decoded Performance of a Two-Stage Coding Approach
Outer Decoder: BCH Code (240,216;7)
Inner Decoder: Convolutional Code; Rate=1/8; K=7
δ=0.00 and No Erasure Information Employed

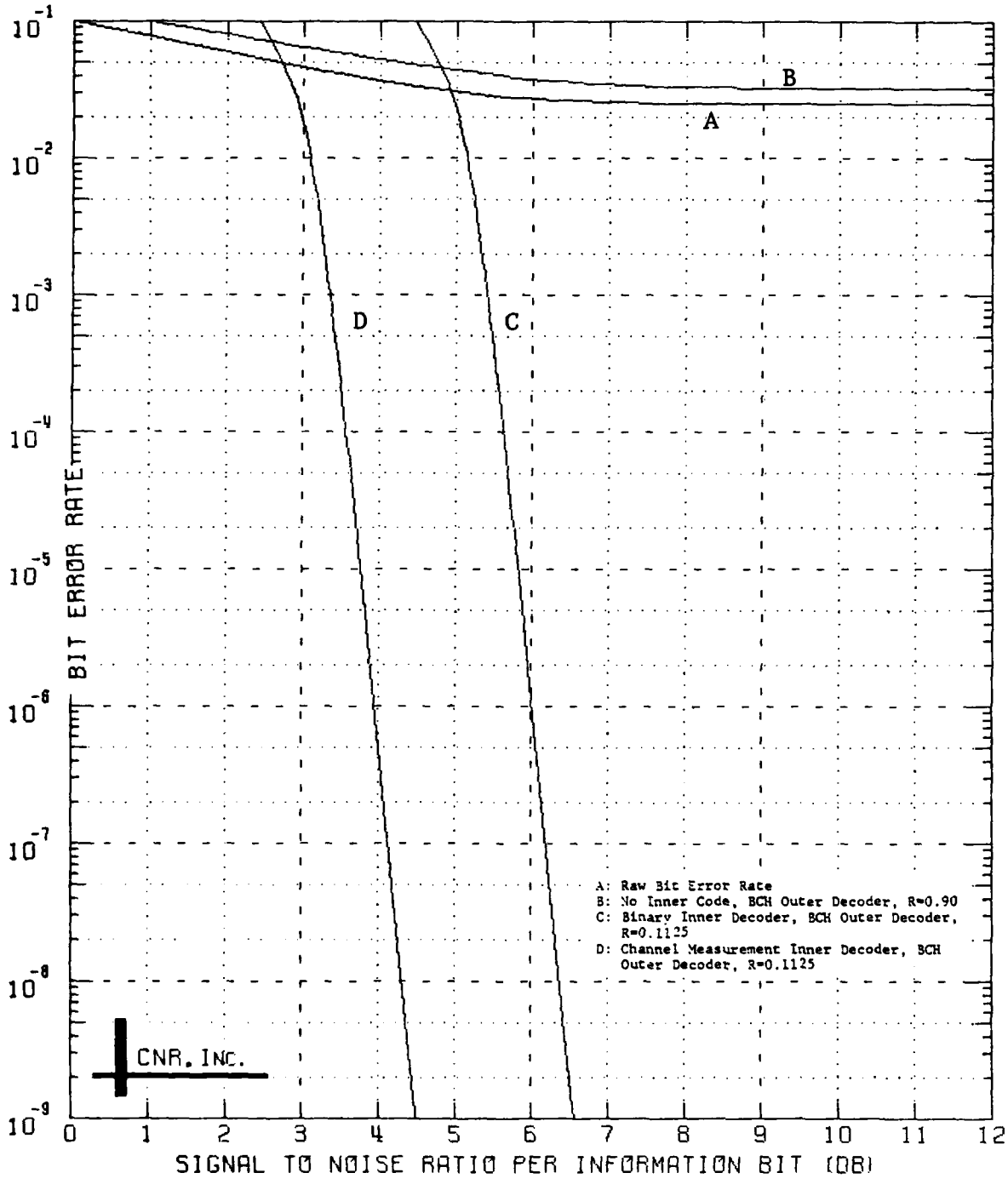


Figure 8.20 Decoded Performance of a Two-Stage Coding Approach
Outer Decoder: BCH Code (240,216;7)
Inner Decoder: Convolutional Code; Rate=1/8; K=7
δ=0.05 and No Erasure Information Employed

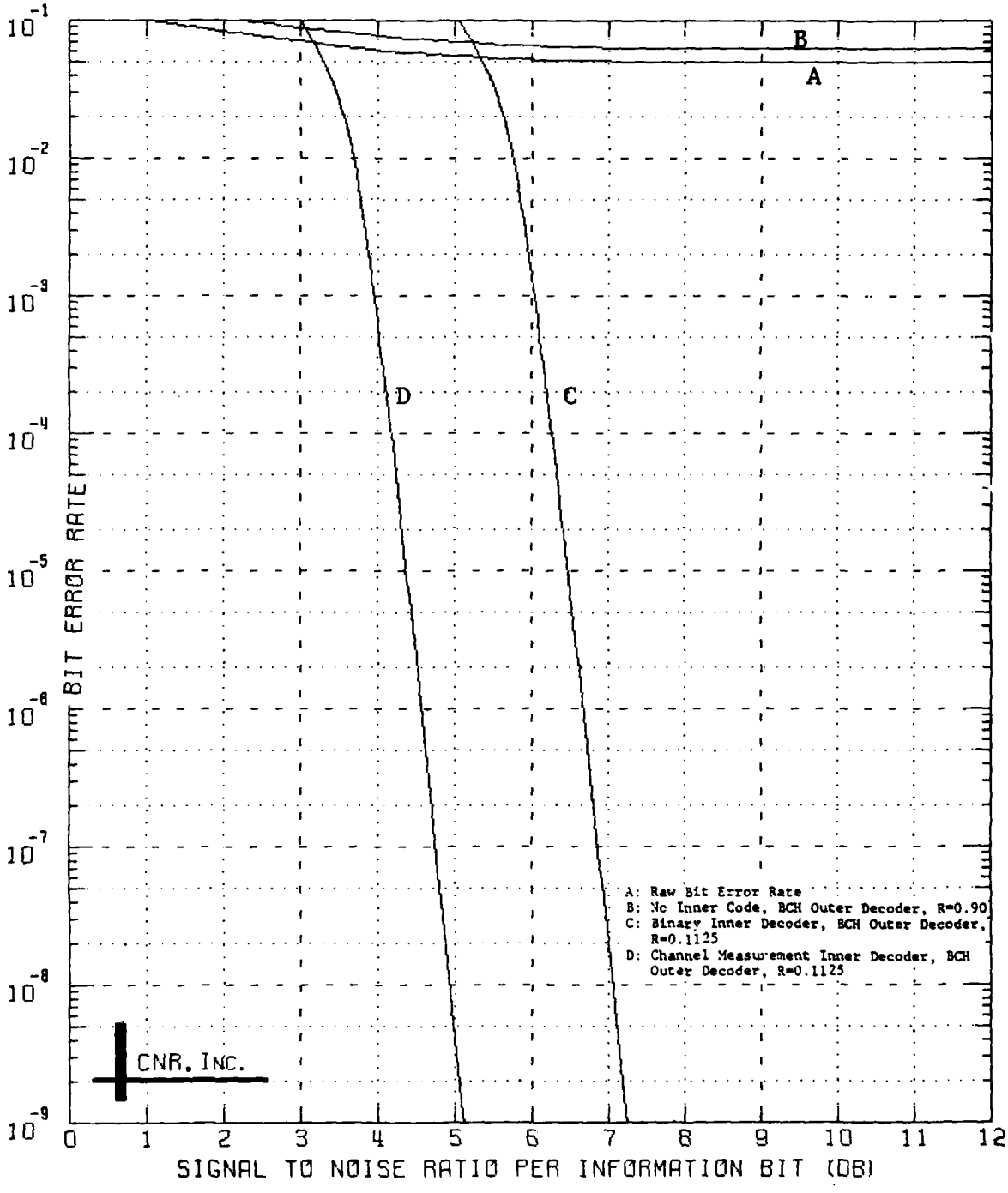


Figure 8.21 Decoded Performance of a Two-Stage Coding Approach
Outer Decoder: BCH Code (240,216;7)
Inner Decoder: Convolutional Code; Rate=1/8; K=7
δ=0.10 and No Erasure Information Employed

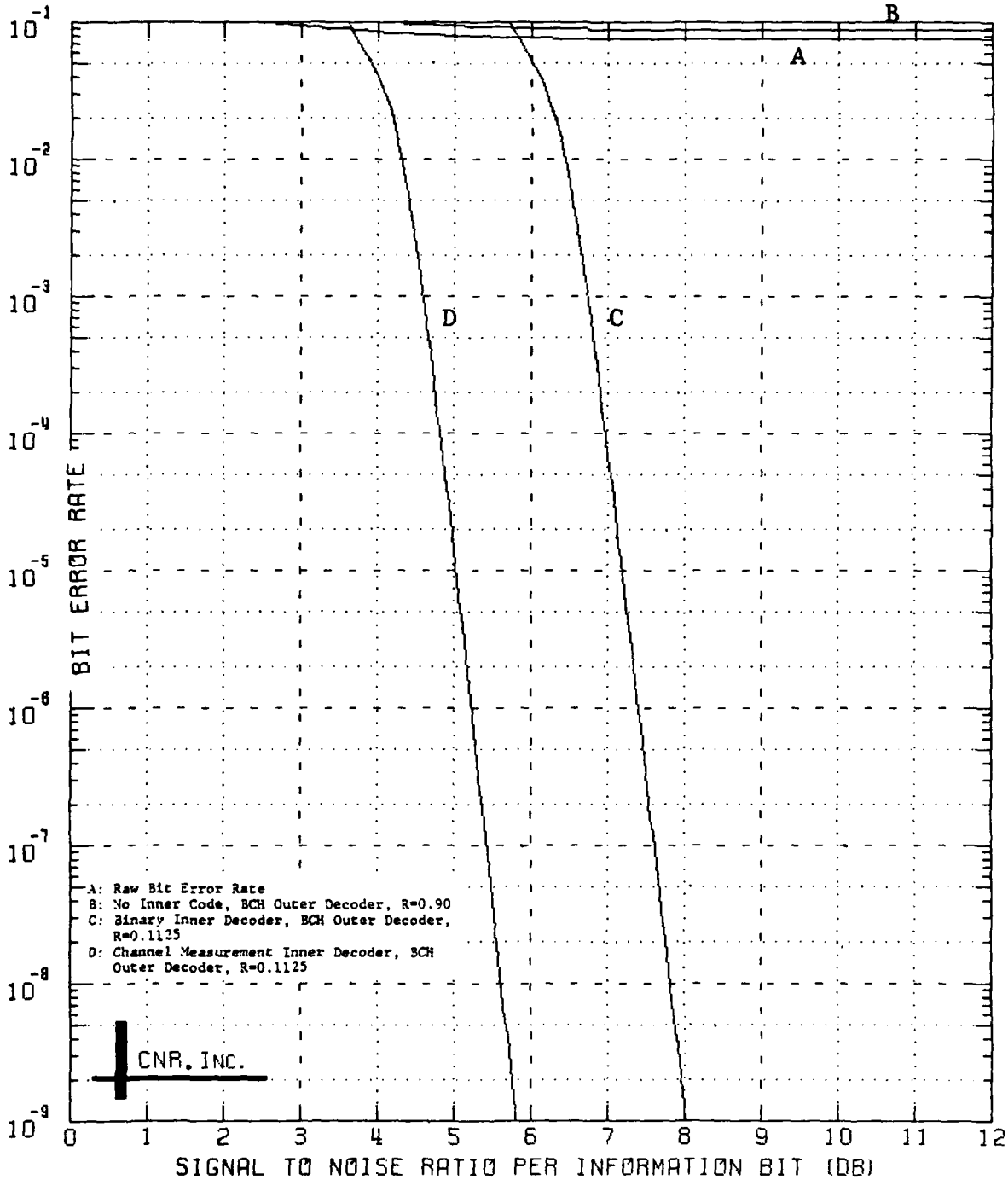


Figure 8.22 Decoded Performance of a Two-Stage Coding Approach
Outer Decoder: BCH Code (240,216;7)
Inner Decoder: Convolutional Code; Rate=1/8; K=7
δ=0.15 and No Erasure Information Employed

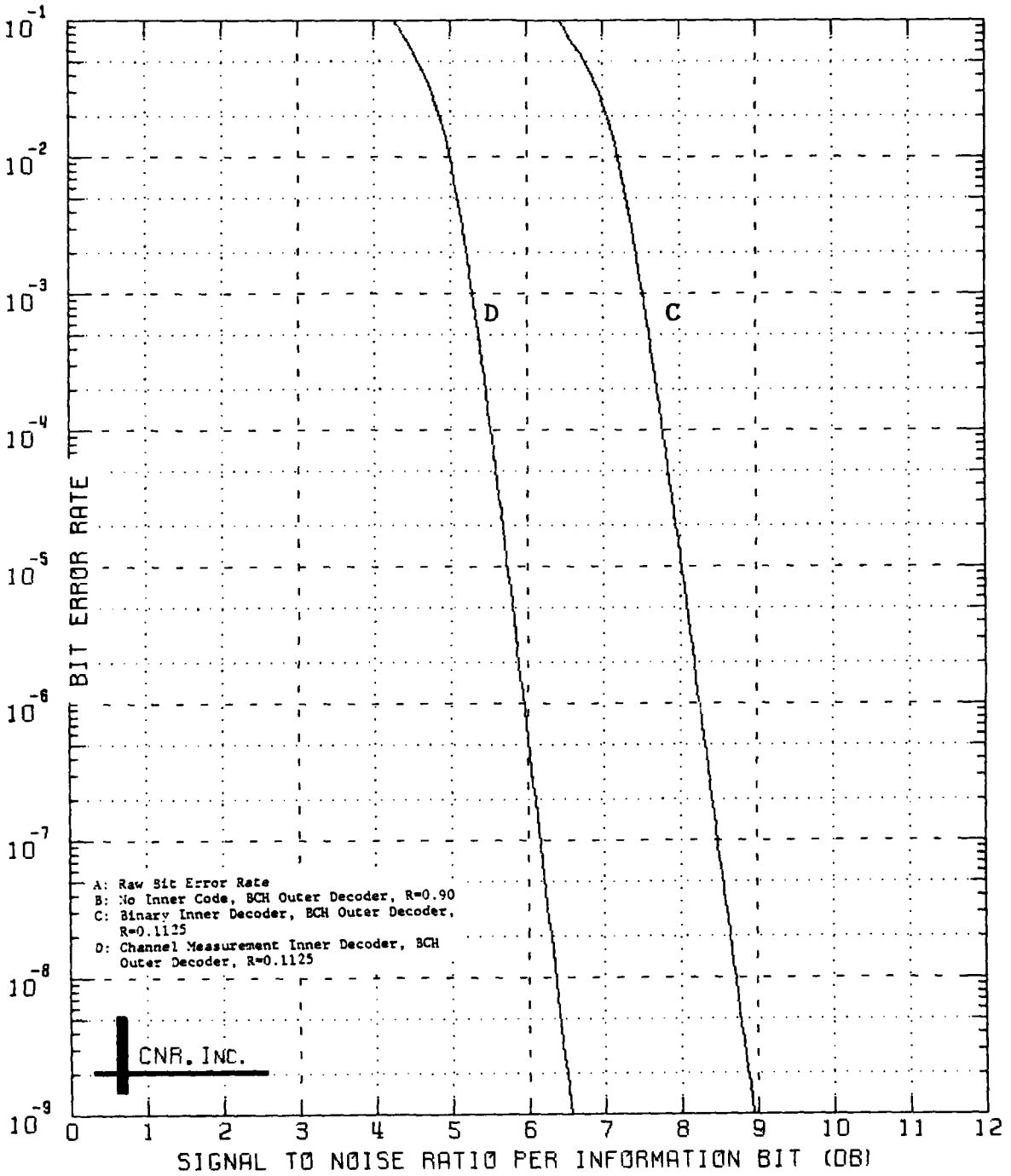


Figure 8.23 Decoded Performance of a Two-Stage Coding Approach
Outer Decoder: BCH Code (240,216;7)
Inner Decoder: Convolutional Code; Rate=1/8; K=7
δ=0.20 and No Erasure Information Employed

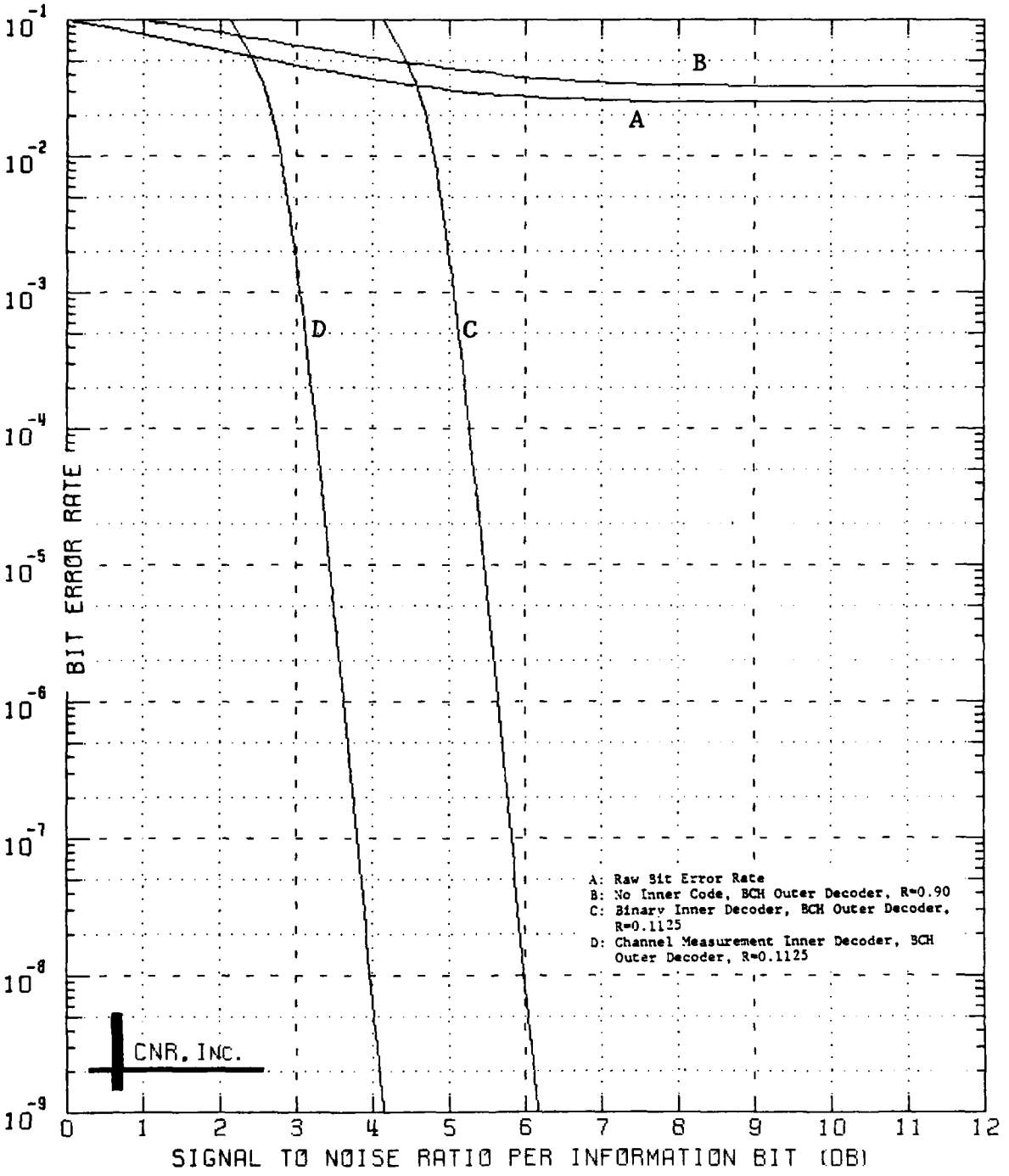


Figure 8.24 Decoded Performance of a Two-Stage Coding Approach
Outer Decoder: BCH Code (240,216;7)
Inner Decoder: Convolutional Code; Rate=1/8; K=7
δ=0.05 and Erasure Information is Employed

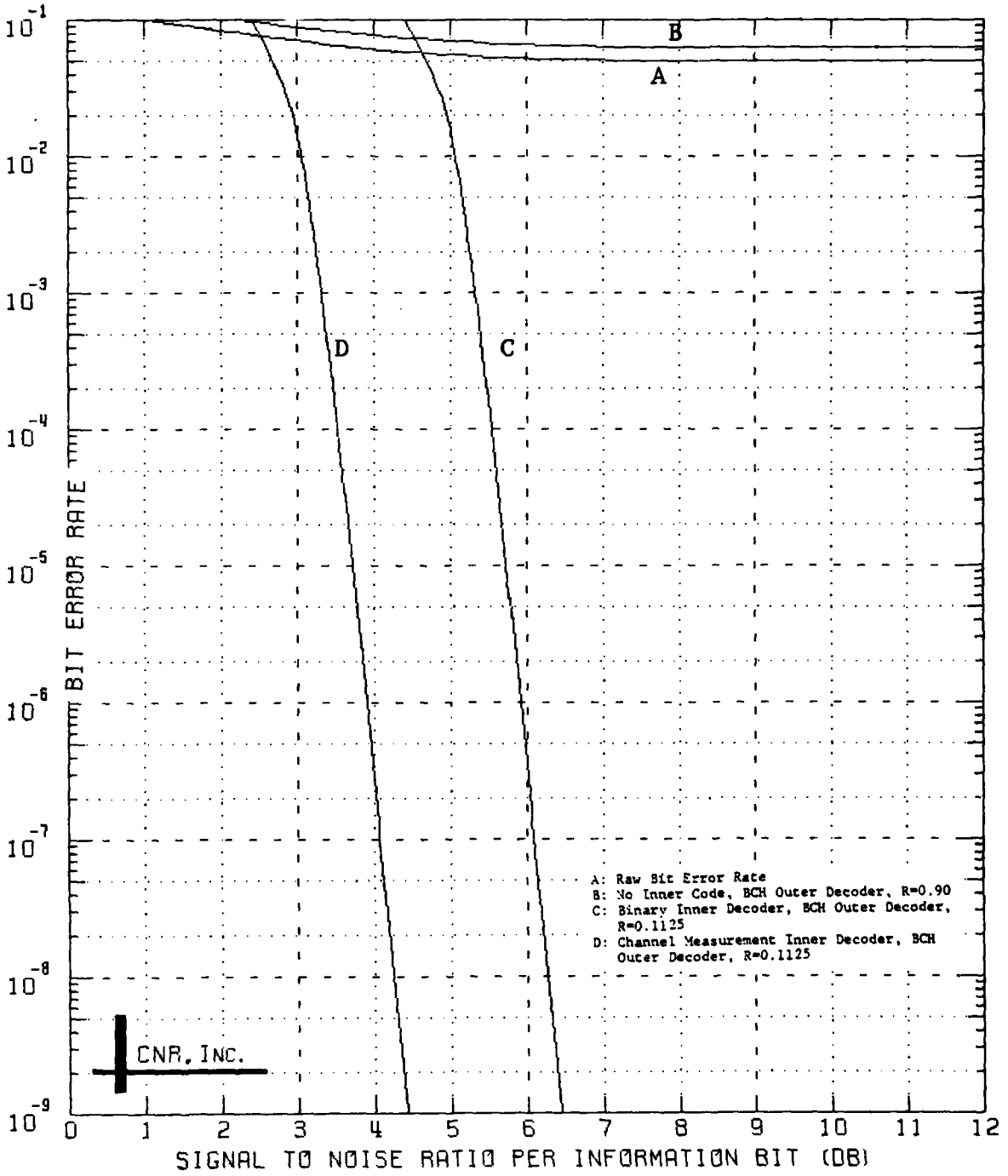


Figure 8.25 Decoded Performance of a Two-Stage Coding Approach
Outer Decoder: BCH Code (240,216;7)
Inner Decoder: Convolutional Code; Rate=1/8; K=7
δ=0.10 and Erasure Information is Employed

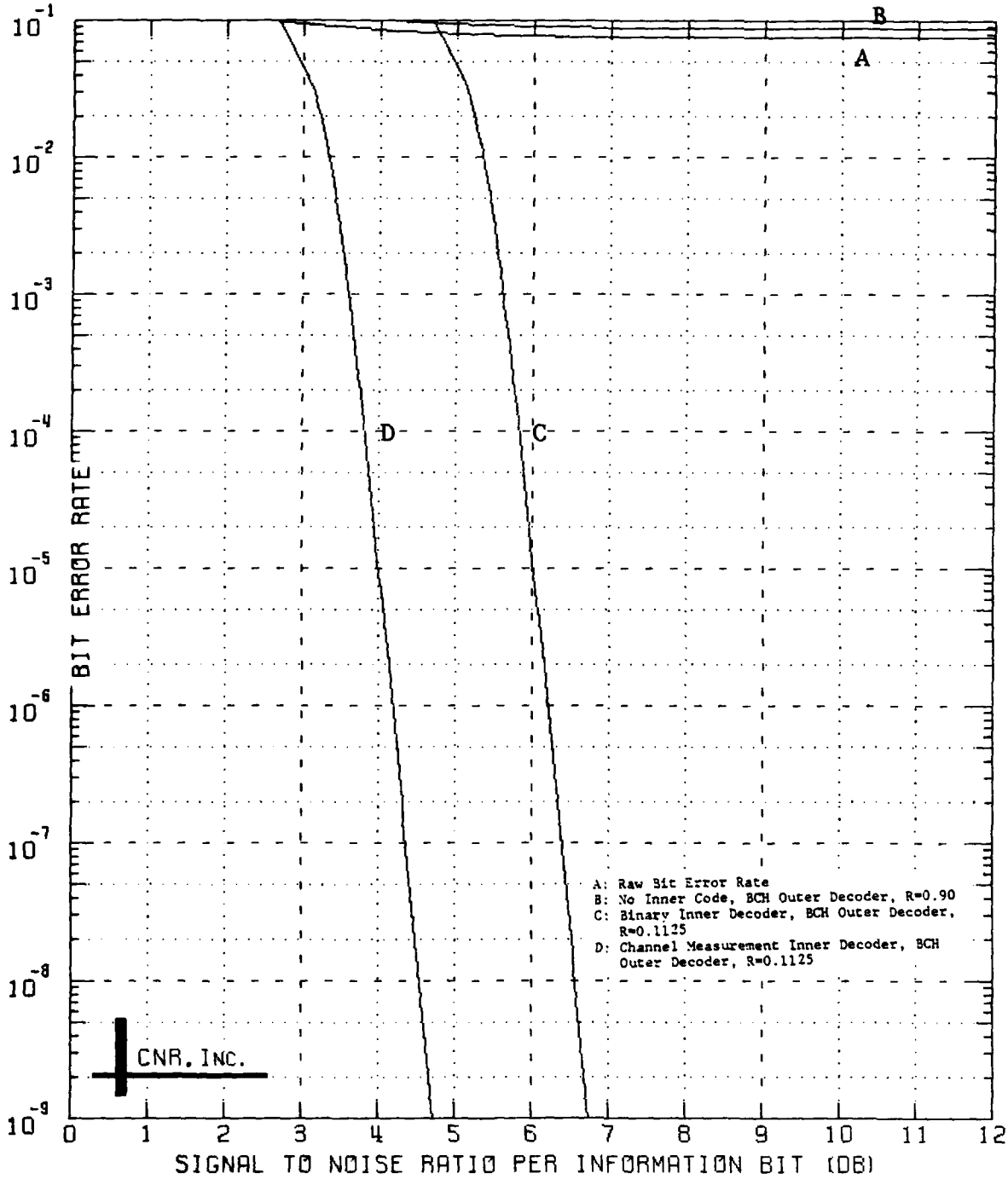


Figure 8.26 Decoded Performance of a Two-Stage Coding Approach
Outer Decoder: BCH Code (240,216;7)
Inner Decoder: Convolutional Code; Rate=1/8; K=7
δ=0.15 and Erasure Information is Employed

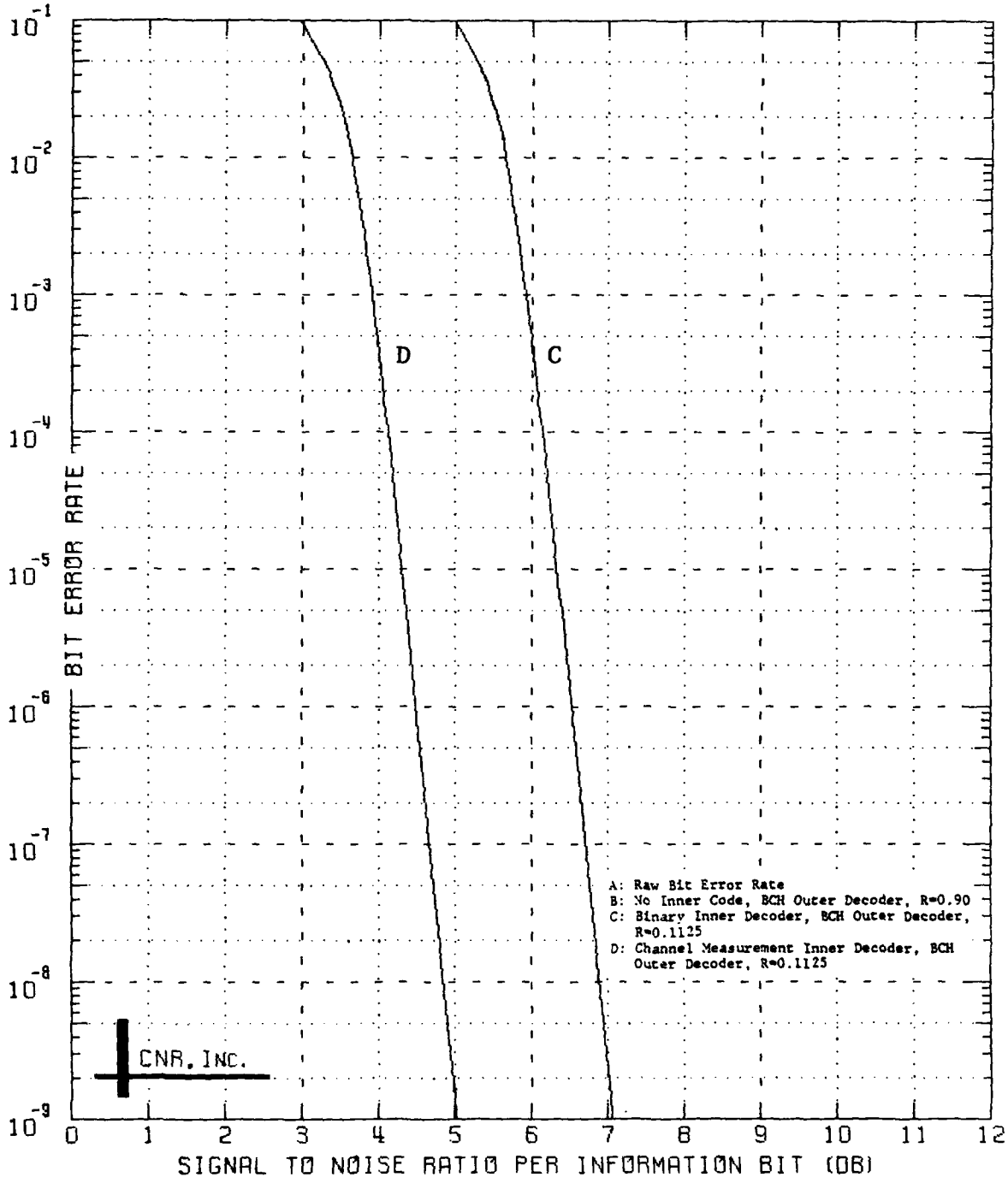


Figure 8.27 Decoded Performance of a Two-Stage Coding Approach
Outer Decoder: BCH Code (240,216;7)
Inner Decoder: Convolutional Code; Rate=1/8; K=7
δ=0.20 and Erasure Information is Employed

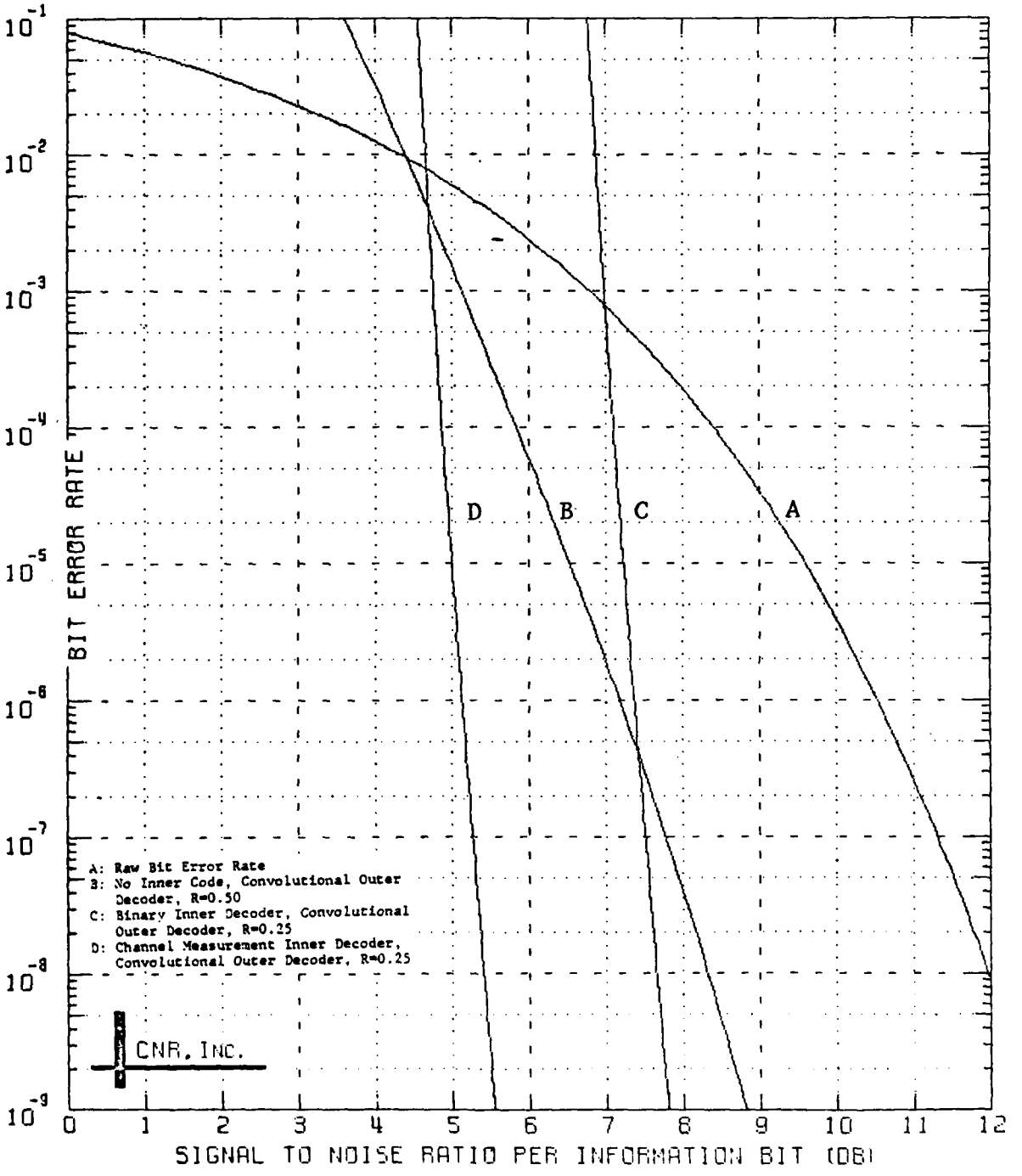


Figure 8.28 Decoded Performance of a Two-Stage Coding Approach
Outer Decoder: Convolutional Code, Rate=1/2; K=7
Inner Decoder: Convolutional Code, Rate=1/2; K=7
δ=0.00 and No Erasure Information Employed

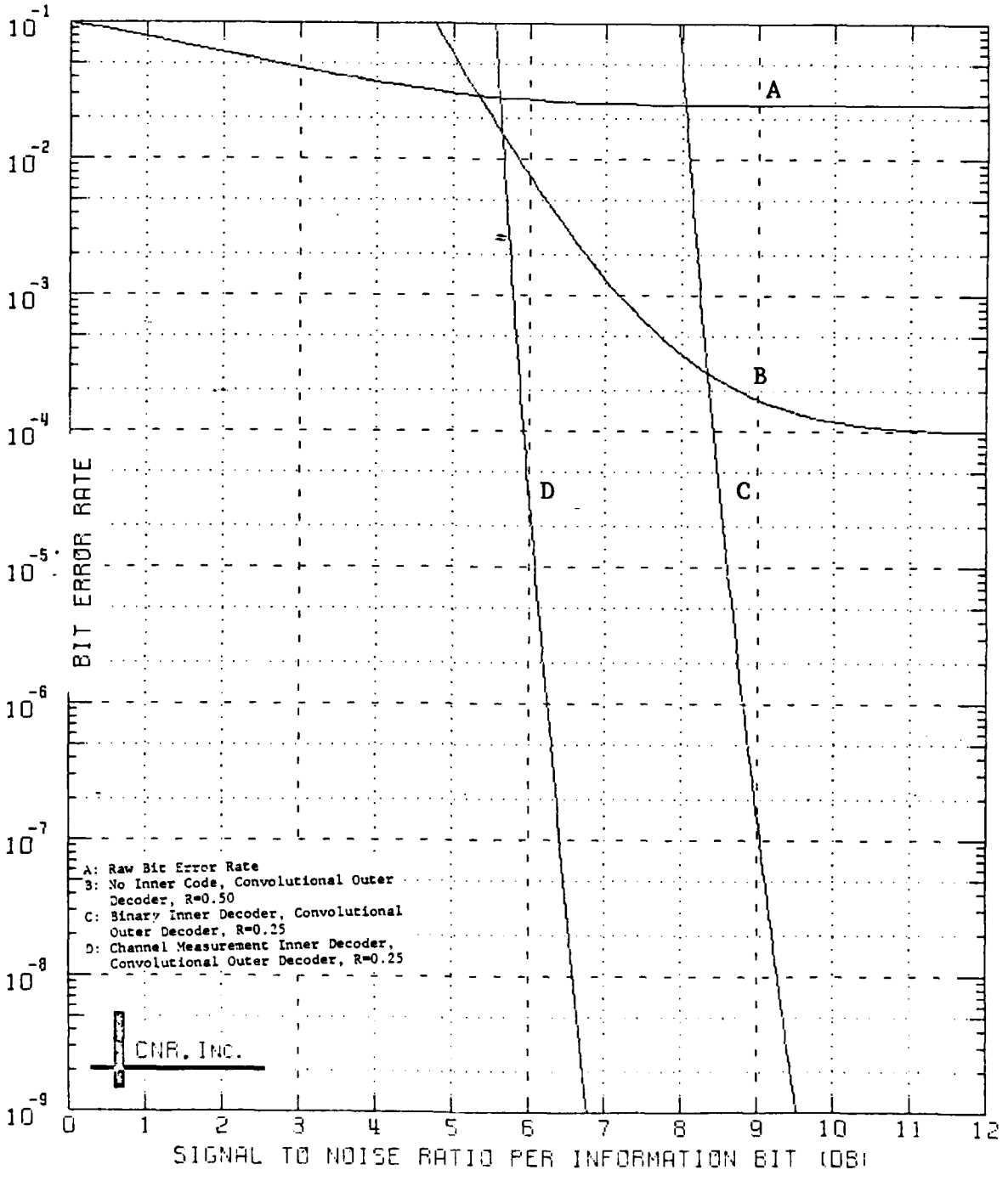


Figure 8.29 Decoded Performance of a Two-Stage Coding Approach
Outer Decoder: Convolutional Code, Rate=1/2; K=7
Inner Decoder: Convolutional Code, Rate=1/2; K=7
δ=0.05 and No Erasure Information Employed

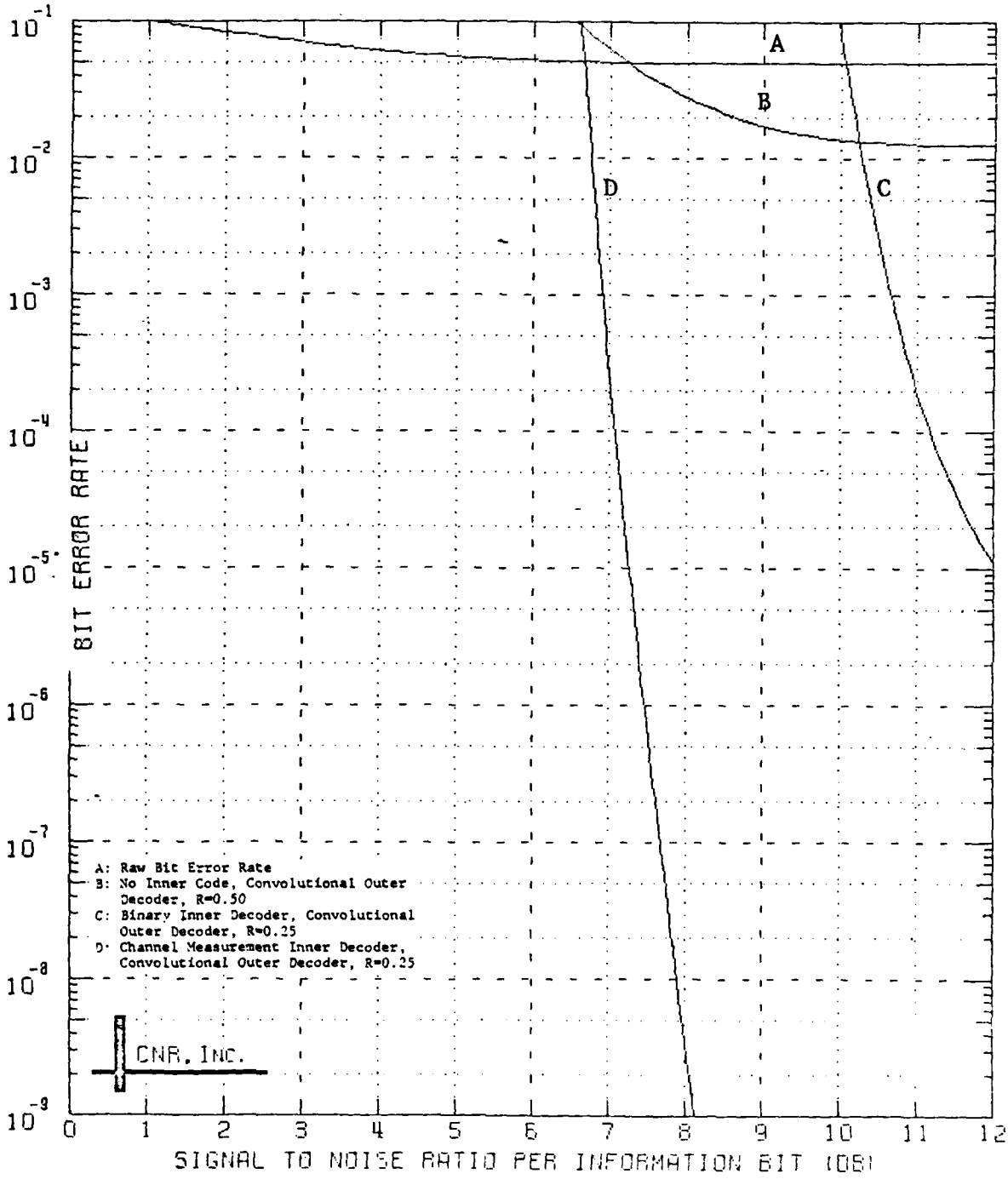


Figure 8.30 Decoded Performance of a Two-Stage Coding Approach
Outer Decoder: Convolutional Code, Rate=1/2; K=7
Inner Decoder: Convolutional Code, Rate=1/2; K=7
δ=0.10 and No Erasure Information Employed

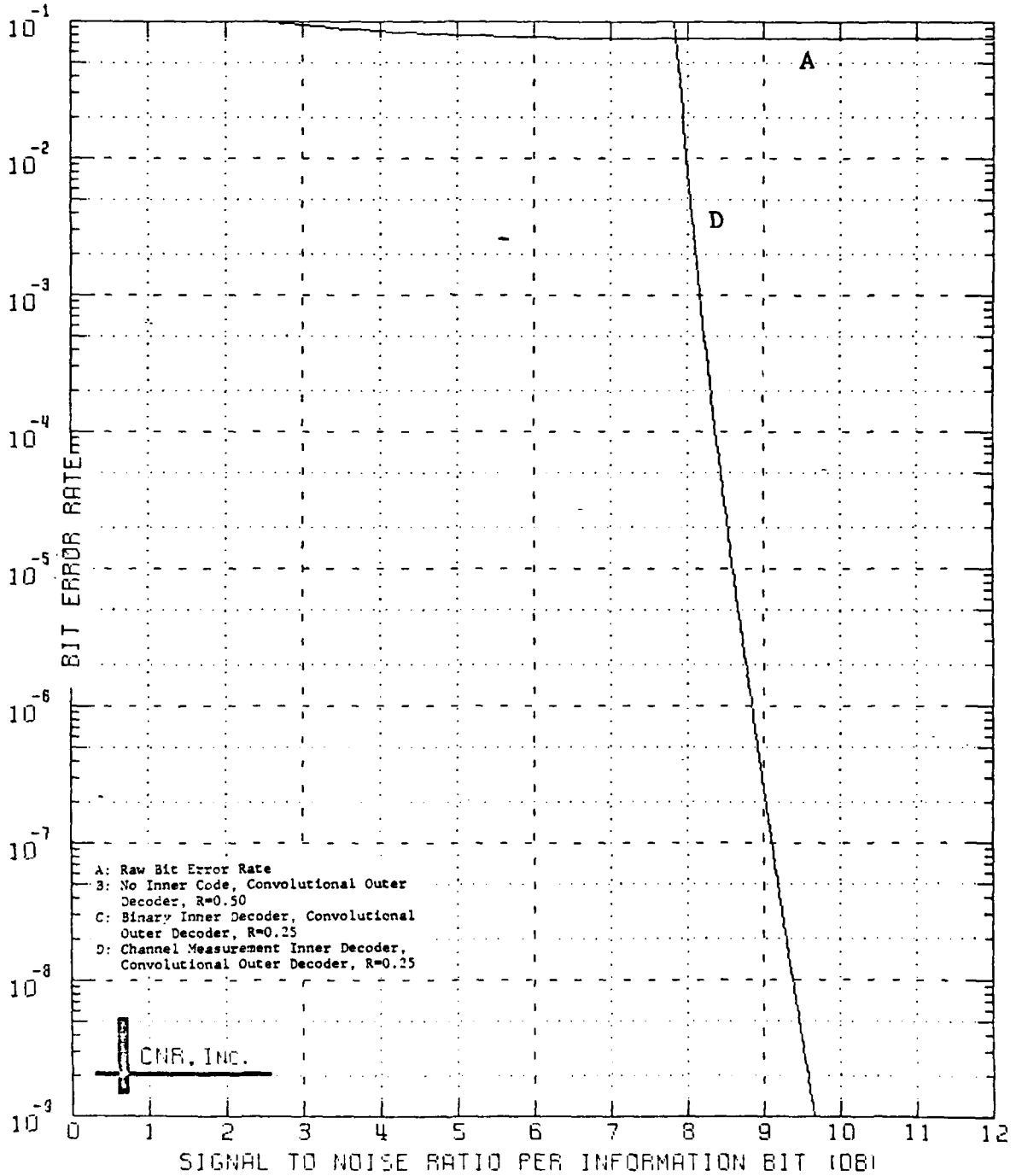


Figure 8.31 Decoded Performance of a Two-Stage Coding Approach
Outer Decoder: Convolutional Code, Rate=1/2; K=7
Inner Decoder: Convolutional Code, Rate=1/2; K=7
δ=0.15 and No Erasure Information Employed

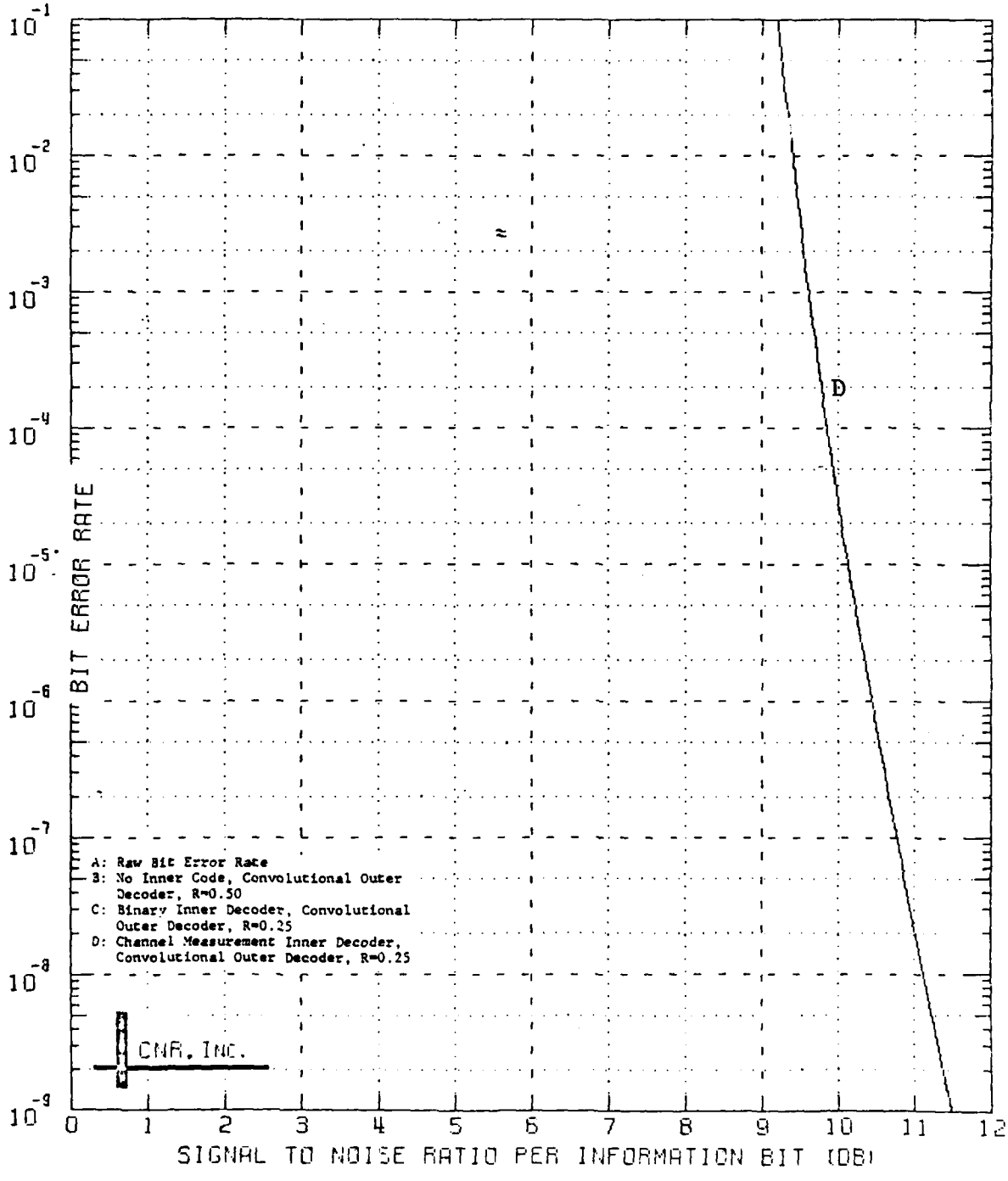


Figure 8.32 Decoded Performance of a Two-Stage Coding Approach
Outer Decoder: Convolutional Code, Rate=1/2; K=7
Inner Decoder: Convolutional Code, Rate=1/2; K=7
δ=0.20 and No Erasure Information Employed

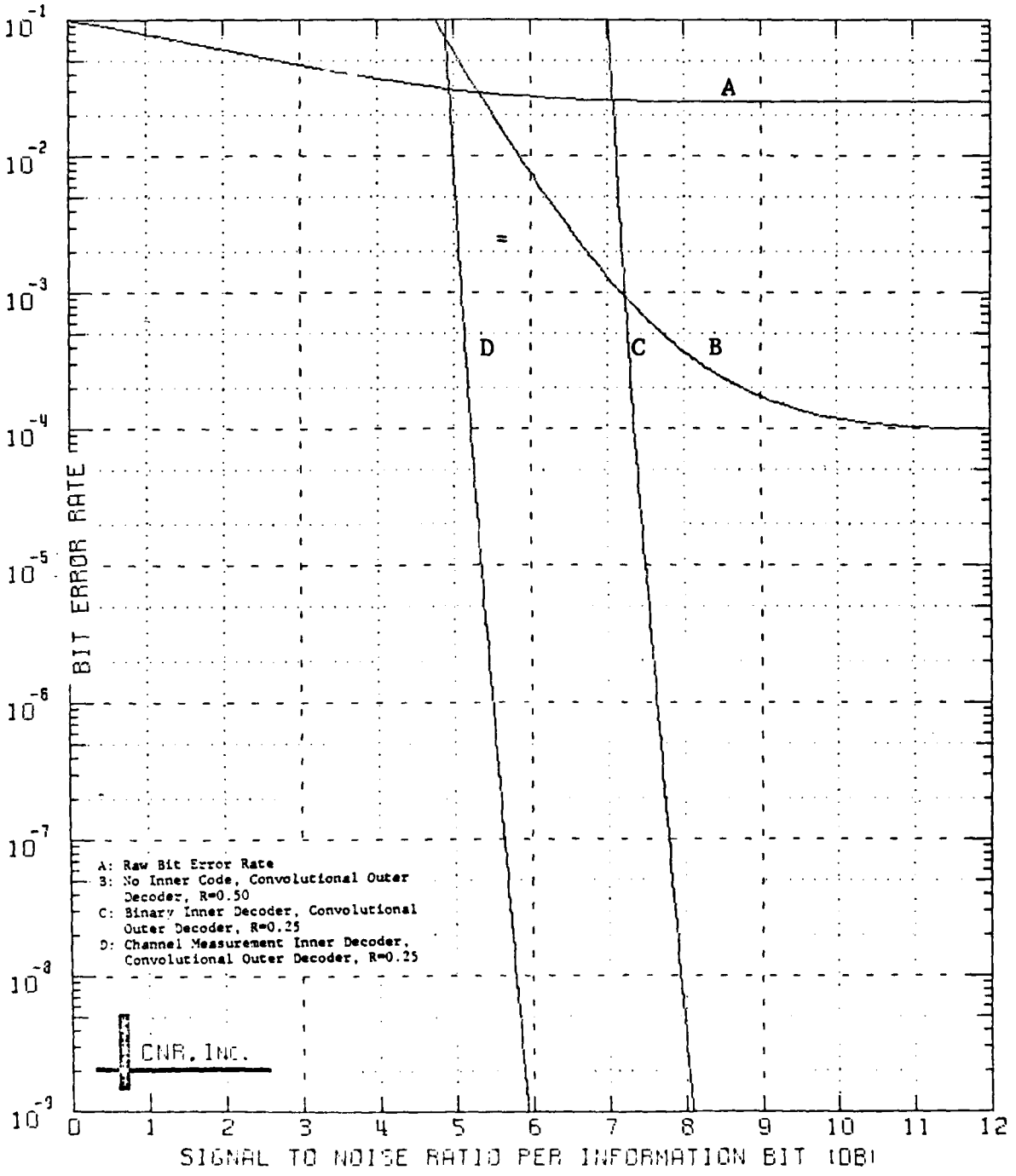


Figure 8.33 Decoded Performance of a Two-Stage Coding Approach
Outer Decoder: Convolutional Code, Rate=1/2; K=7
Inner Decoder: Convolutional Code, Rate=1/2; K=7
δ=0.05 and Erasure Information is Employed

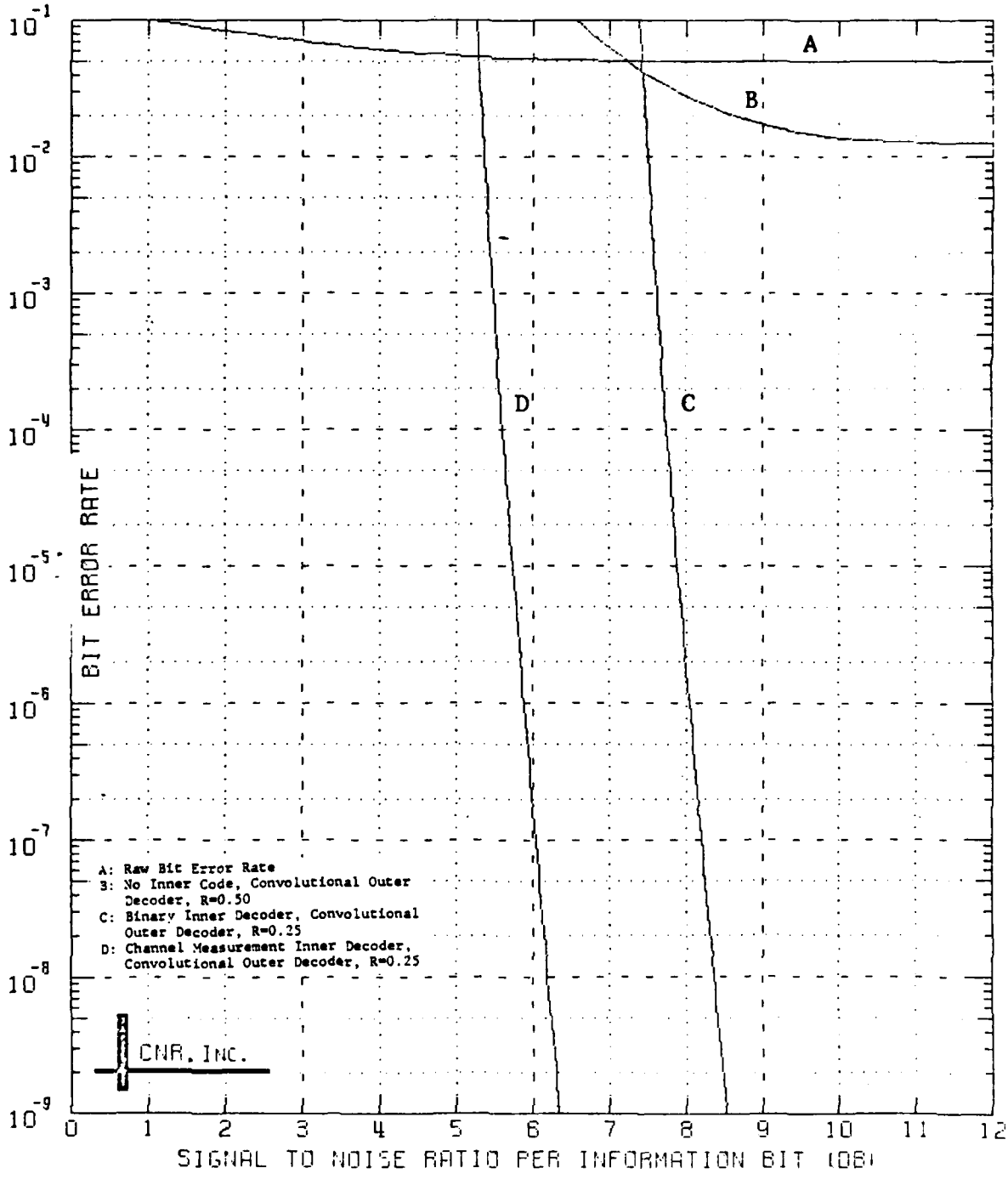


Figure 8.34 Decoded Performance of a Two-Stage Coding Approach
Outer Decoder: Convolutional Code, Rate=1/2; K=7
Inner Decoder: Convolutional Code, Rate=1/2; K=7
δ=0.10 and Erasure Information is Employed

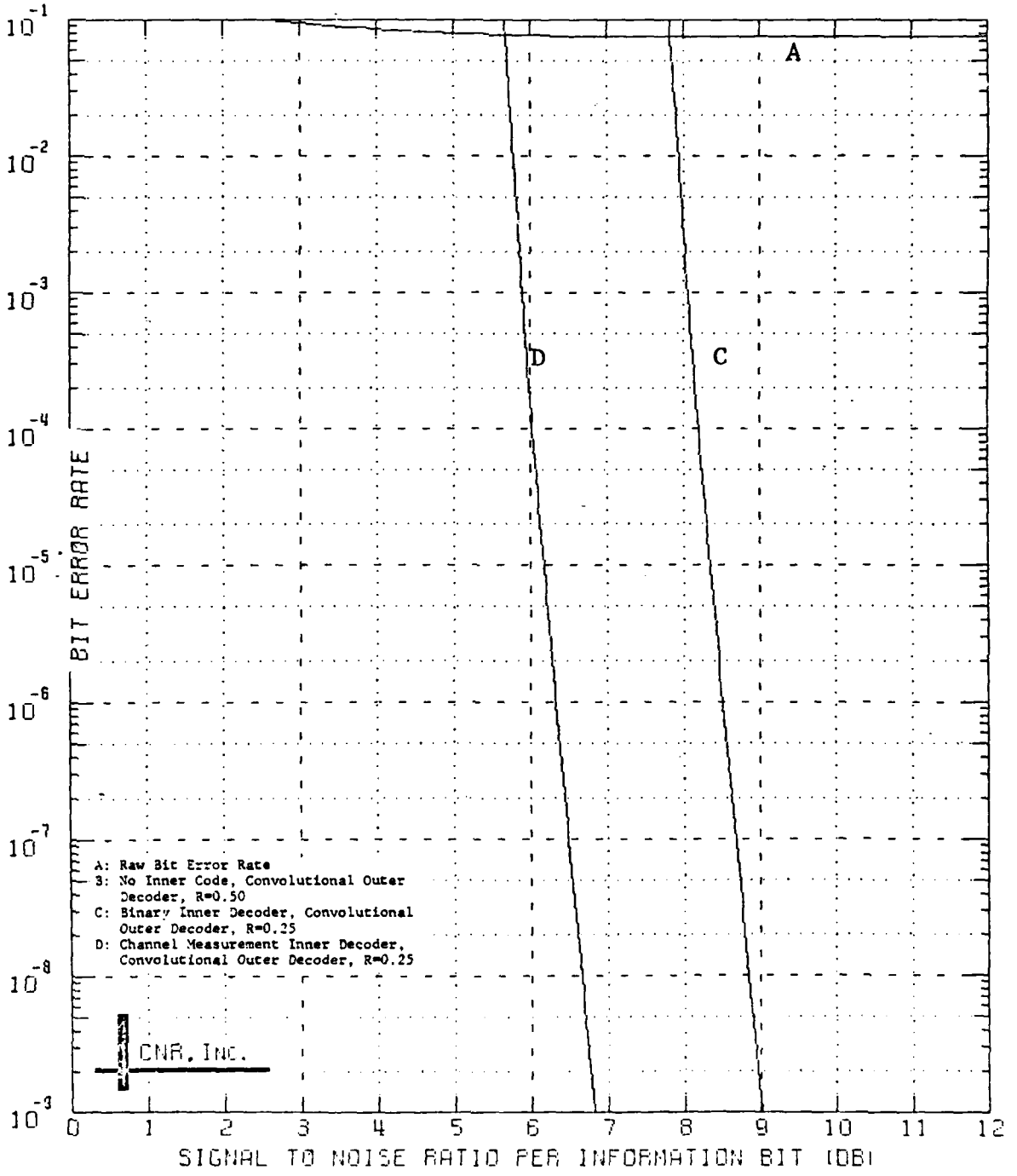


Figure 8.35 Decoded Performance of a Two-Stage Coding Approach
Outer Decoder: Convolutional Code, Rate=1/2; K=7
Inner Decoder: Convolutional Code, Rate=1/2; K=7
δ=0.15 and Erasure Information is Employed

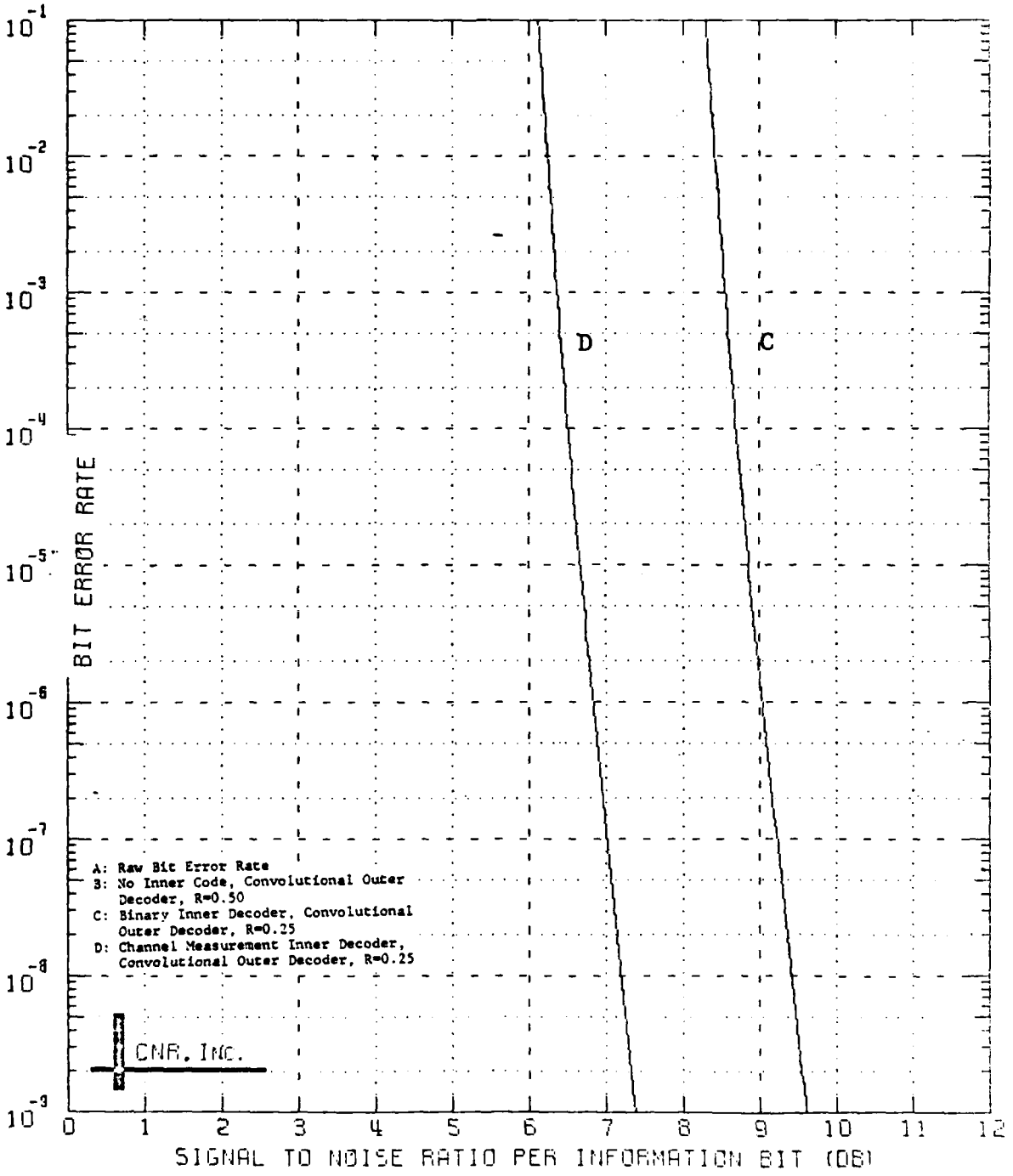


Figure 8.36 Decoded Performance of a Two-Stage Coding Approach
Outer Decoder: Convolutional Code, Rate=1/2; K=7
Inner Decoder: Convolutional Code, Rate=1/2; K=7
δ=0.20 and Erasure Information is Employed

TABLE 8-1

E_b/N_0 (dB) REQUIRED FOR A BIT ERROR RATE OF 10^{-5} FOR A RATE-1/2 INNER CONVOLUTIONAL CODE, WITH RATE-0.9 AND RATE-1/2 OUTER CODES

Inner Decoder/Outer Decoder	Erasure Availability	δ=0.00		δ=0.05		δ=0.10		δ=0.15		δ=0.20	
		BD	CD	BD	CD	BD	CD	BD	CD	BD	CD
Convolutional (K=7)/BCH (240,216;7)	No Erasures	5.5	3.2	7.3	4.5	----	5.9	----	7.5	----	9.5
Rate = 1/2 ⊗ 0.9 = 0.45	Erasures	5.5	3.2	5.8	3.6	6.2	4.0	6.7	4.5	7.3	5.1
Convolutional (K=7)/Convolutional (K=7)	No Erasures	7.2	5.0	8.6	6.1	12.2	7.3	----	8.6	----	10.2
Rate = 1/2 ⊗ 1/2 = 0.25	Erasures	7.2	5.0	7.5	5.3	7.8	5.7	8.3	6.2	8.8	6.7

δ=0.25		δ=0.30		δ=0.35		δ=0.40		δ=0.45		δ=0.50		δ=0.55	
BD	CD	BD	CD	BD	CD	BD	CD	BD	CD	BD	CD	BD	CD
----		----		----		----		----		----		----	
8.1	12.0	9.2	15.6	----	----	----	----	----	----	----	----	----	----
	5.8		6.9	----	----	----	----	----	----	----	----	----	----
----		----		----		----		----		----		----	
9.4	11.9	10.2	14.2	11.2	17.5	13.7	23.8	----	----	----	----	----	----
	7.1		7.8		8.8		11.8		----		----		----

---- Error Rate of 10^{-5} not achievable

TABLE 8-2

E_b/N_0 (dB) REQUIRED FOR A BIT ERROR RATE OF 10^{-5} FOR RATE-1/4 AND RATE-1/8 INNER CONVOLUTIONAL CODE WITH A RATE-0.9 OUTER CODE

Inner Code Rate	Erasure Availability	δ=0.00		δ=0.05		δ=0.10		δ=0.15		δ=0.20		δ=0.25		δ=0.30	
		BD	CD	BD	CD	BD	CD	BD	CD	BD	CD	BD	CD	BD	CD
1/4	Not Available	5.3	3.2	6.1	3.9	7.1	4.7	8.4	5.6	10.7	6.6	----	7.7	----	8.9
	Available	5.3	3.2	5.5	3.4	5.8	3.8	6.2	4.1	6.6	4.5	7.1	4.9	7.5	5.4
1/8	Not Available	5.3	3.2	5.8	3.7	6.5	4.4	7.2	5.0	8.0	5.7	9.1	6.5	10.3	7.4
	Available	5.3	3.2	5.5	3.4	5.7	3.7	6.0	4.0	6.0	4.3	6.3	4.6	6.5	4.9

---- Bit Error Rate of 10^{-5} not achievable
BD - Binary Decoding of Inner Code
CD - Channel Measurement Decoding of Inner Code

TABLE 8-2 (continued)

δ=0.35		δ=0.40		δ=0.45		δ=0.50		δ=0.55		δ=0.60		δ=0.65		δ=0.70		δ=0.75	
BD	CD	BD	CD	BD	CD	BD	CD	BD	CD	BD	CD	BD	CD	BD	CD	BD	CD
----		----		----		----		----		----		----		----		----	
	10.3		12.0		14.1		16.8		21.0		----		----		----		----
8.1		8.7		9.4		10.3		11.7		----		----		----		----	
	5.9		6.5		7.2		8.1		9.4		----		----		----		----
12.1		----		----		----		----		----		----		----		----	
	8.3		9.3		10.5		11.9		13.5		15.5		17.9		21.5		21.9
7.3		7.7		8.1		8.5		9.2		9.9		10.9		12.1		----	
	5.3		5.7		6.1		6.5		7.1		7.9		8.7		9.9		11.8

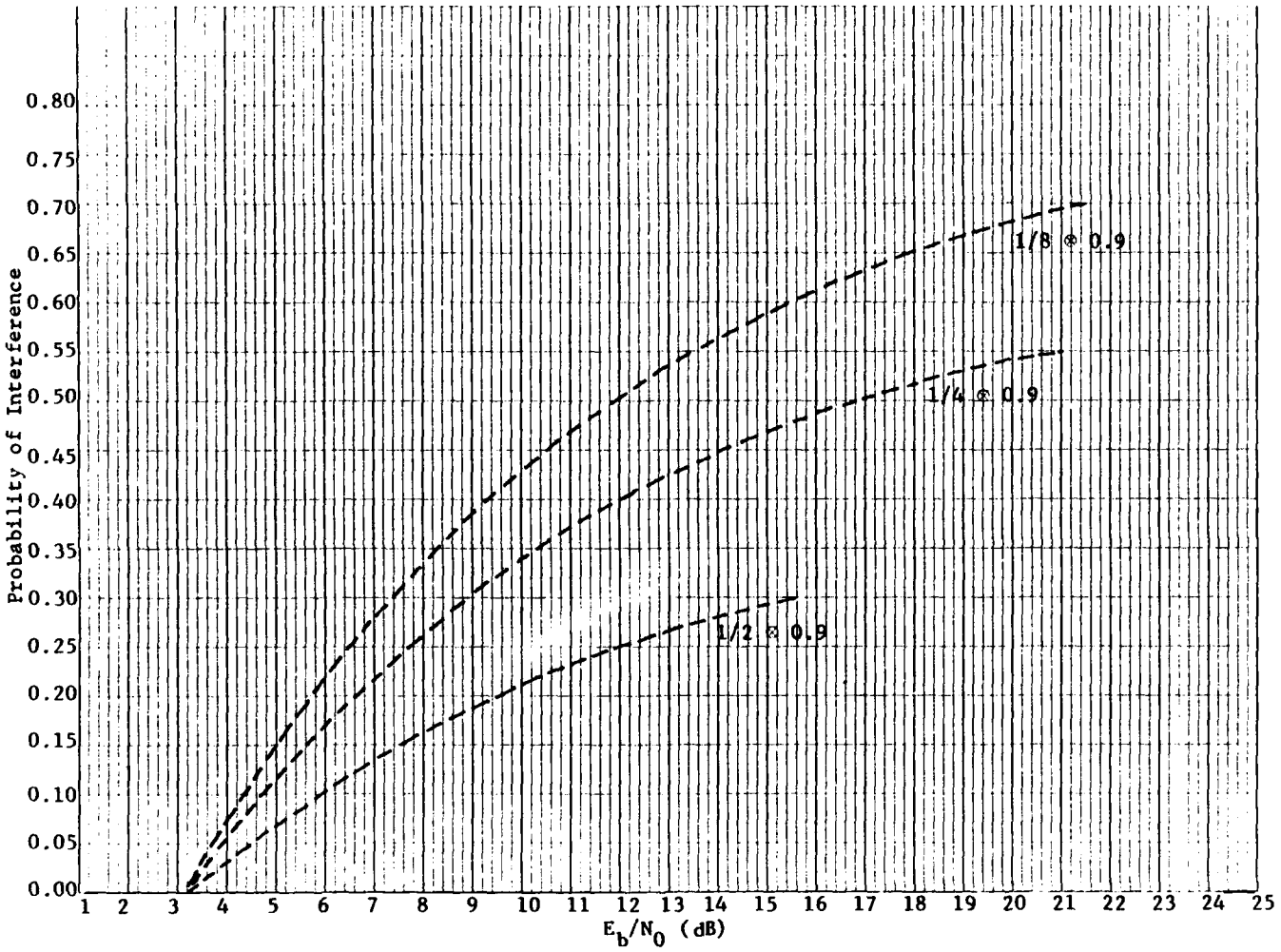


Figure 8.37 Two-Stage Coding Results
Outer Decoder: BCH (240,216;7)
Inner Decoder: Convolutional Code, K=7
Channel Measurement Decoding-No Erasure Information

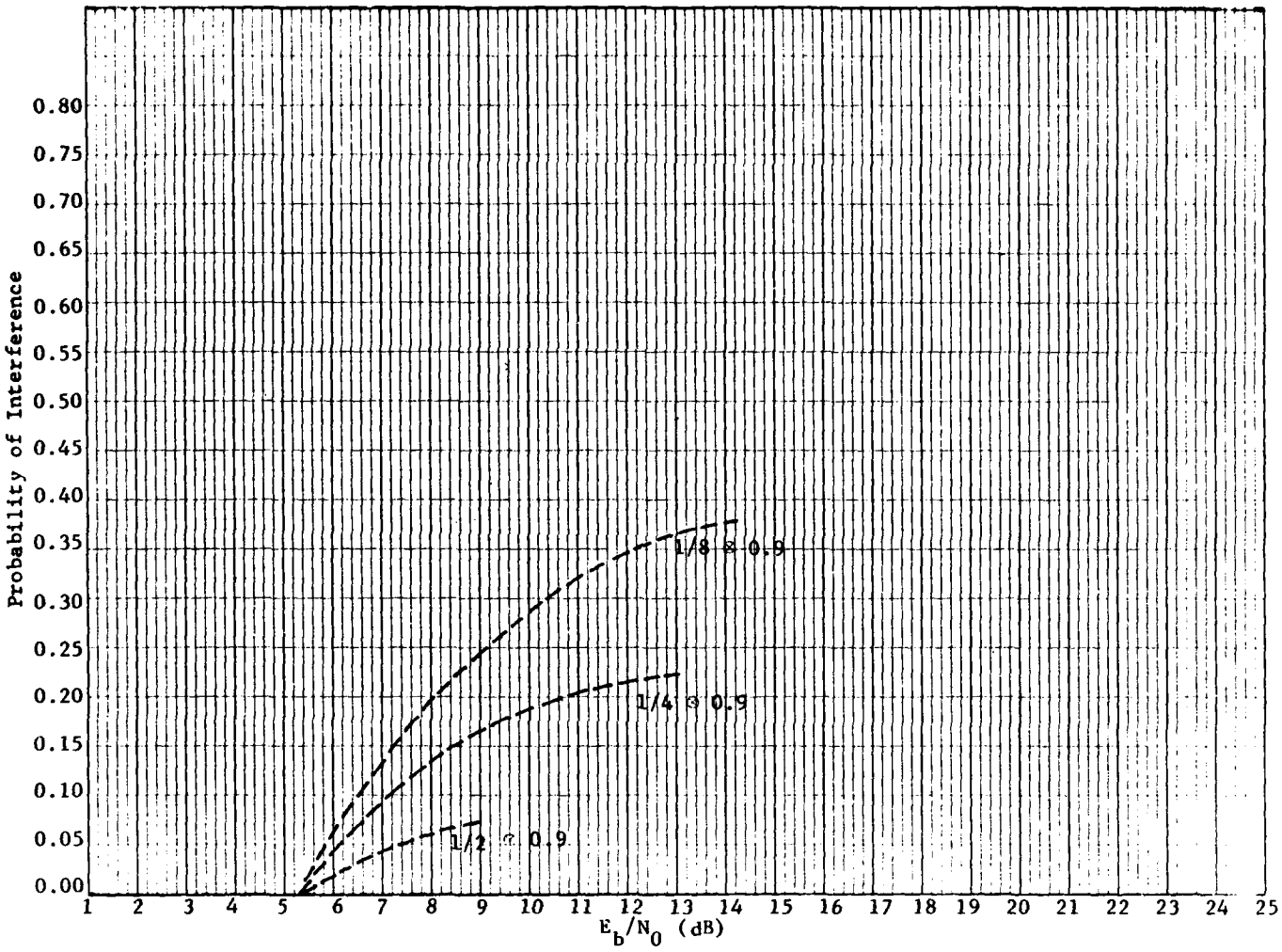


Figure 8.38 Two-Stage Coding Results
Outer Decoder: BCH (240,216;7)
Inner Decoder: Convolutional Code, K=7
Binary Decoding-No Erasure Information

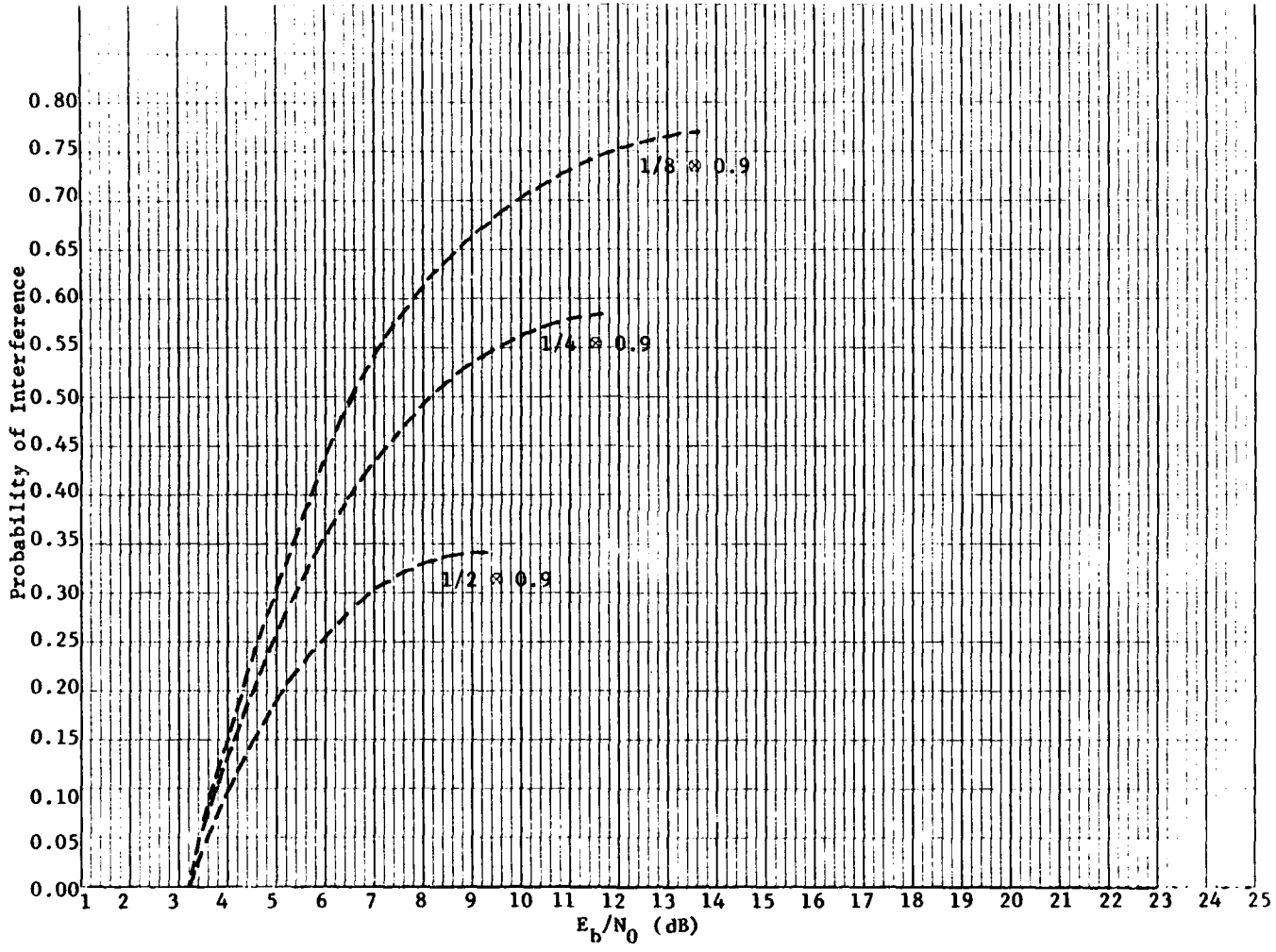


Figure 8.39 Two-Stage Coding Results
Outer Decoder: BCH (240,216;7)
Inner Decoder: Convolutional Code, K=7
Binary Decoding-Erasure Information Employed

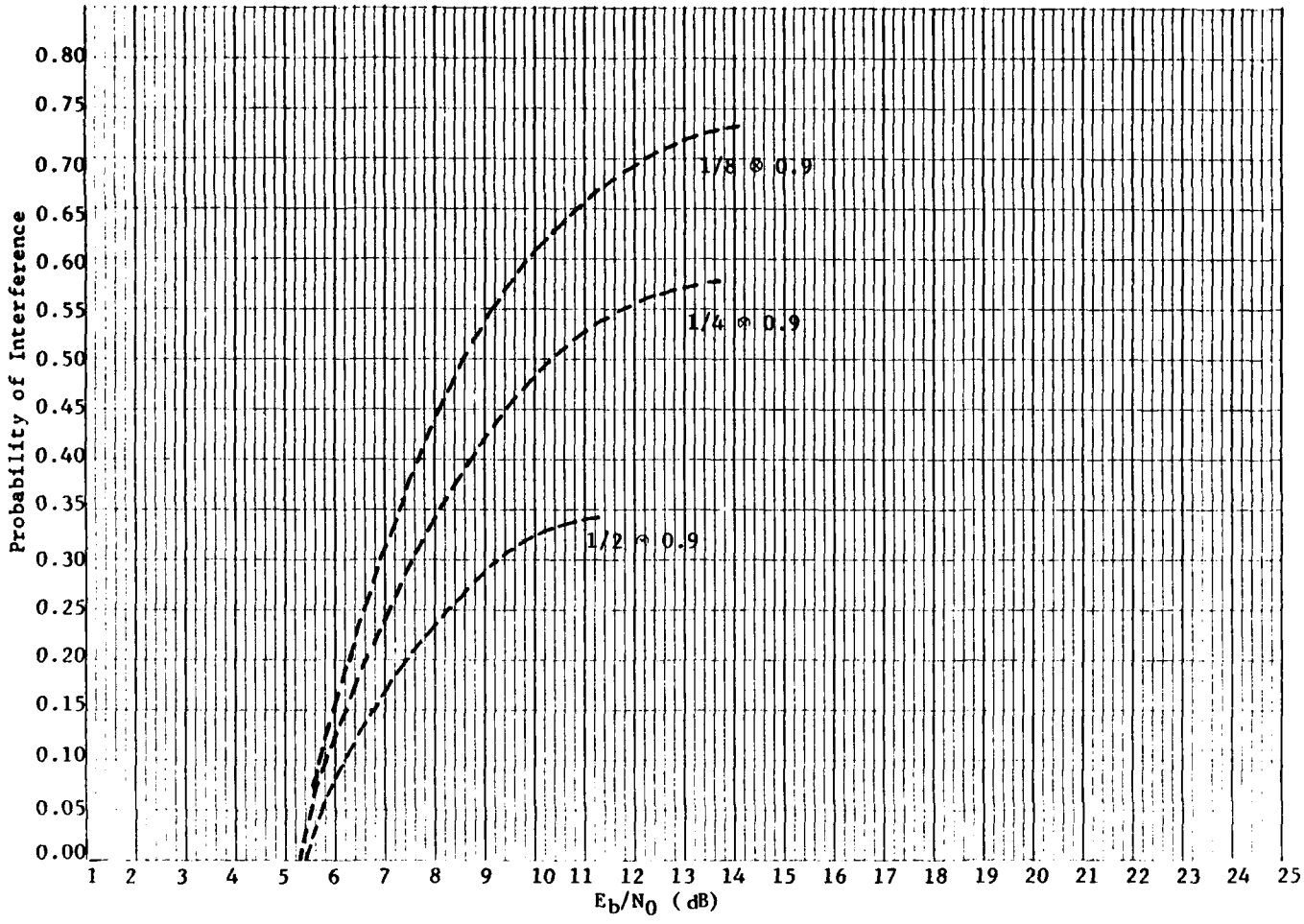


Figure 8.40 Two-Stage Coding Results
Outer Decoder: BCH (240,216;7)
Inner Decoder: Convolutional Code, K=7
Channel Measurement Decoding-Erasure Information Employed

SECTION 9

TWO-STAGE CODING APPROACH BASED ON A REED-SOLOMON OUTER CODE

In this section we present results based on a Reed-Solomon (R-S) outer code of rate-0.9. One R-S code considered is the (60,54;7) code, which has the same minimum distance as the (240,216;7) BCH code but is longer since 360 binary bits are needed to represent this R-S code. The best R-S code of equal binary bit dimensions to the (240,216;7) BCH code is the (40,36;5) R-S code. As discussed in Section 4.5, the (60,54;7) R-S code can outperform the (240,216;7) BCH code if we use symbol interleaving and are guaranteed that burst errors occur with an error rate of 1/2. If bit interleaving is used, the (60,54;7) R-S code offers inferior performance to that possible for the shorter (in binary bits) BCH code. The (40,36;5) R-S code, which is the same length as the BCH code, offers inferior performance for both the cases when a symbol interleaver or bit interleaver is used. For completeness, the input-output curves for these rate-0.9 codes given in Section 4 are repeated as Figure 9.1.

Since the R-S codes are generally inferior to the results possible with the rate-0.9 BCH outer decoder, the R-S results in this section are only applied to the rate-1/2 inner block and convolutional code.

Figures 9.2 to 9.10 illustrate the performance when an inner K=7 convolutional code is used with the (60,54;7) R-S code and bit interleaving is employed. Figures 9.11 to 9.19 illustrate the performance when symbol interleaving is used for the R-S code. Similar results for the (40,36;5) R-S code are given in Figures 9.20 to 9.37.

When a (128,64;22) BCH code is used as an inner code, rather than the K=7 convolutional code, results for a (60,54;7) R-S code and a (40,36;5) R-S code are given in Figures 9.38 to 9.73.

These results clearly show the benefits of symbol interleaving if a R-S code is used. However, as noted in Section 4.5, these benefits are calculated for the case when the symbols are completely destroyed by the interference. The modulation format, jamming scenario, etc., all must be considered to determine the actual benefits of symbol interleaving for a given application.

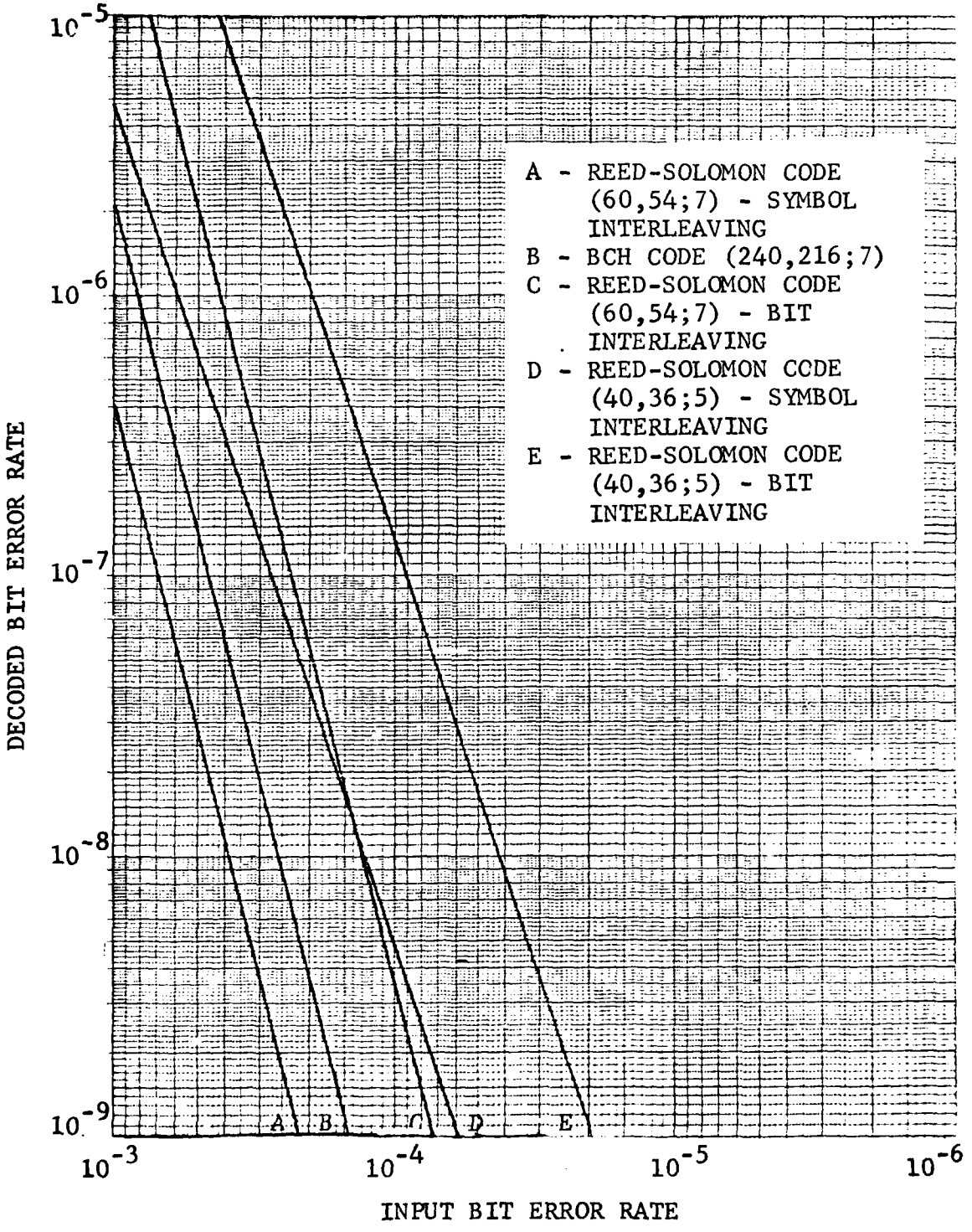


Figure 9.1 Comparison of Error Rate Performance for R = 0.9 Codes

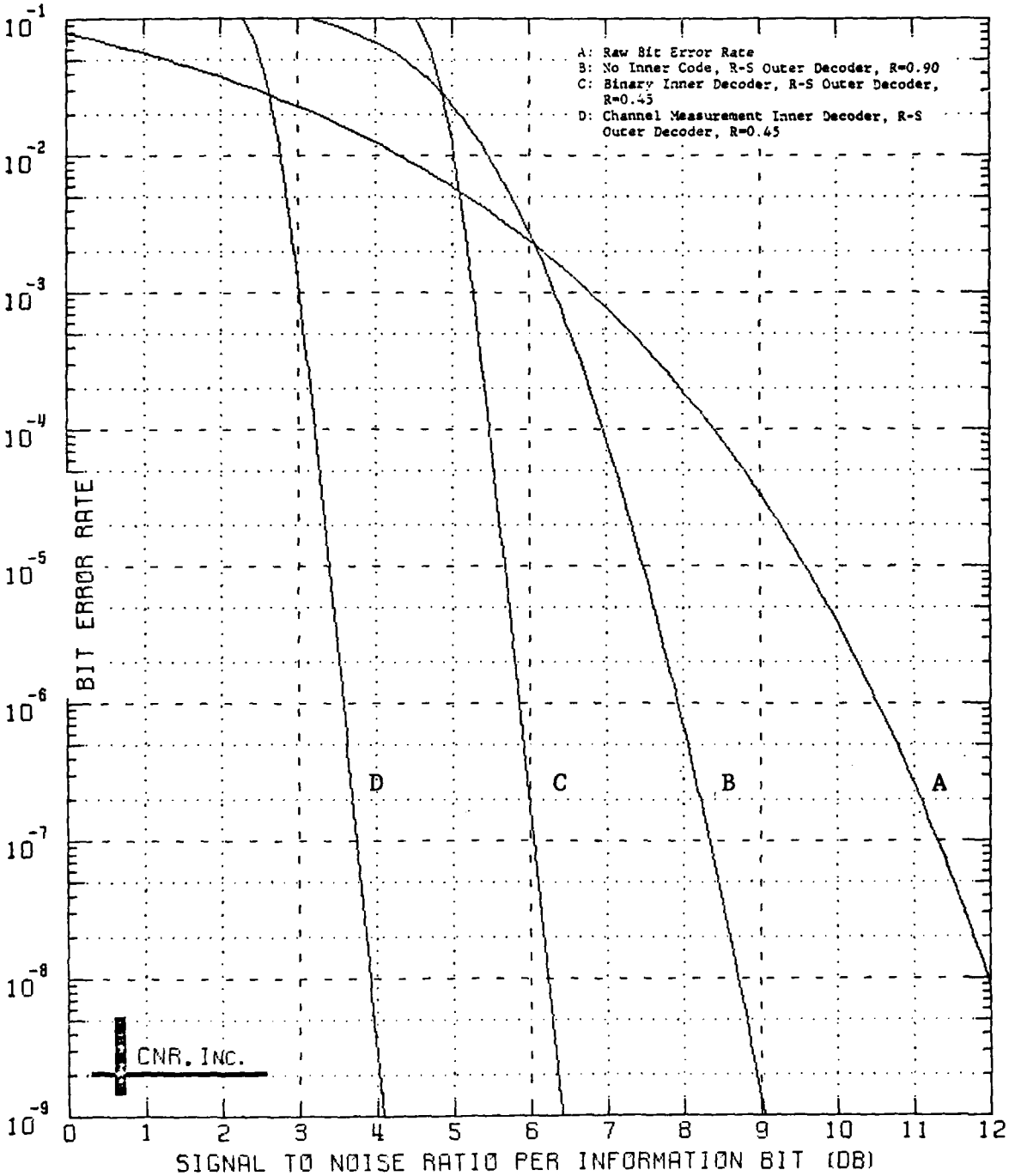


Figure 9.2 Decoded Performance of a Two-Stage Coding Approach
Outer Decoder: Reed-Solomon Code (60,54;7)
Bit Interleaver Employed
Inner Decoder: Convolutional Code, Rate=1/2; K=7
δ=0.00 and No Erasure Information Employed

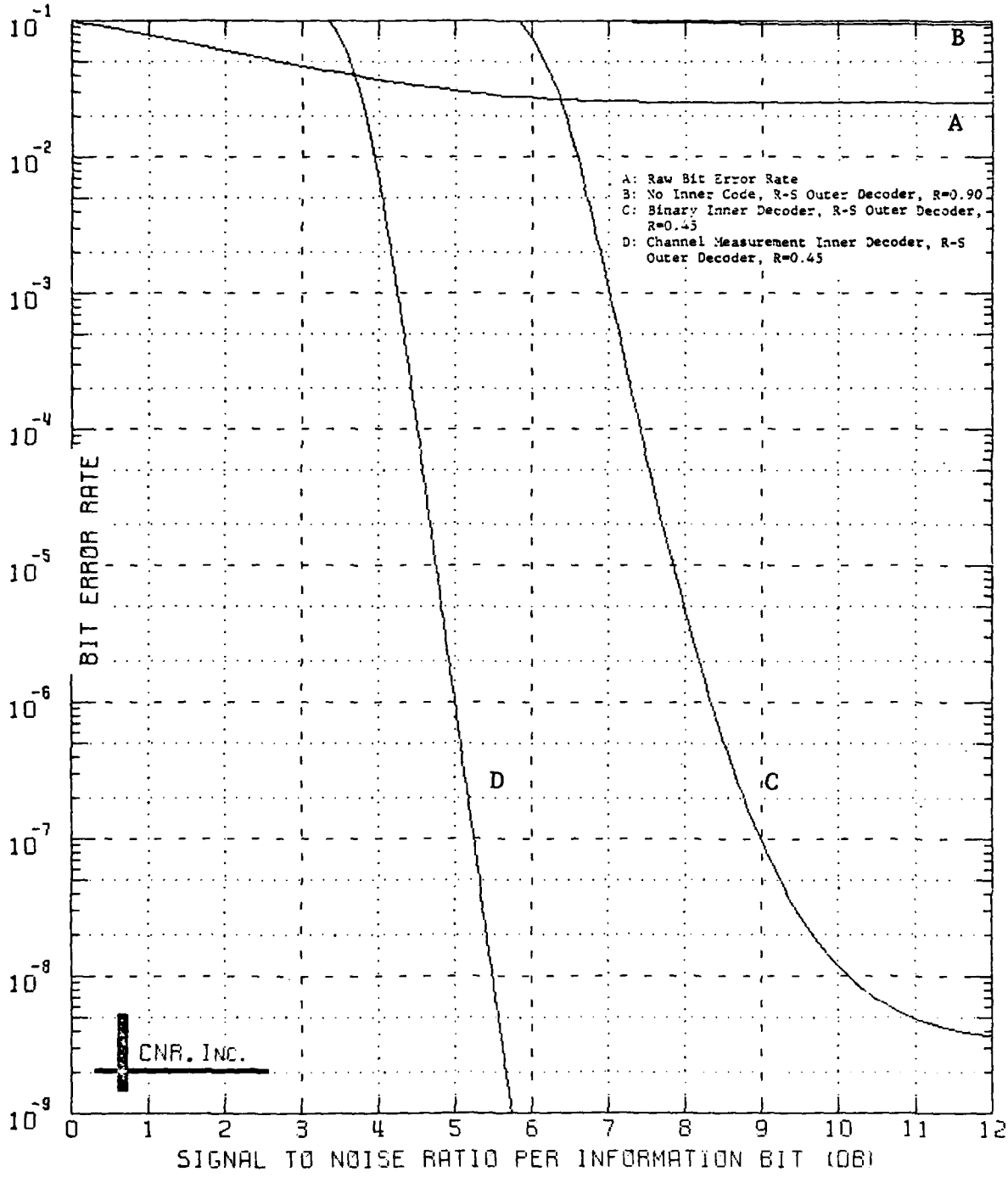


Figure 9.3 Decoded Performance of a Two-Stage Coding Approach
Outer Decoder: Reed-Solomon Code (60,54;7)
Bit Interleaver Employed
Inner Decoder: Convolutional Code, Rate=1/2; K=7
δ=0.05 and No Erasure Information Employed

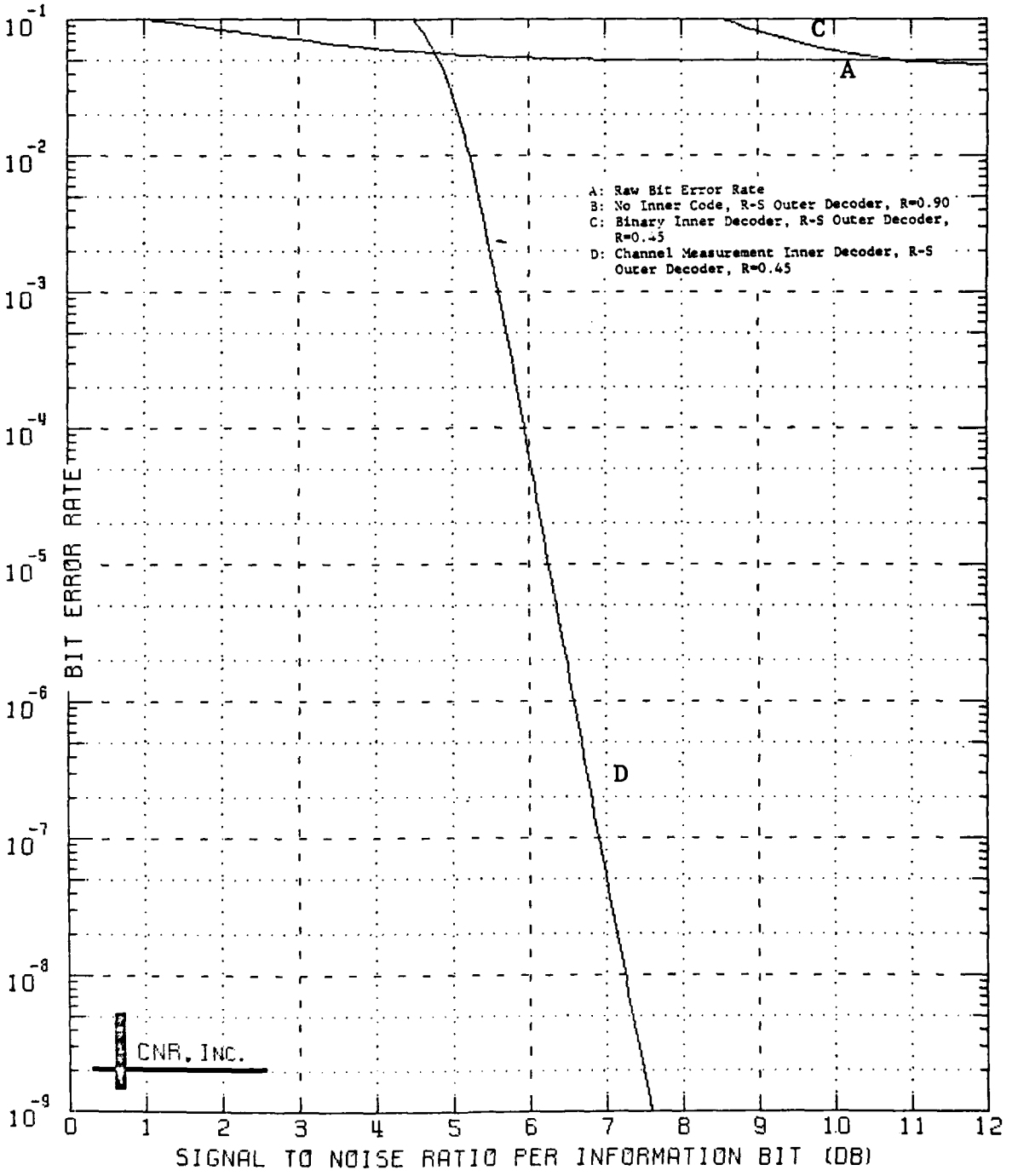


Figure 9.4 Decoded Performance of a Two-Stage Coding Approach
Outer Decoder: Reed-Solomon Code (60,54;7)
Bit Interleaver Employed
Inner Decoder: Convolutional Code, Rate=1/2; K=7
δ=0.10 and No Erasure Information Employed

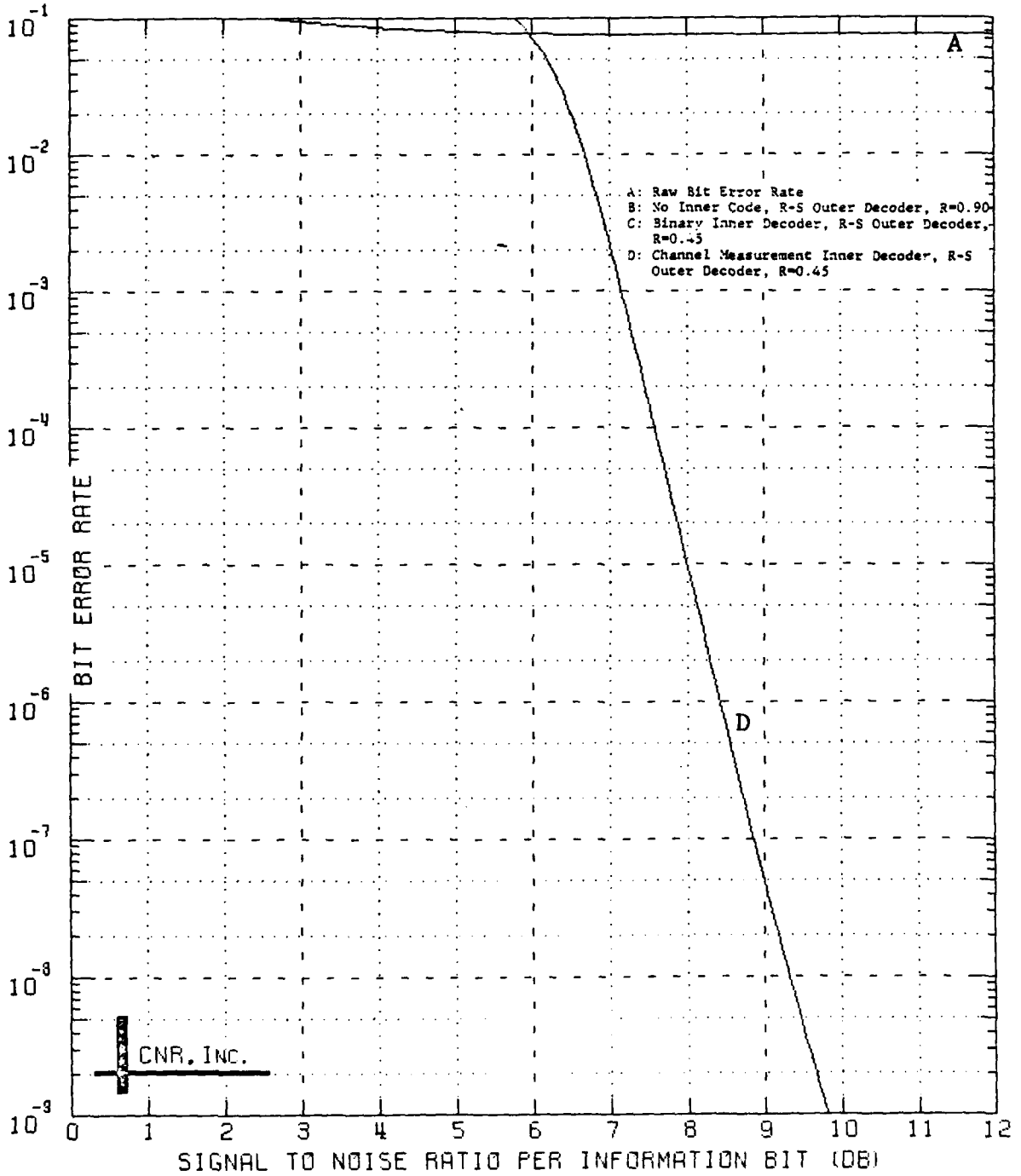


Figure 9.5 Decoded Performance of a Two-Stage Coding Approach
Outer Decoder: Reed-Solomon Code (60,54;7)
Bit Interleaver Employed
Inner Decoder: Convolutional Code, Rate=1/2; K=7
δ=0.15 and No Erasure Information Employed

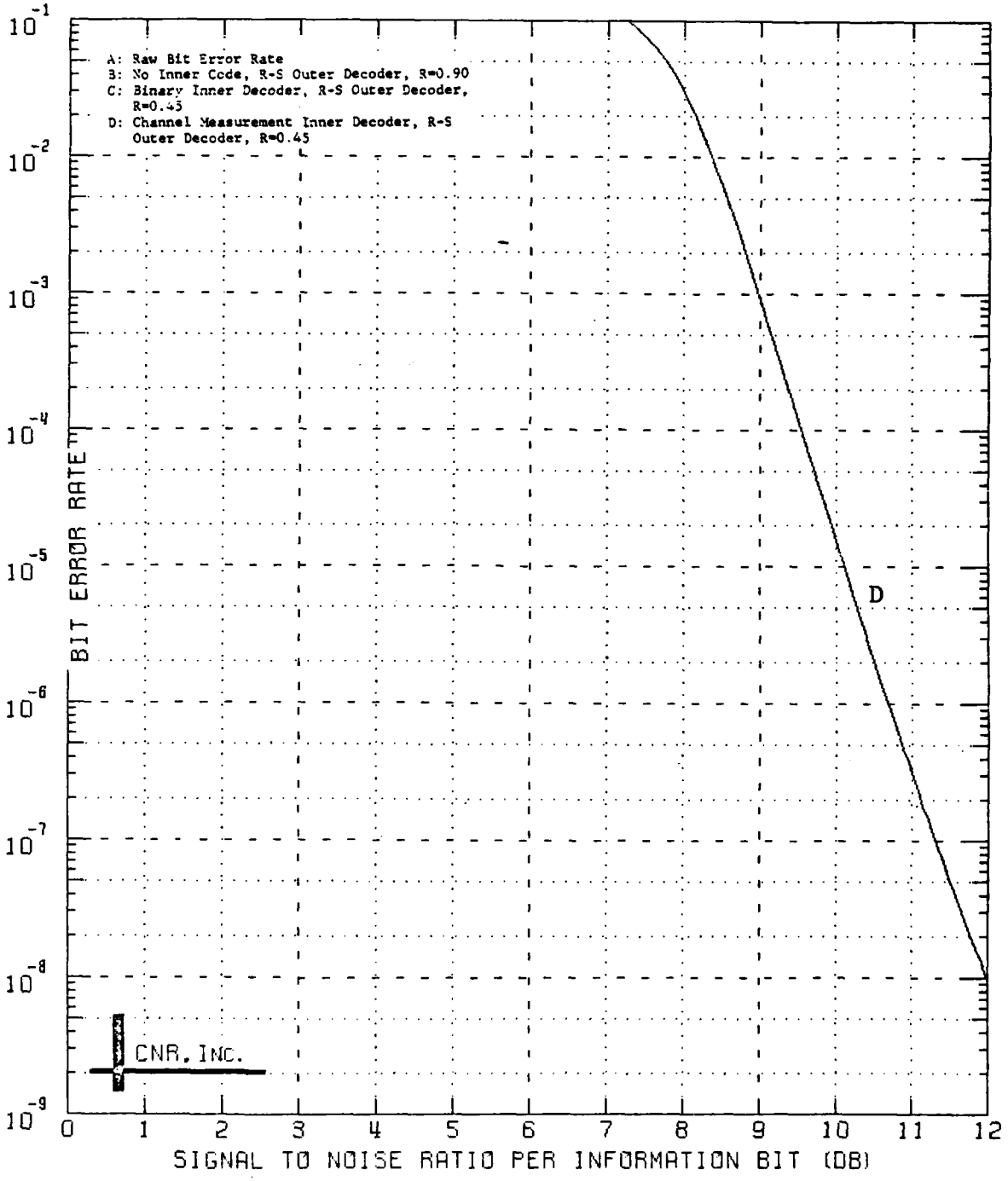


Figure 9.6 Decoded Performance of a Two-Stage Coding Approach
Outer Decoder: Reed-Solomon Code (60,54;7)
Bit Interleaver Employed
Inner Decoder: Convolutional Code, Rate=1/2; K=7
δ=0.20 and No Erasure Information Employed

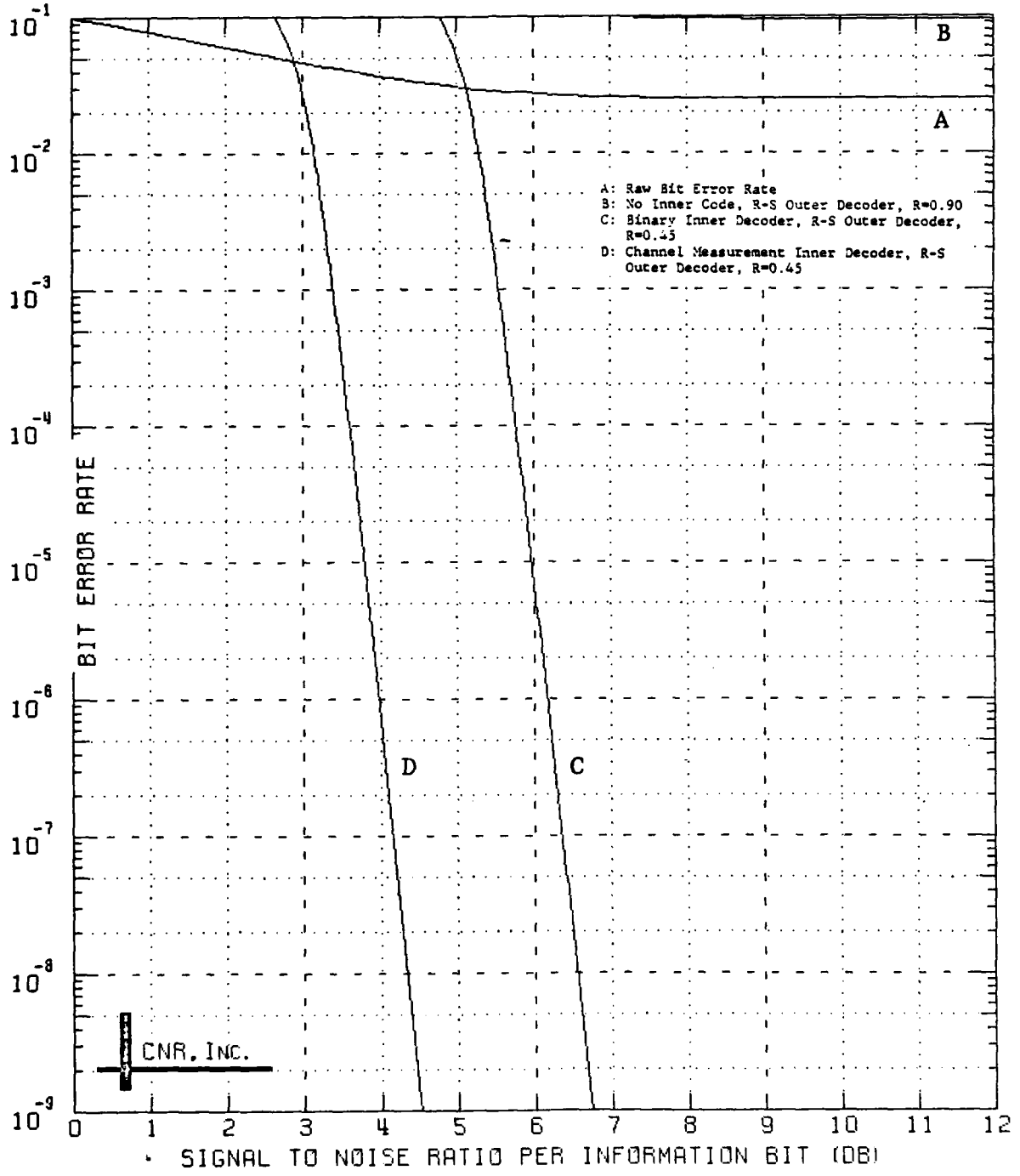


Figure 9.7 Decoded Performance of a Two-Stage Coding Approach
Outer Decoder: Reed-Solomon Code (60,54;7)
Bit Interleaver Employed
Inner Decoder: Convolutional Code, Rate=1/2; K=7
δ=0.05 and Erasure Information is Employed

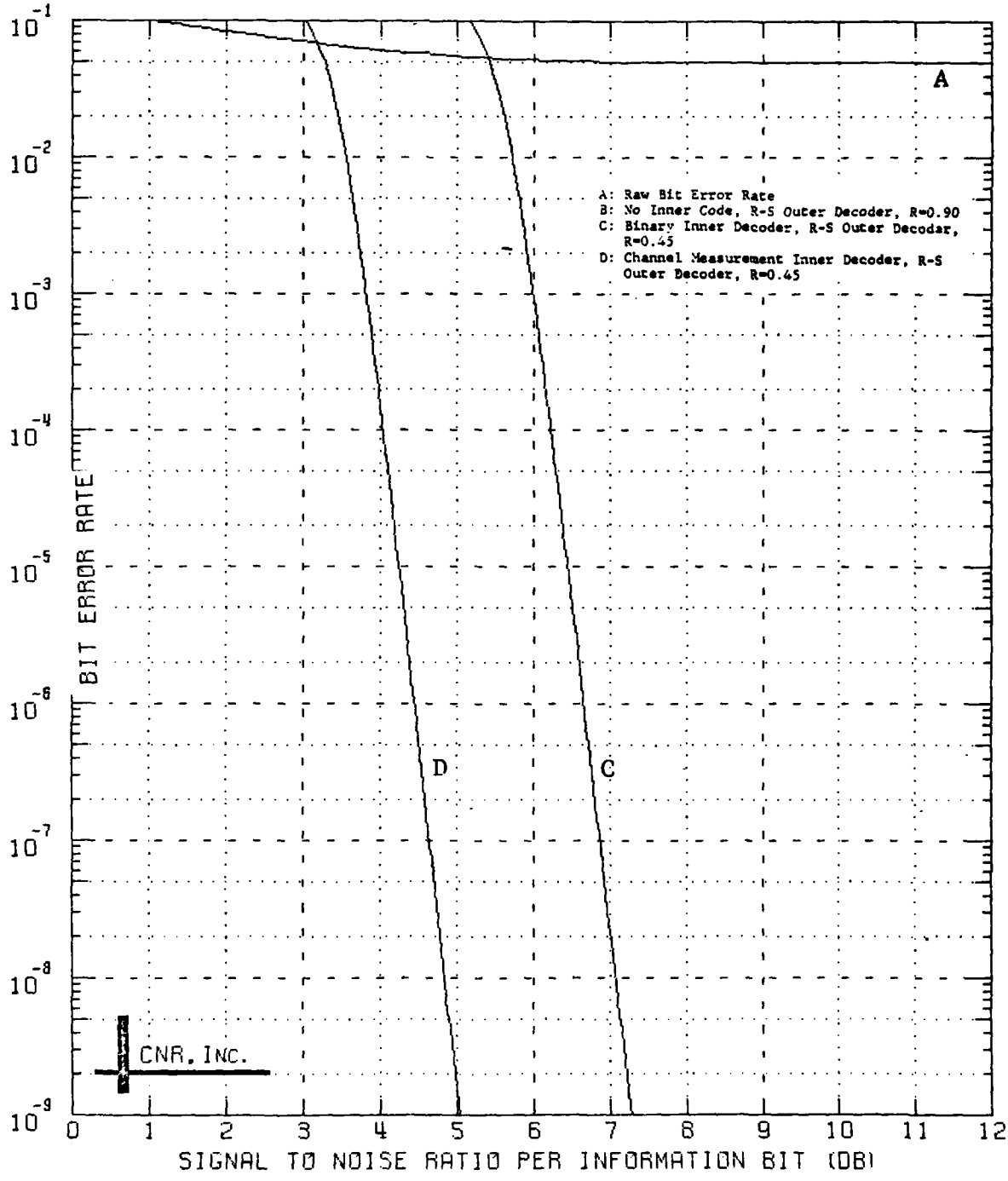


Figure 9.8 Decoded Performance of a Two-Stage Coding Approach
Outer Decoder: Reed-Solomon Code (60,54;7)
Bit Interleaver Employed
Inner Decoder: Convolutional Code, Rate=1/2; K=7
δ=0.10 and Erasure Information is Employed

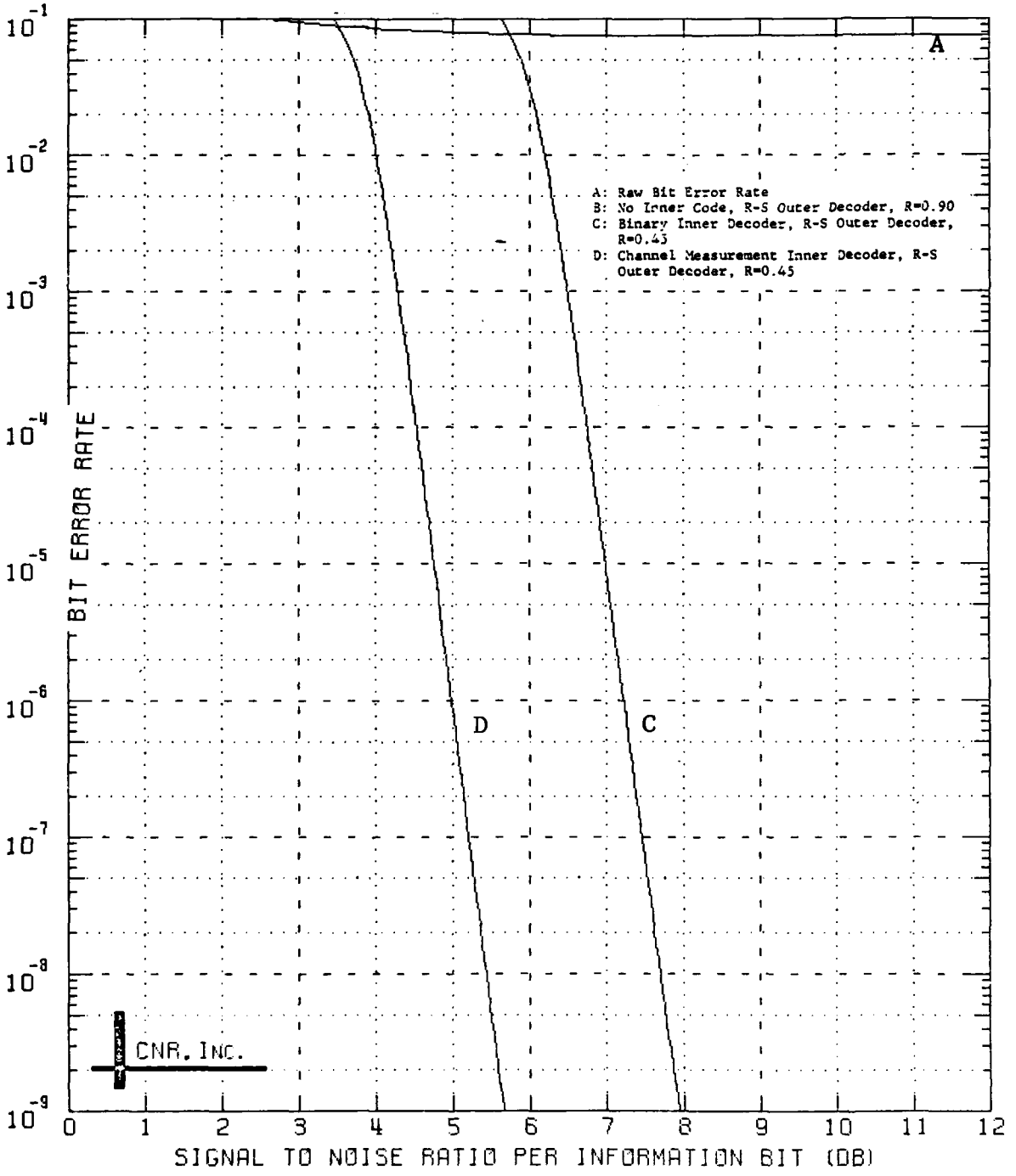


Figure 9.9 Decoded Performance of a Two-Stage Coding Approach
Outer Decoder: Reed-Solomon Code (60,54;7)
Bit Interleaver Employed
Inner Decoder: Convolutional Code, Rate=1/2; K=7
δ=0.15 and Erasure Information is Employed

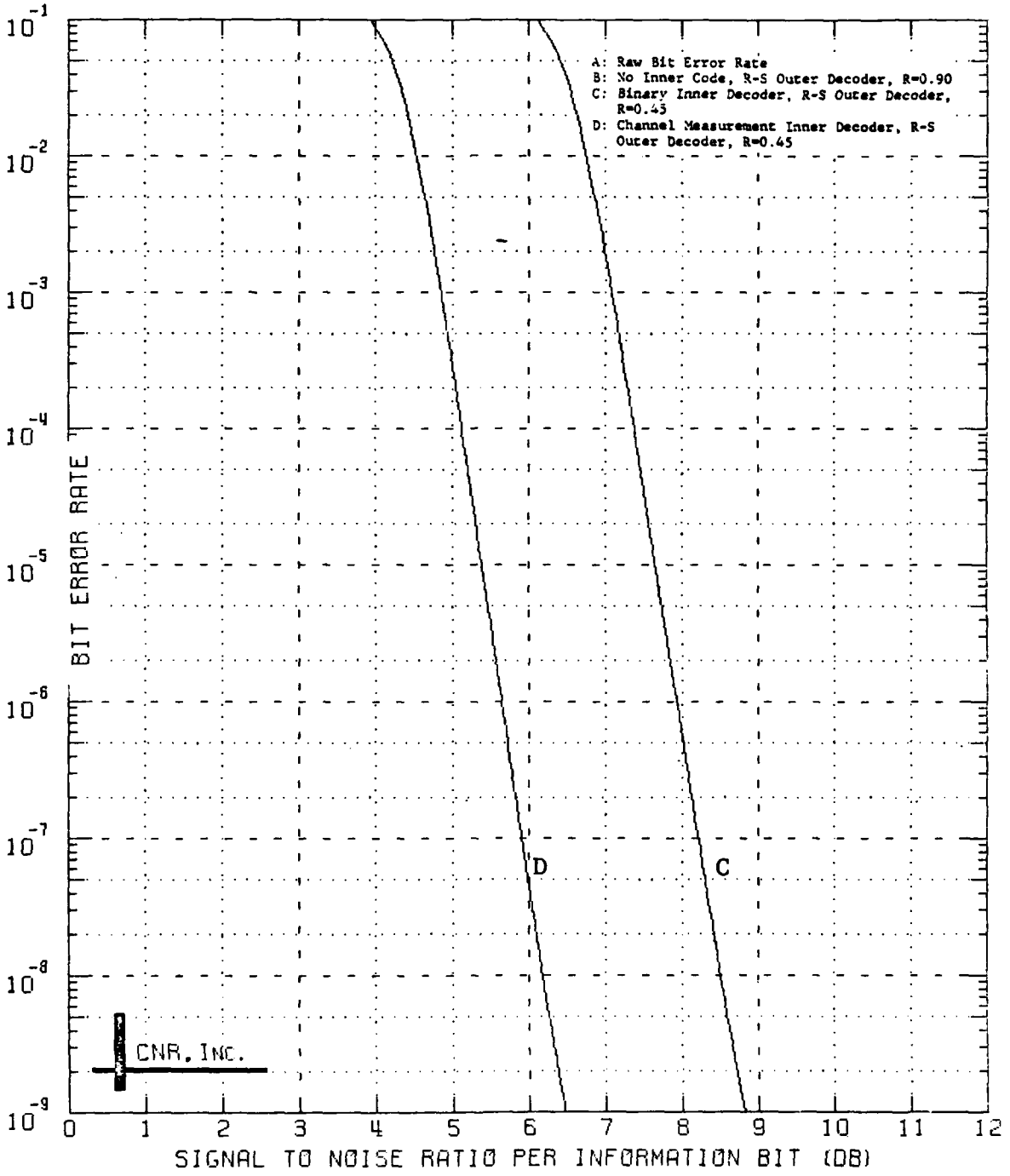


Figure 9.10 Decoded Performance of a Two-Stage Coding Approach
Outer Decoder: Reed-Solomon Code (60,54;7)
Bit Interleaver Employed
Inner Decoder: Convolutional Code, Rate=1/2; K=7
δ=0.20 and Erasure Information is Employed

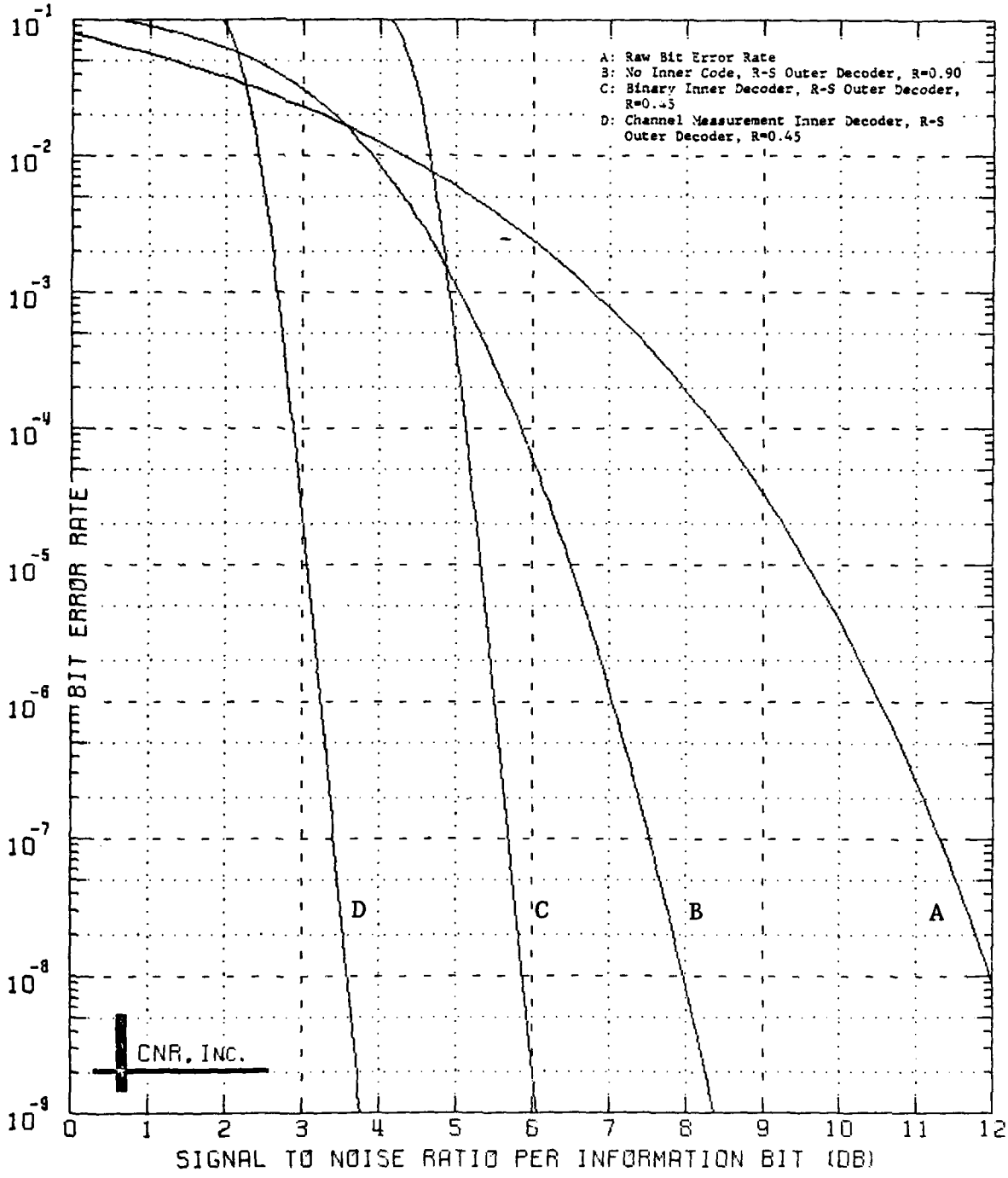


Figure 9.11 Decoded Performance of a Two-Stage Coding Approach
Outer Decoder: Reed-Solomon Code (60,54;7)
Symbol Interleaver Employed
Inner Decoder: Convolutional Code, Rate=1/2; K=7
δ=0.00 and No Erasure Information is Employed

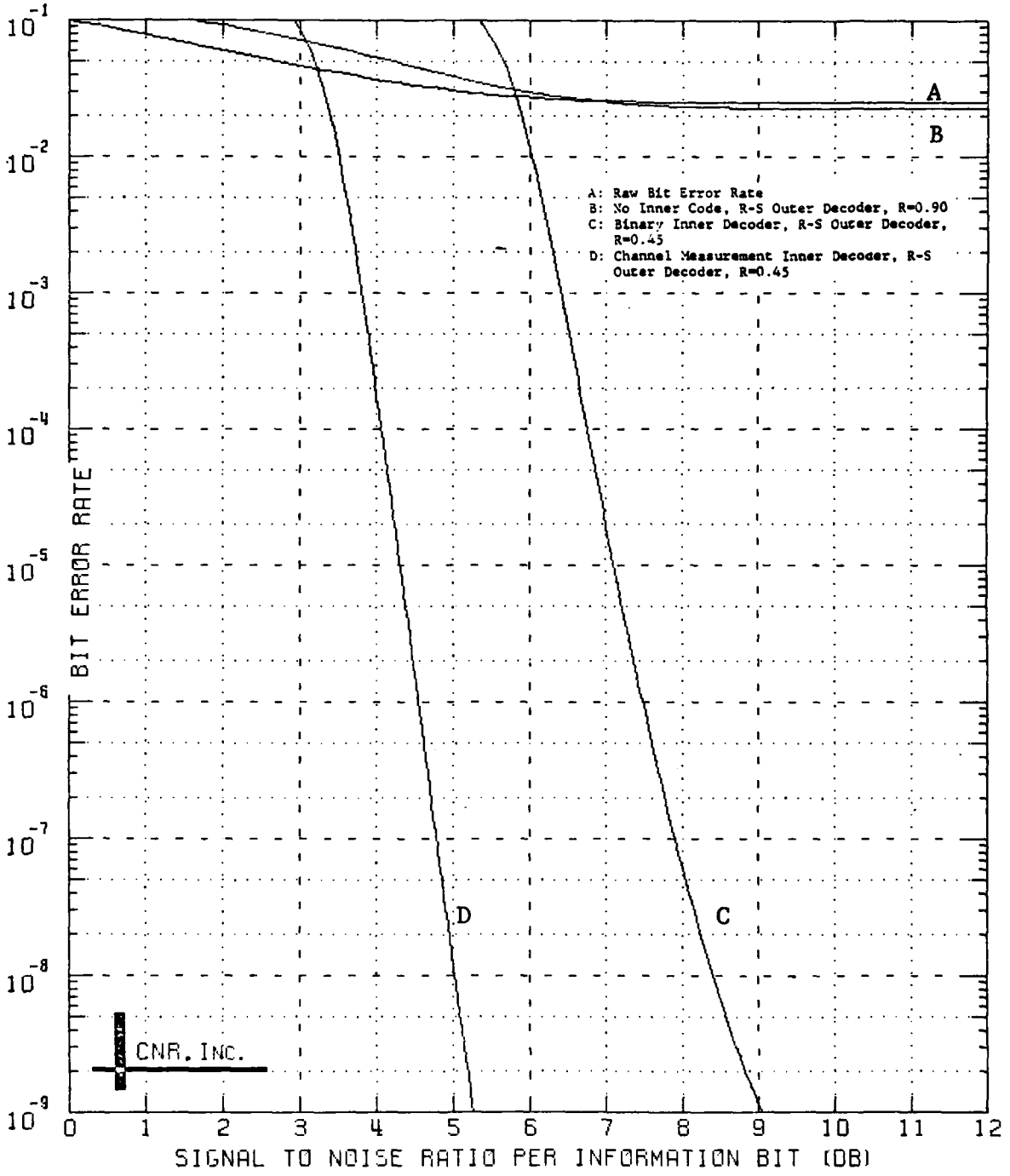


Figure 9.12 Decoded Performance of a Two-Stage Coding Approach
Outer Decoder: Reed-Solomon Code (60,54;7)
Symbol Interleaver Employed
Inner Decoder: Convolutional Code, Rate=1/2; K=7
δ=0.05 and No Erasure Information is Employed

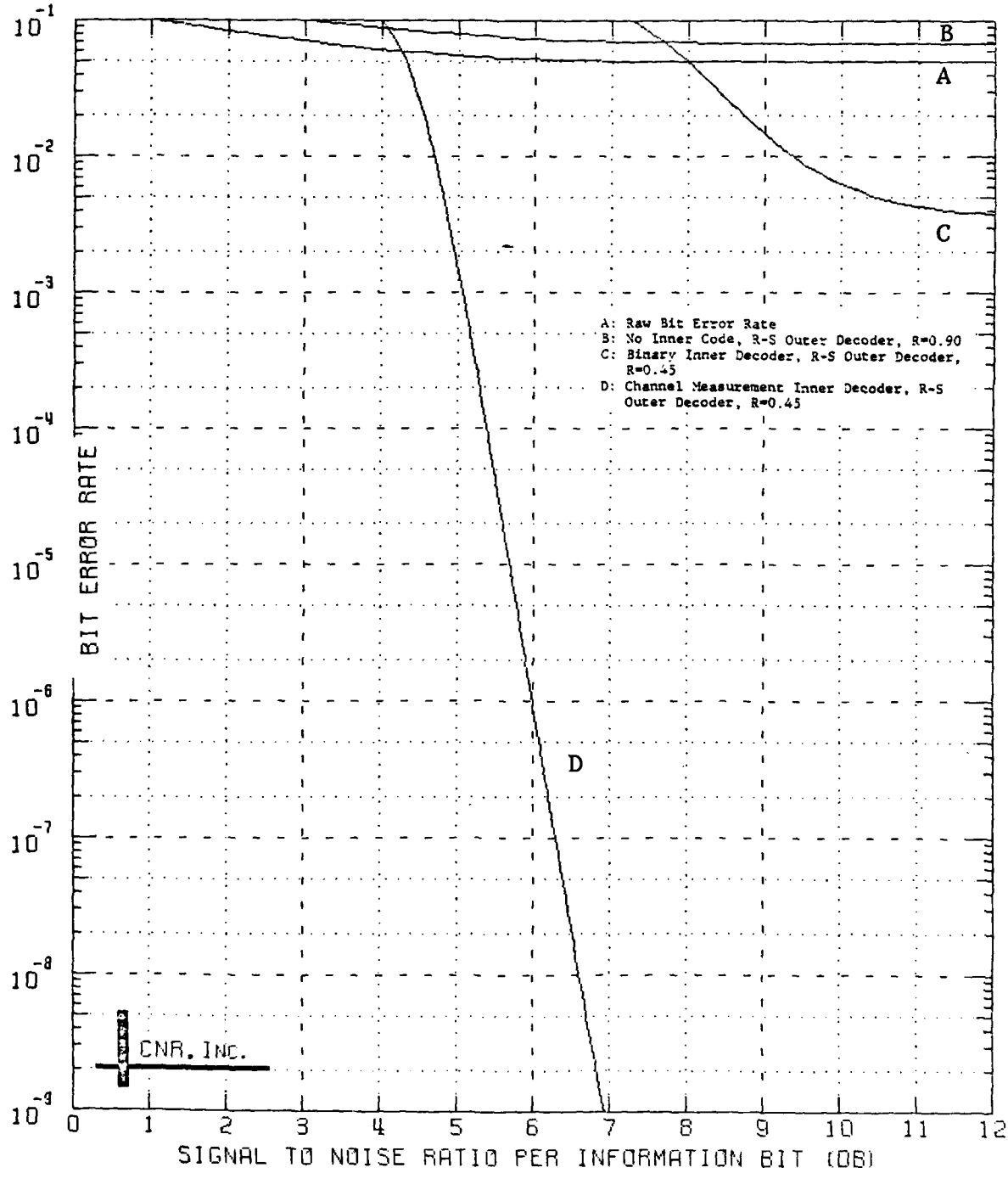


Figure 9.13 Decoded Performance of a Two-Stage Coding Approach
Outer Decoder: Reed-Solomon Code (60,54;7)
Symbol Interleaver Employed
Inner Decoder: Convolutional Code, Rate=1/2; K=7
δ=0.10 and No Erasure Information Employed

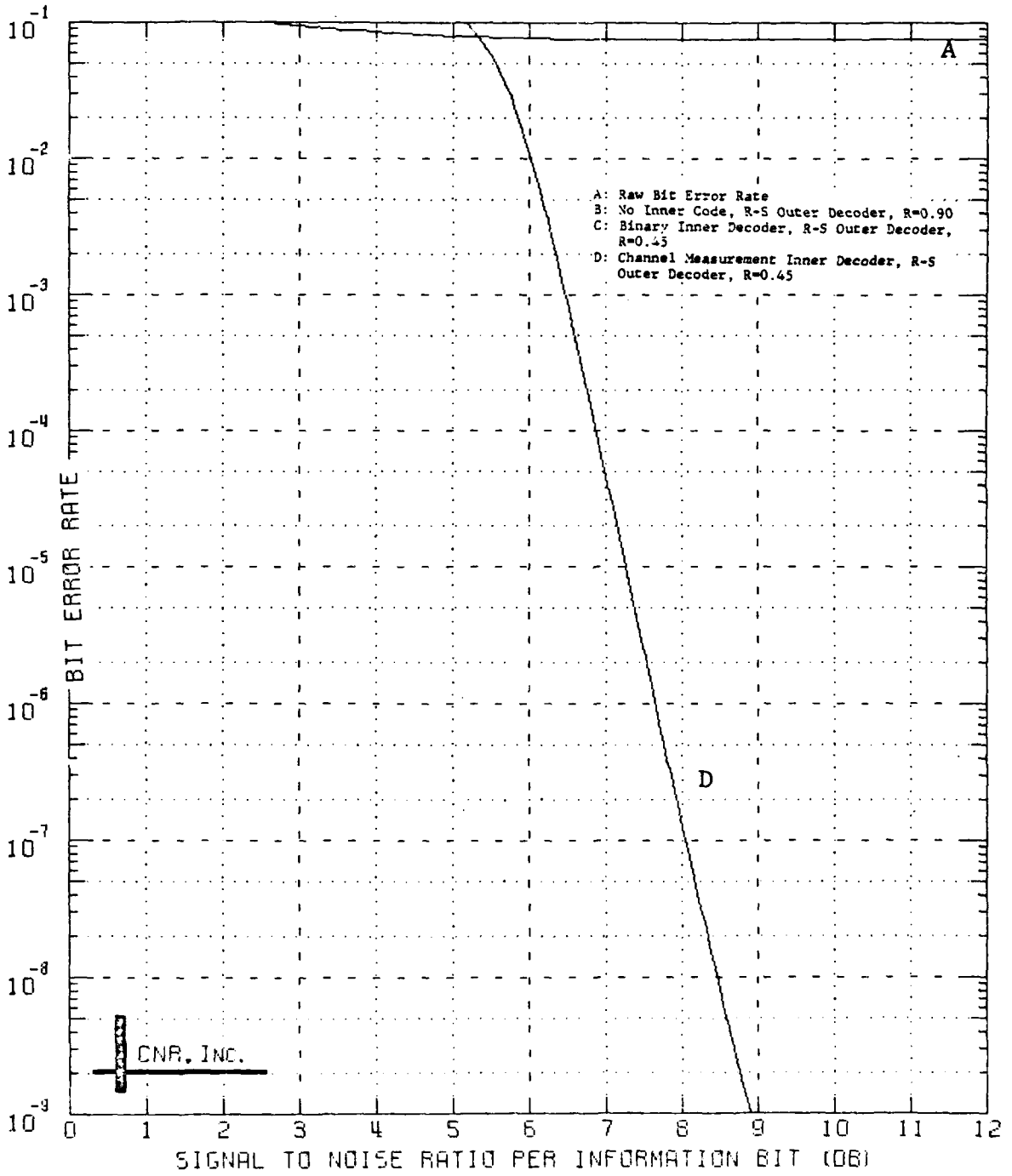
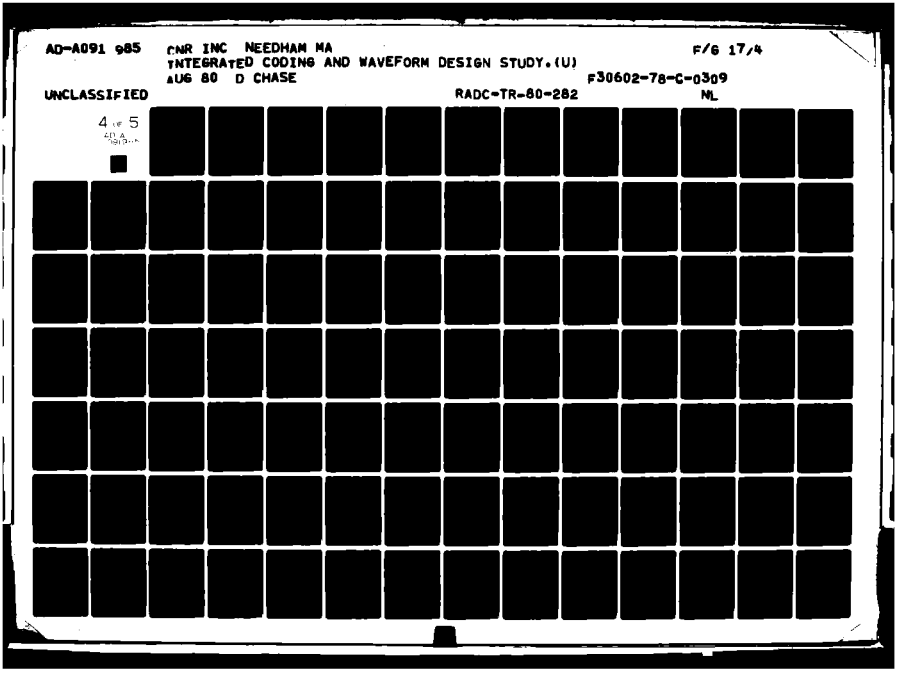


Figure 9.14 Decoded Performance of a Two-Stage Coding Approach
Outer Decoder: Reed-Solomon Code (60,54;7)
Symbol Interleaver Employed
Inner Decoder: Convolutional Code, Rate=1/2; K=7
δ=0.15 and No Erasure Information Employed

AD-A091 985 CNR INC NEEDHAM MA F/G 17/4
INTEGRATED CODING AND WAVEFORM DESIGN STUDY.(U)
AUG 80 D CHASE F30602-78-C-0309
UNCLASSIFIED RADC-TR-80-282 NL



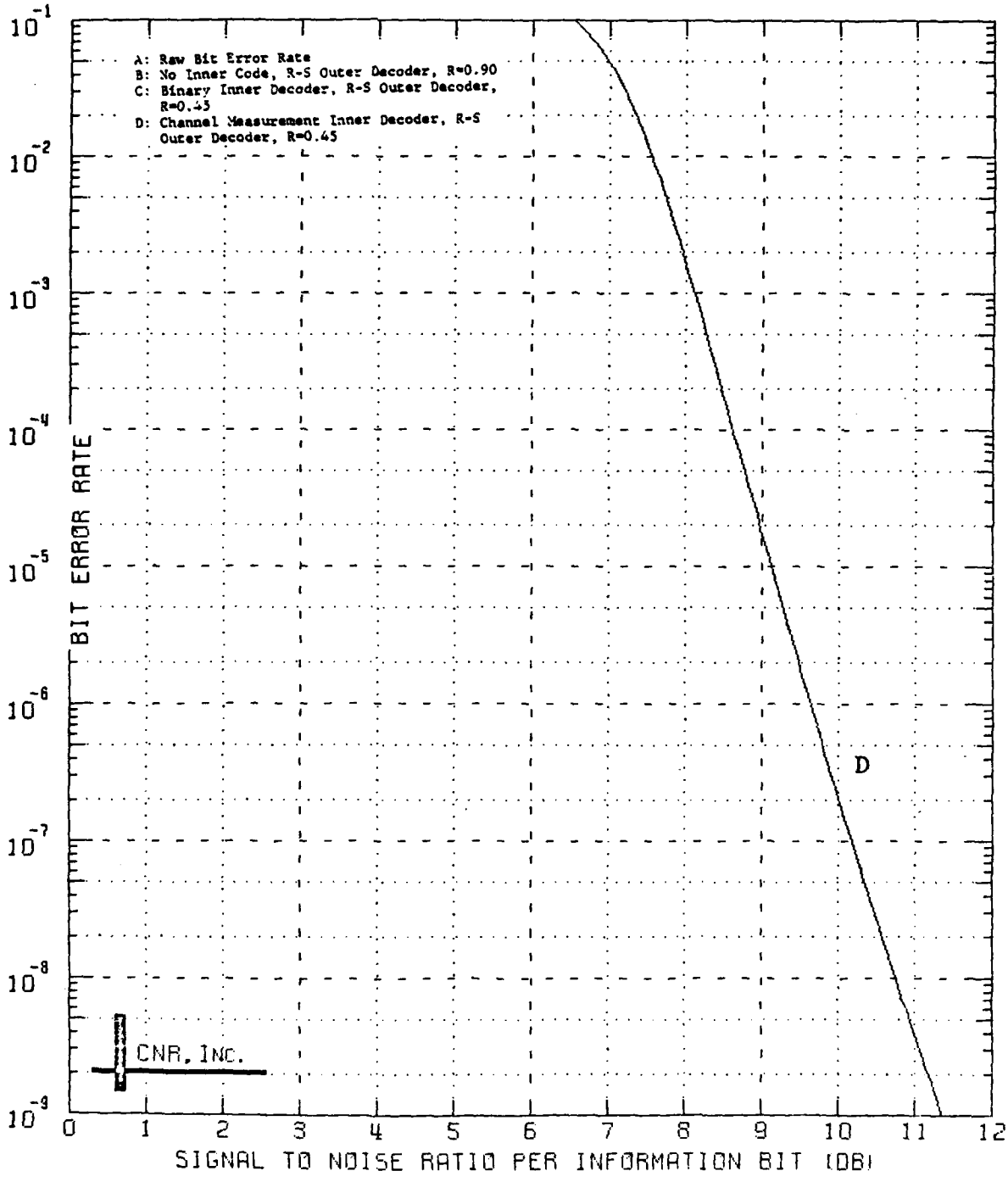


Figure 9.15 Decoded Performance of a Two-Stage Coding Approach
Outer Decoder: Reed-Solomon Code (60,54;7)
Symbol Interleaver Employed
Inner Decoder: Convolutional Code, Rate=1/2; K=7
δ=0.20 and No Erasure Information Employed

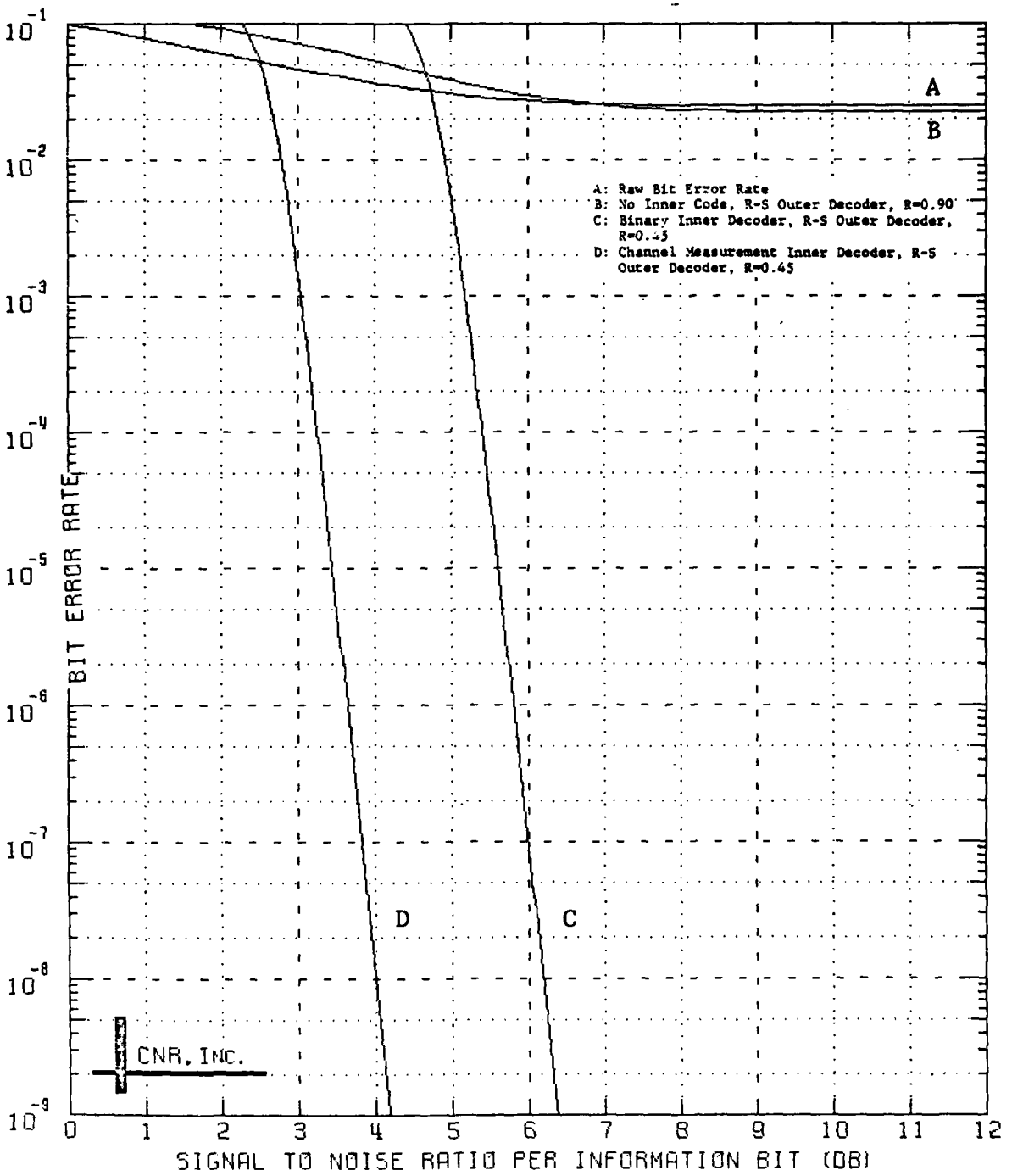


Figure 9.16 Decoded Performance of a Two-Stage Coding Approach
Outer Decoder: Reed-Solomon Code (60,54;7)
Symbol Interleaver Employed
Inner Decoder: Convolutional Code, Rate=1/2; K=7
δ=0.05 and Erasure Information is Employed

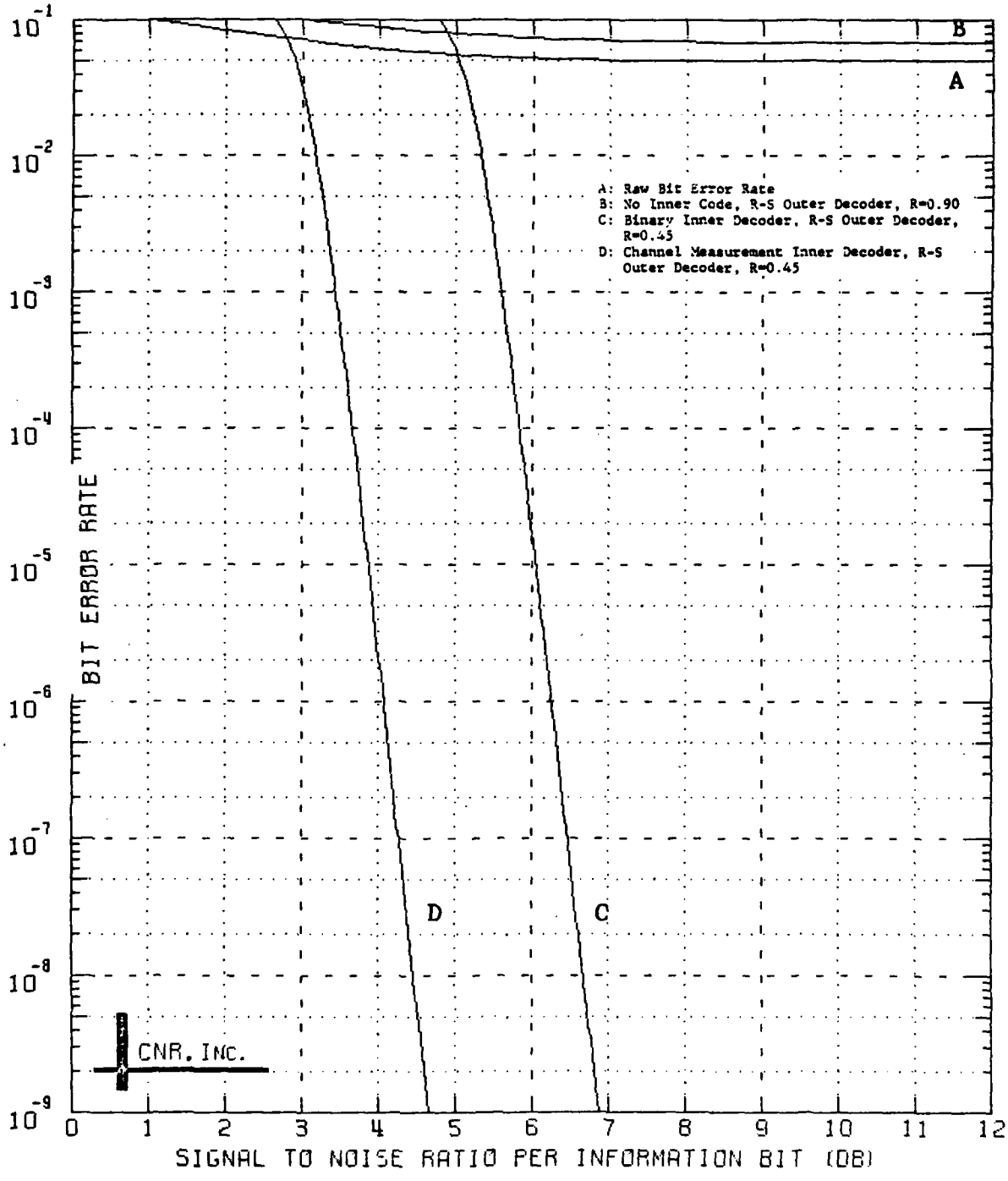


Figure 9.17 Decoded Performance of a Two-Stage Coding Approach
Outer Decoder: Reed-Solomon Code (60,54;7)
Symbol Interleaver Employed
Inner Decoder: Convolutional Code, Rate=1/2; K=7
δ=0.10 and Erasure Information is Employed

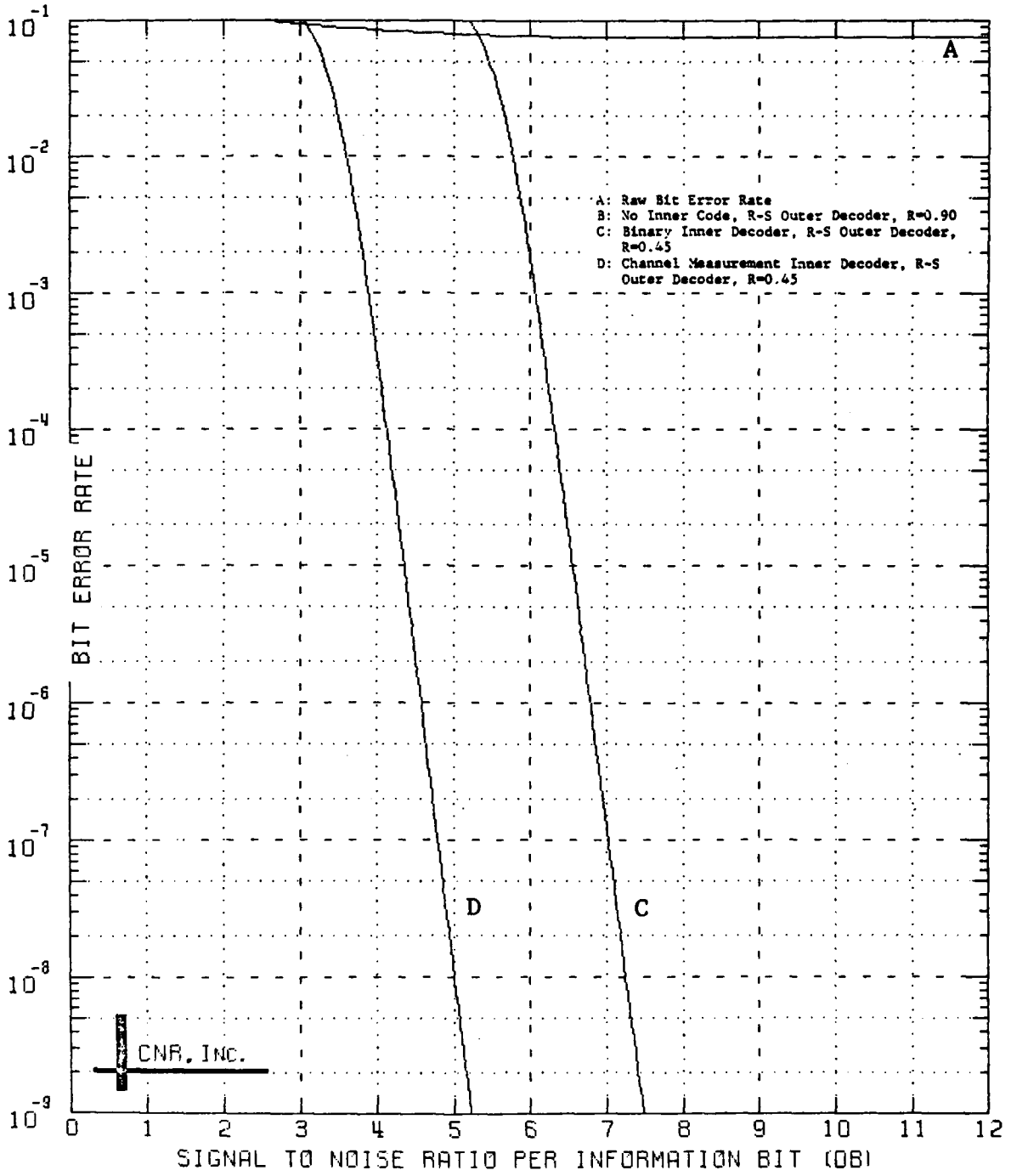


Figure 9.18 Decoded Performance of a Two-Stage Coding Approach
Outer Decoder: Reed-Solomon Code (60,54;7)
Symbol Interleaver Employed
Inner Decoder: Convolutional Code, Rate=1/2; K=7
δ=0.15 and Erasure Information is Employed

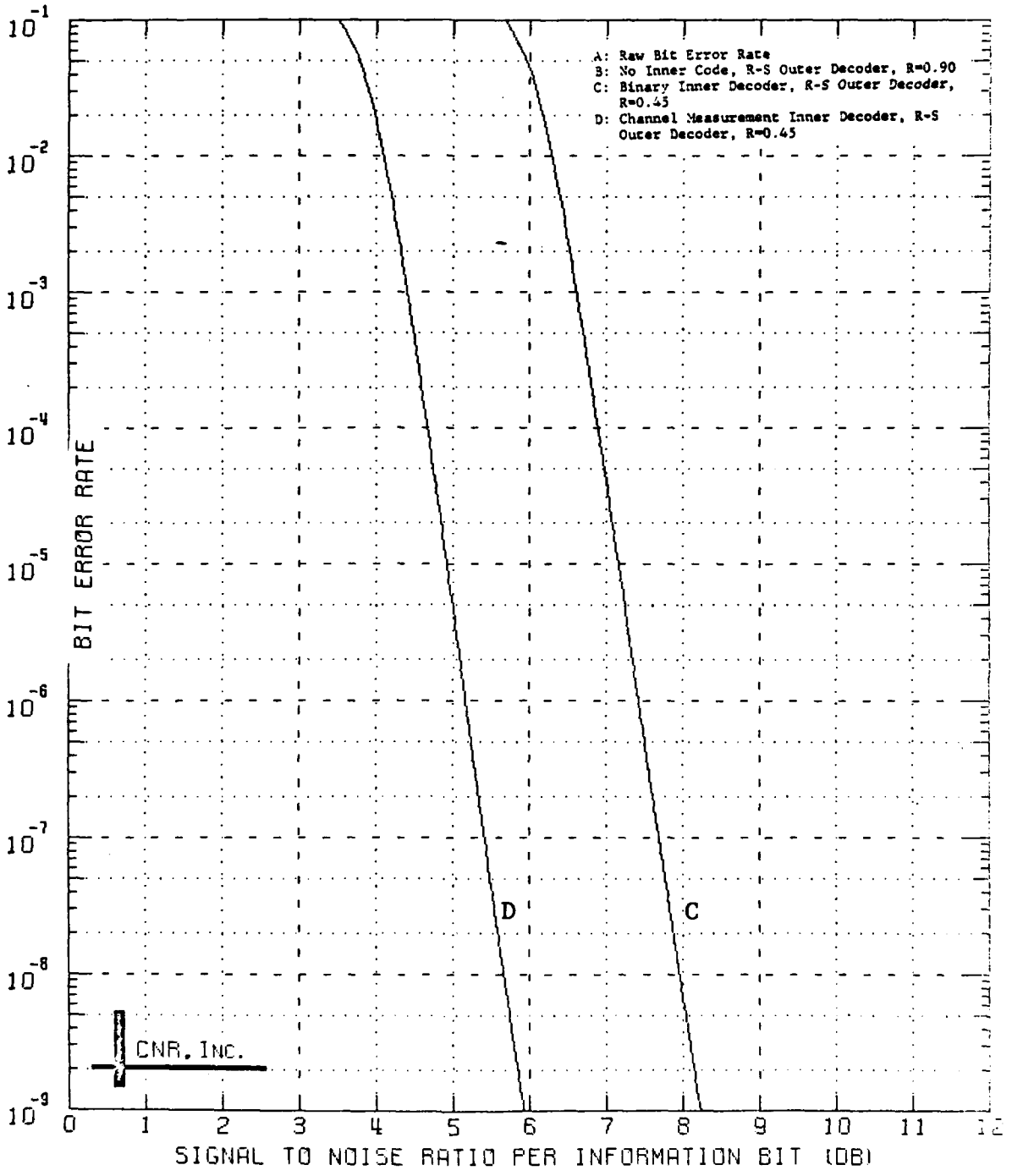


Figure 9.19 Decoded Performance of a Two-Stage Coding Approach
Outer Decoder: Reed-Solomon Code (60,54;7)
Symbol Interleaver Employed
Inner Decoder: Convolutional Code, Rate=1/2; K=7
δ=0.20 and Erasure Information is Employed

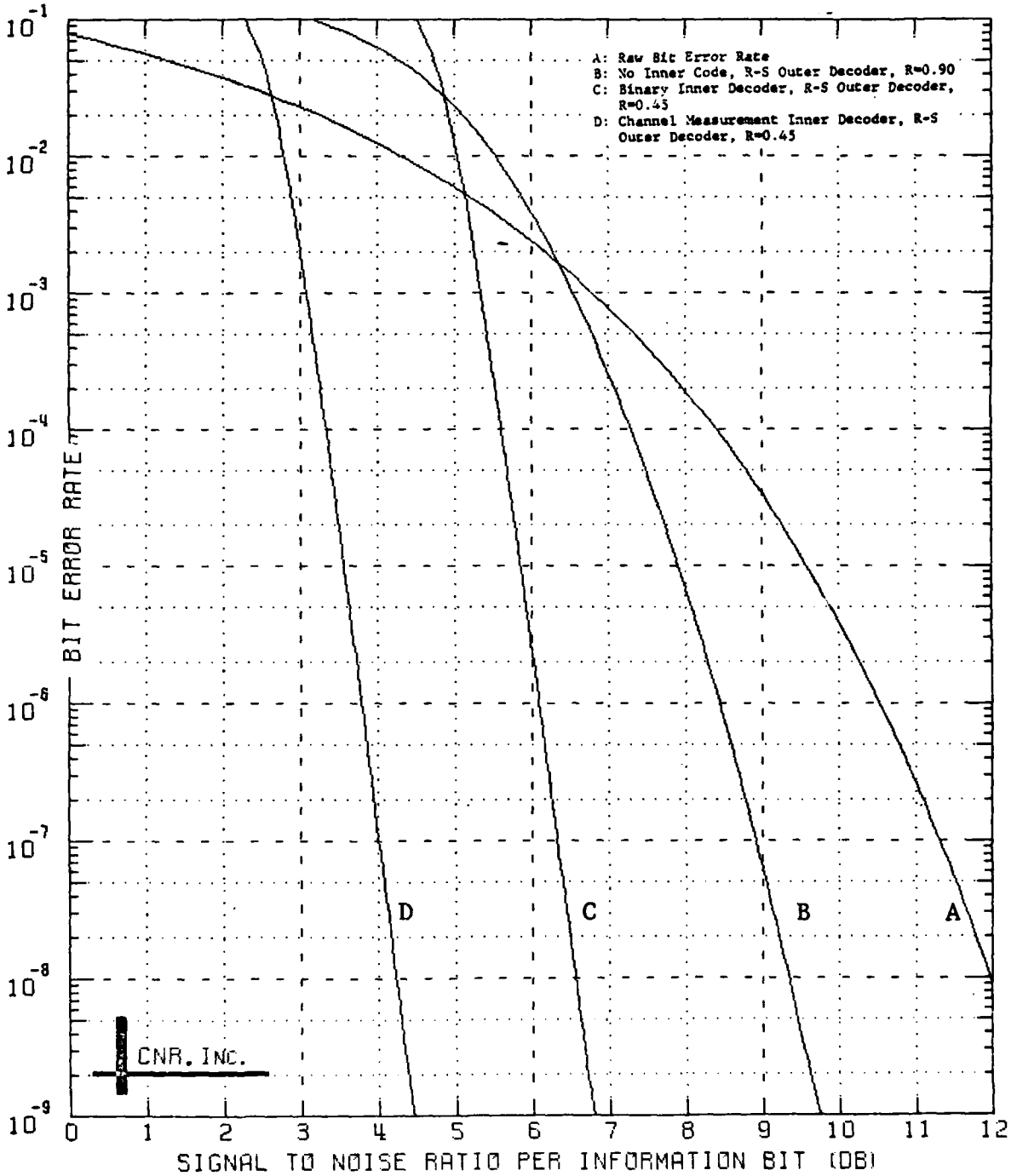


Figure 9.20 Decoded Performance of a Two-Stage Coding Approach
Outer Decoder: Reed-Solomon Code (40,36;5)
Bit Interleaver Employed
Inner Decoder: Convolutional Code, Rate=1/2; K=7
δ=0.00 and No Erasure Information Employed

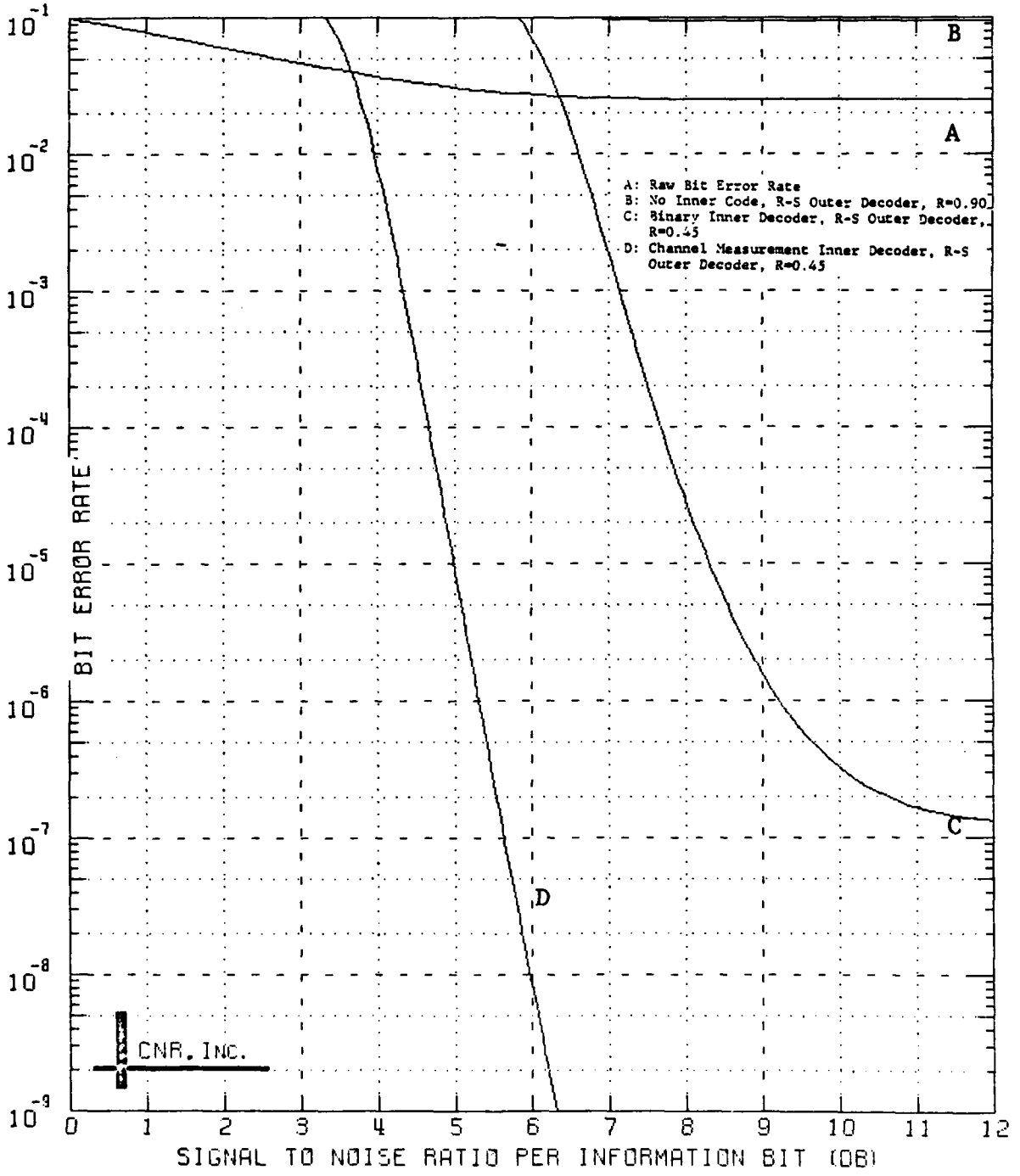


Figure 9.21 Decoded Performance of a Two-Stage Coding Approach
Outer Decoder: Reed-Solomon Code (40,36;5)
Bit Interleaver Employed
Inner Decoder: Convolutional Code, Rate=1/2; K=7
δ=0.05 and No Erasure Information Employed

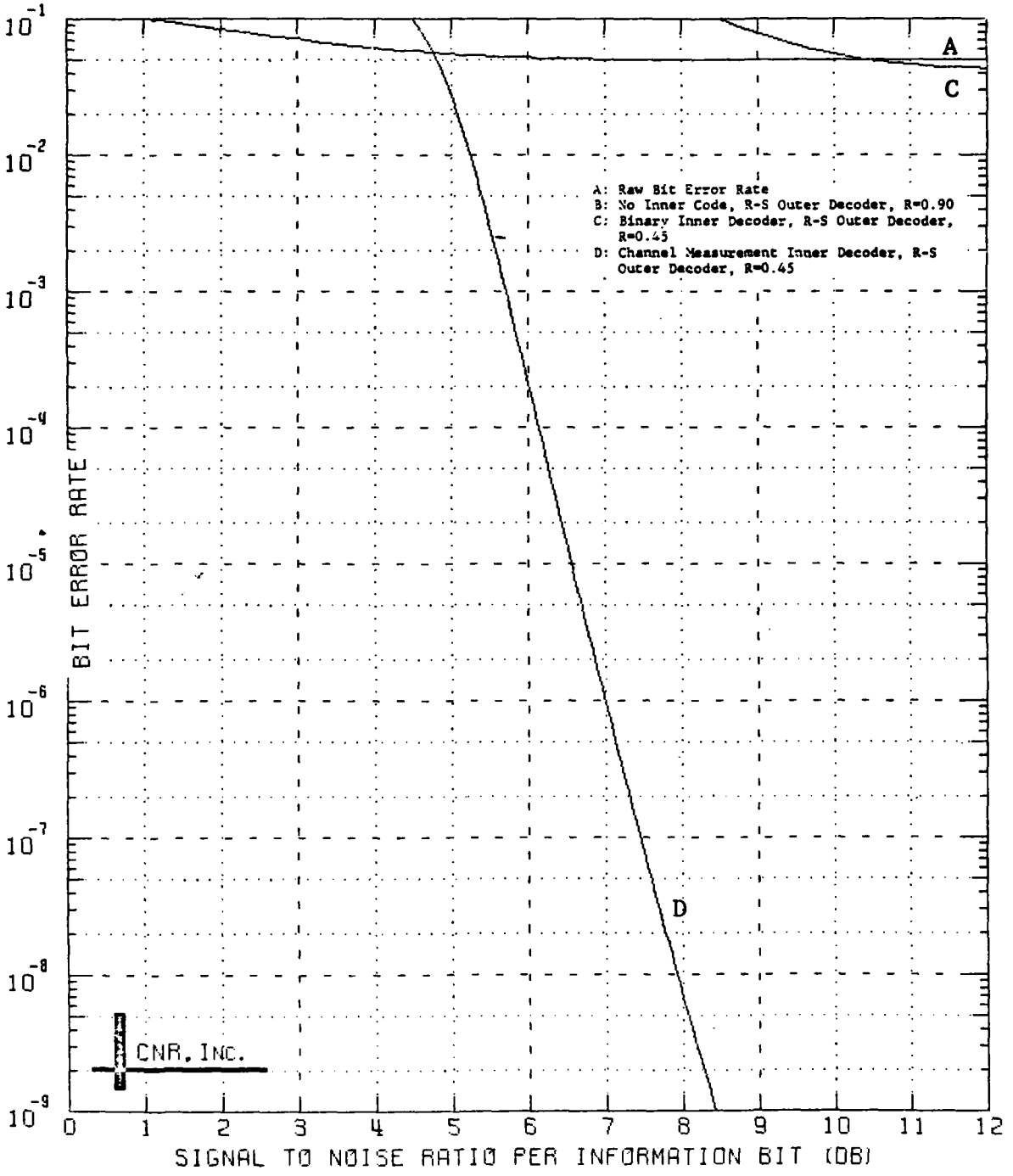


Figure 9.22 Decoded Performance of a Two-Stage Coding Approach
Outer Decoder: Reed-Solomon Code (40,36;5)
Bit Interleaver Employed
Inner Decoder: Convolutional Code, Rate=1/2; K=7
δ=0.10 and No Erasure Information Employed

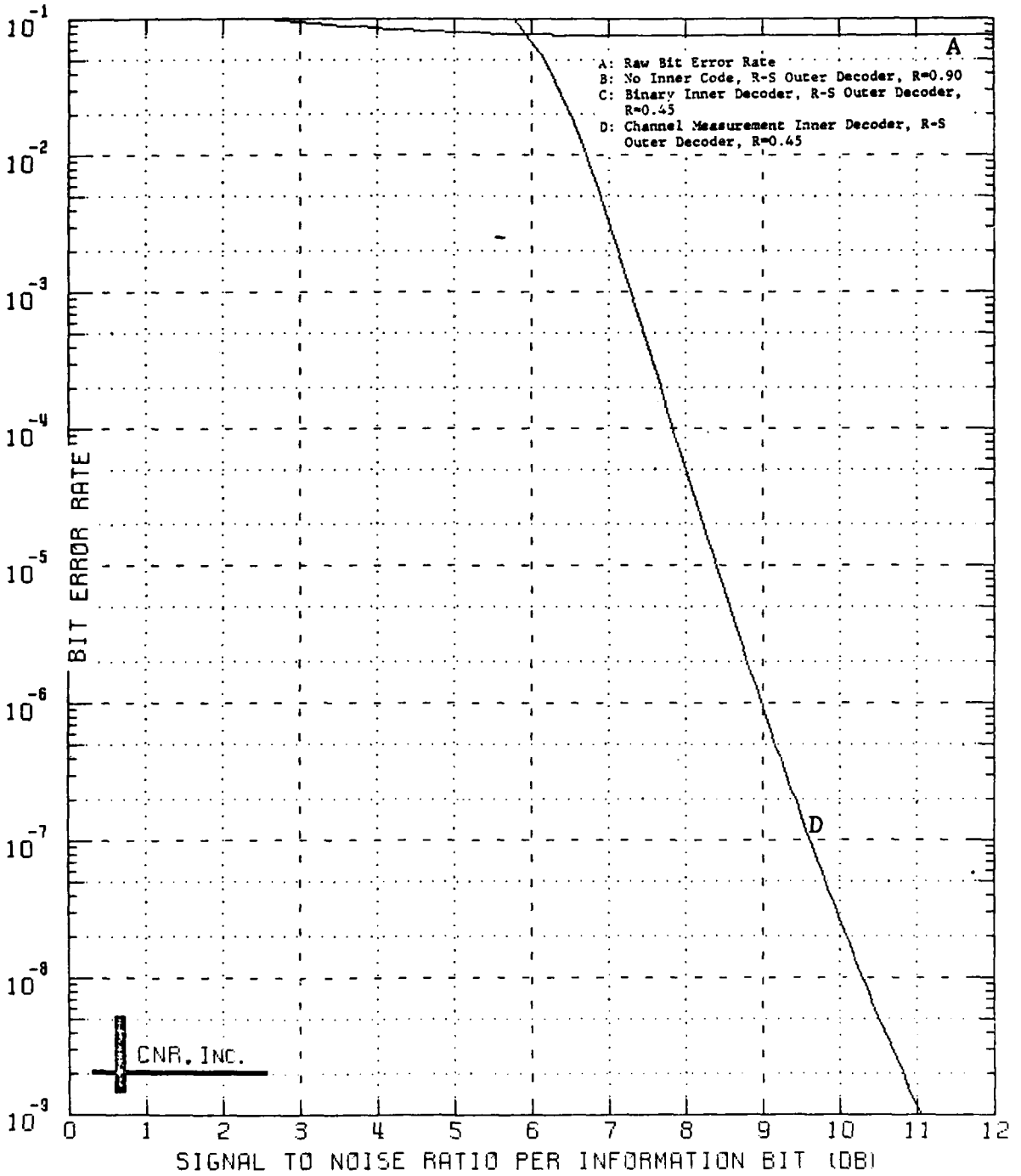


Figure 9.23 Decoded Performance of a Two-Stage Coding Approach
Outer Decoder: Reed-Solomon Code (40,36;5)
Bit Interleaver Employed
Inner Decoder: Convolutional Code, Rate=1/2; K=7
δ=0.15 and No Erasure Information Employed

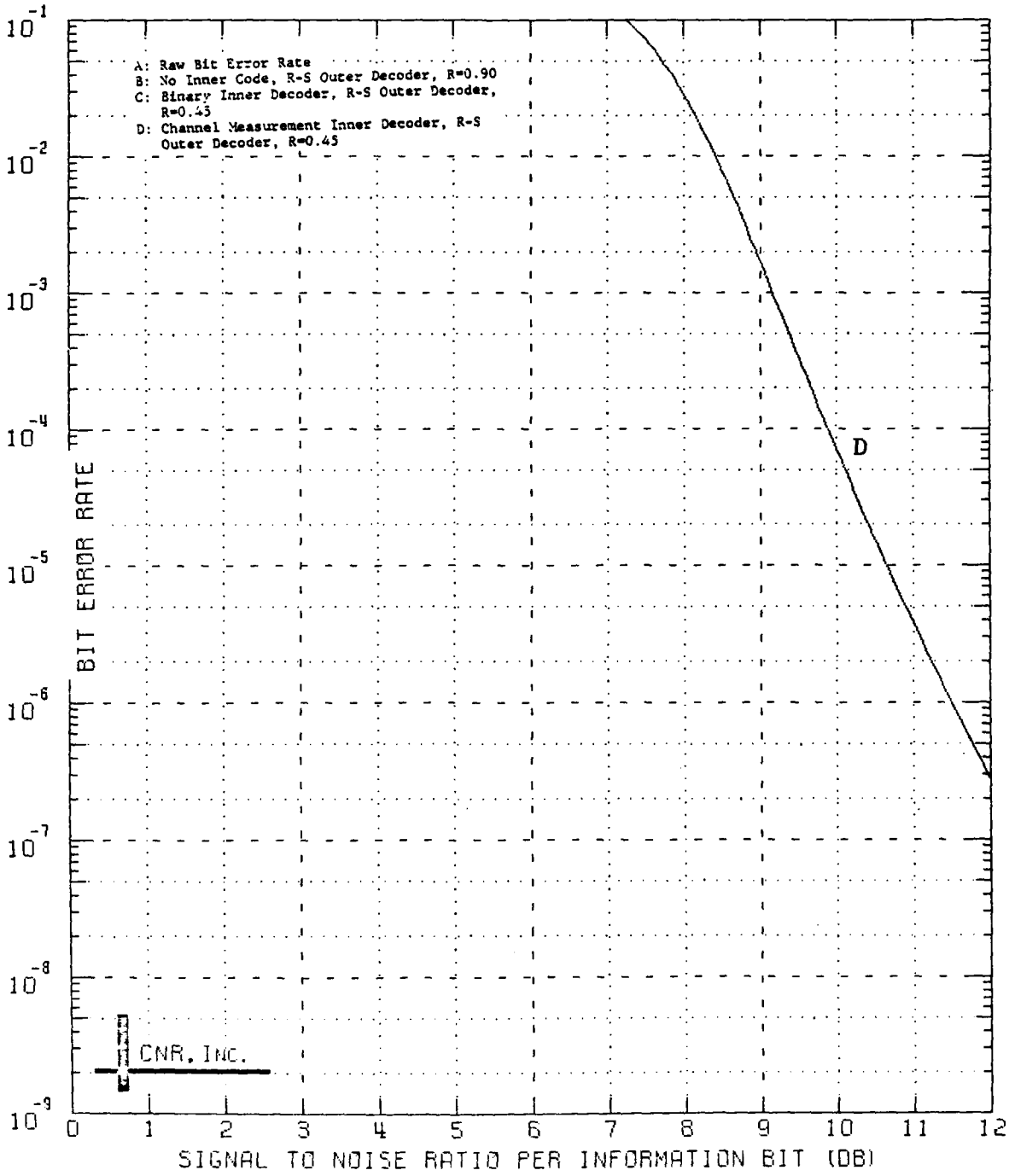


Figure 9.24 Decoded Performance of a Two-Stage Coding Approach
Outer Decoder: Reed-Solomon Code (40,36;5)
Bit Interleaver Employed
Inner Decoder: Convolutional Code, Rate=1/2; K=7
δ=0.20 and No Erasure Information Employed

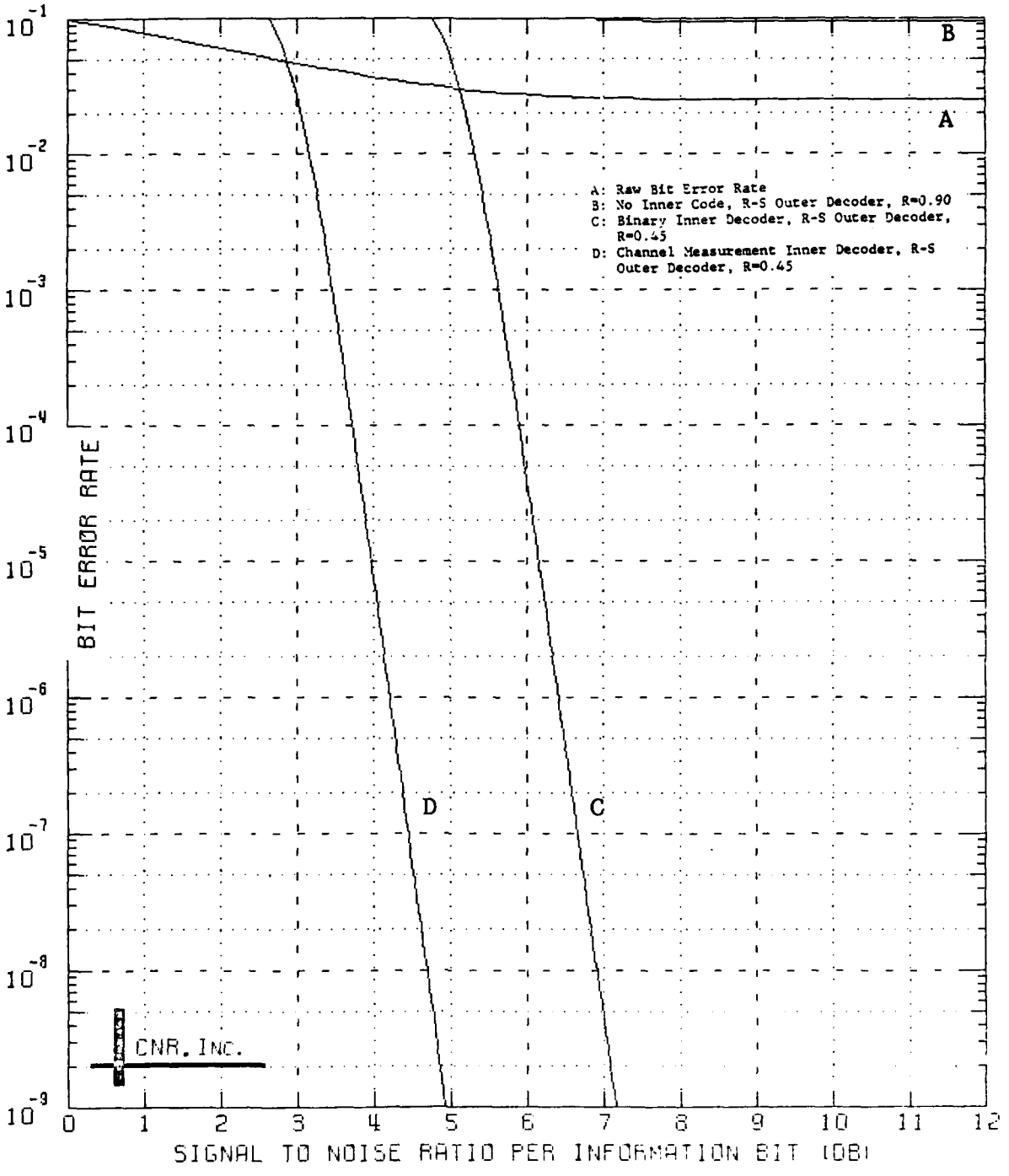


Figure 9.25 Decoded Performance of a Two-Stage Coding Approach
Outer Decoder: Reed-Solomon Code (40,36;5)
Bit Interleaver Employed
Inner Decoder: Convolutional Code, Rate=1/2; K=7
δ=0.05 and Erasure Information is Employed

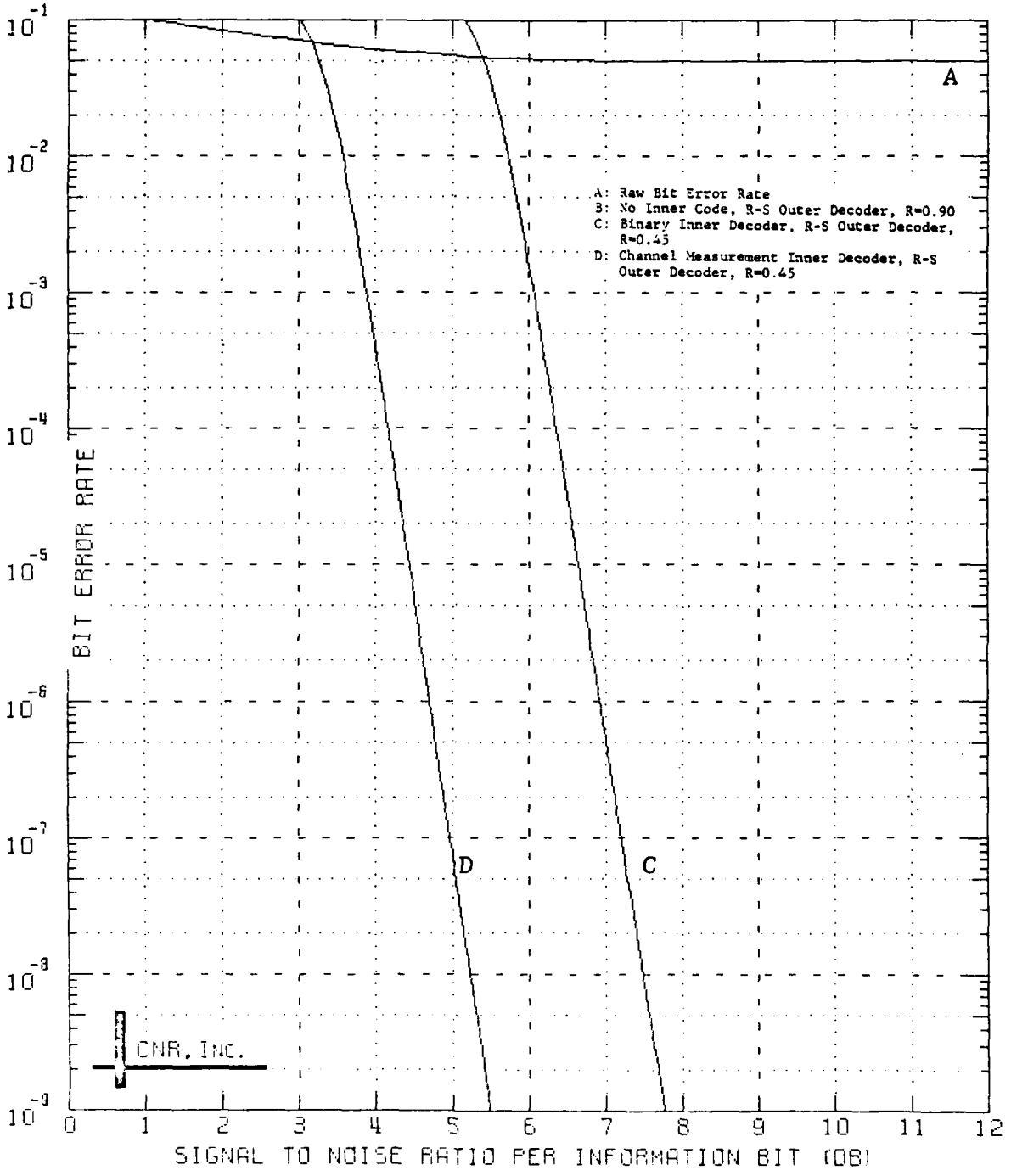


Figure 9.26 Decoded Performance of a Two-Stage Coding Approach
Outer Decoder: Reed-Solomon Code (40,36;5)
Bit Interleaver Employed
Inner Decoder: Convolutional Code, Rate=1/2; K=7
δ=0.10 and Erasure Information Employed

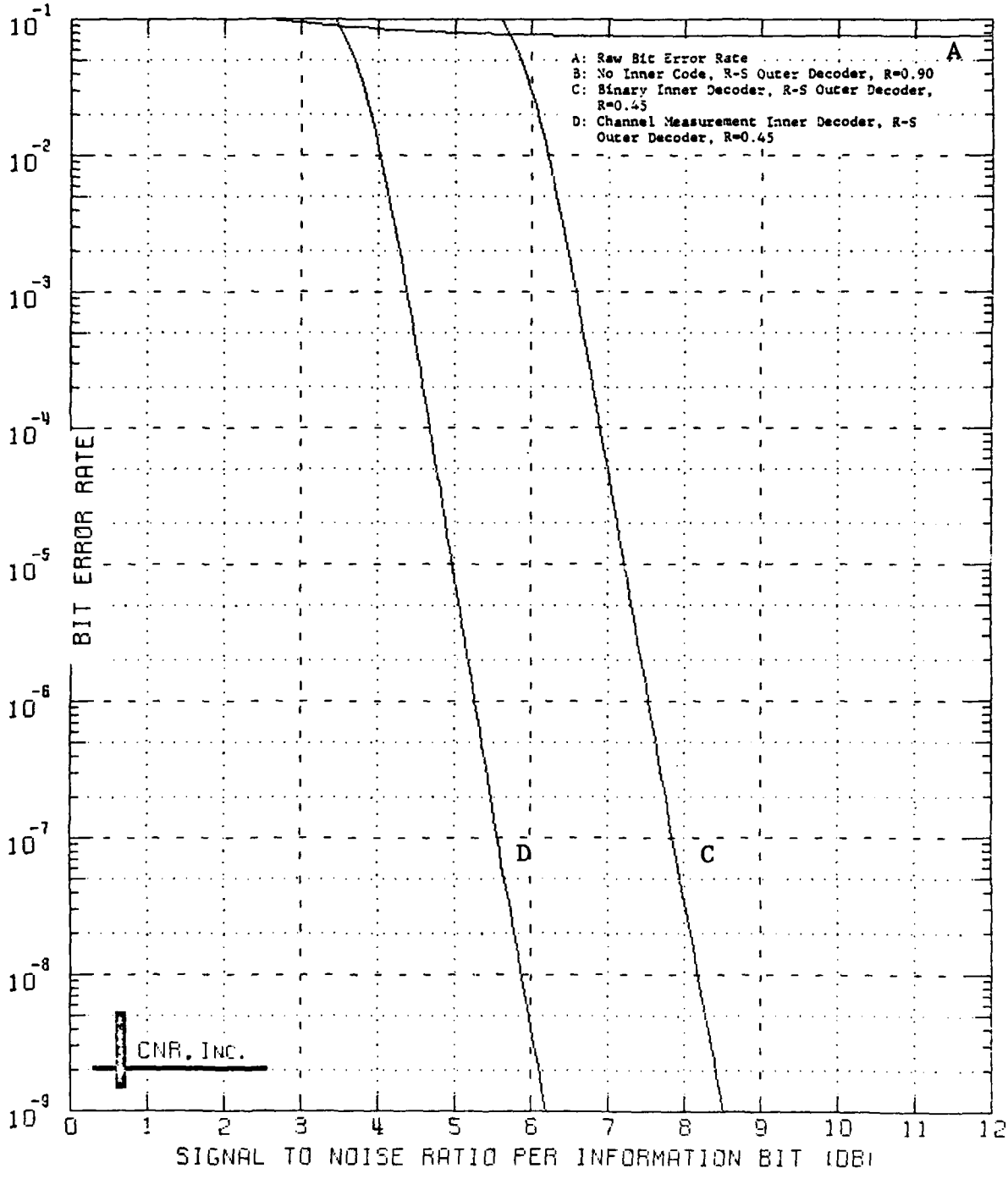


Figure 9.27 Decoded Performance of a Two-Stage Coding Approach
Outer Decoder: Reed-Solomon Code (40,36;5)
Bit Interleaver Employed
Inner Decoder: Convolutional Code, Rate=1/2; K=7
δ=0.15 and Erasure Information is Employed

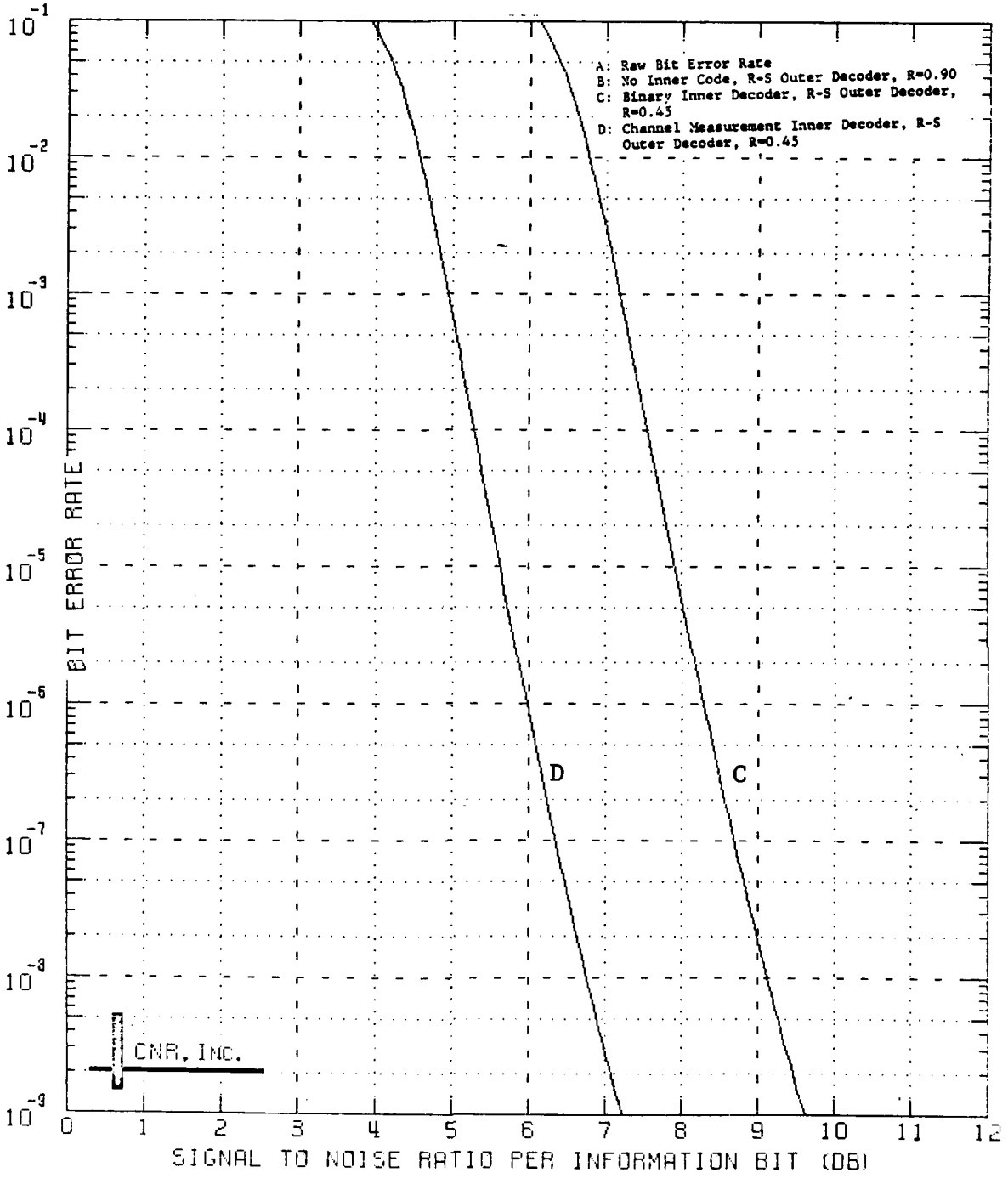


Figure 9.28 Decoded Performance of a Two-Stage Coding Approach
Outer Decoder: Reed-Solomon Code (40,36;5)
Bit Interleaver Employed
Inner Decoder: Convolutional Code, Rate=1/2; K=7
δ=0.20 and Erasure Information is Employed

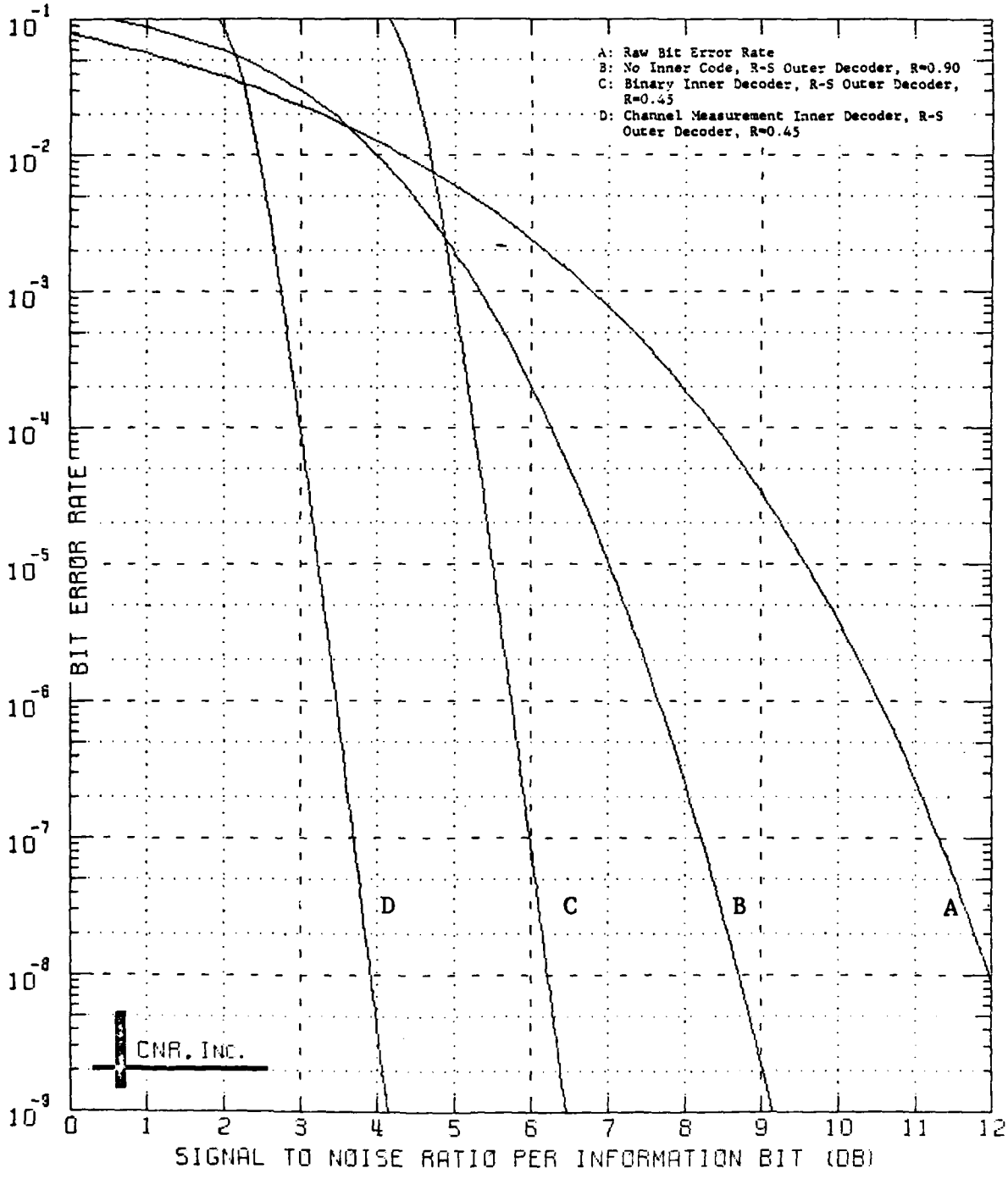


Figure 9.29 Decoded Performance of a Two-Stage Coding Approach
Outer Decoder: Reed-Solomon Code (40,36;5)
Symbol Interleaver Employed
Inner Decoder: Convolutional Code, Rate=1/2; K=7
δ=0.00 and No Erasure Information Employed

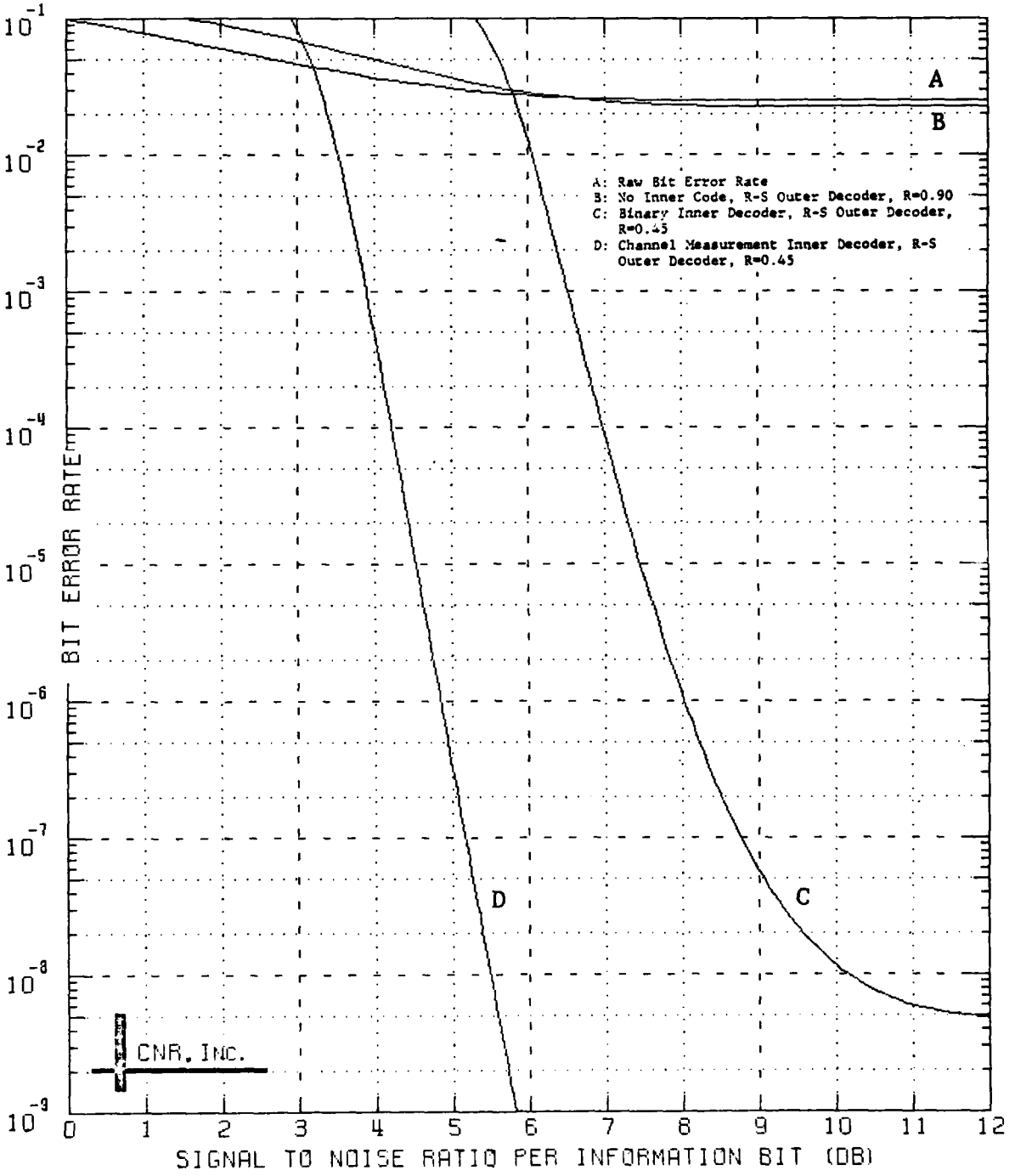


Figure 9.30 Decoded Performance of a Two-Stage Coding Approach
Outer Decoder: Reed-Solomon Code (40,36;5)
Symbol Interleaver Employed
Inner Decoder: Convolutional Code, Rate=1/2; K=7
δ=0.05 and No Erasure Information Employed

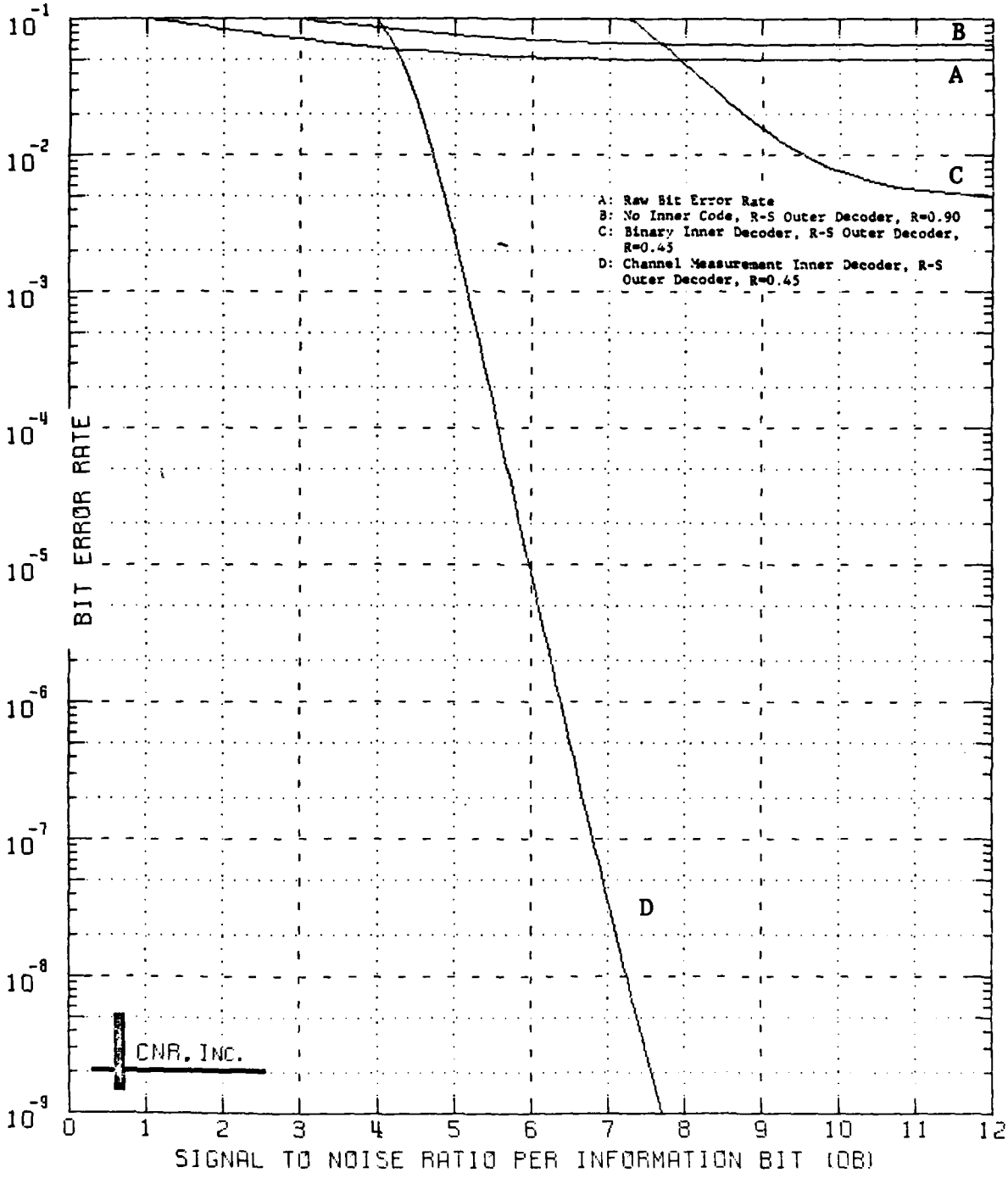


Figure 9.31 Decoded Performance of a Two-Stage Coding Approach
Outer Decoder: Reed-Solomon Code (40,36;5)
Symbol Interleaver Employed
Inner Decoder: Convolutional Code, Rate=1/2; K=7
δ=0.10 and No Erasure Information Employed

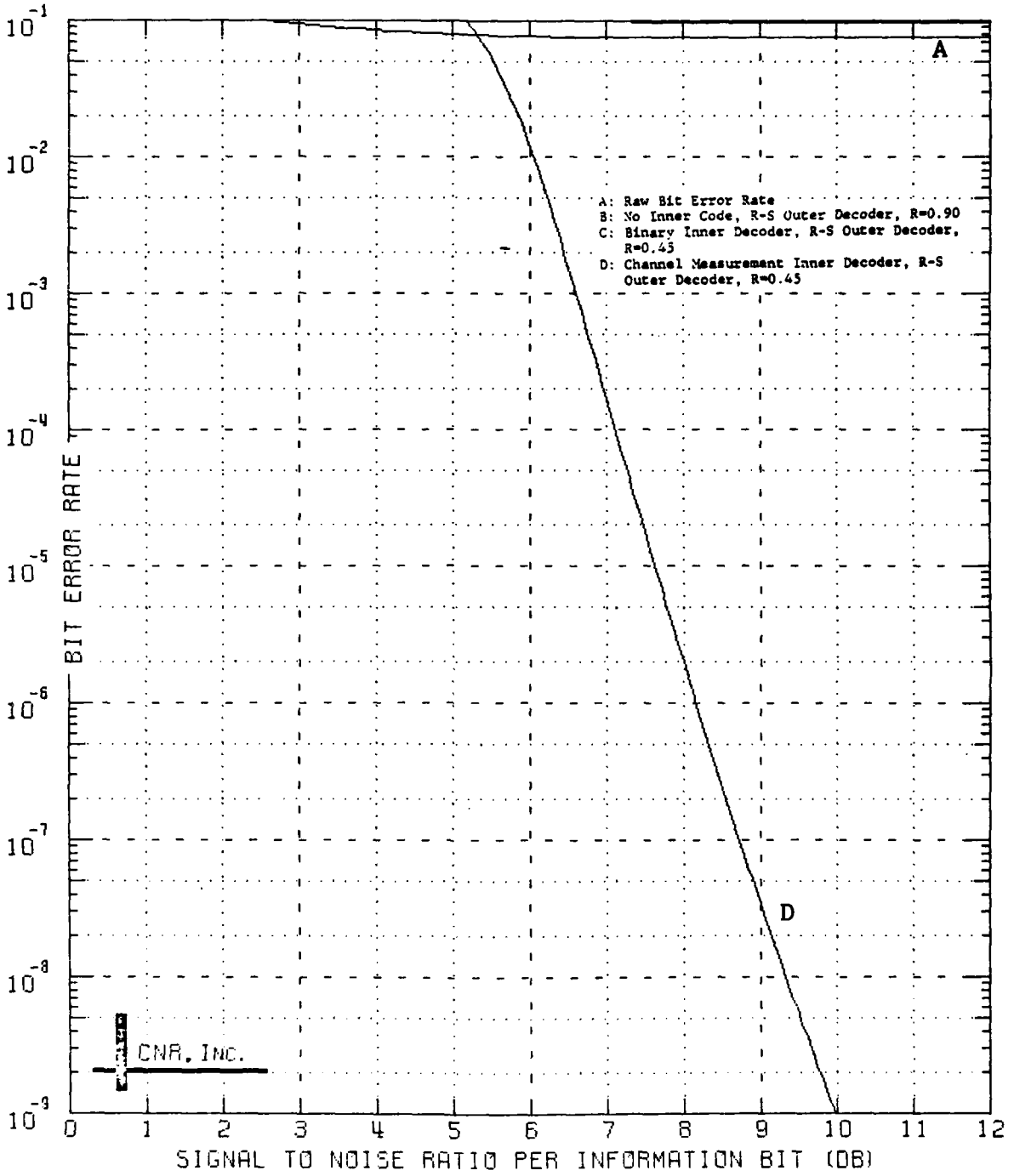


Figure 9.32 Decoded Performance of a Two-Stage Coding Approach
Outer Decoder: Reed-Solomon Code (40,36;5)
Symbol Interleaver Employed
Inner Decoder: Convolutional Code, Rate=1/2; K=7
δ=0.15 and No Erasure Information Employed

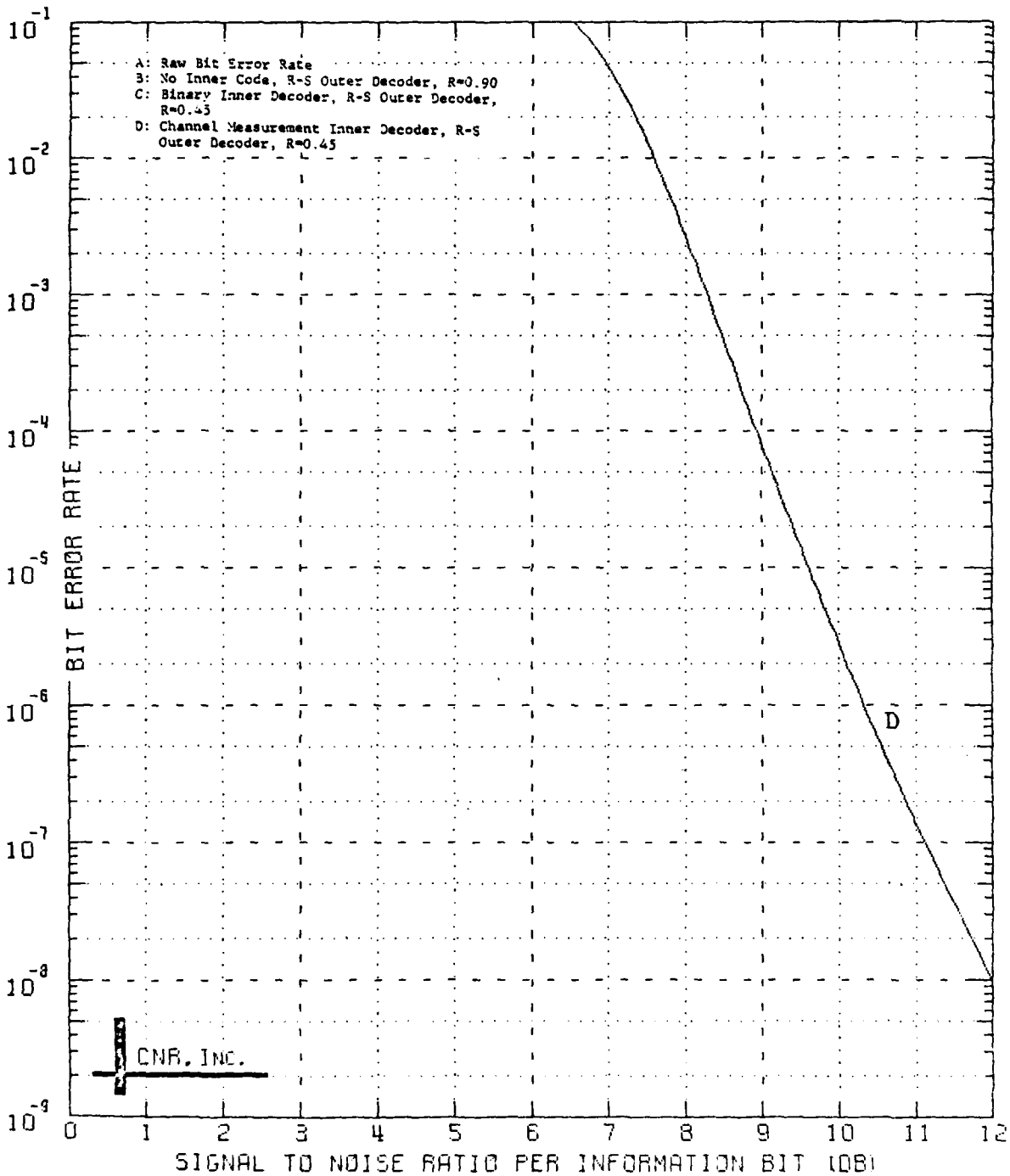


Figure 9.33 Decoded Performance of a Two-Stage Coding Approach
Outer Decoder: Reed-Solomon Code (40,36;5)
Symbol Interleaver Employed
Inner Decoder: Convolutional Code, Rate=1/2; K=7
δ=0.20 and No Erasure Information Employed

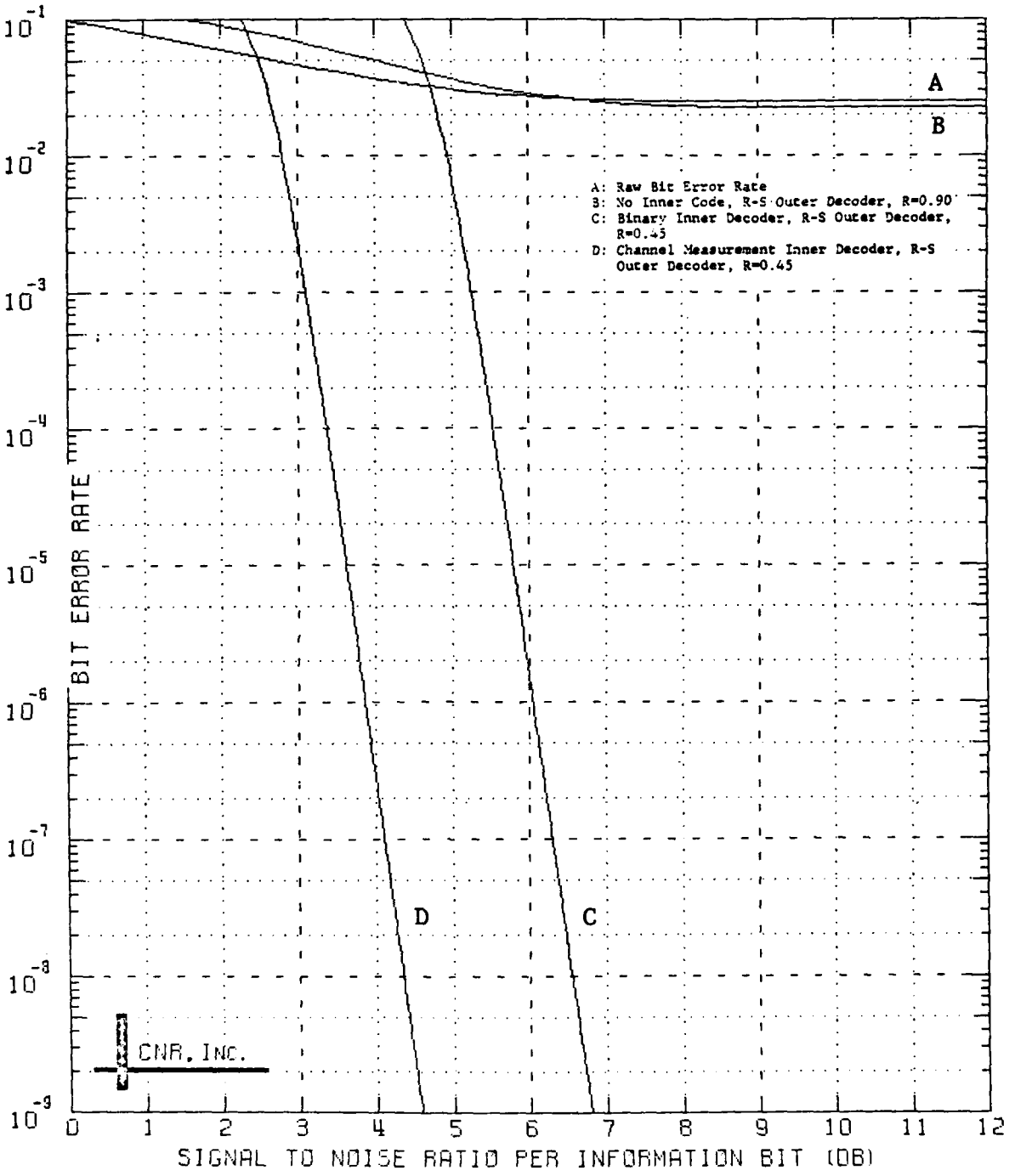


Figure 9.34 Decoded Performance of a Two-Stage Coding Approach
Outer Decoder: Reed-Solomon Code (40,36;5)
Symbol Interleaver Employed
Inner Decoder: Convolutional Code, Rate=1/2; K=7
δ=0.05 and Erasure Information is Employed

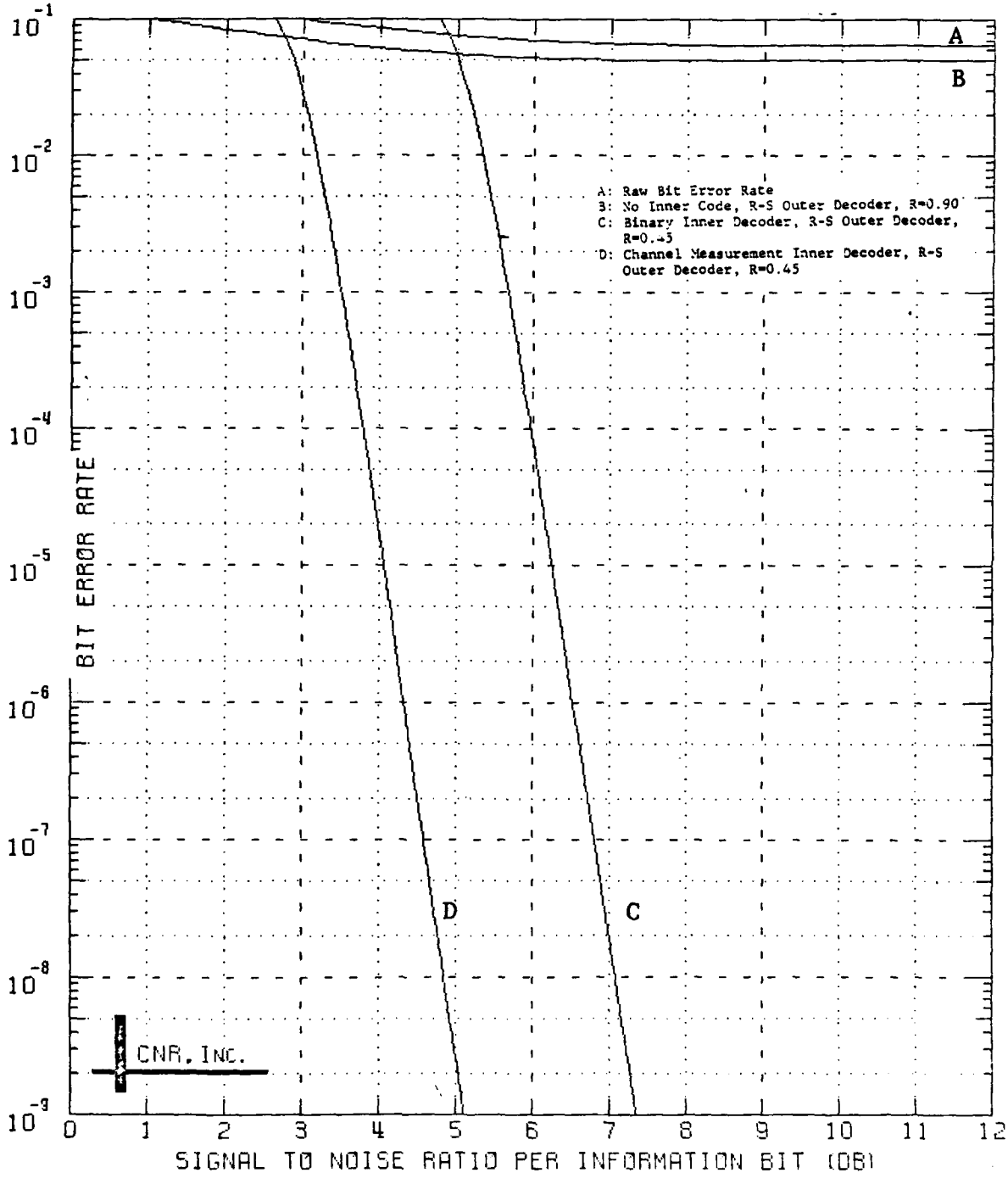


Figure 9.35 Decoded Performance of a Two-Stage Coding Approach
Outer Decoder: Reed-Solomon Code (40,36;5)
Symbol Interleaver Employed
Inner Decoder: Convolutional Code, Rate=1/2; K=7
δ=0.10 and Erasure Information is Employed

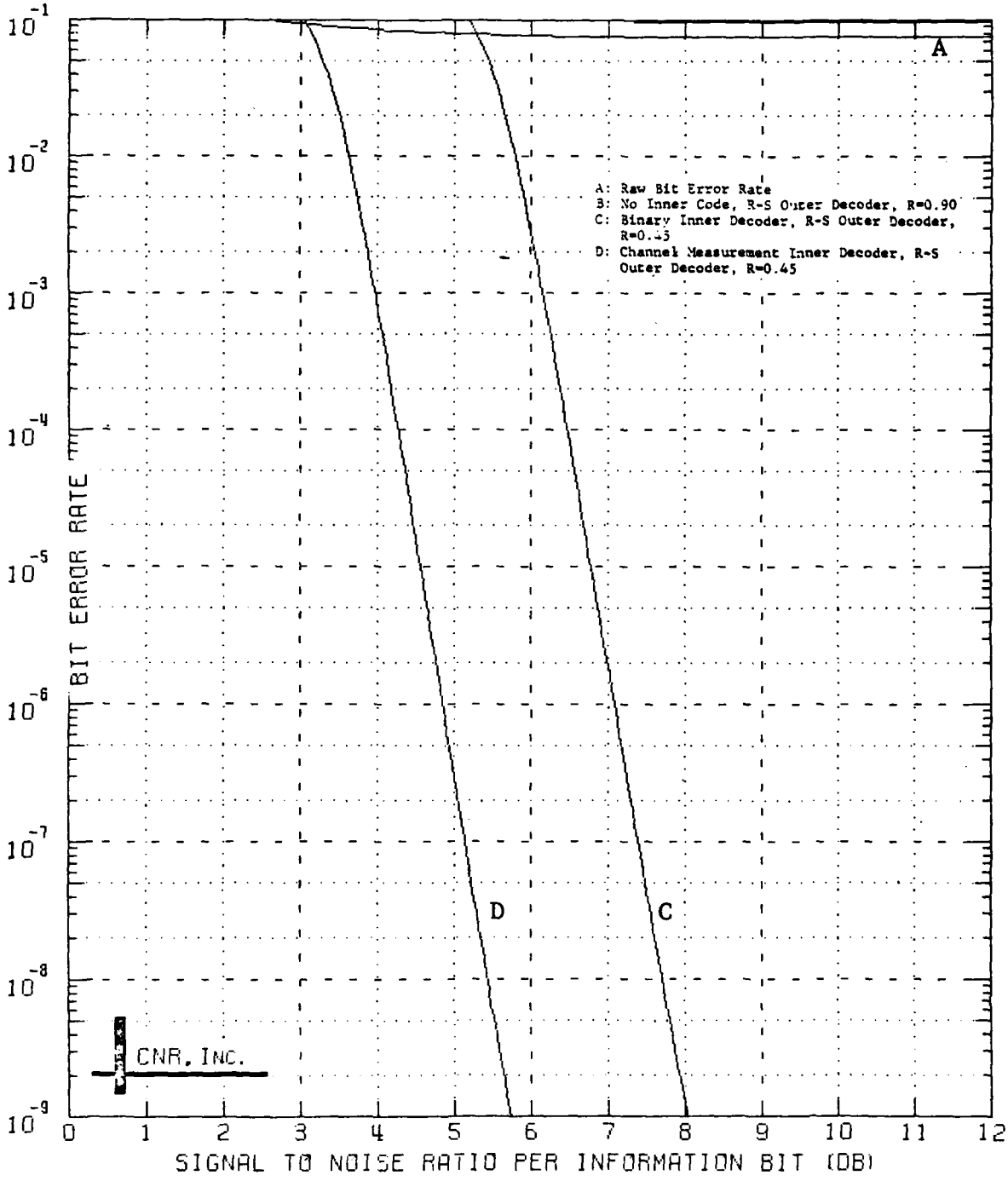


Figure 9.36 Decoded Performance of a Two-Stage Coding Approach
Outer Decoder: Reed-Solomon Code (40,36;5)
Symbol Interleaver Employed
Inner Decoder: Convolutional Code, Rate=1/2; K=7
δ=0.15 and Erasure Information is Employed

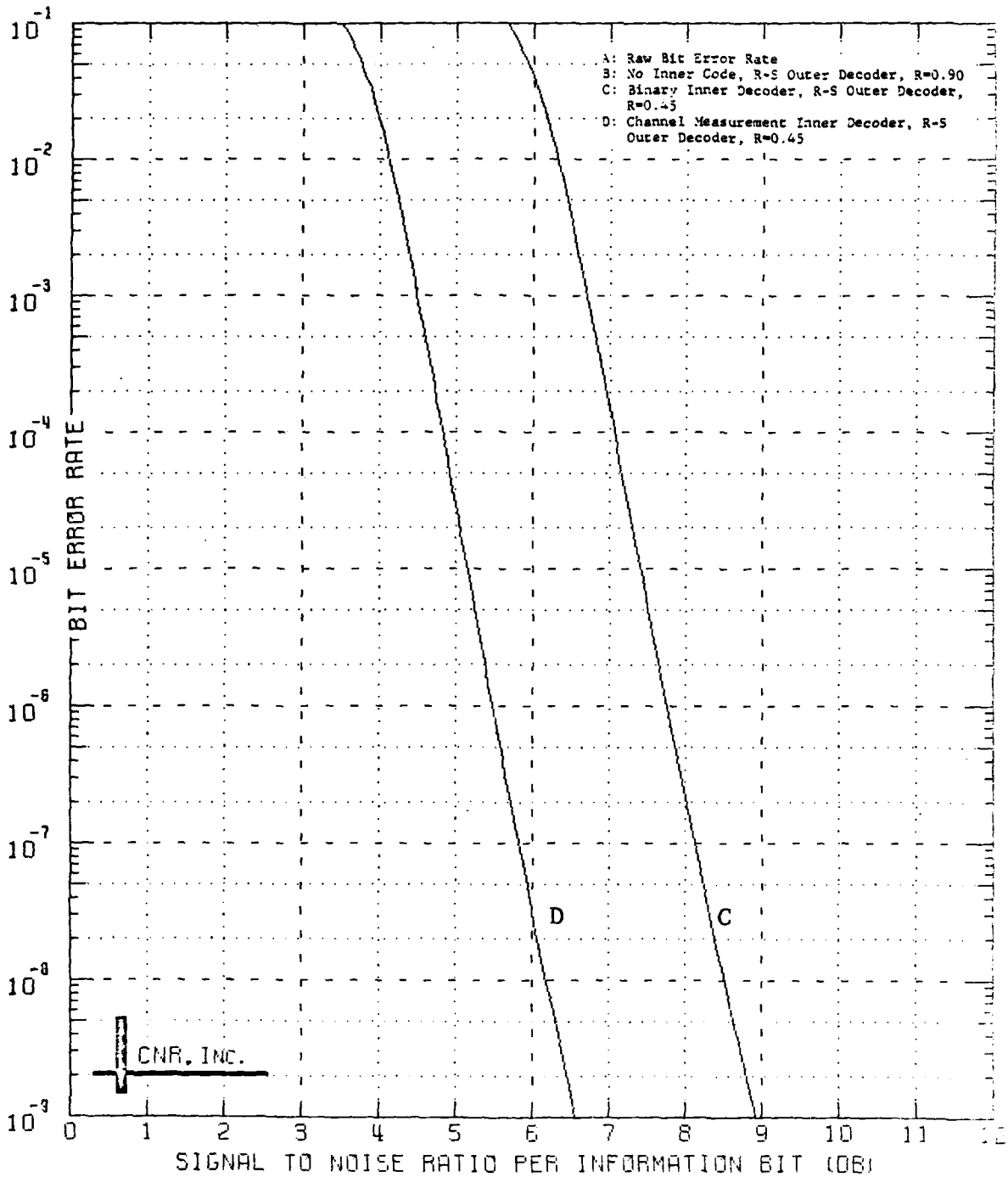


Figure 9.37 Decoded Performance of a Two-Stage Coding Approach
Outer Decoder: Reed-Solomon Code (40,36;5)
Symbol Interleaver Employed
Inner Decoder: Convolutional Code, Rate=1/2; K=7
δ=0.20 and Erasure Information is Employed

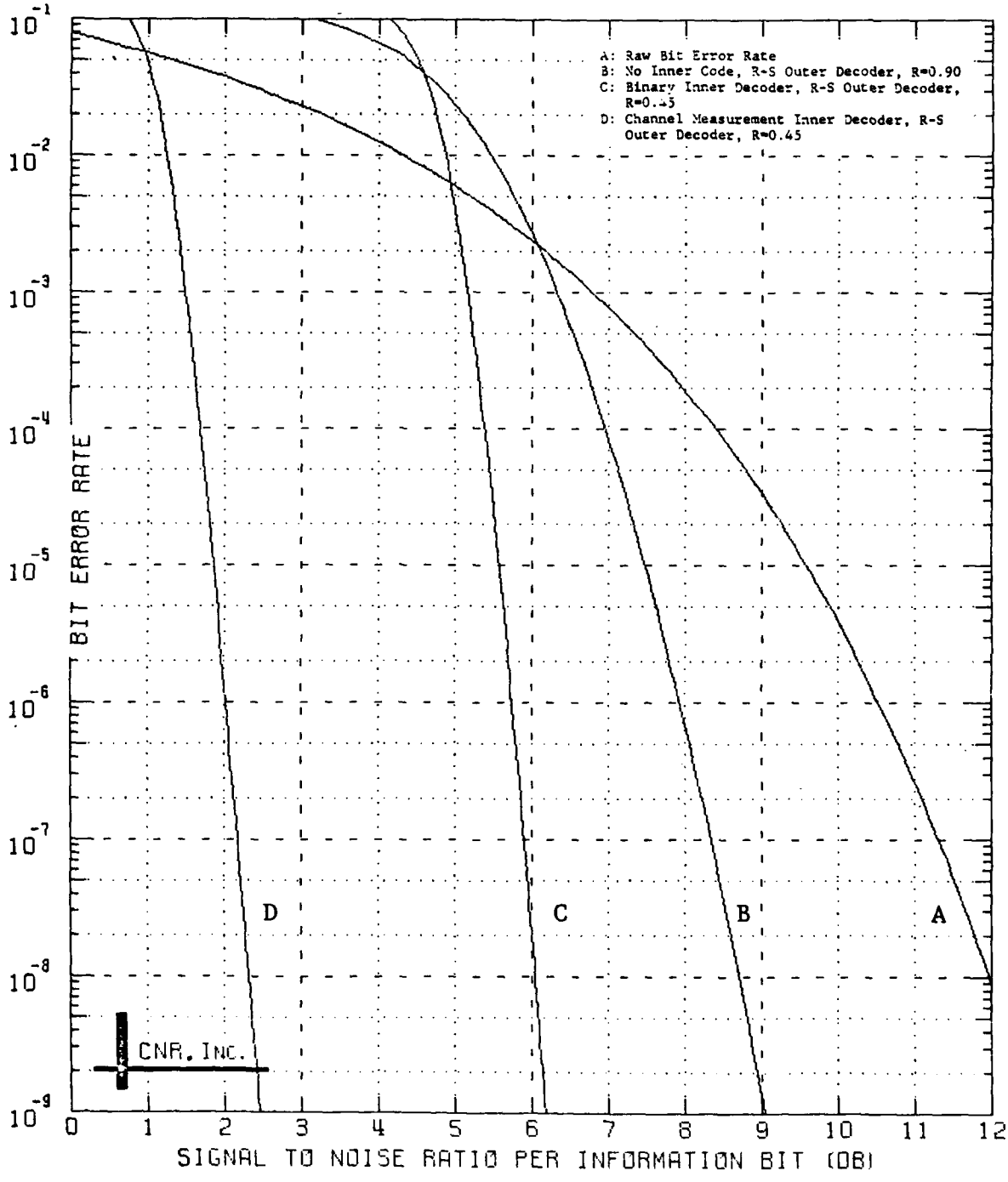


Figure 9.38 Decoded Performance of a Two-Stage Coding Approach
Outer Decoder: Reed-Solomon Code (60,54;7)
Bit Interleaver Employed
Inner Decoder: Block Code (128,64;22)
δ=0.00 and No Erasure Information Employed

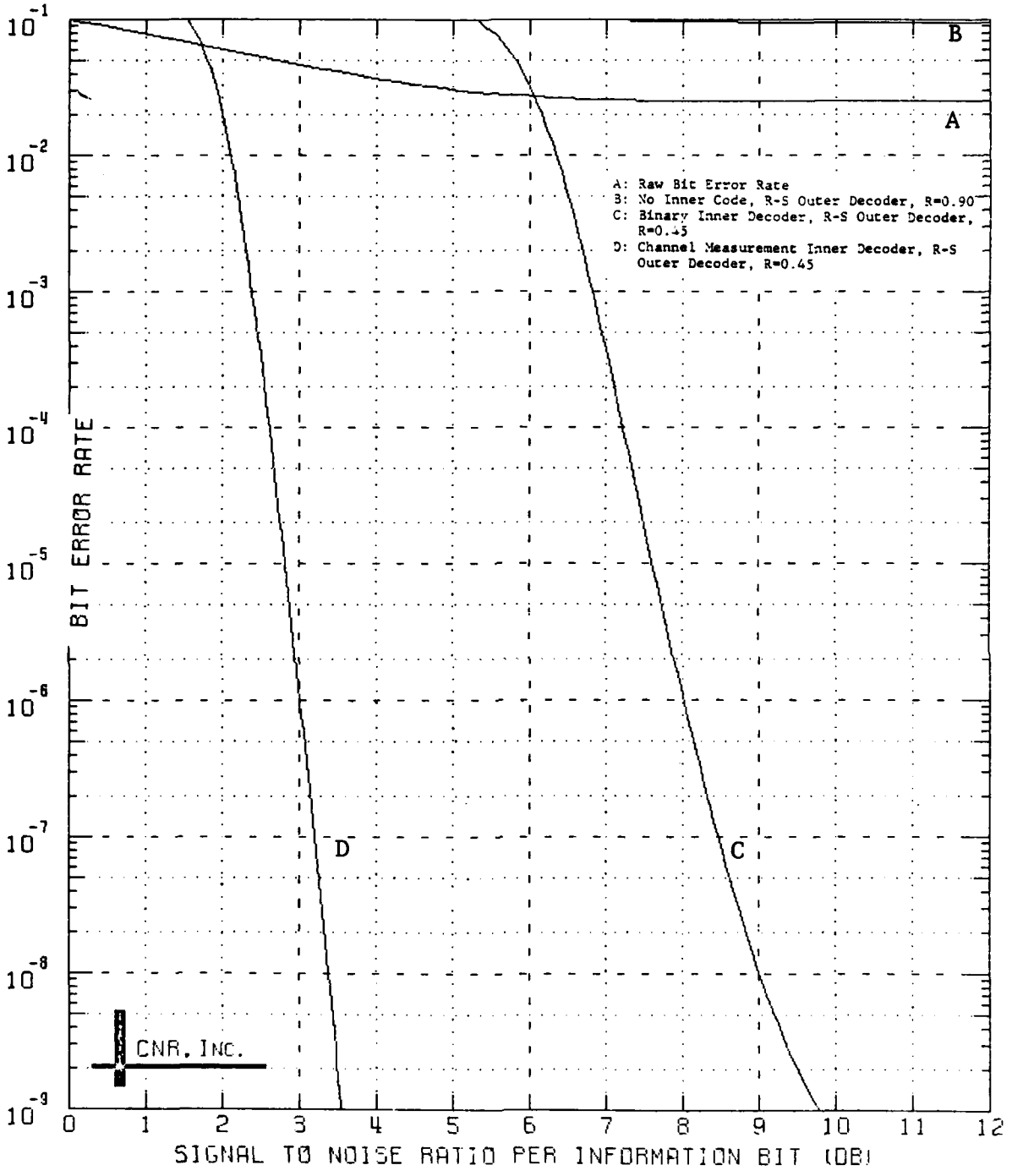


Figure 9.39 Decoded Performance of a Two-Stage Coding Approach
Outer Decoder: Reed-Solomon Code (60,54;7)
Bit Interleaver Employed
Inner Decoder: Block Code (128,64;22)
δ=0.05 and No Erasure Information Employed

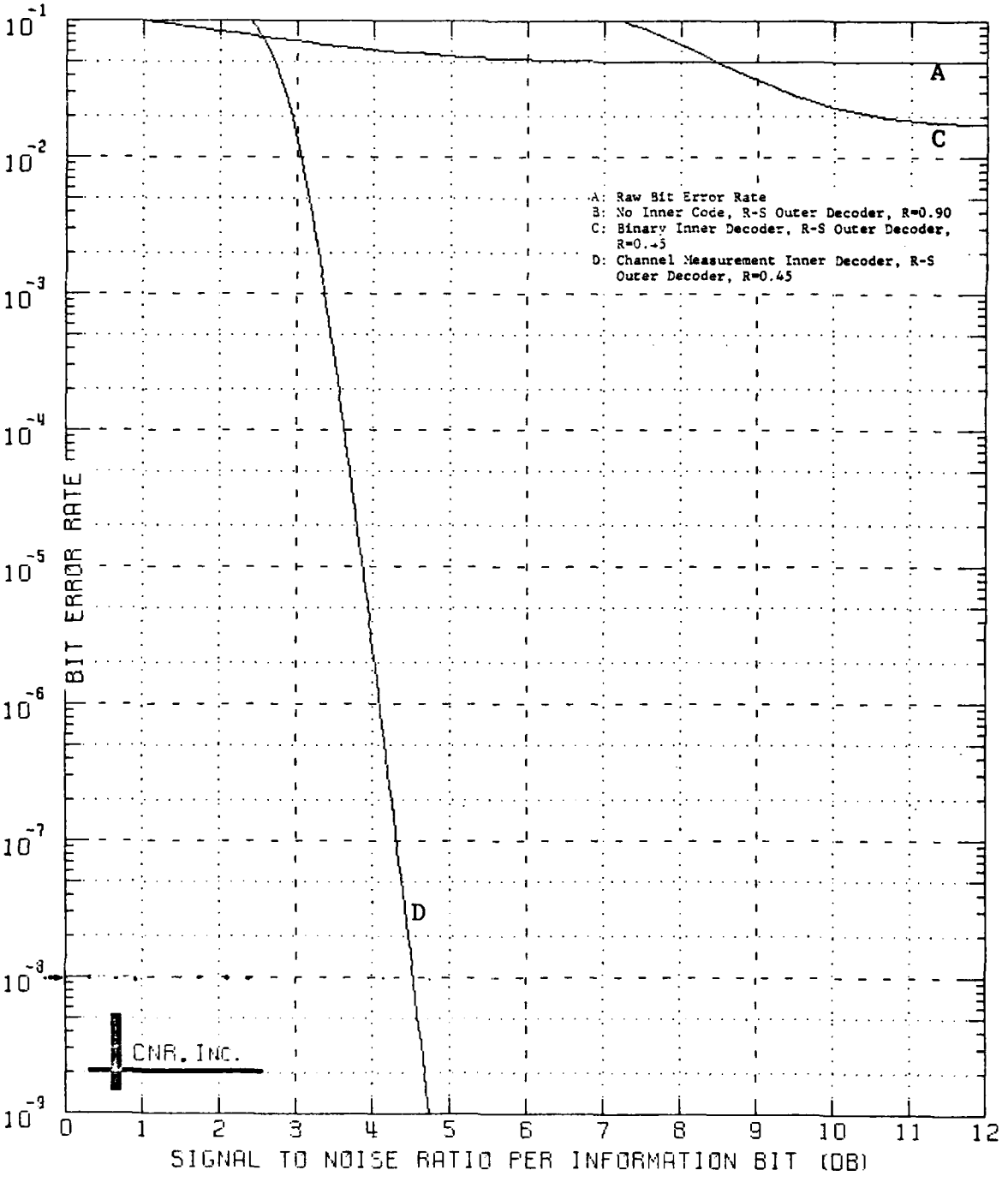


Figure 9.40 Decoded Performance of a Two-Stage Coding Approach
Outer Decoder: Reed-Solomon Code (60,54;7)
Bit Interleaver Employed
Inner Decoder: Block Code (128,64;22)
δ=0.10 and No Erasure Information Employed

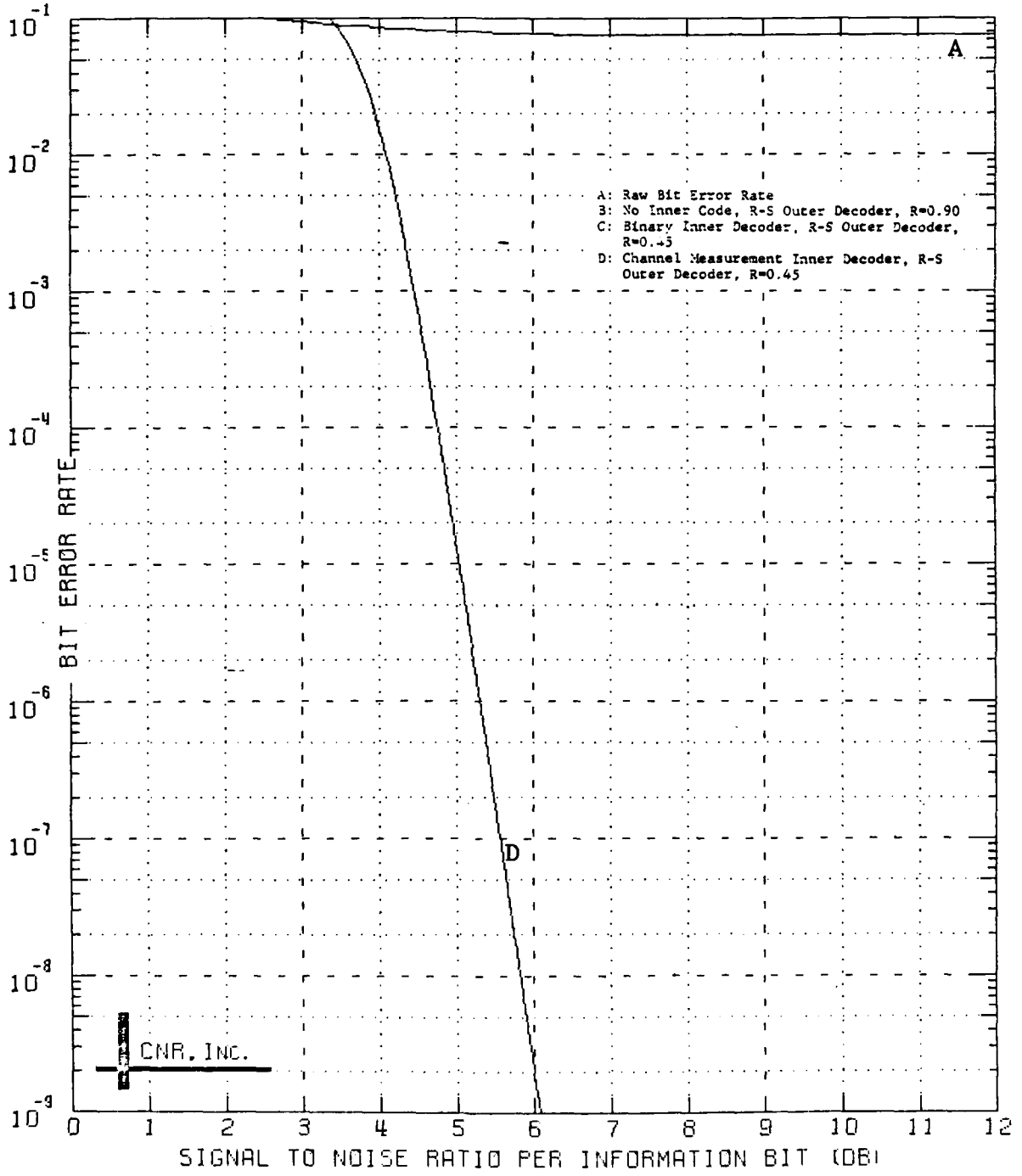


Figure 9.41 Decoded Performance of a Two-Stage Coding Approach
Outer Decoder: Reed-Solomon Code (60,54;7)
Bit Interleaver Employed
Inner Decoder: Block Code (128,64;22)
δ=0.15 and No Erasure Information Employed

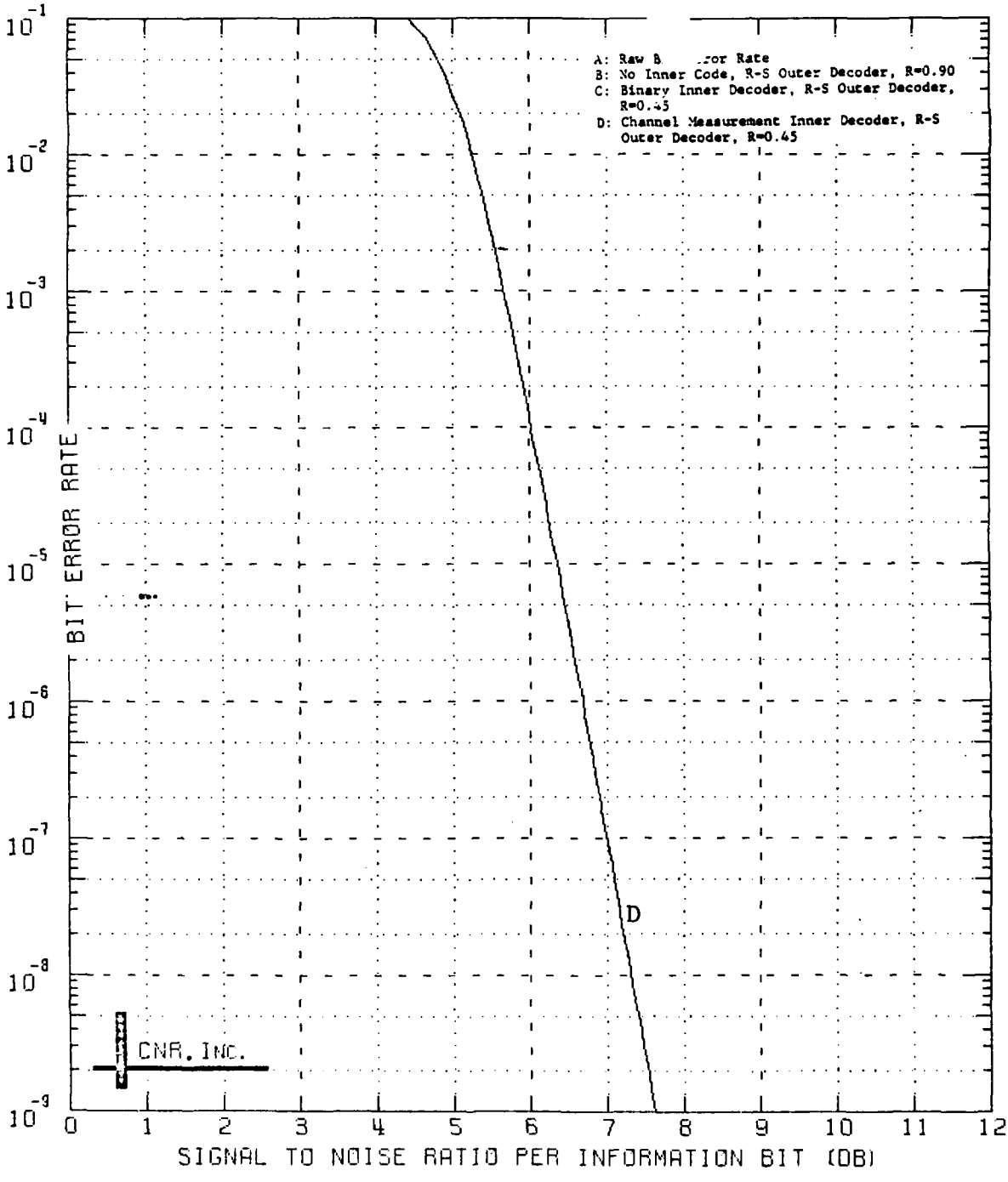


Figure 9.42 Decoded Performance of a Two-Stage Coding Approach
Outer Decoder: Reed-Solomon Code (60,54;7)
Bit Interleaver Employed
Inner Decoder: Block Code (128,64;22)
δ=0.20 and No Erasure Information Employed

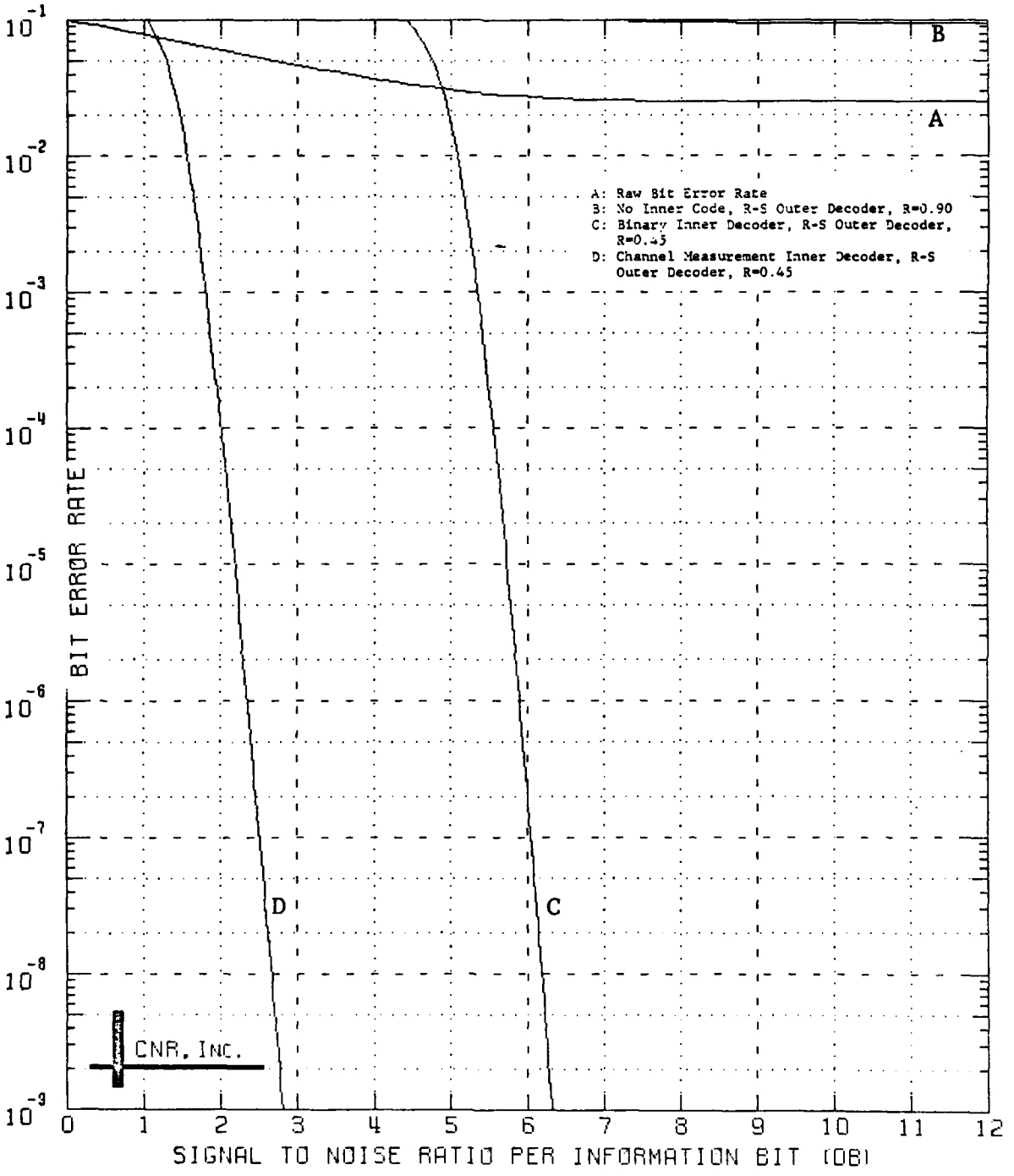


Figure 9.43 Decoded Performance of a Two-Stage Coding Approach
Outer Decoder: Reed-Solomon Code (60,54;7)
Bit Interleaver Employed
Inner Decoder: Block Code (128,64;22)
δ=0.05 and Erasure Information is Employed

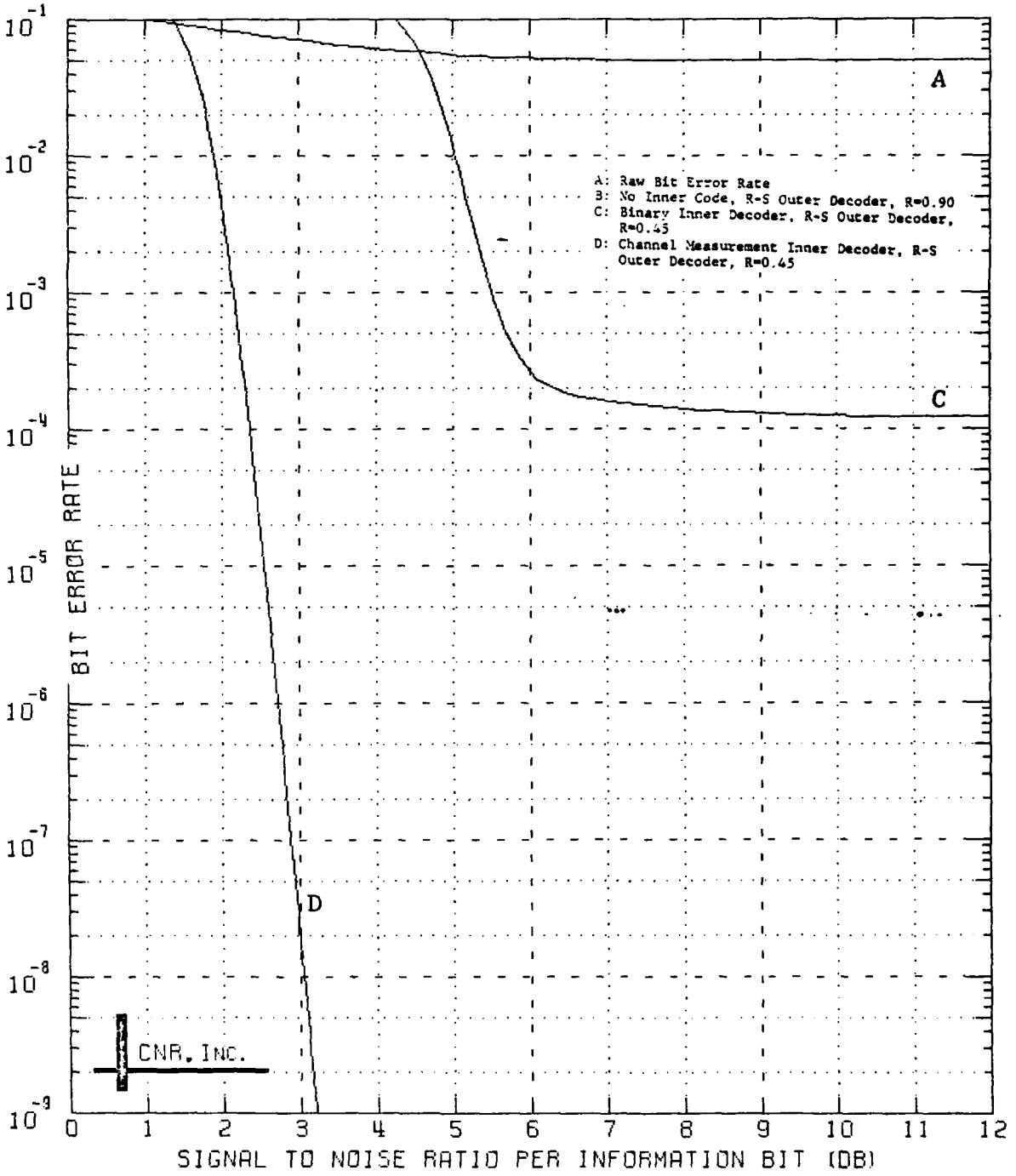


Figure 9.44 Decoded Performance of a Two-Stage Coding Approach
Outer Decoder: Reed-Solomon Code (60,54;7)
Bit Interleaver Employed
Inner Decoder: Block Code (128,64;22)
δ=0.10 and Erasure Information is Employed

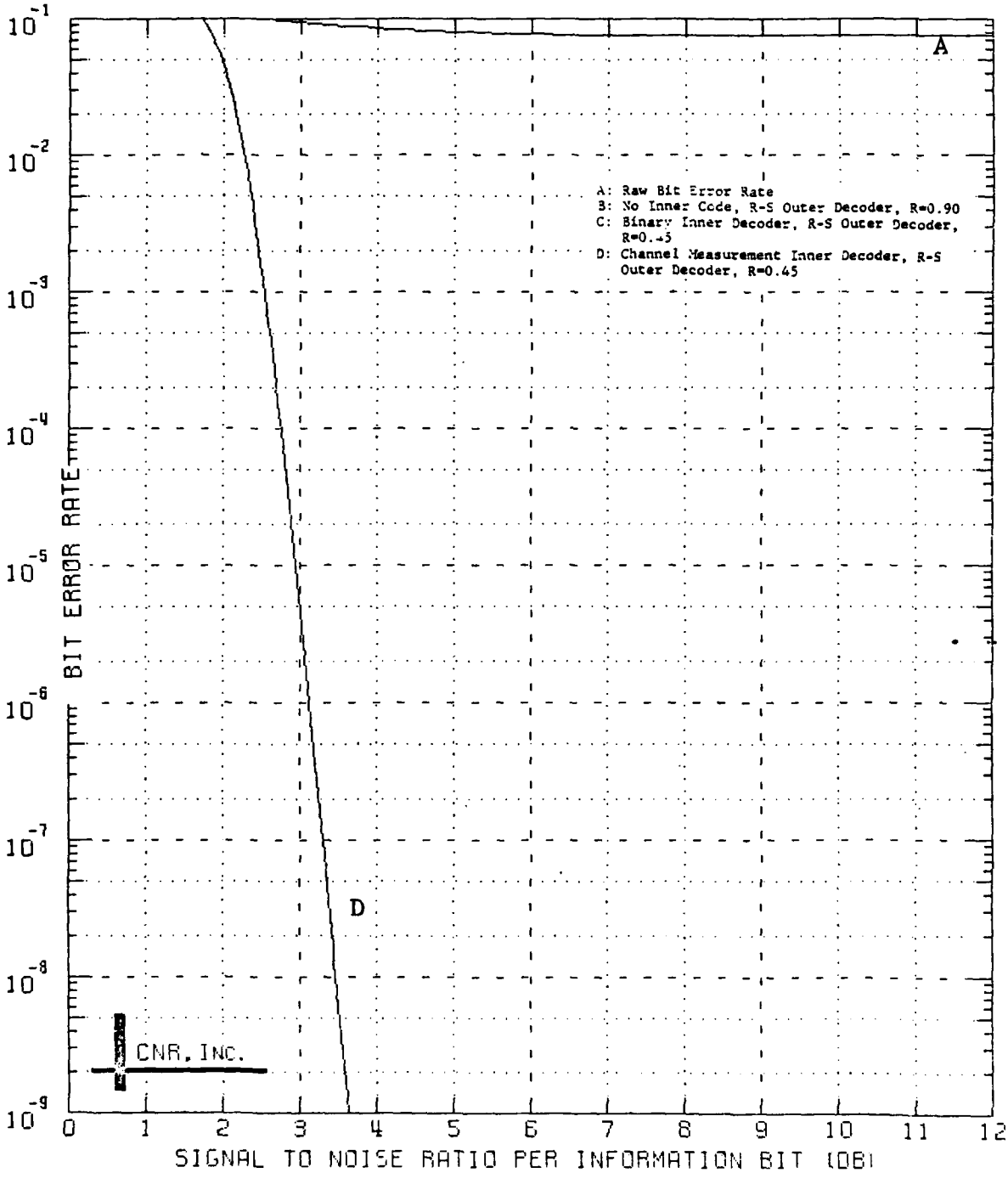


Figure 9.45 Decoded Performance of a Two-Stage Coding Approach
Outer Decoder: Reed-Solomon Code (60,54;7)
Bit Interleaver Employed
Inner Decoder: Block Code (128,64;22)
δ=0.15 and Erasure Information is Employed

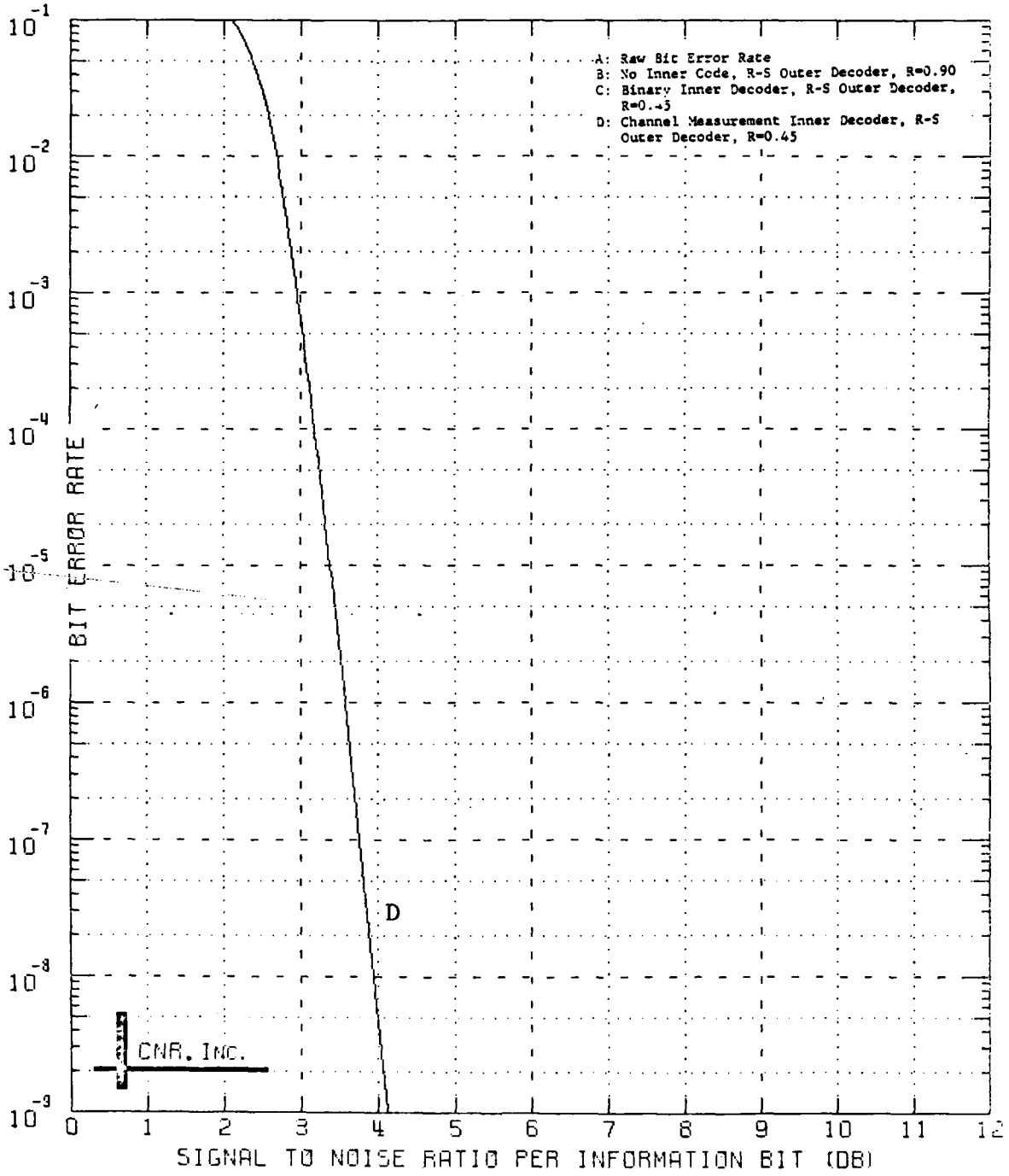


Figure 9.46 Decoded Performance of a Two-Stage Coding Approach
Outer Decoder: Reed-Solomon Code (60,54;7)
Bit Interleaver Employed
Inner Decoder: Block Code (128,64;22)
δ=0.20 and Erasure Information is Employed

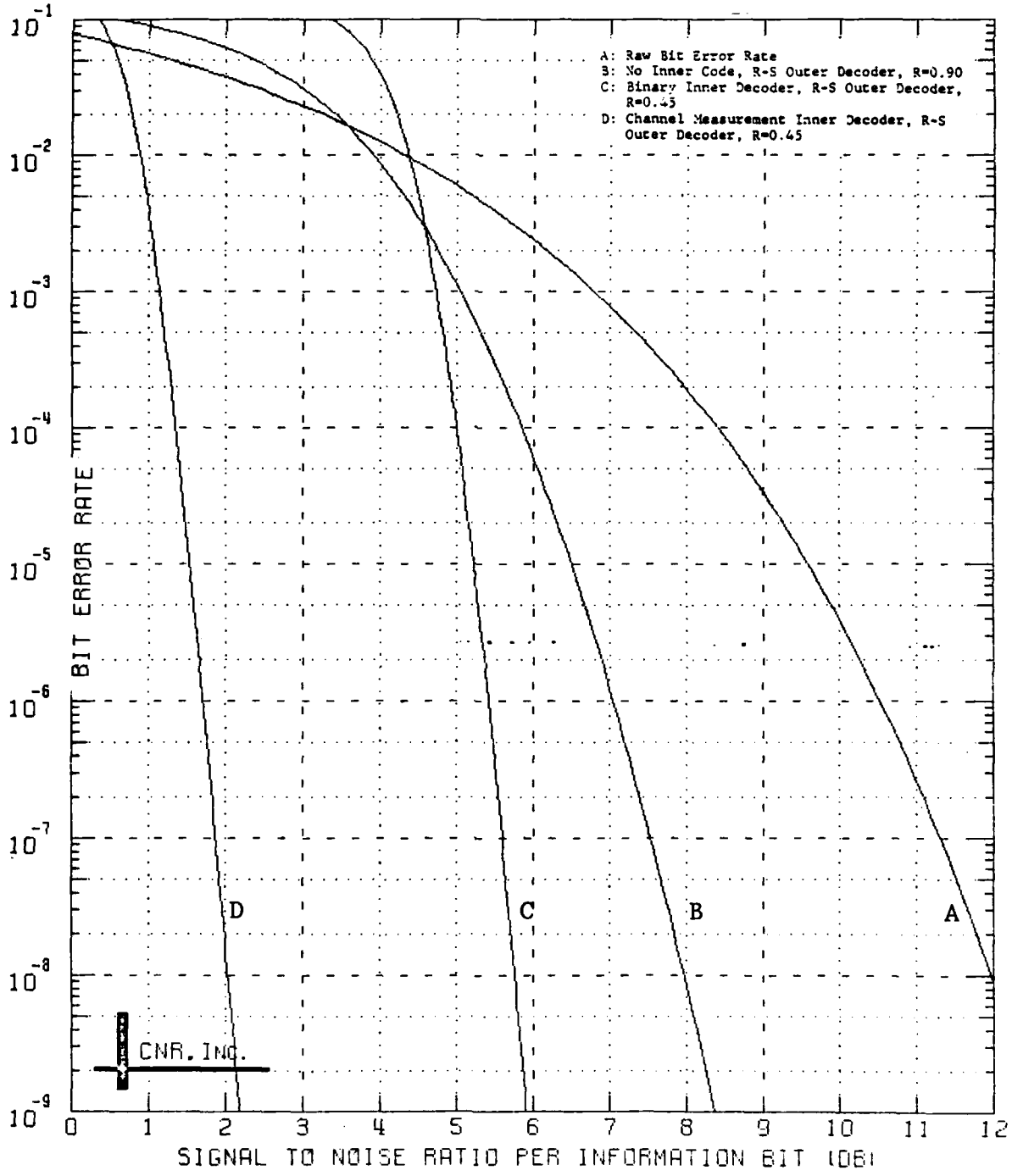


Figure 9.47 Decoded Performance of a Two-Stage Coding Approach
Outer Decoder: Reed-Solomon Code (60,54;7)
Symbol Interleaver Employed
Inner Decoder: Block Code (128,64;22)
δ=0.00 and No Erasure Information Employed

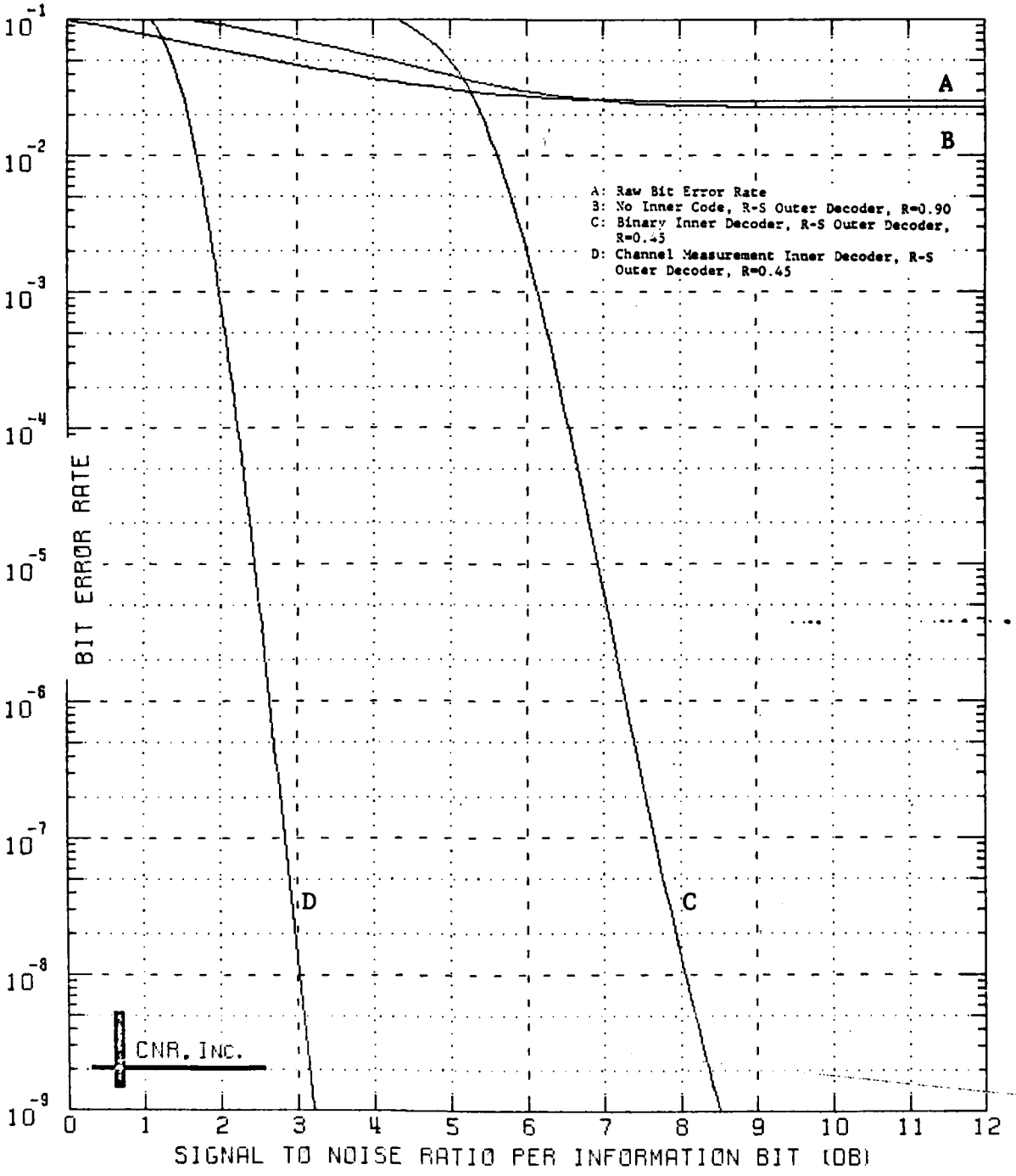


Figure 9.48 Decoded Performance of a Two-Stage Coding Approach
Outer Decoder: Reed-Solomon Code (60,54;7)
Symbol Interleaver Employed
Inner Decoder: Block Code (128,64;22)
δ=0.05 and No Erasure Information Employed

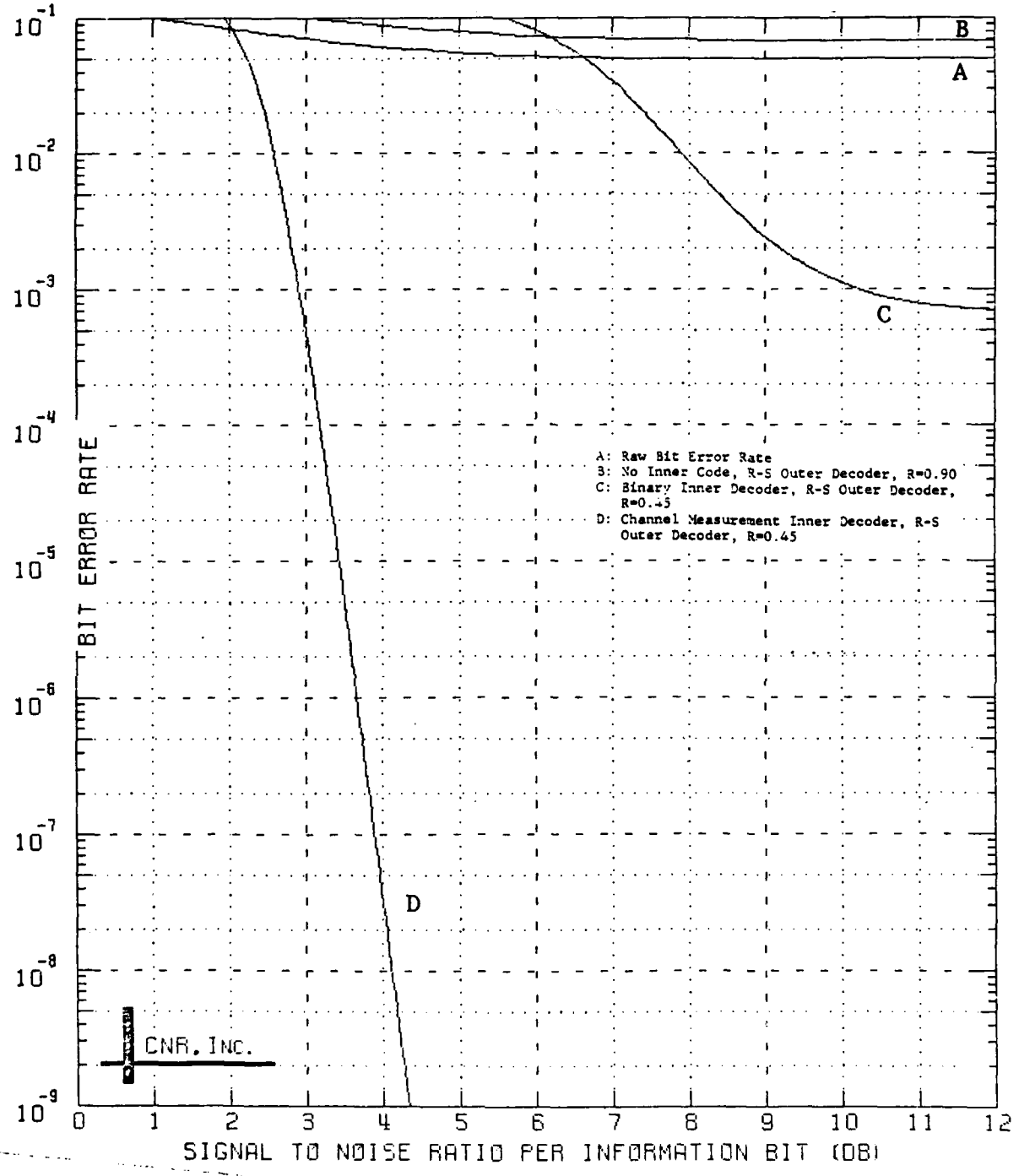


Figure 9.49 Decoded Performance of a Two-Stage Coding Approach
Outer Decoder: Reed-Solomon Code (60,54;7)
Symbol Interleaver Employed
Inner Decoder: Block Code (128,64;22)
δ=0.10 and No Erasure Information Employed

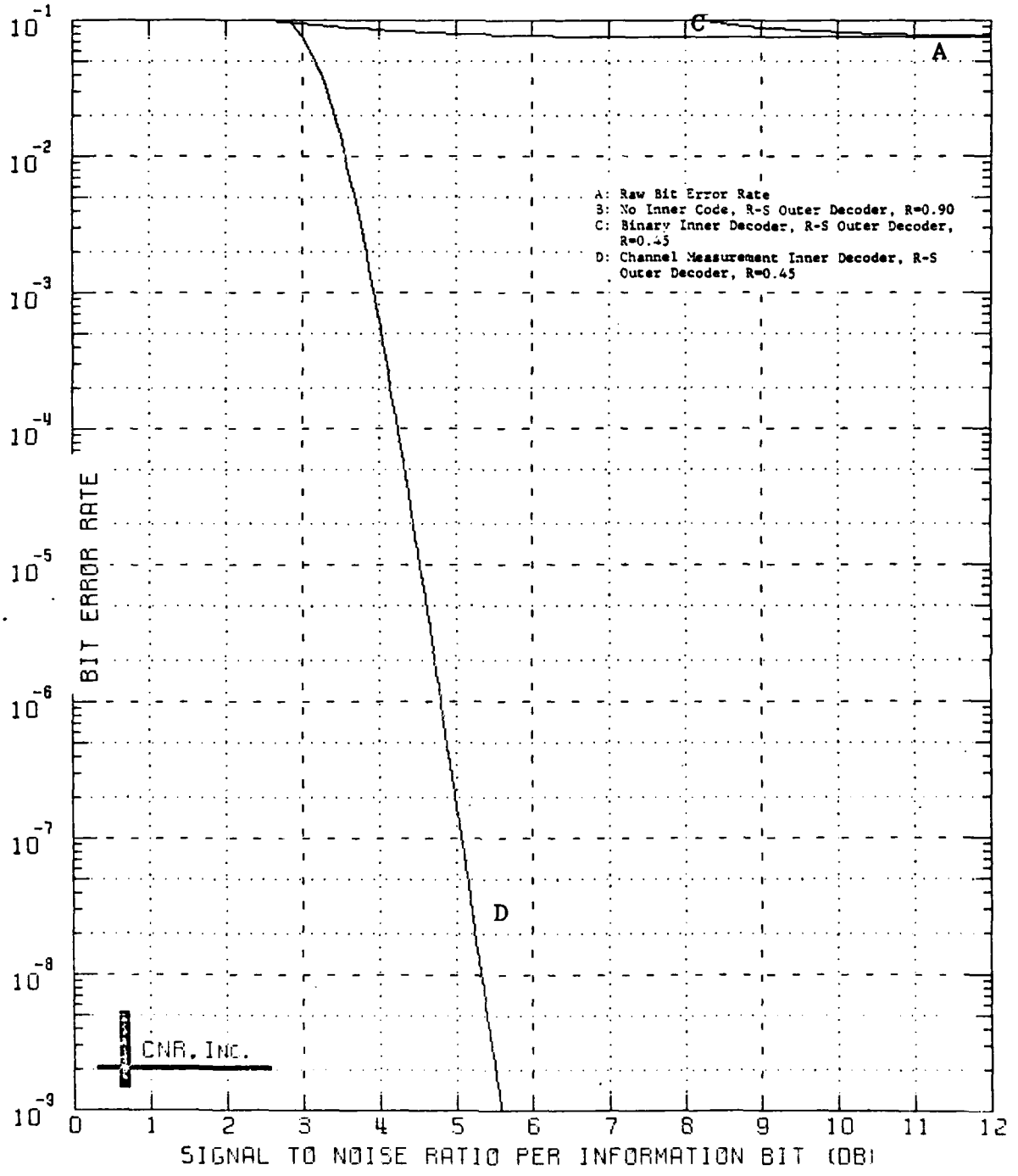


Figure 9.50 Decoded Performance of a Two-Stage Coding Approach
Outer Decoder: Reed-Solomon Code (60,54;7)
Symbol Interleaver Employed
Inner Decoder: Block Code (128,64;22)
δ=0.15 and No Erasure Information Employed

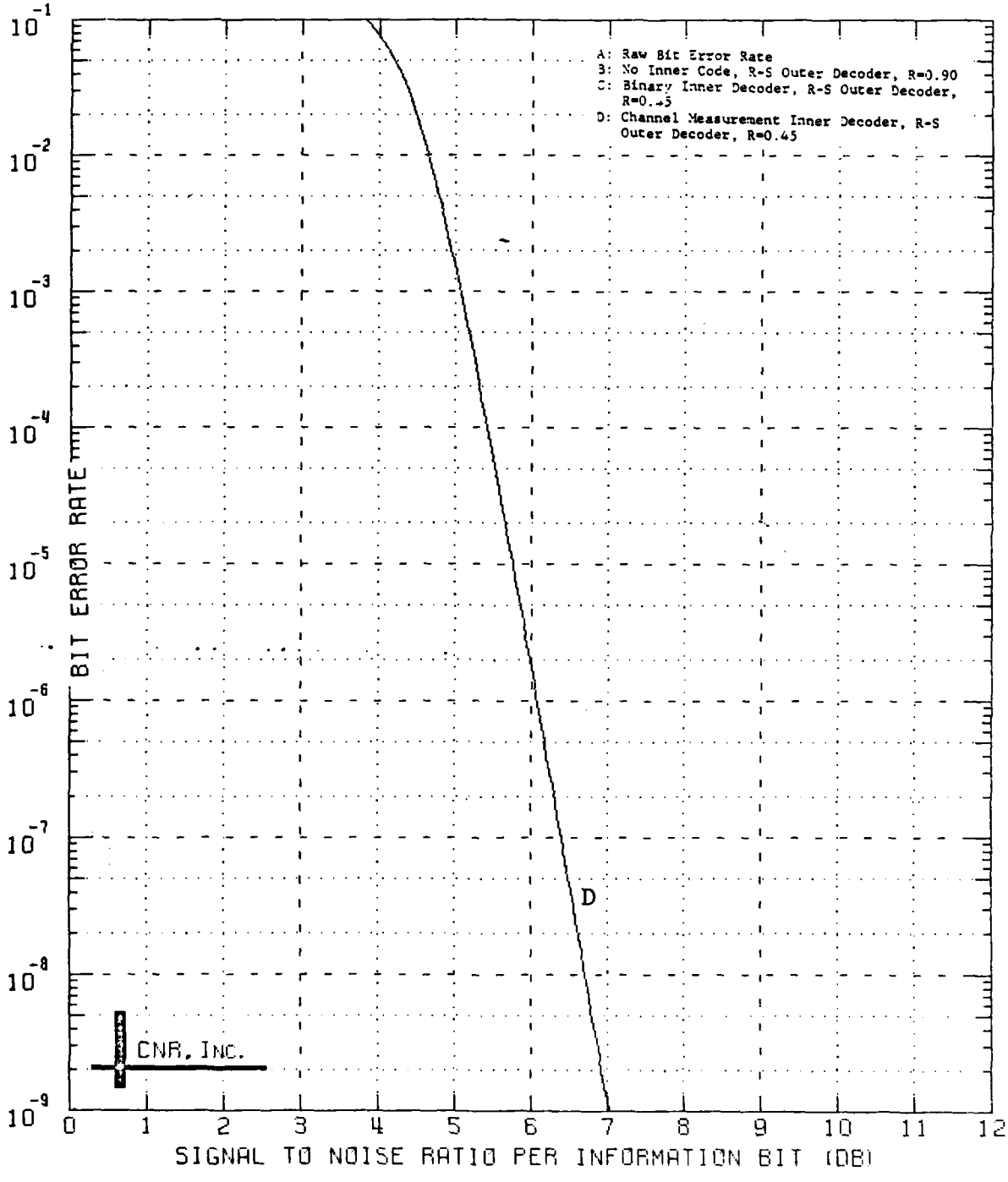


Figure 9.51 Decoded Performance of a Two-Stage Coding Approach
Outer Decoder: Reed-Solomon Code (60,54;7)
Symbol Interleaver Employed
Inner Decoder: Block Code (128,64;22)
δ=0.20 and No Erasure Information Employed

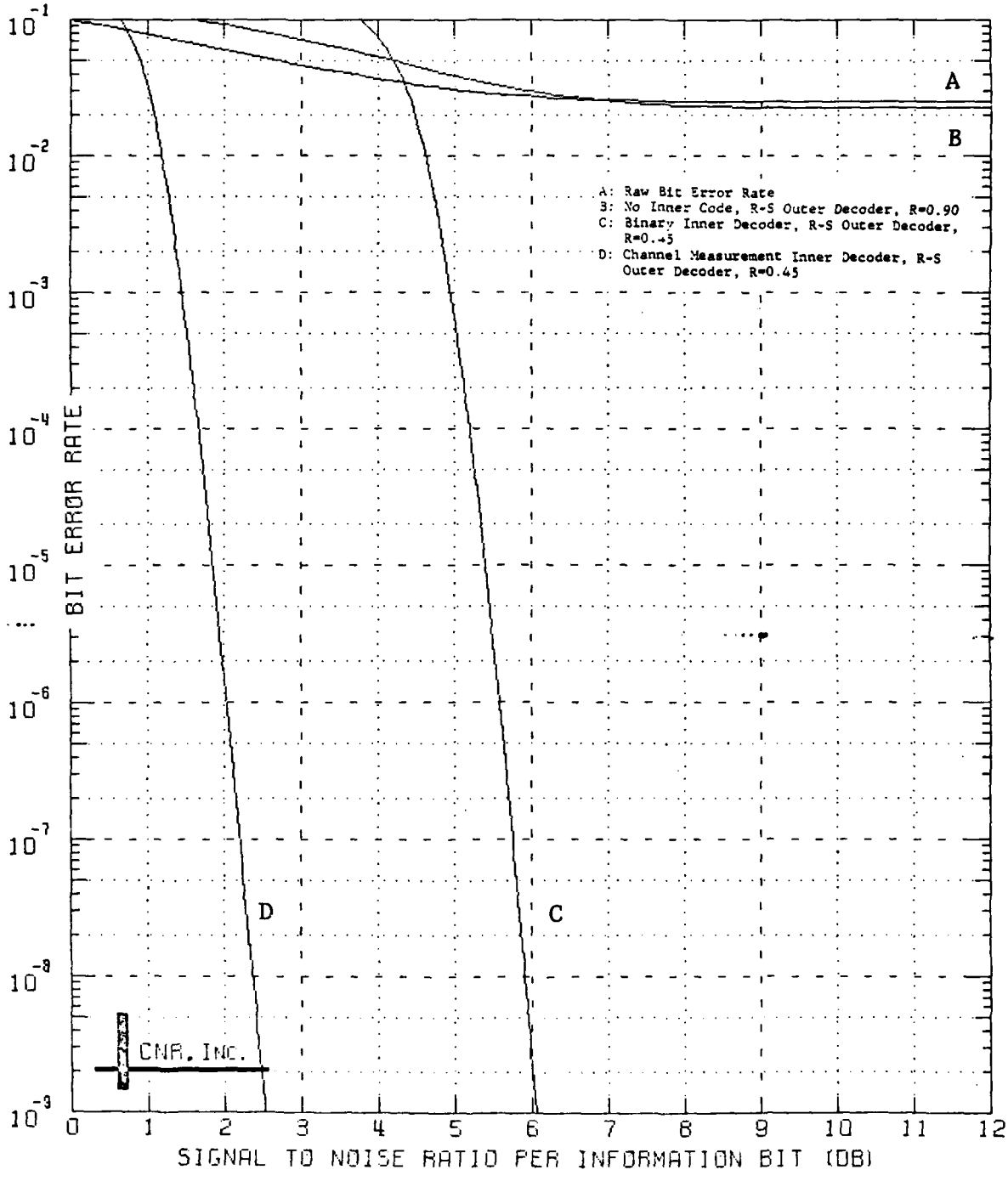


Figure 9.52 Decoded Performance of a Two-Stage Coding Approach
Outer Decoder: Reed-Solomon Code (60,54;7)
Symbol Interleaver Employed
Inner Decoder: Block Code (128,64;22)
δ=0.05 and Erasure Information is Employed

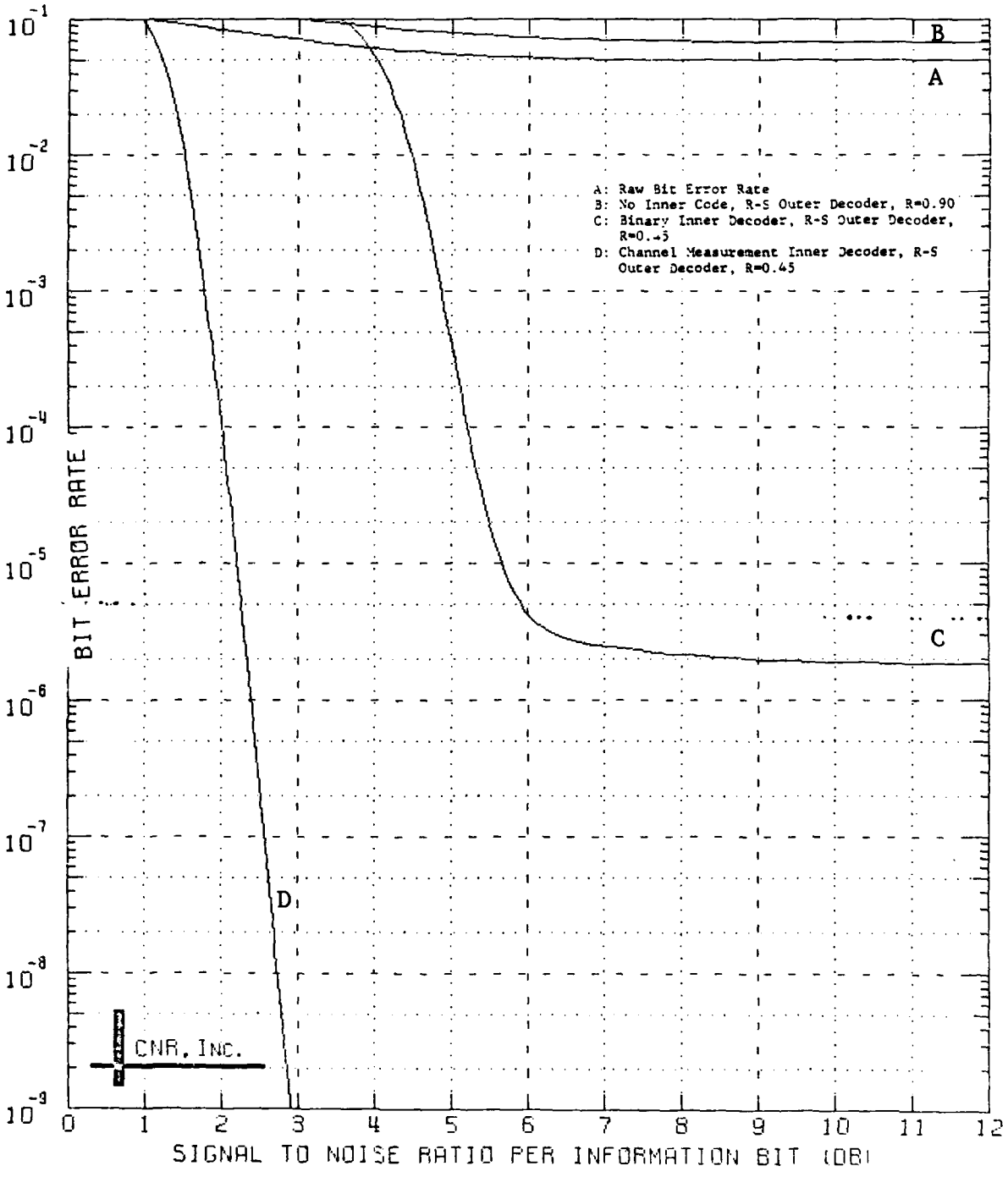


Figure 9.53 Decoded Performance of a Two-Stage Coding Approach
Outer Decoder: Reed-Solomon Code (60,54;7)
Symbol Interleaver Employed
Inner Decoder: Block Code (128,64;22)
δ=0.10 and Erasure Information is Employed

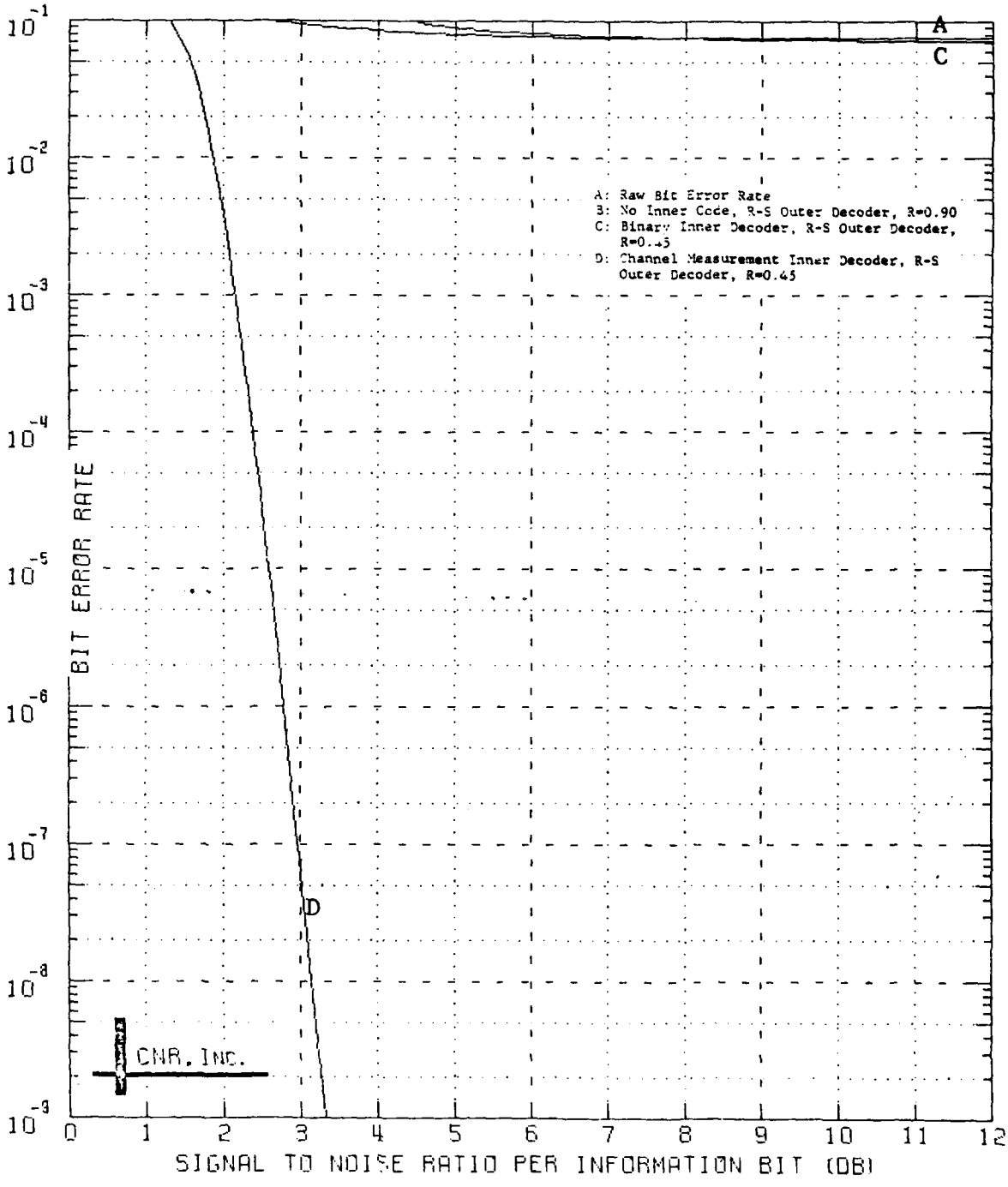


Figure 9.54 Decoded Performance of a Two-Stage Coding Approach
Outer Decoder: Reed-Solomon Code (60,54;7)
Symbol Interleaver Employed
Inner Decoder: Block Code (128,64;22)
δ=0.15 and Erasure Information is Employed

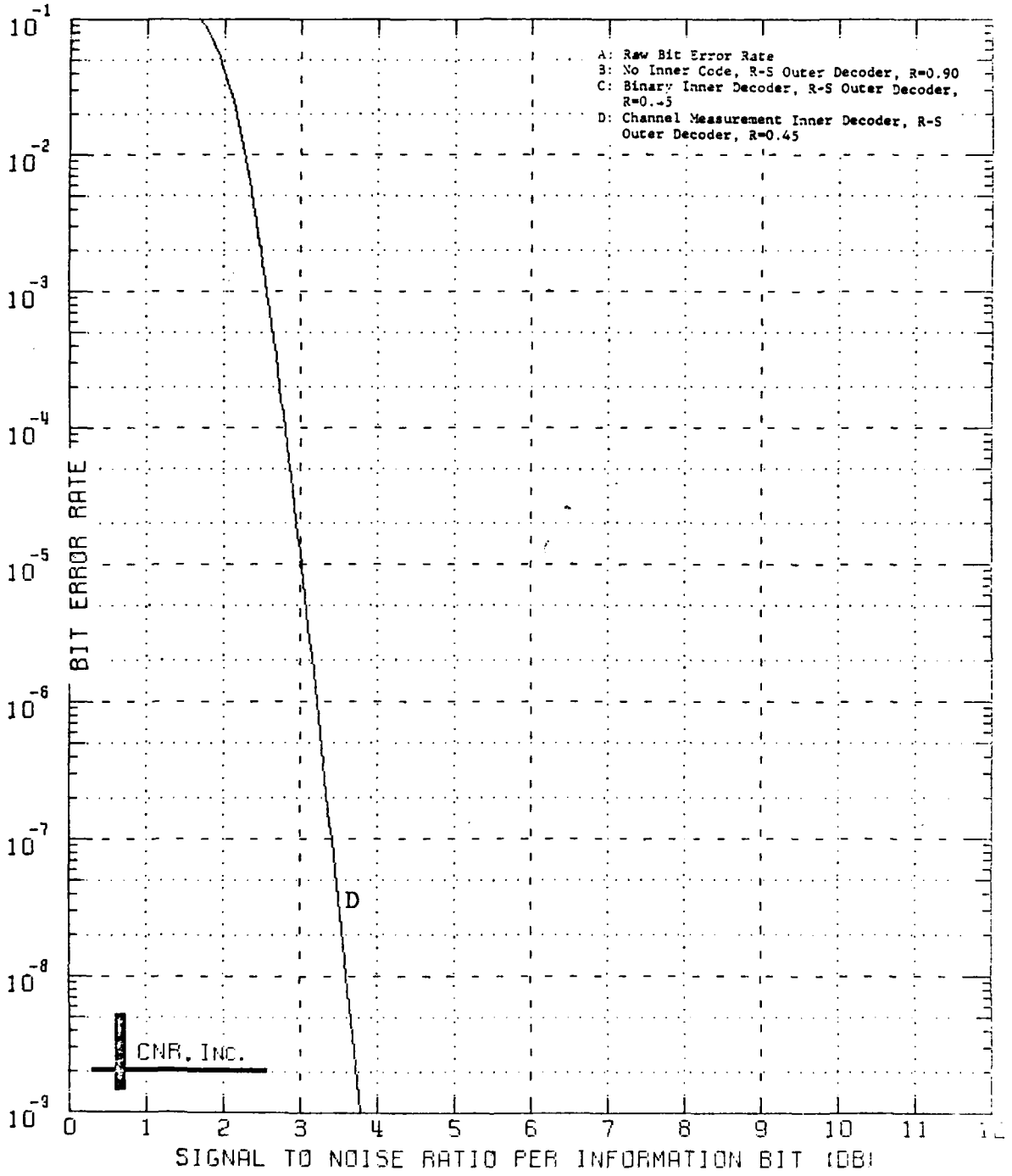


Figure 9.55 Decoded Performance of a Two-Stage Coding Approach
Outer Decoder: Reed-Solomon Code (60,54;7)
Symbol Interleaver Employed
Inner Decoder: Block Code (128,64;22)
δ=0.20 and Erasure Information is Employed

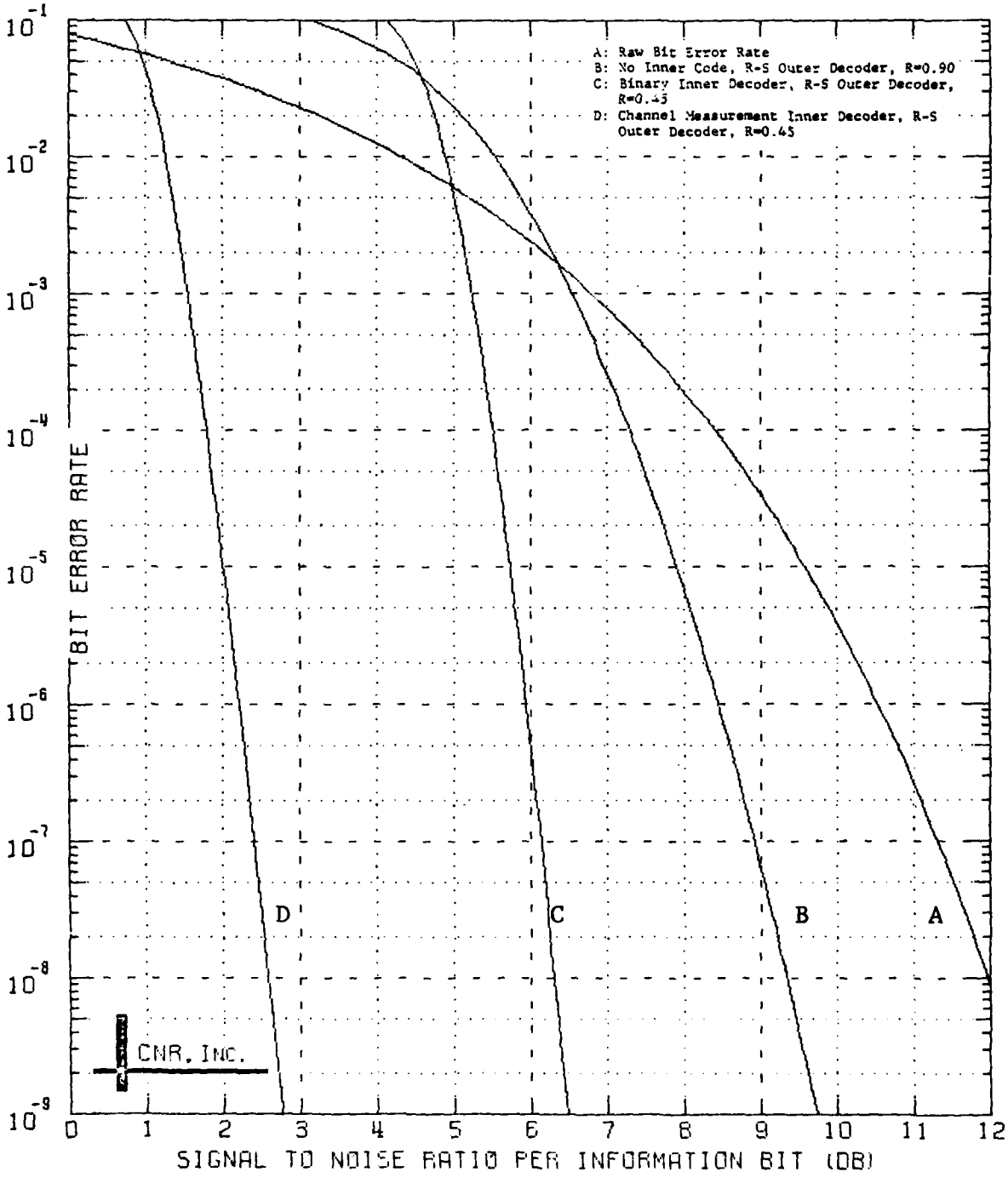


Figure 9.56 Decoded Performance of a Two-Stage Coding Approach
Outer Decoder: Reed-Solomon Code (40,36;5)
Bit Interleaver Employed
Inner Decoder: Block Code (128,64;22)
δ=0.00 and No Erasure Information Employed

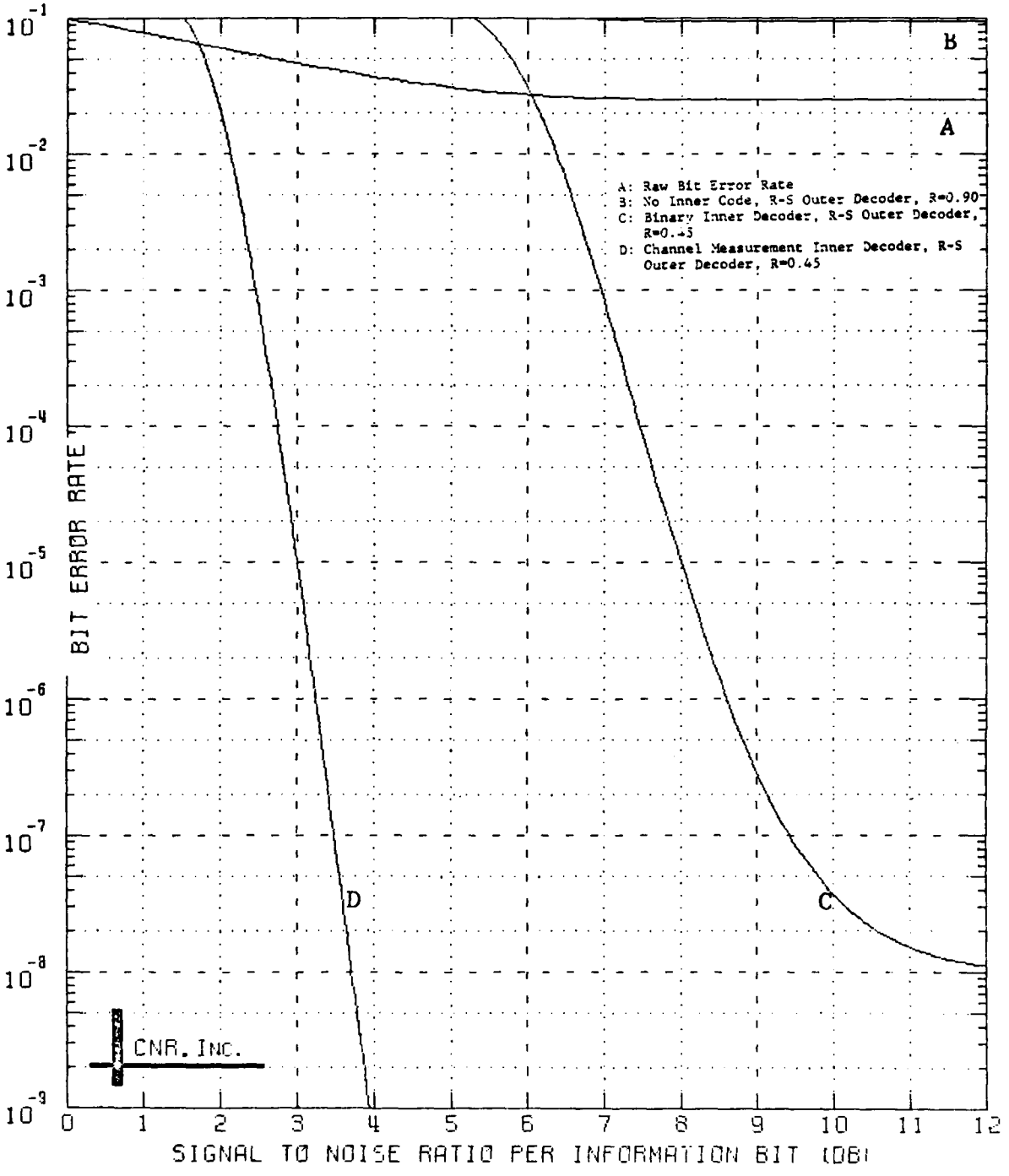


Figure 9.57 Decoded Performance of a Two-Stage Coding Approach
Outer Decoder: Reed-Solomon Code (40,36;5)
Bit Interleaver Employed
Inner Decoder: Block Code (128,64;22)
δ=0.05 and No Erasure Information Employed

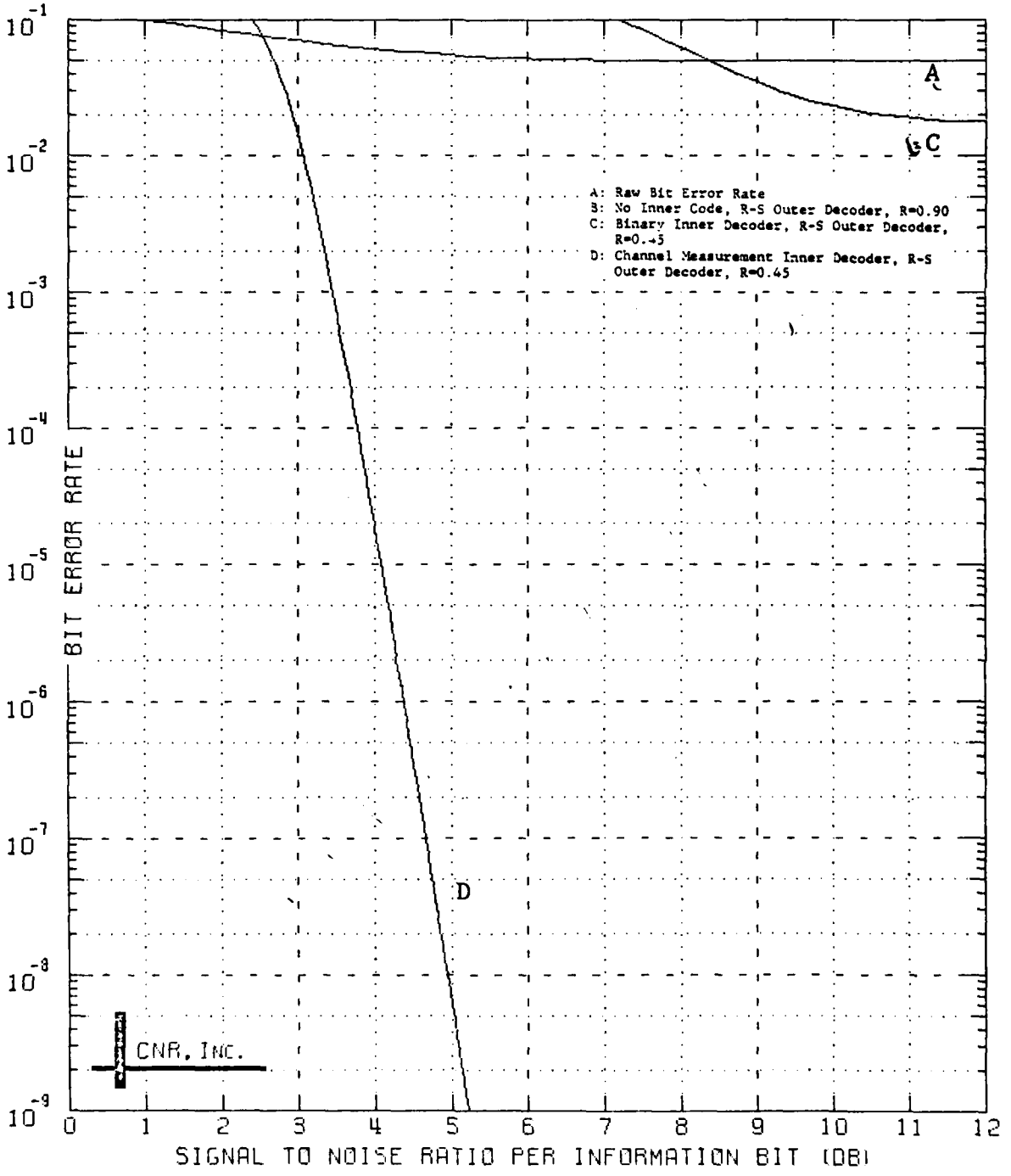


Figure 9.58 Decoded Performance of a Two-Stage Coding Approach
Outer Decoder: Reed-Solomon Code (40,36;5)
Bit Interleaver Employed
Inner Decoder: Block Code (128,64;22)
δ=0.10 and No Erasure Information Employed

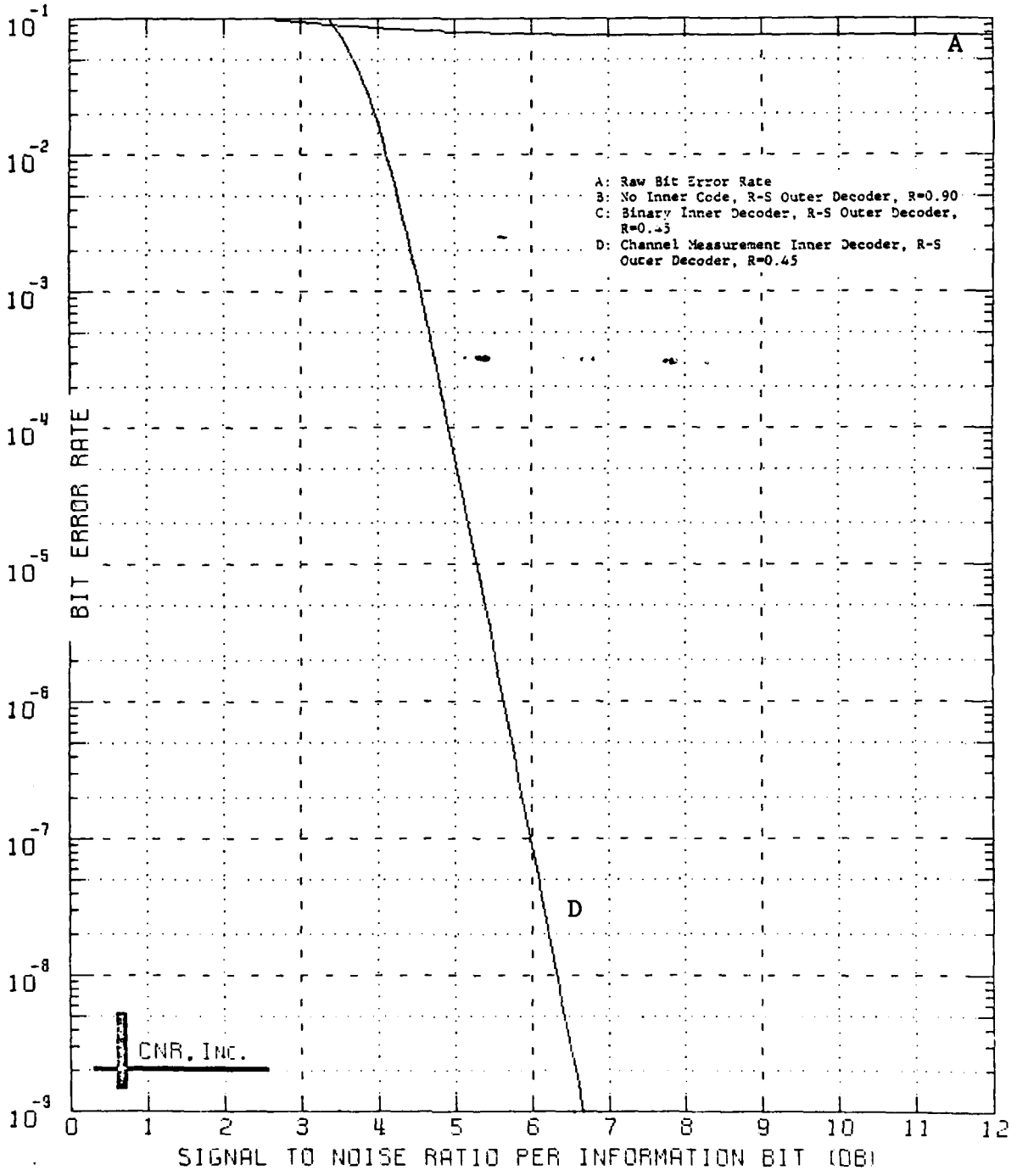


Figure 9.59 Decoded Performance of a Two-Stage Coding Approach
Outer Decoder: Reed-Solomon Code (40,36;5)
Bit Interleaver Employed
Inner Decoder: Block Code (128,64;22)
δ=0.15 and No Erasure Information Employed

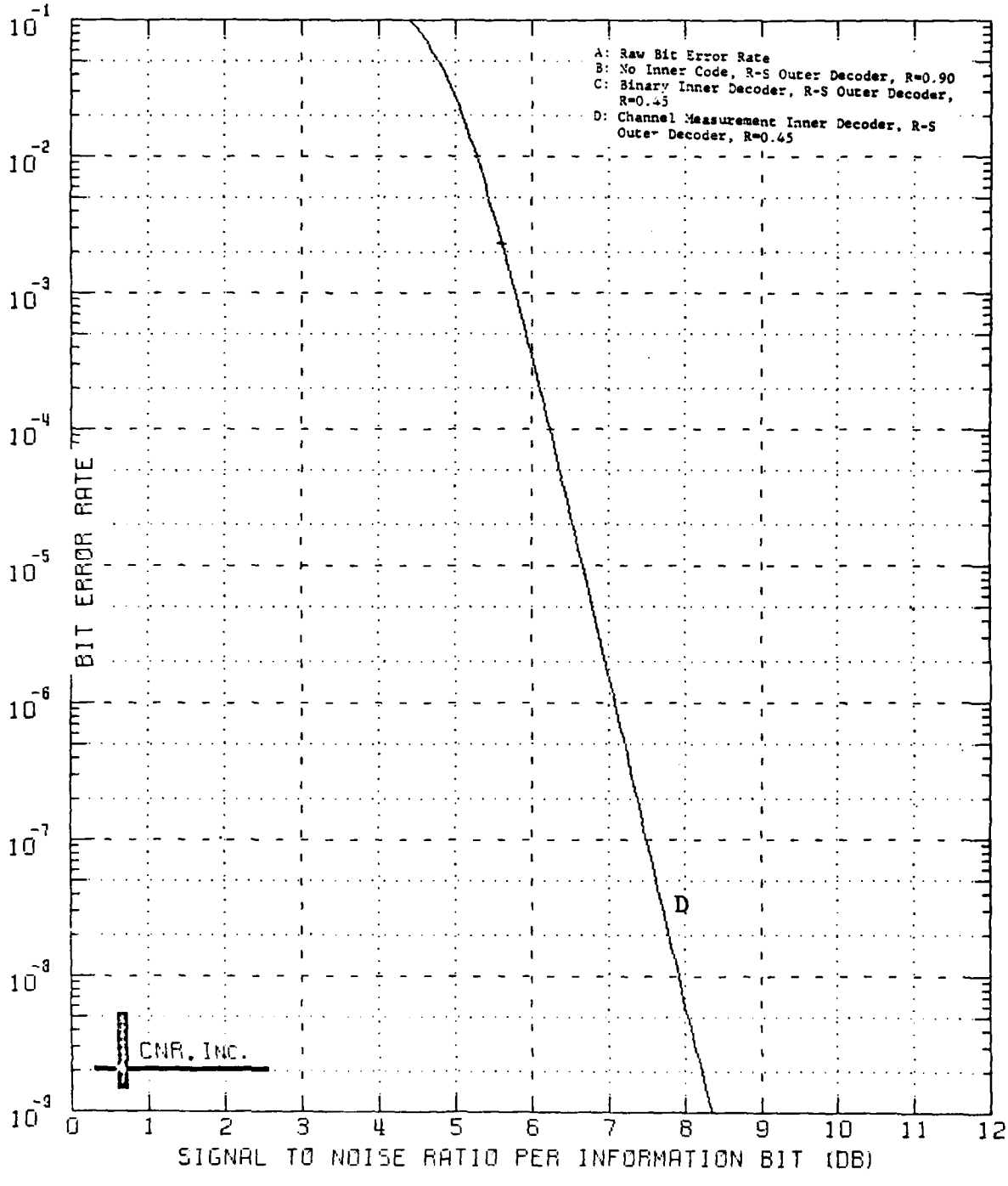


Figure 9.60 Decoded Performance of a Two-Stage Coding Approach
Outer Decoder: Reed-Solomon Code (40,36;5)
Bit Interleaver Employed
Inner Decoder: Block Code (128,64;22)
δ=0.20 and No Erasure Information Employed

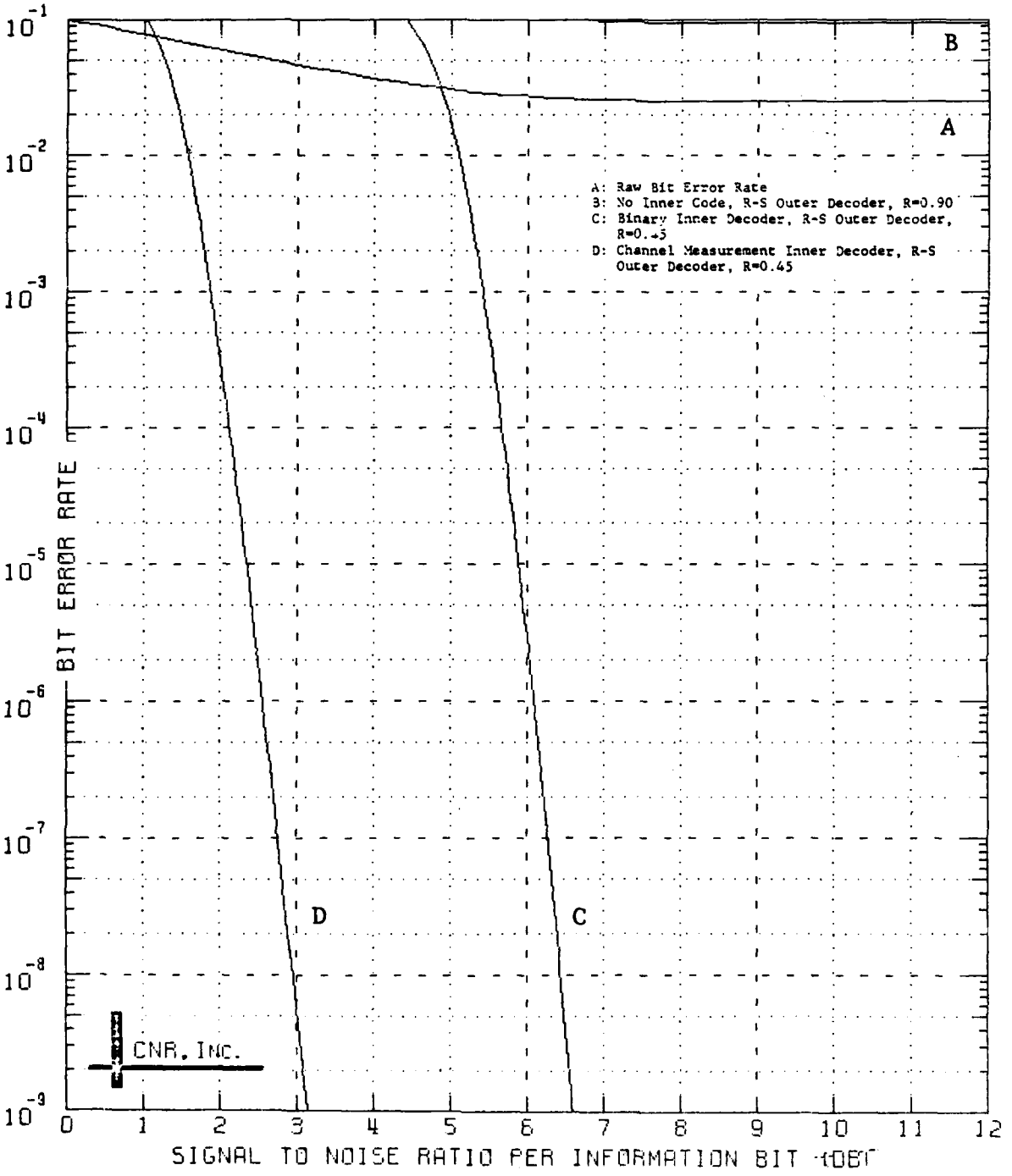


Figure 9.61 Decoded Performance of a Two-Stage Coding Approach
Outer Decoder: Reed-Solomon Code (40,36;5)
Bit Interleaver Employed
Inner Decoder: Block Code (128,64;22)
δ=0.05 and Erasure Information is Employed

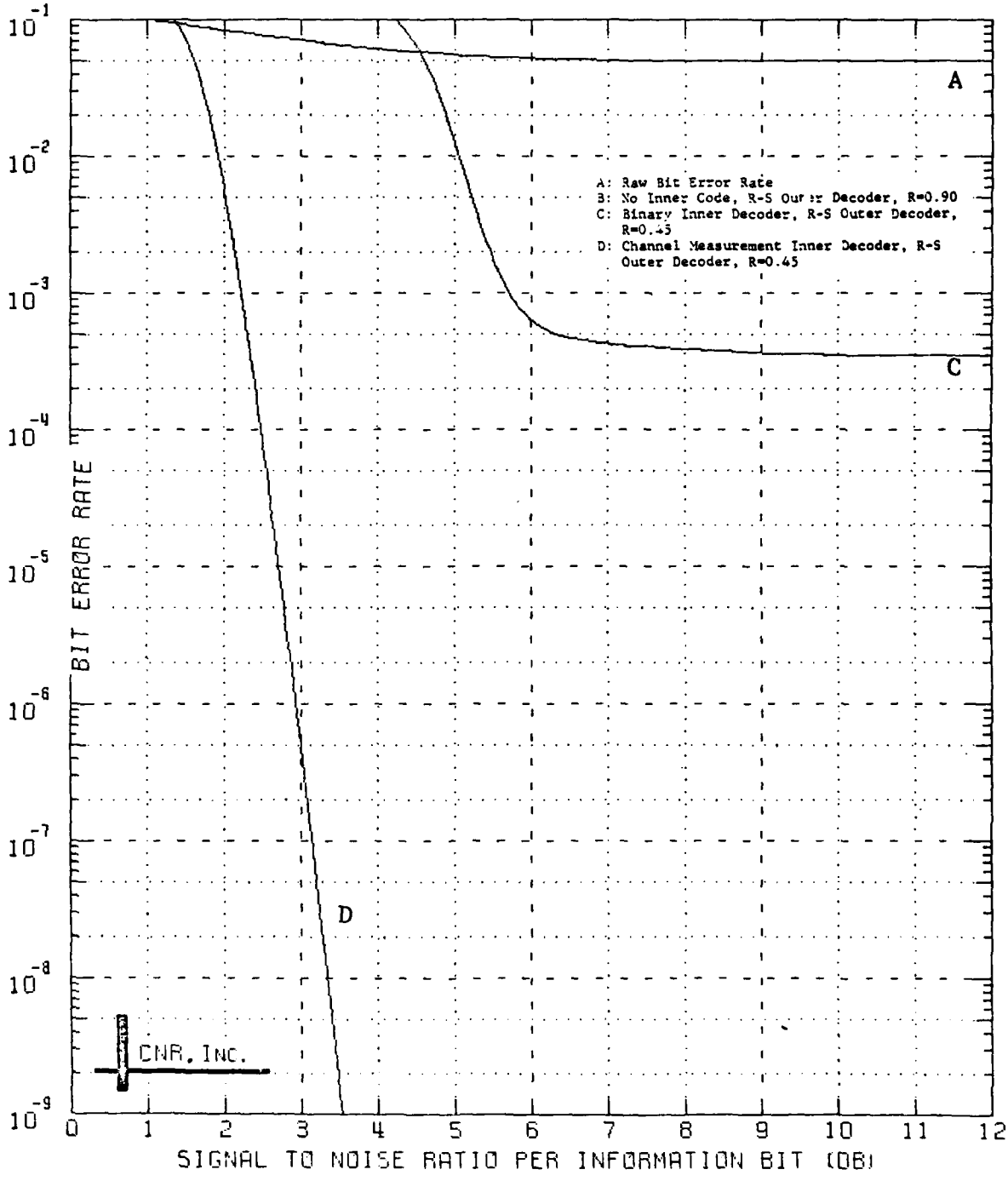


Figure 9.62 Decoded Performance of a Two-Stage Coding Approach
Outer Decoder: Reed-Solomon Code (40,36;5)
Bit Interleaver Employed
Inner Decoder: Block Code (128,64;22)
δ=0.10 and Erasure Information Employed

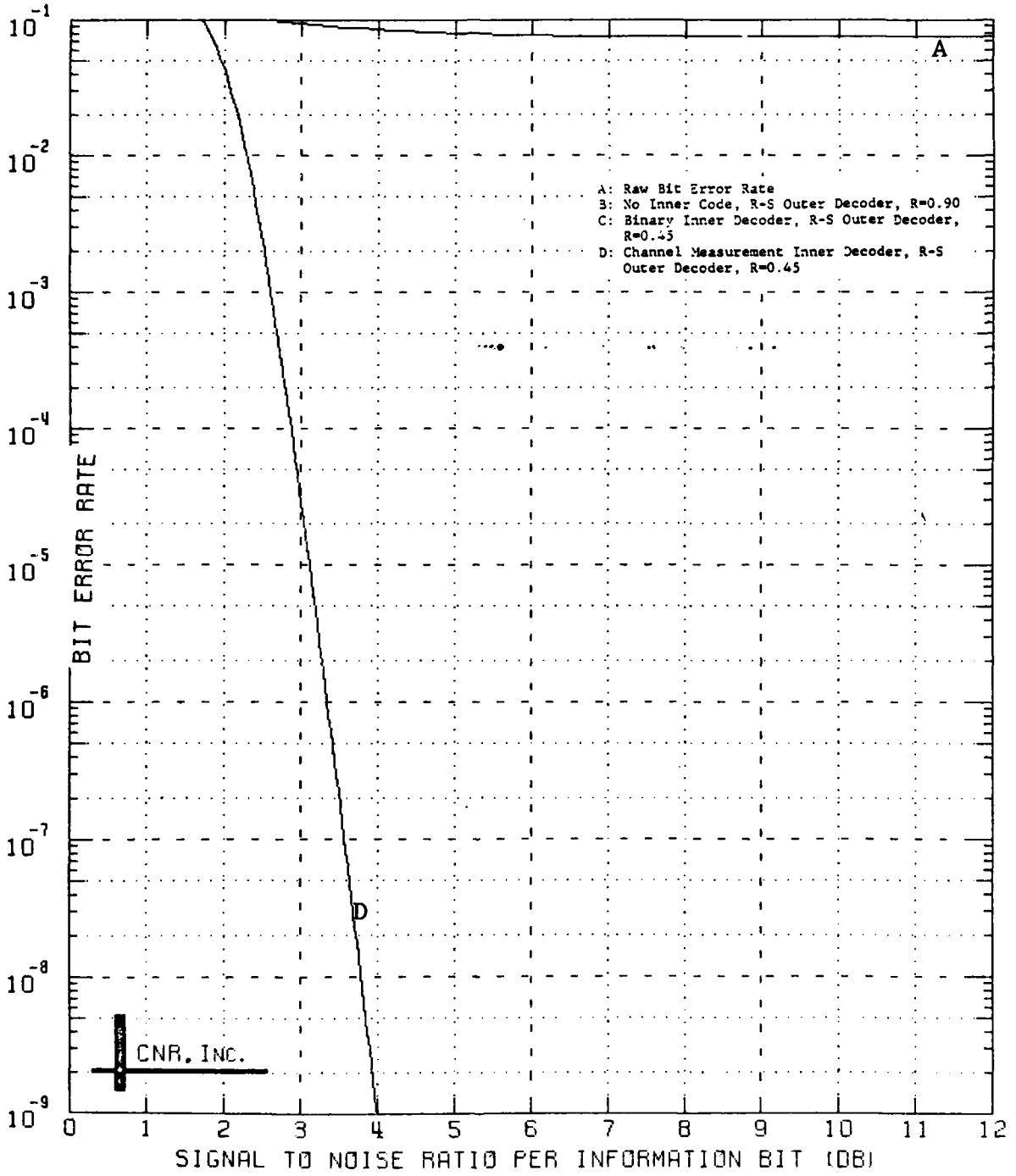


Figure 9.63 Decoded Performance of a Two-Stage Coding Approach
Outer Decoder: Reed-Solomon Code (40,36;5)
Bit Interleaver Employed
Inner Decoder: Block Code (128,64;22)
δ=0.15 and Erasure Information is Employed

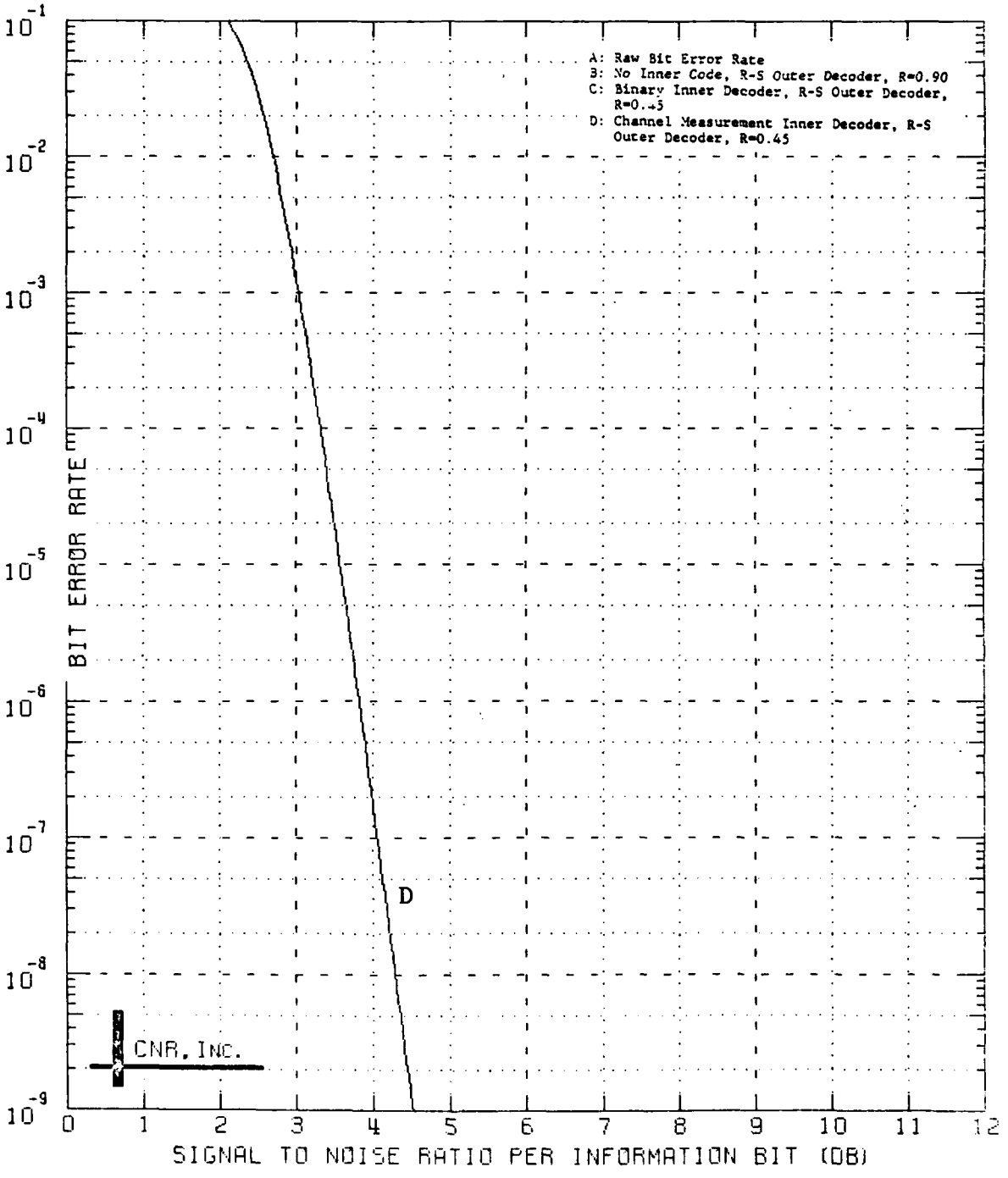


Figure 9.64 Decoded Performance of a Two-Stage Coding Approach
Outer Decoder: Reed-Solomon Code (40,36;5)
Bit Interleaver Employed
Inner Decoder: Block Code (128,64;22)
δ= 0.20 and Erasure Information is Employed

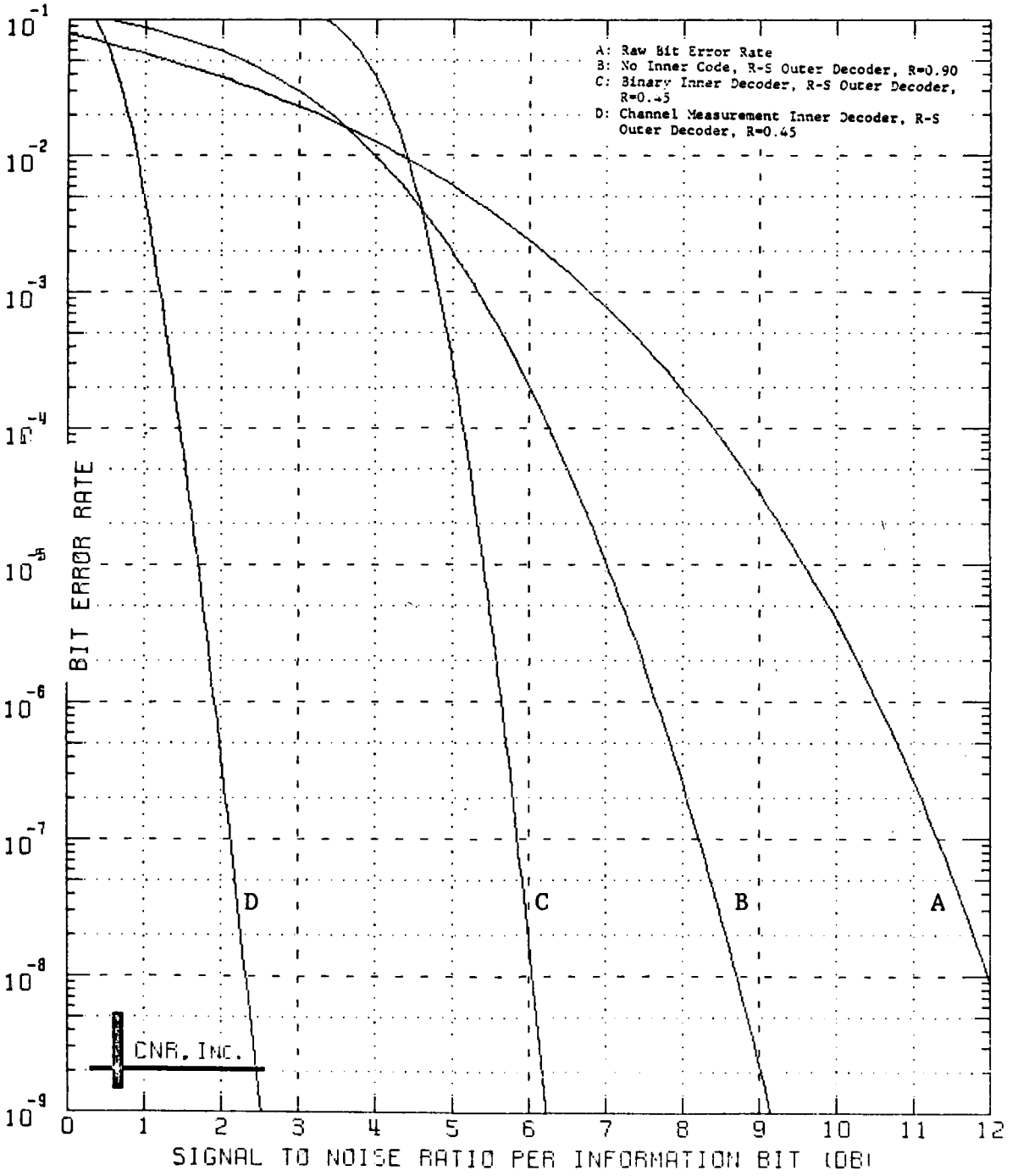


Figure 9.65 Decoded Performance of a Two-Stage Coding Approach
Outer Decoder: Reed-Solomon Code (40,36;5)
Symbol Interleaver Employed
Inner Decoder: Block Code (128,64;22)
δ= 0.00 and No Erasure Information Employed

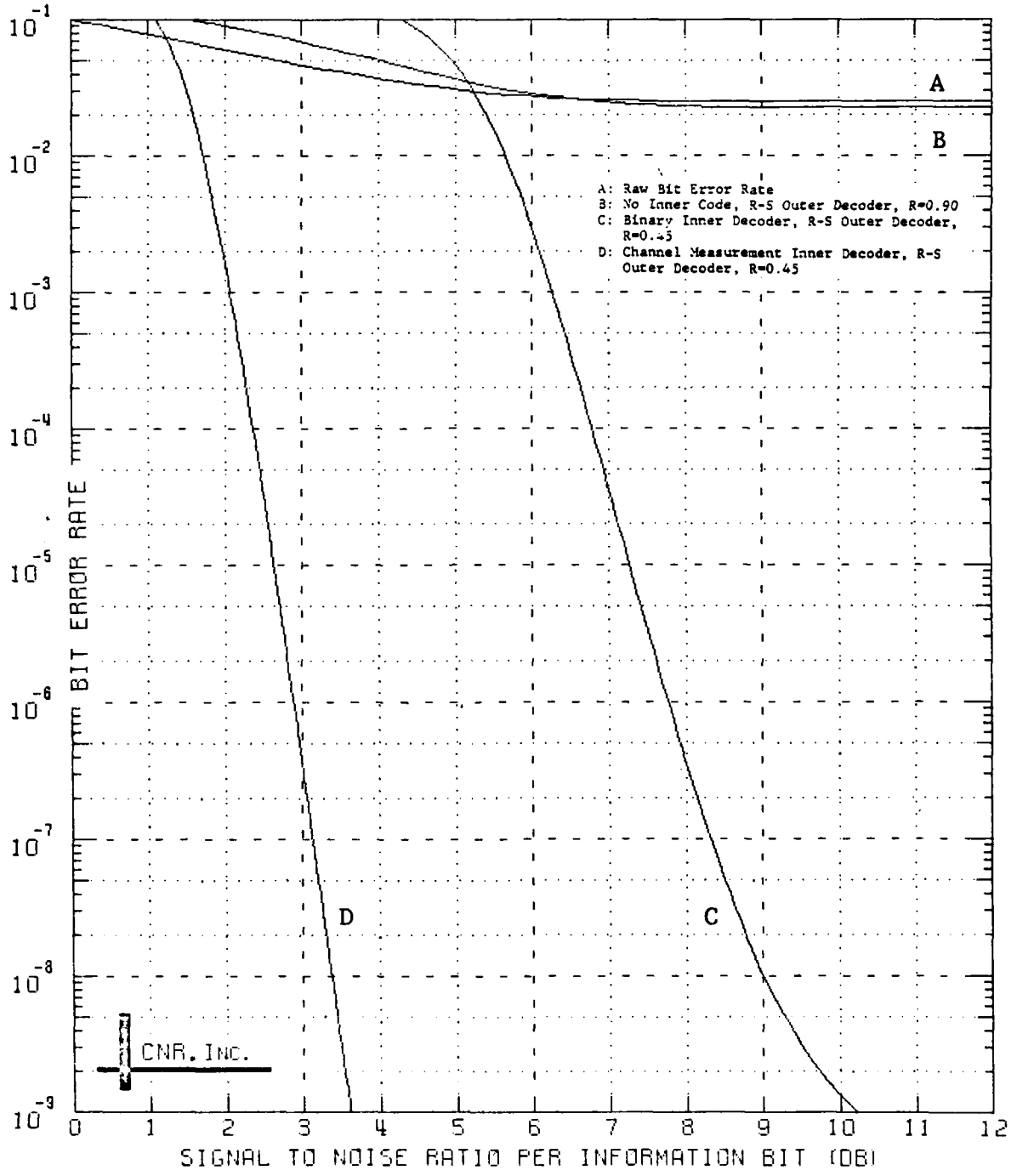


Figure 9.66 Decoded Performance of a Two-Stage Coding Approach
Outer Decoder: Reed-Solomon Code (40,36;5)
Symbol Interleaver Employed
Inner Decoder: Block Code (128,64;22)
δ=0.05 and No Erasure Information Employed

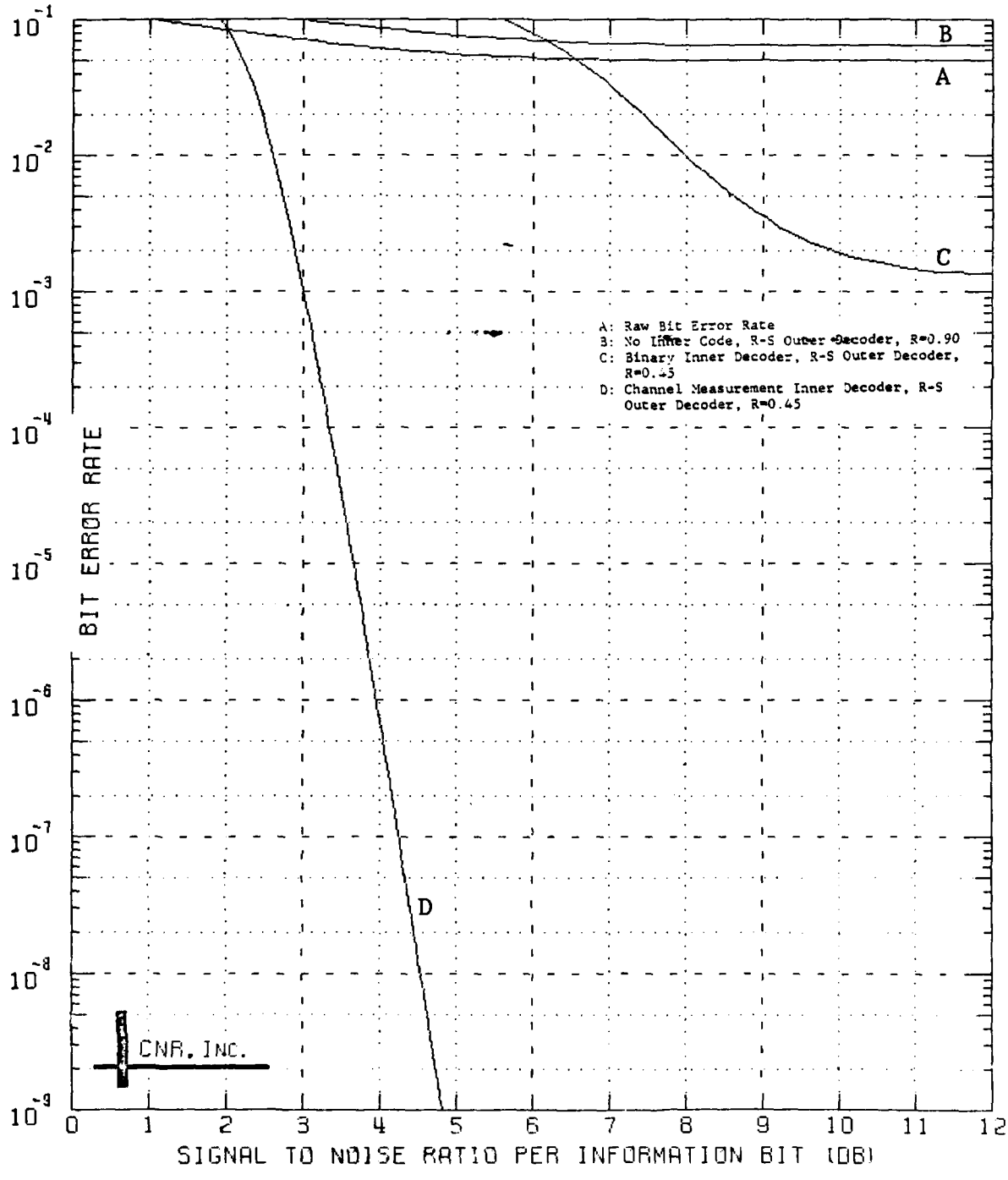


Figure 9.67 Decoded Performance of a Two-Stage Coding Approach
Outer Decoder: Reed-Solomon Code (40,36;5)
Symbol Interleaver Employed
Inner Decoder: Block Code (128,64;22)
δ=0.10 and No Erasure Information Employed

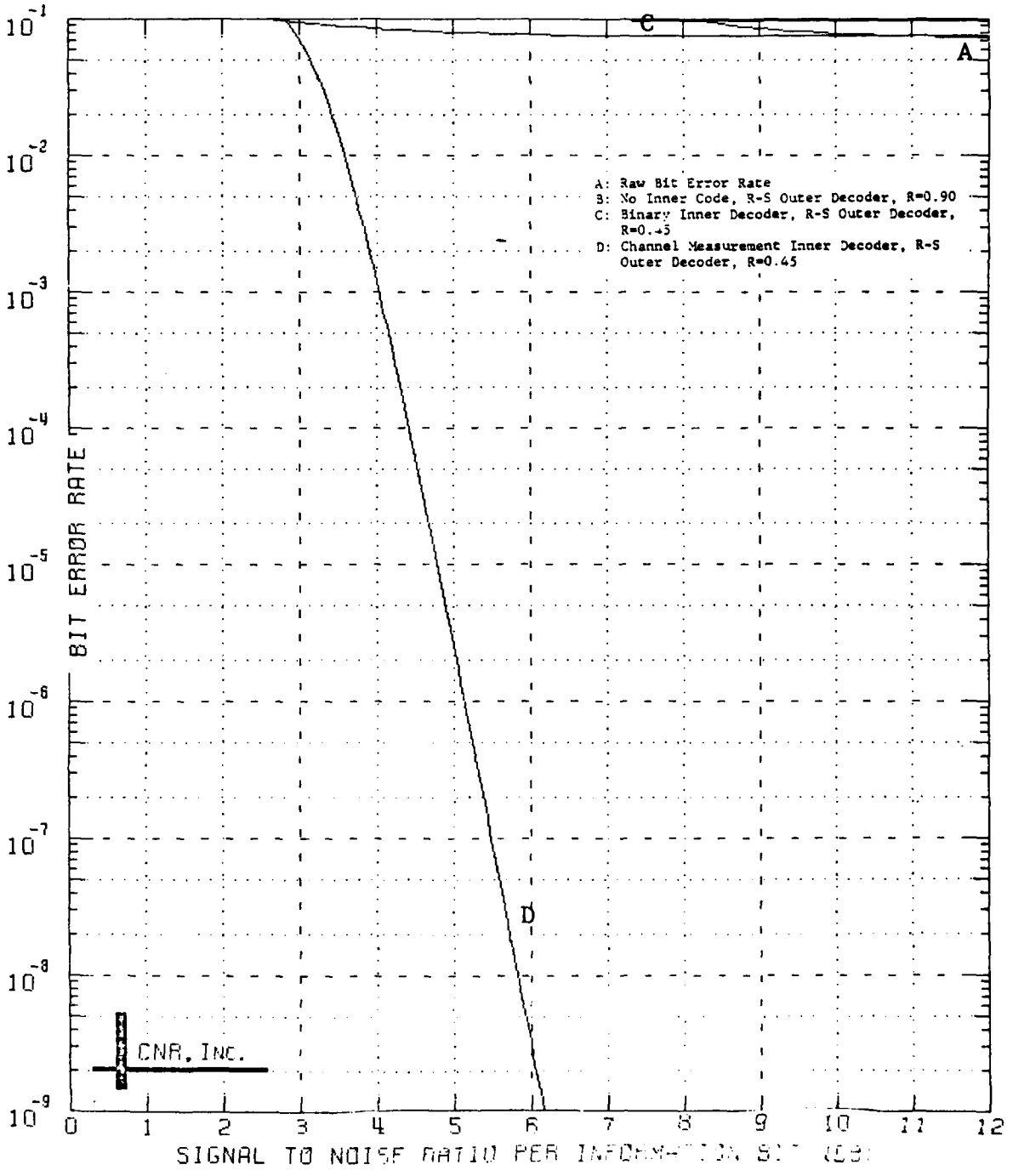


Figure 9.68 Decoded Performance of a Two-Stage Coding Approach
Outer Decoder: Reed-Solomon Code (40,36;5)
Symbol Interleaver Employed
Inner Decoder: Block Code (128,64;22)
δ=0.15 and No Erasure Information Employed

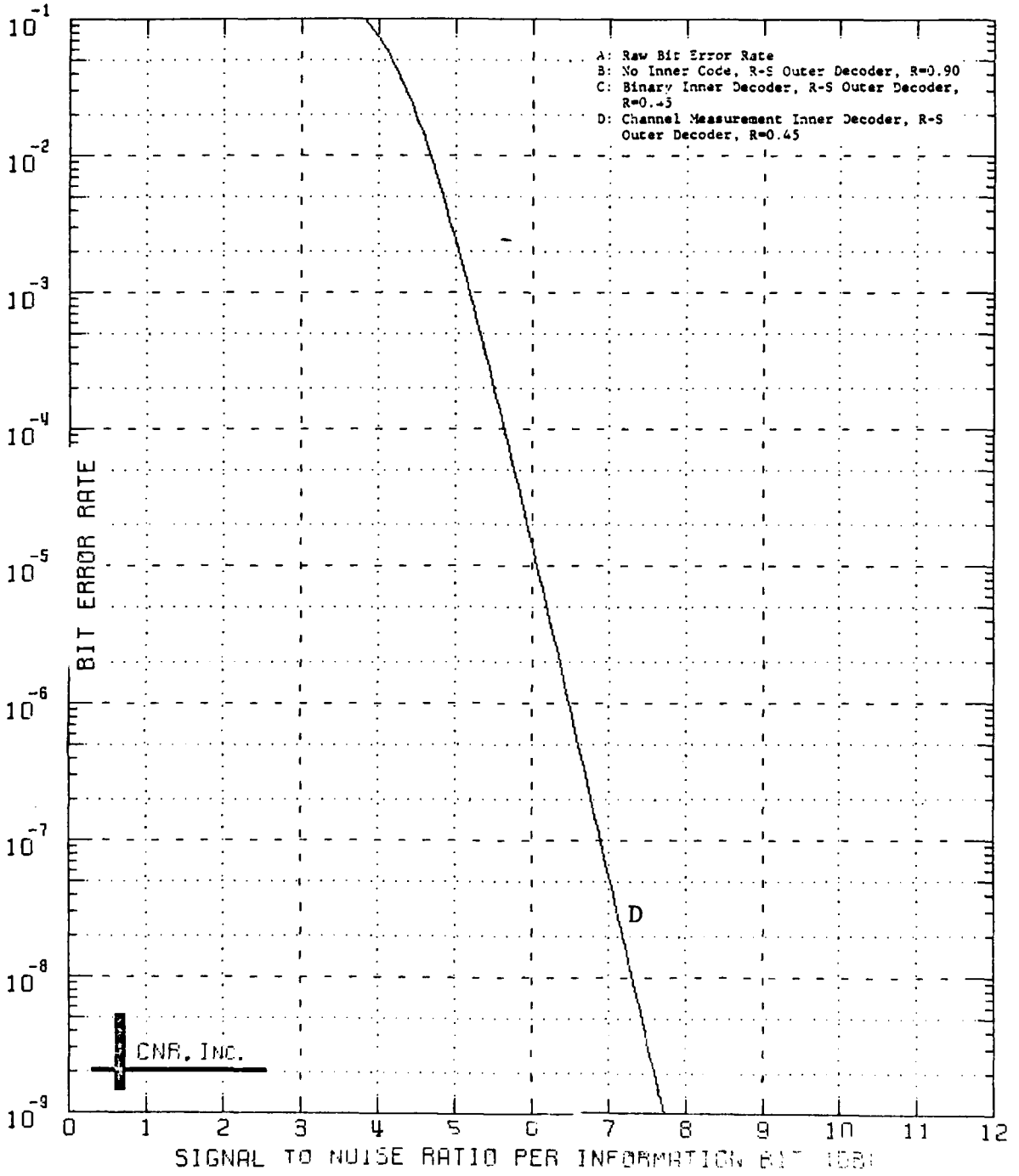


Figure 9.69 Decoded Performance of a Two-Stage Coding Approach
Outer Decoder: Reed-Solomon Code (40,36;5)
Symbol Interleaver Employed
Inner Decoder: Block Code (128,64;22)
δ=0.20 and No Erasure Information Employed

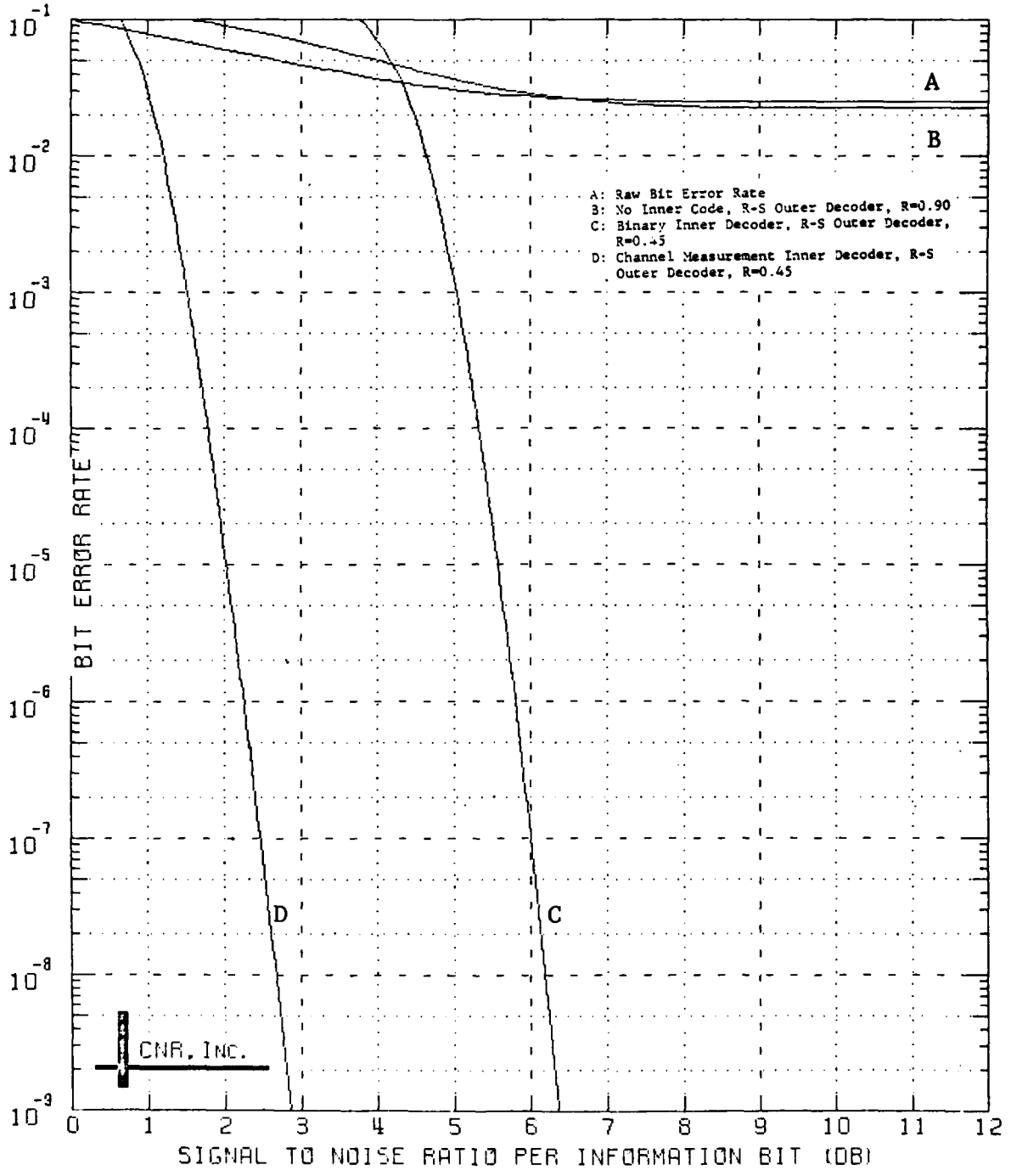


Figure 9.70 Decoded Performance of a Two-Stage Coding Approach
Outer Decoder: Reed-Solomon Code (40,36;5)
Symbol Interleaver Employed
Inner Decoder: Block Code (128,64;22)
δ=0.05 and Erasure Information Employed

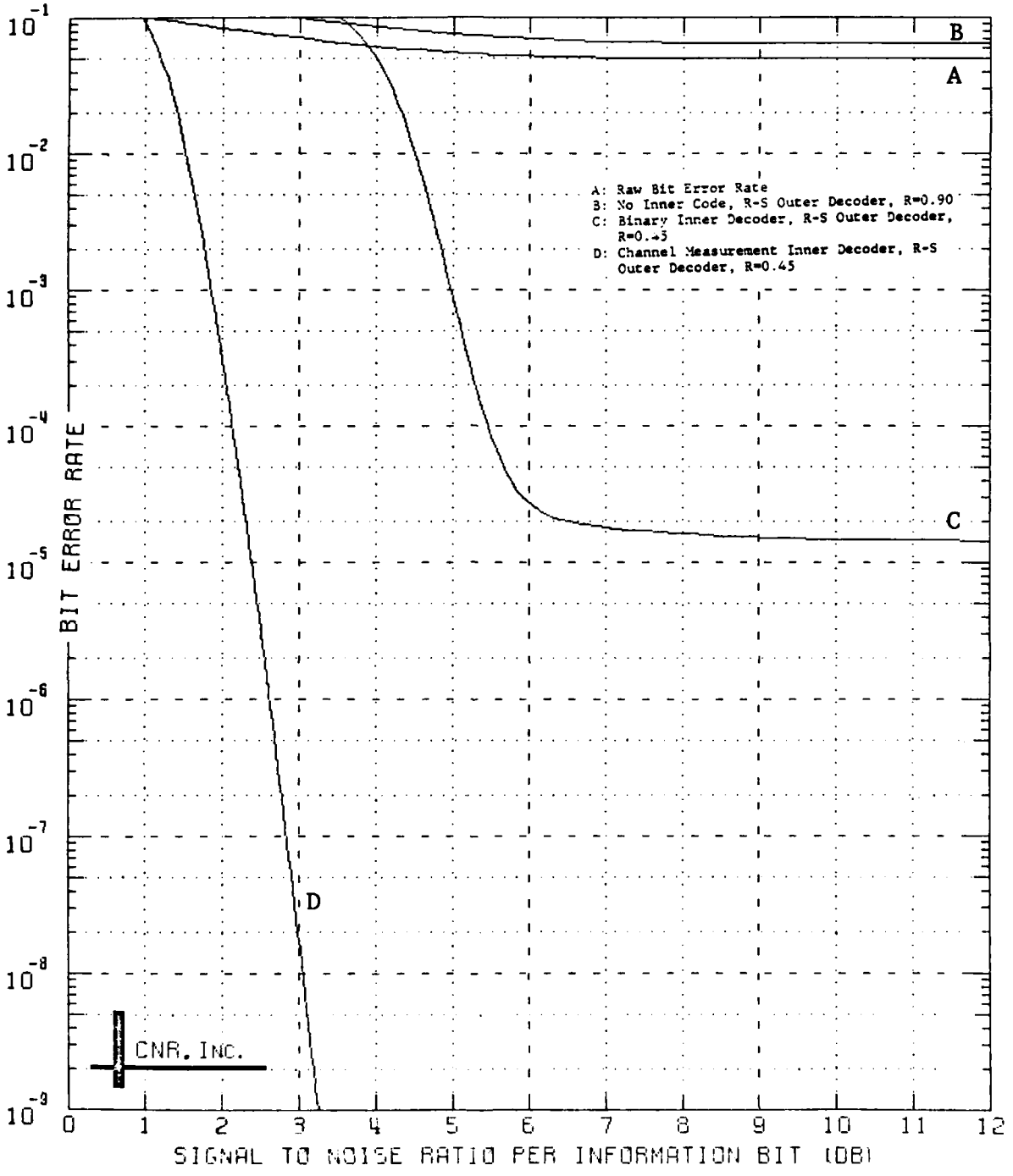


Figure 9.71 Decoded Performance of a Two-Stage Coding Approach
Outer Decoder: Reed-Solomon Code (40,36;5)
Symbol Interleaver Employed
Inner Decoder: Block Code (128,64;22)
δ=0.10 and Erasure Information Employed

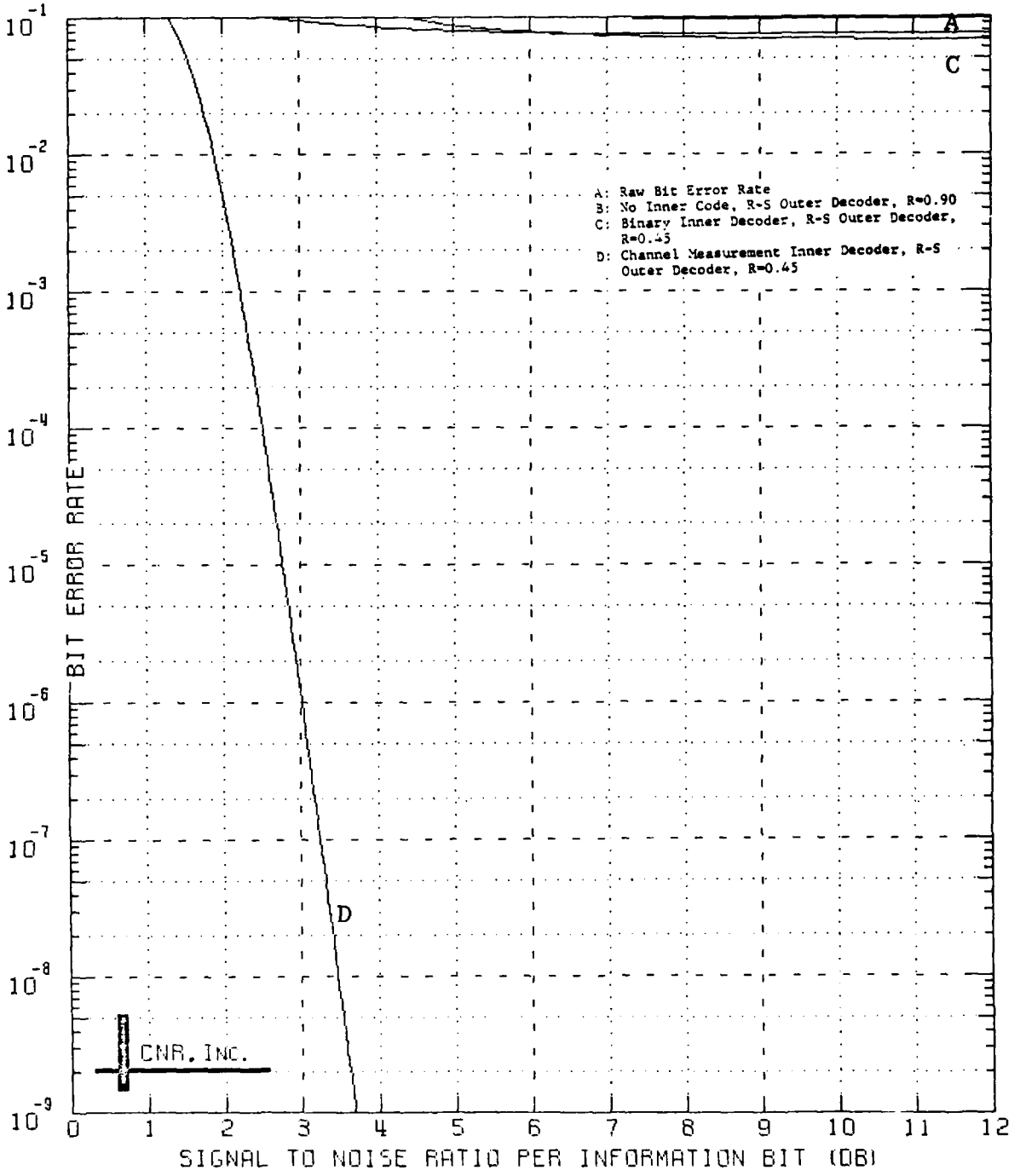


Figure 9.72 Decoded Performance of a Two-Stage Coding Approach
Outer Decoder: Reed-Solomon Code (40,36;5)
Symbol Interleaver Employed
Inner Decoder: Block Code (128,64;22)
δ=0.15 and Erasure Information is Employed

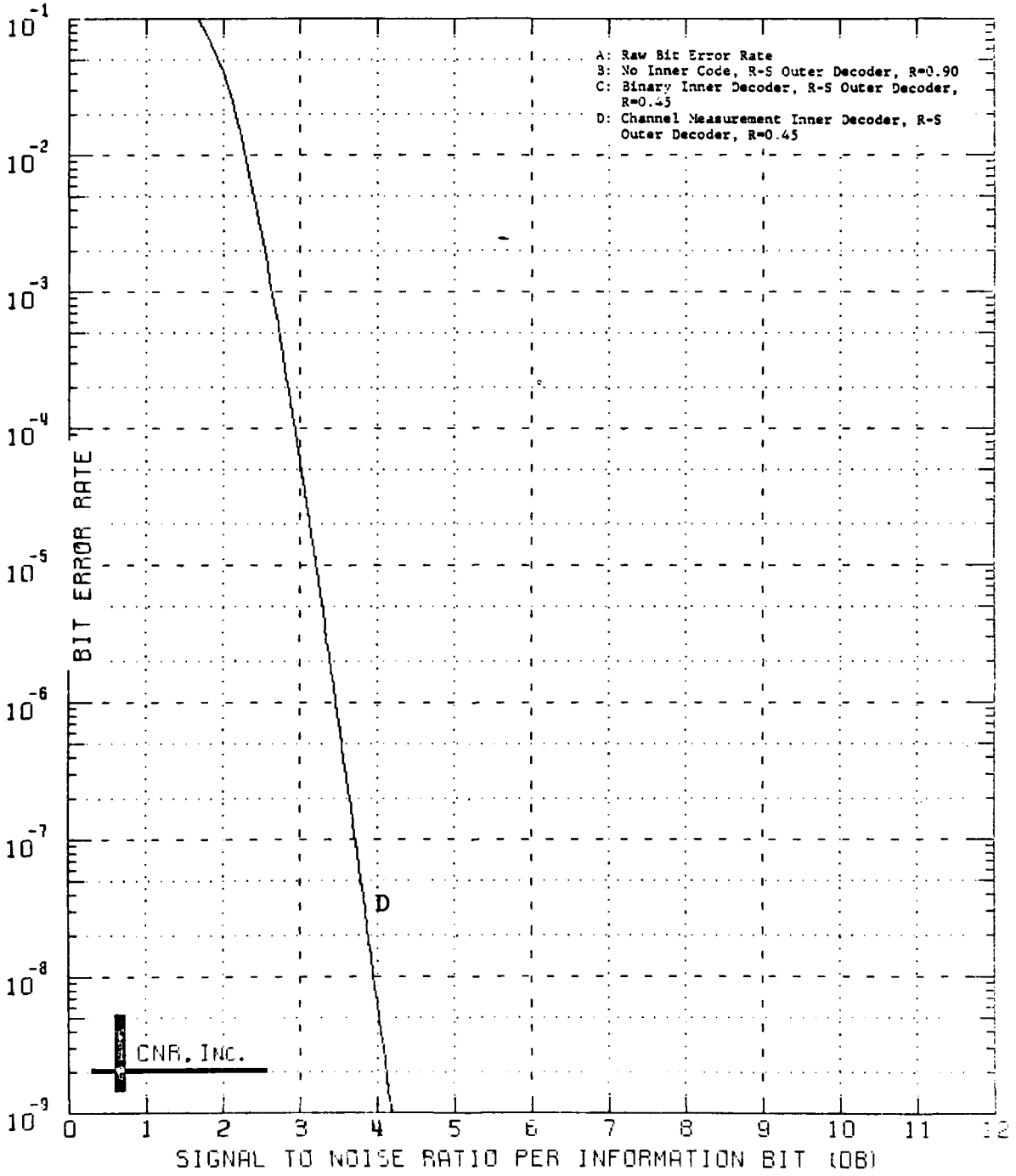


Figure 9.73 Decoded Performance of a Two-Stage Coding Approach
Outer Decoder: Reed-Solomon Code (40,36;5)
Symbol Interleaver Employed
Inner Decoder: Block Code (128,64;22)
δ=0.20 and Erasure Information is Employed

SECTION 10

CONCLUSIONS AND RECOMMENDATIONS FOR FUTURE WORK

The results presented in this report indicate that burst error-correcting codes can be critical components in certain multiple-access and adaptive array systems. With the need for burst error-correcting codes firmly established, a thorough investigation of these codes has been conducted. The interference models used in this investigation are considered to be worst-case models which include random errors as well as intervals where the data is completely destroyed by the assumed interference. Thus, all codes considered are capable of correcting burst errors in the presence of a dense background of random errors. Codes of this nature are applicable to a wide variety of ECCM digital communications systems.

A fundamental result obtained is that essentially error-free communications is possible even when large portions of the data are completely destroyed by interference. For example, with an average of 20% of the data destroyed, an uncoded system is limited to a bit error rate of 10^{-1} regardless of the available SNR. Systems employing burst-correcting codes are capable of yielding an error rate below 10^{-5} at a signal-to-noise ratio measured during the burst-free interval of only 7 dB. As an example, see Figures 5.18, 6.18, 6.23, 7.5, 8.9, and 9.10. The coding gain, defined as the difference in the required SNR between an uncoded and coded system needed to achieve 10^{-5}, is infinite in these examples. While typical coding gains in the presence of just additive noise are in the 5-dB range, coding gains in the presence of interference of 20 dB or more are to be expected. This is even valid for less severe interference models, as discussed in Appendix A.

In a noninterference Gaussian noise environment, the rate-1/2, constraint length 7, convolutional code with three bits of quantization has become an accepted choice. When interference is present, the need for lower rate codes is illustrated directly by the performance results presented. Furthermore, as indicated in Appendix B, the choice of a three-bit soft-decision statistic is not always sufficient in the presence of interference. For this reason, all decoding results are for the unquantized channel

and, thus, the decoders are denoted as channel measurement decoders. If available, erasure information indicating the location of the data that is destroyed by interference can be even more important than soft-decision information when a significant portion of the data is destroyed by interference.

Bounded distance decoding, i.e., decoding based on the minimum Hamming distance, of block codes is an accepted technique for correcting random errors and erasures. The results in Section 5 for the Golay code indicate the importance of true maximum-likelihood decoding, if feasible, when operating in the presence of interference with external erasure information.

The importance of two-stage coding approaches is also enhanced in the presence of interference. The results obtained indicate that a considerably higher percentage of data destroyed by interference can be tolerated if a two-stage coding approach is used instead of a single code of equivalent rate. Coding techniques, such as those discussed in Sections 7 and 8, should be suitable for applications which require a minimum overhead for coding protection against interference.

A quite surprising result obtained is that high-rate BCH codes may be more effective as outer codes in two-stage coding approaches than Reed-Solomon (R-S) codes. The results in Section 4.5 and Sections 7, 8, and 9 indicate that this conclusion is not only true for the interference channel, but even true for a channel with just random errors. The rate-0.9 (240,216;7) BCH code was found to be particularly effective as an outer code. Even the more powerful rate-1/2 outer codes, based on the (128,64) BCH code and the constraint length 7 convolutional code, generally offer inferior performance to this simple rate-0.9 BCH code.

In general, we note that an error-correcting code must span a period greater than the duration of the interference to be effective [10.1],[10.2]. Bit and symbol interleaving, as discussed in Sections 4 and 9, represent an effective approach. The adaptive techniques, discussed in Sections 4 and 7, represent an approach for applications where the decoding delay must be minimized. It should be noted, though, that for certain modulation formats and jamming threats the need for interleaving is minimal. As an example, frequency hopping in the presence of partial band interference yields independent symbol errors; thus, interleaving is required only if symbol errors are to be randomized.

In order to illustrate that these burst error-correcting codes are also cost-effective, an integrated-circuit (IC) count has been compiled in Table 10-1 for several of the coding approaches analyzed in this report. A maximum data rate is also given with each estimate, since in most coding applications the complexity is closely related to the maximum data rate required. Refinements of these estimates can be obtained when the exact amount of interleaving, synchronization requirements, and other system requirements are known. The background material needed to obtain these estimates is given in [10.1], [10.2], and [10.3].

As a note of caution, the maximum effectiveness of burst error-correcting codes is obtained if the coding is designed as an integral part of the system and not added to an existing system to correct a deficiency against certain ECM threats. For the new versatile multiple-access system introduced in Section 2, the waveforms and the system throughput are functions of the actual coding technique considered. For an adaptive array system, erasure and soft-decision information may be available to the decoder. If this information is available, significant performance gains over straight binary decoding is feasible. Fortunately, the four interference models considered in this report enable systems engineers to use the results presented for improving existing digital communications systems as well as for designing new systems.

Many new topics were treated in this report, with the results in almost every Section worthy of future development. However, the most exciting prospect for future work is to directly apply the concepts discussed in this report and other ECCM concepts to an actual communications network requiring multiple-access and ECCM capabilities.

TABLE 10-1

CODING HARDWARE ESTIMATES

Coding Approach	Number of IC's	Maximum Data Rate
Rate-0.9 (240,216;7) BCH Code - Binary Decoding	150	10 Mb/s
Rate-1/2 K=7 Convolutional Code - Maximum-Likelihood Decoding	400	10 Mb/s
Rate-1/2 K=7 Convolutional Code - Maximum-Likelihood Decoding	150	100 kb/s
Rate-1/2 (128,64;22) BCH Code - Binary Decoding	200	10 Mb/s
Rate-1/2 (24,12;8) Golay Code - Maximum-Likelihood Decoding	100	500 kb/s

REFERENCES

[10.1] CNR, Inc., "Troposcatter Interleaver Study Report," RADC-TR-75-19, Phase Report for Rome Air Development Center, February 1975, A008523.

[10.2] CNR, Inc., "Coding/Mux Overhead Study," RADC-TR-75-71, Final Technical Report for Rome Air Development Center, March 1975, A009174.

[10.3] CNR, Inc., "Demod/Decoder Integration," RADC-TR-78-70, Final Technical Report for Rome Air Development Center, April 1978, A053685.

APPENDIX A

EVALUATION OF CONVOLUTIONAL CODES FOR AN AVERAGE POWER-LIMITED PULSE JAMMING MODEL

1. Introduction

The purpose of this appendix is to illustrate that an average power-limited pulse jamming model yields considerably better results than those obtained by our worst-case model. Results for rate-1/2 and rate-1/4 convolutional codes are obtained to demonstrate this point.

2. Channel Model

A two-level jammer, operating at J_{max} with probability δ and J_{min} with probability $(1-\delta)$, and satisfying the following equation,

$$J_{avg} = \delta J_{max} + (1 - \delta)J_{min} \tag{1}$$

is assumed. For a given value of

$$\frac{J_{min}}{J_{avg}} \tag{2}$$

the ratio

$$\frac{J_{max}}{J_{avg}} = \frac{1 - \frac{J_{min}}{J_{avg}} (1 - \delta)}{\delta} \tag{3}$$

is fixed. It is of interest to determine the values of (2) and (3) (or, equivalently, the value of δ) for which the K=7 convolutional code offers the worst possible performance. The jammer power is assumed inversely proportional to E_b/N_0 so that

$$\frac{E_b}{N_0}(\max) = \frac{\frac{E_b}{N_0}(\text{avg})}{\frac{J_{min}}{J_{avg}}} \tag{4}$$

and

$$\frac{E_b}{N_0}(\min) = \frac{\frac{E_b}{N_0}(\text{avg})}{\frac{J_{max}}{J_{avg}}} \tag{5}$$

This assumption is valid for certain pseudo-noise spread-spectrum systems as well as a simple linear system with jammer noise dominating. For the special case when we have an on-off jammer ($J_{min} = 0$), we assume

$$\frac{E_b}{N_0}(\max) \to \infty \tag{6}$$

and

$$\frac{E_b}{N_0}(\min) = \delta \frac{E_b}{N_0}(\text{avg}) \tag{7}$$

3. Performance Bounds

Following the analyses given in Section 4, the probability of a bit error for convolutional codes can be upper bounded in terms of the probability of error between two sequences of Hamming distance d, $P_e(d)$, by

$$P_e < \sum_{d=d_f}^{\infty} a_d \, P_e(d) \tag{8}$$

where d_f is the minimum free distance of a given convolutional

code and a_d is the total number of information bit errors occurring in all sequences of Hamming distance d away from the transmitted sequence.

For binary decoding, assuming statistically-independent errors, we can write

$$P_e(d) = \sum_{i=\frac{d+1}{2}}^{d} \binom{d}{i} p_I^i (1 - p_I)^{d-i} \quad ; \quad d \text{ odd} \tag{9}$$

and

$$P_e(d) = \frac{1}{2} \binom{d}{d/2} p_I^{d/2} (1 - p_I)^{d/2} + \sum_{i=\frac{d}{2}+1}^{d} \binom{d}{i} p_I^i (1 - p_I)^{d-i} \quad ; \quad d \text{ even} \tag{10}$$

For the K=7 case, Eq. (10) will be applicable. The probability P_I is the average interference probability given by

$$P_I = \delta\, Q\left[\sqrt{2R \frac{E_b}{N_0}(\min)}\right] + (1 - \delta)\, Q\left[\sqrt{2R \frac{E_b}{N_0}(\max)}\right] \tag{11}$$

and R is the code rate. For the special on-off case,

$$P_I = \delta\, Q\left[\sqrt{2R \frac{E_b}{N_0}(\text{avg})\ \delta}\right] \tag{12}$$

Results for this case are given on Figures 1 and 2 with δ shown in 0.05 increments. Note that the worst-case value of δ is a function of the available $\frac{E_b}{N_0}(\text{avg})$.

For channel measurement decoding, the probability of errors between two sequences of Hamming distance d is given by

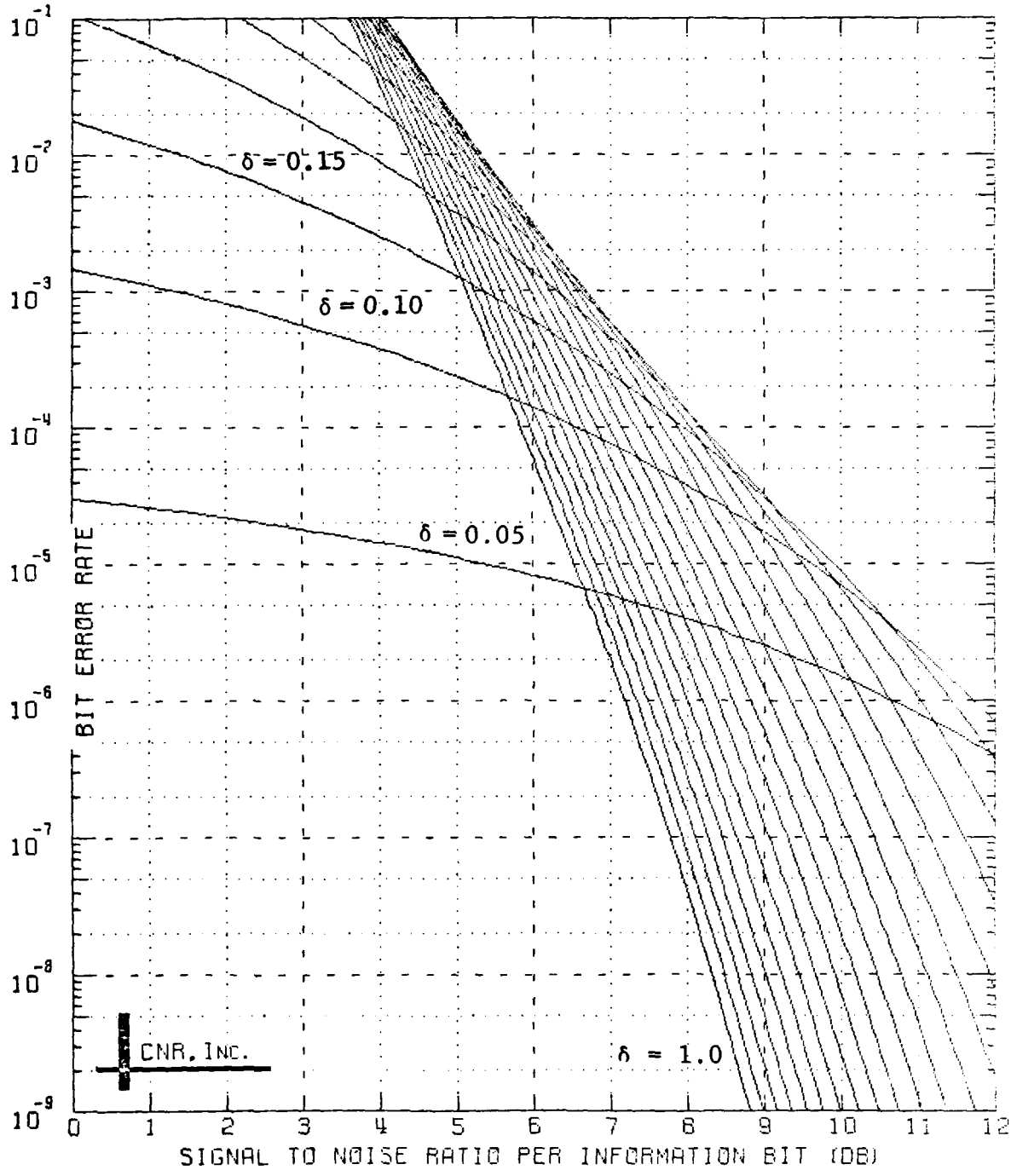


Figure 1 Rate-1/2, K = 7, Binary-Decoding, Average Power-Limited Pulse Jammer Model

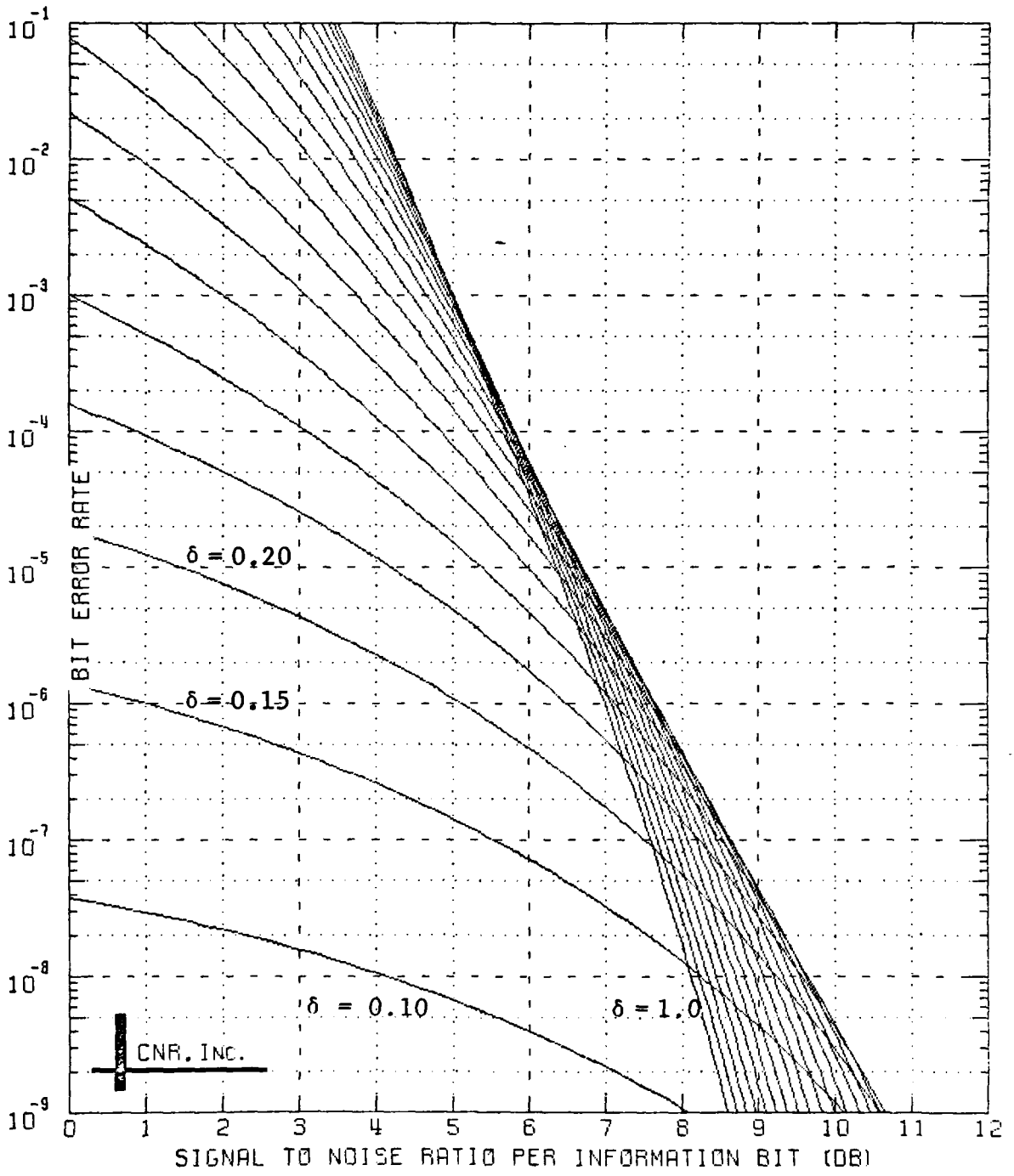


Figure 2 Rate-1/4, K = 7, Binary-Decoding, Average Power-Limited Pulse Jammer Model

$$P_e(d) = \Pr[p(\underline{y}|\underline{\hat{x}}_{m'}) > p(\underline{y}|\underline{\hat{x}}_m)] \tag{13}$$

where, for a Gaussian channel,

$$p(\underline{y}|\underline{x}_m) = \frac{\exp\left\{-\sum_i \frac{\left(y_i - \hat{x}_{m_i}\right)^2}{N_0}\right\}}{\prod_i (\pi N_0)} \tag{14}$$

is the conditional probability density function for the transmitted sequence, and $p(\underline{y}|\underline{\hat{x}}_{m'})$ is the corresponding function for the sequence of distance d from the transmitted sequence. The received decision statistic is

$$y_i = x_{m_i} + n_i \tag{15}$$

which, for convenience, will be assumed such that x_{m_i} is positive for all i. The mean square value of x_{m_i} is a variable with

$$x_{m_i}^2 = \begin{cases} R\,E_b(\max) & - \text{ probability } (1 - \delta) \\ R\,E_b(\min) & - \text{ probability } \delta \end{cases} \tag{16}$$

and the (received) estimated mean square value is

$$\left(\hat{x}_{m_i}\right)^2 = R\,E_b(\text{avg}) \tag{17}$$

which is constant for all values of i. The noise has a constant variance given by $N_0/2$. Note that the signal-to-noise ratio performance curves are in terms of $E_b/N_0(\text{avg})$, which is actually <u>not</u> the average of the two signal-to-noise ratios given in (16).

Equation (13) can be simplified by taking logs and dropping irrelevant terms so that we can write

$$P_e(d) = \Pr\left[\sum_i y_i\left(\hat{x}_{m_i} - \hat{x}_{m_i'}\right) < 0\right] \tag{18}$$

The relevant terms in (18) are composed only of the d terms with i such that $\hat{x}_{m_i} \neq \hat{x}_{m_i'}$.

The case when μ symbols have the minimum value of E_b/N_0 and $(d - \mu)$ have the maximum value of E_b/N_0, occurs with probability

$$p(\mu) = \binom{d}{\mu} \delta^{\mu}(1 - \delta)^{d-\mu} \tag{19}$$

Writing the above as a conditional probability yields

$$P_e(d|\mu) = \Pr\left[\mu\sqrt{E_b(\min)\ R} + (d - \mu)\sqrt{E_b(\max)\ R} + \sum_{i=1}^{d} n_i < 0\right] \tag{20}$$

The term

$$\left(\hat{x}_{m_i} - \hat{x}'_{m_i}\right) = 2\sqrt{E_b(\text{avg})\ R} \tag{21}$$

is factored out of (20).

The conditional probability of an error between two sequences can thus be written as

$$P_e(d|\mu) = Q\left\{\sqrt{\frac{\left[\mu\sqrt{E_b(\min)\ R} + (d - \mu)\sqrt{E_b(\max)\ R}\right]^2}{\frac{d N_0}{2}}}\right\} \tag{22}$$

with the unconditional probability of error given by

$$P_e(d) = \sum_{\mu=0}^{d} P(\mu)\ P_e(d|\mu) \tag{23}$$

For the special case where we have on-off jamming, $E_b(\max) \to \infty$, the only nonzero term in (23) occurs when $\mu = d$. Thus, we can write

$$P_e(d) = \delta^d\ Q\left[\sqrt{\frac{2\,d\,E_b(\text{avg})\,R\,\delta}{N_0}}\right] \tag{24}$$

Figures 3 and 4 illustrate the performance for this case. In the region above 10^{-5}, $\delta = 1$, i.e., the continuous jammer, is essentially the worst-case threat. This is considerably different than the results obtained in Section 6 for convolutional codes. Note that, for the worst-case model, the continuous jammer is represented by the $\delta=0$ case since additive noise is always present in addition to the completed destructive pulse interference.

For completeness, Figures 5, 6, and 7 illustrate the performance of an uncoded (raw bit error rate) system for this average power-limited jamming model. Comparing these results to the results given in Section 6 for the raw bit error rate (curve A), we note that the worst-case model yields an irreducible error of $\delta/2$ regardless of the value of E_b/N_0. For the average power-limited interference model, the probability of error always goes to zero as E_b/N_0 increases. The upper envelope of these curves, which represents the worst-case threats, decreases inversely with E_b/N_0 in a similar manner to that occurring on a Rayleigh fading channel. To obtain a probability of error of 10^{-5}, Figure 7 indicates that a signal-to-noise ratio of around 30 dB is required for the worst-case duty factor. The rate-1/4 coded results achieves 10^{-5} at a signal-to-noise ratio of around 4.5 dB. Thus, even for this interference model, coding gains on the order of 25 dB are feasible.

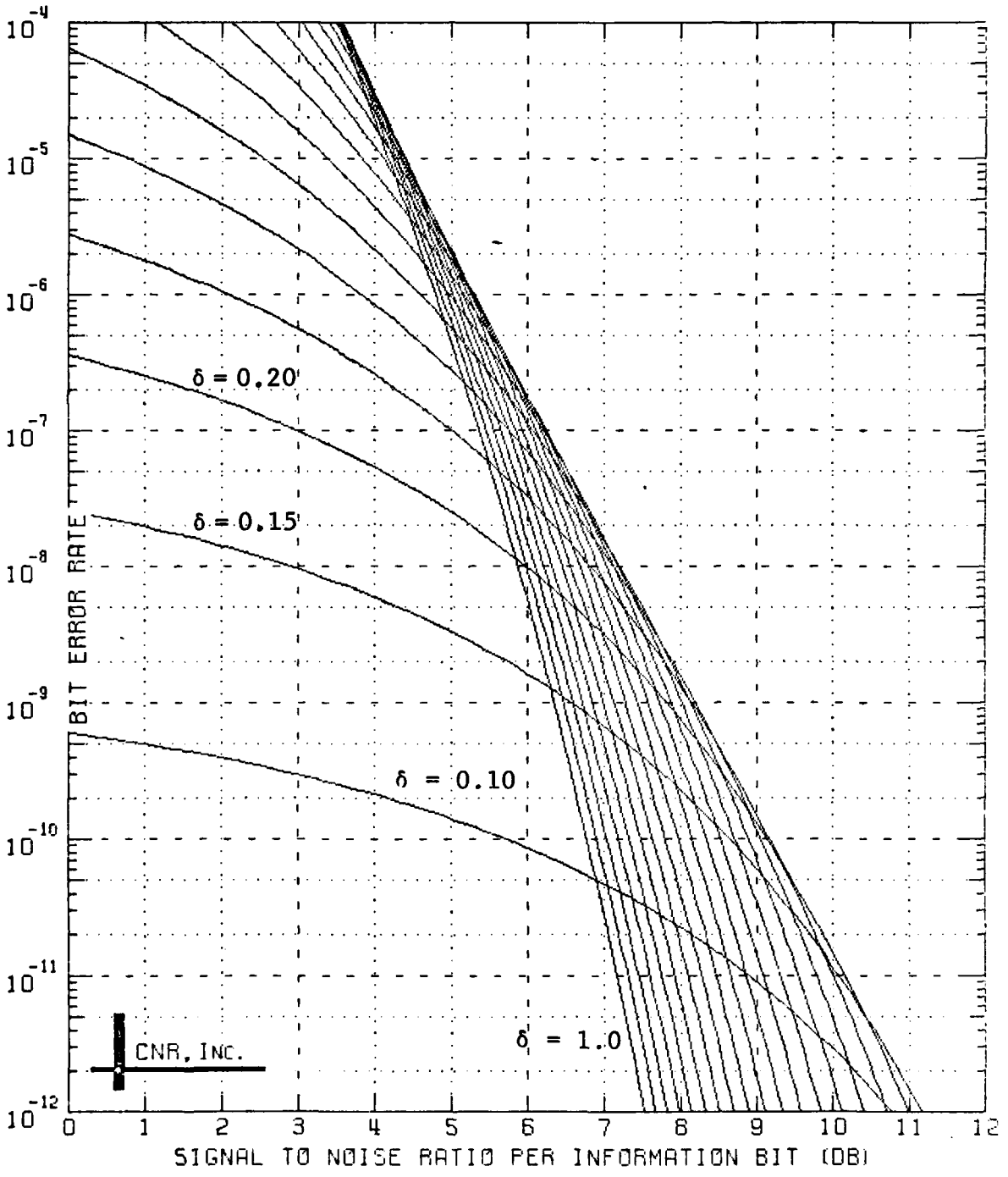


Figure 3 Rate-1/2, K = 7, Channel Measurement Decoding, Average Power-Limited Pulse Jammer Model

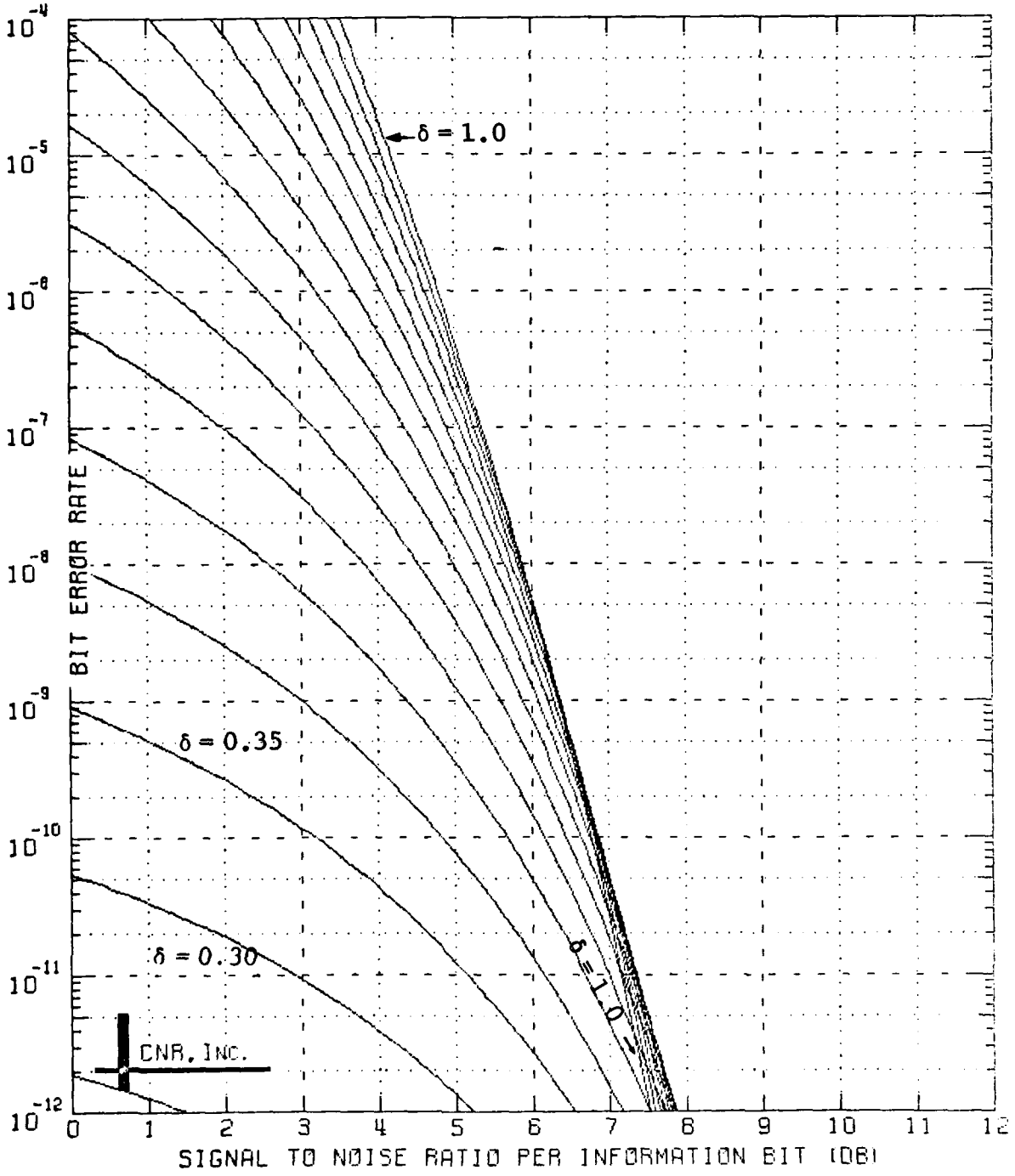


Figure 4 Rate-1/4, K = 7, Channel Measurement Decoding, Average Power-Limited Pulse Jammer Model

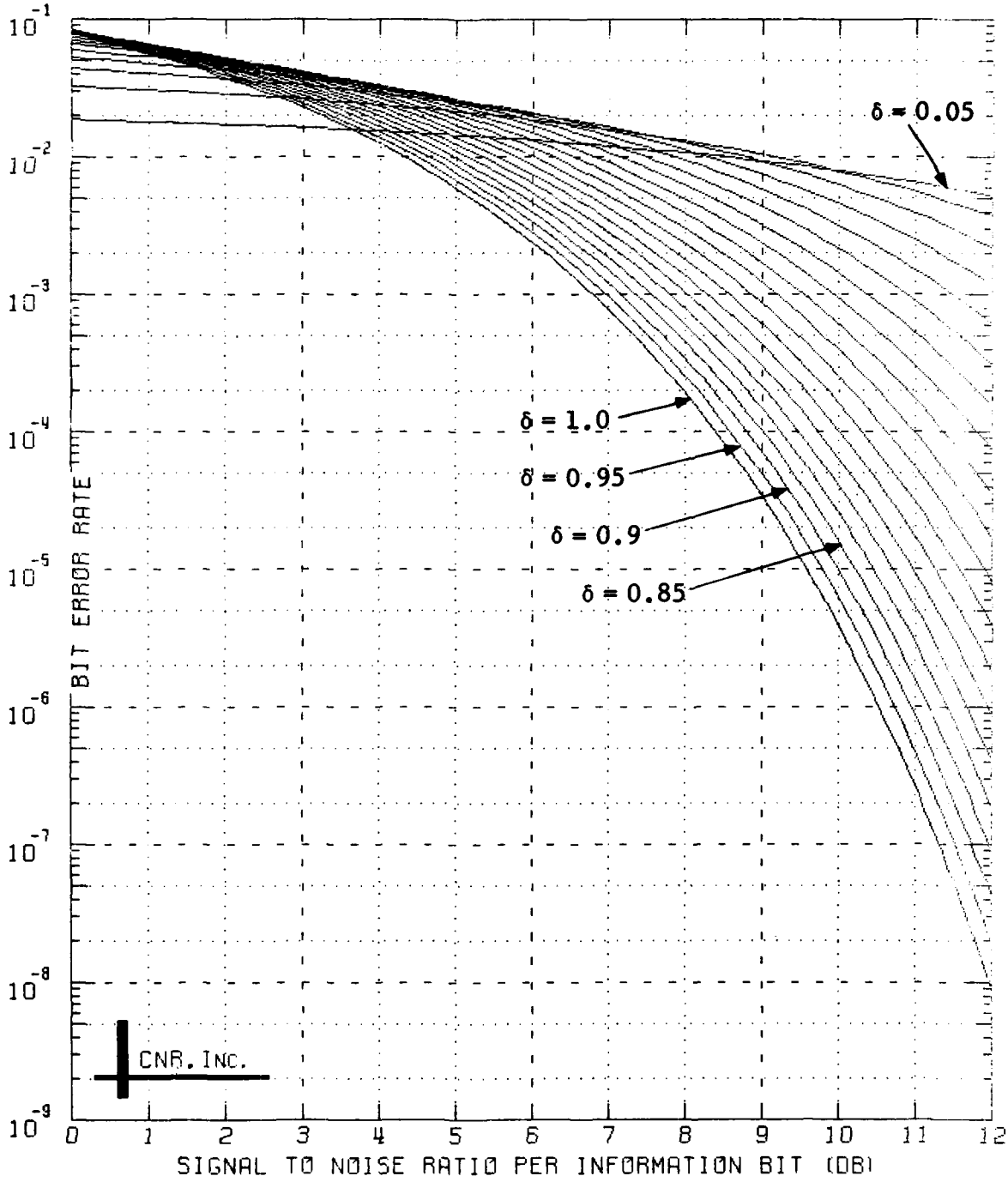


Figure 5 Performance of an Uncoded System for an Average Power-Limited Pulse Jammer Model

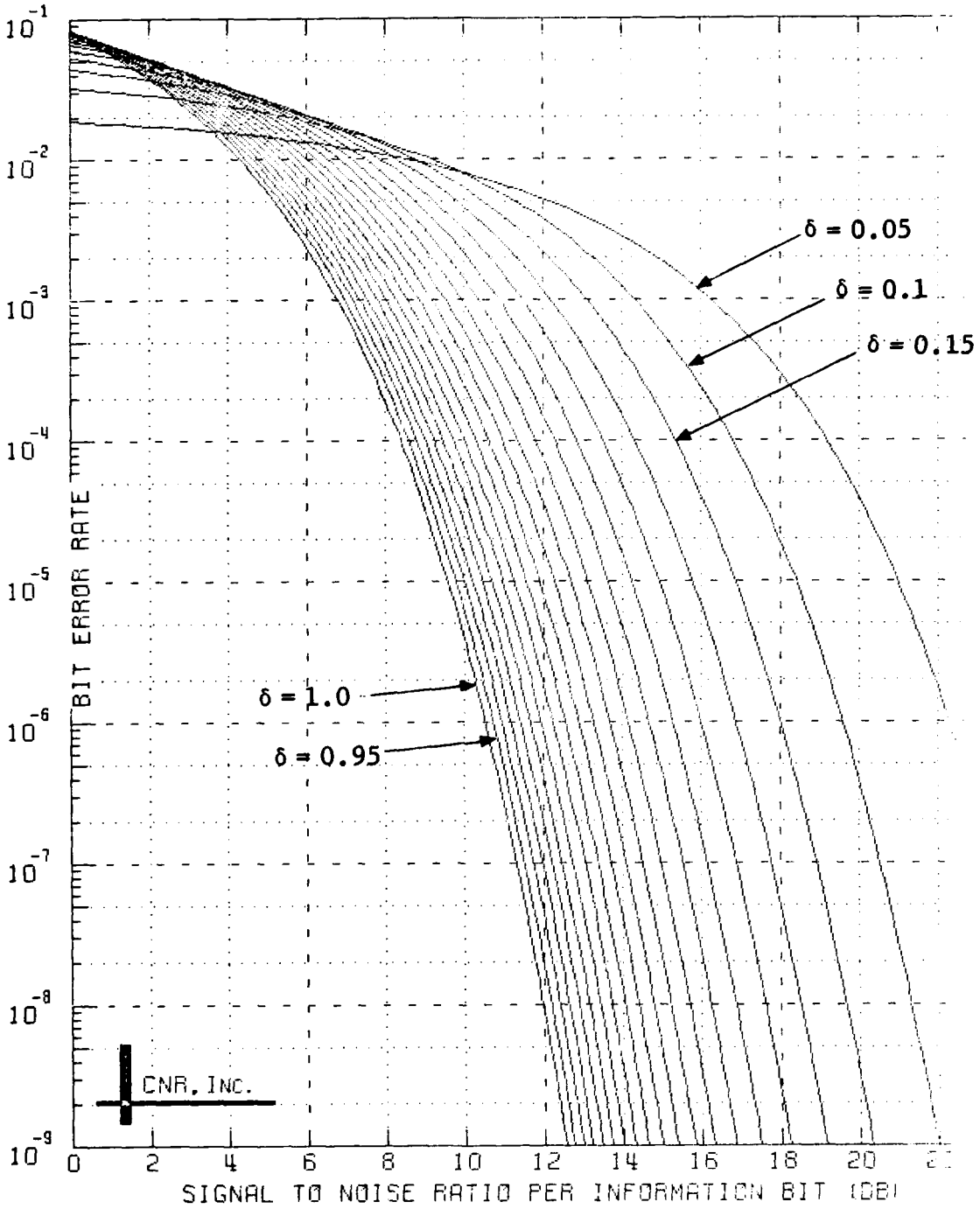


Figure 6 Performance of an Uncoded System for an Average Power-Limited Pulse Jammer Model (Expanded Scale)

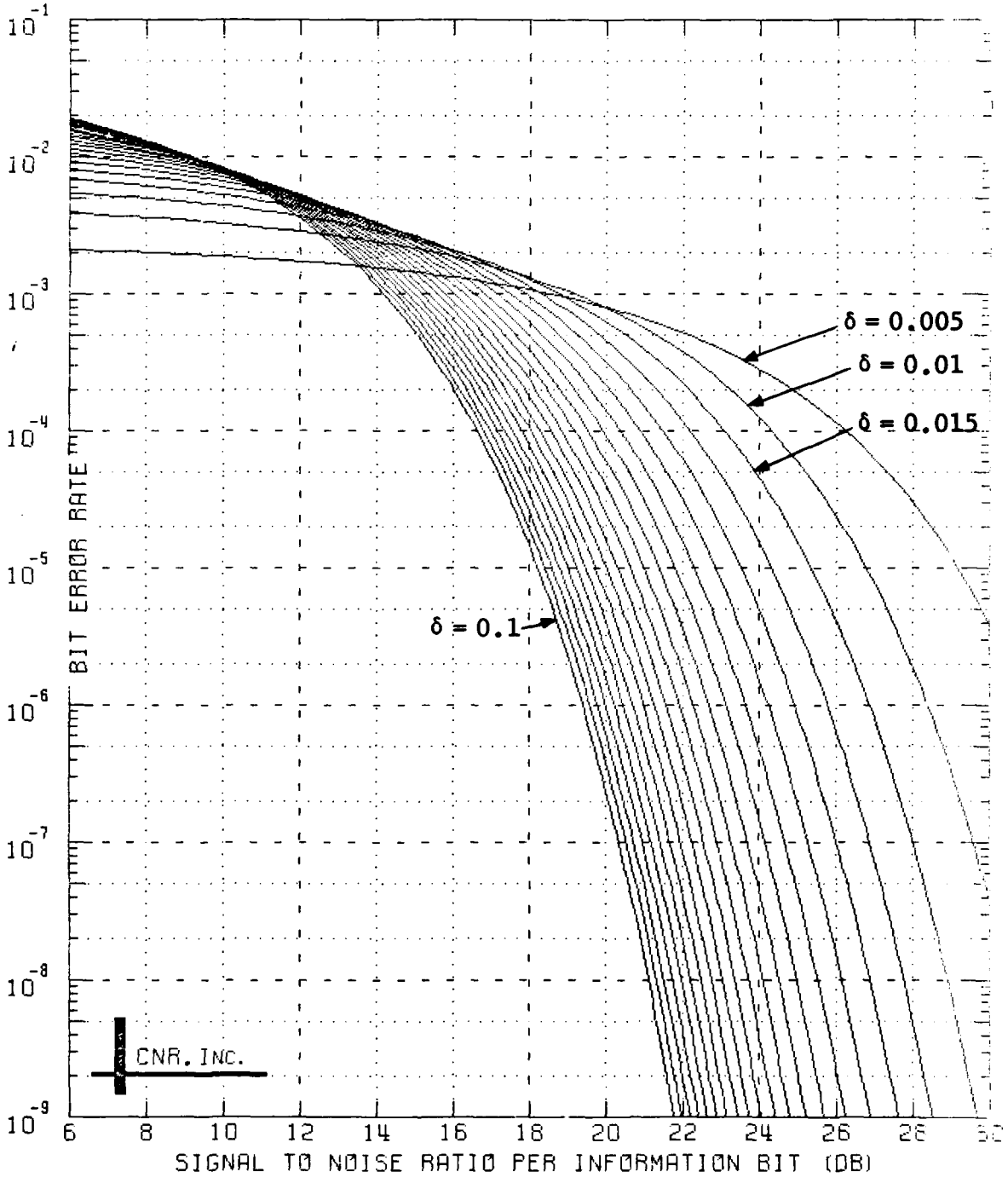


Figure 7 Performance of an Uncoded System for an Average Power-Limited Pulse Jammer Model (for $0.005 < \delta < 0.1$ with $\Delta\delta = 0.005$)

APPENDIX B

EFFECTS OF QUANTIZATION ON THE PERFORMANCE OF CONVOLUTIONAL CODES IN THE PRESENCE OF INTERFERENCE

1. Introduction

In this report the performance of convolutional codes has been obtained for an unquantized receiver. Clearly, it is also of interest to investigate the effects of finite quantization due to an A/D converter such as shown on Figure 1. An interesting question is to determine whether the standard 0.25 dB loss [3] due to 3-bit quantization for the Gaussian channel is also valid in the presence of interference. We will examine the further improvements offered by 4- and 5-bit quantization to determine the number of quantization levels required to achieve satisfactory performance. A brief discussion of the tightness of the bounds we will be using is in order and comparisons with exact results will be shown.

2. Derivation of the Bounds

The first step in determining the soft-decoding bounds is to obtain $P_e(d)$ - the probability of error between two sequences of Hamming distance d. Without loss of generalization, we may assume that the all-zero word is transmitted. Furthermore, since CPSK modulation is used throughout, we assume that a +1 is transmitted for the code symbol 0 and a -1 for the code symbol 1. Once $P_e(d)$ has been obtained, we can make use of the following bound on the bit error probability for convolutional codes:

$$P_e < \sum_{d=d_f}^{\infty} a_d P_e(d) \tag{1}$$

where d_f is the free distance of the code and a_d is the total number of bit errors in all adversaries of weight (distance) d.

An exact expression for $P_e(d)$ can be written [1],

$$P_e(d) = \sum_{y \in Y_d} \prod_{i=1}^{d} P(y_i | x_i = +1) \tag{2}$$

where x_i and y_i are the i^{th} transmitted and received symbols, respectively. $x_i \in \{+1,-1\}$ and $y_i \in Q$ where Q is the set of quantization levels, $Q = \{q_{-\ell},\ldots,q_{-1},q_{+1},\ldots,q_{+\ell}\}$, Y_d is the subspace of all vectors $y = (y_1,y_2,\ldots,y_d)$ for which errors will occur. $P(y_i|x_i)$ is the conditional transition probability of quantizing to level y_i given that symbol x_i was transmitted.

Using Eq. (2) does not constitute an efficient approach to calculate $P_e(d)$ because of the size of the set Y_d. The total space of received vectors, Y, includes all vectors of weight d and there are $(2\ell)^d$ of them if 2ℓ-level quantization is employed. Approximately half of those vectors belong to Y_d. As an example, consider the R=1/2, K=7, convolutional code with 3-bit (8-level) quantization. This code has $d_f = 10$ and we must, therefore, examine on the order of $8^{10} \approx 10^9$ vectors just to evaluate the first term in Eq. (1). In practice, use of Eq. (2) becomes prohibitive for $d > 6$ because of the excessive computation time required.

Since we are using maximum likelihood decoding, we can immediately write an expression for $P_e(d)$ in terms of the likelihood ratios [1],

$$P_e(d) = \Pr\left\{\prod_{i=1}^{d} \frac{P(y_i|x_i=-1)}{P(y_i|x_i=+1)} > 1\right\} \qquad (3)$$

where the RHS of Eq. (3) is simply the probability of the incorrect sequence being more likely than the correct sequence. The set Y_d can be considered to consist of all vectors for which

$$\prod_{i=1}^{d} \frac{P(y_i|x_i=-1)}{P(y_i|x_i=+1)} > 1 \qquad (4)$$

and we can, therefore, state the following bound:

$$P_e(d) < \sum_{y\in Y_d} \prod_{i=1}^{d} P(y_i|x_i=+1)\left[\frac{P(y_i|x_i=-1)}{P(y_i|x_i=+1)}\right]^{1/2} \qquad (5)$$

$$< \sum_{y\in Y} \prod_{i=1}^{d} P(y_i|x_i=+1)^{1/2} P(y_i|x_i=-1)^{1/2} \qquad (6)$$

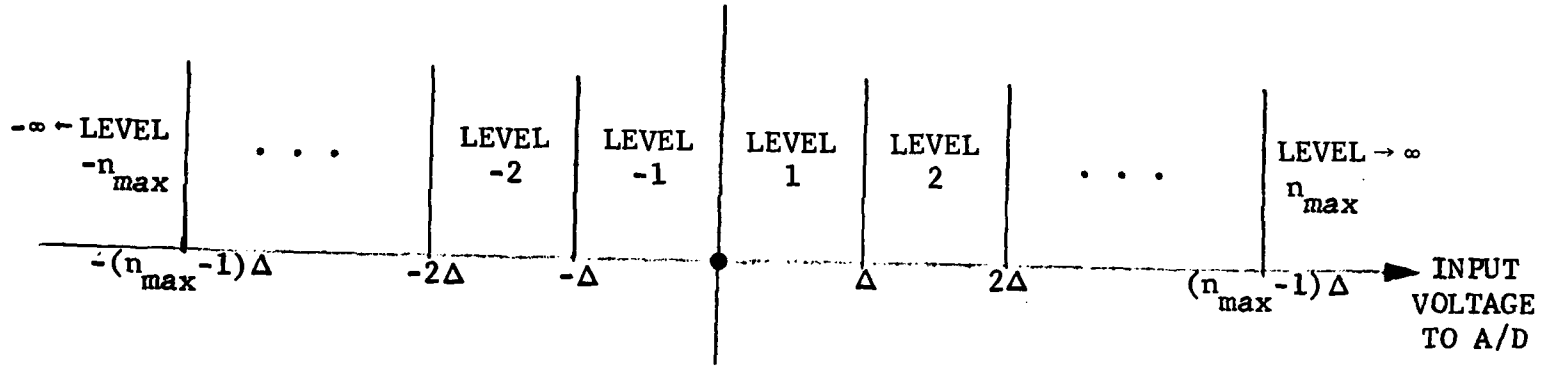


Figure 1 Received Levels for an A/D Converter

The first inequality follows from the fact that we are multiplying each term in the sum by a number greater than one and the second inequality comes about because we have enlarged the set of vectors to be considered. The sum in Eq. (6) is a d-dimensional sum which may be expanded into d one-dimensional sums, each ranging over the set Q. Finally, we may write

$$P_e(d) < \sum_{y_1 \epsilon Q} \sum_{y_2 \epsilon Q} \cdots \sum_{y_d \epsilon Q} \prod_{i=1}^{d} P(y_i|x_i=+1)^{1/2}$$

$$\cdot P(y_i|x_i=-1)^{1/2} \tag{7}$$

$$= \prod_{i=1}^{d} \sum_{y_i \epsilon Q} P(y_i|x_i=+1)^{1/2} \, P(y_i|x_i=-1)^{1/2} \tag{8}$$

The bound implied by Eq. (8) will be used to generate performance estimates for convolutional codes.

One other bounding technique is worth a brief mention. Consider the following Chernoff bound [2],

$$P_e(d) = \Pr\left\{\sum_{i=1}^{d} y_i < 0\right\} \leq \left[E\left(e^{\lambda_0 y_i}\right)\right]^d, \quad \overline{y_i} > 0 \tag{9}$$

where the optimum value of λ_0 can be determined by solving $E\left(y_i e^{\lambda_0 y_i}\right) = 0$. This bound is much weaker than the previous one considered and thus is not of much use for the present application.

3. Results and Conclusions

Using the bound from Eq. (8) in conjunction with the bit error rate bound from Eq. (1), the performance of the R=1/2, K=7, convolutional code was investigated. Results for 3-, 4-, and 5-bit quantizations are shown in Figures 2 to 10. A few observations are worth developing. Notice that there is significant loss in performance for high signal-to-noise ratios when erasure information is not employed. It is also interesting that 3-bit quantization does not offer satisfactory

performance for high SNR while 4-bit quantization performs considerably better. When erasure information is employed, the effects of quantization are not significant and the standard 0.25 dB loss can be expected.

There is some question as to how tight the bound from Eq. (8) really is. In order to investigate the tightness of the bound, comparisons were made with results from Eq. (2) for the R=1/2, K=3 convolutional code. This code has free distance of 5 and all comparisons must be based on the use of only two terms from Eq. (1). Figures 11 to 15 show the results of using both Eq. (2) and Eq. (8) in Eq. (1) with only two terms. Clearly the bound is not very tight, but even when Eq. (2) is used, there are considerable differences in the limiting error probabilities for the channel measurement and soft decoding results.

Table 1 shows the signal-to-noise ratios required to achieve a bit error rate of 10^{-5} for the K=7 convolutional code when 3-bit quantization is used. Results are shown for R=1/2, 1/4 and 1/8. Figures 16 and 17 graphically show the information in Table 1 and comparisons are made between the channel measurement decoding and soft decoding results.

4. Transition Probabilities

In order to evaluate the bounds that were discussed in previous sections, the conditional transition probabilities must be determined. The channel model assumed here is, of course, the interference model where a code symbol is destroyed by interference with probability δ. The quantization step size Δ must also be selected and near optimum values for several quantizers are given below:

Number of Quantizing Levels	Δ
2	Arbitrary
4	1.0σ
8	0.5σ
16	0.3σ
32	0.15σ

where σ^2 is the Gaussian noise variance. A general version of the quantizer is shown in Figure 1.

Note that when a symbol is destroyed by interference and erasure information is not employed, that symbol is assumed to have the Gaussian noise statistics.

The conditional probability of the n^{th} level being chosen is given by the following expressions:

1. $n = n_{max}$

$$P(n|+1) = (1-\delta)Q\left[\frac{(n-1)\Delta-\sqrt{E_s}}{\sigma}\right] + \delta Q\left[\frac{(n-1)\Delta}{\sigma}\right]$$

2. $1 \leq n < n_{max}$

$$P(n|+1) = (1-\delta)\left\{Q\left[\frac{(n-1)\Delta-\sqrt{E_s}}{\sigma}\right] - Q\left[\frac{n\Delta-\sqrt{E_s}}{\sigma}\right]\right\} + \delta\left\{Q\left[\frac{(n-1)\Delta}{\sigma}\right] - Q\left(\frac{n\Delta}{\sigma}\right)\right\}$$

3. $-n_{max} < n \leq -1$

$$P(n|+1) = (1-\delta)\left\{Q\left(\frac{n\Delta-\sqrt{E_s}}{\sigma}\right) - Q\left[\frac{(n+1)\Delta-\sqrt{E_s}}{\sigma}\right]\right\} + \delta\left\{Q\left(\frac{n\Delta}{\sigma}\right) - Q\left[\frac{(n+1)\Delta}{\sigma}\right]\right\}$$

4. $n = -n_{max}$

$$P(n|+1) = (1-\delta)\left\{1-Q\left[\frac{(n+1)\Delta-\sqrt{E_s}}{\sigma}\right]\right\} + \delta\left\{1-Q\left[\frac{(n+1)\Delta}{\sigma}\right]\right\}$$

The identity $P(n|+1) = P(-n|-1)$ holds for all values of n. To simplify notation, the Q-function, defined as

$$Q(x) \triangleq \frac{1}{\sqrt{2\pi}} \int_x^\infty e^{-\frac{t^2}{2}}\, dt$$

has been used.

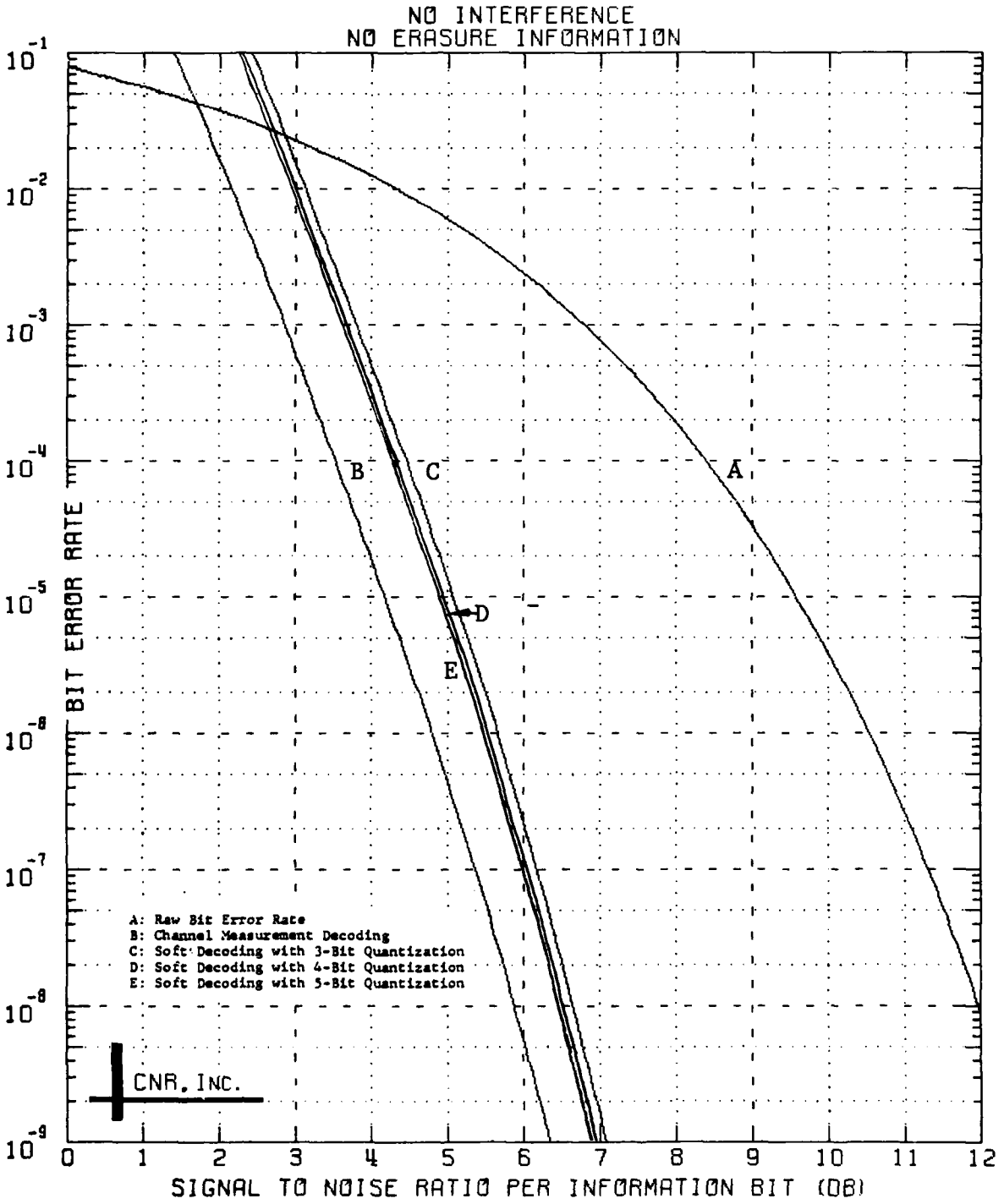


Figure 2 Decoded Performance of a Convolutional Code Rate 1/2; Constraint Length = 7; Gaussian Channel; CPSK Modulation

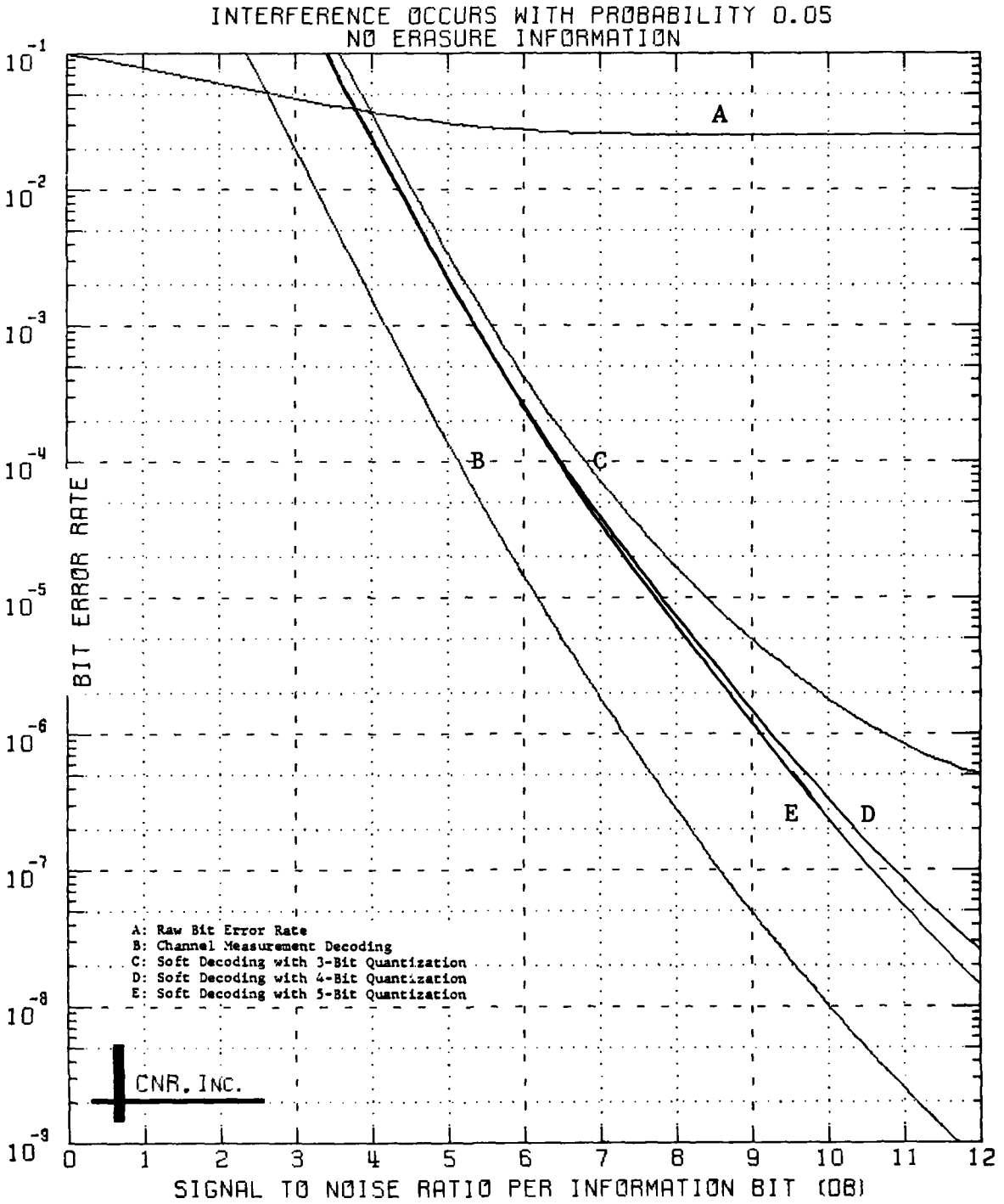


Figure 3 Decoded Performance of a Convolutional Code Rate 1/2; Constraint Length = 7; Gaussian Channel; CPSK Modulation

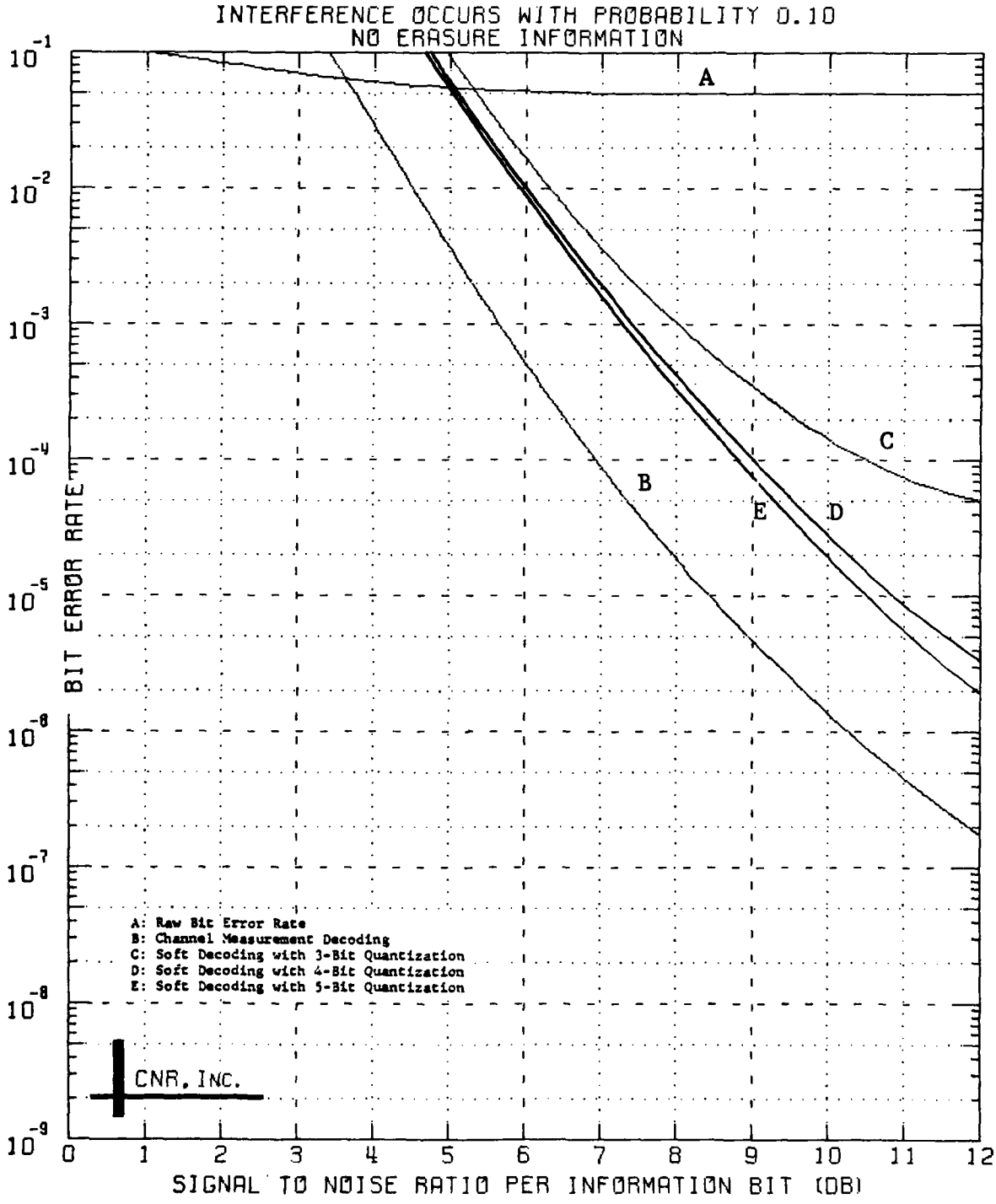


Figure 4 Decoded Performance of a Convolutional Code Rate 1/2; Constraint Length = 7; Gaussian Channel; CPSK Modulation

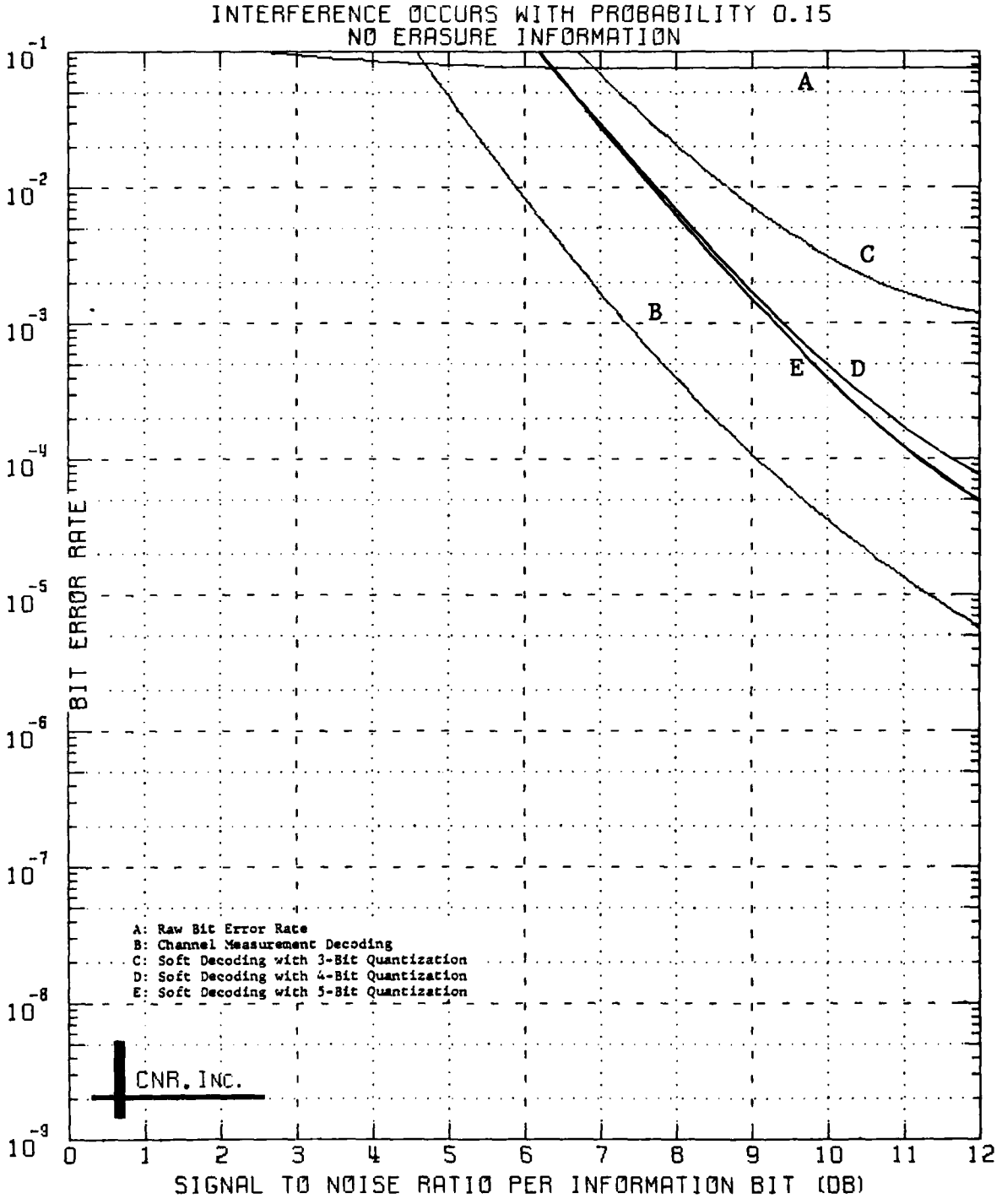


Figure 5 Decoded Performance of a Convolutional Code Rate 1/2; Constraint Length = 7; Gaussian Channel; CPSK Modulation

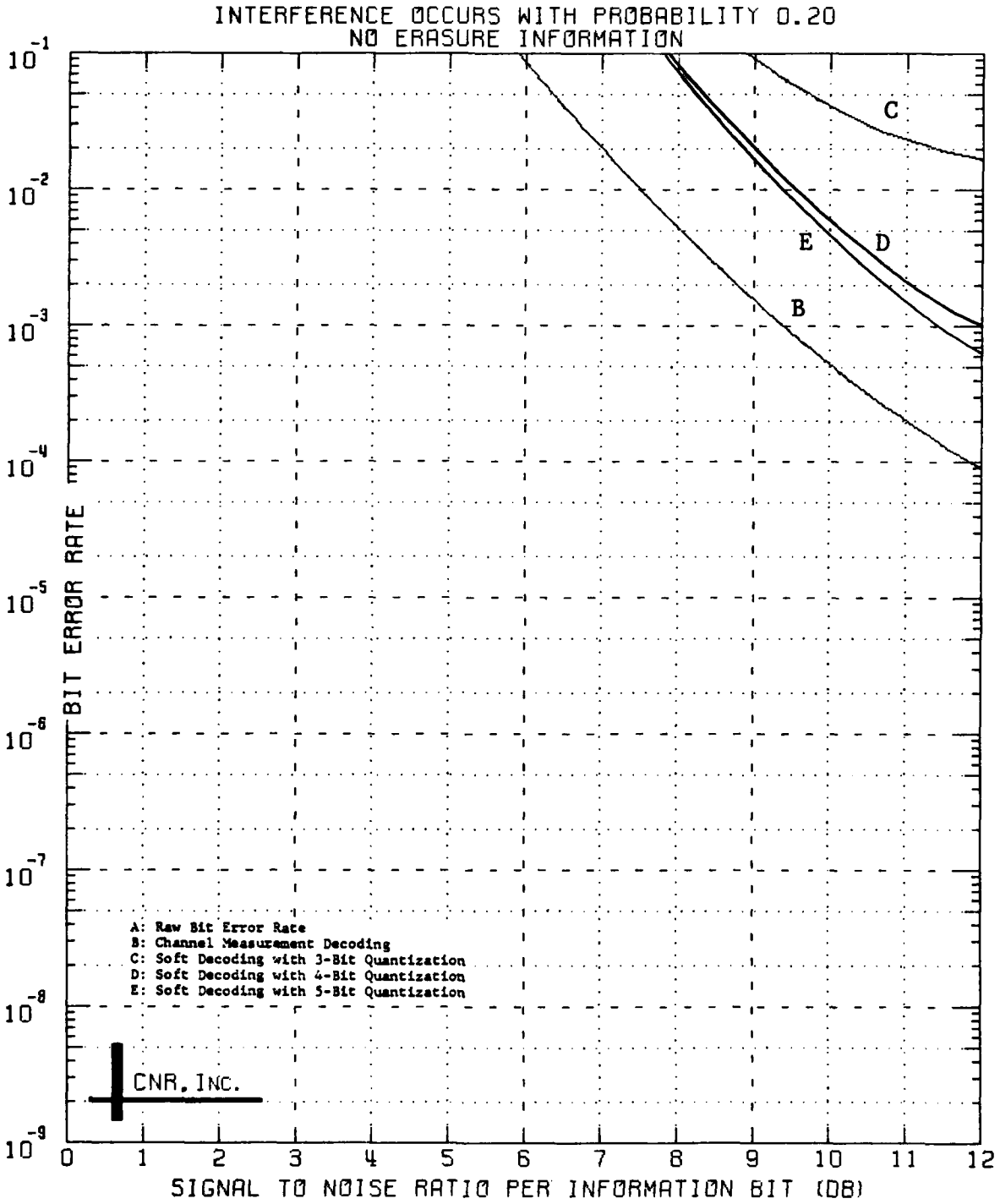


Figure 6 Decoded Performance of a Convolutional Code Rate 1/2; Constraint Length = 7; Gaussian Channel; CPSK Modulation

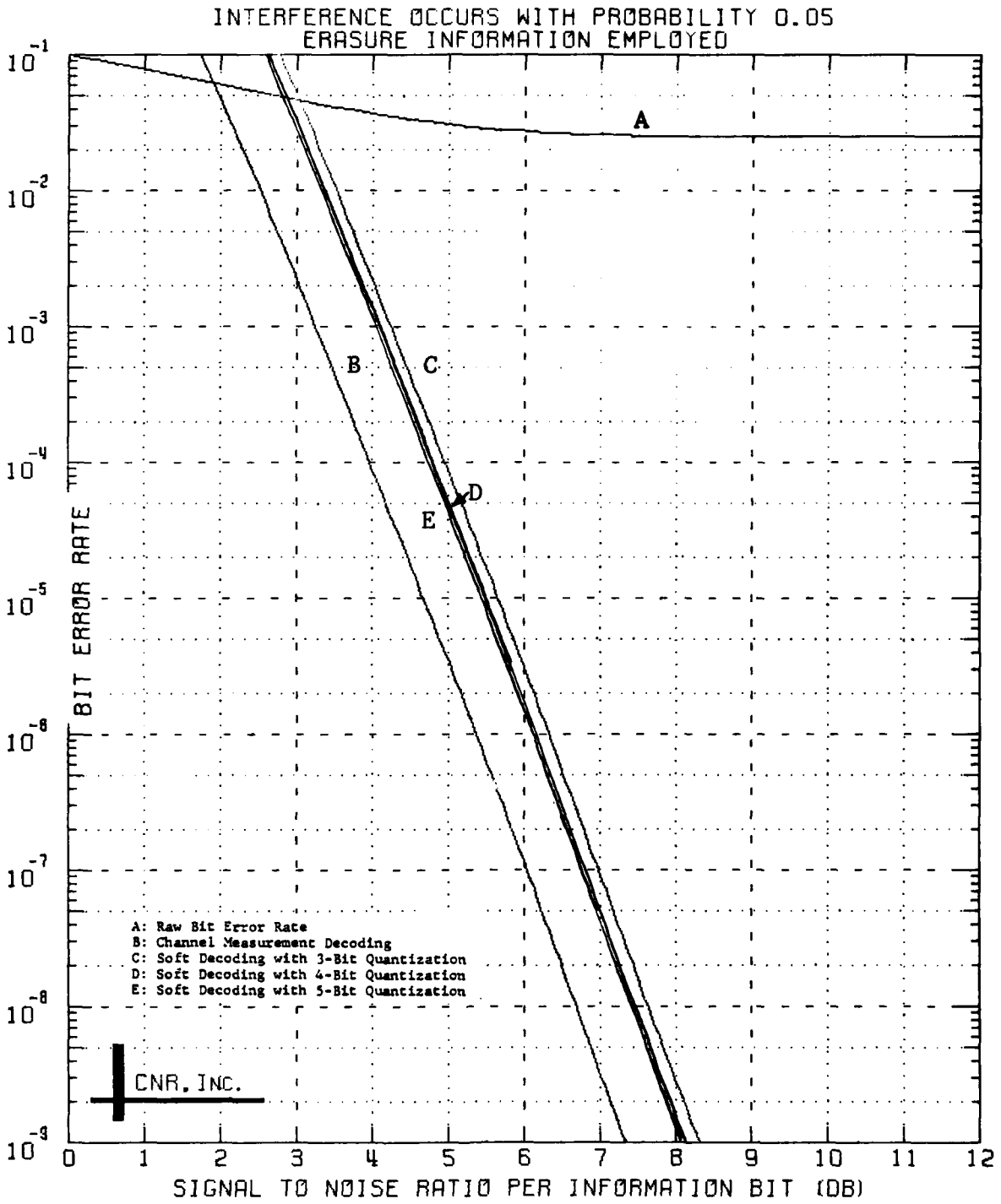


Figure 7 Decoded Performance of a Convolutional Code Rate 1/2; Constraint Length = 7; Gaussian Channel; CPSK Modulation

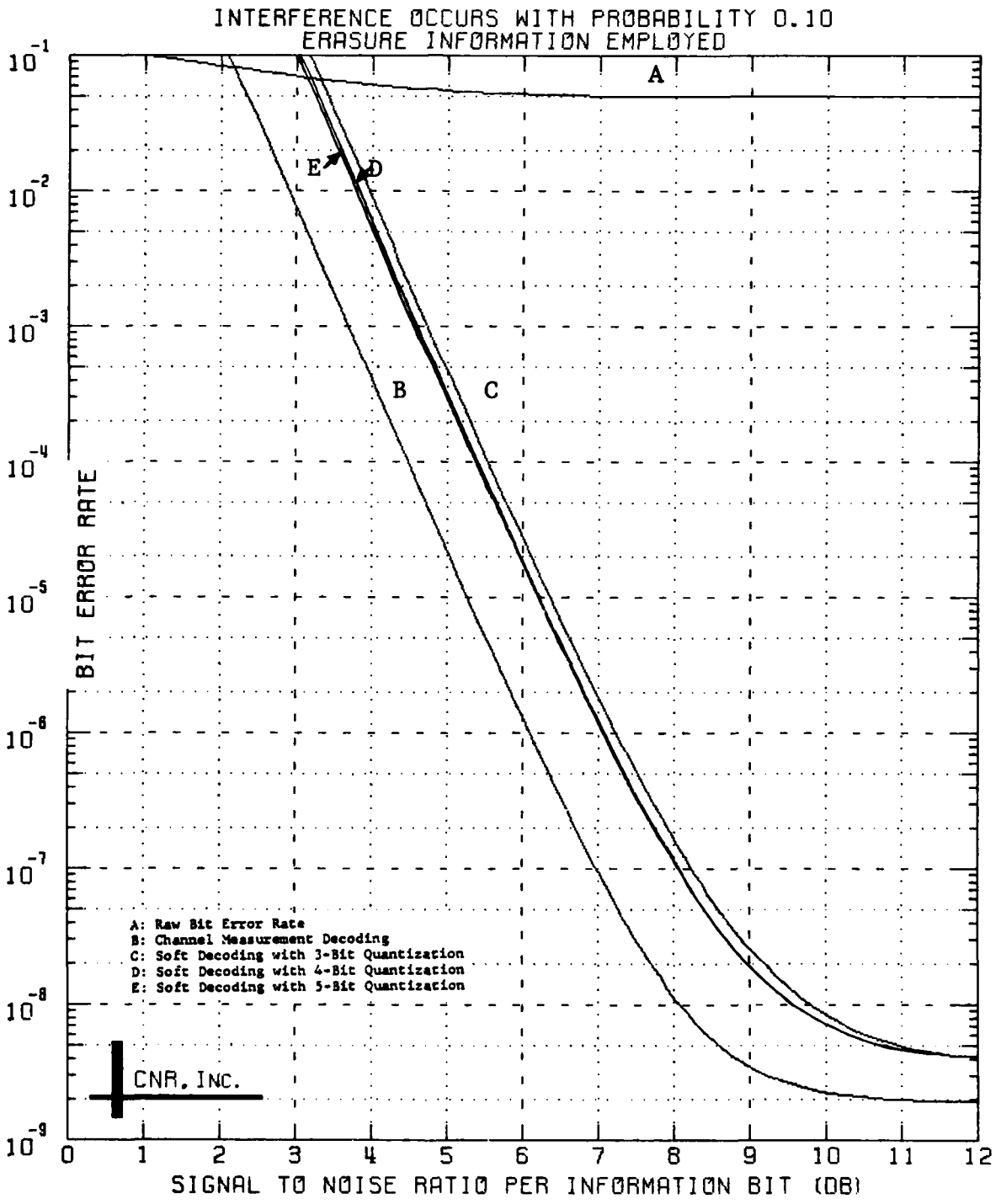


Figure 8 Decoded Performance of a Convolutional Code Rate 1/2; Constraint Length = 7; Gaussian Channel; CPSK Modulation

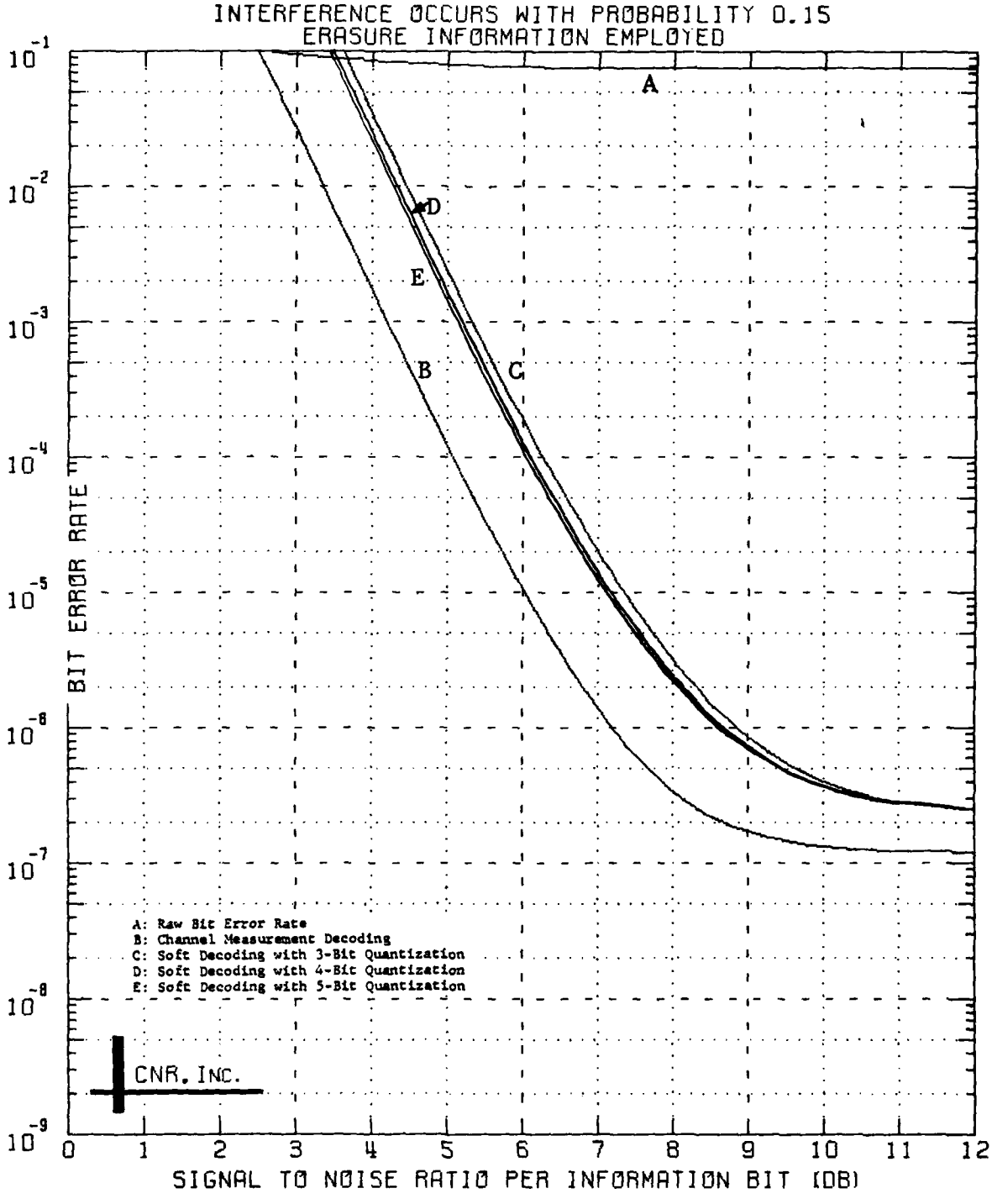


Figure 9 Decoded Performance of a Convolutional Code Rate 1/2; Constraint Length = 7; Gaussian Channel; CPSK Modulation

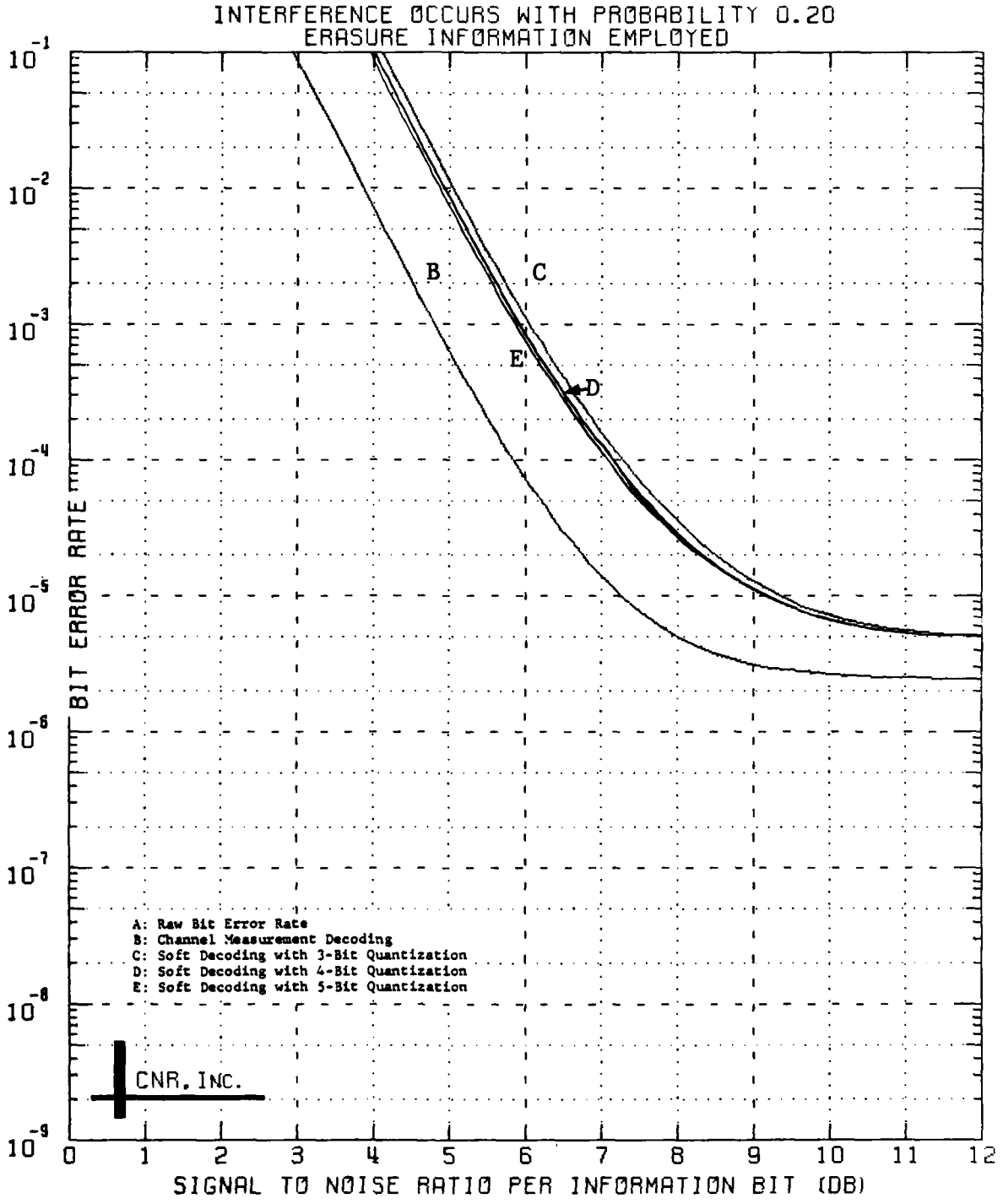


Figure 10 Decoded Performance of a Convolutional Code Rate 1/2; Constraint Length = 7; Gaussian Channel; CPSK Modulation

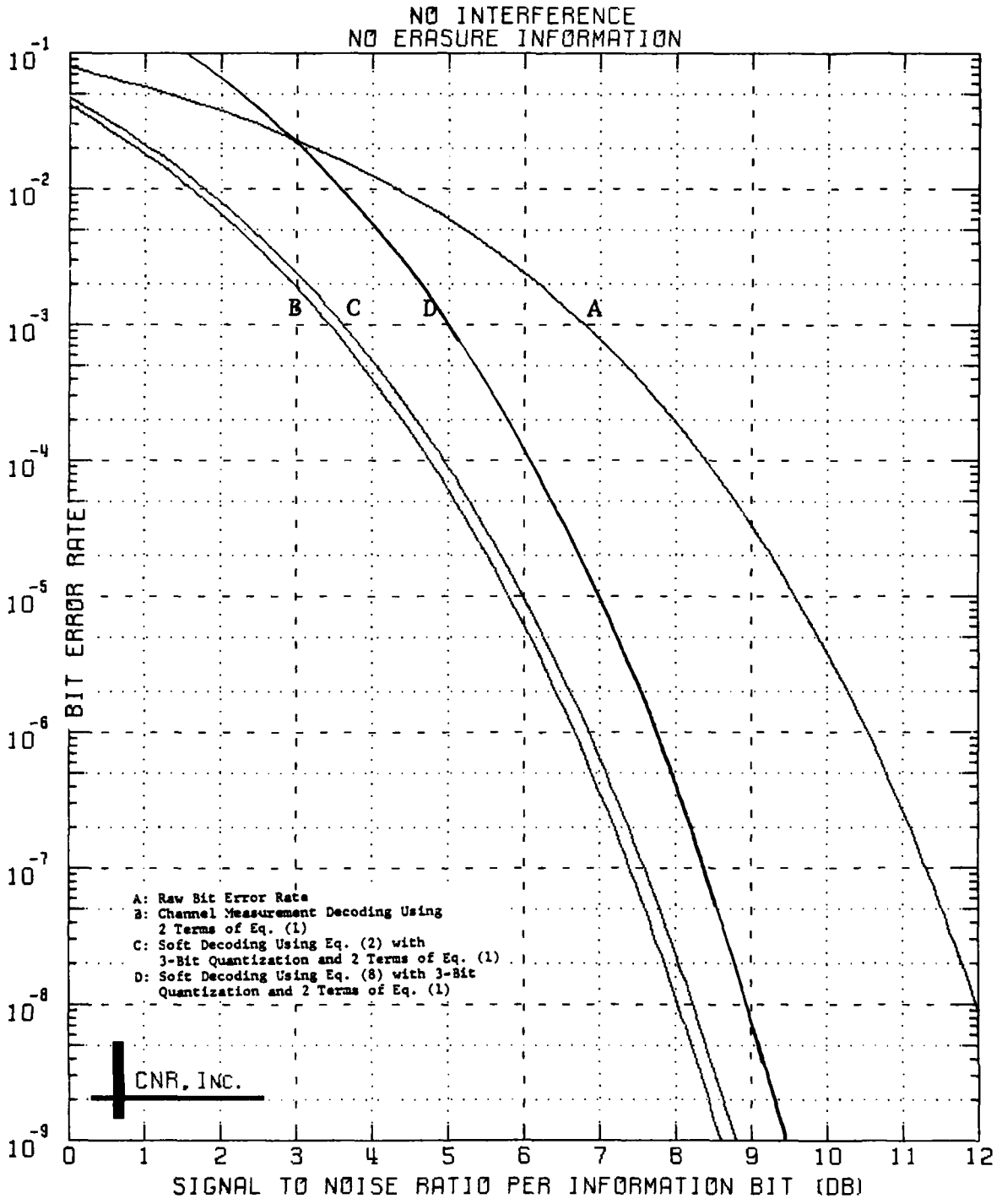


Figure 11 Decoded Performance of a Convolutional Code Rate 1/2; Constraint Length = 3; Gaussian Channel; CPSK Modulation

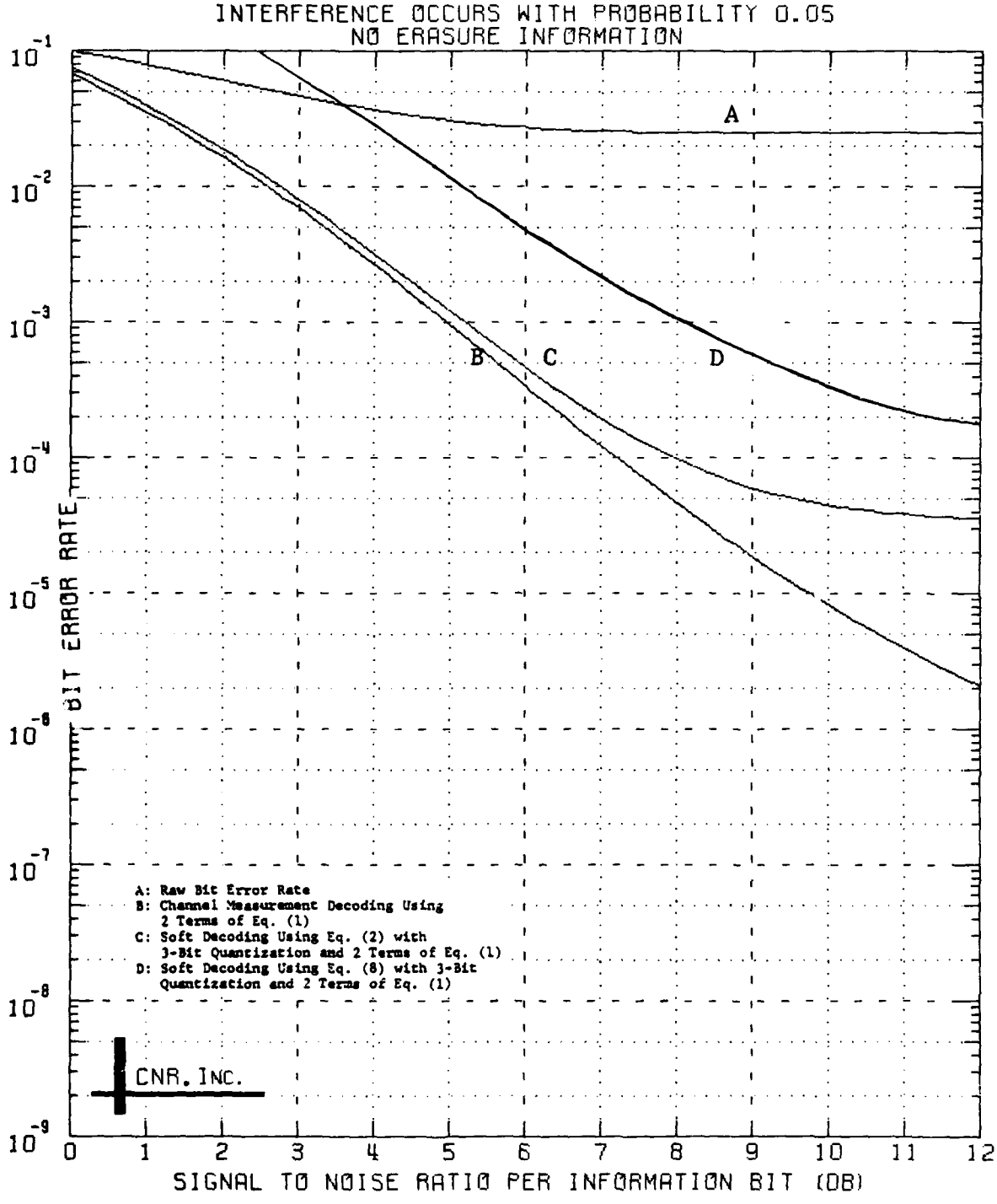


Figure 12 Decoded Performance of a Convolutional Code Rate 1/2; Constraint Length = 3; Gaussian Channel; CPSK Modulation

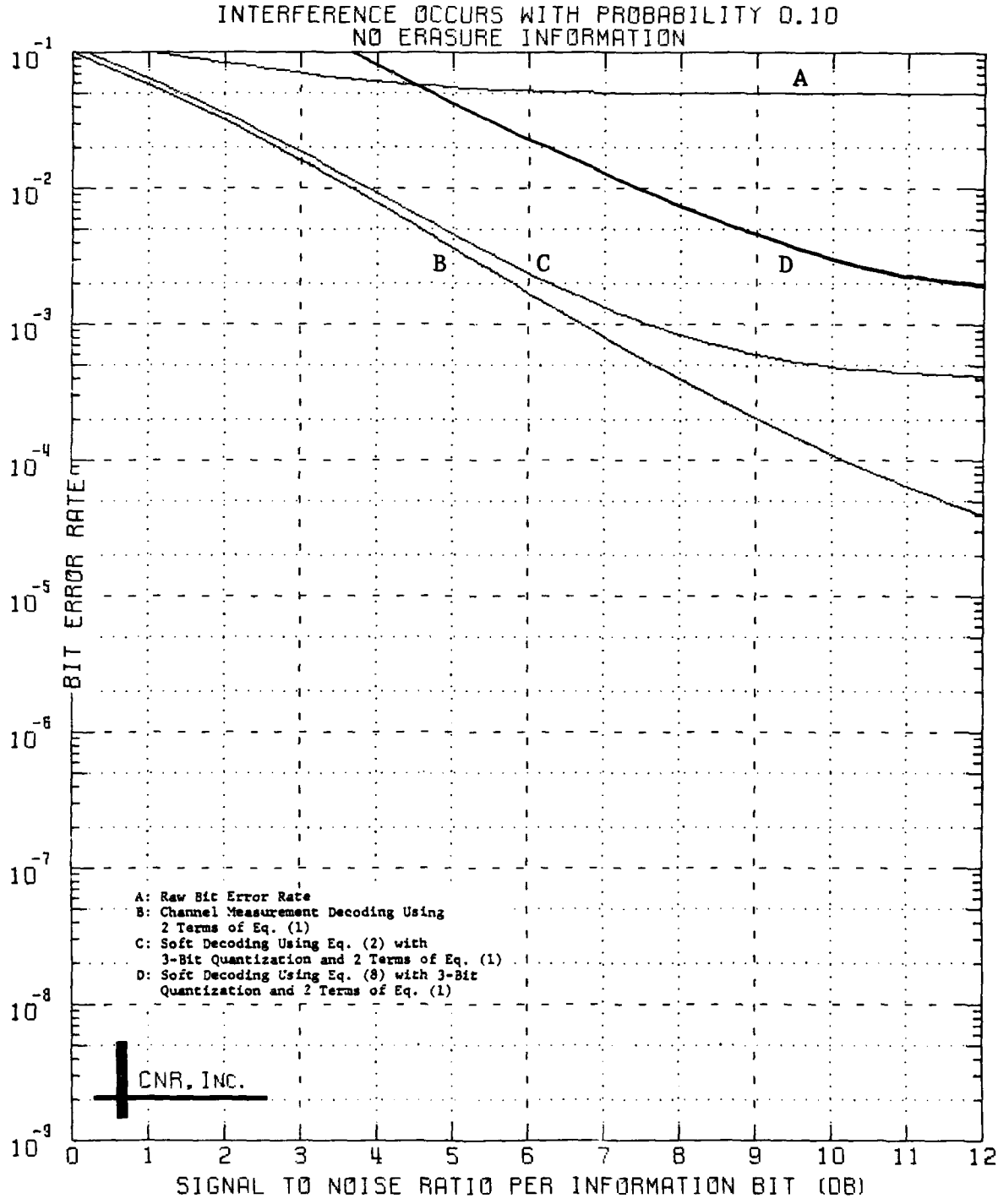


Figure 13 Decoded Performance of a Convolutional Code Rate 1/2; Constraint Length = 3; Gaussian Channel; CPSK Modulation

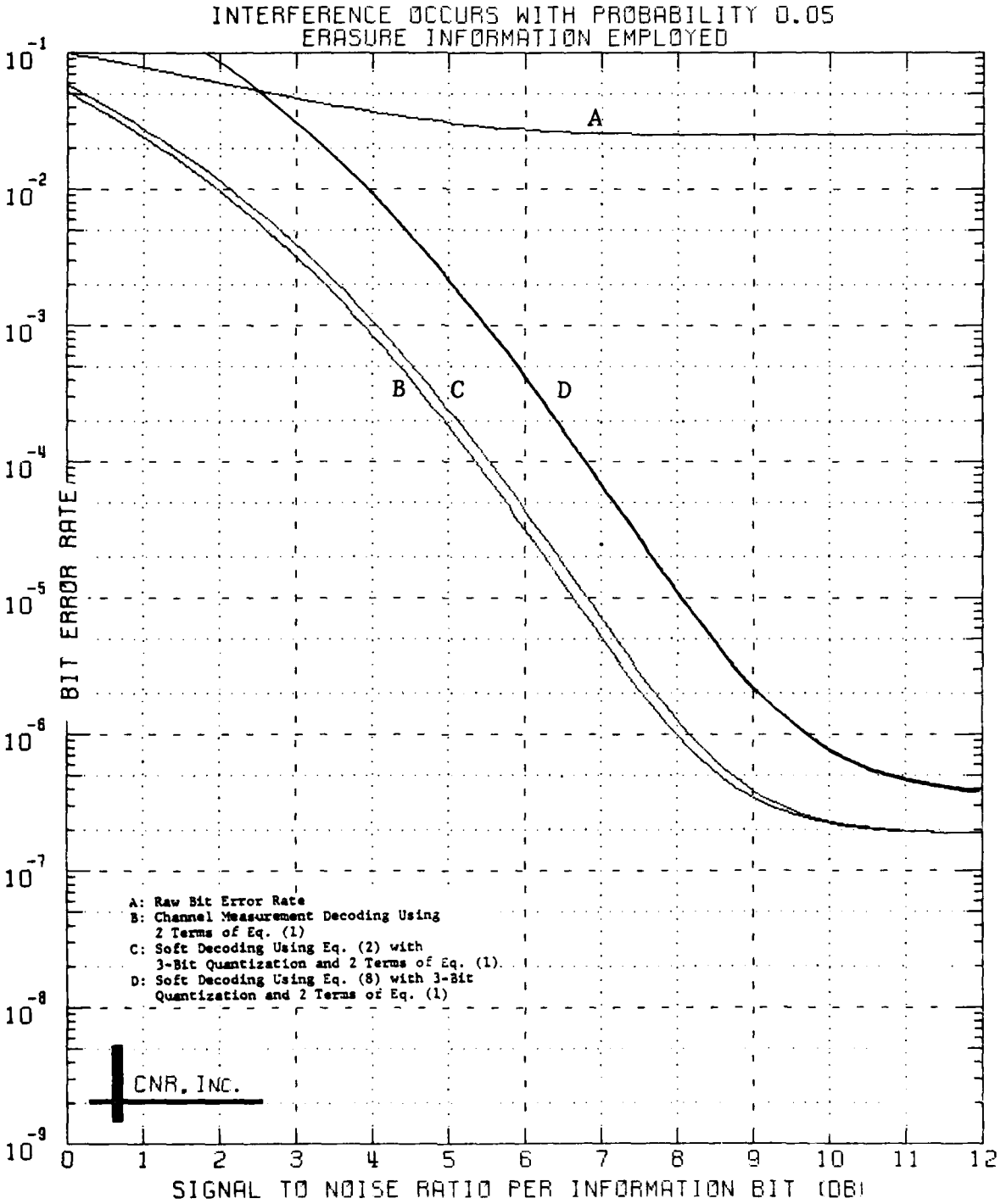


Figure 14 Decoded Performance of a Convolutional Code Rate 1/2; Constraint Length = 3; Gaussian Channel; CPSK Modulation

AD-A091 985 CNR INC NEEDHAM MA F/G 17/4
INTEGRATED CODING AND WAVEFORM DESIGN STUDY.(U)
AUG 80 D CHASE F30602-78-C-0309
UNCLASSIFIED RADC-TR-80-282 NL



END
DATE FILMED
1-81
DTIC

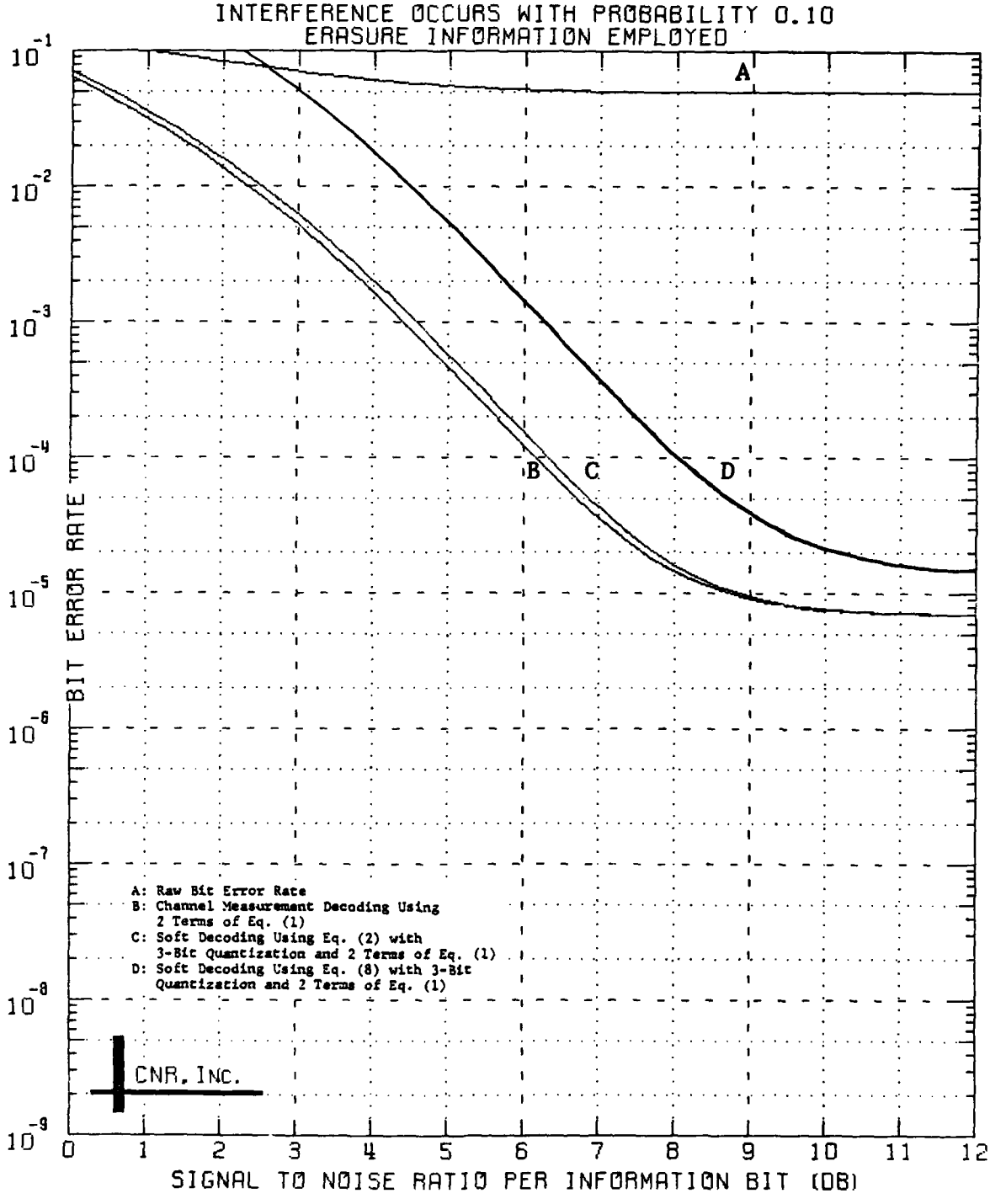


Figure 15 Decoded Performance of a Convolutional Code Rate 1/2; Constraint Length = 3; Gaussian Channel; CPSK Modulation

TABLE 1

UPPER BOUND ON THE SNR (DB) REQUIRED FOR A BIT ERROR RATE OF 10^{-5} FOR THE K = 7 CONVOLUTIONAL CODE USING 3-BIT QUANTIZATION

Code Rate	Erasure Availability	δ=0.0 SD	δ=0.05 SD	δ=0.10 SD	δ=0.15 SD	δ=0.20 SD	δ=0.25 SD	δ=0.30 SD	δ=0.35 SD
R = 1/2	Not Available	5.0	8.3	--	--	--	--	--	--
	Available	5.0	5.6	6.3	7.3	9.2	--	--	--
R = 1/4	Not Available	5.0	6.0	7.2	8.8	10.7	13.4	--	--
	Available	5.0	5.4	5.8	6.2	6.6	7.2	7.8	8.6
R = 1/8	Not Available	5.0	5.7	6.4	7.2	8.2	9.2	10.4	11.8
	Available	5.0	5.3	5.6	5.9	6.2	6.6	7.0	7.5

SD = Soft Decoding

-- Error Rate of 10^{-5} not achievable

TABLE 1 (continued)

δ=0.40	δ=0.45	δ=0.50	δ=0.55	δ=0.60	δ=0.65	δ=0.70
SD	SD	SD	SD	SD	SD	SD
--	--	--	--	--	--	--
--	--	--	--	--	--	--
--	--	--	--	--	--	--
9.8	12.0	--	--	--	--	--
13.4	15.5	--	--	--	--	--
8.0	8.6	9.3	10.1	11.2	13.1	--

SD = Soft Decoding

-- Error Rate of 10^{-5} not achievable

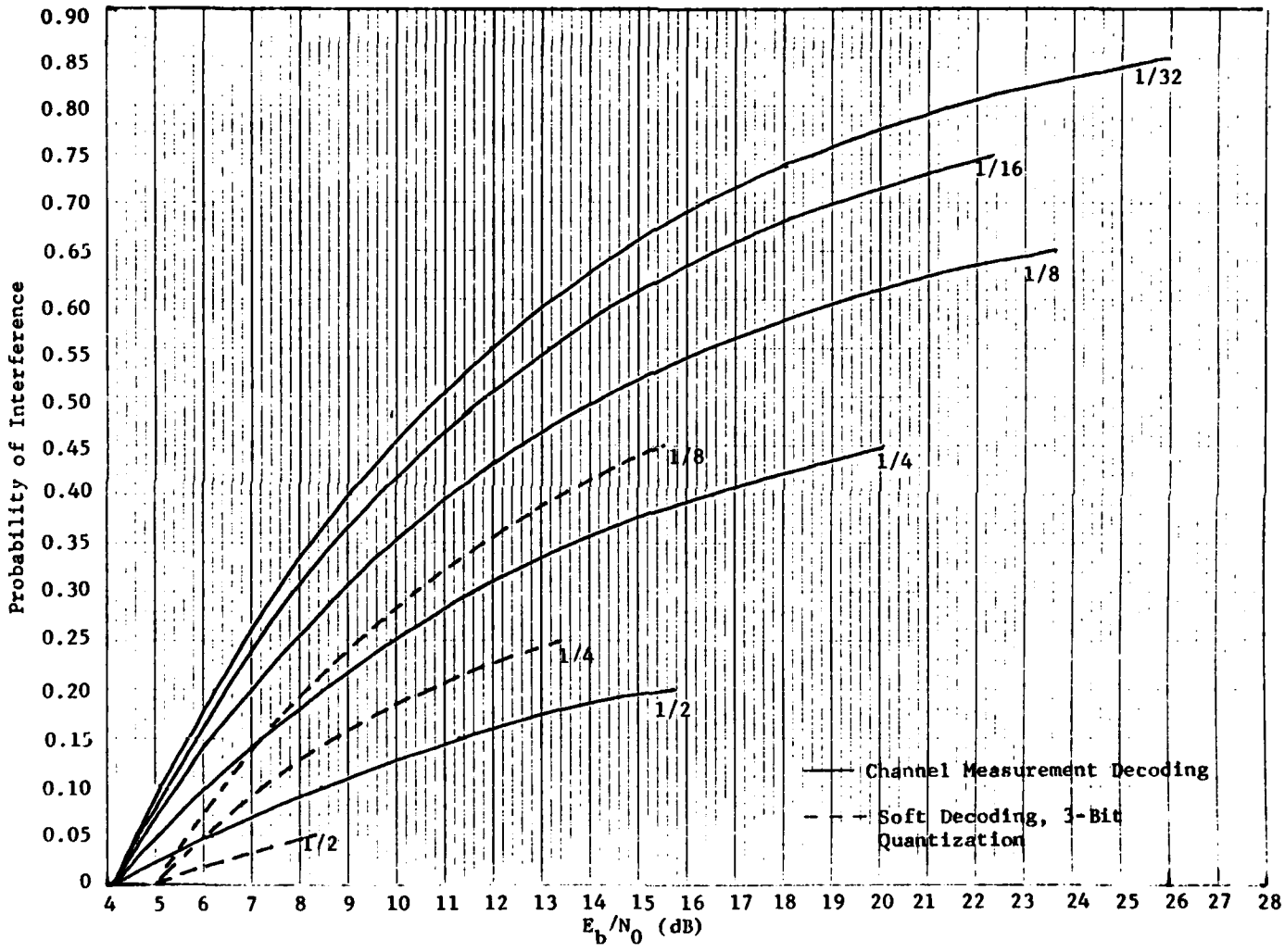


Figure 16 Signal-to-Noise Ratio per Information Bit as a Function of the Probability of Interference for a Bit Error Rate of 10^{-5} using the K=7 Convolutional Code without Erasure Information

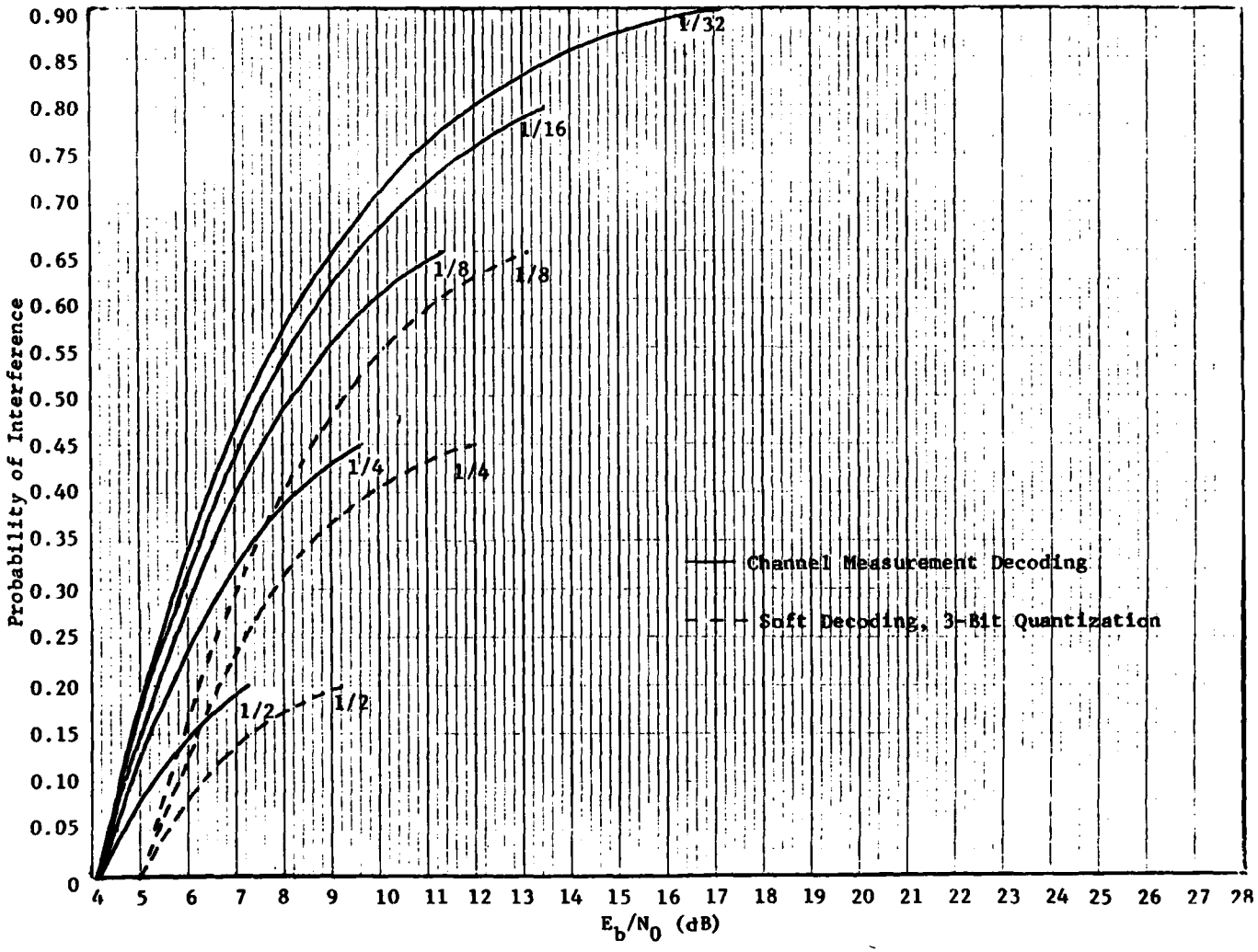


Figure 17 Signal-to-Noise Ratio per Information Bit as a Function of the Probability of Interference for a Bit Error Rate of 10^{-5} using the K=7 Convolutional Code with Erasure Information

REFERENCES

[1] A. J. Viterbi, "Convolutional Codes and Their Performance in Communication Systems," IEEE Transactions on Communications, COM-19, October 1971.

[2] J. Wozencraft and I. M. Jacobs, Principles of Communication Engineering, Wiley, 1965.

[3] J. A. Heller and I. M. Jacobs, "Viterbi Decoding for Satellite and Space Communication," IEEE Transactions on Comm. Tech., Vol. COM-19, No. 5, October 1971.

APPENDIX C

RANDOMIZED INTERLEAVER CONCEPTS

1. Introduction

Significant performance gains have been illustrated by the use of error-correcting codes for the case when the errors within a code are statistically independent. Note that if the interference is such that entire codewords are jammed, the performance of the error-correcting code is comparable to that of the uncoded system, i.e., there is no coding gain. In this appendix two techniques are discussed for approaching statistically independent code digits as assumed throughout this report. A technique for randomizing the digits interleaved by a conventional row-column interleaver is first discussed. The more efficient periodic interleaver is then discussed and a procedure is given for modifying this interleaver for operation in an ECCM environment.

2. Randomized Row-Column Interleaver

Perhaps the most common interleaver is the row-column interleaver.

For a block code of length N, a set of L codewords is first stored in a memory module of dimension L x N, as illustrated in Figure 1. The i^{th} codeword is denoted as

$$\underline{X}_i = X_{1i}, X_{2i}, \ldots, X_{Ni} \tag{1}$$

where i is over the range 1, 2, ..., L. Conventionally, the blocks are first loaded column by column and read out row by row as illustrated below:

$$X_{11}X_{12} \cdots X_{1L}X_{21}X_{22} \cdots X_{2L} \cdots X_{N1}X_{N2} \cdots X_{NL} \tag{2}$$

Thus, every digit in each block codeword is separated by L digits. This same interleaver may be used for convolutional codes providing N is chosen to be several constraint lengths long so that errors in sequences of length N are relatively independent of each other.

$$
\begin{array}{cccc}
X_{11} & X_{12} & \cdots & X_{1L} \\
X_{21} & X_{22} & \cdots & X_{2L} \\
X_{31} & X_{32} & \cdots & \vdots \\
X_{41} & X_{42} & \cdots & \vdots \\
\vdots & & & \vdots \\
X_{N1} & X_{N2} & \cdots & X_{NL}
\end{array}
$$

Figure 1 Row-Column Interleaver

To randomize this interleaver, the L x N digits are first read in as shown on Figure 1, but read out in a pseudo-random manner. At the receiver, these L x N digits are read in an L x N memory module in this same pseudo-random manner.

A randomized interleaver of this nature is effective when the interference is of small duration when compared to the memory of L x N digits. Since the digits in each codeword are randomly distributed among L codewords, we are no longer guaranteed to have L digits separating code digits of each codeword. This loss in conventional burst-correcting capabilities is necessary for ECCM applications since a conventional row-column interleaver is easily defeated by a periodic pulse jammer operating with a period of L.

Depending on the required ECCM capabilities, the pseudo-random readout can vary over every set of L x N digits or be fixed for each set of L codewords. The first approach is harder to jam but is more difficult to synchronize. The latter approach is effective against pulse-type jammers which do not have knowledge of the pseudo-random sequence used to read out the L x N digits.

The memory requirement for this type of interleaver is no greater than*

$$S_T = 2 L x N \tag{3}$$

since as one memory module is read out, a second module may be loaded. The deinterleaver memory is the same if binary decisions are used by the decoder, but is increased if erasure information or channel measurement information is used by the decoder.

3. Continuous-Type Interleavers

For applications where the interleaver memory must be minimized, a periodic interleaver can be shown to minimize the required memory [1],[2],[3]. This class of interleavers will be referred to as continuous-type interleavers since data is always flowing through the memory.

---

*Some reduction in memory may be possible if new digits can be read in as old digits are read out. This is easily achievable if a conventional N x N row-column interleaver is used.

A separation of Q digits for adjacent digits in a codeword is obtained by the interleaver shown in Figure 2. Every block of N bits is fed to the periodic interleaver simultaneously. Digit 0 is passed through path #0; digit 1 is passed through path #1; etc. Therefore, the i^{th} digit in every block is delayed by i(Q-1) digits; thus, the i^{th} and $(i+1)^{th}$ digits are separated by

$$1 + (i+1)(Q-1) - i(Q-1) = Q \text{ digits} \tag{4}$$

In other words, there are Q-1 digits from other code blocks between the i^{th} digit and the (i+1) digits of the code block under consideration.

The periodic deinterleaver is shown in Figure 3. An easy way to understand the operation of deinterleaving is to observe the fact that the total delay of the i^{th} path is

$$D = i(Q-1) + (N-1-i)(Q-1)$$

$$= (N-1)(Q-1) \qquad \text{for all } i \tag{5}$$

Therefore, the combined effect of the interleaver and deinterleaver is to delay every digit by a constant amount of (N-1)(Q-1) digits.

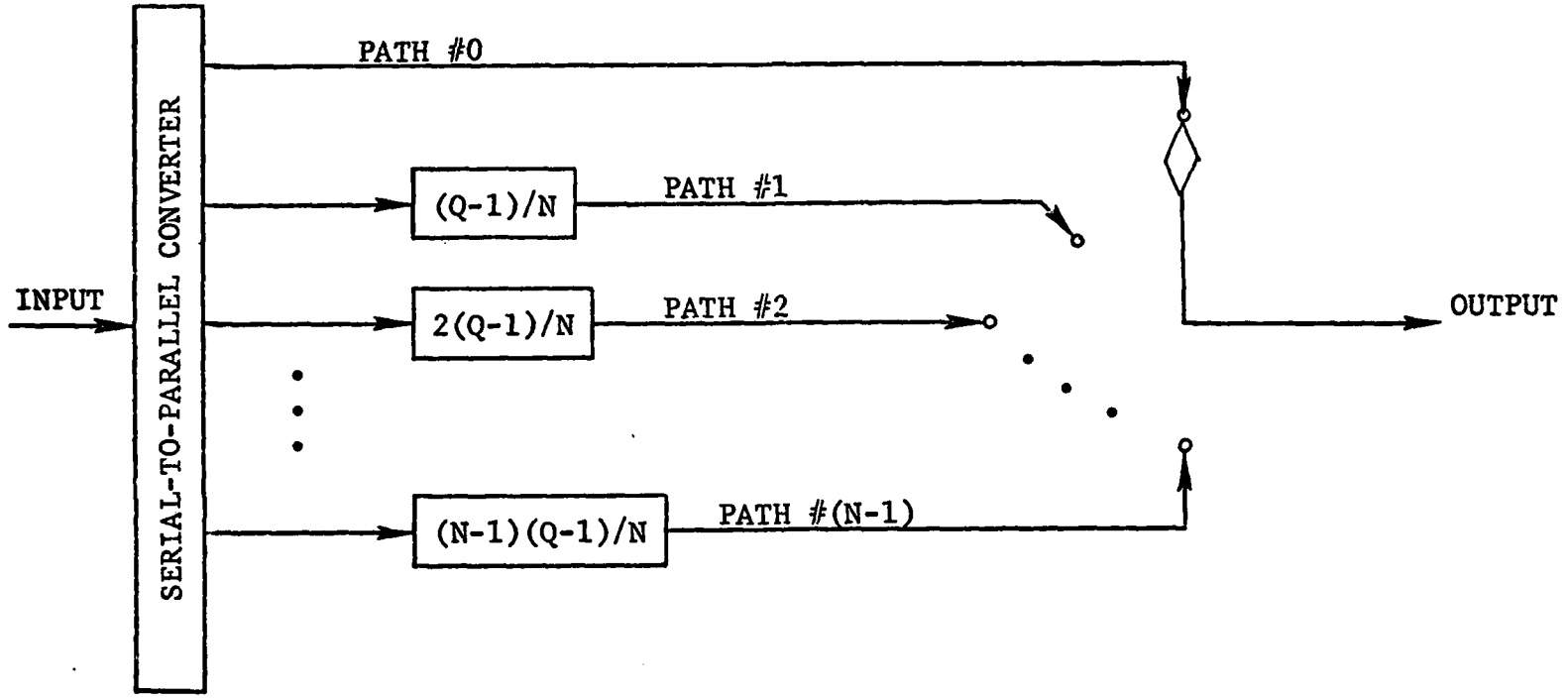
Since each path in the combined interleaver and deinterleaver has exactly (N-1)(Q-1)/N memory units, the total required storage elements in the interleaver and deinterleaver for all N paths are given by

$$S = (N-1)(Q-1) \tag{6}$$

providing a binary decoder is used. It is clear that the required storage elements in the interleaver and deinterleaver are equal, i.e.,

$$S_T = S_R = \frac{1}{2}(N-1)(Q-1) \text{ digits} \tag{7}$$

where S_T and S_R are the respective required storage elements for the transmitter and receiver.



Quantities shown in the boxes are delays. Each unit delay shown in equivalent to a delay of N digits.

Figure 2 A Periodic Interleaver

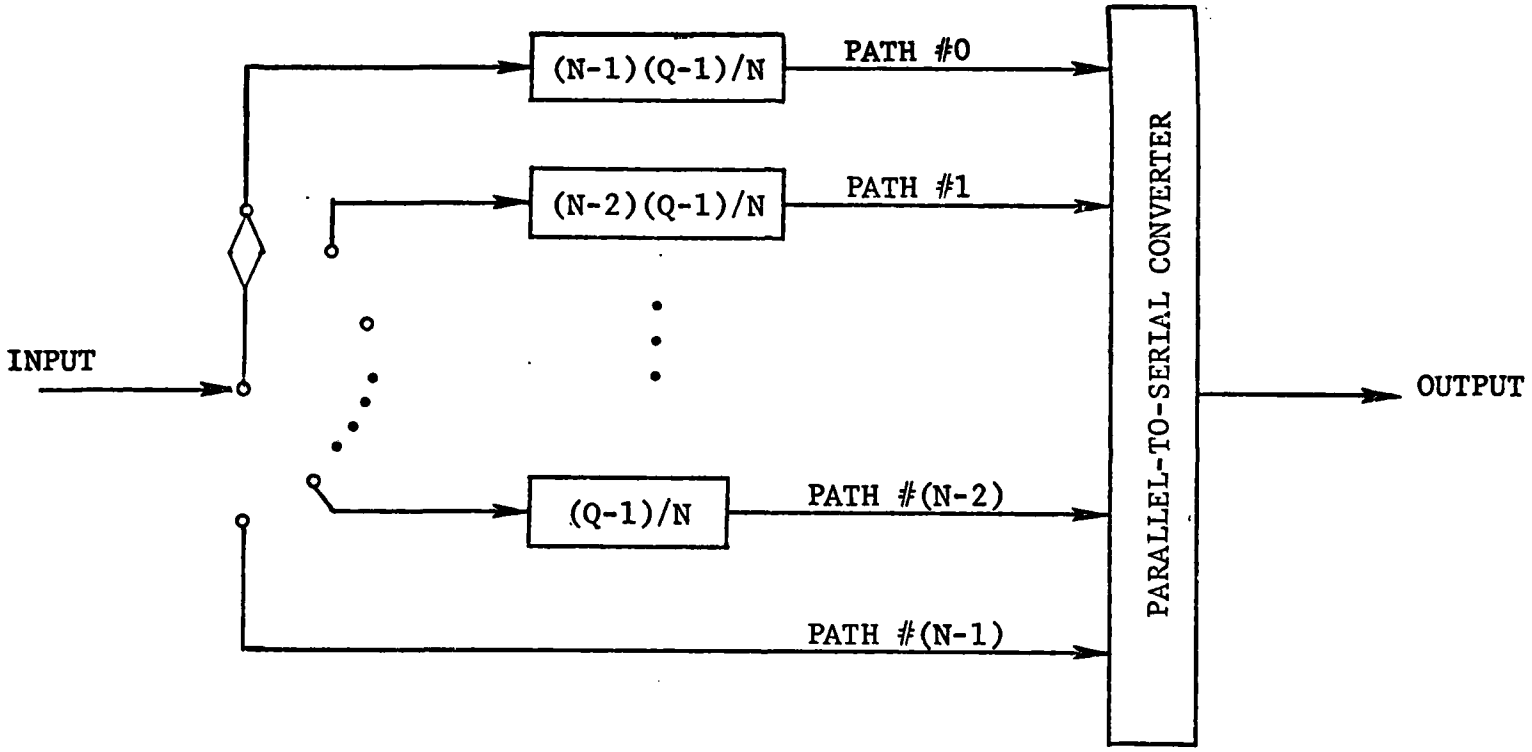


Figure 3 A Periodic Deinterleaver

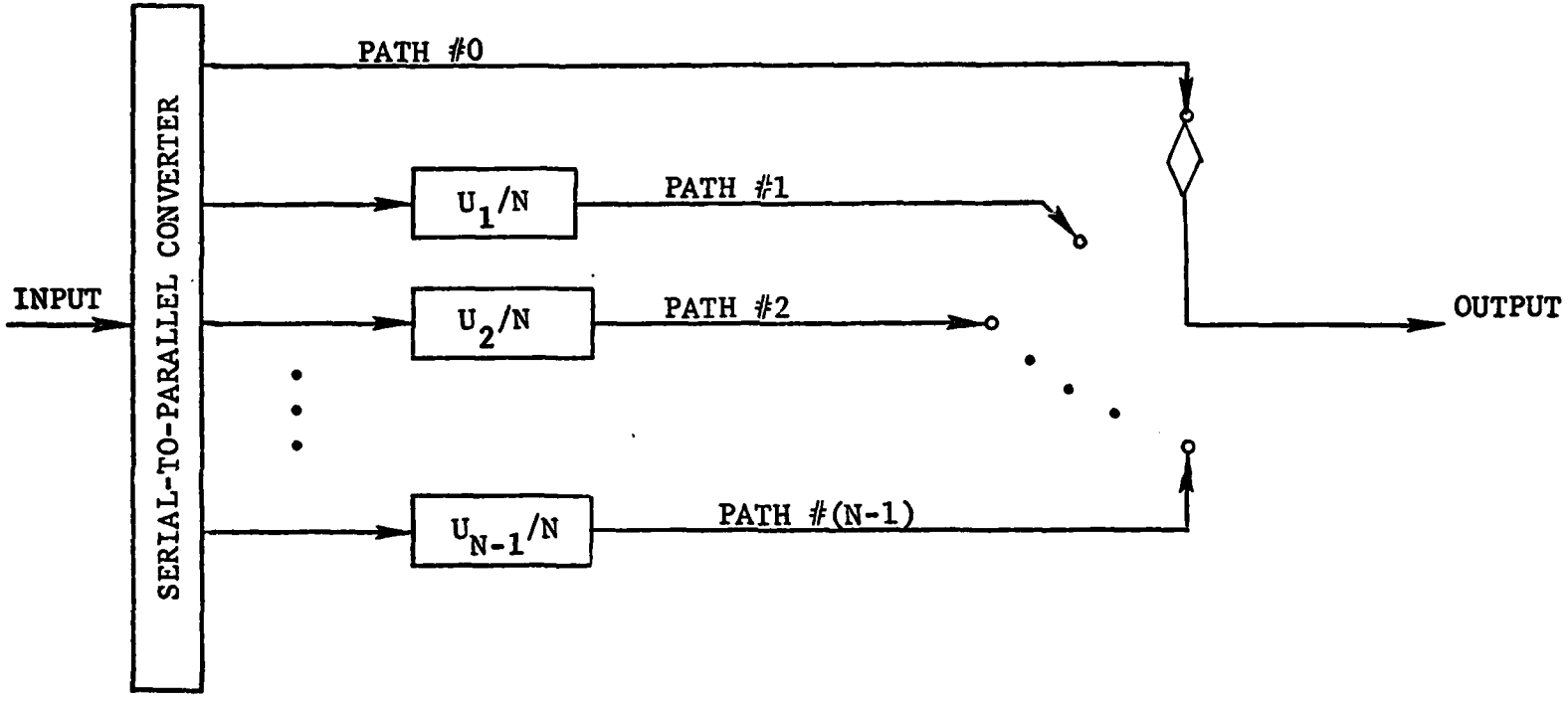
When a channel measurement decoder and/or erasure decoder is used, the storage of the interleaver is still given by (7), but that of the deinterleaver is increased by the number of bits used to represent the soft decisions and erasures.

The advantage of this type of interleaver over the row-column interleaver is the reduction in the required storage. When $L = Q$, comparing Eqs. (2) and (7), we note that the periodic interleaver offers approximately a factor of 4 savings in storage over the row-column interleaver for the same amount of burst-error protection.

To randomize this type of interleaver, one may vary the storage in each of the (N-1) paths, as shown in Figure 4. The deinterleaver is shown in Figure 5. The key property of this interleaver/deinterleaver is that the combined storage for each path is

$$\frac{(N-1)(Q-1)}{N} \tag{8}$$

which corresponds to a total delay of (N-1)(Q-1) digits as is the case for the periodic interleaver/deinterleaver combination. However, the code digit within a code is separated by U_1+1, U_2-U_1+1,.... which can be chosen arbitrarily over the range of 0 to (N-1)(Q-1). For convenience, we assume $U_i > U_{i-1}$. The key disadvantage of this type of interleaver is the difficulty involved in changing the delays U_i for applications where these delays may be known by the jammer. One approach is to use a known synchronizing sequence between each new set of delays. Note that the code digits in the interleaver/deinterleaver must be read out before the memories in each path can be changed. For applications where it is assumed that the pulse jammer does not have knowledge of the durations U_i between code letters, the interleaver/deinterleaver combination, illustrated on Figures 4 and 5, is considerably more efficient, from a storage point of view, than the randomized row-column interleaver.



Quantities shown in the boxes are delays. Each unit delay shown is equivalent to a delay of N digits.

Figure 4 A Continuous Interleaver

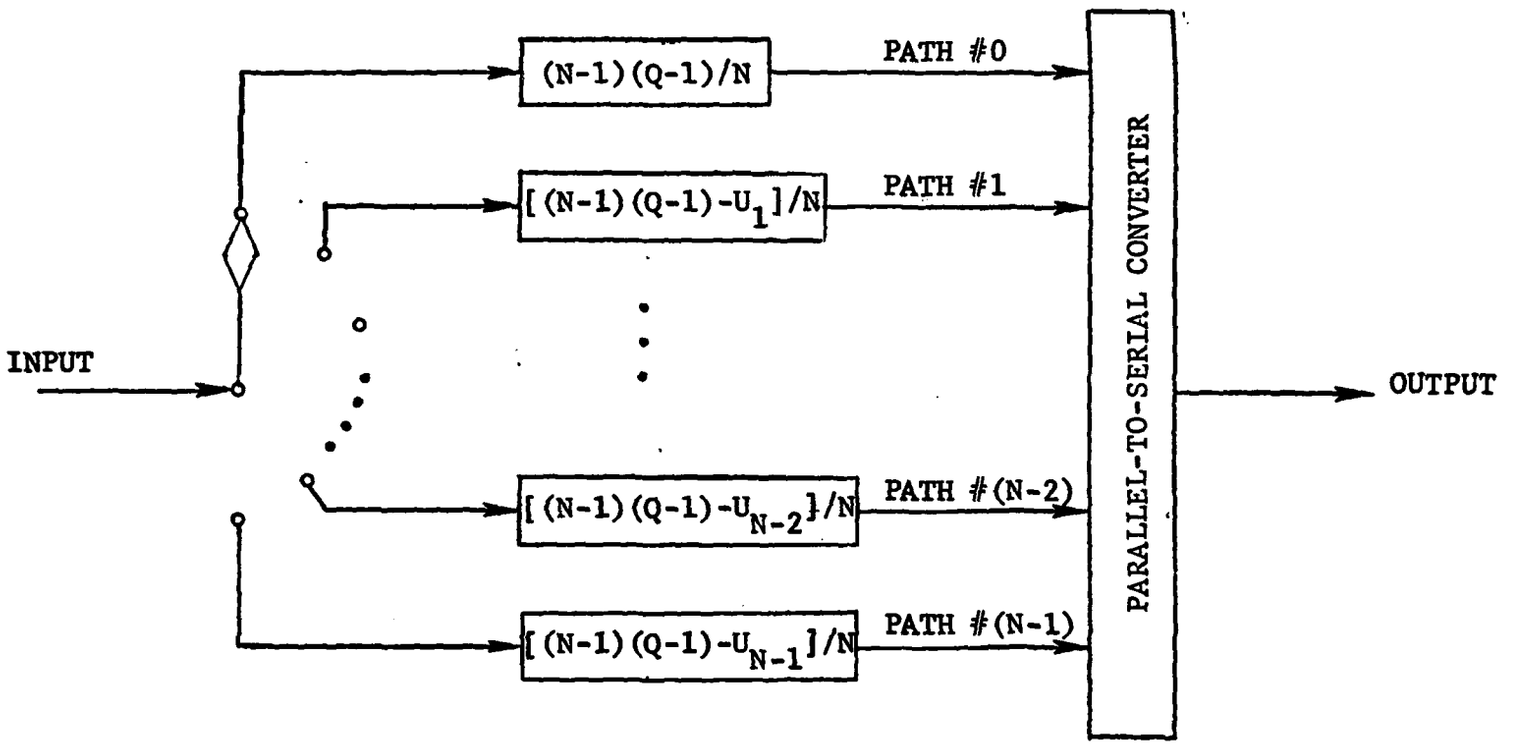


Figure 5 A Continuous Deinterleaver

REFERENCES

[1] G. D. Forney, Jr., "Burst-Correcting Codes for the Classic Bursty Channel," IEEE Trans. on Comm. Tech., Vol. COM-19, No. 5, October 1971, pp. 772-781.

[2] CNR, Inc., "Troposcatter Interleaver Study Report," RADC-TR-75-19, Phase Report for Rome Air Development Center, February 1975.

[3] CNR, Inc., "Coding/Mux Overhead Study," RADC-TR-75-71, Final Technical Report for Rome Air Development Center, March 1975.

MISSION
of
Rome Air Development Center

RADC plans and executes research, development, test and selected acquisition programs in support of Command, Control Communications and Intelligence (C^3I) activities. Technical and engineering support within areas of technical competence is provided to ESD Program Offices (POs) and other ESD elements. The principal technical mission areas are communications, electromagnetic guidance and control, surveillance of ground and aerospace objects, intelligence data collection and handling, information system technology, ionospheric propagation, solid state sciences, microwave physics and electronic reliability, maintainability and compatibility.